REPORT DOCUMENTATION PAGE

Form Approved OMB No. 0704-0188

Public reporting burden for this collection of information is estimated to average 1 hour per response, including the time for reviewing instructions, searching existing data sources, gathering and maintaining the data needed, and completing and reviewing the collection of information. Send comments regarding this burden estimate or any other aspect of this collection of information, including suggestions for reducing the burden, to Department of Defense, Washington Headquarters Services, Directorate for Information Operations and Reports (0704-0188), 1215 Jefferson Davis Highway, Suite 1204, Arlington, VA 22202-4302. Respondents should be aware that notwithstanding any other provision of law, no person shall be subject to any penalty for failing to comply with a collection of information if it does not display a currently valid OMB control number.
PLEASE DO NOT RETURN YOUR FORM TO THE ABOVE ADDRESS.

1. REPORT DATE *(DD-MM-YYYY)*	2. REPORT TYPE	3. DATES COVERED *(From – To)*
27-11-2006	Conference Proceedings	16 October 2006 - 20 October 2006

4. TITLE AND SUBTITLE

Biological Effects of Electromagnetic Fields

5a. CONTRACT NUMBER
FA8655-07-1-5026

5b. GRANT NUMBER

5c. PROGRAM ELEMENT NUMBER

6. AUTHOR(S)

Conference Committee

5d. PROJECT NUMBER

5d. TASK NUMBER

5e. WORK UNIT NUMBER

7. PERFORMING ORGANIZATION NAME(S) AND ADDRESS(ES)

University of Ioannina
Panepistimioupolis
IOANNINA GR45110
Greece

8. PERFORMING ORGANIZATION REPORT NUMBER

N/A

9. SPONSORING/MONITORING AGENCY NAME(S) AND ADDRESS(ES)

EOARD
PSC 821 BOX 14
FPO AE 09421-0014

10. SPONSOR/MONITOR'S ACRONYM(S)

11. SPONSOR/MONITOR'S REPORT NUMBER(S)
CSP 07-5026

12. DISTRIBUTION/AVAILABILITY STATEMENT

Approved for public release; distribution is unlimited. (approval given by local Public Affairs Office)

13. SUPPLEMENTARY NOTES

14. ABSTRACT

The Final Proceedings for Biological Effects of Electromagnetic Fields, 16 October 2006 - 20 October 2006

15. SUBJECT TERMS

Biology, Radio Frequency Safety and Health

16. SECURITY CLASSIFICATION OF:			17. LIMITATION OF ABSTRACT	18, NUMBER OF PAGES	19a. NAME OF RESPONSIBLE PERSON
a. REPORT	b. ABSTRACT	c. THIS PAGE			ROBERT N. KANG, Lt Col, USAF
UNCLAS	UNCLAS	UNCLAS	UL	1510	19b. TELEPHONE NUMBER *(Include area code)* +44 (0)20 7514 4437

EMF EFFECTS ON MICROCIRCULATORY SYSTEM

CHIYOJI OHKUBO

RAD, WORLD HEALTH ORGANIZATION, GENEVA CH1211, SWITERLAND

Abstract

The speaker reviews the importance of studying the effects of electromagnetic fields on microcirculatory system, especially in respect of possibility that vasculature may have direct and indirect role in interaction of static magnetic fields. It outlines the physiological importance of microcirculation and relatively new methods of evaluation technique in vivo and explains in details the local and/or whole body exposure effects of static magnetic field with range of 0.3–180 mT, power frequency electromagnetic fields with range of 0.1-30 mT and microwaves at 1.5 GHz with range 0.08 - 8 W/kg brain average SARs on microcirculatory systems in different tissues in experimental animals.

Introduction

The circulatory system is the transport system of the organism that supplies O_2, ions, hormones, and substances absorbed from the gastrointestinal tract to the tissues, and returns CO_2 to the lungs and other products of metabolism to the liver and kidneys. It also has a central role in the regulation of body temperature, and the distribution of the hormones and other agents that regulate tissue and cell function. The principal function of microcirculation is exchanging physiological substances between blood and tissues, and the compensatory adjustments should contribute to the efficacy of the exchange process: lumen dimensions, length, tortuosity, diameter of branch ratios, vascular density, wall thickness, vessel diameter (vasomotion), blood flow velocity, blood viscosity, intramicrovascular hematocrit, leukocyte-endothelial cell interaction and others.

Microcirculation consists of structurally and functionally differentiated small blood vessels: small muscular arteries, arterioles, metarterioles, capillaries, postcapillary venules, venules, and lymphatic capillaries. In the cutaneous microvascular beds, the connection between the arterioles and the venules is made by some thoroughfare channels including capillaries or arteriolar-venular shunts. In most vascular beds, the precapillary resistance vessels are responsible for the largest function of the resistance in a vascular bed, and hence are the major components that influence regional hemodynamics and total peripheral resistance. Smooth muscle cells are found in all of these except the blood capillaries and lymphatic capillaries. The blood capillary wall is composed of a single layer of endothelial cells. The lymphatic capillaries are composed of endothelium-lined vessels similar to blood capillaries. Fluid and protein that have extravasated from the blood capillaries partially enter the lymphatic capillaries and are transported via the lymphatic system back to the blood vascular system. Postcapillary venules play an important role in fluid and cellular exchange and are the major site of leukocyte migration into tissue spaces.

Rhythmical and spontaneous changes in both the diameter of arterioles and the volume and velocity of blood flow due to constriction and dilation of the vascular smooth muscle are known as vasomotion (1). The quantitative description of spontaneous arteriolar vasomotion requires data on frequency, amplitude, diameter, and branching order of the vessels observed. Fluid absorbed into lymphatic capillaries is passively transported through dynamic changes due to arteriolar vasomotion in cutaneous tissue. Frequency and amplitude of spontaneous vasomotion could play an important role in disease. In microangiopathies, lymphedema, and essential hypertension, altered patterns of arteriolar vasomotion could constitute an additional pathogenetic factor (2). Extracellular control of the smooth muscle cells is exerted through neurogenic, hormonal, local and myogenic mechanisms (3).

For evaluating EMF exposure effects on microcirculatory system, various microcirculatory preparations, e.g., rabbit ear chamber (REC) (4), dorsal skin fold chamber (DSC) in mice (5) and cranial window (CW) in mice and rats (6-7), have been used to observe and analyze microcirculation in our group. These preparations allow non-invasive, continuous measurement of hemodynamics, blood velocity, angiogenesis, metabolites, e.g., pH and pO2, transport of molecules and particles, and cell to cell interactions in vivo (8).

Static fields

The REC offers the advantage of superior optical quality. Due to the longer duration of an individual measurement, we have exclusively utilized REC to investigate the effects of SMFs on microcirculation using microphotoelectric plethysmography (MPPG) monitoring system. REC is a round-table chamber made of acryl resin for disk with an observing table and three holding pillars, a sustaining ring, and a glass window. The

methods for installation of REC and its availability to the bioelectromagnetic research have been published in detail (9-12). Blood Pressures (BPs) in a central artery contralateral to that of an ear lobe having the REC, fixed on the stage of the microscope, were monitored by a BP monitoring system.

1. Local exposure on the ear lobe to SMF (1.0 mT, 10 min) in conscious rabbits
Experimental Procedures: The SMF of 1.0 mT were generated by a C-shaped electromagnet device. An animal set on the observing stage of a microscope, laid prone in a holder without anesthesia. An intact central artery of the ear lobe fixed on an observing stage of the microscope was applied to analyzing the temporal changes of microcirculation in MPPG monitoring system. Two experimental procedures were randomly categorized: (1) sham exposure (CTL) and SMF exposure (SMF). MPPG profiles including DC levels and amplitudes of MPPG and/or BPs just before (pre-) exposure were compared with those during exposure and post-exposure.
Results: SMFs had a biphasic effect upon the microcirculatory system; when the vascular tone was low, the SMF induced vasoconstriction, and when it was high, the SMF induced vasodilation (9).

2. Whole-body exposure to SMF (5.5 mT, 30 min) in conscious rabbits
Experimental Procedures: The SMFs of 5.5 mT (Bmax) were generated by a doughnut-shaped annular electromagnet device. A rabbit in a holder was placed into the annular electromagnets. The measured magnetic flux densities were 5.0–5.5 mT in the trunk, 0.5–4.0 mT in the head, 1.0–4.0 mT in the throat, and<1.0 mT in the ear lobe, respectively. Two experimental procedures were randomly categorized: sham exposure (CTL) and SMF exposure (SMF). These values pre-exposure were compared with those during exposure and post-exposure.
Results: Comparing SMF with CTL, there were no significant changes in MPPG values throughout the experiment. For BPs, comparing SMF with CTL, there were no significant changes throughout the experimental period (13).

3. Local exposure on the ear lobe to SMF (1.0 mT, 10 min) in pharmacologically treated rabbits with REC
This study is attempted to demonstrate the vasoconstrictor effect as well as the vasodilating effect by local exposure on the cutaneous microcirculation within a REC under pharmacologically modified vascular tone. Based on the hypothesized effects, nor-adrenaline (NA) and acetylcholine (ACh) were chosen to enhance and reduce the vascular tone pharmacologically.
Experimental Procedures: Cutaneous microcirculation of REC exposed to SMF was studied under pharmacological treatment using MPPG method. NA and ACh were used for increase sympathetically and decrease parasympathetically in vascular tone, respectively.
Results: The temporal changes of MPPG profiles during and after exposure were quantitatively analyzed. In NA group, the vasoconstriction with reduced vasomotion was observed throughout the experimental period. In NA+SMF group, the vasoconstrictor effects with reduced vasomotion followed by NA infusion were significantly reduced. In contrast, in ACh group, the vasodilation with increased vasomotion was observed throughout the experimental period. In ACh+SMF group, however, the vasodilator effect with increased vasomotion followed by ACh infusion were significantly reduced. In mean amplitudes of MPPG between ACh+SMF and ACh groups, there were significant differences for up to 60 min after cessation of SMF exposure. In CTL group, there were no significant changes throughout the experimental period (11).

4. Local exposure on the ear lobe to SMF (1.0 mT, 30 min) in pharmacologically treated rabbits without REC
The purpose of this study is to elucidate the hypothesized homeostatic effects of SMF on BPs, and to show that it can alter the microcirculation in a cutaneous tissue and hence modify the BPs. This study was designed to investigate the effects of SMF on a Ca^{2+} channel blocker, nicardipine (NIC)-induced hypotension as well as a nitric oxide synthase (NOS) inhibitor, Nx-nitro-L-arginine methyl ester (L-NAME)- induced hypertension.
Experimental Procedures: The effects of SMF on BPs in rabbits were investigated under pharmacological treatment. Hypotensive and vasodilator actions were induced by NIC. Hypertensive and vasoconstrictor actions were induced by L-NAME.
Results: In NIC alone, the acute and intense vasodilation with increased vasomotion resulting in increases of both MPPG parameters was observed. In SMF + NIC, by contrast, the vasodilating effect with increased vasomotion following NIC injection was reduced. In mean amplitude between SMF+NIC and NIC, there was a significant difference during SMF exposure. In L-NAME alone, 10 min after L-NAME infusion, the vasoconstriction resulting in decreases of mean DC level was observed. In SMF + L-NAME, by contrast, the vasoconstrictor effect following L-NAME infusion was reduced. In mean amplitude between SMF + L-NAME and L-NAME, however, there were no significant differences throughout the experimental period. In NIC alone, BPs decreased from baseline immediately after NIC injection. In contrast, in SMF + NIC, the reduction of BPs was suppressed. In L-NAME alone, BPs gradually increased from baseline after L-NAME infusion. In contrast, in SMF + L-NAME, the elevation of BPs was suppressed during exposure and post-exposure (14).

5. Local exposure on the neck or pelvic to SMF (1.0-5.5 mT, 30 min) in pharmacologically treated rabbits
Experimental Procedures: Magnetic flux densities were up to 5.5 mT and the spatial magnetic gradient peaked in neck (carotid sinus baroreceptor) region at the level of 0.06 mT/mm. The duration of exposure was 30 min and the effects on BP were investigated up to 100 min post-exposure. BPs were pharmacologically modulated by norepinephrine (NE)-induced hypertension as well as an L-type voltage-gated Ca^{2+} channel blocker, nicardipine (NIC)-induced hypotension. Baroreflex sensitivity (BRS) was estimated from invasive recordings of systolic BP and pulse interval.
Results: Neck exposure to 5.5 mT significantly attenuated the pharmacologically induced vasoconstriction or vasodilation, and subsequently suppressed the increase or decrease in BP compared with sham exposure. In contrast, pelvic exposure to 5.5 mT did not significantly antagonized NE-elevated BP or NIC-reduced BP. The neck exposure to 5.5 mT has a biphasic and restorative effect on vascular tone and BP acting to normalize the tone and BP. The neck exposure to 5.5 mT caused a significant increase in BRS in NE-elevated BP compared with sham exposure. The buffering effects of the SMF on increased hemodynamic variability under NE-induced high vascular tone and NIC-induced low vascular tone might be, in part, dependent on baroreflex pathways, which could modulate NE-mediated response in conjunction with Ca^{2+} dynamics (15).

6. Whole-body exposure to SMFs (0.3, 1.0, and 10.0 mT, 10 min) in anesthetized mice
This study was designed to investigate the effects of SMFs for modulating the muscle capillary mirocirculation under pentobarbital-induced hypnosis.
Experimental Procedures: SMFs were generated by a C-shaped electromagnet device. Muscle capillary microcirculation of mice exposed to SMFs (0.3, 1.0, and 10.0 mT, 10 min) was studied under pentobarbital anesthesia. FITC-labeled dextran was used for an in vivo fluorescent plasma marker of the muscle capillaries.
Results: Significant increases of the peak blood velocities by SMFs of at least 1.0 mT were observed, whereas those of the mean blood velocities were not. In CTL or SMF exposure at 0.3 mT, on the other hand, there were no significant changes throughout the experimental period within either of the peak blood velocities (16).

7. Whole-body exposure to SMF (10 or 25 mT, 12 weeks) in reserpine-induced hypotensive rats
This study investigated the interrelated antihypotensive effects of static magnetic fields (SMF) and plasma catecholamine levels in reserpine-induced hypotensive Wistar-Kyoto rats.
Experimental Procedures: Seven-week-old male rats were exposed to two different ranges of SMF intensities, 3.0-10 mT (Bmax) or 7.5-25 mT (Bmax) for 12 weeks. Six experimental groups of 10 animals each were examined: (1) no exposure with intraperitoneal (ip) saline injection (sham exposed control); (2) 10 mT SMF exposure with ip saline injection (10 mT); (3) 25 mT SMF exposure with ip saline injection (25 mT); (4) no exposure with ip reserpine injection (RES); (5) 10 mT SMF exposure with ip reserpine injection (10 mT + RES); (6) 25 mT SMF exposure with ip reserpine injection (25 mT + RES). Reserpine (5 mg/kg) was administered three times a week for 12 weeks, and 18 h after each injection, arterial blood pressure (BP), heart rate, skin blood flow, plasma nitric oxide metabolites, plasma catecholamine levels, and behavioural parameters of a functional observational battery (FOB) were monitored.
Results: The reserpine idministration significantly decreased BP, reduced plasma norepinephrine (NE), increased the FOB hunched posture score and decreased the number of rearing events in the RES group, compared with the respective age-matched control group. Exposure to 25 mT, but not 10 mT, for 2-12 weeks significantly prevented the reserpine-induced decrease of BP in the 25 mT + RES group compared with the respective RES group. Moreover, exposure to 25 mT for 5 weeks partially suppressed the reserpine-induced NE reduction, but did not bring about a complete reversal of reserpine effects. NE levels for the 25 mT + RES group for 5 weeks were significantly higher compared with the RES group, but still lower compared with the control group. In addition, the FOB hunched posture score for the 25 mT + RES group was significantly lower and the number of rearing events was higher compared with the RES group, but these behavioural parameters did not revert to control levels. There were no significant differences in any of the physiological or behavioural parameters measured between the 10 mT + RES and RES groups, nor between the two different SMF groups and the control group (17).

8. Whole-body exposure to SMF (5.5 mT, 30 min) in pharmacologically induced hypertensive rabbits
The purpose of our study is to elucidate the hypothesized hypotensive or antipressor effects of SMFs, and to show that it can alter the microcirculation in a cutaneous tissue and hence normalize the BPs. More particularly, this study was designed to investigate the effects of SMF on pharmacologically induced hypertension via NA-mediated increases in sympathetic nerve activity, or a NOS inhibitor in vascular endothelial cells and/or neurons.
Experimental Procedures: Hypertensive and vasoconstrictor conditions were induced by NA or a NOS inhibitor, L-NAME. As a preliminary intensity-finding experiment using SMFs ranging 1.0–50.0 mT in NA-induced hypertension, whole-body exposure to SMFs under 5.5 mT did not significantly induce antipressor effects.

Results: In NA alone, just after NA infusion, the acute and intense vasoconstriction resulting in reduction of mean DC level of MPPG was observed. In SMF + NA, by contrast, the vasoconstrictor effect following NA infusion was antagonized. In L-NAME alone, the vasoconstriction resulting in decreases of mean DC level was observed. In SMF+L-NAME, the vasoconstrictor effect following L-NAME infusion was reduced. Comparing mean amplitude of MPPG between SMF+L-NAME and L-NAME; however, there were no significant differences throughout the experimental period. In NA alone, BPs increased from baseline after NA infusion. In contrast, in SMF + NA, the elevation of BPs was antagonized and hypotension was induced. After withdrawal of SMFs, there were significant differences between SMF+NA and NA in BPs. In L-NAME alone, BPs increased from baseline after L-NAME infusion. In contrast, in SMF + L-NAME, the elevation of BPs was suppressed during exposure and post-exposure. For plasma vasoactive substances, comparing between NA and SMF + NA in pre- and post-exposure, there were no significant changes in any catecholamines, angiotensin II and aldosterone levels (13).

9. Whole-body exposure to SMF (1, 5, 10 and 25 mT, 12 weeks) for genetically hypertensive rats
The purpose of our study is to elucidate the hypothesized antipressor effects of SMFs with mT levels on a genetically hypertensive animal.
Experimental Procedures 1: A SMF exposure device was composed of a pair of rectangular magnetic plates (strontium-ferrite) externally placed in parallel. Four types of SMF exposure devices with different magnetic flux densities were used. The mean flux densities in the center of a cage were ranging from 3.0 to 10.0 mT (Bmax) here referred to as SMF 10 mT and ranging from 8.0 to 25.0mT(Bmax) as SMF 25mT. Effects of SMFs on development of hypertension were investigated using young male stroke-resistant spontaneously hypertensive rats (SHRs) beginning at 7 weeks of age. SHRs were randomly assigned to two different exposure groups or an unexposed group. A rat in a cage with magnetic plates was exposed to either SMF continuously for 12 weeks, except during the short period of measuring BPs and heart rate and blood sampling. The BPs and heart rate in each rat were determined weekly using tail-cuff method.
Results 1: The changes of systolic BP with continuous exposure to either SMF for 12 weeks and with crossover exposure to SMF 25 mT for 6 weeks were indicated, as compared with sham exposed group. The rats exposed to SMFs displayed suppression and retardation in the development of systolic BP during 2–9 weeks. However, at least 1 week after crossover exposure for 6 weeks, significant differences between systolic BP disappeared. Similar suppressions of development of hypertension exposed to SMFs also occurred in diastolic BP during 5–6 weeks in SMF 10 mT and during 3–6 weeks in SMF 25 mT. Moreover, antipressor effects on mean BP were observed during 3–5 weeks in both SMFs. Exposure to SMFs for 5 weeks significantly reduced the concentrations of plasma angiotensin II and plasma aldosterone concentration, as compared with sham exposed group. There were no detectable effects of SMFs on the other measured vasoactive substances (renin activity, angiotensin I, arginine vasopressin and angiotensin I-converting enzyme concentrations) (18).
Experimental Procedures 2: Seven-week-old SHRs were exposed to three different ranges of SMF intensity, ranging from 0.3 to 1.0 mT (Bmax) here referred to as SMF 1 mT, ranging from 1.5 to 5.0 mT (Bmax) here referred to as SMF 5 mT, for 12 weeks and sham exposure. Arterial BP, hear rate, skin blood flow and plasma NO metabolites (NOx) and plasma cathecholamine levels were monitored.
Results 2: SMF 5 mT, but not SMA 1 mT, significantly suppressed and retarded the early stage development of hypertension for several week, compared with the age matched, unexposed (sham exposed) control. Exposure to 5 mT resulted in reduced plasma NOx concentrations together with lower level of anigiotensin II and alsosteron in SHR (19).

10. Local-body exposure on the baroreceptor region to SMF (180 mT, 6 and 14 weeks) in genetically hypertensive rats
The purpose of our study is to elucidate the hypothesized antipressor effects of SMFs with mT levels on SHRs special regard to exposure region to the baroreceptor.
Experimental Procedures: This study investigated the combined effects of a moderate intensity SMF and a Ca^{2+}channel blocker, nicardipine in stroke-resistant SHRs. A disc-shaped permanent magnet or a dummy magnet was implanted in the vicinity adjacent to the left carotid sinus baroreceptor region in the neck of each rat. Five-week-old male rats were exposed to SMF intensity up to 180 mT (Bmax) with a peak spatial gradient of 133 mT/mm for 14 weeks. Four experimental groups of 14 animals each were examined: (1) sham exposure with intraperitoneal (ip) saline injection (control); (2) SMF exposure with ip saline injection (SMF); (3) sham exposure with ip nicardipine injection (NIC); (4) SMF exposure with ip nicardipine injection (SMF+NIC). Nicardipine (2 mg/kg ip) was administered three times a week for 14 weeks, and then 15 min after each injection, arterial blood pressure (BP), heart rate (HR), baroreflex sensitivity (BRS), skin blood flow (SBF), skin blood velocity (SBV), plasma nitric oxide (NO) metabolites (NOx), plasma catecholamine levels and behavioural parameters of a functional observational battery were monitored.

Results: The action of nicardipine significantly decreased BP, and increased HR, SBF, SBV, plasma epinephrine and nor-epinephrine in the NIC group compared with the control respective age-matched group without changing plasma NOx levels. Neck exposure to SMF alone for 5–8 weeks significantly suppressed or retarded the development of hypertension together with increased BRS in SMF group. Furthermore, the exposure to SMF for 1–8 weeks significantly promoted the nicardipine-induced BP decrease in the SMF+NIC group compared with the respective NIC group. Moreover, the SMF induced a significant increase in plasma NOx in the nicardipine induced hypotension. There were no significant differences in any of the physiological or behavioural parameters measured between the SMF+NIC and the NIC groups, nor between the SMF and the control groups (20-21).

Summary of Static Field Effects

Microcirculation and BPs were modulated by SMFs with mT levels in pharmacologically treated animals and genetically hypertensive animals. By contrast, these physiological parameters were not changed by SMFs in normal animals. Appreciable minimum level for modulating microcirculation and BPs was 1.0 mT in pharmacologically treated animals. For the minimum exposure duration of 1.0 mT, it took 10 min to change microcirculation and 30 min to modulate BPs in these animals. To induce antipressor effects of SMFs on pharmacologically induced hypertensive animals, the whole-body exposure to SMF of 5.5 mT for 30 min was needed. To induce antipressor effects of SMFs on genetically hypertensive animals, whole-body exposure to SMFs of 5.0 mT for at least 2 weeks was required.

The effects of SMFs in the mT range were mediated by antagonizing the action of biochemical substances, there by inducing homeostatic effects biphasically:

1. Suppression of an adrenergic neurotransmitter, NA-induced vasoconstriction, and hypertension
2. Suppression of a cholinergic neurotransmitter, ACh-induced vasodilation
3. Suppression of reserpine-induced hypotension and bradykinesia.
4. Suppression of an anesthetic agent, pentobarbital-induced decrease in the peak blood velocities
5. Suppression of a Ca2+ channel blocker, nicardipine-induced vasodilation and hypotension
6. Suppression of a NOS inhibitor, L-NAME-induced vasoconstriction and hypertension
7. Suppression of early BP elevation via inhibition of elevation of vasopressor hormones, Ang II and Ald
8. Suppression of delay BP elevation via the NO pathway and hormonal regulatory systems
9. Enhancement of nicardipine-induced antipressor effects in SHRs which partially related to NOx activity

The effects of SMFs with mT levels on microcirculation and BPs obtained from different mammals would be used in possible explanation for the therapeutic effects on many ischemic diseases related to dysfunction in circulation and microcirculation. Furthermore, the SMFs might exert regulatory effects on BPs.

ELF EMFs

1. Whole body exposure effects to threshold levels of 50 Hz EMFs (0.3-30 mT, 30 min or 15 days) in mice

Whole body exposure effects to threshold levels of 50 Hz electromagnetic fields (3.0, 10.0, 30.0 mT for acute exposure and 0.3, 1.0, 3.0 mT for subchronic exposure) on intramicrovascular behaviour of leukocytes in the cutaneous microcirculation was evaluated by newly developed dorsal skin fold chamber (DSC) technique in mice under conscious conditions. The results indicated that the exposure intensity at 3.0 mT is a threshold level for increasing leukocyte adhesion to the endothelial walls. Effects of 50Hz electromagnetic fields (EMF) exposure on leukocyte are mainly performed *in vitro*, however, little information of these is available *in vivo* experiments. In order to investigate the acute and subchronic exposure effects of threshold levels of 50Hz EMF on leukocyte behaviour *in vivo* system, we measured the behaviour of intra-microvascular leukocytes in the cutaneous microcirculation in mice.

Experimental Procedures: Male mice (BALB/c) having the DSC were subjected to intravital-microscopic study. We have developed the DSC with non-metal materials of Duracon resin, which could not be physically affected by EMF exposure. For visualization of intra-microvascular leukocytes, fluorescent dye (rhodamine 6G; 0.3mg/kg, iv) was injected. The numbers of leukocyte rolling or adhering to the venular walls were measured by confocal laser microscopy and recorded into VCR and analyzed from the images. The magnetic flux densities used for the acute exposure (30 minutes) were controlled at 3, 10, 30 mT at the centre of animal body(n=10 each), respectively. For subchronic exposure study, mice were divided into 4 groups (n=10 each), i.e., exposure group with 50 Hz EMF at 0.3, 1.0 and 3.0 mT and control group with sham exposure. The 50Hz EMF exposure was intermittently performed everyday from 16:00 to 12:00(20hours/day) for 15 days. Plasma cytokine (IL-1β, TNF-α) concentration was measured by ELISA.

Results: Acute Effects (3, 10, 30 mT, 30 min): A tendency to increase the adherent cell count of leukocytes due to the 50 Hz EMF exposure toward higher magnetic field intensity was recognized. Following the exposure at 30 mT, the counts of adherent cell was significantly higher than those obtained before exposure. Subchronic Effects (0.3, 1.0 and 3.0 mT, 15 days): Following subchronic exposure to 50Hz EMF, no significant changes in arteriolar blood flow velocity and diameter were noticed in both groups, however, statistically significant

increases($p<0.05$) in adherent leukocyte counts at 3.0 mT were noticed. There was no change in IL-1β and TNF-α plasma levels between before and after exposures in any group. No noticeable changes in the adherent cell counts were observed between before and after sham exposures in the control group.
Conclusion: The results indicated that 50 Hz EMF exposure may influence cell to cell interaction between venular endothelial cells and leukocytes. Previous observations using human monocyte in *in vitro* system indicated that changes in cytokine profile of monocyte were induced by exposures of 50 Hz EMF. We hypothesize that 50 Hz EMF exposure effects on leukocyte and endothelial cell interaction due to change in cytokine levels, however, IL-1β and TNF-α may not be involved in this phenomenon (5, 22-23).

2. Whole body exposure effects to 50Hz EMFs (3mT, 15 days) on mammary tumour proliferation in mice
The tumor vasculature consists of both vessels recruited from the pre-existing network from the angiogenic response of host vessels to cancer cells. In the process of cancer promotion, angiogenesis is one of the key issues to proliferate their cells into host tissue. We have intravital-microscopically found that 50Hz electromagnetic fields(EMF) as well as static magnetic field exposure(>1mT) might modify the microvascular tone in rabbits under conscious conditions. If 50Hz EMF can affect on hemodynamic parameters of pre-existing microvasulature, 50Hz EMF may also affect on tumor vasculature or angiogenic process, hence, growth rate of tumor cells which implanted into the animals.
Experimental Procedures: Mammary tumour cells (MMT06562: MMT) were grafted into DSC. The area occupied by tumour tissue within a DSC was measured by PC image analysis with NIH image. Mice were divided into 2 groups (n=10-12 each), i.e., exposure group with 50 Hz EMF at 3 mT and control group with sham exposure. The 50Hz EMF exposure was intermittently performed everyday (22hours/day) for 15 days. Bood vessel diameter, blood flow velocity, adherent leukocyte counts to venular wall were evaluated by comparison between these values of pre- and post-exposure within group, or these of exposure group and control group.
Results: After MMT grafting, almost one week required to initiate the angiogenic response. During 2 weeks' whole body exposure to 3 mT, 50 Hz EMF, successive changes of angiogenesis including vascular density and growth of the tumor were compared with non-exposed control animals. The area occupied by tumor tissue within DSCs of the exposure group is smaller than its control group, however, no significant difference was found between them.
Conclusion: The results indicated that 50 Hz EMF exposure at 3 mT induced no effects on the mammary tumour cell proliferation in tumour bearing animals (24).

3. Whole body exposure effects to 50Hz EMFs (3mT, 15 days) with or without transient magnetic fields (7.4 kHz with 50 msec, 162 μT) on brain tumour proliferation in SCID mice
This study evaluates whole body exposure effects to ELF-EMF with transient magnetic field on the implanted brain tumour growth and tumour microcirculation within a mice cranial window (CW).
Experimental Procedures: Male SCID (Severe combined immuno-deficiency) mice were used in this study. One week after installation of CW, the window was opened and a small piece of human glioma U87 tissue which grown in source mouse was implanted into the centre of CW. Then, mice were divided into two groups: exposure and sham group. In exposure group, mice were subchronically exposed to combination of 50 Hz EMF with repetitive transient magnetic fields (1 burst/s, 7.4 kHz waves with duration of 50 msec and peak magnet density of 162 μT) for 15 days (15 hours/day: 7 p.m. to 10 a.m.) following tumour implantation. During and after the exposure, we measured the size of tumour, microcirculatory parameters of angiogenic vessels in the growing tumour by real-time confocal microscopy, and vascular permeability of rhodamine-labelled albumin using a photon counting system.
Results: Although tumour size increased markedly following implantation, tumour growth did not show any significant difference between the exposure group and control group. Tumour angiogenesis was also induced inside and around the tumour tissue, however, ELF-EMF with transient magnetic fields did not affect any of the microcirculatory parameters of these angiogenic vessels, for instance, vascular density, mean diameter and branched numbers of vessels.
Conclusion: No possible pathophysiological effect in the brain tumour microcirculation can be induced by the subchronic and combined exposures of 50 Hz (3 mT) and transient magnetic fields. The growth rate of implanted brain tumour tissue was not also affected by the present exposure conditions (6).

4. Whole body exposure effects to ELF EMFs (10, 16 and 50 Hz, 28 mT, 10 min) on cutaneous microcirculation in mice
Experimental Procedures: Three different ELF EMFs, e.g., 10, 16 and 50 Hz, were used in this study. Following caudal vein injection of FITC-dextran 250 kDa, the microvasculature (initial arteriole diameter of 45–80 μm), was examined by intravital microscopy and video images were recorded. Measurements of blood vessel diameter within a DSC were continuously monitored for 33 min including pre-, during and post- exposure of ELF-EMF

and every 389 ms blood vessel diameter were calculated.
Results: During and post-exposure to 16 Hz EMF, arteriolar diameters increased significantly compared with the pre-exposure period, and the changes were larger during post-exposure. No noticeable changes in arteriolar diameters were obtained from exposure to sham, 10 Hz and 50 Hz EMFs.
Conclusion: This study indicates that frequency specific interation may be evoked by ELF EMF (16 Hz), however, further research is needed to confirm this phenomenon (25).

RF EMFs
Local exposure to 1.5 GHz RF-EMF (0.08 - 35 W/kg brain average SARs, 10, 50, 80 min or 4 weeks) in rats

There is little information are available about the exposure effects of EMF on cerebral microcirculation. In this study we developed a cranial window method for evaluating the exposure effects of EMF on the BBB function, hemodynamics of pial microcirculation and behaviour of intramicrovascular leukocytes by using an intravital microscopy in rats.
Experimental Procedures 1: In the monopole antenna experiment, the exposure system consisted of a small anechoic chamber and a monopole antenna. The head of each rat was positioned toward the central antenna and was locally exposed to 1,439MHz electromagnetic near-field TDMA (time division multiple access) signal for PDC (Personal Digital Cellular, Japanese cellular telephone standard) system. The degree of intensity of RF exposure was controlled by mean specific absorption rate (SAR) of the brain. The SAR values were 1, 4, and 8 W/kg for acute effect experiment, and 4 W/kg for sub-chronic effect experiment, respectively. The EMF exposure duration was 10 minutes for the acute exposure experiment and was 60 minutes everyday, 5 days a week for 4 weeks for the subchronic exposure experiment. The pial microcirculation including vascular diameters, plasma velocities, leukocyte behaviour and BBB-function within the cranial window was investigated by a fluorescence microscope equipped with an SIT camera.
Results 1: Acute Exposure Experiment: The values in the diameters and maxmal plasma velocity of the pial venule of pre- and post-exposures did not significantly differ from each other for any SARs tested. Corresponding to the increase in SAR, the number of rolling leukocytes on the venular endothelia tended to decrease, however, no significant differences were recognized between the values for pre- and post-exposures. No extravasation of two kinds of fluorescence dyes, FITC-Dx (MW: 250,000) and sodium-fluorescein (MW: 376), from the pial venule was noticed due to any SARs. Subchronic Exposure Experiment: The values in the diameters and maxmal plasma velocity of the pial venule of pre- and post-exposures did not significantly change. No significant differences were recognized between the values for pre- and post-exposures in vascular diameters, plasma velocities and adherent leukocyte counts. No extravasation of the two kinds of fluorescence dyes from the pial venule was noticed (7).
Experimental Procedures 2: In the loop antenna experiment, the head of rat was positioned 2mm under the loop antenna and was locally exposed to 1,439MHz electromagnetic near-field TDMA signal for PDC system. The degree of intensity of EMF exposure was controlled by average specific absorption rate (SAR) of the brain at 0.2, 2.0, and 7.5W/kg for acute effect experiment, and 2 W/kg for subchronic effect experiment, respectively. Other experimental procedures were same with the monopole antenna experiment mentioned above.
Results 2: Acute Effect Experiment: No significant differences were recognized between the values for pre- and post-exposures in maximal plasma velocities and adherent leukocyte counts. No extravasation of two kinds of fluorescent dyes, FITC-Dx and sodium-fluorescein, from the pial venule was noticed due to any SARs. Sub-chronic Effect Experiment: The infection of piamater, the regeneration of dura mater and the serpiginous change of vessel were not observed within a cranial window of each group throughout the experiment. There was no significant difference in the maximal plasma velocity of the pial venule of each group at 4th week. No extravasation of two kinds of fluorescence dyes, FITC-Dx and sodium-fluorescein, from the pial venule was noticed in any group (7).
Experimental Procedures 3: Rat's head was locally exposed to 1,457MHz electromagnetic near-field TDMA (time division multiple access) signal for PDC (Personal Digital Cellular, Japanese cellular telephone standard) systems by an "8"-shaped loop antenna placed 4 mm upward to the cranial window. RF-EMF exposure intensity was maintained at an averaged SAR (2.0W/kg) in parietal targeted area. During 80 min experimental period including 50 min RF-EMF exposure, three microcirculatory parameters (BBB-function, plasma velocities and vessel diameters) in pial venules were measured every 10 min, and the results were compared between those of RF and Sham groups. Other experimental procedures were same with the monopole antenna experiment mentioned above.
Results 3: No statistical changes were observed between RF group and Sham group in any microcirculatory parameters (26).
Experimental Procedures 4: Possible adverse health effects of radiofrequency electromagnetic field (RFEMF) exposure during mobile phone uses on the developing brain in children are one of the important public health issues. The aim of the present study is to investigate whether RF-EMF exposure induces transient effects on

brain microcirculation being observed only during RF-EMF radiation period in juvenile rats. As juvenile and adult rats, we used 4 and 8 weeks male Sprague-Dawley rats, respectively. Both juvenile and adult rats were divided into two groups: RF group was exposed to RF-EMF and Sham group was not exposed to any RF-EMF. Other experimental procedures were same with the "8"-shaped loop antenna experiment mentioned above.
Results 4: We succeeded to directly observe pial microcirculation through the cranial windows during RF-EMF exposure in juvenile rats. In 4 weeks juvenile rats, no changes in any of the three microcirculatory parameters were elicited by the RF-EMF exposure. No statistical changes were recognized between RF group and Sham group. These negative effects obtained from RF-EMF exposure in juvenile rats were also confirmed in 8 weeks adult rats. No transient effects of RF-EMF exposure on the brain microcirculation in either juvenile or adult rats were recognized (27).
Conclusion: These results from acute and subchronic exposure to RF EMF suggested that no noticeable changes in the cerebral microcirculatory parameters, at least on BBB-function, plasma velocities or vessel diameters, in either juvenile or adult rats under present exposure conditions.

There is an importance of understanding the effects of magnetic fields on microcirculatory system. It may have direct and indirect role in interaction of magnetic fields with different tissues. The results from our studies could be useful in applying them for microcirculatory disorders. In addition, results obtained from exposure to ELF and RF EMFs failed to show any changes in microcirculatory system except for leukocyte and endothelial cell interaction. Levels of EMFs used in our studies are very higher than the international exposure guidelines. These animal studies can contribute to evaluate possible health risks of EMFs.

Acknowledgements
All the studies were performed at Department of Environmental Health (former Department of Physiological Hygiene), National Institute of Public Health, Japan from which I have retired in March 2004. I sincerely express my greatest appreciations to all members of the Department.

References
1. Asano M, Branemark PI. Microphotoelectric plethysmography using a titanium chamber in man. In: Harders H, ed. Advances in Microcirculation. Vol.4. Basel: S. Karger, 1972:131–160.
2. Funk W, Intaglietta M. Spontaneous arteriolar vasomotion. In: Messemer K, Hammersen F, eds. Progress in applied microcirculation. Vol. 3. Basel: Karger, 1983:66–82.
3. Mulvany MJ. Functional characteristics of vascular smooth muscle. In: Messemer K, Hammersen F, eds. Progress in applied microcirculation. Vol. 3. Basel: Karger, 1983:4–18.
4. Asano M, Yoshida K, Tatai K. Microphotoelectric plethysmography using a rabbit ear chamber. J Appl Physiol. 1965; 20:1056–1062.
5. Ushiyama A, Yamada S, Ohkubo C. Microcirculatory parameters measured in subcutaneous tissue of the mouse using a novel dorsal skinfold chamber. Microvascular Research. 2004; 68:147– 152
6. Ushiyama A, Masuda H, Ohkubo C. Effects of subchronic exposure to extremely low frequency electromagnetic fields on the cranial microcirculation in the brain tumor bearing mouse. Abstract book of 25th Annual Meeting of the Bioelectromagnetics Society. 2003: 89.
7. Masuda H, Hirota S, Ushiyama A, Wake K, Watanabe S, Taki M, Ohkubo C. In vivo evaluation of exposure effects to radio-frequency electromagnetic fields on the cerebral circulation in rats. Abstract book of the Blood-Brain Barrier (BBB) Workshop of COST281-Potential health implications from mobile communication systems; 2003 Nov 2-6; Reisensburg: Germany; 2003. p.28-29.
8. Jain RK. The Eugene M. Landis Award Lecture 1996. Delivery of molecular and cellular medicine to solid tumors. Microcirculation. 1997; 4:1–23.
9. Ohkubo C, Xu S. Acute effects of static magnetic fields on cutaneous microcirculation in rabbits. In Vivo. 1997; 11:221–225.
10. Xu S, Okano H, Ohkubo C. Subchronic effects of static magnetic fields on cutaneous microcirculation in rabbits. In Vivo. 1998; 12:383–389.
11. Okano H, Gmitrov J, Ohkubo C. Biphasic effects of static magnetic fields on cutaneous microcirculation in rabbits. Bioelectromagnetics. 1999; 20:161–171.
12. Gmitrov J, Ohkubo C, Okano H. Effect of 0.25 T static magnetic field on microcirculation in rabbits. Bioelectromagnetics. 2002; 23:224–229.
13. Okano H, Ohkubo C. Anti-pressor effects of whole-body exposure to static magnetic field on pharmacologically induced hypertension in conscious rabbits. Bioelectromagnetics. 2003; 24: 139-147
14. Okano H, Ohkubo C. Modulatory effects of static magnetic fields on blood pressure in rabbits. Bioelectromagnetics. 2001; 22:408–418.
15. Okano H, Ohkubo C. Effects of neck exposure to 5.5mT static magnetic field on pharmacologically modulated blood pressure in conscious rabbits. Bioelectromagnetics. 2005; 26:469–480.

16. Xu S, Okano H, Ohkubo C. Acute effects of whole-body exposure to static magnetic fields and 50-Hz electromagnetic fields on muscle microcirculation in anesthetized mice. Bioelectrochemistry. 2000; 53:127–135.
17. Okano H, Ohkubo C. Effects of 25 mT static magnetic fields on blood pressure in reserpine-induced hypotensive Whiter-Kyoto rats. Bioelectromagnetics. 2005; 26:36-48.
18. Okano H, Ohkubo C. Effects of static magnetic fields on plasma levels of angiotensin II and aldosterone associated with arterial blood pressure in genetically hypertensive rats. Bioelectromagnetics. 2003; 24:403-412.
19. Okano H, Masuda H, Ohkubo C. Decreased plasma levels of nitric oxide metabolites, angiotensin II, and aldosterone in spontaneously hypertensive rats exposed to 5 mT static magnetic field. Bioelectromagnetics. 2005; 26:161-172.
20. Okano H, Ohkubo C. Exposure to a moderate intensity static magnetic field enhances the hypotensive effect of a calcium channel blocker in spontaneously hypertensive rats. Bioelectromagnetics. 2005; 26:611-23.
21. Okano H, Ohkubo C. Elevated plasma nitric oxide metabolites in hypertension: synergistic vasodepressor effects of a static magnetic field and nicardipine in spontaneously hypertensive rats. Clin Hemorheol Microcirc. 2006; 34:303-308.
22 Ushiyama A, Ohkubo C. Acute effects of low-frequency electromagnetic fields on leukocyte-endothelial interaction in vivo. In vivo. 2004; 18:125-132
23. Ushiyama A, Masuda H, Hirota S, Ohkubo C. Subchronic effects on leukocyte-endothelial interactions in mice by whole body exposure to extremely low frequency electromagnetic fields in vivo. In vivo. 2004; 18: 425-432.
24. Ushiyama A, Ohkubo C. Effects of whole body exposure to 50 Hz electromagnetic fields on the microcirculatory system and the proliferative process of mammary tumor cells in mice. EBEA 2001 (5th International Congress of the European Bio Electromagnetics Association), Helsinki, 2001: 46-48.
25. Traikov L, Ushiyama A, Lawlor G, Sasaki R, Ohkubo C. Subcutaneous arteriolar vasomotion changes during and after ELF-EMF exposure in mice *in vivo.* The Environmentalist. 2005; 25: 93–101.
26. Masuda H, Ushiyama A, Hirota S, Watanabe H, Wake K, Watanabe S, Yamanaka Y, Taki M, Ohkubo C. Real-time measurement of brain microcirculation during RF-EMF exposure using an ‘‘8’’-shaped loop antenna. In: Abstract book of the 28th General Assembly of International Union of Radio Science; 2005 Oct 23-29; New Delhi, India. 2005. K03.5 (097) in CD-ROM.
27. Masuda H, Ushiyama A, Takahashi Y, Hirota S, Tanaka S, Kawai H, Wake K, Watanabe S, Taki M, Ohkubo C. No transient effects of RF-EMF exposure on the brain microcirculation in either juvenile or adult rats. Abstract book of 28th Annual Meeting of the Bioelectromagnetics Society. 2006: 104.

SUPPRESSION OF NO PRODUCTION IN MACROPHAGES BY ELF ELECTRO-STIMULATION

MUNEYOSHI KAGAWA, TOSHIYUKI SHIMOOKA, YUJI KURACHI and KOICHI SHIMIZU

GRADUATE SCHOOL OF INFORMATION SCIENCE AND TECHNOLOGY, HOKKAIDO UNIVERSITY

Abstract

We have pursued the possibility to control immune functions by ELF electro-stimulation. As the first step, the effect of electro-stimulation on the NO producing ability of macrophages was examined. The decrease of NO production due to the electro-stimulation was observed with statistical significance. To elucidate the mechanism of this phenomenon, the amount of the NO synthesizing enzyme was measured. The measurement showed the decrease in the emergence of the enzyme with statistical significance, as well. These facts suggested that the ELF electro-stimulation suppressed the emergence of the NO synthesizing enzyme and that the amount of NO production was consequently decreased by the electro-stimulation. To analyse the association between the amount of the NO synthesizing enzyme and the amount of NO production, the dose-response of this effect was investigated by changing the electric current density of the electro-stimulation. The rates of the decrease in NO synthesizing enzyme and the NO production were found to be very close. These results showed that the change in the NO synthesizing enzyme is closely involved in the mechanism of the suppression of NO production by electro-stimulation. This suggested the feasibility to control the immune function by applying electro-stimulation from outside the body.

Introduction

The influence of ELF electromagnetic field on various physiological functions has been reported, and much study has been conducted mainly from the view point of adverse effects. On the other hand, there is a clinical application such as therapeutic instruments using ELF electric field. With the view towards the immune control by ELF electric field exposure, we have studied the effect of electro-stimulation on cell functions. Macrophages play important roles in a human immune system. We have examined the effect of electro-stimulation on the phagocytic activity and the active oxygen production ability of macrophages. Through this study, it has been found that the both activities are suppressed by the capacitively coupled electro-stimulation[1,2]. The electric current induced in the suspension of cells was in the similar order to that induced in the human body with the therapeutic instrument of electric field exposure.

In the current study, we have examined the effect of electro-stimulation on the production capacity of nitric oxide (NO). The NO is a kind of the same radicals as the active oxygen and is produced in the immune function of a macrophage. The NO is produced to kill bacteria but can destroy normal cells when produced excessively. Moreover, it reacts with the active oxygen and becomes the peroxynitrite ($ONOO^-$). The $ONOO^-$ is more toxic and damages normal cells. Therefore, if we can control the NO production, it will contribute to the prevention and the treatment of various diseases. We have examined this possibility by the ELF electro-stimulation in vitro.

Materials and Methods

macrophage preparation

Peritoneal exudate macrophages were used in all the experiments. The thioglycollate medium (4.05%, 2 ml) was injected in the peritoneal cavity of a normal mouse (Std:ddy, female, 7-11weeks). After 3 or 4 days, the cells were harvested from the mouse abdomen. Then, macrophages were collected from the cells in the established method. [3] We prepared the cell culture solution (RPMI 1640 with L-Glutamine , Sodium Bicarbonate and 10%Fetal Bovine Serum: RPMI 1640, hereafter) with 0.5×10^5IU penicillin G potassium and 50mg streptomycin sulfate added. The collected macrophages were suspended in the cell culture solution to make the cell density of 2×10^6cells/ml. When electro-stimulation was applied to the cells, the IFN-γ(10U/ml) and the LPS(1μg/ml) were added as stimulants to both the stimulation group and sham group.

electrostimulation system

The macrophage cells were stimulated by the electric current in the container insulated electrically from the electrodes to simulate the condition of electro-stimulation from outside the human body. Figure 1 shows the structure of the sample container.

Two plane electrodes were kept parallel with 3 mm distance by a plexiglass separator. The electrodes were square cupper plates (24mm×24mm×6mm top and 32mm×32mm×6mm bottom). The top electrode was insulated with a 0.15 mm thick cover-glass, and the bottom one with 0.10 mm thick silicone film. The outline of the electrostimulation system is shown in Fig.2. Two electrodes were connected to a high-voltage power source through a noise filter. As the power source, the power supply of a commercial apparatus for the electric field therapy was used (Healthtron , Hakuju Inst. Health Science, maximum supply voltage 10kV). A sinusoidal AC signal of 50Hz was supplied to the apparatus with a waveform generator to make the high-voltage with the sinusoidal waveform of 50Hz. In the experiment, the cell suspension was placed in the container, and electro-stimulation was applied in a CO_2 incubator (38ºC, $CO_2$5%). The cell suspension of the sham group was kept in another incubator of the same condition.

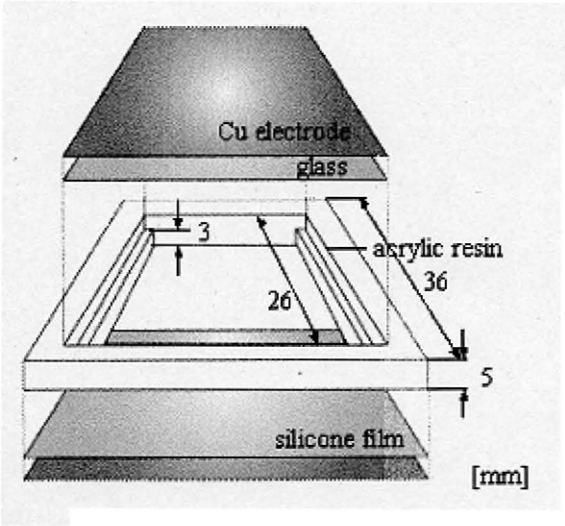


Fig.1 Sample container

Fig.2 Schematic diagram of electro-stimulation system.

Effect on NO production

We stimulated macrophages in the suspension with IFN-γ and LPS, and applied the electro-stimulation for the exposure group. The sham group was treated in the same way except connecting to the power source. The amount of NO produced outside the cell was measured as fluorescent intensity (495nm excitation and 515nm emission) using fluorescent reagent Diaminofluorescein-2(DAF-2) for the NO detection.

Macrophages were collected in the established method, and washed three times with Hanks' Balanced Salt Solution (HBSS) in centrifugation (400G) for 5 minutes. Then, they were suspended in the culture liquid RPMI 1640 again, and the electro-stimulation (50Hz, 35μA/cm^2, 16h) was applied. After the electro-stimulation, the macrophages were washed with HBSS in centrifugation, and cultured in HBSS suspension with DAF-2(10μM) and L-arginine(1mM) two hours without electro-stimulation. After the two hour culturing, the supernatant part was separated in centrifugation. With a fluorescent photometer, the fluorescent spectrum of the supernatant was measured. The supernatant of the sham group was collected in the same process except for the electro-stimulation, and the fluorescent spectrum was measured in the same way as the stimulation group.

Figure 3 shows an example of the measured result. The abscissa is the wavelength and the ordinate is the fluorescent intensity. The wavelength of the intensity peak was around 515 nm in both cases. There was no significant change in the shape of the spectrum, but 30% decrease in the intensity was observed in the stimulation group. This suggest the suppression of NO production by the electro-stimulation. The same experiments were repeated nine times. Figure 4 shows the reduction ratios of the fluorescent intensity between the stimulation and the sham groups. In all the nine cases, the fluorescent intensity was decreased by the electro-stimulation. The p-value of the paired-t test was 1.79×10^{-2}, which suggested the suppression of NO production by the electro-stimulation with a statistical significance.

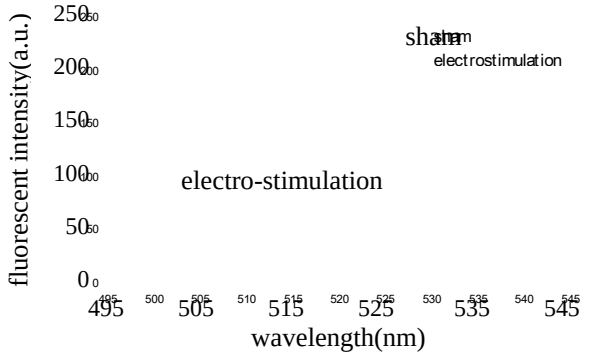


Fig3. Example of measured NO production by fluorescence spectroscopy.

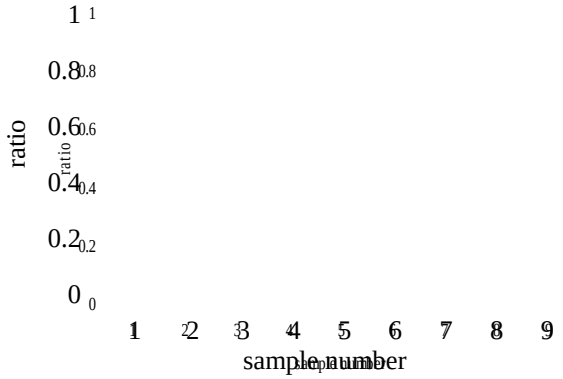


Fig.4 Suppression of NO production.

Effect on iNOS expression

NO is synthesized in a macrophage by the inducible nitric oxide synthase (iNOS). To elucidate the mechanism of the suppression in the NO production, the effect of the electro-stimulation on the iNOS expression was examined. The amount of the iNOS expression was evaluated by measuring the fluorescent intensity in the indirect immunity fluorescent method. [5, 6]

In the same way as the one mentioned above, macrophages were collected, separated into two groups, and electro-stimulation (50Hz, 35μA/cm^2, 16h) was applied to the stimulation group. After the electro-stimulation, the macrophages were collected in the centrifugation. With 70% ethanol, the cell membrane was processed to enhance its permeation. After three times centrifugation (400G, 5 minutes), macrophages were suspended in HBSS. We added the rabbit anti-iNOS antibody (BD Biosciences) and kept it in a shaker bath at 4 ºC in 30 minutes. Then we added 20μg/ml of the FITC tagged hircine anti-rabbit Ig antibody (MP Biomedicals Inc.) and kept it in the shaker bath. Finally, we fixed the suspension with 1% paraformaldehyde, and measured the fluorescent intensity with a flow cytometer (FACS Calibur Becton Dickinson and Company).

Figure 5 shows an example of the results. The abscissa is the fluorescent intensity in an arbitrary unit, and the ordinate is the number of the cell. The broken line in the figure shows the average intensity of all the cells. The average values were 79 and 65 for the sham (a) and the stimulation (b) cases, respectively. This result showed the decrease in iNOS expression by the electro-stimulation. The same experiments were repeated eleven times. Figure 6 shows the ratio of the average intensity between the simulation and the sham cases. As shown in the figure, the decrease in fluorescent intensity was observed in all the eleven trials. The p-value of the paired-t test was 5.52×10^{-5}. This suggested that the iNOS expression was suppressed by the electro-stimulation with statistical significance.



Fig.5 Example of measured iNOS expression by fluorescence spectroscopy.

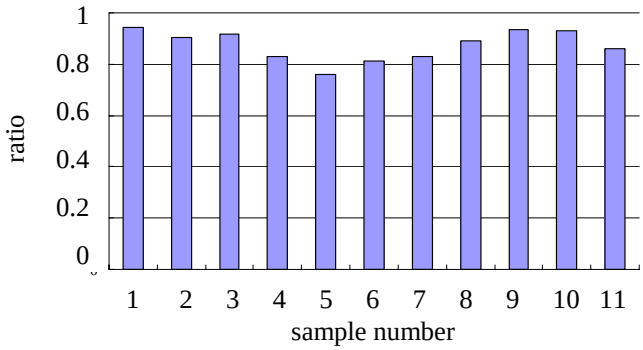


Fig.6 Suppression of iNOS expression.

Analysis of dose-response

As the first step of quantitative evaluation, the dose-response of these phenomena was analysed. In experiments, the amounts of the NO production and the iNOS expression in different current densities (0.35μA/cm^2, 0.675μA/cm^2, 3.5Aμ/cm^2) were measured. After the electro-stimulation in 16 hours, the cell suspension was divided into two. One was used for the measurement of the NO production, and another is for that of iNOS expression. Figure 7 shows the results of the measurements. The abscissa is the current density and the ordinate is the fluorescent intensity normalized by that of the sham case. The number of repeated measurements were 4, 6 and 4 for the cases of 0.35μA/cm^2 , 0.675μA/cm^2 and 3.5μA/cm^2, respectively. The result of 35μA/cm^2 case was added, in which the numbers of the repeated experiments were 11 and 9 for NO and iNOS cases, respectively.

With the current density of 0.35μA/cm^2, we could not observe apparent decrease in either of the NO or the iNOS. With 0.675μA/cm^2, about 5% decrease was observed. With the current density of more than 3.5μA/cm^2, more than 15% decrease was observed. In both of the NO and the iNOS, the threshold of the suppression seems to exist between 0.35μA/cm^2 and 3.5μA/cm^2. The similar characteristics in the dose-response strongly suggested the close correlation between the suppression of iNOS expression and that of NO production.

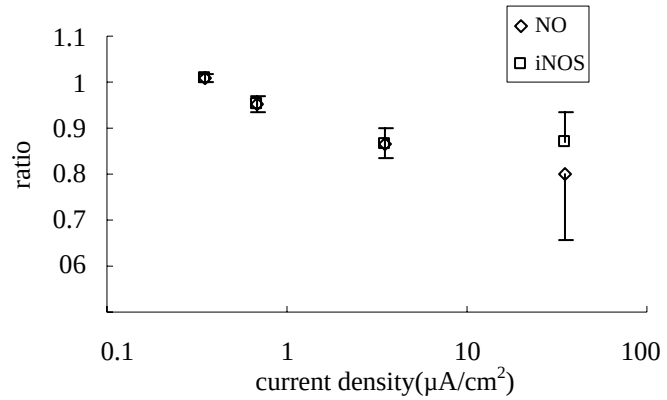


Fig.7 Analysis of NO and iNOS suppression effect by electro-stimulation.

Discussion

In the in-vitro experiments, it was found that the NO production is significantly suppressed by the ELF electro-stimulation. This suggested the possibility to control the functions of macrophages by the electro-stimulation applied from outside the body using the apparatus for the electric field therapy. Since a macrophage plays an important role in the first stage of the immune response, the electro-stimulation can influence the entire immune reaction. For example, we can expect the relief from the following diseases. They include the chronic inflammation and the autoimmune diseases caused by an excessive immune response. We can also expect the relief from the endotoxin shock due to the excessive NO production, the etiologic vasodilation, the cardio-vascular ischemia, the cerebral hemorrhage and the cancers. Moreover, we have confirmed the suppression of the active oxygen production by the electro-stimulation.[2] Therefore, we can also expect the control of $ONOO^-$

production which shows high cell-toxicity.

However, the finding of this study is only the result of in-vitro experiments using macrophages. We need further investigation to confirm this effect with human macrophages, and the investigation on this effect in-vivo where other kinds of cells are closely interacted. Yoshikawa and his co-workers reported the increase of NO production in the liver when LPS (2 mg/kg) was administered by abdominal injection and the magnetic field (60Hz, 0.1mT) was exposed in 5.5 hours. The current density induced by this magnetic field inside the body is estimated at $1.1\times10^{-8}A/cm^2$. This result is opposite to our result. It seems that the direct comparison between these two cases is not appropriate, since the object cell and the current density is greatly different among them.

Besides this, there have been few reports on the effect of ELF electromagnetic fields on the NO production, and little has been known on its mechanism. We consider that the arginine metabolism, iNOS activity and iNOS expression are closely associated with the decrease in the NO production. To investigate this mechanism, we have compared the amounts of NO production and the iNOS expression.

Figure 7 shows the coincidence in the reduction ratio of fluorescent intensity between NO and iNOS by the same electro-stimulation. This result suggests that the electro-stimulation affects the NO production through iNOS expression. The signal transmission pathway for the iNOS expression is stimulated by LPS and IFN-γ through receptors on a cell membrane. As the result, a transcription factor is activated and the iNOS is transcribed. In our study, the electro-stimulation was applied from the beginning when we started the stimulation with LPS and IFN-γ. Therefore, it is most plausible that the electro-stimulation affects this process.

However, the following possibility cannot be neglected. In the peritoneal exudate cells used in this study, about 10% cells were not macrophages. Since these non-macrophage cells can affect the signal transmission pathway of the NO production, they might influence the mechanism of the suppression of the NO production. Therefore, we have to examine this point in the experiment using the pure macrophage cells separated from other cells.

In our experiment, the threshold of the effect was found between $0.35\mu A/cm$ and $3.5\mu A/cm^2$. In the study for the biological effects of ELF electromagnetic fields, the minimum threshold of magnetic field exposure has been reported. [7] According to the report, the threshold current density for the characteristic change in tissues and cells was in the order of $10mA/m^2$ or $1\mu A/cm^2$. Though this threshold is for the electric current induced by magnetic field, it is very close to our result in which the electric current was induced by the electric field.

Conclusion

With the view toward the control of immune functions by ELF electric field exposure, the effect of the electro-stimulation on the NO production of macrophages was examined in vitro. The decrease of NO production due to the electro-stimulation was observed with statistical significance. In experiments, it was found that the expression of NO synthesizing enzyme or iNOS was suppressed in the same rate as NO in the electro-stimulation. Further investigation is required to ascertain this mechanism of NO suppression and to verify the feasibility of the immune control by electro-stimulation.

Reference

[1] I. Fujii, T. Shimooka, Y. Morita and K. Shimizu, "Experimantal verification for the effect of capacitively coupled electrostimulation on macrophage's endocytosis," Tec. Report IEICE., MBE2001-101, pp.97-102,2002.(in Japanese)

[2] Takeshi Tatebe, Toshiyuki Shimooka, Muneyoshi Kagawa, Koichi Shimizu, "Effect of ELF electrostimulation on reactive oxygen generation of macrophage", Tec. Report IEICE, MBE2003-131, pp.13-18, 2004.(in Japanese)

[3] Stohlman SA, Frelinger JA, Weiner LP. Resistance to fatal central nervous system disease by mouse hepatitis virus, strain JHM. II Adherent cell-mediated protection. J Immunol., 124(4):1733-9, 1980.

[4] Wataru Yoshida, Minori Ogawa, Yuko Furuoya, Yu Igarashi, Rumi Sato, Akiko Hayashi, Kazuya Hirano, Masatoshi Beppu, "Effect of Estrogenic Compounds on Superoxide and Nitric Oxide Production by Activated Macrophages Assessed by Sensitive Microplate Assays", Journal of Health Science, 48(5), pp.455-459, 2002.

[5] Oh-Deog KWON, Chang-Yeol YIM, Kyu-Shik JEONG, Kyu-Yong JUNG, John R. McGREGOR, Neil R.BASTIAN Wolfram R. SAMLOWSKI, "Suppression of Cytokine-Inducible Nitric Oxide Synthesis During Intraperitoneal Meth A Tumor Growth" , J Vet Med Sci., 66, pp.357-365, 2004.

[6] Wolfram E. Samlowski, Jhon R. McGregor, Gregory J. Litton, "Liver Sequestration of Murine Lymphokine Activated Killer Cells Is Mediated by Carbohydrate-specific Receptor", Regional immunology Vol.2, pp.254-265, 1989.

[7] ICNIRP Guidelines : "Guidelines for limiting exposure to time-varying electric, magnetic, and electromagnetic fields(up to 300GHz)", Health Physics, Vol.74, No.4, pp494-522.1998.

[8] Yoshikawa T, Tanigawa M, Tanigawa T, Imai A, Hongo H, Kondo M, "Enhancement of nitric oxide generation by low frequency electromagnetic field" , Pathophysiology, pp.131-135, Jul;7(2), 2000.

THE ANALYSIS OF VARIOUS APPROACHES TO ASSESSMENT OF SPATIALLY HETEROGENEOUS EMF EXPOSURE IN THE WORKPLACE

JOLANTA KARPOWICZ, PATRYK ZRADZIŃSKI, KRZYSZTOF GRYZ, MARCIN MOLENDA

CENTRAL INSTITUTE FOR LABOUR PROTECTION – NATIONAL RESEARCH INSTITUTE, LABORATORY OF ELECTROMAGNETIC HAZARDS WARSZAWA, POLAND, e-mail: jokar@ciop.pl

Abstract

The subject of presented investigations is a spatial distribution of electromagnetic field (EMF) in the workplace, in the vicinity of dielectric heaters where worker's exposure occurs. Detailed spatial distribution of *E*-field in the vicinity of 4 dielectric heaters of various constructions was measured and taken as reference data: 2 dielectric heaters of low emitted field (1 not shielded and 1 shielded) and 2 dielectric heaters of high emitted field (1 not shielded and 1 shielded). Numerical simulations of EMF emitted by numerical model of such devices were carried out with the use of specialized software packages for EMF simulations based on various numerical methods. The comparative analysis of various principles for limitation on workers' exposure to spatially heterogeneous EMF was taken into consideration (EC Directive, IEEE, IEC and EN standards, Polish occupational regulation and standards). The results of measurements and numerical modeling of worker's exposure were discussed, as well as the discussion concerning the worker's protection level corresponding to the use of various spatial averaging protocols while exposure assessment. The obtained results have proved the practical usefulness of various calculations methods for intermediate frequency EMF exposure assessment. The use of the Protection Level Factor, defined by authors for the analysis of the protection level associated with various exposure assessment protocols has been demonstrated at the example of a detailed analysis of electric field from dielectric heaters and its various assessment methods. For example, following the comparison of exposure assessment rules from IEEE standards, EC Directive and Polish regulations - IEEE rules, which seems to be the most liberal for 1 MHz, become to be the most restrictive for the frequency of 27 MHz.

Keywords: EMF exposure, exposure assessment, measurements, numerical calculations, dielectric heaters

1. Introduction

Electromagnetic field's (EMF's) exposure assessment can be required for various purposes, like occupational safety and health (OSH) engineering, epidemiological studies of EMF-exposed groups, environmental monitoring. For all of those purposes, EMF exposure assessment adequate to the real exposure level is the crucial step towards appropriate risk assessment. The highest requirements concerning detailed EMF exposure assessment come from the legislations concerning mandatory control of occupational or environmental EMF exposure. The highest influence on the legislative rules concerning EMF in particular countries come from European Directive 2004/40/EC, ICNIRP's guidelines and IEEE standards. There are also many national regulations implementing various additional rules concerning the protecting of workers against EMF overexposure.

The provisions of the Directive 2004/40/EC are based on the ICNIRP's guidelines in which the limit values of external measures of EMF exposure refer to the electromagnetic fields spatially averaged over the human body. Up to now, it is a lack of European Standards (EN) from CENELEC, harmonized with the Directive 2004/40/EC and focused on details of measurement's procedures and assessment of workers exposure. Various examples of procedures for spatial averaging of electromagnetic fields affecting human body were taken from the existing standards in order to analyze the possible practical consequences of various approaches to solving this problem. Analyzed procedures may be considered as a possible statement for future harmonized standards.

The assessment of the EMF exposure while hand-operating of the dielectric heaters is exactly a practical example of the above-mentioned problems. Dielectric heater's operation involves putting sticking/gluing components from thermoplastic foil between electrodes (upper – powered and lower - grounded) and switching

on the RF power (usually of the frequency of 27 MHz). In the case of manual operation, the worker is sitting or standing in front of the device, in the distance of 30 – 50 cm from the electrodes.

During the heating process, the worker is exposed to a spatially heterogeneous field of high electric field strength and relatively weak magnetic component. Usually, it is a sinusoidal time-varying field. Theses exposure conditions cause that protocol for EMF hazard's assessment should include the real characteristic of exposure and that exposure effects in the worker's body depend on the spatial distribution of the exposure. Such effects are well illustrated by differences in results of calculation of *SAR*, which are shown on figure 1 and in table 1. The calculations were done with a homogeneous model of worker's body, in a sitting position, grounded and exposed to electric fields from the model of dielectric heater or in spatially uniform (homogeneous), vertically polarized field. Both fields are of the same field strength at reference point located in vertical axe of torso of the body model, at height of powered electrode of a dielectric heater. The calculations results of *SAR* values were normalized by the whole body SAR (taken as 100%) in worker's body exposed to an uniform field, because such exposure scenario is usually taken for calculations of relation between external (*E* field) and internal (*SAR*) limitations for permissible EMF exposure.

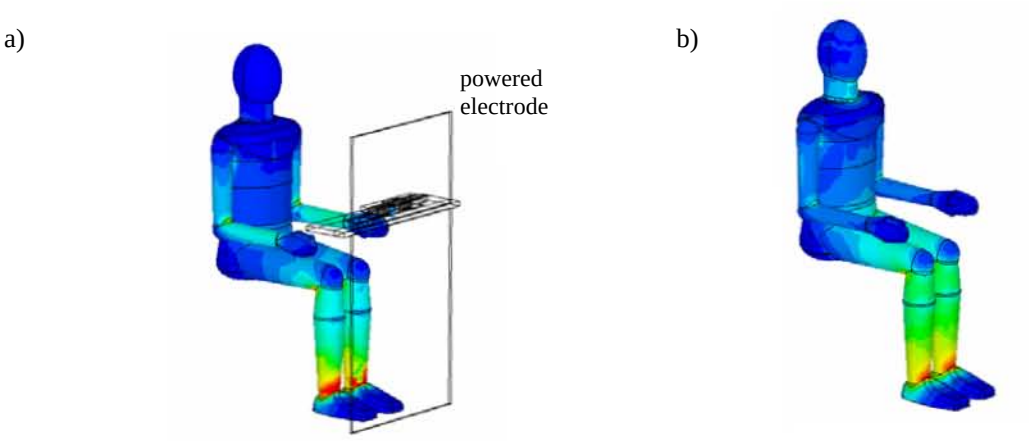


Fig 1. *SAR* distribution in homogeneous grounded model of sitting worker exposed to EMF: a) in front of dielectric heater; b) in vertically polarized uniform field

Table 1.
Results of *SAR* calculations for homogeneous grounded model of sitting worker

	SAR, relative value, %	
	exposure from dielectric heater	exposure in vertically polarized uniform field
SAR - max (10g) local value in the body model	170	1350
SAR - value averaged over whole body	14	100

However, the spatial distribution of *SAR* calculated for both cases is rather comparable with the highest exposure effects localized in ankles, the absolute level of *SAR* values are app. 10-fold higher in the case of uniform field exposure. Various approaches to assessment of spatially heterogeneous EMF exposure in the workplace, where exposure conditions are similar to that in the vicinity of dielectric heaters, were analysed. Exposure limitations and exposure assessment protocols fixed by the EC Directive, EN, IEC, IEEE standards and occupational regulation and standards established in Poland, were taken into consideration.

2. European Directive 2004/40/EC and European Standards

European Directive 2004/40/EC on minimum health and safety requirements regarding the exposure of workers to the risk arising from electromagnetic fields (EMFs) was established in 2004 as the 18th individual Directive within the meaning of Article 16(1) of Framework Directive 89/391/EEC [1]. The EMF's Directive requires that employers undertake risk/exposure assessments using detailed procedures from harmonized European Standards given by the European Committee for Electrotechnical Standardisation (CENELEC), which have not been published yet. This Directive specifies the minimum requirements, thus giving Member States the option of

maintaining or adopting more favorable provisions for the protection of workers, in particular the fixing of lower values for the action values or the exposure limit values for electromagnetic fields. The implementation of this Directive should not serve to justify any regression in relation to the situation which already prevails in each Member State.

The Member States should implement the provisions of the Directive into national legislation by April 2008 and should consider them as minimal requirements against occupational risks due to exposure to EMFs. Detailed comparative analysis of protection levels coming from the Directive's provisions and provisions of existing national regulations and existing national and international standards is very impeded because of the lack of above mentioned European Standards. From the formal point of view, until harmonized European standards from CENELEC cover all relevant assessment, measurement and calculation situations, worker's EMF exposure assessment may be carried out in accordance with other, e.g. national scientifically-based standards and guidelines. Such practice is not guaranteeing that results of exposure assessment carried out according to various protocols will provide comparable conclusions concerning the level of EMF hazard in the workplace.

2.1. EMF exposure limitations established by Directive 2004/40/EC

The employer shall assess and, if necessary, measure and/or calculate the levels of EMFs to which workers are exposed. According to the obligations arising out of the Directive, workers shall not be exposed above the exposure limit values in any event. Additionally, action values were defined for testing and assessing environmental conditions in the workplace. On the basis of the assessment of the levels of EMF, if the action values (external measures as: electric field strength, E, and magnetic field strength, H, in the workplace) are exceeded, the employer shall assess and, if necessary, calculate whether the exposure limit values (internal measures of maximum permissible exposure effects in exposed worker's body as: induced current density, J, and specific energy absorption rate SAR) are exceeded.

The action values are obtained from the exposure limit values according to the rationale presented in ICNIRP's guidelines [3]. External measures are provided strictly as an aid for practical exposure assessments, to determine whether the internal measures are likely to be exceeded. Overexposure concluded from EMF measurements in the workplace do not guarantee that limit values are exceeded in exposed body.

The limit values for electric field strength from the intermediate frequency range are presented within frequency ranges from table 2. The same values were mentioned in the ICNIRP's guidelines, as reference values.

Table 2.
The exposure limitations referring to external measures of the EMF exposure (unperturbed RMS values) - action values from the Directive 2004/40/EC

Frequency range	Electric field strength, E [V/m]
0.82 kHz - 1 MHz	610
1 – 10 MHz	$610/f$
10 – 400 MHz	61

f - frequency in MHz

As these values were calculated for the frequencies above 100 kHz to protect against the thermal effect inside the exposed body, electric field from the workplace should be spatially - and time - averaged for the analysis of the compliance with the internal measures' limitations. Currently, there is a lack of European exposure standards harmonized with above mentioned directive. Protocols from existing product standard concerning the analysis of compliance with ICNIRP's guidelines for general public exposure assessment, obligatory for testing products emitting EMF before entrance to European market (emission product standard), can be considered as a possible source of the protocol for the analysis of compliance with the Directive's provisions.

2.2. Spatial averaging from the EN/IEC product standards

The method of spatially averaging of the results of measurements of EMF is presented in the European standard EN 50357 [2] and IEC Standard 62369-1 [4] for testing the compliance with reference values (external measures published by ICNIRP). Following the provisions of these standards, the torso is the most appropriate part of the body to be assessed and the grid from Figure 2 should be used. The position of the grid in relation to the unit

under test can vary according to the typical usage of the EMFs emitting unit, e.g. the height *Z* should be modified for the assessment of a sitting person exposure. The layout and dimensions of the grid shall remain identical.
For assessment referring to the EMF exposure of torso, the EMF's spatial distribution should be measured in 45 grid points. The result of the arithmetic average of the measured *E* values should be compared with the limit value from ICNIRP's guidelines. In the exceptional cases where the exposure is predominately to the head, then the grid located in a position referring to the head must be used.

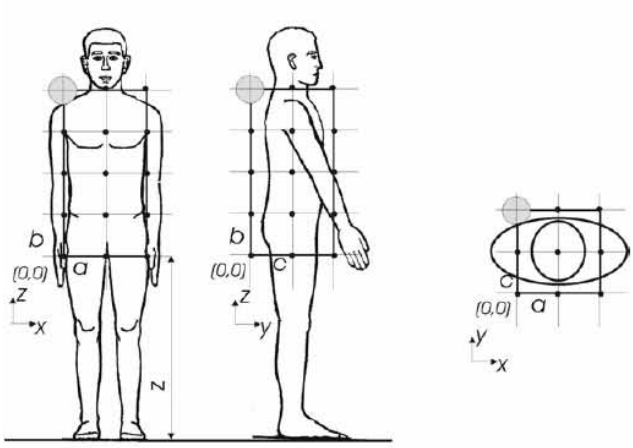


Fig. 2. Torso measurement grid for spatially averaged measurements according to EN 50357 or IEC 62369-1 (normative dimensions: a, b, c = 15 cm; Z = 85 cm)

3. EMF exposure limitations and assessment by IEEE standards

IEEE Std C95.1-2005[5] provides the recommendations to minimize aversive or painful electro stimulation in the frequency range of 3 kHz to 5 MHz and to protect against adverse heating in the frequency range of 100 kHz to 300 GHz similar to ICNIRP's rationale. The recommendations are expressed in the terms of basic restrictions (BRs) and maximum permissible exposure (MPE) values. The BRs are limits on fields induced in the body, specific absorption rate (SAR), and current density. The MPEs are derived from the BRs. The MPE values for electric field strength from the intermediate frequency range are presented within frequency ranges from table 3.

Table 3.
Electric field maximum permissible values (MPE) from IEEE STd C95.1-2005

Frequency range	Electric field strength, *E* [V/m]
3 kHz – 1 MHz	1842
1 – 30 MHz	1842/*f*
30 – 100 MHz	61.4

f - frequency in MHz

For spatially heterogeneous exposures, the mean values of the incidental fields should be obtained by spatially averaging the squares of the field strengths. The IEEE Std C95.3-2002 [6] standard provides details concerning exposure assessment protocol for testing compliance with IEEE Std C95.1-2005 provisions.

3.2. Spatial averaging from the IEEE exposure assessment standard

According to IEEE Std C95.3-2002 [6], for the measurement of electric or magnetic fields, carried out for the assessment of the whole-body exposure, spatial averaging of the measurement's results means the root mean square of the field over an area equivalent to the vertical cross section of the adult human body. The spatial average can be measured by scanning (with a suitable measurement probe) a planar area equivalent to the area occupied by a standing adult human (projected area). In the majority of cases, a simple vertical, linear scan of the fields over a 2 m height through the center of the projected area will be sufficient. IEEE document doesn’t describe details how to do spatial averaging.

4. Workers EMF exposure limitations and assessment standards in Poland

The occupational safety and health (OSH) legislation in Poland concerns, among others, ambient environmental factors, electromagnetic fields at workplace. Regulations concerning occupational exposure to EMF of 0 Hz - 300 GHz frequency range have been in force since 1972 in Poland as mandatory legislation (current ed. - PL Journal of Laws 217/2002, item 1833 [8]). Regulations are periodically revised and, if necessary, updated under the umbrella of Interdepartmental Commission for Maximum Admissible Concentrations and Intensities for Agents Harmful to Health in the Working Environment, which is the scientific advisory body established by the Prime Minister of the Polish Government.

The main base for all EMF regulations in Poland was taken from the thresholds of thermal and nerve excitation effects, similarly to ICNIRP's approach implemented by the Directive 2004/40/EC. As periodical assessment of EMF exposure level in the workplace is mandatory in Poland, the regulations refer directly to external measures only (*E*, *H*). The internal measures (*J*, *SAR*) were not directly introduced into published regulations since there is no possibility to measure them in real conditions. However, the permissible internal measures of exposure effects defined by ICNIRP's guidelines (EC Directive) and IEEE Standards were used as an important contribution to theoretical rationale for the level of prohibited exposure to EMF's of various frequencies, drafted as scientific background for above mentioned national legislation.

Following the above-mentioned regulation and Polish Standard, the strength of electric and magnetic fields (*E*, *H*), the frequency of these fields (*f*) and workers' exposure duration (*t* and exposure factor *W*), should be taken into consideration for occupational EMF exposure assessment. The main provisions include:

- high exposure - Workers without protective clothes should not have been allowed to access to the area of EMF higher than the level of prohibited exposure (table 4) – the exposure level harmonized with the permissible internal measures from ICNIRP/EC Directive.

- medium exposure - The range of exposure level of permissible EMF exposure duration shorter than 8 hours. In the case that both electric and magnetic fields are relatively high, the exposure factor defining the permissible exposure duration is the sum of components from both fields of the frequency up to 3 GHz. The 8-hours permissible exposure level is the equivalent for ICNIRP/EC Directive external measures' limitation (table 4).

Table 4.
Electric field strength – exposure limitation established in Poland (external measures)

Frequency range	Electric field strength, *E* [V/m]	
	prohibited exposure	8 hours exposure
1 kHz < $f \leq$ 3 MHz	1000	100
3 MHz < $f \leq$ 15 MHz	3000/f	300/f
15 MHz < $f \leq$ 150 MHz	200	20

f - frequency in MHz

4.1. Protocol from the Polish Standard PN-T-06580 for workers exposure assessment

Polish Standards determine the protocols how to do EMF measurements and workers exposure assessment (PN-T-06580:2002, revised in 2002 [7]). Worker's exposure assessment should be performed on the results of spot measurements of RMS value of electric and/or magnetic field strength. The maximum value over the worker's body position in the workplace should be considered for testing the compliance of EMF exposure condition with OSH regulations. In practice, it is usually the maximum value of measured electric or magnetic field strength in the vertical axis of worker's body, up to 2 m height.

5. Method

The EMF exposure of workers can be evaluated following the results of calculations in the case when for a particular workplace the exposure assessment on the basis of EMF measurements is not adequate. Such situations occur when EMF's distribution is highly heterogeneous, a worker operates close to the field source or his body is in contact with it. Such exposure assessment needs appropriate modeling of EMF source - for

assessment considering external measures and additionally appropriate modeling of workers body - for assessment considering internal measures limitation.
The subject taken for the investigations presented has been a spatial distribution of electric field in the workplace in the vicinity of dielectric heaters where worker's exposure occur.
A detailed spatial distribution of *E*-field in the vicinity of 4 dielectric heaters of various construction was executed: 2 dielectric heaters of low level of emitted field - 1 not shielded (M-m1) and 1 shielded (M-m2); 2 dielectric heaters of high level of emitted field - 1 not shielded (M-d1) and 1 shielded (M-d2). Measurements were done by RMS value meter with isotropic probe. Three dimensional components (X, Y and Z) of electric field strength have been recorded online using notebook computer. The recording system is shown on figure 3. A measuring probe was placed in succeeding appointed points along measuring lines. The registration of only one single pulse was done at each measurement point.

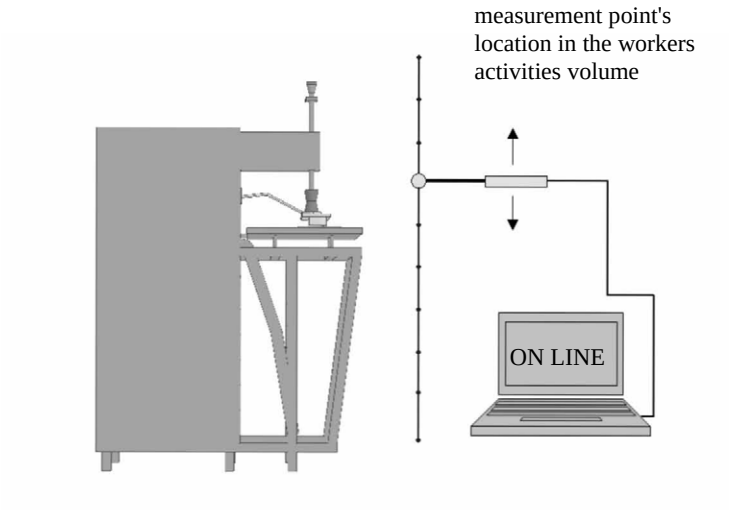


Fig. 3. Online registration system used for EMF measurement for data – acquisition in the vicinity of real dielectric heater.

Numerical simulations were carried out with the use of specialized software packages for EMF simulations based on various numerical methods:
- OPERA 3D v. 8.7 (Vector Fields Ltd, United Kingdom) – specialized for finite element method – FEM
- CST MICROWAVE and EM STUDIO (CST – Computer Simulation Technology - Germany) - specialized for finite integration technique – FIT.

The geometrical model of dielectric heater is shown in figure 4. EMF's source for this numerical modeling was created by powered electrode of 1 kV electrical potential.

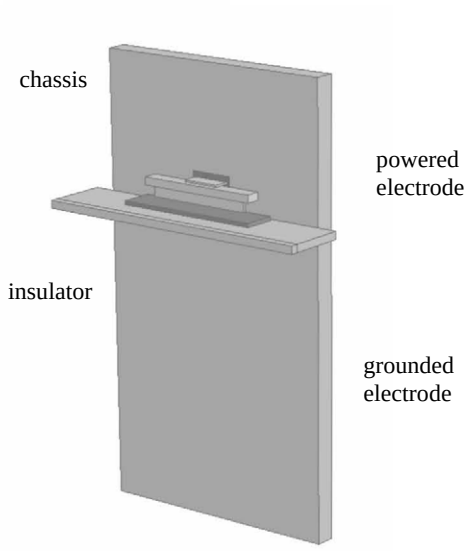


Fig. 4. Geometrical model of dielectric heater.

6. Results

Spatial distribution of *E* field in the vicinity of dielectric heater obtained from calculations and measurements have been averaged over the volume of worker's torso (following EN/IEC standards' protocol) and over the vertical axis of workers body position (following IEEE standard protocol). Averaging of measurements results have been carried out on the base of maximum values registered from each welding pulses. The results were presented in fig. 5 as values relative to the maximum value over the workers body which is taken for exposure assessment following the protocol established by Polish Standard PN-T-06580. Bars representing various measurements result's averaging are labeled in figure 5 as M-m1; M-m2; M-d1 and M-d2 (with above mentioned meaning). Bars representing averaging of calculation's results are labeled as follow: C-s1 - from Opera software, C-s2 - from CST MW and C-s3 - CST EM.

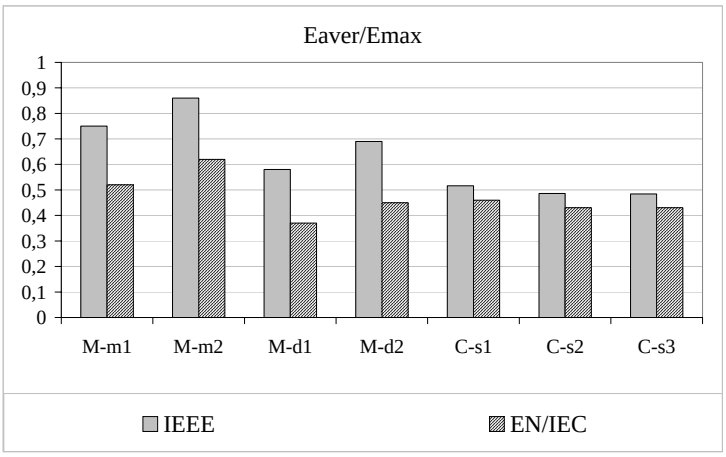


Fig. 5. Spatial averaging over the workplace the *E*-field from dielectric heaters

The data concerning *E*-field spatial distribution, obtained from simulations with the use of very simple model of EMF source and various software, averaged over the workers body presented the similar relation to maximum value of *E* field at workplace (0.43-0.51) as the ratio observed among the measurement results from real workplace (0.35-0.85). Thanks to this fact, obtained results of calculations suggest that various numerical simulations' methods could be acceptable for calculations executing for the assessment of intermediate frequency EMF occupational exposure. Very simple models of EMF source can be also accepted, but "calibration" of the calculation results has to be done by the comparison with measurement results to obtained confirmation concerning the absolute values of exposure level (*E*-field).

For a deeper analysis of the practical consequences of the use of various exposure assessment protocols and limit values, the protection level coefficient can be consider. Protection Level Factor (PLF) can be define as the ratio of the exposure estimator taken for exposure assessment on the basis of particular exposure assessment protocols (e.g. various spatial averaging protocols above mentioned), divided by exposure limitation harmonized with this protocol (e.g. E field averaged following the protocol from IEEE C95.3 divided by limit value fixed by IEEE C95.1). With such definition, PLF of higher value correspond to the more restrictive exposure assessment rules, or in other word, higher protection level.

The practical usefulness of the analysis of various exposure assessment rules with the use of PLF value can be show at the example of electric fields of spatial distribution like in the vicinity of dielectric heaters and maximum value at the axis of worker's torso of 1000 V/m, assessed following the limit values from tables 2-4. The field taken for the analysis can be described by max value of 1000 V/m, value averaged following IEEE rules of 700 V/m and value averaged following EN/IEC rules of 500 V/m. For such values, in the case of electric field of frequency of 1 MHz, PLF values are: for the exposure assessment rules established by the European Directive and EN/IEC standards – PLF(EC, 1MHz) = 0.8; for exposure assessment rules established by IEEE standards – PLF(IEEE, 1MHz) = 0.4 and for exposure assessment rules established in Poland as the threshold of prohibited exposure – PLF(PL, 1MHz) = 1. In the case of electric field of 27 MHz PLF values have different order: PLF(EC, 27MHz) = 8; PLF(IEEE, 27MHz) = 10; PLF(PL, 27MHz) = 5 – IEEE rules, which seems to be the most liberal for 1 MHz, become to be the most restrictive for the frequency of 27 MHz.

7. Conclusion

These investigations can support the work on methods of numerical simulations for the routine assessment of worker's exposure to EMF from intermediate frequency range. There is relatively a wide gap of experience of "numerical" assessment of worker's exposure to EMF from intermediate frequency range in comparison with the huge amount of data concerning power frequency and microwave.
The selection of geometry of EMF source's models, as well as the selection of numerical simulations methods can significantly influence on the level of obtained results, however the relative spatial distribution of E-field could be similar.
Presented methodology of analysis of the protection level which is associated with various exposure assessment protocols can be use for detailed comparative analysis of various exposure limitation standards, legislation or guidelines. The overall analysis should consider not only the spatial averaging of incidental fields but also rules of time-averaging of non-continuous exposure, calibration of measurement devices for non-sinusoidal fields, etc. components of exposure assessment protocols.

Acknowledgment
This paper has been prepared within the investigations supported by the State Committee for Scientific Research and Ministry of Economy, Labour and Social Policy of Poland (grant 1.A.02).

References

[1] Directive 2004/40/EC of the European Parliament and of the Council of 29 April 2004 on the minimum health and safety requirements regarding the exposure of workers to the risks arising from physical agents (electromagnetic fields) (18th individual Directive within the meaning of Article 16(1) of Directive 89/391/EEC), O.J. nr L-184 of 24 May 2004.
[2] EN 50357:2001 Evaluation of human exposure to electromagnetic fields from devices used in Electronic Article Surveillance (EAS), Radio Frequency Identification (RFID) and similar applications.
[3] ICNIRP *Guidelines for Limiting Exposure to Time-Varying Electric, Magnetic, and Electromagnetic Fields (up to 300 GHz)*, Health Physics, vol. 74, No. 4 (April), 494-522, 1998.
[4] IEC Draft 62369-1. Evaluation of human exposure to electromagnetic fields from Short Range Devices (SRDs) in various applications over the frequency range 0-300 GHz. Part 1: Fields produced by devices used for Electronic Article Surveillance, Radio Frequency Identification and similar systems (September 2004).
[5] IEEE Std C95.1-2005, Standard for Safety Levels with Respect to Human Exposure to Radio Frequency Electromagnetic Fields, 3 kHz to 300 GHz. Published by the Institute of Electrical and Electronics Engineers, New York, USA, 2006.
[6] IEEE Std C95.3-2002 Recommended Practice for Measurements and Computations of Radio Frequency Electromagnetic Fields With Respect to Human Exposure to Such Fields, 100 kHz–300 GHz. Published by the Institute of Electrical and Electronics Engineers, New York, USA, 2002.
[7] Polish Standard PN-T-06580:2002. Labour protection in electromagnetic fields and radiation of the frequency range from 0 Hz to 300 GHz. Part 1: Terminology. Part 3. Methods of measurement and evaluation of the field on the work stands (in Polish).
[8] Regulation of the Minister of Labour and Social Policy, Permissible occupational conditions, Journal of Laws 217/2002, item 1833 (in Polish).

ACTIVE SUPPRESSION OF AN INDUSTRIAL FREQUENCY ELECTROMAGNETIC FIELD (EMF): THE PRACTICAL REALIZATION

A.SHENKMAN, N. SONKIN, E. NEEMAN, V. KAMENSKY,
R. ZEMAH

HOLON INSTITUTE OF TECHNOLOGY,
52 GOLOMB ST., P.O.B. 305, HOLON 58102, ISRAEL

ABSTRACT

The present work deals with the active suppression of an electromagnetic field (EMF) of complicated multi-circuit transmission lines and its practical realization. This research is the continuation of a previous one [1], in which more simple case of only one (single) transmission line EMF was investigated and a method of its suppression proposed.

In double circuit transmission systems, for instance, the EMF has an elliptic space-time characteristic, as the big and small axes of the ellipse can be approximately of the same lengths.

The active suppression of an EMF in such cases can be carried out by means of two loops installed in parallel to the transmission lines having independent automatic control of the currents in each loop.

The method of calculating the EMF of the transmission system and of the loops and the computer program for performing such calculations, have been developed in this work. Based on these calculations, loop parameters and their arrangement in space may be determined.

As a result of the research, a practical application (pilot installation- see the pictures) of the suppression of EMF, induced by a high voltage (160kV) double transmission line in an office building of an industrial zone of the city of Rosh Haayin has been performed. Two loops located along the protected office have been installed and activated by a control system. The experimental results of such protection were in very good agreement with the theoretical predictions. The electromagnetic field in various points of the protected office has been reduced 3-10 times, so that the suppressed EMF became less than the permissible value.

INTRODUCTION

In the previous research [1] it was shown that the space-time characteristic of the EMF of a single transmission line has very narrow elliptic form. It was also shown that the suppression of such EMF could be done by using a single loop, whose space-time characteristic is a straight line. The suppression is achieved when the parameters of the loop (its ampere-turns and position in the space) are chosen in such a way that its straight-line-characteristic coincides with the big axis of the elliptic-characteristic of the transmission line EMF and equals it in length. The two EMF's of the line and the loop of course have to be of opposite phases.

ELECTROMAGNETIC FIELD GENERATED BY A COMPLICATED POWER LINE

Let us now analyze a double-circuit transmission line having any phase sequence. Fig. 1 shows such a line going in parallel to a four story building.

Fig.1 Three-phase double-circuit power line and a protected building

Let $P(y,z)$ be the point, where we wish to calculate the magnetic field (the point of observation), where y, z are the coordinates of the point of observation. (In this case the observation point is located on the third floor).

In accordance to the Biot-Savart law the magnetic flux density produced by an infinite conductor is:

$$B(y,z,t) = \frac{\mu_0}{2\pi} \frac{I_m \sin(\omega t - \alpha)}{R(y,z)} \quad (1)$$

where μ_0 is the magnetic permeability of air, $I_m \sin(\omega t - a)$ is the current carried by the conductor and $R_i(x,z)$ is the distance from *i*-phase to the point of observation.

$$R_i(y,z) = \sqrt{(y_i(y)^2 + (z_i(z))^2}\ , \quad (2)$$

where $y_i = y - Y_i$, $z_i(z) = z - Z_i$ and Y_i *and* Z_i are coordinates of an *i*-phase.

Then the vertical and horizontal components of EMF are defined by the expressions:

$$BV_i(y,z,t) = B_i(y,z,t) \frac{y_i(y)}{R_i(y,z)}$$
$$BH_i(y,z,t) = B_i(y,z,t) \frac{z_i(z)}{R_i(y,z)} \quad (3)$$

The sum of the vertical and horizontal components at point $P(y,z)$ for a three-phase double-circuit line is given by:

$$BV(y,z,t) = \sum_{i=1}^{6} BH_i(y,z,t)$$
$$BH(y,z,t) = \sum_{i=1}^{6} BH_i(y,z,t) \quad (4)$$

With the vertical and horizontal components (4) the space-time characteristic of the transmission lines EMF is built and shown in Fig.2. As can be seen, the obtained ellipse is pretty wide so that the successful suppression of EMF by use of only one loop cannot be achieved.

Fig. 2 An elliptic characteristic of EMF

In Fig.3 the above two components (4) are shown as functions of the distance from the office wall, parallel to the transmission lines, along the *y*-axes, and in Fig. 4 they are shown along the *z*-axis from the floor up to the ceiling. The origin of these coordinates is located at the point of the location of the sensor, which activates the control system).

Fig. 3 Effective values of transmission lines' EMF inside the office: 1-horisontal, 2-vertical components

Fig. 4 Effective values of transmission lines' EMF in the office versus height: 1-horisontal, 2-vertical components

Both components of the EMF, of course, can be measured and compared with the one computed and, if the line currents and the phase sequences are presented by their actual values, the computed values (Figs 3 and 4) should be in agreement with the measured ones. Now, being sure that the picture of the EMF is correct we can design the compensation loops.

ELECTROMAGNETIC FIELD GENERATED BY COMPENSATING LOOPS

Since the EMF of a two-circuit transmission system is expressed by the wide ellipse, as is mentioned above, the suppression of such a field should be performed by means of two perpendicular loops, as shown in Fig. 5. In this case the protected area is the office of ECTEL Company. (The position of the sensor, whish activates the automatic control system, is indicated by ©)

Fig. 5 The position of the protecting loops

The EMF of these loops is calculated as a sum of the vertical and horizontal components of all four lines:

$$BV_l(y,z,t) = \sum_{i=1}^{4} BV_{li}(y,z,t)$$
$$BH_l(y,z,t) = \sum_{i=1}^{4} BH_{li}(y,z,t) \qquad (5)$$

The suppressed field $(BVs(y,z,t),\ BHs(y,z,t))$ is then obtained as a sum of the vertical and horizontal components of the transmission line system $(BV(y,z,t),\ BH(y,z,t))$ and the loop system $(BVl(y,z,t),\ BHl(y,z,t))$:

$$BVs(y,z,t) = BV(y,z,t) + BVl(y,z,t)$$
$$BHs(y,z,t) = BH(y,z,t) + BHl(y,z,t) \qquad (6)$$

As it was already mentioned, the vertical loop (loop 1) should be positioned in such a way that its characteristic (line 2 in Fig. 6a) will coincide with the big axes of the ellipse (line 1 in Fig. 6a). The resulting EMF is also shown in Fig. 6a as line 3, which actually is an ellipse, but due to the relatively small scale looks as a line. Then the horizontal loop (loop 2) is designed and positioned in such a way that its characteristic (line 2 in Fig. 6b) coincides with the small axis of the original ellipse (line 1 in Fig. 6a). Note that this small axes after the first compensation turns into the big one, as shown in Fig. 6b (1). (Also note that line 3 in Fig. 6a now looks like an ellipse in Fig. 6b due to the larger scale). After the second compensation (by loop 2) the resulting EMF is suppressed up to the very small ellipse (3), which again looks like a straight line.

(a) (b)

Fig. 6 The field characteristics of the transmission lines (1) and the loops (2 and 3)

The resulting curves of the suppressed field (curves 1) and the curves of the original field (curves 2) are shown in Fig.7a and b. It should be mentioned that the minimum point of the suppressed EMF is at the position of the sensor. Therefore, by choosing this position we can influence the distribution of the suppressed field along the office/home.

(a) (b)

Fig. 7 The EMF distribution inside the office: versus the distance from the wall (a) and the height (b) (1-original field, 2-suppressed field)

PRACTICAL REALIZATION

For checking and proving the proposed method of EMF suppression an experimental sample of a suppressing system to protect an office (of ECTEL Company in Rosh Haain) was projected and installed. The front of the office building and the loop installation is shown in Fig. 8. The same installation as seen from the corner of the building and the transmission line are shown in Fig.9.

The resulting curves of the suppressed EMF along the protected office along with the original EMF (before the compensation) are shown in Fig. 10a and b: the calculated curves (a) and measured (b). As can be seen, there is a good agreement between the theoretical and practical results. The remaining EMF inside the office does not exceed 2.5mG, which is the required norm [3].



Fig. 8 The picture of the protecting loops in the front of the building



Fig. 9 The picture of the protecting loops and the transmission lines from the corner of the building

(a) (b)

Fig. 10 The resulting curves of the EMF: calculated (a) and measured (b) (1-original field, 2-suppressed field)

SUMMARY

The method of active suppression of the EMF induced by a complicated system of high voltage, large power transmission lines is developed and practically performed.

It is shown that in such cases the protecting system comprises two compensating loops, which should be arranged in space perpendicularly to each other, usually one lies in the vertical plane and the second one in the horizontal plane.

The pilot installation, based on the proposed method, was performed and tested on one of the offices in the building, located near to a high voltage transmission system.

The pilot performances are very successful: the original EMF has been suppressed 3-7 times, so that the remaining EMF is of 2-2.5mG, which is required the norm.

REFERENSCES

[1] A. Schenkman, N. Sonkin V.Kamensy“ Transmission lines as a source of industrial frequency electromagnetic field (EMF) radiation and a device for its active suppression”, *Proceedings of 3-th International Workshop Biological effects of EMFs*, pp. 593-599, 4-8 October2004, Kos, Greece.

[2] A. Schenkman, N. Sonkin V.Kamensy“ Active protection from electromagnetic field hazards of a high voltage power line” *HAIT Journal of Science and Engineering B, Volume 2, Issues 1-2*, pp. 254-265, 2005 Holon Academic Institute of Technology, Israel.

[3] “ELF Electromagnetic Fields and the Risk of Cancer” *Documents of the NRPB*, Volume 12, No 1, 2001

MEASUREMENT OF THE MAGNETIC FIELD AND INDUCED VOLTAGE IN 217Hz COMPONENT AND ITS HARMONICS DUE TO THE CELL PHONE

M. LAK
YOUNG RESEARCHERS CLUB, ISLAMIC AZAD UNIVERSITY, SCIENCE AND RESEARCH BRANCH, TEHRAN, IRAN
mahdilak@yahoo.com

M. KAVIANI MOGHADAM
DEPARTMENT OF MEDICAL PHYSICS, TARBIAT MODARES UNIVERSITY, TEHRAN, IRAN
kaviani_mm@yahoo.com

M. JANAHMADI
DEPARTMENT OF PHYSIOLOGY, SHAHEED BEHESHTI MEDICAL SCIENCES, TEHRAN, IRAN
mjanahmadi@yahoo.com

S.M.P. FIROOZABADI
DEPARTMENT OF MEDICAL PHYSICS, TARBIAT MODARES UNIVERSITY, TEHRAN, IRAN
pourmir@modares.ac.ir

Abstract

The quick growth of mobile communication has led to investigate the possible adverse effects on public health. It spite of security regulation norm for public exposure by governments from different country all around the world, the current controversy lies now on the possibility that the ELF could produce biological non-thermal effects. Nowadays some scientists are concerned about the possible impact of ELF fields of mobile phone. Magnetic ELF component are mainly generated by supply current in the phone.

In order to achieve a practical conclusion about sensitivity of nervous system to cell phone, the magnetic flux density in 217Hz and its harmonics from cell phone battery current were measured and these data will be used for stable magnetic field coil that made electrically for studying the effects of environmental ELF fields on bioelectric activity of nerve cell.

For measuring ELF fields of cell phone resulted from battery current, an on-made search coil was provided and calibrated precisely under several experimental conditions. Using Fast Fourier Transform (TNM-DSO Software) the power spectrum of induced voltage in search coil was analyzed and the amplitudes of 217Hz and its harmonics were extracted, considering the difference between induced voltage in search coil and magnetic

flux density of cell phone in 217Hz component and its harmonics, we measured a range of power variation in different times of the day.

The results of this study suggest that, ELF B-field of cell phone was not the same in different points. These findings emphasize the need for caution and regard all variations of power range during the different time of the day when biological effect of magnetic fields from cell phone is studied. To reach windowing effect, we must consider the physical characteristics of fundamental component wave (217Hz) and its harmonics produced by mobile phone accurately near to real one in exposure system.

Keywords: Mobile phone, ELF magnetic fields, 217Hz

Introduction

Modern technology offers powerful tools to stimulate a range of benefits for society, in addition to economic development. However, technological progress in the broadest sense has always been associated with hazards and risks [1].

Radio frequency transmitted by digital GSM telephones in the 900MHz band (890-915MHz) belongs to the "heating" category of the frequency spectrum. Hand-held digital mobile phones generate pulsed magnetic fields resulted from battery current, they transmit information in burst of microwaves and operate in one of the eight time slots, i.e. sending the information to the base station in 0.577 ms bursts with 217 bursts per second. This pulsed magnetic field (MF) of extremely low frequency (ELF) mainly include 217Hz (pulse their harmonics and subharmonics) [2]. It is quite possible that living organism have two- fold sensitivity to the pulsed GSM signal, to both the microwave carrier and lower frequency pulsing “time division multiple access”(TDMA)[3]. Besides a large number of researches which have been focused on high frequency components much less attention has been paid on the low frequency pulsed magnetic fields associated with pulsed battery current characteristic for GSM-type mobile phone [4,5,6,7,8,9,10,11].

The pulsed ELF-MF in mobile phone signals could exert influence on biological systems through non-thermal effects and this ELF emission is itself capable of causing significant biological effects [4]. In contrast to heating, which relies on an organism’s ability to absorb energy from irradiating field, the possibility of non-thermal effects arises from an “oscillatory similitude” between the radiation and living organism to respond to low-intensity pulsed via its ability to recognize certain frequency characteristics of that radiation, in fact non-thermal effects are non-linear [3].

The existence of specific amplitude and frequency values at which the response of the object was more pronounced. The sensitivity of the biological systems to weak MF has been described elsewhere, mainly in respect to the dependence of bioeffects on the amplitude or the frequency of the applied fields. More and more studies have suggested that for non-ionizing radiation cannot be applied the principle of ionizing radiation when the increase of the dose enhance the effects [12].

Thus in this paper we monitored the environment intensities of magnetic field emitted by one model of digital cell phone to settle the experimental conditions in order to reproduce the pattern of waves of mobile phones in a configuration closer to real condition.

These ranges of intensities will be used for studying the effects of environmental ELF battery’s fields on bioelectrical activities of nerve cell.

Material and Methods

The assessment ELF fields of GSM mobile phones requires a search coil, according to Faraday's induction law the variable magnetic field induces a voltage in wire winding. The average diameter of on-made search coil was 5mm with 500 turns wire with 0-260kHz frequency response. For RF immunity the probe was shielded with aluminum foil.

To obtain calibration factor, the search coil was exposed with known magnetic field. It was done with a system when an accurately known current with 217Hz frequency was injected through the circular coil (drived by known signal). The flux density of magnetic field was measured by a hand-held digital magnetic field meter (TES 1394, Electronic Electrical Corp.).

The calibration factor (μT/mV) was the ratio between flux density (B) and induced voltage in search coil that measured with the analog oscilloscope (Topward 7046A).

For scanning the surface B-field (flux density) distribution on the back side of the mobile phone a 10×10mm grid (Figure 1), in a way that the search coil was situated 4mm far from battery surface, was used. With considering the surface of battery we had 15 points on the back side of phone and we measured induced voltage in three axes in different times of the day in each points. The amplified induced voltage (root mean square) in search coil was measured with digital oscilloscope (DSO, TNM Electronics). By using Fast Fourier Transform (FFT) method (TNM-DSO software), the power spectrum of induced voltage was analyzed and the power of 217Hz component and its harmonics were extracted and saved in computer. Then, the B-field in 217Hz calculated with calibration factor.



Figure 1- 10×10mm grid for scanning B-field of mobile phone

Results

Ten experiments were carried to calculate calibration factor. The magnetic flux densities in 6 cm far from the circular coil were measured with digital magnetic field meter and induced voltage in search coil measured with the analog oscilloscope. According to the ratio B/V, where B is the B-field of circular coil and V is the induced voltage in the search coil, we calculated the calibration factor (Figure 2). The calibration factor was 51.57 μT/mV with .997 regression coefficient.

Figure 2- Measured magnetic flux density (B) and induced voltage (V) at 6 cm far from the circular coil

The induced voltages (rms) in 217Hz component of the sum vector of all three axes ($Bs=\sqrt{B_x^2+B_y^2+B_z^2}$) in different times of day in 15 points on the back side of phone were measured (Table 1). The measured induced voltage waveform is shown in Figure 2. It consists of pulses train. The duration of pulse is 0.577ms and the repetition interval is 4.61ms that are the same of sending information to the base station with 217 Hz (Figure 3).

Table 1-The sum vector of three axes of induced voltage in 217Hz in different times of day

Induced Voltage (rms in mV)	**Maximum**	**Minimum**	**Average**
Morning	2.77	0.25	1.39
Afternoon	1.62	0.19	0.80
Evening	2.09	0.23	0.81

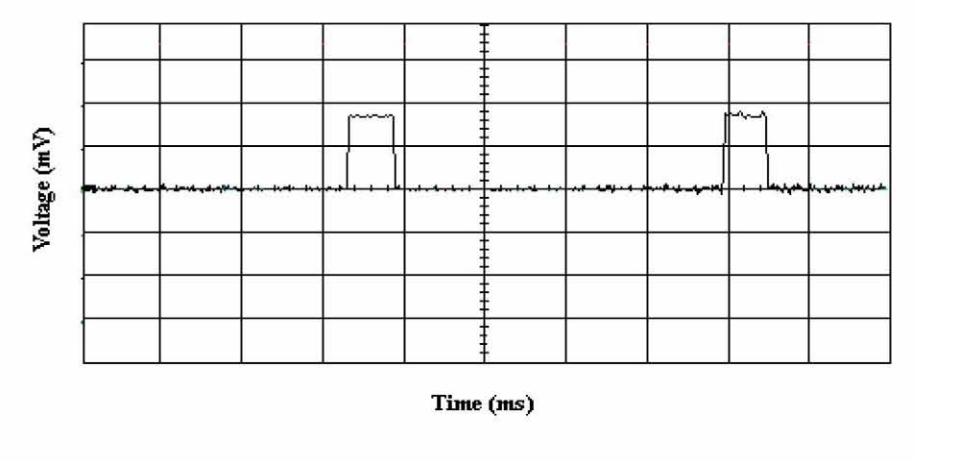


Figure 3: Induced voltage waveform in 217 Hz

The power spectrum of induced voltage was analyzed by Fast Fourier Transform (FFT) method and the amplitude of induced voltage in 217Hz and its harmonics were extracted (Table 2)(Figure 4).

Table 2- The sum vector of three axes of induced voltage in 433Hz and 650 Hz in different times of day

Induced Voltage (rms in mV)		Maximum	Minimum	Average
433Hz	Morning	2.57	0.24	1.31
	Afternoon	1.54	0.13	0.74
	Evening	1.99	0.22	0.77
650Hz	Morning	2.24	0.19	1.10
	Afternoon	1.21	0.07	0.61
	Evening	1.68	0.18	0.64

B-field distribution on back side of mobile phone is the result of the surface scan with 4mm distance between the phone's surface and search coil. The distribution pictures show the 217 Hz component of sum vector of all three axes of induce voltage(rms) times calibration factor (MATLAB software, version6.5, the Math Works Inc.)

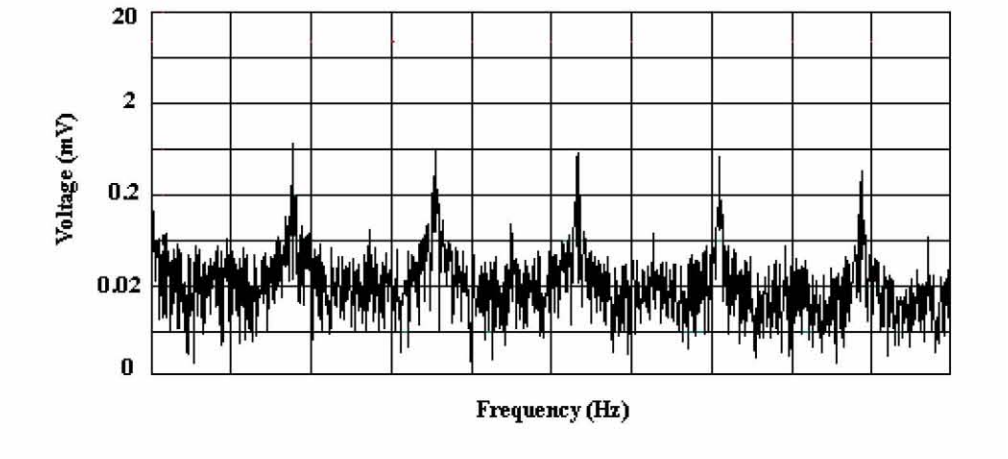


Figure 4- The power spectrum of induced voltage in 217 Hz and its harmonics

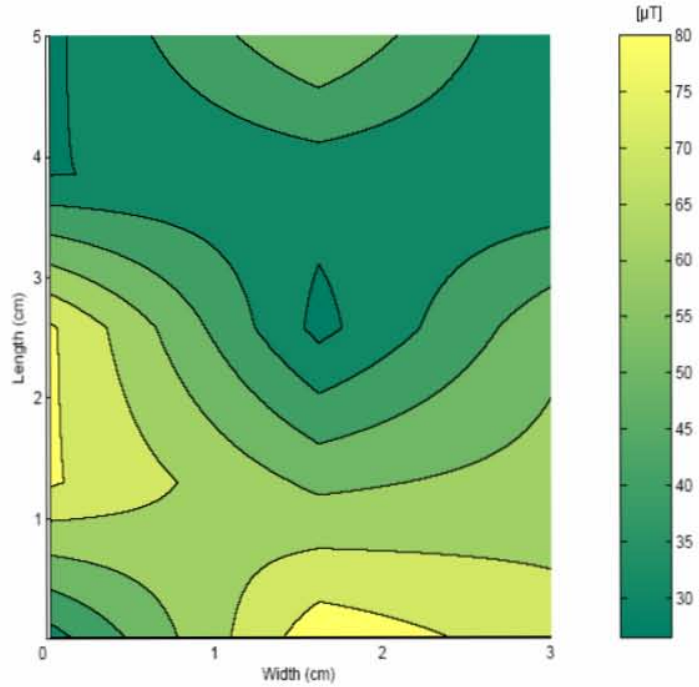


Figure 5- B-field distribution on back side of mobile phone

Discussion and Conclusion

The obtained results clearly show that the amplitude of induced voltage (rms) in 217 Hz and its harmonics considerably varies in different points of handset's battery back side. In this study, the results of changing magnetic fields from battery phone are not new and our research outputs were similar to the other works [5].

In addition to the other works we measured the B-fields in different parts of the day (Morning, Afternoon and Evening) according to network jam. So, we obtained a power range of induced voltage from 0.07 to 2.77 mV and B-fields between 26.40μT to 86.52μT. We had done our experiments in Iran workplace.

Furthermore the relative powers of two main harmonics to fundamental component were 94% and 78%.

As it may be interesting to know that all early publication made a link between "windows" and information transfer it is better to consider a range of intensities. So, for reasonable approach to the ELF "windows" problem we must consider a range of parameters such as magnetic flux density (amplitude) or frequency. In this way it appears reasonable to claim the existence of "window effect".

Besides considering the rage of intensities, it should be stressed that for biological studying of mobile phone, according to the power spectrum analysis, we must consider the intensities of higher harmonics of fundamental component, in addition to 217Hz signals, in ELF exposure systems.

To properly assess the validity of any experimental results demonstrating cell phone bioeffects, it is necessary to understand the mechanism by which these effects may occur.

Further investigation is on the way to settle the experimental condition in order to reproduce the pattern of the waves of mobile phones in a configuration closer to real one and examining the effects of low-frequency component of mobile phone on nervous system.

References

[1] WHO. WHO hand book on establishing a dialogue on risks from electromagnetic fields. World Health Organization, Geneva, Switzerland, 1992.

[2] Tuor M., Ebert S., Schuderer J., Kuster N. Assessment of ELF exposure from GSM handsets and development of an optimized RF/ELF exposure set up for studies of human volunteers. Bag Reg. No. 2.23.02-18 /02.001778. Final Report 2005.

[3] Gandhi OP., Kang G. Some present problems and proposed experimental phantom for SAR compliance testing of cellular telephones at 835 and 1900 MHz. Phys Med Biol 47:1501-1518; 2002.

[4] Hyland G.J. Physics and biology of mobile telephony. The Lancet 356: 1833- 36; 2000.

[5] Kuster N., Kastle R., Schmid T. Dosimetric evaluation of handheld mobile communications equipment with known precision. IEICE Trans E80-A (5):1-8; 1997.

[6] Jokela K., Puranen L., Sihvonen A.P. Assessment of the magnetic field exposure due to the battery current of digital mobile phones. Health Physics. 86(1): 56-66; 2004.

[7] Azenza M.J., Del Moral A. Cell membrane biochemistry and neurobiological approach to biomagnetism. Prog. Neurobiol. 44: 517-601; 1994.
[8] Cranfield C., Wieser H.G., Madan J., Dobson J.AL. Preliminary evaluation of nanoscale biogenic magnetite-based ferromagnetic transduction mechanisms for mobile phone bioeffects. IEEE Transactions on nanobioscience. 2(1): 40-43; 2003.
[9] Ilvonen S., Sihvonen A-P., Käkkäinen K., Sarvas J. Numerical assessment of induced ELF currents in the human head due to the battery current of a digital mobile phone. Bioelectromagnetics 26:648-656; 2005.
[10] Linde T., Mild K.H. Measurement of low frequency magnetic fields from digital cellular telephones. Bioelectromagnetics 18: 184-186;1997.
[11] Pedersen G.F, Andersen J.B. RF and ELF exposure from cellular phone handsets: TDMA and CDMA systems. Radiation Protection Dosimetry 83(1-2): 131-138; 1999.
[12] Marko S.M. Myosin phosphrylation –A plausible tool for studying “Biological window”. 3rd International Workshop “Biological Effects of Electromagnetic Fields, 2004. Oct 4-8; Kos, Greece.p.1-9.

AN INVESTIGATION OF THE DEPENDENCE BETWEEN MAXIMUM LEVEL OF OUTPUT POWER MOBILE PHONE AND RECEIVING LEVEL

NIKOLAY TODOROV ATANASOV[1], GABRIELA LACHEZAROVA ATANASOVA[2]

[1]DEPARTMENT OF WIRELESS COMMUNICATIONS AND BROADCASTING, HIGHER COLLEGE OF TELECOMMUNICATIONS AND POSTS, 1 "ACAD. STEFAN MLADENOV" STR., 1700 SOFIA, BULGARIA, e-mail: natanasov@hctp.acad.bg
[2]DEPARTMENT OF TELECOMMUNICATION TECHNOLOGIES, HIGHER COLLEGE OF TELECOMMUNICATIONS AND POSTS, 1 "ACAD. STEFAN MLADENOV" STR., 1700 SOFIA, BULGARIA, e-mail: ghristova@hctp.acad.bg

Abstract
RF power control is used to minimize the transmit power required by the mobile or base station subsystem while still maintaining the quality of the radio links. By minimizing the transmit power levels, interference among co-channel users can be reduced.

For circuit-switched services in GSM system, the mobile is commanded by the base station to change its power level. The base station directs this process with the help of the uplink receiving level and quality measurements.

In this paper we consider dependence between maximum output power level of GSM mobile phone and receiving level.

The measurements were performed with GSM mobile phones, which used service software in the networks of the three PLMNs (Public Land Mobile Network) in Bulgaria.

Our results indicate the receiving levels in those the GSM mobile phone transmit with maximum output power.

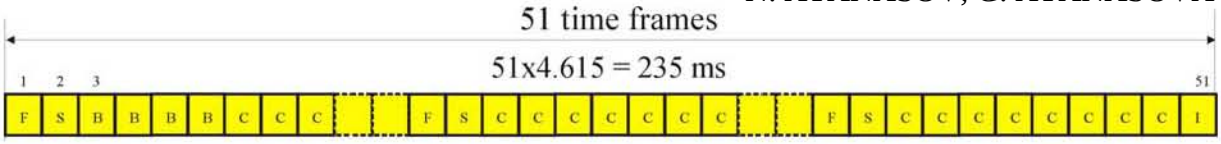
Introduction
The adaptive power control allows the mobile station (MS) to increases or decreases output power level for provides of reliable communications. It also decreases interference with other co-channels users and, through dense frequency reuse, improves spectral efficiency, while maintaining an adequate communications quality and facilities a reduction in power consumption, which is particularly important in hand-held MSs. And not the lastly place decrease of the output power level provides to decrease of absorbing energy (decrease of Specific Absorption Rate SAR) in the head of a user, which is particularly important for the users of mobile phones.

The power control procedure is accomplished by during a call (when the MS is in Traffic CHannel – TCH) and it controls from base station (BS). Output power level of MS for GSM900 can be reduced in 15^{th} steps from 33dBm (2W) to 5dBm (3.2mW) and each step is 2dBm [1].

The adaptive power control procedures rely on measurements of the received RF signal strength (RXLEV), the received signal quality (RXQUAL) [2].

RXLEV is evaluated by measuring the received level of the broadcast control channel (BCCH) carrier, which is continuously transmitted by the BS on all time slots of the B frame in Fig. 1 and without variations of the RF level. An MS measures the received signal level from the serving cell and from the BSs in all adjacent cells by tuning and listening to their BCCH carriers. The root mean squared level of the received signal is measured over a dynamic range of -103dBm to -41dBm for intervals of one slow associated control channel (SACCH) multiframe (480 ms). The RXLEV parameters are then coded into 6-bit words for transmission to the serving BS via the SACCH.

RXQUAL is estimated by measuring the bit error rate (BER) before channel decoding, using the Viterbi channel equalizer's metrics and/or those of Viterbi convolutional decoder [3]. Eight values of RXQUAL span the logarithmically scaled BER range of 0.2% to 12.8% before channel decoding.



F: Frequency Control Channel;
S: Synchronisation CHannel;
B: Broadcast Control CHannel;
C: Common Control CHannel (Access Grant/Paging CHannel);
I: Idle Frame

Figure 1. Multiframe 51 in GSM system

The adaptive power control is based on RXLEV and RXQUAL measurements. In every SACCH multiframe the BS compares the RXLEV readings reported by the MS, or obtained by the base station, with set thresholds. The exact strategy for RF power control is determined by the network operator with the aim of providing an adequate quality of service for speech and data transmissions while keeping interferences low.

Most of the investigations were performed to determinate transmission levels of BSs [4, 5], but a small amount of investigations are performed to determinate output power levels of MS in real operating conditions [6]. That's provoking us to set following aims.

Aims of the investigation

1. Estimation of the received levels (RXLEVs) in those output power level (TXLEV) of the mobile station is 33 dBm (2 W) for GSM900 for every one PLMNs Bulgarian operator.
2. Estimation of output power levels (TXLEVs) of the mobile station on occupation of different logical channels during a call in the GSM900.

Schema of the investigation

For achieved of the traced aims were measured receiving levels of the BCCH carrier (RXLEVs) and TCH carrier (RXLEV_TCHs), quality of a receiving signal (RXQUAL), output power levels of the mobile phone (TXLEVs) and absolutely distance between mobile phone and base station (DISTANCE).

The investigation was performed using two mobile phones type NSE-1 and service software for network monitoring.

The measurement was made whit that set up:

1. The both mobile stations were connected to a personal computer through interface cables for observing and reading the values of the RXLEVs, RXLEV_TCHs, TXLEVs, RXQUALs, and DISTANCEs in the radio interface by service software for network monitoring;
2. For elimination of the influence from operator's hand and head on the values of the measurement parameters, the both mobile phones were raised from the ground surface of 1.5 meters on the set ups and the set ups were placed at distance with radius 5 meters of the operator.

The schema of the measurements:

1. The measurements were performed in the three points displayed in Fig. 2, marked like point A, point B, and point C (the point C is farthest away from the base station). These points are in outskirts whit hilly relief and trees.
2. The values of RXLEV, RXLEV_TCH, TXLEV, RXQUAL and DISTANCE were measured in every one of the three points in two deference days, for the three network operators.
3. The measurements were realized by making ten originated calls from the one mobile station and reading of RXLEV_TCH, TXLEV, RXQUAL, and DISTANCE, and the second mobile station continuously measured the level of the BCCH carrier (RXLEV). Every originated call was with period of sixty seconds, and the reading of the values on measurement parameters was made of every five seconds.
4. There were measurements carried out in the two accidentally selected points in the urban area. In the every one of these points were made ten originated calls and measurements of RXLEV, RXLEV_TCH, TXLEV, RXQUAL, and DISTANCE by the pointing above schema. The aim is to compare values of parameters from points in the urban area, when the mobile station and subscriber are too close to base station (some hundred meters) to values of parameters from points in the thinly populated places, when the mobile station and subscriber are too far away from base station (some kilometres).
5. For every one of the network operator the output power levels of the mobile station on occupation of different logical channels during an originated call was determinate. The logical channels in GSM

system during an originated call are occupy as following [7]:

BCCH/CCCH	Broadcast Control CHannel/ Common Control CHannel	
RACH	Random Access CHannel	**Start a call**
AGCH	Access Grant CHannel	
SDCCH	Stand-alone Dedicated CHannel	
TCH	Traffic CHannel	
…	…	**…**
TCH	Traffic CHannel	**Stop a call**
BCCH/CCCH	Broadcast Control CHannel/ Common Control CHannel	

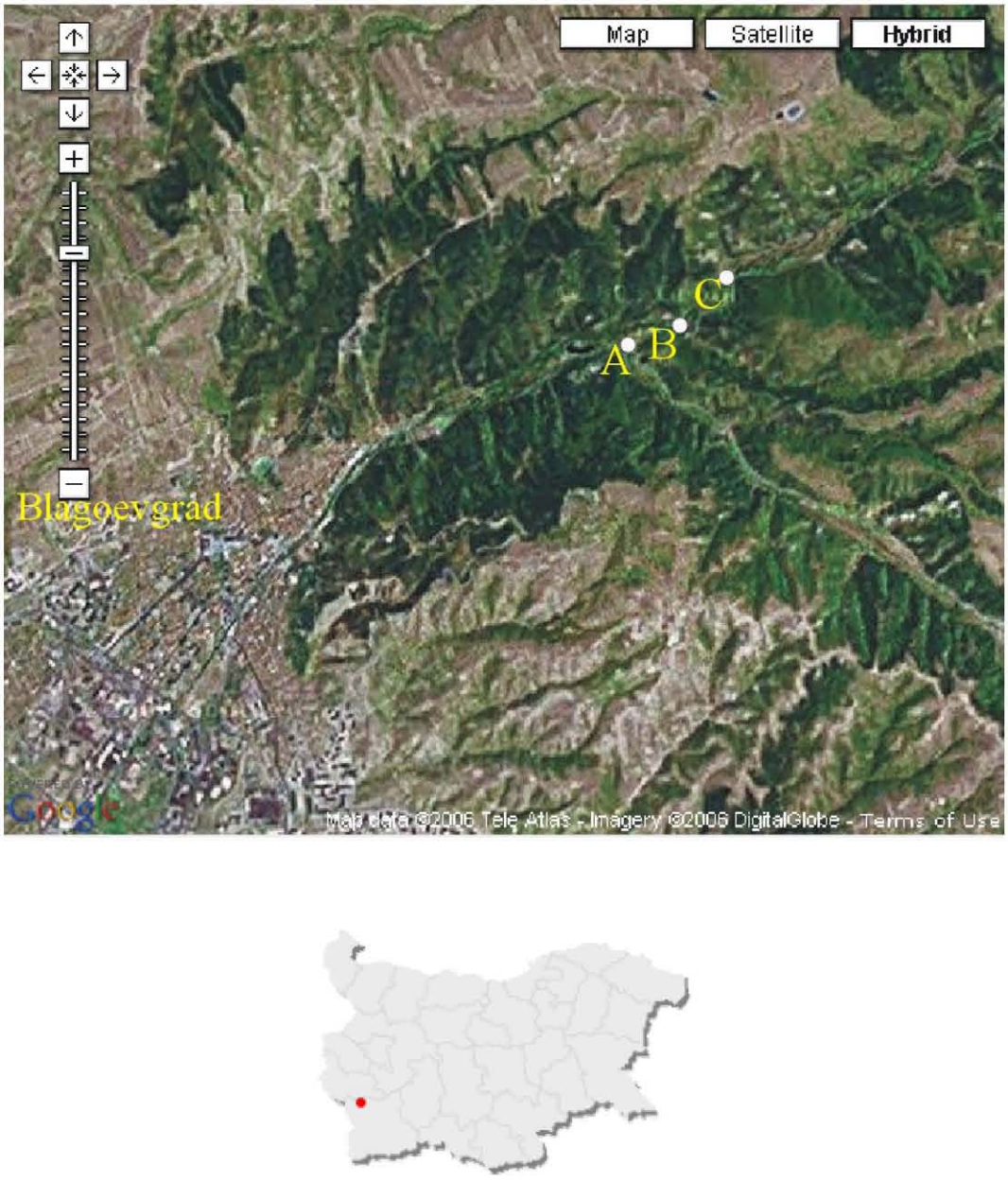


Figure 2. Placement of the points of measurements in outskirts with hilly relief and trees.



Figure 3. Placement of the first point of measurements in urban area.

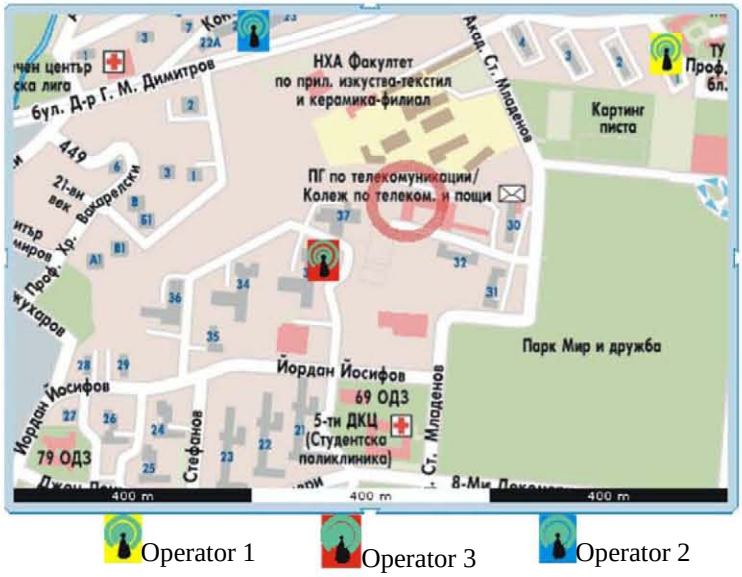


Figure 4. Placement of the second point of measurements in urban area.

Results

The results of the measurements are displayed of Figs. 5…19.

"Pointing" assessments for showing of the uncertainty of the measurement were determinate [8]. "Directed" assessment of statistical moments of the investigated accidental value and more specific – of the mathematical expectation $\hat{m}_x$ and dispersion $\hat{\sigma}_x^2$ [9] were performed.

The point assessments of performed n (where n=10) independent measurements with registration implementations $x_1, x_2, \ldots, x_i, \ldots, x_n$ of the accidental value X is as following:

$$\hat{m}_x = \frac{1}{n}\sum_{i=1}^{n} x_i \,, \hat{\sigma}_x^2 = \frac{n}{n-1}\left[\frac{1}{n}\sum\left(x_i\right)^2 - \hat{m}_x^2\right] \tag{1}$$

The root mean squared deviation $\hat{\sigma}_x$ was evaluated.

The "interval" assessments for specific cases displayed of Figs. 8(a, b), 9(a, b), and 10(a, b) were determinate on the base of the "pointing" assessments of $\hat{m}_x$ and $\hat{\sigma}_x$ by (1).

THE DEPENDENCE BETWEEN MAXIMUM LEVEL OF OUTPUT POWER MOBILE PHONE AND RECEIVING LEVEL

The half-magnitude of the confidential interval $\varepsilon = \frac{I_{m_x}}{2}$ and confidential boundaries were determinate, as following:

$$m_1 = \hat{m}_x - \frac{\hat{\sigma}_x}{\sqrt{n}} A',\ m_2 = \hat{m}_x + \frac{\hat{\sigma}_x}{\sqrt{n}} A', \qquad (2)$$

where $A' = 1.960$ with $p_I = 0{,}95$.

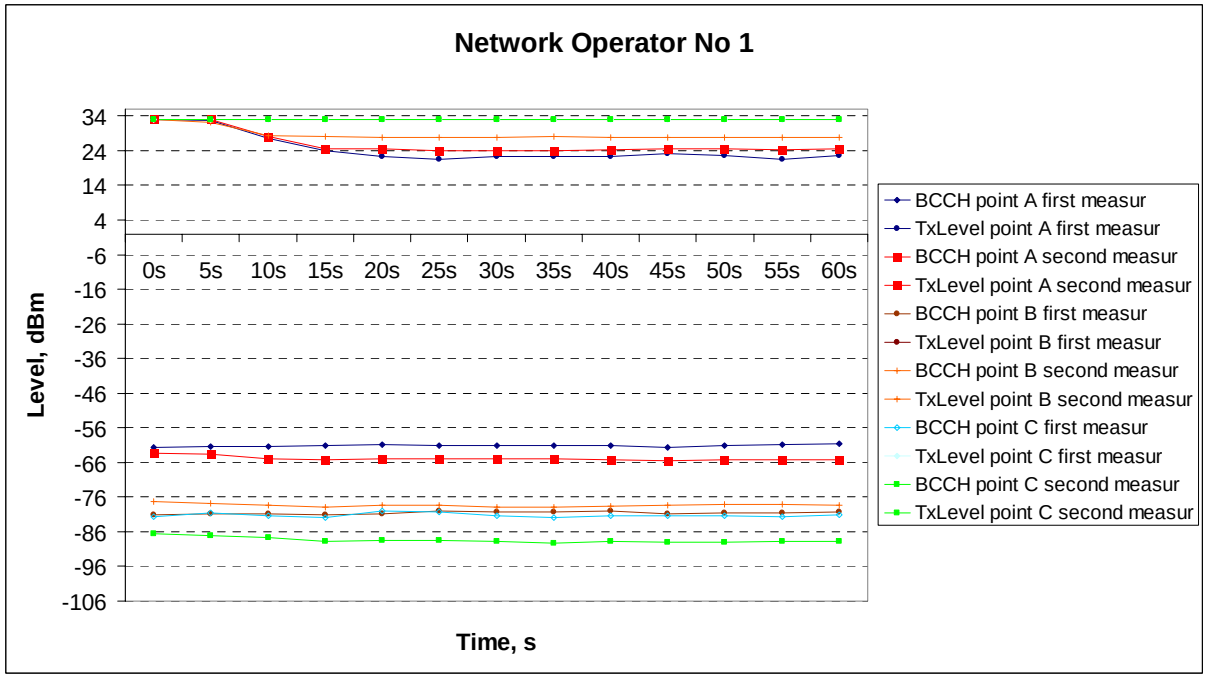


Figure 5. Dependence between RXLEV and TXLEV of MS in the time, for Network Operator 1.

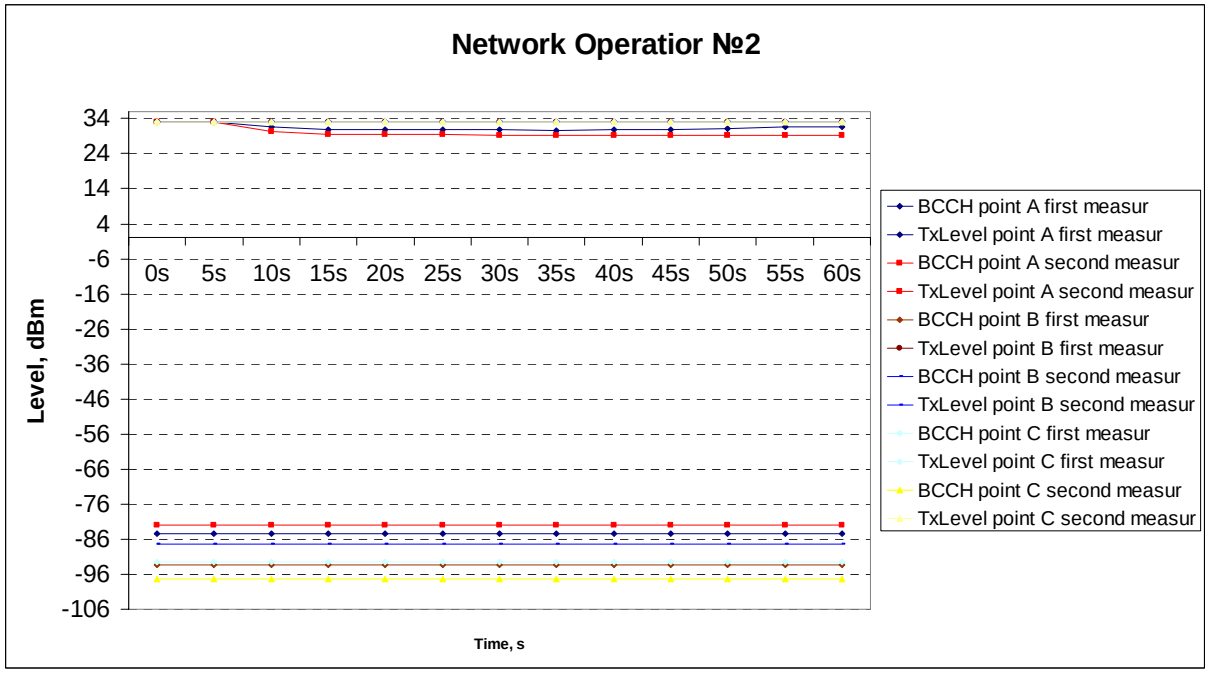


Figure 6. Dependence between RXLEV and TXLEV of MS in the time, for Network Operator 2.

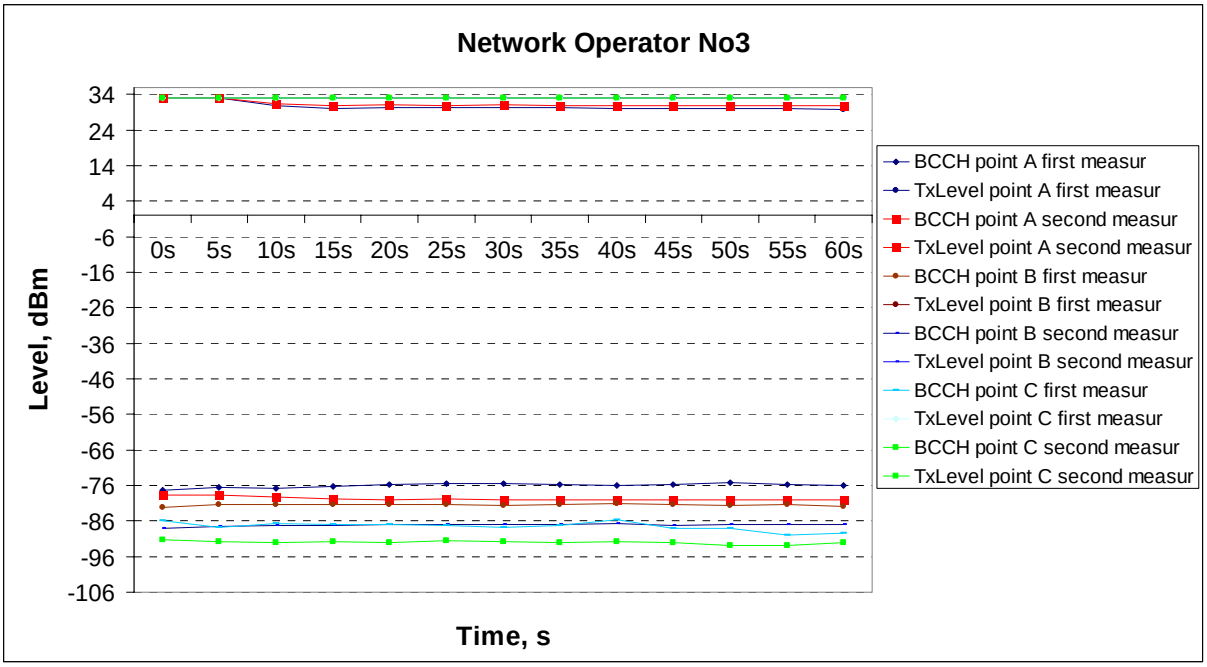
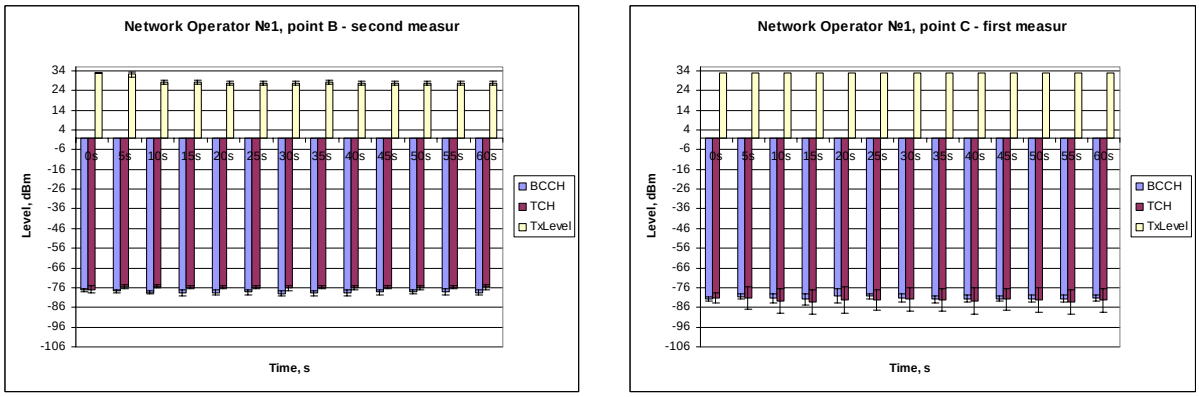


Figure 7. Dependence between RXLEV and TXLEV of MS in the time, for Network Operator 3.

From the results displayed of Fig. 5 can be seen the two boundary cases for network operator 1 – *TxLevel point B second measure* and *TxLevel point C first measure*. In the first case TxLevels of MS are very close to the maximum levels. In the second case TxLevels of MS are always 33dBm; its RXLEVs are highest from another cases in those TxLevel is also always 33dBm. These two cases correspond of two points from Fig. 2. The values measured in these two cases and two points are displayed graphically in Figs. 8(a, b).



(a) **(b)**

Figure 8. Presentation of average data of RXLEV, RXLEV_TCH, and TXLEV for Network Operator 1 in points indicated in Fig. 2: **(a)** point B; **(b)** point C.

In Table 1 and Table 2 are presented: confidential boundaries m_1 and m_2 of confidential interval I_{m_x}; the error ε (a half-magnitude of confidential interval) by n=130 independent measurements and confidential stochastic p_I=0.95. The results presented in Table 1 and Table 2 corresponded to the results from Figs. 8(a, b) respectively.

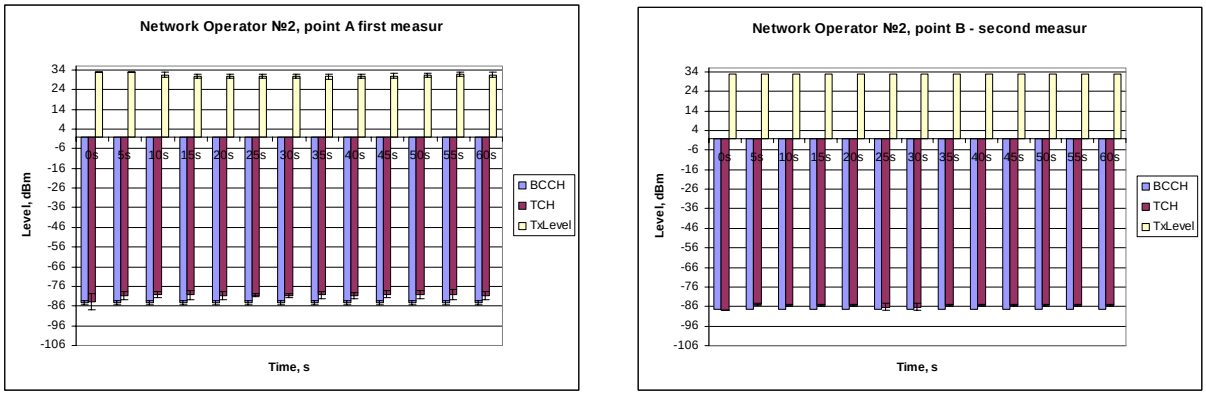
Table 1

	BCCH	TxLevel
m_1	-78.598	28.272
m_2	-78.084	29.069
ε	0.257	0.398

Table 2

	BCCH	TxLevel
m_1	-81.608	33.000
m_2	-80.930	33.000
ε	0.339	0.000

From the results displayed of Fig. 6 can be seen the two boundary cases for network operator 2 – *TxLevel point A first measure* and *TxLevel point B second measure*. In the first case TxLevels of MS are very close to the maximum levels. In the second case TxLevels of MS are always 33dBm; its RXLEVs are highest from another cases in those TxLevel is also always 33dBm. These two cases correspond of two points from Fig. 2. The values measured in these two cases and two points are displayed graphically in Figs. 9(a, b), respectively.



(a) **(b)**

Figure 9. Presentation of average data of RXLEV, RXLEV_TCH, and TXLEV for Network Operator 2 in points indicated in Fig. 2: **(a)** point A; **(b)** point B.

In Table 3 and Table 4 are presented: confidential boundaries m_1 and m_2 of confidential interval I_{m_x}; the error ε by n=130 independent measurements and confidential stochastic p_I=0.95. The results presented in Table 3 and Table 4 corresponded to the results from Figs. 9(a, b) respectively.

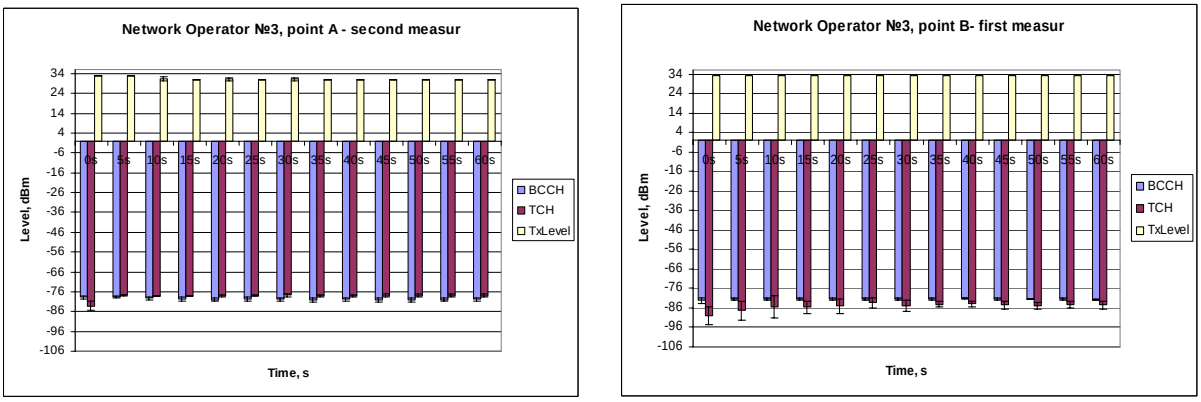
Table 3

	BCCH	TxLevel
m_1	-81.115	31.217
m_2	- 80.347	31.647
ε	0.384	0.214

Table 4

	BCCH	TxLevel
m_1	-85.878	33.000
m_2	-85.276	33.000
ε	0.339	0.000

From the results displayed of Fig. 7 can be seen the two boundary cases for network operator 3 – *TxLevel point A second measure* and *TxLevel point B first measure*. In the first case TxLevels of MS are very close to the maximum levels. In the second case TxLevels of MS are always 33dBm; its RXLEVs are highest from another cases in those TxLevel is also always 33dBm. These two cases correspond of two points from Fig. 2. The values measured in these two cases and two points are displayed graphically in Figs. 10(a, b), respectively.



(a) **(b)**

Figure 10. Presentation of average data of RXLEV, RXLEV_TCH, and TXLEV for Network Operator 3 in points indicated in Fig. 2: **(a)** point A; **(b)** point B.

In Table 5 and Table 6 are presented: confidential boundaries m_1 and m_2 of confidential interval I_{m_x}; the error ε by n=130 independent measurements and confidential stochastic p_I=0.95. The results presented in Table 5 and Table 6 corresponded to the results from Fig. 10(a, b) respectively.

Table 5

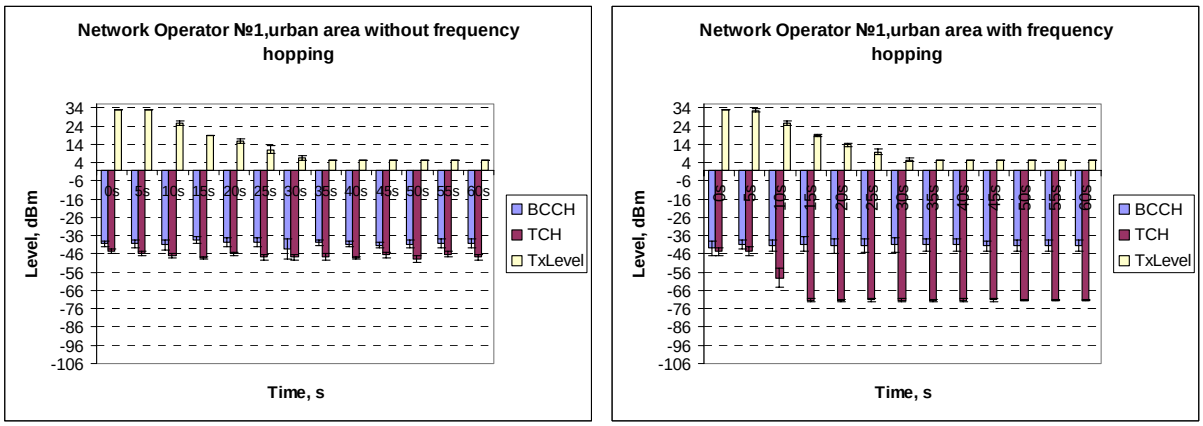
	BCCH	TxLevel
m_1	-79.876	31.235
m_2	- 79.557	31.503
ε	0.157	0.134

Table 6

	BCCH	TxLevel
m_1	-81.600	33.000
m_2	- 81.345	33.000
ε	0.128	0.000

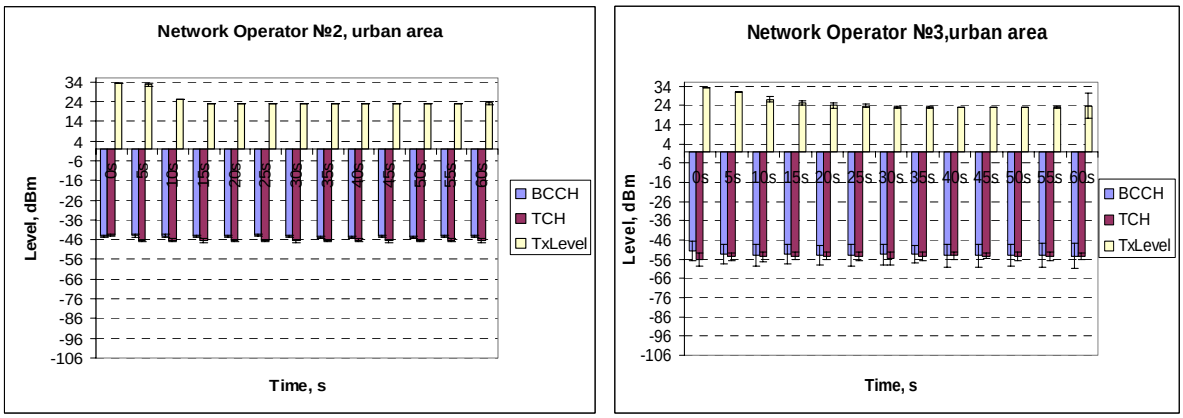
The received data in course of the present investigation (Figs. 5…10; Tables 1…6) showed that received level RXLEV in that output power level TXLEV of the mobile station is 33dBm for:

- Network operator 1 is approximate: - 81dBm;
- Network operator 2 is approximate: - 85dBm;
- Network operator 3 is approximate: - 81dBm.



(a) **(b)**

Figure 11. Presentation of average data of RXLEV, RXLEV_TCH, and TXLEV for Network Operator 1 in points indicated in Fig. 3: **(a)** without frequency hoping; **(b)** with frequency hoping.



(a) **(b)**

Figure 12. Presentation of average data of RXLEV, RXLEV_TCH, and TXLEV in points indicated in Fig. 3: **(a)** for network operator 2; **(b)** for network operator 3.

Analysis of the data from Figs. 11 and 12 showed that in the urban area output power level of the MS decrease during a call. The boundaries of the lowest output power levels of the MS are different, from 5dBm for network operator 1 to 23dBm for network operators 2 and 3. Based on these results can be seen, that values of the received levels of BCCH carrier for network operators are between -54dBm …-40dBm. Therefore, BSs of the operators are equally distant from the point of measurement. In the same time the alterations of output power level of the MS are different for the network operators. The different strategies for RF power control of the network operators are confirm from these results.

Adaptive power control of MS for the network operators starts after initial 10 seconds (see Figs. 8(a), 9(a), 10(a), 11, and 12). The reason for this is that during these seconds MS occupied controls channels; it is confirmed form the results illustrated of Fig. 13.

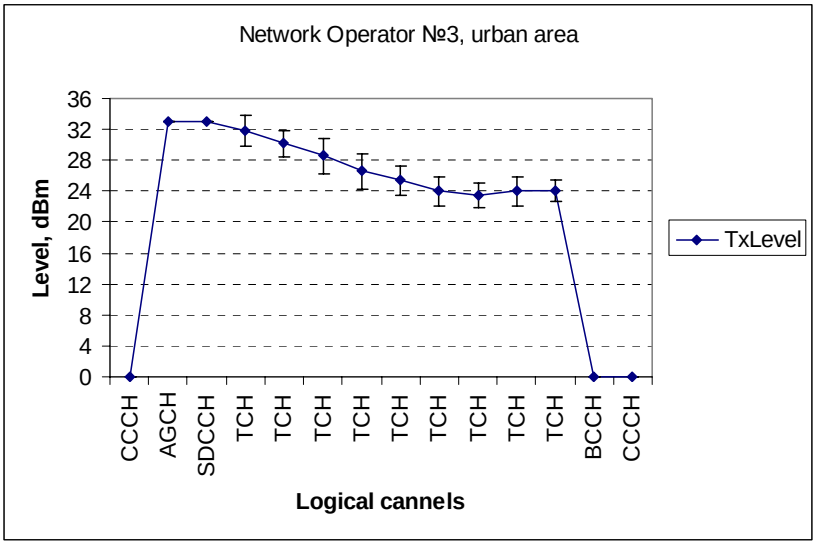


Figure 13. Presentation of average data of TXLEV in points indicated in Fig. 4.

In Fig. 11(a) TCH and BCCH channels using the same carrier, and have similar levels.

In Fig. 11(b) the TCH carrier is different from the BCCH carrier. In this case received level of TCH carrier is lower than level of BCCH carrier, it's mean that transmission power of BS is lower compared with the case from Fig. 11(a).

Summary

On the basic of the results of measurements of RXLEV, RXLEV_TCH, TXLEV, RXQUAL, and DISTANCE in the three points from Fig. 2 were established average value on the received levels RXLEVs in those output power level TXLEV of the mobile station is 33dBm (2W). Therefore, the received values (RXLEV ≈ - 85dBm …-81dBm) can be used to provide a reference levels.

These results can be applied to found the areas (points) in those output power level TXLEV of the mobile station is 33dBm (2W).

The results from the investigation demonstrated that adaptive power control of MS depended on level of BCCH carrier, but not of the level of TCH carrier (see Figs. 11(a, b)).

The results received via measurements in real operating conditions can be useful for further *in Vitro* and *in Vivo* investigations for the influence of the GSM mobile phones on the man.

Finally, according to reference from [10] to necessary to determine a complex of hygienic requirements to a mobile telephone, allowing the subscriber to realize the right of a voluntary choice of a comprehensible risk level and according by the World Health Organization recommendations to subscriber can be suggest: 1. During the first 10 seconds the mobile phone transmitted with maximum power 2 Watts, therefore, in this time the mobile phone must be distant from subscriber's head; 2. When the bars displaying receiving level strength of the mobile phone display are smaller from the maximum number, then the mobile phone will be transmit with maximum power during a call.

References

[1] N. Atanasov, "An Investigation of Adjusting Output Power Transmitter in Mobile Station for GSM900," *Telecom*, pp388-394, October, 2004.

[2] L. Hanzo, P. Sherriman, and J. Streit, *Wireless Video Communications Second to Third Generation Systems and Beyond*. New York: IEEE Press, 2001.

[3] R Steele and L. Hanzo, eds., *Mobile Radio Communications*. New York: IEEE Press-John Wiley, 2nd ed., 1999.

[4] Base Stations & wireless networks: Expose and helth consequences, *WHO*, Geneva, 15-16 June 2005.

[5] L. Guliani and B. Francesco, "The monitoring of BTS in Italy shows lower environmental limits are achievable" *Mobile communication and health: medical, biological and social problems*, pp. 89-90, September 2004.

[6] M. Wuschek, "Investigations into the power control of a GSM mobile phone under real operating conditions," *FGF Newsletter*, vol. 1, pp. 40-50, April 2005.

[7] G. Atanasova, "An Investigation of Signaling in Air Interface for GSM900," *Telecom*, pp327-333, October, 2004.

[8] H. Radev and V. Bogoev, *Uncertainty of the result of the measurement*. Sofia: Softtrade, 2001.
[9] E. Ferdinandov and B. Patchedgieva, *Stochastic and Statistics methods in the Communications.* Sofia: Ciela, 2005.
[10] Somov, "Ecological and technical characteristics of mobile communication networks," *Mobile communication and health: medical, biological and social problems*, pp. 119-120, September 2004.

STRESS HORMONE REACTIVITY IN MEDICAL STAFF EXPOSED TO ELECTROMAGNETIC RADIATION

MICHEL ISRAEL, KATIA VANGELOVA, DESIMIRA VELKOVA, MICHAELA IVANOVA

NATIONAL CENTER OF PUBLIC HEALTH PROTECTION,
15 ACAD. IVAN GESHOV BLVD., 1431 SOFIA, BULGARIA

Abstract

The **aim** of the investigation was to study the effect of electromagnetic radiation (EMR) on stress hormone reactivity of medical staff in physiotherapies. The excretion rates of stress hormones cortisol, adrenaline and noradrenaline were followed during morning shift in 15 female physiotherapists using RIA kits and a spectrofluorimetric method. The mean number of treatments with EMR emitting devices per month and the emission of each device was followed. A control group of nurses, matched by age, sex and work task was followed. The psychosocial factors were followed and showed no differences between the two groups. Significantly higher excretion rates of cortisol ($F_{(1,69)} = 7.171$, $p = 0.009$), adrenaline ($F_{(1,69)} = 7.869$, $p = 0.007$) and noradrenaline ($F_{(1,69)} = 10.643$, $p = 0.002$) with the studied physiotherapists in comparison with the control group of nurses was found. In conclusion, our data showed that EMR influenced stress hormone reactivity of medical staff in physiotherapies.

Key words: Cortisol, adrenaline, noradrenaline, medical staff, EMR exposure.

Introduction

Stress at work and work related changes in health and well being of the medical staff have been subject to growing concern in recent years (Deane et al. 2002, Elfering et al. 2002, Fujiwara et al. 2004). Little is known about stress at work of the medical staff in physiotherapies, exposed to some common for the medical staff stressors as risk of infections, emotional load of dealing with patients, heavy lifting, exposure to chemicals, but also some specific stressors as the exposure to electromagnetic radiation (EMR) from different devices as equipment for microwave and high frequency diathermy, pulsed magnets, d'Arsonvale devices, optical sources (UV, IR and visible), lasers etc.

Several studies investigated the effects of radiofrequency EMR emitted from GSM, broadcasting and TV transmitters on hypothalamic-pituitary adrenal axis and sympathetic adrenomedullary system. Mann et al. (1998) studied several endocrine parameters in humans exposed at night to a low level (0.2 W/m^2) radiofrequency field from GSM at 900 MHz and found a transient 1 hour increase in cortisol during the first hour of the exposure. Radon et al. (2001) failed to find an effect of low level pulsed radiofrequency EMR (carrier frequency 900 MHz, pulsed frequency 217 Hz, average power flux density of 1 W/m^2) on the salivary cortisol. Our earlier data (Vangelova et al. 2002) showed a trend for increase in 11-oxycorticosteroid (11-OCS) excretion rates in operators, working under low-level radiofrequency EMR. Next our study (Vangelova and Israel 2005) showed dose-effect relationship in the excretion of stress hormones and radiofrequency EMR. There are no data for the effect of EMR on stress hormone reactivity in medical staff in the physiotherapies, exposed to high level EMR, but for very short periods of time.

The **aim** of the investigation was to study the effect of EMR on stress hormone reactivity of medical staff in physiotherapies.

The study is a part of complex investigation of health risk in medical staff exposed to EMR.

Material and methods

Subjects

We investigated 15 female physiotherapetists, aged 49.5 ± 7.4 years with average length of service 26.4 ± 7.7 years, working in 4 hospital physiotherapies in Sofia. A control group of nurses, matched by age up to three years, work organization and having similar job task was studied. The control group was of mean age 48.9 ± 6.9 years and length of service 25.8 ± 7.3 years. All the investigated subjects worked fast-rotating two-shift system:

morning shifts (7:30 a. m- 2:00 p.m) and afternoon shifts (1:30 - 08:00 p.m). The investigated subjects have signed informed consent for participation in the study.

EMR exposure and confounding physical factors
EMR exposure
The method for EMR exposure assessment is presented in details elsewhere /9/. In general, the method is based on the following:
Parameters for exposure assessment
In order to establish unified conditions for exposure assessment for different frequencies (over the overall frequency range) we apply a general unified indicator associated with the energetic irradiation dose, according to the ICNIRP Guidelines /8/, ACGIH TLVs /15/, and the Bulgarian National Standards /1,2/.

Conditions for applying the wave impedance
We can consider a prevailingly directed flow at distances from the emitter to the object not shorter than 6 wavelengths and an entirely homogeneous flow of electromagnetic energy – at about 100 wavelengths. In the far field the conductivity of the medium is proportional to the squared distance from the emitter. At approaching it the value of this quantity increases proportionally to the volume between the emitter and the object, reaching maximum through areas obtained along the main diagonal of the volume. This reflects on an undefined value of the wave impedance.

Dimensions of values related to energy load
The energy load of the human organism is defined for three cases as a derived quantity of energy falling at external irradiation: $\boldsymbol{W_E = E^2.T,\ (V/m)^2.h}$, $\boldsymbol{W_H = H^2.T,\ (A/m)^2.h}$ and $\boldsymbol{W_S = S.T,\ \mu W/cm^2.h}$, based on dispersed energy per unit time on human body during the official working shift. Measurable quantities are used – intensities and power density according to the distance from the generator to the measuring device and the respective frequency range of the single photon.
As ***SAR*** is introduced by the dimension of base metabolism of an adult man (175 cm/70 kg) the dimension of ***SA*** is the dimension of ***SAR*** by the time.
The two types of quantities - $\boldsymbol{W_E}$, $\boldsymbol{W_H}$ and $\boldsymbol{W_S}$ on the one side, and ***SAR, SA*** on the other do not differ substantially in conditions of air equivalent environment and a human body situated in it.
SAR is introduced through Human Equivalent Antenna. If the respective effective area is $\boldsymbol{A_e}$, then through relationships between the dimensions of the quantities ***W*** and ***SA*** following by the definition for power and from the way of determining human body exposure, the quantity ***W*** corresponds to whole body value of ***SA*** at constant body weight and unchanging mean conductivity of the tissue, standardized to the effective exposure area $\boldsymbol{A_e}$. The magnitude of the latter on its part depends on the mutual orientation of a standing person and the intensity of the falling electric field ***E***.
The measurable quantity in all cases is the same – ***E [V/m].*** Consequently $\boldsymbol{W_E}$ will incorporate the definition of ***SA*** and vice versa.

Determination of the exposure duration
We divide the time of being in the working environment with NIR into two sets of intervals for exposure duration: real exposure time at work with a device $\boldsymbol{T_{app}}$ ***[h]***, and a total duration of the working shift ***T [h]***. The difference between them is so called "void time" when there is no real exposure.
We use the method of the "chronometer scenario" because the void time has no equipartitioned averaged evaluation. The duration time is introduced by the number of devices and the number of patients serviced by the individual.

Measurement method
The method is unified as far as three parts of its nature are unified: Equipment; Distances to the particular device, mandatory for the measurement – 6 distances depending on the frequency range; list with the mandatory restrictions to the behavior of the physicist/engineer, performing the measurement.
The major characteristics of the method are the 6 mandatory distances to the different types of generators determined depending on the frequency range of the radiation. They conform to two conditions: Requirements for measurement in the far and near field zones; Requirements for determination of ***SAR*** in different cases of electromagnetic energy falling on a standing human.

General relationships for assessment of individual exposure
The dose is a function of the squared mean measured intensity and can be presented by the ***SAR*** quantity.
Our calculation formulation is based on the vision of the averaged dose: the dose (calculated with the actual measured values of the field and exposure time) multiplied by the mean geometric value of the partial doses on

the distance from the physician/nurse to the patient r_1 and the dose of the same to another characteristic distance (one of the cited – r_i, i ≠ 1). Thus a characterizing quantity is obtained which is a non-dimensional growing sum $\overline{D}$:

$$\overline{D} \approx \sum \frac{1}{q} \sqrt{D(r_1)} \sqrt{D(r_{i\neq 1})}$$

Here $1/q$ is a non-dimensional quantity – ratio.
The squared field strength (E^2) used for the dose assessment is equal to the product of the measured intensity of the field at distance r_1 and the sum of weighed intensities of the other 5 distances.
The method allows, at unified measurements, the elaboration of individual exposure assessment for each person in physiotherapy through calculations depending on the number of devices, number of patients and the actual configuration of the ward.
SAR is calculated for the relevant frequency directly through the calculated dose multiplied by the individual's mass:
$SAR = D.m + B(f) + C$,
where m is the mass of the exposed person; B is a frequency -depending ratio, and C is a constant.
The method was used for assessment of the exposure in several physiotherapy units. Assessment of the exposure in several physiotherapy units by devices is shown on Table 1. Calculating the relative values for the whole frequency range in the studied physiotherapies the obtained quota is much larger than 1.

Table 1

Frequency	Devices	Calculated parameter	Basic restriction
≤ 2 kHz	Magnets	j ≈ 0,28 – 0,31 A/m^2	j ≤ 2 mA/m^2
≤ 2 kHz	Interferentz	j ≈ 0.69 mA/m^2	j ≤ 2 mA/m^2
f ≤ 2.5 MHz	UHF generator for ultrasound therapy	j ≈ 3.8 mA/m^2	j ≤ 2 mA/m2
≤ 100 kHz	Diadynamik (Bulgaria)	j ≈ 0.15 mA/m^2	j ≤ 1 A/m^2
≤ 100 kHz	Galvanostat	j ≈ 0.15 mA/m^2	j ≤ 1 A/m^2
150 ÷ 300 kHz	D'Arsonval	SAR ≤ 0.4 W/kg	0,4 W/kg
27,12 MHz	UHF devices	SAR = 3,71 – 9,78 W/kg	0,4 W/kg
2450 MHz	Medical radar	SAR = 0,31 – 5,3 W/kg	0,4 W/kg whole body 20 W/kg for limbs 10 W/kg for head

Light sources (polychromatic) - restrictions according to ACGIH (2004):
IR: S ≤ 1.8.t$^{-3/4}$ W/cm^2 (for cornea and lens)
IR: S ≤ 0.6/α W/cm^2.sr (for retina protection)
IR (with blue light filter – B1): 1 μW/cm^2, and : t_{max} ≤ 10 (mJ/cm^2)/S(W/cm^2)
UV and visible light: t_{max} ≤ 0.003 (J/cm^2)/S (W/cm^2)

Quartz (UVB-1, UVB, UVA, Visible: S ≈ 17.6 mW/cm^2
Solux Infrarouge, without filters: S ≈ 286.1 mW/cm^2
Solux Infrarouge, with filter B1: S ≈ 4.9 mW/cm^2

Noise and microclimate
The noise and microclimate were followed, too, and were within hygienic norms with no differences between the groups.

The psychosocial factors
The psychosocial factors were assessed by the questionnaire "My job", based on checklists, containing five subscales (Kompier et al. 1994). The working condition scale contains items about work posture, lighting, noise, vibrations, temperature, humidity, flow, dust, odours, etc. The job content scale sums eighteen items as a monotony, tasks, requiring intense concentration, time pressure, work organization, etc.). The job control scale (ten items) includes questions about novelties at work, ability to influence the pace, methods of work, promotion, etc. The work related social support scale sums ten items: five ones concerning support from coworkers and five from supervisors. Health complaints scale is the sum of sixteen items.

The excretion rates of stress hormones
The excretion rates of stress hormones were followed during the morning shift (7:30 – 14:00). The following

three periods were studied: early morning (6:30 – 8:30), second period (8:30 – 11:00) and third period (11:00 – 13:30). The urine aliquids were stored at –20°C and the subsamples for catecholamine assay were acidified to pH 3 with 6N HCL prior refrigeration. Urine free cortisol was assessed by radioimmunological kit (Orion Diagnostica, Espoo, Finland): interassay CV 5.2, 5.2, 6.1 % for low, mean and high value urine samples. The catecholamines adrenaline and noradrenaline were measured with spectrofluorimetric method (Vangelova 2000).

Statistics

The time-of-day variations of the studied stress hormones were analyzed for the effect of radiofrequency EMR exposure and time-of-day by tests of between-subjects effects (SPSS). Variation analysis (one-way ANOVA) and correlation analysis were used to calculate the psychosocial factors and the relationships between the studied variables.

Results

Our data show no significant differences of psychosocial factors between the exposed and control group (Table 2). The studied physiotherapists and control group of nurses had a feeling of strain at work and emotional load of dealing with patients, increased risk of infections, heavy lifting and work tasks, requiring concentration. The working conditions were described as moderate, but the physiotherapists found the lighting unsatisfactory. The number of psychosomatic complaints were comparatively high with both studied groups, slightly higher with the physiotherapists in comparison to the control group of nurses. The main psychosomatic complaints were musculoskeletal disorders (pain in the back, bones and muscles), numbness and/or timbling sensation in the limbs, physical and mental exhaustion, fatigue, dizziness, etc.

Table 2.
The psychosocial factors in exposed to EMR physiotherapists and control group

Scales/Groups	Maximal scores	Physiotherapists	Control group (nurses)
Working conditions	17	7.1 ± 3.0	7.1 ± 9.8
Work content	16	5.4 ± 3.2	7.0 ± 3.2
Control	10	2.9 ± 2.02	5.3 ± 1.8
Social support	10	2.3 ± 1.9	2.6 ± 2.4
Psychosomatic complains	16	9.4 ± 3.3	8.9 ± 2.7

Significantly higher excretion of cortisol with the physiotherapists in comparison to the control group of nurses (Figure 1) was found ($F_{(1,69)} = 7.171$, $p = 0.009$). The excretion rates of cortisol followed the typical diurnal rhythm with highly significant time-of-day variations ($F_{(2,69)} = 12.231$, $p = 0.000$).

The adrenaline excretion rates (Figure 2) were significantly higher in the studied physiotherapists in comparison to the control group of nurses ($F_{(1,69)} = 7.869$, $p = 0.007$). Also, significantly higher excretion rates of noradrenaline (Figure 3) with the physiotherapists in comparison to the nurses ($F_{(1,69)} = 10.643$, $p = 0.002$) were found. The time-of-day variations of adrenaline and noradrenaline were not significant.

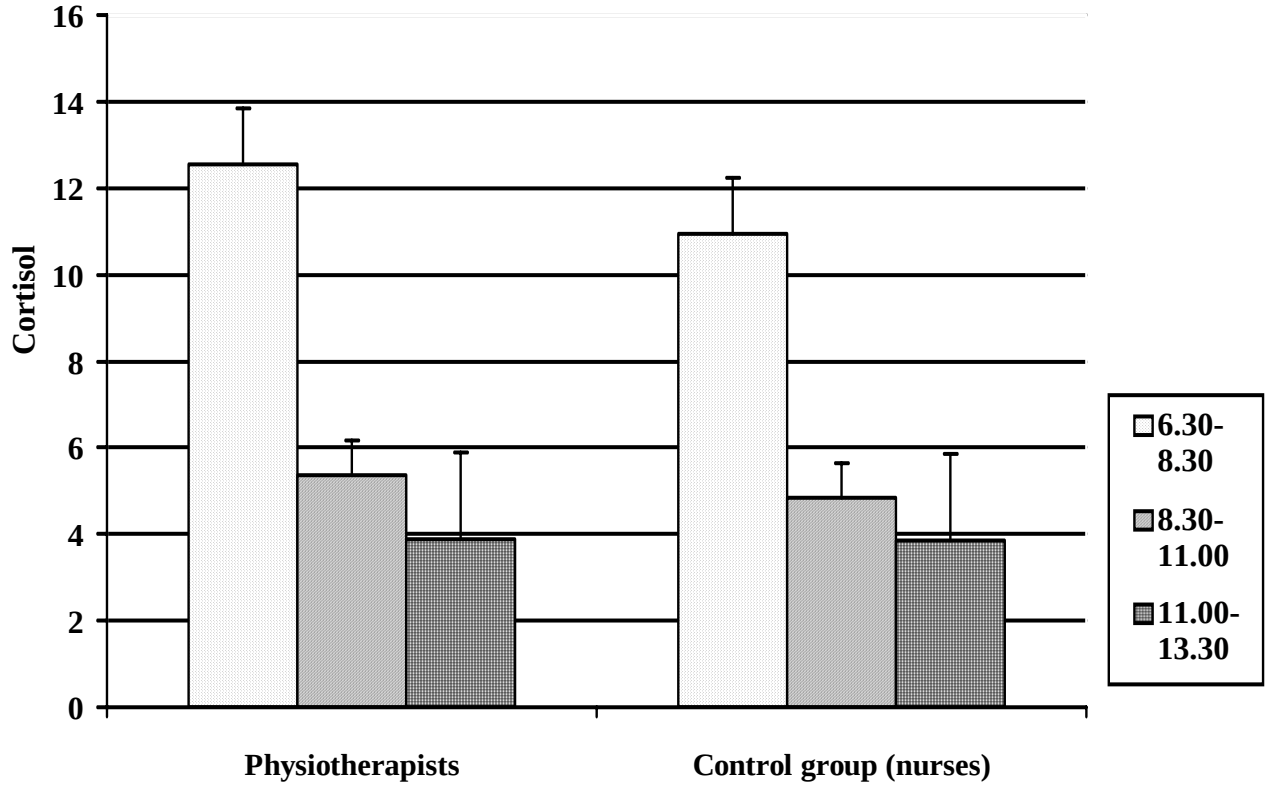


Figure 1. The excretion rates of cortisol in physiotherapists exposed to EMR and control group.

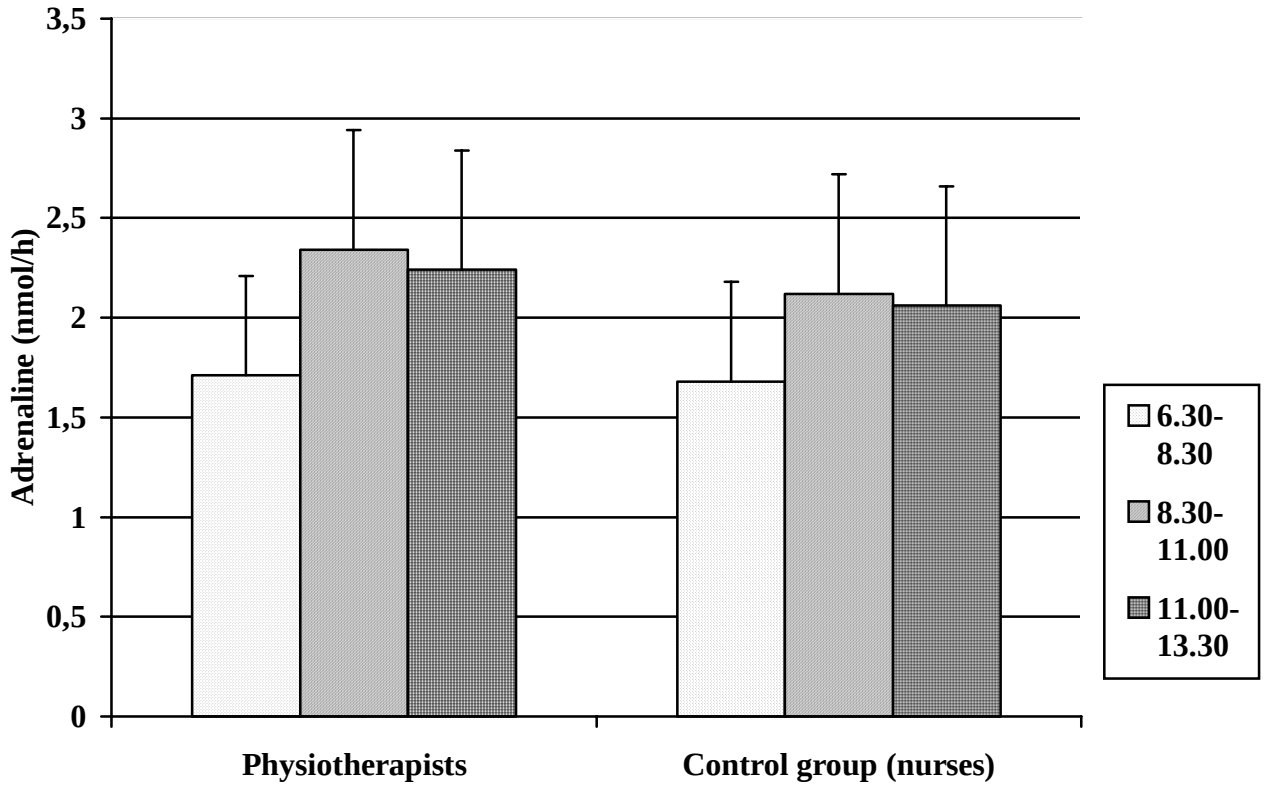


Figure 2. The excretion rates of adrenaline in physiotherapists exposed to EMR and control group.

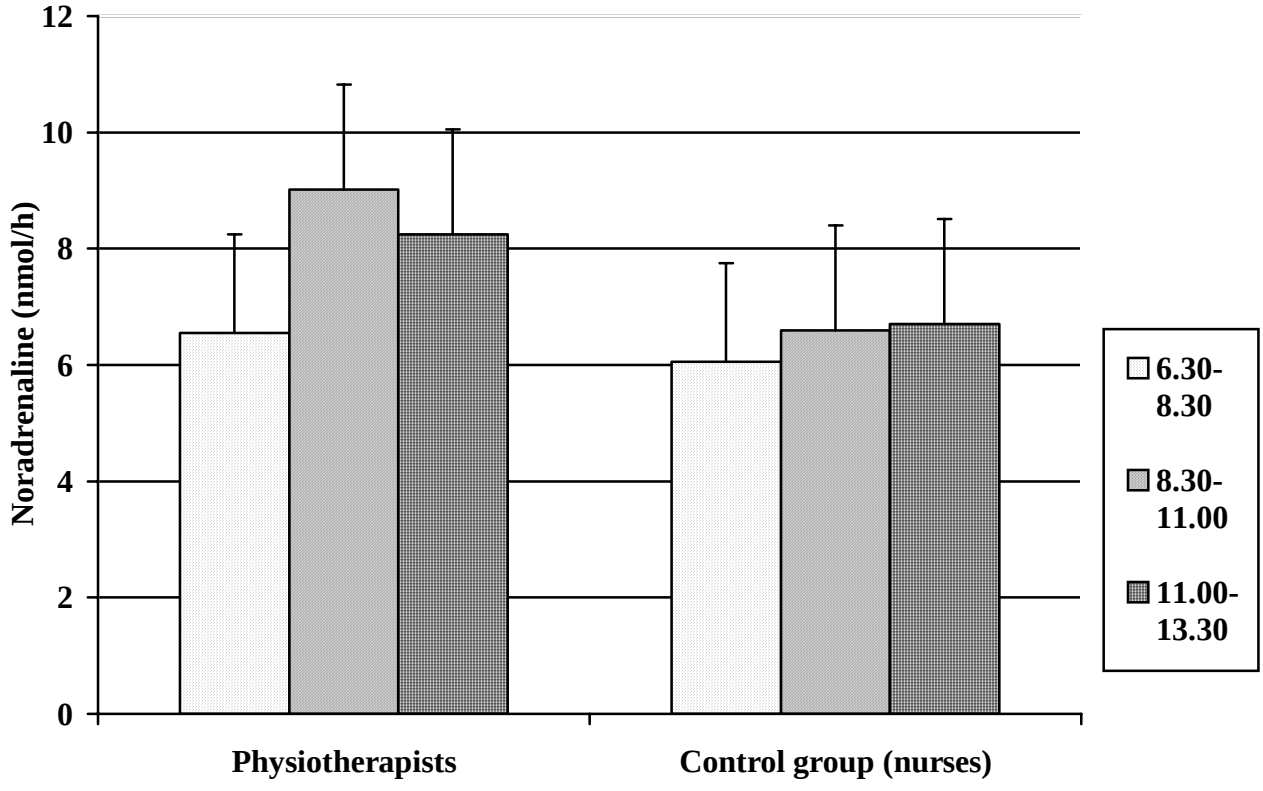


Figure 3. The excretion rates of noradrenaline in physiotherapists exposed to EMR and control group.

Discussion

Our data show significant effect of non-ionising radiation on the excretion rates of stress hormones during the working day. The work conditions, work content, work control and psychosocial support showed no significant differences between the exposed and control group. No acute incidents and changes in the task requirements among the groups during the period of the study were registered. The number of treatments in the studied physiotherapies did not exceed the number of treatment by the studied control group of nurses. The studied physiotherapist had no complains concerning the EMR emissions and were not aware of the level of the exposure during the study.

The present study confirmed our previous data (Vangelova et al. 2002, Vangelova and Israel 2005) for effect of EMR exposure on stress hormones reactivity, with the highest effect on noradrenaline excretion rates. The stress hormones are important biomarkers for allostatic load (McEwen 1998, Chrousos 2000, Tsigos and Chrouos 2002) and the long term effects of increased secretion of stress hormones are associated with health implications. The effects of catecholamines on the cardiovascular function are well known. The excessive and sustained cortisol secretion has been for long associated with depression, osteoporosis, immunosuppression and the entire spectrum of the metabolic syndrome (Fraser et al. 1999, Rosmond et al 1998).

Summing up, significantly higher excretion rates of stress hormones with the medical staff under EMR exposure in physiotherapies were found. As outlined above, the chronic elevation of stress hormones may be associated with health implications. Reduction of EMR exposure in physiotherapies both by technical solutions and limiting the time of exposure should be encouraged.

References

1. Bulgarian National Standard 14425 –90. Labour protection. Electromagnetic fields – radiofrequency range. Admissible values and requirements for control (in Bulgarian).
2. Bulgarian National Standard 17137-90. Labour protection. Electromagnetic fields – microwave range. Admissible values and requirements for control (in Bulgarian).
3. Chrousos, G.P. The role of stress and the hypothalamic-pituitary-adrenal axis in the pathogenesis of metabolic syndrome: neuroendocrine and target tissue-related causes. Intern. J. Obesity 2000; 24 (Suppl. 2): S50-5.
4. Deane R, Chummun H, Prashad D. Differences in the urinary stress hormones in male and female nurses at different ages. Journal of Adv. Nurs. 2002; 37 (3): 304-310.
5. Elfering A, Grebner S, Semmer NK, Gerber H. Time control, catecholamines and back pain among young nurses. Scandinavian Journal of Work and Environmental Health 2002; 28 (6): 386-393.
6. Fraser, R., Ingram, M.C., Anderson, N., Morrison, C., Davies, E., Connell, J.M.C. Cortisol effects on body mass, blood pressure, and cholesterol in general population. Hypertension 1999; 3: 1374-8.
7. Fujiwara K, Tsukishima E, Kasai S, Masuchi A, Tsuts A, Kawakami N, Miyake H, Kishi R. Urinary catecholamines and salivary cortisol on workdays and days off in relation to job strain among female health providers. Scandinavian Journal of Work and Environmental Health 2004; 30, 2, 129-138.
8. ICNIRP. Guidelines for limiting exposure to time-varying electric, magnetic and electromagnetic fields (up to 300 GHz). Health Physics 1998; 74(4): 494–522.
9. Israel, M., Tschobanoff, P. Exposure to non-ionizing radiation of personnel in physiotherapies. In: Bioelectromagnetics. S. N. Ayropetyan and M. S. Markov (eds.), Springer Press, 2006: pp.367-376
10. Kompier M, Levi L. Stress at work: causes, effects and prevention. A guide for small and medium sized enterprises. European Foundation for Improvement of Living and Working Conditions. 1994, Geneva.
11. Mann K, Wadner P, Brunn G, Hassan F, Hiemke C, Roschke J. Effects of pulsed high frequency electromagnetic fields on the neuroeudocrine system. Neuroendocrinol 1998; 67: 139-44.
12. McEwen BS. Protective and demaging effects of stress mediators. New England Journal of Medinine 1998: 338(3): 171-179.
13. Randon K, Parera D, Rose D–M, Jung D, Vollrath L. No effects of pulsed radiofrequency electromagnetic fields on melatonin, cortisol and selected markers of the immune system in men. Bioelectromag 2001; 22: 280-7.
14. Rosmond, R., Dallman, M.F., Bjorntorp, P. Stress related cortisol secretion in men: Relationships with abdominal obesity and endocrine, metabolic and hemodinamic abnormalities. J. Clin Endocrinol. Metab. 1998; 83: 1853-1859.
15. Threshold Limit Values for Chemical Substances and Physical Agents & Biol. Exp. Indices, ACGIH, Signature Publications, 2004.
16. Tsigos C, Chrousos GP. Hypothalamic-pituitary-adrenal axis, neuroendocrine factors and stress. Journal of Psychosomatic Medicine, 2002; 53 (4): 865-871.
17. Vangelova K. Method for assessment of catecholamines adrenaline and noradrenaline in urine. In: Methods for Investigations in Hygiene. National Center of Hygiene, Medical Ecology and Nutrition, Sofia, 2000; 2:

2-4 (in Bulgarian).
18. Vangelova K., Israel M., Mihailov S. The effects of low level radiofrequency electomagnetic radiation on the excretion rates of stress hormones in operators during 24 hour shifts. Centr. Eur. J. Public Health 2002; 10, 23-27.
19. Vangelova K., Israel M. Variations of melatonin and stress hormones under extended shifts and radiofrequency electromagnetic radiation. Rev. Environ. Health 2005, 20 (2): 151-161.

EFFECTS OF ELF-EMF EXPOSURE ON BODY WEIGHT GAIN, HAEMOPOIESIS AND MAMMARY CARCINOGENESIS IN BALB/c and BALB NeuT MICE.

IEZZI M.[1,4], FELICETTI P.[1,4], BORGIA L.[1,4], PANNELLINI T.[1,4], MARIGGIO' M.A.[2,4], PIETRANGELO A.[2,4], MEZZETTI A.[3,4], CUCCURULLO F.[4], FANO' G.[2,4], MUSIANI P.[1,4]

[1] IMMUNO-ONCOLOGY LAB, [2] CELL PHYSIOLOGY LAB, [3] ATHEROSCLEROSIS LAB, [4]AGING RESEARCH CENTER, G. d'ANNUNZIO UNIVERSITY FOUNDATION, VIA COLLE DELL'ARA, 66013 CHIETI, ITALY.

ABSTRACT

Several epidemiological studies have pointed to a positive correlation between Extremely Low Frequency ElectroMagnetic Fields (ELF-EMFs) exposure and the incidence of haematological or solid tumors. To better clarify its effects on haemopoiesis and cancer development, we exposed to continuous and intermittent ELF-EMF young and adult BALB/c mice or inbred BALB Neu T mice: the latter constitute a transgenic model of HER-2-dependent mammary carcinogenesis. We monitored the body weight trend and studied haemopoietic lineages and mature immune cells in bone marrow and lymphoid organs by morphologic and FACS analysis.

In young but not in adult male and female BALB/c mice there was a transient decrease of body weight and a decrease in bone marrow and splenic myelopoietic cells, whereas there were no haematological differences between treated and control young or adult BALB NeuT mice, probably because of the cancer-driven haematological dysregulation. Histological and Whole Mount grading showed that ELF-EMF do not influence mammary carcinogenesis.

This study demonstrates that ELF-EMF produce a biological stress that affects growth. Healthy subjects are able to both adapt to and compensate it. Further in vivo studies are needed to determine the consequences of ELF-EMFs exposure combined with other known stress factors.

INTRODUCTION

There is a large body of epidemiological evidence in favour of a significant positive correlation between exposure to magnetic fields and the risk of cancer [1, 2, 3, 4, 5] and the International Agency for Research on Cancer (IARC) has classified extremely low frequency electro) magnetic fields (ELF-EMF) as possible sources of human cancer [6]. Subsequent in vitro, in vivo and epidemiological studies, however, have not yet substantiated this correlation and its extent.

Carcinogenesis is a complex process and ELF-EMFs could be involved in any of its steps [7]. They do not induce direct DNA damage in vitro, but may synergize with compounds that induce DNA modification [8]. It has been shown, for example, that ELF-EMFs exposure co-promotes the rat mammary tumors induced by 7,12-dimethylbenz[a]anthracene (DMBA) [9, 10].

The central role of the immune system in the natural history of carcinogenesis makes it essential to determine the immunological consequences of exposure to ELF-EMFs. Some studies show that ELF-EMFs have no effect on or do not suppress the immune system, whereas others have found proliferative effects. Exposure of murine bone marrow cells to a magnetic field causes proliferation and differentiation/reduction of the granulocyte-macrophage progenitor, whereas its effect on the proliferation of stromal stem cells proliferation is not clear [11]. Leukopenia and neutropenia have been observed in mice after long exposure to ELF-EMFs [12]. In another report, ELF-EMFs had no effect on the cytotoxic activities of NK and LAK cells, nor on the production of IFN-γ, TNF-α, IL-2 and IL-10 production by human PBMC [13].

These discrepancies can readily be assigned to the use of dissimilar cell systems, mouse models, magnetic flux

densities, and exposure units and periods.
The present study set out to determine whether a striking relationship exists between carcinogenesis and exposure to ELF-EMF, and how far the immune system is affected.
A pair of Helmholtz coils was used to deliver variable, homogeneous, sine-wave AC magnetic fields at 50 Hz with an intensity of 0.5-1.0 mT. The apparatus comprises plastic cages in which the animals are exposed to the ELF-EMFs and is located in an insulated room with the control animals outside the EMF area (see appendix- Instrument).
BALB/c and BALB NeuT mice were employed. BALB/c is one of the most frequently used inbred strains owing to its good breeding performance and long reproductive lifespan. It is particularly well known for the production of plasmacytomas on injection of mineral oil and widely used for studies on lymphoma.
BALB-neuT are transgenic for the rat transforming HER-2/neu oncogene [14, 15]. Its transforming mutated form under the transcriptional control of a mammary tumour virus causes fast and aggressive mammary carcinogenesis. Tumours become spontaneously evident after the progression of tumorigenesis and their relationship with the surrounding tissues is preserved. Reproduction of the development of autologous tumours, the occurrence of invasion and metastasis, and the presence of an intact immune system are other key features of these genetically modified mice [16]. At 10 weeks of age, they display advanced cancerization, especially around the nipple where the side buds become in situ carcinomas and an increasing number of hyperplastic foci form along the mammary tree. The in situ carcinomas become invasive between the 15th and the 20th week and metastasize after the 30th week [17].
Our experiment was designed to answer the following questions.

Initially:
* Whether ELF-EMFs influence the growth and the haemopoietic system of BALB/c and BALB NeuT mice
* Whether male and female animals are equally responsive
* Whether young and adult animals are equally responsive
Subsequently:
* Whether the effects were transient or persistent
* Whether a dose-response relation or a threshold value for the ELF-EMF intensity is apparent
* Whether continuous and intermittent (night-time only) exposure exert the same effects

Lastly the effect of ELF-EMFs effect on mammary carcinogenesis in BALB NeuT mice was investigated.

Mice were randomised as explained in the Appendix. Briefly, groups of female and male BALB/c and female BALB-neuT were exposed continuously and intermittently to ELF-EMF at 0.5 or 1mT at 6 weeks of age (young mice) and 10 weeks of age (adult mice).
Animal body weight was recorded at the beginning of the experiment and every 15 days.
After 4 and 12 weeks from the beginning of the exposure mice were sacrificed and primary and secondary lymphoid organs were analyzed by histology, immunohistochemistry and flow cytometry.
Tumour burden in BALB neuT mice was assessed by Whole Mount analysis, histology and immunohistochemistry.

Since no differences were evident between 0,5 and 1 mT ELF-EMF exposure, only data referring to 0,5 mT will be shown below.

ELF-EMFs slow down the body weight gain of young, but not of adult BALB/c mice.
Young male and female BALB/c mice were treated for 12 weeks. The controls were housed in the same room. Their body weight was recorded at the beginning of the experiment and every 15 days.
After 4 weeks of exposure, a significant decrease in body weight was observed in both continuously and intermittently treated mice (Fig.1, 2). This was made up later.

ELF-EMF EXPOSURE AFFECTS BODY WEIGHT GAIN AND HAEMOPOIESIS IN YOUNG BALB/C MICE.

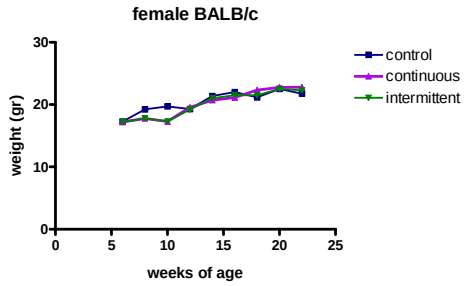


Fig.1

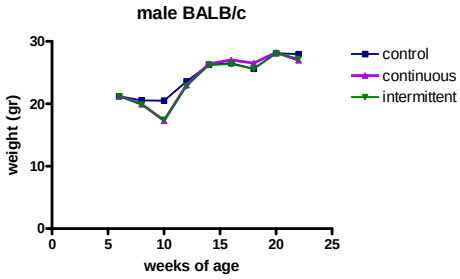


Fig.2

There was no comparable decrease in the adult animals.

ELF-EMFs impaired bone marrow myelopoiesis and splenic lymphoid compartment in the young BALB/c mice.

Several bone marrow and spleen alterations were found after 4 weeks' exposure.
No comparable changes were noted in the adult animals.

Bone marrow haemopoiesis.
Morphometrical analysis of cytological bone marrow samples showed that myeloid progenitors were reduced in both continuously and intermittently exposed mice (Tab 1). Myelocytes are large cells with specific granules in the cytoplasm and an indented nucleus, usually
displaced from the center. Metamyelocytes are similar to the myelocyte stage except that they are smaller and demonstrate a deeply indented, kidney shaped nucleus. In spite of the reduction in the total myeloid compartment (see Segmented cells in Tab 1), the ratio between mature neutrophils and immature myelocytes was normal (data not shown). The decrease of segmented cells was coupled with a relative increment in the proportion of red cells and lymphocytes. However the bone marrow cellularity was normal, as well as the differentiation in all the lineages, so neither maturative blocks nor dysplasia were evident.

Table 1. Bone marrow cell count in 10 week old mice.

	Controls	**Intermittent ELF-EMFs exposure**	**Continous ELF-EMFs exposure**
Myeloid Immature Cells	13 ± 3.1*	8 ± 3.1†	7± 4.1†
Segmented cells	33 ± 9.1	23 ± 8†	24 ± 7.1
Erythroid Cells	45 ± 7.3	54 ± 10.6†	53 ± 11.6
Lymphoid Cells	12 ± 5.1	18 ± 3.1	16± 6

*The values (mean ± SD from 16 mice per group) are expressed as cell percentages
†Significantly different values (a: p≤ 0.001) from those of WT littermates

Histological and immunohistochemical analysis of lymphoid organs.
The volume of the spleens of treated and untreated mice was determined from the following formula: "(transverse diameter)2 * longitudinal diameter/transverse diameter". No differences were found (data not shown). No splenomegaly or other macroscopic pathological aspects were observed.
Despite their normal size, the spleens of treated mice revealed a reduction in the white pulp area (Tab. 2).

Table 2. Extension of the white pulp in the H&E stained spleens.

	Controls	**Intermittent ELF-EMFs exposure**	**Continous ELF-EMFs exposure**
White pulp	52 ± 1.1*	46 ± 2°	43 ± 3°

*The values (mean ± SD from 16 mice per group) are expressed as the percentage of the area occupied by
White pulp area [%= (White pulp area*100)/total spleen area].
° Significantly different values ($P \leq 0.01$) from those of WT littermates.

The same results were obtained when we correlated the CD4, CD8 and B220 positive areas with the total spleen area, showing that the reduction involved all the lymphoid subsets.
No architectural nor cytopathological alterations were observed in the lymphoid (black arrows) or haemopoietic (green arrows) compartments. (Fig.4)

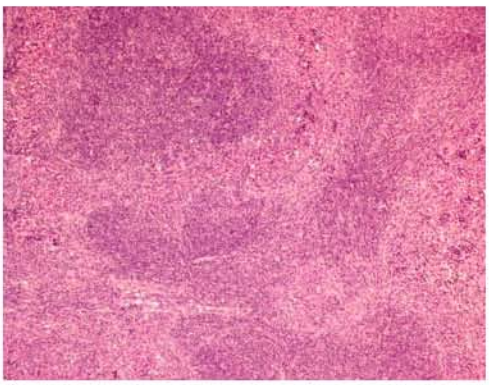


Fig. 4

The percentages of the CD4, CD8 and B220 positive areas in the lymph nodes did not differ in the treated and untreated mice.

The effects of ELF-EMFs exposure on the immune system are reversible.
Bone marrow and spleen samples were collected from the treated and untreated BALB/c mice after 12 weeks. The haematological parameter values of treated mice are not significantly different with respect to the controls. Count of bone marrow cells on cytological smears shown a normalization in percentage of myeloid compartments and quantitation of white pulp area percentage in the spleen showed no differences between experimental groups (data not shown).
FACS analysis of spleen and bone marrow from 18-week-old mice.
To obtain a clearer picture of any slight effects of ELF-EMF, at the end of the treatment we performed FACS analysis of bone marrow and spleen cells at the 18th week of age; a statistically significant reduction in CD11b+ granulocyte and monocyte lineages was observed in the male (Fig. 5, 6), but not the female mice.

ELF-EMF EXPOSURE AFFECTS BODY WEIGHT GAIN AND HAEMOPOIESIS IN YOUNG BALB/C MICE.

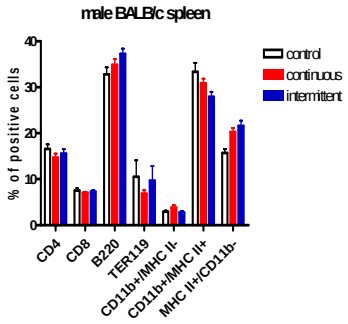


Fig 5

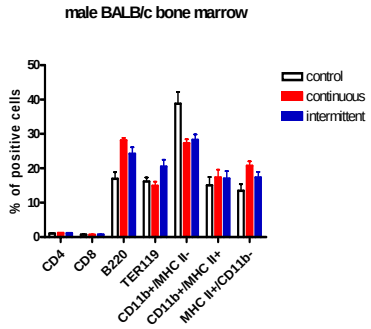


Fig 6

ELF-EMFs slow down the body weight gain of young but not of adult BALB/neuT mice.
Young and adult female BALB/neuT mice were exposed the same ELF-EMF for 12 weeks.
After 4 weeks, a slight decrease in body weight was observed in both continuously and intermittently treated young mice. This was made up later.

ELF-EMFs exposure does not affect bone marrow myelopoiesis and splenic lymphoid compartment in young and adult female BALB/neuT mice.
As for BALB/c mice we analyzed hematological parameters as well as the structure of hematopoietic and lymphoid organs. A progressive increase in the number of monocytes and granulocytes was found in the peripheral blood of BALB/neuT mice after 4 and 12 weeks of exposure. Cytological examination of bone marrow smears revealed a predominance of segmented cells when compared to treated or untreated BALB/c mice (Table 3, compare to Table 1), coupled with a relative decrease in the proportion of red cells and lymphocytes.

Table 3 Bone marrow counts in 12-week-old BALB/neuT mice.

	Controls	**Discontinous ELF-EMFs treated mice**	**Continous ELF-EMFs treated mice**
Myeloid Immature Cells	20 ± 4.1*	21 ± 6.1	24± 3.1
Segmented cells	42 ± 9.1	47 ± 3	39 ± 5.1
Erythroid Cells	35 ± 7.3	36 ± 10.6	33 ± 11.6
Lymphoid Cells	10 ± 6.0	12 ± 9.2	14± 4.0

At 18 weeks of age, FACS analysis of the spleen and bone marrow revealed a pronounced increase of CD11b+ granulocyte and monocyte lineages in all treated and untreated BALBneuT mice when compared to BALB/c mice. All the alterations were proportional to the tumor burden and not to the treatment.

ELF-EMF exposure does not modify the occurrence and progression of BALB-neuT mammary tumors.
To assess the effects of ELF-EMFs exposure on tumor occurrence and progression, mammary glands of control and treated mice were analysed by Whole Mount preparation, histology and immunohistochemistry.
Fig 7 and 9 show representative whole mount pictures of the inguinal mammary gland from a control (a), a continuously (b) and an intermittently (c) exposed BALB Neu T mouse at 10 and 18 weeks of age. Fig 8 and 10 show their respective histological aspects.
These pictures show that ELF –EMS exposure didn't modify the occurrence, the progression or the histological features of the HER-2 dependent tumors.

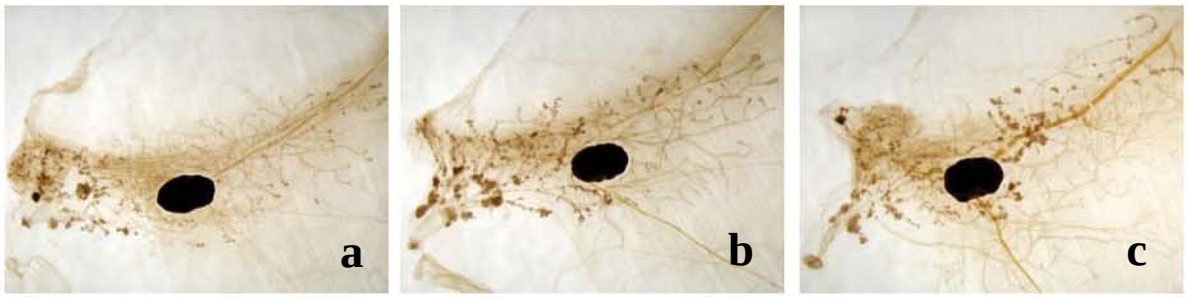


Fig 7

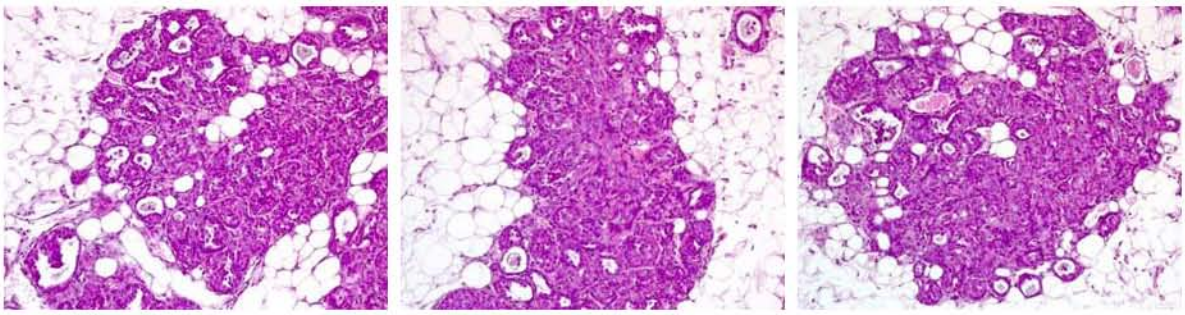


Fig 8



Fig 9

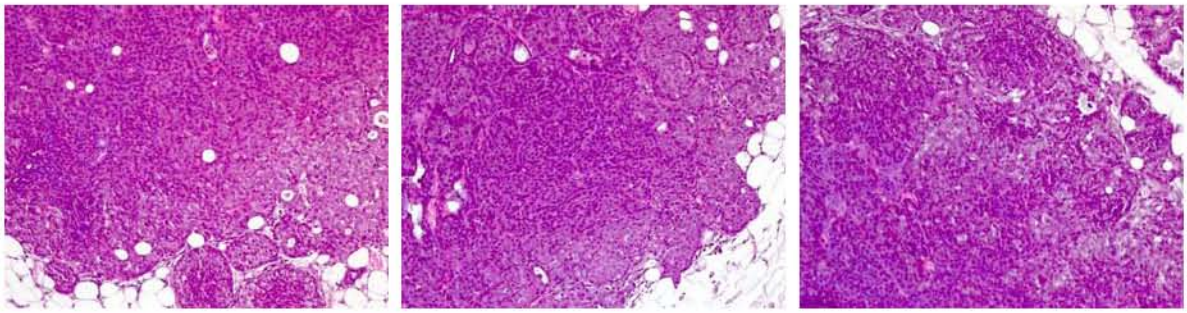


Fig 10

ELF-EMF EXPOSURE AFFECTS BODY WEIGHT GAIN AND HAEMOPOIESIS IN YOUNG BALB/C MICE.

SUMMARY

This study was performed on a large number of animals (a total of 720 mice) with an innovative dedicated generator of ELF-EMF to answer the following questions:

* Whether ELF-EMFs influence the growth and the haemopoietic system of BALB/c mice
* Whether male and female animals are equally responsive
* Whether young and adult animals are equally responsive

Our results clearly indicate that ELF-EMF exposure slow down the body weight gain and alter the haemopoietic system of young, but not of adult BALB/c mice resulting more effective on male compared to female animals.

Subsequently we wondered:

* Whether these effects are transient or persistent
* Whether a dose-response relation or a threshold value for the ELF-EMF intensity is apparent
* Whether continuous and intermittent (night-time only) exposure exert the same effects

Interestingly we found that after the first 12 weeks of exposition gain loss and alterations of spleen and bone marrow cell count were almost completely recovered persisting only a reduction of granulocyte and monocyte lineages in the male mice exposed from the young age.
We were not able to find a dose-response relation or a threshold value for the ELF-EMF intensity nor a difference between continuous and intermittent exposure.

Lastly the effect of ELF-EMF exposure on BALB NeuT mice growth, hemopoietic system and mammary carcinogenesis was investigated.

Only a slight loss of weight during the first month of treatment was reproduced in the BALB NeuT system. Spleen and bone marrow cell count as well as tumoral occurrence and growth appeared not to be influenced by ELF-EMF exposition probably because of the aggressiveness of this model of mammary cancerogenesis and of cancer-driven haematological dysregulation.

This study demonstrates that ELF-EMF produce a biological stress that affects weight gain and haemopoiesis of growing mammalian organisms. Healthy subjects are able to both adapt to and compensate it. Further studies are requested to elucidate the role of oncosuppressors or repair systems in this scenario.

ACKNOWLEDGMENTS

This study was supported by grants from the Italian Ministry of Environment and Territorial Protection (5377/2002/SIAR, 5378/2002/SIAR, DSA/2004/0026779, DSA/2004/0026778)

REFERENCES

[1**]** Sandler DP, *Recent studies in leukemia epidemiology.* Curr Opin Oncol, 7(1):12-18, 1995
[2] Gurney JP et al, *Extremely low frequency electromagnetic fields (EMF) and brain cancer in adults and children: review and comment.* Neuro-oncol. 1(3):212-20, 1999
[3] McBride ML et al, *Power-frequency electric and magnetic fields and risk of childhood leukemia in Canada.* Am J Epidemiol, 149(9):831-42, 1999
[4] Shuz JP et al, *Residential magnetic fields as a risk factor for childhood acute leukaemia: results from a German population-based case-control study.* Int J Cancer. 91(5):728-35, 2001
[5] Kliukiene J et al, *Residential and occupational exposures to 50-Hz magnetic fields and breast cancer in women: a population-based study.* Am J Epidemiol, 159(9):852-61, 2004

[6] Mild KH et al, *Occupational Carcinogens: ELF MFs.* Environmental Health Perspective, vol.113 (11), 2005
[7] Juutilinen J et al, *Possible Cocarcinogenic effects of ELF electromagnetic fields may require repeated long-term interaction with known carcinogenic factors.* Bioelectromagnetics, 21:122-128, 2000
[8] Scassellati Sfarzolini G et al, *Evaluation of genotoxic effects in cell exposed in vitro to extremely-low frequency electromagnetic fields.* Ann. Ig, 16(1-2): 321-340, 2004

[9] Baum A et al, *A histopathological study on alterations in DMBA-induced mammary carcinogenesis in rats with 50Hz, 100 muT magnetic field exposure.* Carcinogenesis, 16, 119-125, 1995
[10] Thun-Battersby S et al, *Exposure of Sprangue-Dawley rats to 50-Hertz, 100-μTesla magnetic field for 27weeks facilitates mammary tumorigenesis in the 7,12-dimethylbenz[a]-anthracene model of breast cancer.* Cancer Research, 59, 3627-2633, 1999
[11] Van Den Heuvel R et al, *Haemopoietic cell proliferation in murine bone marrow cells exposed to extreme low frequency (ELF) electromagnetic fields.* Toxicology in vitro, 15, 351-355, 2001
[12] Bonhomme-Faivre L et al, *Alterations of biological parameters in mice chronologically exposed to low-frequency (50Hz) electromagnetic fields.* Life Sciences, 62 (14): 1271-1280, 1998
[13] Ikeda K et al, *No effects of extremely low frequency magnetic fields found on the cytotoxic activities and cytokine production of human peripheral blood mononuclear cells in vitro.* Bioelectromagnetics, 24: 21-31, 2003
[14] Muller WJ et al, *Single-step induction of mammary adenocarcinoma in transgenic mice bearing the activated c-neu oncogene.* Cell, 54: 105-115, 1988
[15] Stern DF et al, *p185, a product of the neu proto-oncogene, is a receptorlike protein associated with tyrosine kinase activity.* Mol Cell Biol, 6: 1729-1740, 1986
[16] Finn OJ et al, *Prophylactic cancer vaccine.* Curr Opin Immunol, 14: 172-177, 2002
[17] Pannellini T et al, *Immunobiology of her-2/neu transgenic mice.* Breast Dis., 20:33-42, 2004.

APPENDIX

Instrument. The 50Hz electromagnetic fields were generated by a pair of Helmholtz coils. This device was planned and built to deliver variable, homogeneous, sine-wave alternate current magnetic fields with 50 Hz frequency and intensities ranging between 0.1-1.0 mT±2%. The pair of Helmholtz coils, (r=630mm, distance between coils=700mm), parallel to the ground and producing homogeneous magnetic field over the specified volume-under-test corresponding to the plastic cage in which where the animals to be exposed, were located in an isolated room containing also the control animals out of the electromagnetic fields exposure area. The coils were connected to a power supply Elgar Electronics (mod. CW 2501P) and were used to generate 0.1-1.0mT ELF for long time animal exposure (up to 16 weeks).



The Helmholtz coils connected to the power supply

Mice.

Female and male Balb-c and Balb-neuT mice transgenic for the activated rat *neu* oncogene have been generated in our laboratories.

Four-week old females were routinely screened for the transgene by PCR, as previously described ([ ]Muller Cell 1988).

120 male,120 female BALB/c and 120 BALB-neuT mice entered the study at 6 and 10 weeks of age. Each group of 120 mice was divided into 3 groups of 40 mice: control group, intermittently exposed group and continuously exposed group. Mice exposed intermittently were exposed during the night only (active period of mice). Half of the

mice were selected for the sacrifice after 4 weeks of exposition. The remaining 20 mice were sacrificed after 12 weeks of treatment. GraphPad Software was used to secure uniform randomization.
All the procedure was repeated twice for the experiments with 0,5mT and 1mT intensity ELF-EMF.

Analysis of body weight trend
Mice were weighted before they entered the study and start the exposition to the ELF-EMF. The body weight was checked each 15 days and the body weight trend was plotted and analyzed by GraphPad.

Blood and bone marrow smear
Peripheral blood was collected via intra-cardiac extraction.
Bone marrow was flushed from femur and tibia and suspended in PBS 1X. A small drop of blood or bone marrow suspension is placed on the surface of a clean glass slide near the end. An edge of the spreader slide is placed on the first slide to the left of the drop of blood and is pulled to the edge of the drop. When the smear was completely dried, it was stained by May-Grunwald Giemsa.

Histology and Immunohistochemisty
For histologic evaluation, tissue samples were fixed in 10% neutral-buffered Formalin, embedded in paraffin, sectioned at 4 µm, and stained with H&E. For immunohistochemistry, paraffin-embedded or acetone-fixed cryostat sections were immunostained with anti-p185 (clone C-18) (Santa Cruz Biotechnology), anti-proliferative cell nuclear Ag (PCNA) (clone PC10) (DakoCytomation), anti-endothelial cells (CD31, PECAM-1, clone MEC13.3) (BD Pharmingen), anti-Mac-1 (CD11b/CD18, clone M1/70.5), anti-CD8 (Ly/T2, clone YT5 169.4) and anti-CD4 (LT34, clone YT5.191.1.2; all from Sera-Lab, Crawley Down, Sussex, United Kingdom), or anti-CD11c (clone N418; Chemicon International Inc., Temecula, CA), anti-CD45R/B220 (clone RA3-6B2; all from PharMingen, San Diego, CA),Abs. After washing, sections were overlaid with biotinylated goat-anti-rat and anti-rabbit Ig (Vector Laboratories) for 30 min. Unbound Ig was removed by washing, and slides were incubated with avidin-biotin complex /alkaline phosphatase (DakoCytomation). To quantify germinal centers (GC), each spleen was transversely dissected into four segments from which semiserial sections were obtained. The GC in the total area of each section were counted. Morphologic studies were conducted independently by three pathologists in a blind fashion.

Whole mount and image analysis
Whole mounts of all mammary glands were done as indicated in http://ccm.ucdavis.edu/tgmouse/HistoLab/wholmt1.htm. Digital images were acquired by dividing the whole mount of each gland into 10 quadrants. Ten points were randomly chosen on the duct surface in each quadrant and the corresponding lesions were measured. All lesions with a diameter >150 µm on the same quadrant were counted. Images of whole-mount preparations were taken with a Nikon Coolpix 950 digital camera (Nital Spa, Turin, Italy) mounted on a stereoscopic Leica MZ 6 microscope (Leica Microsystems, Milan, Italy). A 0.63 objective were used to obtain images with a total magnification of x630 and a resolution of 1,600 x 1,200 pixels. Images were acquired within Adobe Photoshop version 6.0 graphic software (Adobe Systems, San Jose, CA). Glands larger than a single imaging area were captured by photographing contiguous microscopic fields in a raster pattern. Each captured image was merged using the layer technique in Adobe Photoshop to form a single composite image for analysis. Spatial calibration was determined by photographing a 1 mm stage using the same parameters as those for image capturing of whole-mount preparations. The distance drawn on the 1 mm calibration image was divided by 1,000 to find the number of pixels per micrometer. In each image, 100 discrete points were randomly chosen on the duct surface and lesion widths in micrometer were measured perpendicular to duct direction. Points with no lesion were ranked as zero. Lesion measurements were recorded on an Excel spreadsheet and mean and SE were calculated for each treatment group. Statistics were obtained with a two-tailed Student's *t* test.

Flow Cytometry
Single cell suspensions of bone marrow and spleen were prepared. The cells were washed in PBS with 1%FCS (staining buffer). Aliquots of $0.5-1.0\times10^6$ cells were then stained for 30 min on ice with monoclonal antibodies conjugated with fluorescein isothiocyanate (FITC) or phycoerythrin (PE). The antibodies used in these experiments included reagents specific for: B220 (CD45R), TER-119, CD4, CD8α, MHC-classII (all antibodies were purchased from Miltenyi). Cells were washed once in staining buffer and multicolor flow-cytometric analysis was done with a FACScan (Becton-Dickinson). A minimum of 10 000 events were acquired and the data was analyzed using CellQuest software. Statistics were obtained with two-tailed Student's t test.

SUPPRESSION OF NO PRODUCTION IN MACROPHAGES BY ELF ELECTRO-STIMULATION

MUNEYOSHI KAGAWA, TOSHIYUKI SHIMOOKA, YUJI KURACHI and KOICHI SHIMIZU

GRADUATE SCHOOL OF INFORMATION SCIENCE AND TECHNOLOGY, HOKKAIDO UNIVERSITY

Abstract

We have pursued the possibility to control immune functions by ELF electro-stimulation. As the first step, the effect of electro-stimulation on the NO producing ability of macrophages was examined. The decrease of NO production due to the electro-stimulation was observed with statistical significance. To elucidate the mechanism of this phenomenon, the amount of the NO synthesizing enzyme was measured. The measurement showed the decrease in the emergence of the enzyme with statistical significance, as well. These facts suggested that the ELF electro-stimulation suppressed the emergence of the NO synthesizing enzyme and that the amount of NO production was consequently decreased by the electro-stimulation. To analyse the association between the amount of the NO synthesizing enzyme and the amount of NO production, the dose-response of this effect was investigated by changing the electric current density of the electro-stimulation. The rates of the decrease in NO synthesizing enzyme and the NO production were found to be very close. These results showed that the change in the NO synthesizing enzyme is closely involved in the mechanism of the suppression of NO production by electro-stimulation. This suggested the feasibility to control the immune function by applying electro-stimulation from outside the body.

Introduction

The influence of ELF electromagnetic field on various physiological functions has been reported, and much study has been conducted mainly from the view point of adverse effects. On the other hand, there is a clinical application such as therapeutic instruments using ELF electric field. With the view towards the immune control by ELF electric field exposure, we have studied the effect of electro-stimulation on cell functions. Macrophages play important roles in a human immune system. We have examined the effect of electro-stimulation on the phagocytic activity and the active oxygen production ability of macrophages. Through this study, it has been found that the both activities are suppressed by the capacitively coupled electro-stimulation[1,2]. The electric current induced in the suspension of cells was in the similar order to that induced in the human body with the therapeutic instrument of electric field exposure.

In the current study, we have examined the effect of electro-stimulation on the production capacity of nitric oxide (NO). The NO is a kind of the same radicals as the active oxygen and is produced in the immune function of a macrophage. The NO is produced to kill bacteria but can destroy normal cells when produced excessively. Moreover, it reacts with the active oxygen and becomes the peroxynitrite ($ONOO^-$). The $ONOO^-$ is more toxic and damages normal cells. Therefore, if we can control the NO production, it will contribute to the prevention and the treatment of various diseases. We have examined this possibility by the ELF electro-stimulation in vitro.

Materials and Methods

macrophage preparation

Peritoneal exudate macrophages were used in all the experiments. The thioglycollate medium (4.05%, 2 ml) was injected in the peritoneal cavity of a normal mouse (Std:ddy, female, 7-11weeks). After 3 or 4 days, the cells were harvested from the mouse abdomen. Then, macrophages were collected from the cells in the established method. [3] We prepared the cell culture solution (RPMI 1640 with L-Glutamine , Sodium Bicarbonate and 10%Fetal Bovine Serum: RPMI 1640, hereafter) with 0.5×10^5IU penicillin G potassium and 50mg streptomycin sulfate added. The collected macrophages were suspended in the cell culture solution to make the cell density of 2×10^6cells/ml. When electro-stimulation was applied to the cells, the IFN-γ(10U/ml) and the LPS(1μg/ml) were added as stimulants to both the stimulation group and sham group.

electrostimulation system

The macrophage cells were stimulated by the electric current in the container insulated electrically from the electrodes to simulate the condition of electro-stimulation from outside the human body. Figure 1 shows the structure of the sample container.

Two plane electrodes were kept parallel with 3 mm distance by a plexiglass separator. The electrodes were square cupper plates (24mm×24mm×6mm top and 32mm×32mm×6mm bottom). The top electrode was insulated with a 0.15 mm thick cover-glass, and the bottom one with 0.10 mm thick silicone film. The outline of the electrostimulation system is shown in Fig.2. Two electrodes were connected to a high-voltage power source through a noise filter. As the power source, the power supply of a commercial apparatus for the electric field therapy was used (Healthtron , Hakuju Inst. Health Science, maximum supply voltage 10kV). A sinusoidal AC signal of 50Hz was supplied to the apparatus with a waveform generator to make the high-voltage with the sinusoidal waveform of 50Hz. In the experiment, the cell suspension was placed in the container, and electro-stimulation was applied in a CO_2 incubator (38ºC, $CO_2$5%). The cell suspension of the sham group was kept in another incubator of the same condition.

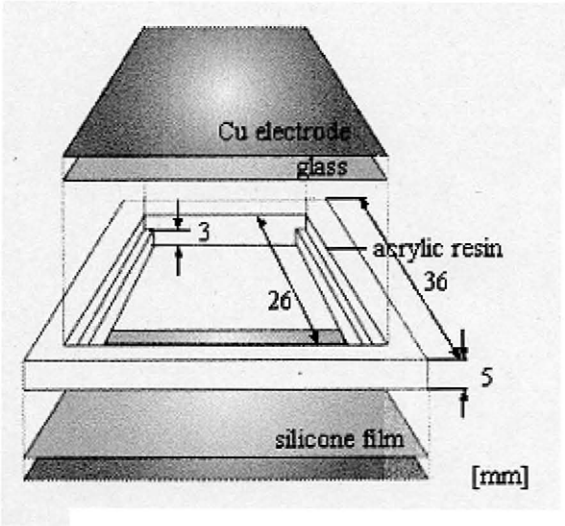


Fig.1 Sample container

Fig.2 Schematic diagram of electro-stimulation system.

Effect on NO production

We stimulated macrophages in the suspension with IFN-γ and LPS, and applied the electro-stimulation for the exposure group. The sham group was treated in the same way except connecting to the power source. The amount of NO produced outside the cell was measured as fluorescent intensity (495nm excitation and 515nm emission) using fluorescent reagent Diaminofluorescein-2(DAF-2) for the NO detection.

Macrophages were collected in the established method, and washed three times with Hanks' Balanced Salt Solution (HBSS) in centrifugation (400G) for 5 minutes. Then, they were suspended in the culture liquid RPMI 1640 again, and the electro-stimulation (50Hz, 35μA/cm^2, 16h) was applied. After the electro-stimulation, the macrophages were washed with HBSS in centrifugation, and cultured in HBSS suspension with DAF-2(10μM) and L-arginine(1mM) two hours without electro-stimulation. After the two hour culturing, the supernatant part was separated in centrifugation. With a fluorescent photometer, the fluorescent spectrum of the supernatant was measured. The supernatant of the sham group was collected in the same process except for the electro-stimulation, and the fluorescent spectrum was measured in the same way as the stimulation group.

Figure 3 shows an example of the measured result. The abscissa is the wavelength and the ordinate is the fluorescent intensity. The wavelength of the intensity peak was around 515 nm in both cases. There was no significant change in the shape of the spectrum, but 30% decrease in the intensity was observed in the stimulation group. This suggest the suppression of NO production by the electro-stimulation. The same experiments were repeated nine times. Figure 4 shows the reduction ratios of the fluorescent intensity between the stimulation and the sham groups. In all the nine cases, the fluorescent intensity was decreased by the electro-stimulation. The p-value of the paired-t test was 1.79×10^{-2}, which suggested the suppression of NO production by the electro-stimulation with a statistical significance.

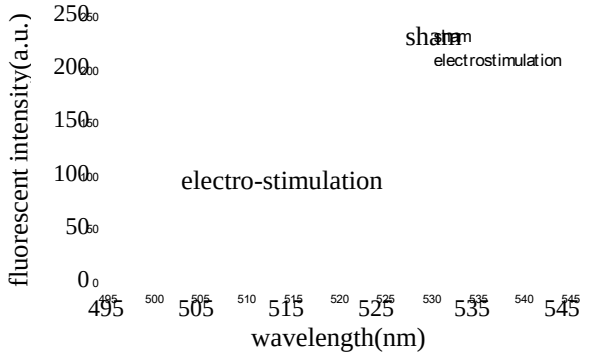


Fig3. Example of measured NO production by fluorescence spectroscopy.

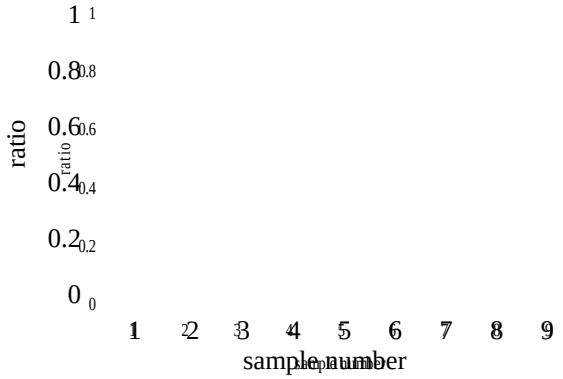


Fig.4 Suppression of NO production.

Effect on iNOS expression

NO is synthesized in a macrophage by the inducible nitric oxide synthase (iNOS). To elucidate the mechanism of the suppression in the NO production, the effect of the electro-stimulation on the iNOS expression was examined. The amount of the iNOS expression was evaluated by measuring the fluorescent intensity in the indirect immunity fluorescent method. [5, 6]

In the same way as the one mentioned above, macrophages were collected, separated into two groups, and electro-stimulation (50Hz, 35μA/cm^2, 16h) was applied to the stimulation group. After the electro-stimulation, the macrophages were collected in the centrifugation. With 70% ethanol, the cell membrane was processed to enhance its permeation. After three times centrifugation (400G, 5 minutes), macrophages were suspended in HBSS. We added the rabbit anti-iNOS antibody (BD Biosciences) and kept it in a shaker bath at 4 ºC in 30 minutes. Then we added 20μg/ml of the FITC tagged hircine anti-rabbit Ig antibody (MP Biomedicals Inc.) and kept it in the shaker bath. Finally, we fixed the suspension with 1% paraformaldehyde, and measured the fluorescent intensity with a flow cytometer (FACS Calibur Becton Dickinson and Company).

Figure 5 shows an example of the results. The abscissa is the fluorescent intensity in an arbitrary unit, and the ordinate is the number of the cell. The broken line in the figure shows the average intensity of all the cells. The average values were 79 and 65 for the sham (a) and the stimulation (b) cases, respectively. This result showed the decrease in iNOS expression by the electro-stimulation. The same experiments were repeated eleven times. Figure 6 shows the ratio of the average intensity between the simulation and the sham cases. As shown in the figure, the decrease in fluorescent intensity was observed in all the eleven trials. The p-value of the paired-t test was 5.52×10^{-5}. This suggested that the iNOS expression was suppressed by the electro-stimulation with statistical significance.



Fig.5 Example of measured iNOS expression by fluorescence spectroscopy.

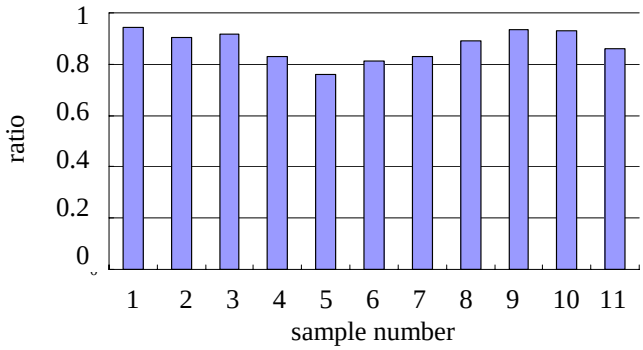


Fig.6 Suppression of iNOS expression.

Analysis of dose-response

As the first step of quantitative evaluation, the dose-response of these phenomena was analysed. In experiments, the amounts of the NO production and the iNOS expression in different current densities (0.35μA/cm^2, 0.675μA/cm^2, 3.5Aμ/cm^2) were measured. After the electro-stimulation in 16 hours, the cell suspension was divided into two. One was used for the measurement of the NO production, and another is for that of iNOS expression. Figure 7 shows the results of the measurements. The abscissa is the current density and the ordinate is the fluorescent intensity normalized by that of the sham case. The number of repeated measurements were 4, 6 and 4 for the cases of 0.35μA/cm^2 , 0.675μA/cm^2 and 3.5μA/cm^2, respectively. The result of 35μA/cm^2 case was added, in which the numbers of the repeated experiments were 11 and 9 for NO and iNOS cases, respectively.

With the current density of 0.35μA/cm^2, we could not observe apparent decrease in either of the NO or the iNOS. With 0.675μA/cm^2, about 5% decrease was observed. With the current density of more than 3.5μA/cm^2, more than 15% decrease was observed. In both of the NO and the iNOS, the threshold of the suppression seems to exist between 0.35μA/cm^2 and 3.5μA/cm^2. The similar characteristics in the dose-response strongly suggested the close correlation between the suppression of iNOS expression and that of NO production.

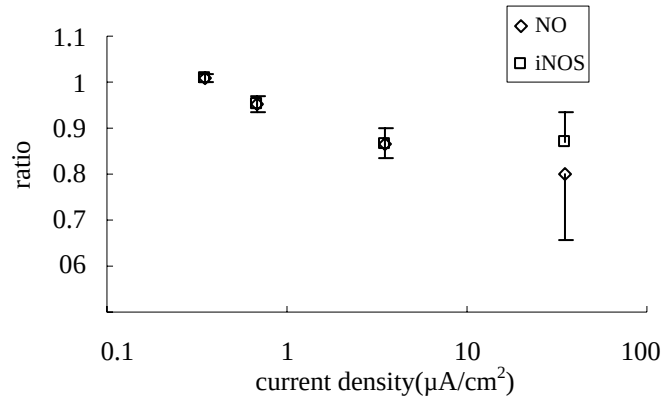


Fig.7 Analysis of NO and iNOS suppression effect by electro-stimulation.

Discussion

In the in-vitro experiments, it was found that the NO production is significantly suppressed by the ELF electro-stimulation. This suggested the possibility to control the functions of macrophages by the electro-stimulation applied from outside the body using the apparatus for the electric field therapy. Since a macrophage plays an important role in the first stage of the immune response, the electro-stimulation can influence the entire immune reaction. For example, we can expect the relief from the following diseases. They include the chronic inflammation and the autoimmune diseases caused by an excessive immune response. We can also expect the relief from the endotoxin shock due to the excessive NO production, the etiologic vasodilation, the cardio-vascular ischemia, the cerebral hemorrhage and the cancers. Moreover, we have confirmed the suppression of the active oxygen production by the electro-stimulation.[2] Therefore, we can also expect the control of $ONOO^-$

production which shows high cell-toxicity.

However, the finding of this study is only the result of in-vitro experiments using macrophages. We need further investigation to confirm this effect with human macrophages, and the investigation on this effect in-vivo where other kinds of cells are closely interacted. Yoshikawa and his co-workers reported the increase of NO production in the liver when LPS (2 mg/kg) was administered by abdominal injection and the magnetic field (60Hz, 0.1mT) was exposed in 5.5 hours. The current density induced by this magnetic field inside the body is estimated at $1.1\times10^{-8}A/cm^2$. This result is opposite to our result. It seems that the direct comparison between these two cases is not appropriate, since the object cell and the current density is greatly different among them.

Besides this, there have been few reports on the effect of ELF electromagnetic fields on the NO production, and little has been known on its mechanism. We consider that the arginine metabolism, iNOS activity and iNOS expression are closely associated with the decrease in the NO production. To investigate this mechanism, we have compared the amounts of NO production and the iNOS expression.

Figure 7 shows the coincidence in the reduction ratio of fluorescent intensity between NO and iNOS by the same electro-stimulation. This result suggests that the electro-stimulation affects the NO production through iNOS expression. The signal transmission pathway for the iNOS expression is stimulated by LPS and IFN-γ through receptors on a cell membrane. As the result, a transcription factor is activated and the iNOS is transcribed. In our study, the electro-stimulation was applied from the beginning when we started the stimulation with LPS and IFN-γ. Therefore, it is most plausible that the electro-stimulation affects this process.

However, the following possibility cannot be neglected. In the peritoneal exudate cells used in this study, about 10% cells were not macrophages. Since these non-macrophage cells can affect the signal transmission pathway of the NO production, they might influence the mechanism of the suppression of the NO production. Therefore, we have to examine this point in the experiment using the pure macrophage cells separated from other cells.

In our experiment, the threshold of the effect was found between $0.35\mu A/cm$ and $3.5\mu A/cm^2$. In the study for the biological effects of ELF electromagnetic fields, the minimum threshold of magnetic field exposure has been reported. [7] According to the report, the threshold current density for the characteristic change in tissues and cells was in the order of $10mA/m^2$ or $1\mu A/cm^2$. Though this threshold is for the electric current induced by magnetic field, it is very close to our result in which the electric current was induced by the electric field.

Conclusion

With the view toward the control of immune functions by ELF electric field exposure, the effect of the electro-stimulation on the NO production of macrophages was examined in vitro. The decrease of NO production due to the electro-stimulation was observed with statistical significance. In experiments, it was found that the expression of NO synthesizing enzyme or iNOS was suppressed in the same rate as NO in the electro-stimulation. Further investigation is required to ascertain this mechanism of NO suppression and to verify the feasibility of the immune control by electro-stimulation.

Reference

[1] I. Fujii, T. Shimooka, Y. Morita and K. Shimizu, "Experimantal verification for the effect of capacitively coupled electrostimulation on macrophage's endocytosis," Tec. Report IEICE., MBE2001-101, pp.97-102,2002.(in Japanese)

[2] Takeshi Tatebe, Toshiyuki Shimooka, Muneyoshi Kagawa, Koichi Shimizu, "Effect of ELF electrostimulation on reactive oxygen generation of macrophage", Tec. Report IEICE, MBE2003-131, pp.13-18, 2004.(in Japanese)

[3] Stohlman SA, Frelinger JA, Weiner LP. Resistance to fatal central nervous system disease by mouse hepatitis virus, strain JHM. II Adherent cell-mediated protection. J Immunol., 124(4):1733-9, 1980.

[4] Wataru Yoshida, Minori Ogawa, Yuko Furuoya, Yu Igarashi, Rumi Sato, Akiko Hayashi, Kazuya Hirano, Masatoshi Beppu, "Effect of Estrogenic Compounds on Superoxide and Nitric Oxide Production by Activated Macrophages Assessed by Sensitive Microplate Assays", Journal of Health Science, 48(5), pp.455-459, 2002.

[5] Oh-Deog KWON, Chang-Yeol YIM, Kyu-Shik JEONG, Kyu-Yong JUNG, John R. McGREGOR, Neil R.BASTIAN Wolfram R. SAMLOWSKI, "Suppression of Cytokine-Inducible Nitric Oxide Synthesis During Intraperitoneal Meth A Tumor Growth" , J Vet Med Sci., 66, pp.357-365, 2004.

[6] Wolfram E. Samlowski, Jhon R. McGregor, Gregory J. Litton, "Liver Sequestration of Murine Lymphokine Activated Killer Cells Is Mediated by Carbohydrate-specific Receptor", Regional immunology Vol.2, pp.254-265, 1989.

[7] ICNIRP Guidelines : "Guidelines for limiting exposure to time-varying electric, magnetic, and electromagnetic fields(up to 300GHz)", Health Physics, Vol.74, No.4, pp494-522.1998.

[8] Yoshikawa T, Tanigawa M, Tanigawa T, Imai A, Hongo H, Kondo M, "Enhancement of nitric oxide generation by low frequency electromagnetic field" , Pathophysiology, pp.131-135, Jul;7(2), 2000.

IMMUNE STIMULATION IN FISH AND FARM ANIMALS THROUGH WEAK LOW FREQUENCY ELECTROMAGNETIC FIELDS: A. HYPOTHESIS

J.J.M. Cuppen[1], H.K. Parmentier[2], H.F.J. Savelkoul[2]

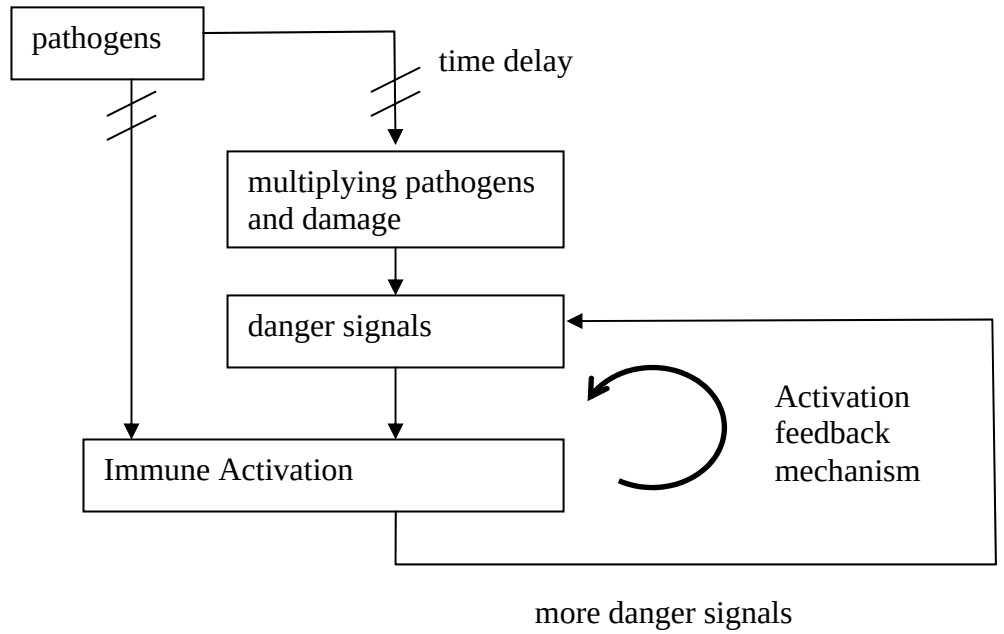
1: Immunent BV, 2: Wageningen University, The Netherlands

Abstract
A hypothesis is proposed how LF EMF treatment can stimulate an immune response, based on recent insights in immunology. Danger signals have been shown in the last decade to be an essential factor in the coordinated response of the immune system to pathogens. We hypothesize that the EMF treatment induces mild stress to cells in the body, which then produce danger signals for the immune system. In this way EMF treatment takes the place of multiplying pathogens and the damage these cause in the triggering of an immune response.

Introduction
Immunent has developed a signal for advancing and elevating the immune response to pathogens (multiple LF components, 0.1-50 µT, 30 minutes per day) which we have tested at various experimental conditions. Pilot findings with this signal (proprietary, but available for research purposes) were presented at the 2004 Kos meeting (Cuppen and Vink 2004). In subsequent experiments with carp, goldfish and chickens significant and often strong effects of immune stimulation have been observed. The effects include: 40% increased oxidative burst of isolated phagocyting cells ($p<0.001$), 60% decreased mortality in infected fish ($p<0.001$), 5% decreased feed consumption for equal growth in chicken ($p<0.05$) comparable to the use of preventive antibiotics and 40% decreased intestinal lesions in chicken ($p<0.01$) due to Eimeria infections. These results are reported in detail at this conference in one presentation and two posters.
In this paper we take the liberty to hypothesize about the observed strong responses of the immune system of this broad range of animals. The hypothesis regards the possible mechanism of action and attempts to answer the question how such weak, short duration EMF signals can induce an effective immune response.

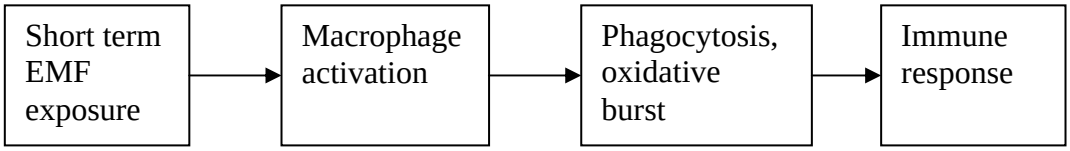
Hypothesis
During last decade in immunology a hypothesis has been developed that immune response is not only due to the presence of non-self cells but also needs the presence of promoters (e.g. Matzinger 2002, Kapsenberg 2003, Shi et al 2003). This holds in particular for the innate immune response to pathogens not earlier encountered. Such promoters are called “danger” signals. An example might be Heat Shock Proteins (prime examples of cell response to injury or insult), as well as Interferon, Interleukins and other cytokines. Danger signals are formed when cells get stressed or damaged, and this is “presumed by the cells” to be caused by harmful pathogens. The idea behind the view is that strange DNA that does not cause damage, such as a foetus or food, does not and should not trigger an immune response. Support for this view has been obtained from the new approach to transplants that originated from it: after surgery the transplant organ contains lots of danger signals due to the cell damage caused by surgery or the trauma of the donor. Flushing of the transplant organ, which eliminates danger signals from the organ tissue, led to an enormous decrease in rejection reactions from the receiving patient. With this technique, a strong reduction in immune suppressing medication could be achieved.
In immunology other factors besides damage due to pathogens have been identified that stimulate the production of danger signals, such as stress or shock from salt, cold or heat. See Engelsma, Hougee and Nap (2003), and Huising, Guichelaar and Hoek (2003).
The danger signal hypothesis can be schematically represented as in Figure 1.

Figure 1. Matzinger Hypothesis



Several authors (see Blank, Khorkova, and Goodman 1992, Goodman, Blank and Lin 1994, Blank, Lin and Goodman 1995, Simkó and Mattsson (2004), Monselise, Parola and Kost 2003, de Bruyn and de Jager 1994, Mevissen, Haussler, Szamel, Emmendorffer, Thun-Battersby and Loscher 1998, Markov, Nindl, Hazlewood and Cuppen 2006) discussing the effects initiated by various EMF signals have demonstrated the production of cytokines, increased immune parameters and stress effects and concluded that EMF causes stress at the cellular level and that this leads to production of cytokines and consequently biological response, including immune response. This has led Mattson and Simkó (2004) to formulate a hypothesis that proposes a mechanism for immune activation due to short term EMF exposure (see Figure 2) and a mechanism for cell damage due to long term EMF exposure.

Fig 2. Simkó and Mattsson hypothesis



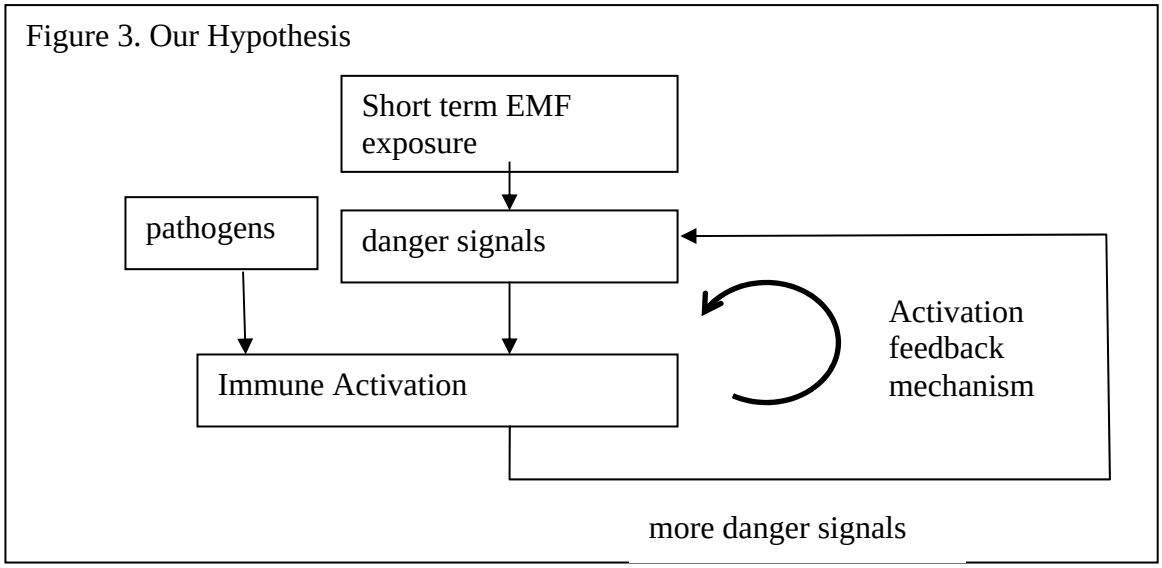
Based on published theoretical and experimental studies, as well as our own experience we propose a hypothesis, that combines and extends the views quoted, by

a) the observation that an immune response is a self stimulating process, at least in the initial stages. Macrophages become activated under the influence of danger signals, and thus have a higher statistical chance and a lower expected time until they actually encounter and recognise pathogens. Once this happens they themselves produce cytokines that increase the immune response etcetera
b) the observation that for chronic infection apparently the feedback cycle stated in a) does not gain sufficient momentum for the infection to reach acute phase
c) the observation that for new infections a more active and alert immune system will start the feedback

loop in a) earlier, thus slowing down the multiplication of pathogens and reducing damage.

Therefore we propose an extended hypothesis which can be schematically represented as in Figure 3.

Figure 3. Our Hypothesis



The core of the proposed Hypothesis is that short term LF EMF exposure, possibly repeated, can produce danger signals that can trigger the immune system activation feedback mechanism in the presence of pathogens. As such the EMF induced danger signals take the place of the danger signals that would be produced by multiplying pathogens and the damage they cause to cells and tissues. In this way a timely EMF treatment can avoid the delay given by the time it takes for enough damage to occur and danger signals to be produced in a normal disease development. Thus the immune response to pathogens can be advanced in time and damage and a well developed pathogen attack can be avoided.

In our own in vivo experiments (Cuppen et al. 2004, 2006c, 2006d) we have observed immune stimulation effects after repeated exposures of 30 minutes per day. There is evidence in literature and there are anecdotal indications that continuous exposure to EMF leads first to increased immune parameters, but later to decreased immune parameters, which can be interpreted as exhaustion (Mevissen et al. 1998, Jager et al. 2004).

References

Blank M., Khorkova O. and Goodman, R. (1992): Changes in polypeptide distribution stimulated by different levels of electromagnetic and thermal stress. Bioelectrochem. Bioenerg. 33, 109-114, 1992

Blank M., Lin H. and Goodman, R. (1995) Increased expression of heat shock genes in cells exposed to 60 Hz electromagnetic fields. Mol. Biol. Cell 6, 466a, 1995.

Monselise E. B.-I., Parola A.H., Kost D. (2003): Low-frequency electromagnetic fields induce a stress effect upon higher plants, as evident by the universal stress signal, alanine. Biochem Biophys Res Commun. 2003 Mar 7;302(2):427-34.

Bruyn L. de, de Jager L. (1994) Electric field exposure and evidence of stress in mice. Environ Res. 1994 Apr;65(1):149-60.

Cossarizza A., Angioni S.,Petraglia F., Genazzani A. R., Monti D., Capri M., Bersani F., Cadossi R. and Franceschi C. (1993) Exposure To Low Frequency Pulsed Electromagnetic Fields Increases Interleukin-1 And Interleukin-6 Production By Human Peripheral Blood Mononuclear Cells. Exp Cell Res 204(2):385-387 1993

Cuppen J.J.M. and Vink A. (2004): Effects of ELF exposure on weight and immune parameters in young turkey broilers, 3rd Intl workshop on Biological Effects of EMFs, Kos, 2004, p 1203.

Cuppen J.J.M, Wiegertjes G.F., Geervliet J., Smink W., Beynen A.C., Elmusharaf M.A. and Grooten H.N.A. (2006b): Immune Stimulation In Fish And Farm Animals Through Weak Low Frequency Electromagnetic Fields, B. Experiments, this proceedings.

Cuppen J.J.M., Wiegertjes G.F., Molenaar M., Geervliet J., Smink W. (2006c): Immune Stimulation In Fish And Fish Immune Cells Through Weak Low Frequency Electromagnetic Fields With Variable Field Strength, this proceedings

Cuppen J.J.M., Beynen A.C., Elmusharaf M.A., Grooten H.N.A. and Smink W. (2006d): Immune Stimulation In Chicken Broilers Through Weak Low Frequency Electromagnetic Fields With Coccidia Infection, this proceedings

Engelsma M.Y., Hougee S., Nap D. et al. (2003) Multiple acute temperature stress affects leucocyte populations and antibody responses in common carp, Cyprinus carpio L, Fish Shellfish Immunol, 15 (5), 397-410

Goodman R., Blank M., Lin H. et al. (1994) Increased levels of hsp70 transcripts induced when cells are exposed to low frequency electromagnetic fields, Bioelectrochemistry and Bioenergetics, 33 (2), 115.

Huising M.O., Guichelaar T., Hoek C. et al. (2003) Increased efficacy of immersion vaccination in fish with hyperosmotic pretreatment, Vaccine, 21 (27-30), 4178-93.

Jager L. de, Bruyn L. de (2004) Long-term Effects of Time Varying Extremely Low Frequency Magnetic Fields, 3rd Intl workshop on Biological Effects of EMFs, Kos, 2004, p 573.

Kapsenberg M.L. (2003): Dendritic-cell control of pathogen-driven T-cell polarization. Nature Rev Immunol 2003;3:984-93.

Markov M.S., Nindl G., Hazlewood C.F. and Cuppen J.J.M. (2006) Interactions between electromagnetic fields and immune system: possible mechanism for pain control. In: S.N. Ayrapetryan and M.S. Markov (eds.), Bioelectromagnetics, Springer 2006, pp 213-225.

Matzinger P. (2002): The danger model: a renewed sense of self. Science 2002;296:301-5.

Mevissen M., Haussler M., Szamel M., Emmendorffer A., Thun-Battersby S. and Loscher W. (1998). Complex Effects of Long Term 50 Hz Magnetic Field Exposure In Vivo on Immune Functions In Female Sprague - Dawley Rats Depend on Duration of Exposure. Bioelectromagnetics 19:259-270.

Shi Y., Evans J.E., Rock K.L. (2003): Molecular identification of a danger signal that alerts the immune system to dying cells. Nature 2003;516-21.

Simkó, M. and Mattsson M.O. (2004): Extremely low frequency electromagnetic fields as effectors of cellular responses in vitro: possible immune cell activation. J. Cell. Biochem. 93:83-92, 2004.

IMMUNE STIMULATION IN FISH AND FARM ANIMALS THROUGH WEAK LOW FREQUENCY ELECTROMAGNETIC FIELDS: B. EXPERIMENTS

J.J.M. Cuppen[1], G.F. Wiegertjes[2], J. Geervliet[3], W. Smink[3], M.A. Elmusharaf[4], A.C. Beynen[4], H.N.A. Grooten[3]

1: Immunent BV, 2: Wageningen University, 3: FIS BV, 4: Utrecht University, The Netherlands

Abstract

Most of the publications in the bioelectromagnetics are related to animal/human studies, very few to effects of magnetic fields on plants and practically no studies were performed on small farm animals and fish. Our goal is to examine how properly selected magnetic fields can decrease the potential of development of infectious diseases in farm animals.

Experimental results presented and discussed here are set up to (indirectly) test the hypothesis that low frequency electromagnetic field (LF EMF) treatment can stimulate an immune response through the creation of danger signals which are necessary to trigger an immune reaction in the presence of pathogens.

The reported cell experiments show that the treatment stimulates oxygen burst in phagocytes which supports the notion that danger signals are indeed formed. Experiments with goldfish demonstrate a large decrease of mortality caused by infectious disease (gill parasites and accompanying microbial infections). This result is consistent with the idea that the exposure to EMF increases the strength of the immune reaction, so that a larger percentage of animals sufficiently combats the disease early enough to prevent disease to develop and that these animals are therefore able to return to health. Finally experiments with chicken broilers with coccidia infection, induced after starting the EMF treatment, show both less intestine damage due to the disease and a better growth to feed ratio. This demonstrates the effectiveness of the treatment in prevention of disease: the results indicate that, in the presence of pathogens, a self stimulating immune response originates sooner and more strongly than without the EMF treatment. An infection is then counteracted earlier, with less opportunity for pathogens to multiply and to cause damage.

All results combined support our hypothesis that the Immunent LF EMF treatment induces the formation of cytokines (danger signals) that put the immune system in a state of higher alertness and activity.

Introduction

In aquaculture and farming, infectious disease is one of the biggest, if not the biggest problem and challenge, economically as well as in terms of animal welfare and environmental pressure. "Disease is the biggest single impediment to aquaculture development," said Rohana Subasinghe, Senior Fisheries Research Officer at the United Nations' Food and Agriculture Organization (FAO). Total damage in aquaculture of infectious disease is estimated at $9 billion yearly. In Ecuador in 1999 70% of the crop of farmed shrimp was lost due to a single virus infection that led to a national crisis and a loss of 150.000 jobs.

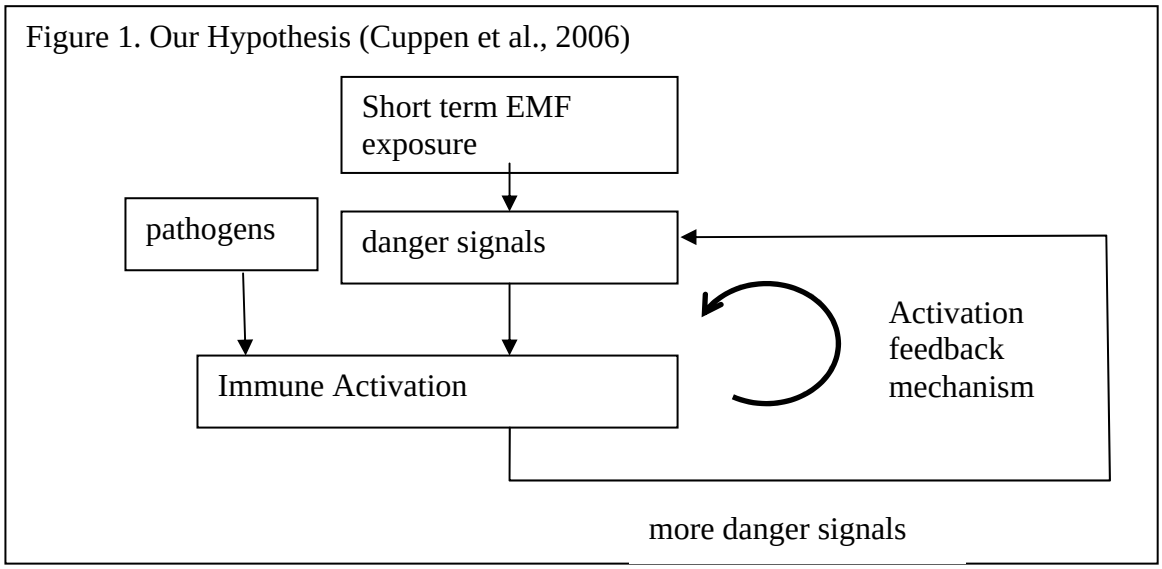
For chicken farmers infectious diseases form the biggest problem they face. Economically, for animal welfare, environmentally and for acceptance in the market and in society. Preventive antibiotics have been used not only to prevent infectious disease, but also as a growth promoter. The antibiotic use could prevent or eliminate infectious disease at an early stage, before the pathogens strongly multiply in the animals and the animals have to spend substantial energy to combat the disease. In general 5 to 10% decrease of feed necessary to support equal growth could be achieved with preventive antibiotics. However, preventive antibiotics have been banned in Europe from animal feed since 2006, with similar developments in other countries, because of development of microbial resistance related to humans. Therefore the agriculture and aquaculture sectors are urgently searching for other disease inhibitors to substitute antibiotics.

Environmentally, infectious disease causes a lot of pressure: by the chemicals and pharmaceuticals used, by the pathogens that multiply in farms and increase disease pressure on the surrounding wildlife, and by the pressure on aqua farmers to abandon farms with disease and start new farms in nature areas.

It has been shown that various EMF signals are capable of influencing the immune system (Markov, Nindl, Hazlewood, Cuppen, 2006).

Immunent has developed an EMF signal for advancing and elevating the immune response to pathogens (multiple LF components, 0.1-50 µT, 30 minutes per day) which have been tested at various experimental conditions. Pilot findings with this signal (proprietary, but available for research purposes) were presented at the 2004 Kos meeting (Cuppen and Vink 2004).
In immunology during the last decade the view has been developed that an immune reaction to pathogens needs promoters to be present in addition to the presence of pathogens (or other non-self cells) (Matzinger 2004).
In a companion paper at this conference (Cuppen et al. 2006a) the hypothesis was proposed that the enhanced immune reaction observed after LF EMF treatment is due to the fact that LF EMF induces the formation of such (a level of) danger signals, cytokines such as heat shock proteins (HSP's), Interferon, Interleukins, that an immune response can occur earlier and/or stronger than without the treatment. The treatment triggers the self-sustaining feedback mechanism in the immune reaction which otherwise would occur much later, when pathogens significantly multiplied and caused more damage.

Figure 1. Our Hypothesis (Cuppen et al., 2006)



Materials and results

This paper describes three different types of experiments conducted with the Immunent signal applied with different configurations on the subjects of research. For that reason the paper is written in three section describing the methods and results, followed by a discussion section.

In vitro cell experiments

Phagocytes (Macrophages and dendrites) from Carp were isolated as described in (Cuppen et al. 2006c, which also contains detailed descriptions of the other materials and methods) and stimulated in the different ways as described below. Oxygen burst was measured with a NBT assay as a measure of immune activity. and in vitro subjected to the treatment.
In 20 runs 48 samples each were divided over six test groups. Three groups had no chemical pre-stimulation (called negative), three (called positive) received chemical pre-stimulation with 10 µl 0.01 µg/µl PMA (Phorbol 12-myristate 13-acetate). Pairs of groups were formed (a positive and a negative). One pair was exposed for 30 minutes to sham: called control, one to a signal with 5 µT field strength: called low, and one to a signal with 1.5 mT field strength: called medium as indicated in Table 1.

Table 1. Summary of the in vitro experiment setup

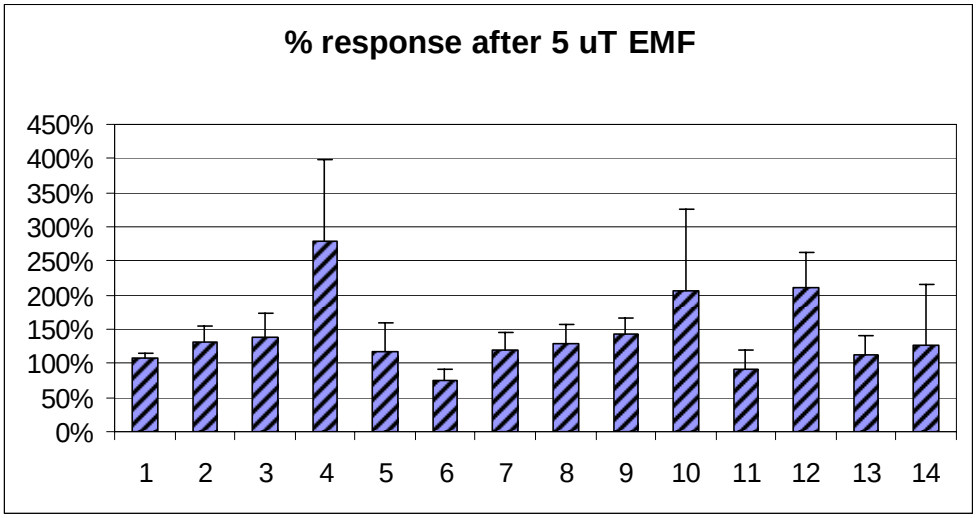
	No EMF treatment	EMF treatment with field strength	
	Control	5 µ Tesla	1.5 m Tesla
No chemical pre-stimulation	negative control	negative low	negative medium
Pre-stimulation with PMA	positive contr	positive low	positive medium

In each run the 48 samples are taken from a single fish and therefore the oxygen burst activity numbers in different test groups of that same run can be compared to each other. However for different runs different fish are used and the cells of one fish may show large differences in their baseline reactivity and activation capacity to the cells of another fish. Therefore the absolute numbers between different runs are not comparable. This complication can be overcome by normalizing all data to the average negative control value in each run, and positive EMF data to the positive control.

Six out of 20 runs were discarded on the (sole) basis that positive control average did not exceed negative control average by more than 50%. This means that cell preparation must be considered to have failed.

The Oxygen burst was increased in 12 out of 14 cases after 5 µT treatment (see Figure 2), and in 11 out of 14 cases after 1.5 mT treatment. With pre stimulation with PMA, oxygen burst was further increased in 9 out of 14 cases at 5 µT, and in 12 out of 14 cases at 1.5 mT.

Figure 2.



All results together are summarized in Table 2.

Table 2. Summary in vitro results, averaged over all runs (Average % increase in oxygen burst.)

	No EMF treatment	EMF treatment with field strength	
	control	5 µ Tesla	1.5 m Tesla
no chemical pre-stimulation	negative control = 100%	142 %	133 %
pre-stimulation with PMA	positive control = 276% of negative control	118% of positive control	122% of positive control

Statistical analysis (ANOVA) was carried out with SAS via a meta-analysis of the 14 datasets. A significant ($p<0.0001$) increase by EMF on the response of the exposed cells was found. As can be seen in Figure 2, the numbers given in Table 2 are averages of strongly varying results. It cannot therefore be concluded that the effect is stronger at 5 µT than at 1.5 mT or vice versa, but rather that the effects may be of the same order of magnitude at these two field strengths.

A second point we wish to make is that a treatment at or below 5 µT is in the practice of farm applications (large areas and volumes to be treated) much easier and less costly to achieve than at 1.5 mT.

The data achieved at 1.5 mT are in line with those reported for 50 Hz, sinusoidal, 1 mT fields in murine and human macrophages by Simkó, Droste, Kriehuber and Weiss 2001 and Lupke, Rollwitz and Simkó 2004.

In vivo experiments with diseased goldfish

To evaluate the potential of LF EMF to prevent or decrease the infections caused by ecto parasites (gill parasites) such as *dactylogyrus/ gyrodactylus, trichodina, chilodinella* and *costia* a series of 4 experiments was executed using fantail goldfish (*Carrassius auratus spp*.). Infection with those parasites occurs consistently at the grower and increases during storage, packing and international transport due to crowding. This and

subsequent secondary bacterial infections cause high mortality if not treated. The progress of the diseases can be measured by daily counting and removing from the tank any dead fish over a period of a few weeks. In the reported experiments, running 3 or 4 weeks, fish are divided over 12 to 20 tanks per experiment. Each tank is an experimental unit, and these are divided over a control group (usually 4 tanks) and test groups (usually 4, sometimes 2 tanks each) that are exposed to different EMF treatments, always for 30 minutes per day. In the early experiments we used 12 fish per tank, which was increased first to 21 and then to 30 fish per tank in order to increase the statistical power of the experiments once it became clear that this is feasible.

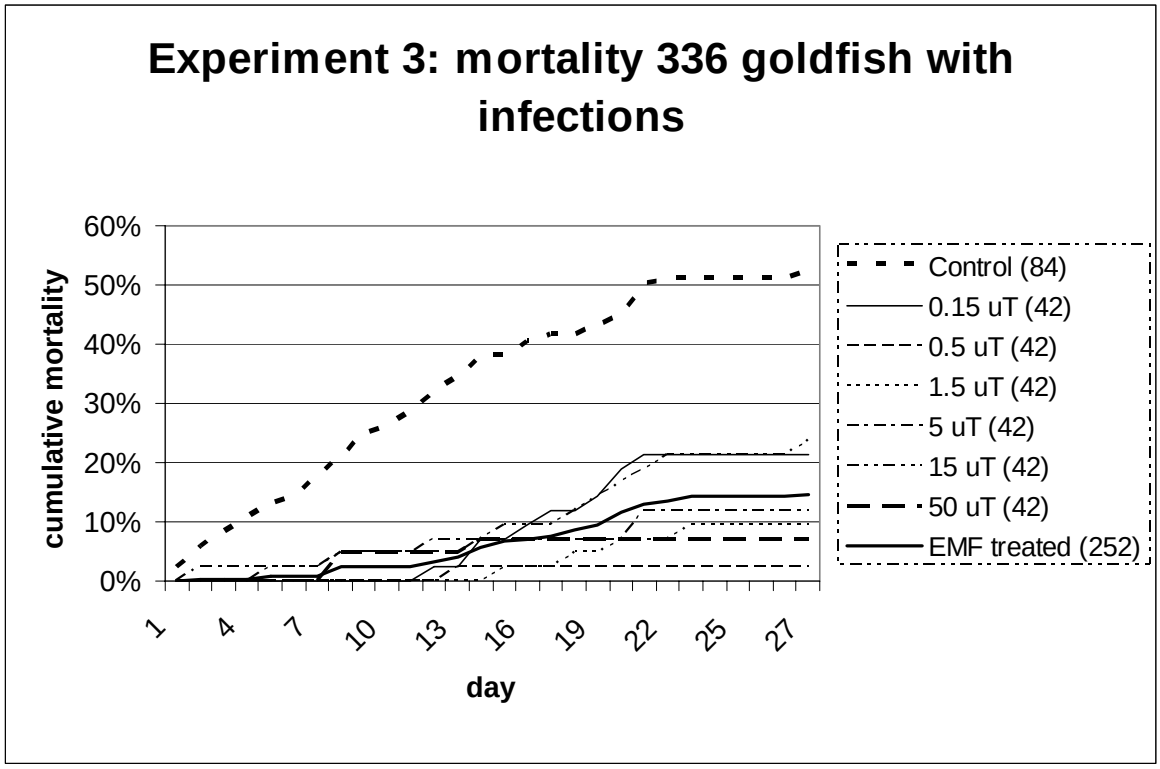
Tanks are exposed to uniform, vertical AC electromagnetic fields, with a (proprietary) Immunent signal consisting of several components with base frequencies between 100 and 10.000 Hz. The treatment is given daily for 30 minutes in each tank, by an automated Immunent signal generator that continuously monitors current output that was calibrated to magnetic field strength. For a detailed discussion of materials and methods, and more data, see (Cuppen et al. 2006c) in these proceedings.

The treatment is aimed at boosting the fish immune defense and, thereby, decreasing the mortality. The experiment is powerful because large numbers of animals can be used and the measurement is easy and accurate. For example, results in Figure 3 account for a total of 336 fish in the experiment, 84 in control and 252 in the six experimental series.

In experiments 1 and 2 (see Cuppen 2006c) mortality after 17 days was decreased by LF EMF from 52% ± 14% untreated to 19% ± 10%, and from 52% ± 8% untreated to 26% ± 19%. Moreover the intermediate day values had a comparable ratio to the end values so that the quoted standard deviations probably strongly underestimate statistical significance. In these experiments there were 8 control tanks and 15 experimental tanks at 5 μT with 12 fish initially each.

Next, experiments were performed at different field strengths. Figure 3 shows the typical mortality curves in an experiment with 4 control tanks and 2 experimental tanks per field strength with 21 fish initially per tank.

Figure 3 Mortality with treatment on different field strength levels

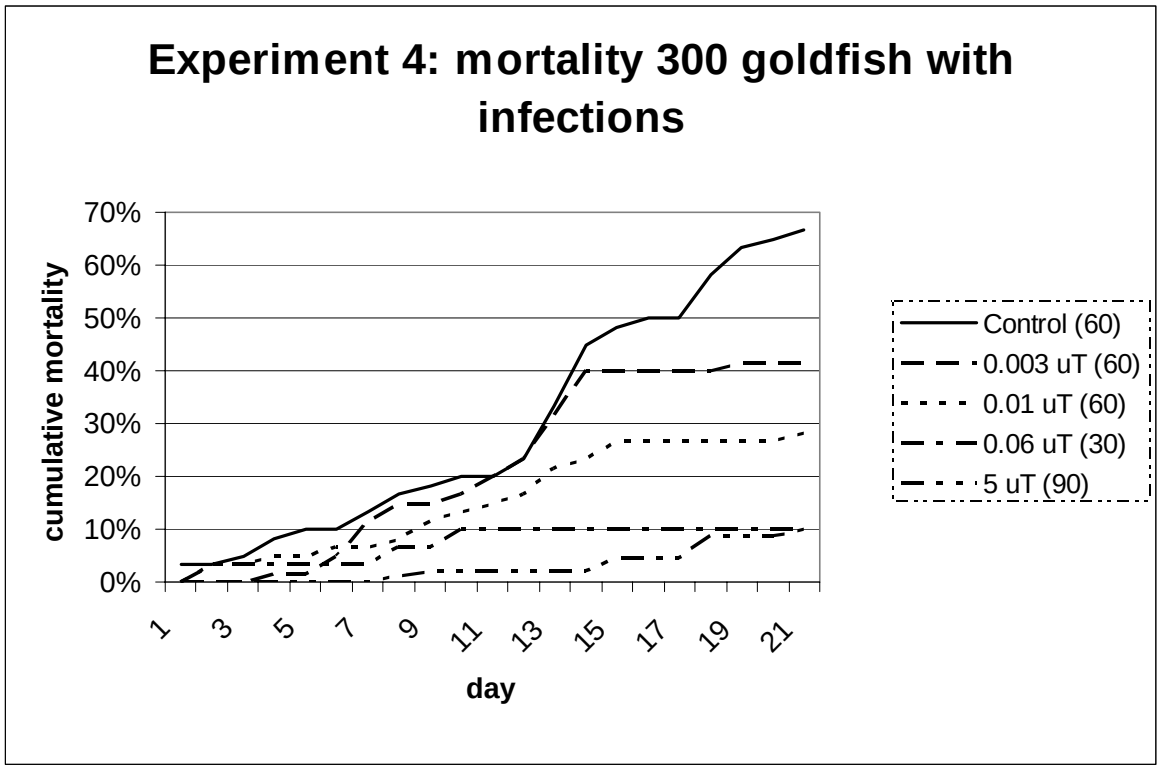


At only two replicates per field strength these results indicate that the treatment is effective in the whole window of field strength between 0.15 and 50 μT (and probably beyond). The average line of all treated tanks (solid, thick) corresponds very well, or is even better than the results of experiments 1 and 2. Together they show that a surprisingly strong improvement of the survival of these fish with this disease can be achieved with this form of EMF.

Because of its interest for practical application in farming and aquaculture, we investigated further at the lower field strength level. Since these field strengths cannot be reliably produced directly in our setup (too low

voltages, too low currents, and therefore too high electronic noise levels) this was done using the stray fields of our coils around tubs at 5 µT. These are solenoid coils which produce the desired field, sufficiently uniform, at 50 cm, 100 cm and 120 cm distance from the (outside) of the coil. Figure 4 gives the results.

Figure 4. Treatment results at extremely low field strengths.



A dose response pattern is visible between 0.003 and 0.06 µT with the latter value delivering a result not far from our reference value of 5 µT.

The results obtained demonstrate that the treatment with EMF drastically reduced the mortality in fish that is due to above-mentioned parasites and secondary microbial infections. These results indicate that even in strongly diseased fish the stimulation with LF EMF mobilizes the immune system for fighting the invaders possibly because it puts the immune system in a higher state of activity, thus giving it a better chance of fighting the disease.

The dose response values given in Figure 4 indicate that some effect of the treatment remains even at field strengths as low as 3 nT. Therefore in experiments large distances must be maintained between control tanks and experimental tanks, so that the stray fields are below 1 nT or less.

This observation raises questions for the experimental setups with sham controls. The field cancellation between the opposing currents in the sham coils must be extremely good. It can be doubted if the required cancellation is ever reached in practice.

Using Helmholtz pairs of coils should also be surrounded with careful measurements of the stray fields, which can be substantial.

In vivo experiments with chicken broilers, exposed to infection pressure from coccidia parasites

A universal infection in fattening chicken is coccidiosis, with *Eimeria* parasites that live and explosively multiply in a particular part of the intestines of a particular host for each *Eimeria* specie. Number of studies has suggested that the immune response to *Eimeria* infection among other is mediated through the release of cytokines. Breed et al. (1997) reported that chicken peripheral blood leucocytes of *E. tenella* infected chickens produce interferon-γ after in vitro re-stimulation. Moreover, it has been shown that treatment chickens with interferon-γ preceding infection with *E. acervulina* decrease the negative effect of infection on weight gain (Lowenthal et al., 1997).

For the three subsequent experiments 192, 288 and 272 one-day old female broilers (Ross 308) were purchased from the hatchery. On day of arrival, they are wing-banded, weighed and randomly housed in wire-floor, suspended cages. Each cage is provided with thick foil and litter. Under the floor of each cage a 16-loop coil was located to deliver LF EMF for 30 minutes per day to chicken within the cage. No attempt was made to create a

uniform field since in a preliminary experiment it was determined that effective field strengths lie between 0.1µT and 50 µT. Moreover the practical application that is our goal will also not allow complete uniformity of the field strengths. The field strength (rms) in the middle of the cage was set at 6,5 micro Tesla, measured with an F.W.Bell 5180 Tesla meter. Dosimetry control during the experiment was ensured by constantly monitoring the (rms) current through the coil. The applied signal was designed by Immunent, which contains several LF components with frequencies between 100 and 10.000 Hz.
In the experiment 1, infection pressure was provided with Campylobacter jejuni on day 6, in the experiment 2 high level infection pressure was given on day 15 with Coccidia, containing a controlled mixture of different Eimeria species, and in experiment 3, a low level of the same infection pressure was given at day 15. Detailed information about materials and methods, as well as more data, are provided in (Cuppen et al. 2006d this proceedings).
It has been common practice (now illegal) to include preventive antibiotics in chicken feed in order to fight potential infection. This caused infections to be suppressed from the start, so keeping the chicken healthy they will properly develop and gain weight. This is usually estimate in what is called “feed conversion”, the number of kilograms of feed required for 1 kilogram of growth of the animal. To determine whether EMF could replace preventive antibiotics by providing enhanced immune response as a preventive measure, the feed uptake and growth were carefully measured per cage during the experiment, and corrected for the number of chickens actually present every day.

At the end of the growing cycle chickens were normally slaughtered and intestines evaluated for lesions as caused by the infection in a blind setup.

The results obtained are given in Tables 3 and 4.

Table 3: Feed conversion of broilers (kg feed consumed / kg weight increase).

	Negative control	Positive control	EMF no infection	EMF w infection
Experiment 1	1.78 ± 0.02	1.73 ± 0.04	not in experiment	1.61± 0.03*
Experiment 2	1.58 ± 0.04	1.63 ± 0.04	1.57 ± 0.05	1.52 ± 0.06 *
Experiment 3	1.83 ± 0.03	1.84 ± 0.05	1.73 ± 0.03*	1.72 ± 0.03*

∗ significant ($p<0.05$) vs. the relevant control

Feed conversion for the EMF treated groups was significantly improved in 4 out of 5 cases compared with non-treated groups. This result indicates that this EMF treatment has a similar effect as preventive antibiotics on feed conversion in the chickens. Of course this could be the result of an as yet unknown effect of EMF, but we consider it likely that the mechanism is through an enhanced immune competence of the chicken, and that therefore these results support our hypothesis.

Economically, these results are important as well, since 10 points feed conversion translate into a cost reduction of about 5 euro cents per chicken.

In experiment 3, we could also measure (blind) the damage of the infection in terms of lesions in the chicken intestines. The results are shown in Table 4.

Table 4: Mean lesion scores of intestines in chicken broilers after Coccidiosis infection at day 16.

	Control		EMF	
	- cocc	+ cocc	- cocc	+ cocc
E. acervulina				
day 21	0.44 ± 0.22	2.44 ± 0.15	0.44 ± 0.18	2.00 ± 0.16*
day 29	1.06 ± 0.27	1.69 ± 0.09	0.31 ± 0.13*	1.50 ± 0.15*
day 36	1.38 ± 0.26	1.75 ± 0.19	0.94 ± 0.24*	1.22 ± 0.10*
E. maxima				
day 21	0.13 ± 0.08	2.25 ± 0.19	0.06 ± 0.06*	1.67 ± 0.13*
day 29	0.56 ± 0.20	1.63 ± 0.08	0.00 ± 0.00*	1.33 ± 0.21*
day 36	1.50 ± 0.38	2.10 ± 0.12	0.50 ± 0.25*	1.22 ± 0.21*
E. tenella				
day 21	0.13 ± 0.08	1.50 ± 0.09	0.06 ± 0.06	1.42 ± 0.11
day 29	0.19 ± 0.09	1.31 ± 0.13	0.06 ± 0.06*	1.00 ± 0.11*
day 36	0.56 ± 0.15	1.42 ± 0.15	0.13 ± 0.08*	1.17 ± 0.11*

The reductions in pathology after EMF treatment are significant in all measurements more than 5 days after infection showing less damage due to the disease and therefore indicating a better immune response with EMF treatment.

Discussion and conclusions

The in vitro and in vivo results clearly indicate that LF EMF treatment induces an enhanced immune response. It is not clear at present what the exact mechanism is of this EMF stimulation. In (Markov et al. 2006) we discussed that one of the key players of the immune system (T-lymphocytes) has a very specific response to EMF stimulation: react only when lymphocytes are activated. “Activation” means that the immune system gets the signal that some thing wrong is coming or going on. Then lymphocytes would be in high state of alert, ready to react. In Fig. 1, it is suggested that EMF stimulation and pathogens actually in combination trigger the immune system, giving it the signal that something “wrong” is indeed coming..

Moving from biology to fish and chicken farming, the results reported have extraordinary importance: by helping the immune system to handle infections in fish tanks, ponds or chicken barns, the LF EMF stimulation drastically reduces mortality and increases the efficiency of feed conversion. This is even more important since the preventive antibiotics are being banned for further application as feed supplement in the EU and other countries.

An additional advantage of the LF EMF stimulation reported on in this study is that it is achieved with a very low magnetic flux density which is a) economically and technically feasible in large areas and b) makes it unlikely that adverse effects would be initiated by this EMF stimulation.

All results above were obtained at levels less than 6.5 µT field strength (except one in vitro series at 1.5 mT) and in the one case tested, the effects were maintained even to a level of 0.006 µT. At these levels a direct effect on the pathogens is highly unlikely and the effect can only take place though resonance and the triggering of a system ready to react. A comparison might be made with a car stopping for a red light. No sufficient amount of energy was transferred to make any meaningful change in the process of the driving car. Nevertheless the signal was detected and a response generated that causes the car to stop. Likewise the minute signal required to generate the effects reported indicates that a physiological process was triggered that was waiting to go off.

In summary, our in vitro results indicate that the Immunent signal indeed increases immune activity on cell level and that ROS production is increased causing oxygen stress at cell level. The in vivo experiments show a) reduced mortality and b) increased growth and reduced pathology after LF EMF treatment. The effects are strong, up to being actually relevant for animal management in farms. The effects measured support the hypothesis that LF EMF creates stress at cell level that can trigger an immune response that sustains itself after the immune system becomes active enough to attack a sufficient number of pathogens.

References

Breed D.G., Dorrestein J., Schetters T. P., Waart L. V., Rijke E., and Vermeulen A. N.. (1997). Peripheral blood lymphocytes from Eimeria infected chicken produce gamma-interferon after stimulation in vitro. Parasite Immunol. 19:127-135.

Cuppen J.J.M. and Vink A. (2004): Effects of ELF exposure on weight and immune parameters in young turkey broilers, 3rd Intl workshop on Biological Effects of EMFs, Kos, 2004, p 1203.

Cuppen J.J.M., Parmentier H.K. and Savelkoul H.F.J. (2006a): Immune Stimulation In Fish And Farm Animals Through Weak Low Frequency Electromagnetic Fields, A. Hypothesis, this proceedings.

Cuppen J.J.M., Wiegertjes G.F., Molenaar M., Geervliet J., Smink W. (2006c): Immune Stimulation In Fish And Fish Immune Cells Through Weak Low Frequency Electromagnetic Fields With Variable Field Strength, this proceedings

Cuppen J.J.M., Beynen A.C., Elmusharaf M.A., Grooten H.N.A. and Smink W. (2006d): Immune Stimulation In Chicken Broilers Through Weak Low Frequency Electromagnetic Fields With Coccidia Infection, this proceedings

Lowenthal J.W., York J.J.,. ŐNeill T.E, Rhodes S., Prowse S. J., Strom D.G., and Digby M.R.. (1997). In vivo effects of chicken interferon-gamma during infection with Eimeria. J. Interferon Cytokine Res. 17:551-558.

Lupke M., Rollwitz J. and Simkó M. (2004) 50 Hz magnetic fields induce reactive oxigen intermediates in human monocytes and in Mono Mac 6 cells. Free Radic. Res. 38, 985-993

Markov M., Nindl G., Hazlewood C., Cuppen J. (2006) Interactions between electromagnetic fields and immune system: Possible mechanism for pain control. In: Ayrapetyan S and Markov M (eds.) Bioelectromagnetics: Current concepts. Springer, Dordrecht, The Netherlands. 213-226

Matzinger P. (2002): The danger model: a renewed sense of self. Science 2002;296:301-5.

Maxey B.W and Page R.K., (1977) Efficacy of lincomycin feed medication for the control of necrotic enteritis in broiler-type chickens. Poult Sci., 56: 1909-13.

Simkó M., Droste S., Kriehuber R. and Weiss D.G. (2001): Stimulation of phagocytosis in murine macrophages by 50 Hz electromagnetic fields. Eur. J. Cell Biol. 80, 562-566

PULSED ELECTROMAGNETIC FIELDS EFFECTS ON MEMBRANE PARAMETERS OF ATTACHED CELLS IN CULTURE

MIHAELA G. MOISESCU[1,4], EUGENIA KOVACS[1], TUDOR SAVOPOL[1], IRINA STOIAN[2], PHILIPPE LEVEQUE[3], LLUIS M MIR[4]

[1] BIOPHYSICS AND CELL BIOTECHNOLOGY DEPT., "CAROL DAVILA" MEDICAL UNIVERSITY, BUCHAREST, ROMANIA, MMOISESC@UNIVERMED-CDGM.RO

[2] BIOCHEMISTRY DEPT., "CAROL DAVILA" MEDICAL UNIVERSITY, BUCHAREST, ROMANIA

[3] XLIM, UMR 6615 CNRS -UNIVERSITE DE LIMOGES, FRANCE, LEVEQUE@UNILIM.FR

[4]UMR 8121 CNRS, INSTITUT GUSTAVE-ROUSSY, VILLEJUIF, FRANCE, LUISMIR@IGR.FR

Abstract

The effects of pulsed electromagnetic fields (EMFs) were studied on processes and parameters of cell membrane of B16 metastatic murine melanoma cells and DC-3F transformed Chinese hamster lung fibroblasts. The fluid phase endocytosis were quantified on attached cultured cell under EMFs exposure.

The pulsed EMFs used were trains of low amplitude 900 MHz EMFs at a 217Hz envelope frequency, 580µs pulse duration, for times up to 30 minutes. Cells grown on Petri dishes were exposed at subconfluence using a wire-patch antenna or a TEM antenna. Endocytosis is critical for cellular functions like nutrition, signaling, transmembrane transport or surface area control. Fluid phase endocytosis is one main type of endocytosis corresponding to the liquid media engulfment in intracytoplasmic vesicles (endosomes) formed on the inner cell surface. Fluid phase endocytosis can be monitored by the Lucifer Yellow (LY, a fluorescent non diffusible dye) uptake and we previously showed that exposure of the cells to GSM microwaves significantly increases LY uptake in the absence of a temeperature increase. The results here reported confirm and extend our previous observations. Indeed, we confirm that GSM microwaves increase LY uptake using another exposure system, a TEM irradiation antenna. Using known inhibitors of endocytotic pathways, we have identified, among the various cellular mechanisms resulting in external molecules engulfment, the mechanism that is actually affected by the exposure to the EMFs. Indeed, our data show that only the clathrin-dependent pathway is perturbed by the EMFs pulses while the potocytosis is not affected.

Introduction

Endocytosis is one of the basic cellular mechanisms participating to molecule exchange between the cell and its environment. Various ways of endocytosis mediate essential cell processes among which: extracellular molecules incorporation, membrane renewal and surface area control, antigen presentation, membrane receptor expression, etc. [1]. In the fluid phase endocytosis and the receptor mediated endocytosis, vesicles are constantly formed on the inner surface of the membrane and correspond to the absorption of extracellular medium into intracytoplasmic vesicles (endosomes). They detach in the cytoplasm and fuse with other internal cellular vesicles. The cytoplasmic surface of these vesicles is covered by a specialized protein, the chlatrin. Pinocytosis is another related endocytosis process in which the vesicles also detach from the cell membrane even though they are not covered by the chlatrin. Membrane area is restored by exocytosis, which corresponds to the fusion of internal vesicles to the plasma membrane. In the potocytosis, the vesicles (termed caveolae, and surrounded by a protein known as caveolin) formed at the inner cell surface do not detach but allow for active transport of molecules towards the cell inside. Apart from these general endocytotic pathways, specialized cells possess specialized endocytotic functions like the phagocytosis of the macrophages.

We previously showed that the incorporation of the Lucifer Yellow, a non permeant molecule that enter normal cells only by endocytosis, was increased under pulsed electromagnetic fields exposure (EMFs) using a standardised wire-patch antenna (Fig. 1). Here we confirm the increase in endocytosis using another exposure system, a TEM irradiation antenna. Moreover we have identified, among the various cellular mechanisms resulting in external molecules engulfment, the mechanism that was actually affected by the EMFs exposure.

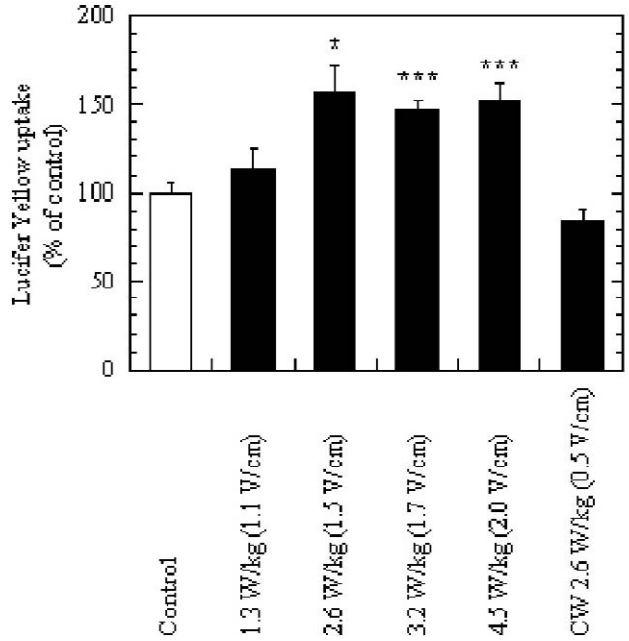


Fig.1. Increase of LY uptake by B16F1 cells after 10min of incubation at 30°C, caused by GSM-EMFs exposure to various SAR into the wire-patch antenna. CW: exposure to EMFs without 217Hz modulation. Values in brackets: peak electric field intensities of the EMFs electric component. 100% correspond to $(9\pm2.2)x10^6$ LY molecules by cell. Unpaired Student's t-test: * $p<0.05$, ** $p<0.01$, *** $p<0.001$ (from [2]).

Materials and methods

Wire-patch antenna experimental set-up The experimental exposure system is described in figure 2.

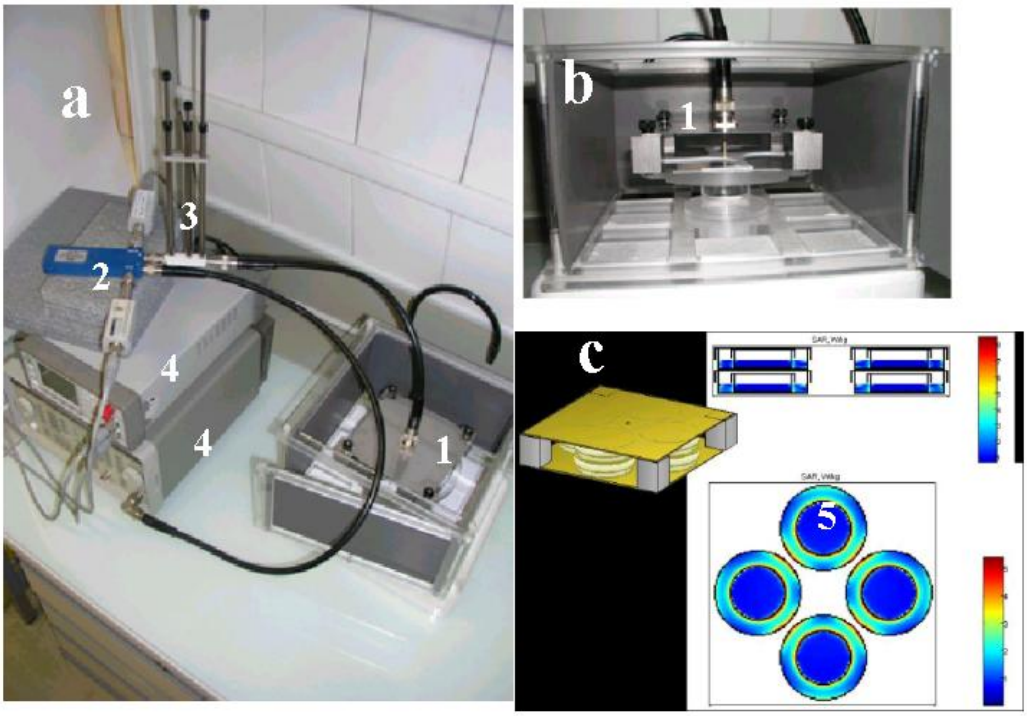


Fig.2**a** and 2**b**. **1** - wire-patch antenna, **2** - bidirectional coupler for forward and reflected power monitoring, **3** - impedance matcher, **4** – wattmeters;

Fig.2**c**. Modelling of field homogeneity in 4 samples exposed to GSM-EMFs: **5** - 35mm Petri dishes with attached cells in culture in 50mm Petri dishes with water.

TEM antenna experimental set-up The experimental exposure system is described in figure 3.



Fig.3**a** and 3**b**. **1** - TEM antenna, **2** - bidirectional coupler for forward and reflected power monitoring, **3** – 50Ω load, **4** - wattmeter **5 –** temperature, CO_2 and humidity control systems;
Fig. 3**c**. 900 MHz CW / GSM generator of adjustable powers;
Fig.3**d**. Modelling of TEM antenna with 35mm Petri dish with attached cells in culture to be exposed to GSM-EMFs.

Cells
F10 or F1 metastatic B16 murine melanoma cells and DC-3F transformed Chinese hamster lung fibroblasts were used. They were cultured at 37°C, 5% CO_2, in Eagle MEM (Gibco) supplemented with 10% foetal calf serum (Life Technologies), 100 units/ml of penicillin and 100 µg/ml of streptomycin (Gibco).
Exposure to EMFs
Two kinds of EMFs waves were used: (i) pulsed waves (GSM-EMF because they correspond to the EMFs delivered by the GSM mobile phones) consisting in 580µs-long square pulses delivered with a low frequency envelope at 217 Hz and with a high-frequency carrier sine wave at 900 MHz ; (ii) continuous wave (CW-EMF) consisting in a high-frequency sine wave at 900 MHz.
The signal generator RF S 900-60 (RFPA, Bordeaux,France) was delivering these two kinds of signals at adjustable powers ranging from 1 to 7 W (mean incident powers) for GSM-EMF and from 1 to 56 W for CW (mean or peak incident powers being identical for the CW-EMF).
EMFs in vitro exposure devices were a wire-patch or a TEM antennas.
Into the TEM antenna a single 35mmPetri dish with cells attached to was placed in the middle of the antenna.
Into the wire-patch antenna four Petri dishes were simultaneously exposed. Each 35mm Petri dish with the cultured cells was placed inside a 50mm Petri dish, used as a sample holder and both dishes were placed above another 50mm Petri dish. Both 50mm Petri dishes were containing water in order to preserve the same depth of the medium volume and the dielectric properties continuity. Therefore, a fair homogeneity of the EMF was achieved for the whole of the cells reducing the edge effects at the periphery of the 35mm dish [5].
For all experiments, cells were subjected to either EMFs exposure or sham exposure, under identical experimental conditions, in particular regarding to the location of the dishes in the wire-patch / TEM antennas and the location of the antennas in the incubator.

Media temperature was measured immediately before and after each exposure, using a digital thermometer and no significant rise in temperature was found at the powers used in the experiments, in agreement with the theoretical calculations.
Exposures were characterized by the **SAR** (Specific Absorption Rate) or power density absorbed by cell unit mass: SAR = $\sigma E^2/\rho$, [SAR] = W/Kg with **E** = local electric field intensity, **σ** = electric conductivity and **ρ** = absorbing material density.

Endocytosis rate determination
The endocytosis rate was quantified by the accumulation of Lucifer Yellow (LY, Sigma), a non diffusible fluorescent dye. 24h before the experiment, the cells were seeded into 35mm Petri dishes in order to have a cell monolayer in exponential growth at the time of exposure. Cells were incubated for various time durations (ranging from 10 to 30 min) with 2 ml of culture medium containing 2 mM LY, in the presence or the absence of the applied EMFs. The incubations and EMFs exposures were done at 30°C. Immediately after the incubation, the cells were rapidly washed three times with 3 ml of NaCl 0.09%, trypsinized (Trypsin-EDTA 0.05%, Gibco), centrifuged (1000rpm, 10min, room temperature) and the cellular pellets resuspended in 1ml H_2O. Then, the cell suspension was sonicated 2x15s, at 100 W, on ice or chemically lysed. (Promega Lysis Reagent kit). The total fluorescence was measured using a spectrofluorometer (SFM 25, Kontron Instruments) at excitation and, respectively, emission wavelengths of 423 and 536 nm. The baseline was obtained for cells not exposed to the fluorescent dye. 20µl of cellular lysis was used for protein dosage (MicroBCA Protein Assay kit, Pierce).
For the experiments with endocytosis inhibitors, before the EMF exposure, the cells were incubated for 30 min at 37°C with Chlorpromazine Hydrochloride (Sigma) or Filipin III from Streptomyces filipinensis (Sigma). The two chemicals were also present into the media during the EMF exposure.
Viability of the cells incubated with 15µM Chlorpromazine or 1µg/ml Filipine III was 90 to 95%.of the viability of the controls (data not shown).

Results

The cells in the TEM antenna were exposed to SARs of 2.7 W/kg and 5 W/kg for 20 minutes. Indeed from previous work using the wire-patch antenna and the same cells, we knew that the exposed B16-F1 melanoma cells could display an increased dye uptake compared to the control cells after incubations times as short as 10min and we also knew that exposure to SARs between 0.6 and 1.3 W/kg had no significant effect on LY uptake while exposure to SARs between 2.6 and 4.5 W/kg significantly increased the LY uptake. Above an apparent threshold value under which no effect was detected, the increase of the fluorescent dye uptake was independent of the delivered GSM-EMF power, with a constant increase of approximately 1.5-fold with respect to control cells incubated under the same conditions but in the absence of the EMF exposure.
Cell viability after cells exposure to EMFs in the TEM antenna was similar to the viability in the controls (data not shown).
The results of cells exposure to GSM microwaves in the TEM antenna are reported in figure 4. Experiment was repeated 8 times, including each time an exposed and an unexposed Petri dish. As for the exposure in the wire-patch antenna, an statistically significant increase in the LY uptake was detected when cells were exposed at 5 W/kg ($p<0.05$, paired t-Student's test). No significant increase was detected at 2.7 W/kg, a SAR value close to the threshold in the wire-patch antenna exposure system. These results confirm thus our previous observations.

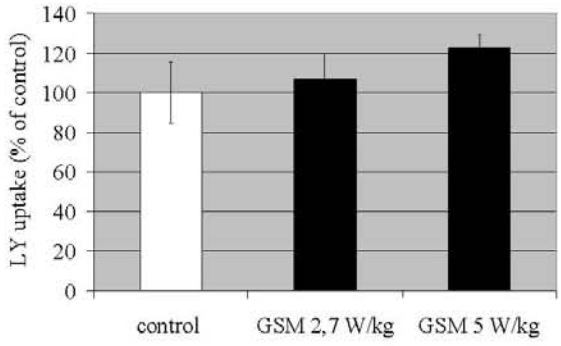


Fig.4. Increase of LY uptake by B16F10 cells after 20min of incubation at 30°C, caused by GSM-EMFs exposure to various SAR (2.7 and 5 W/kg) into the TEM antenna. 100% correspond to (19.8± 3.04)x10^6 LY molecules by cell. Each value is the average of 8 samples ± SD.

To determine whether the increased LY uptake is due to a increase in classical endocytosis (mediated by the chlatrin coated vesicles) or by potocytosis (mediated by the caveolin coated vesicles), the cells were preincubated with drugs selectively inhibiting these two endocytotic pathways: We used chlorpromazine that is a known inhibitor of the clathrin-dependent pathway [3], and Filipin III that is a known inhibitor of the potocytosis, that is of the caveolae-dependent pathway [4]. Results are reported in figures 5 and 6. Exposures were performed in the wire-patch antenna exposure system because several Petri dishes can be simultaneously exposed and because our previous experience using this exposure system.

Figure 5 shows that chlorpromazine slightly decreased LY uptake in the control unexposed cells. More interesting, chlorpromazine completely blocked the increase in LY uptake provoked by the exposure of the cells to the GSM microwaves. This results that the LY uptake pathway stimulated by the GSM microwaves is a chlatrin dependent pathway.

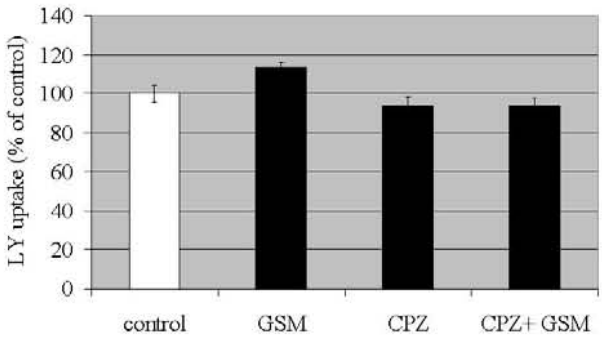


Fig.5. LY uptake by B16F10 cells after 20min of incubation at 30°C, in the presence or not of GSM-EMFs pulses and/or 15µM chlorpromazine (CPZ). GSM-EMFs exposure of 3.2W/kg SAR into the wire-patch antenna. Each value is the average of 8 samples ± SD.

Figure 6 shows that an increased endocytosis rate under EMFs exposure was still detected in the filipin III-treated cells. Thus the inhibition of the caveolin dependent pathway does not prevent the stimulation of the LY uptake by the GSM microwaves, suggesting that only the clathrin-dependent pathway is perturbed by the EMFs pulses.

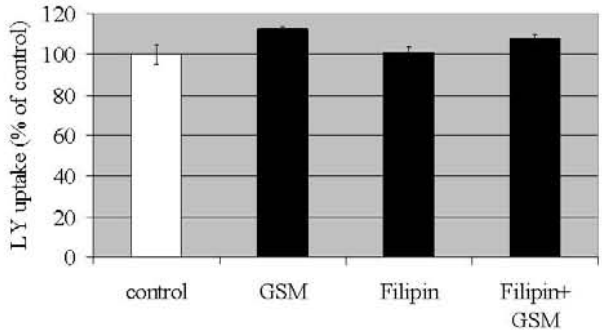


Fig.6. LY uptake by B16F10 cells after 20min of incubation at 30°C, in the presence or not of GSM-EMFs pulses and/or 1µg/ml filipin III. GSM-EMFs exposure of 3.2W/kg SAR into the wire-patch antenna. Each value is the average of 8 samples ± SD.

Summary
The results here reported confirm and extend our previous observations [2]. Indeed, we confirm that GSM microwaves increase LY uptake using another exposure system, a TEM irradiation antenna. Results are similar to those obtained using the wire-patch antenna even though significant increase at a SAR of 2.6 W/kg was detected with the wire-patch antenna and no significant increase was detected at a SAR of 2.7 W/kg with the TEM antenna. Indeed, these SAR values result mainly from models of energy deposition in the two exposure systems, approximately validated by measurements of temperature increase. Precision of both the models and of the measurements does not allow precise comparisons between the two exposure systems. At a SAR of 5 W/kg with the TEM antenna there is a statistically significant increase in the LY uptake. In the experiments here reported, the LY uptake increase in the cells exposed to the GSM microwaves was lower than 1.5 times the uptake in the control cells but this increase was still statistically significant.
The effects of the GSM microwaves on the endocytosis (LY uptake) are also confirmed by the effects of the two inhibitors used. Indeed, one of the two molecules tested actually inhibited the increase in LY uptake, while the other not. This excludes a non-specific effect of the addition of a chemical in the incubation medium. Simultaneously, the inhibition provoked by a known inhibitor of one of the endocytosis pathways confirms our previous observations and conclusions, namely that the exposure of the cells to the GSM microwaves affects the endocytosis pathways.
Moreover we have identified, among the various cellular mechanisms resulting in external molecules engulfment, the mechanism that is actually affected by the exposure to the EMFs. Indeed, our data demonstrate that only the clathrin-dependent pathway is perturbed by the EMFs pulses. Thus the potocytosis is not affected, while the classical endocytosis is actually modified by the cell exposure to the GSM microwaves.

Acknowledgements
Nous remercions le Conseil Scientifique de l'ACI "effets biologiques de la radiotéléphonie mobile" et le ministère chargé de la recherché qui a finance ce projet, ainsi que les opérateurs de téléphonie mobile qui ont complété ce financement en concertation avec le Conseil Scientifique de l'ACI et le ministère chargé de la recherche. We also thank M.A. Verjus for technical assistance and the Romanian Ministry of Research for grant CEEX n° 67/2005 to Pr E. Kovacs.

References
[1] Alberts B.; Johnson A.; Lewis J.; Raff M.; Roberts K.; Walter P., *Molecular Biology of the Cell*, 4th edition, Garland Publishing, New York, **2002**, 711-766;
[2] Mahrour N.; Pologea-Moraru R.; Moisescu M.G.; Orlowski S.; Leveque P.; Mir L.M., In-vitro increase of the fluid phase endocytosis induced by pulsed radiofrequency electromagnetic fields : importance of the electric field component, *Biochim. Biophys Acta*, **2005**, *1668*, 126-137;
[3] S. B. Sieczkarski, G. R. Whittaker, Dissecting virus entry via endocytosis, *J. Gen. Virology*,**2002,** *83*, 1535 – 1545;
[4] P.A.Orlandi, P.H. Fishman**,** Filipin-dependent inhibition of cholera toxin: evidence for toxin internalisation and activation through caveolae-like domains, *J.Cell Biol.*, **1998**, *141* ,905-915;
[5] L. Laval, P. Leveque, A new in vitro exposure device for the mobile frequency of 900 MHz, *Bioelectromagnetics*, **2000**, *21*, 255– 263.

TEM CELL IN BIOMEDICAL EXPERIMENTS

TOMASZ DLUGOSZ, HUBERT TRZASKA

WROCLAW UNIVERSITY OF TECHNOLOGY,
INSTITUTE OF TELECOMMUNICATIONS, TELEINFORMATICS & ACOUSTICS
WYBRZEZE WYSPIANSKIEGO 27, 50-370 WROCLAW, POLAND
tomasz.dlugosz@pwr.wroc.pl, hubert.trzaska@pwr.wroc.pl

Abstract

This paper deals with application of Transverse ElectroMagnetic (TEM) cell as an exposure system in technical and biomedical studies. In many publications is described problem of influence of an object upon the electromagnetic field (EMF) distribution inside a exposure system while inverse effect - influence of exposure system on tested object is overlooked. The problem plays primary role if a correlation between investigations carried out in an enclosure (eg TEM cell) and that in the free space is looked for.

Introduction

TEM cell was proposed by Myron L. Crawford in 1970 [3] as a new way of establishing standard, uniform EMF in a shielded environment and until now it is one of the most frequently applied EMF standard and exposure system. TEM cell is based on the idea that a TEM wave propagates inside a transmission line. Inside can be immersed an object that susceptibility to the EMF is tested. It is used for probes' calibration, electromagnetic compatibility and biomedical investigations (Fig. 1). The reasons of such popularity of TEM cell are its advantages: quite homogeneous EMF distribution inside the cell, similar to plane wave, wide frequency range, field intensity independent from frequency, simple EMF intensity estimations, etc.

However, "in the pot of honey is a spoon of a ter". Even not to mention the mutual interactions between the cell and object tested in it, these are: nonideal EMF distribution, moreover disturbed by the object, limited volume of the cell and the volume decrease with frequency increase, problems with larger objects testing in wide frequency range, etc. The former are discussed then while the latter are illustrated bellow. A concept of the homogeneity improvement by the way of covering the cell walls with a dielectric material is shown in Fig. 2. An approach to the frequency range widening is presented in Fig. 3. The slots limit tangential currents and, as a result, higher modes in the cell.

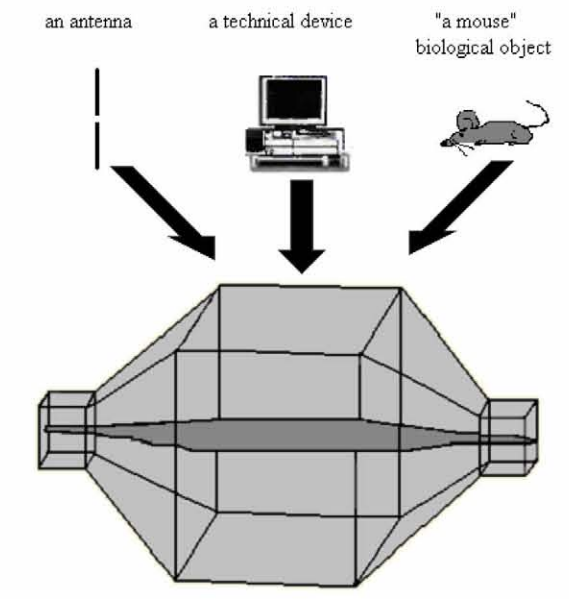


Fig. 1. A different way of using TEM cell.

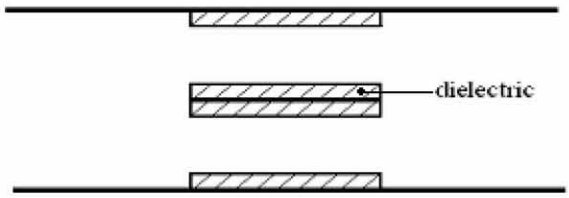


Fig. 2. Dielectric sheets in a cell.

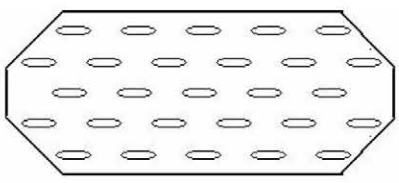


Fig. 3. A center conductor of a TEM cell.

What are the feelings of an antenna inside a cell?

Before we start our considerations related to biomedical experiments we would like to remind a problem of antenna's calibration in the cell, it would illustrate the role of mirror reflections phenomenon and then our way to farther considerations.

The answer to the question in the title is: due to infinite large number of mirror reflections (Fig. 5) the single antenna feels as an element of antenna system. If consider a cell without side walls, as in Fig. 1, and take into account only two plates, as shown in Fig. 4, the input reactance of a short dipole antenna X_i is expressed by:

$$X_i = X_{11} - \Delta X = X_{11} - 2\sum_{i=2}^{\infty}(-1)^{i-1} X_{1i} \tag{1}$$

where: X_{11} – input reactance of the antenna in free space, ΔX – input reactance change due to a mutual couplings, X_{1i} - mutual reactance of the antenna and its i-th mirror reflection.

Presence of the mirror reflections, and their result ΔX, leads to a calibration error δ in relation to the free space conditions, the error we'll formulate in the form:

$$\delta = \frac{\Delta X}{X_i} . \tag{2}$$

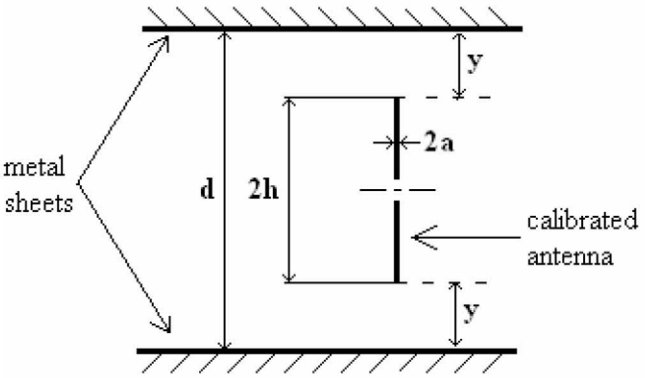


Fig. 4. Geometry of calibration.

Fig. 5. Mirror reflections caused by metal sheets.

The input reactance of the antenna as well as the mutual reactances of the antenna and its mirror reflections is a function of its slenderness ratio. The slenderness ratio is a function of the relation of the antenna's length (2h) to diameter of it's arm (2a). Calculated runs of the error δ versus b/2h for h/a = 30, 300 and 1000 are shown in Fig. 6 [9]. In the estimations the plates were assumed infinitely large and perfectly conducting. The case while h/a=30 was reestimated on analytical and numerical way [4]. Results are presented in Fig. 7.

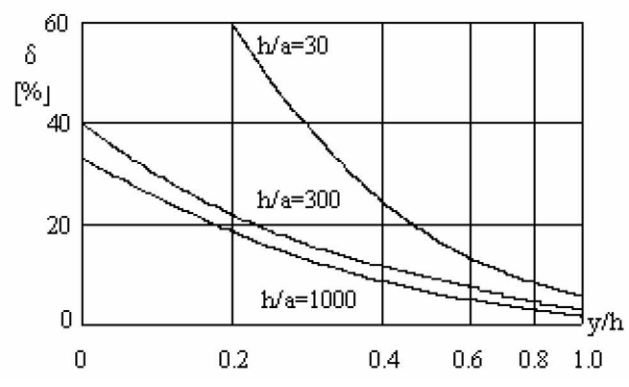


Fig. 6. Error δ versus y/h as a function of slenderness

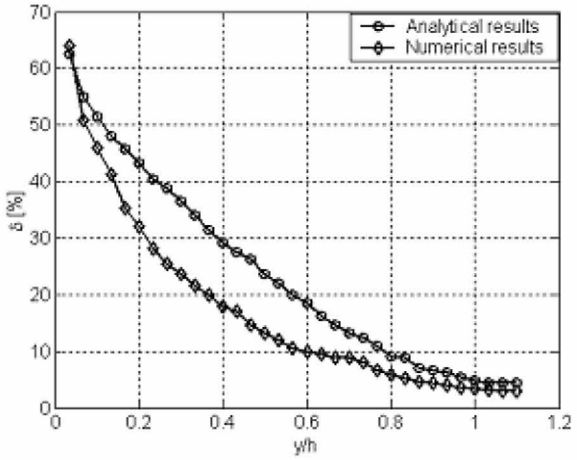


Fig. 7. Error δ versus y/h for h/a=30.

ratio.

The above considerations allow several conclusions:

- real error of calibration is remarkably limited by presence at the input of a probe a capacitive divider,
- the phenomenon is of deterministic character and appropriate correction factors may be used to eliminate the error discussed,
- if the phenomenon exists in the presented case of an antenna calibration, a similar phenomenon should exist while in the cell any other material medium is immersed,
- if in the case of antennas a correction factor may improve accuracy of calibration similar approach should exist in the case of the medium investigations in order to find a way to refer the exposure conditions (and results of measurements) in the cell to that in the free space.

Numerical methods in biomedical dosimetry

An estimation of EMF energy absorption in any case may be done on the ground of the Maxwell equations solution. Unfortunately, analytical solutions are known only for the simplest structures. Even above presented estimations of input impedance of a dipole antenna required an assumption of it's perfect conductivity and sinusoidal current distribution along the antenna. The assumption may be accepted only for very thin structures. What to say about biological media where not only shapes may be arbitrary ones but the electrical parameters of the media are different for different tissues, organs and even parameters of the same tissues may be different depending upon a history of their donator. These limitations have lead, not only at our field, to necessity to use substitutional methods, i.e.: numerical ones. Along with the computer technology development and computers availability more and more sophisticated numerical methods and models were worked out.

The above is well illustrated by development of models applied in numerical dosimetry. In Fig. 7 are presented different models of a mouse (Fig. 7a). The oldest ones are spheroidal (Fig. 7b) [11] and cube (Fig. 7c) models. Follows them (Fig. 7d) a block model, containing of several cages, that allows bit better representations of the mouse's shapes and different electrical parameters. Now the most sophisticated model allows almost ideal reflection of investigated animal.

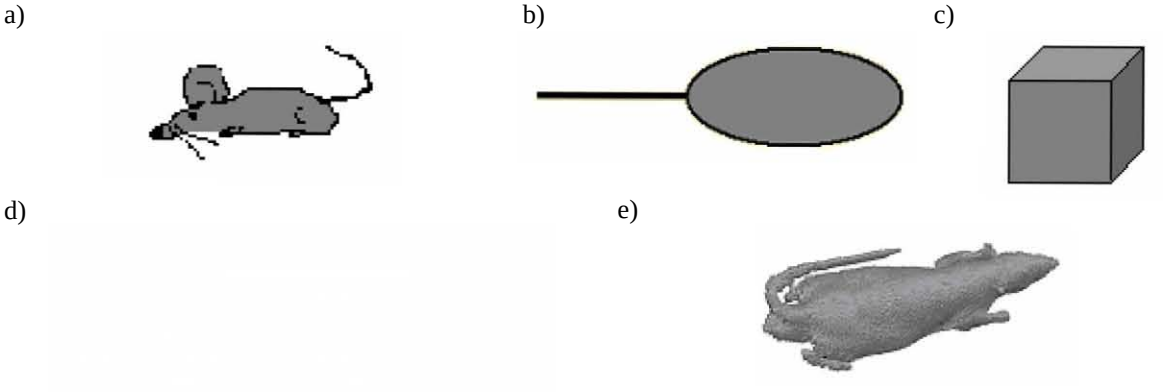


Fig. 7. Models of a mouse: a) real object, b) spheroidal model, c) cube model, d) block model, e) voxel model.

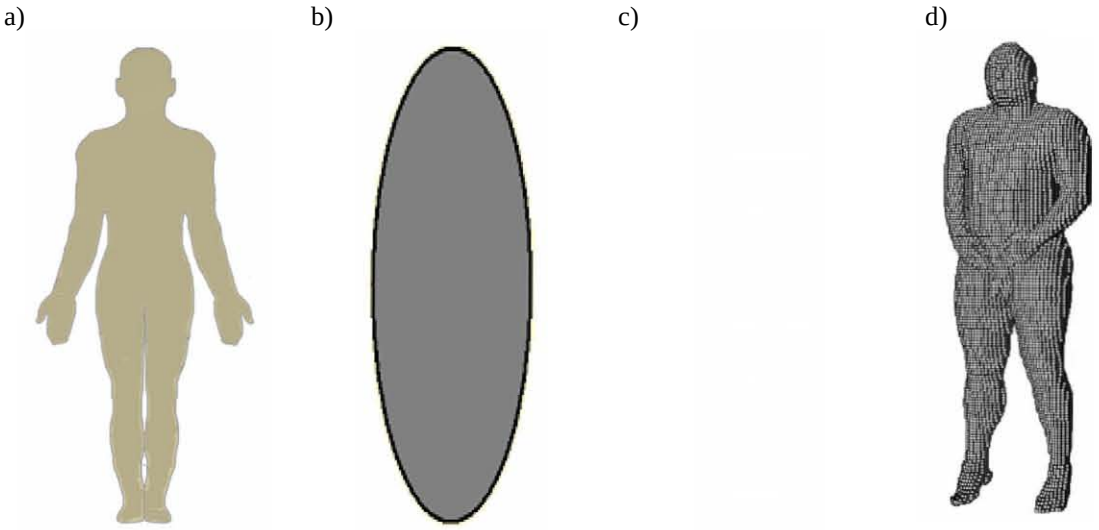


Fig. 8. Models of a man: a) real object, b) spheroidal model, c) block model, d) voxel model.

Similar development, as regards as a model of the man, is presented in Fig. 8 [6] [7] [8] [10]. We may only remind here that homogeneous spheroidal and block models were applied in analytical studies, block model of a man was proposed by Guy and Johnson [10] and the most sophisticated "millimeter resolution" model of a man was developed by Gandhi [7].

It is evident that more sophisticated models require more sophisticated hard- and software. Both of them were not fully available to the authors. Thus, our estimations are limited to the use of rather simple codes (Maxwell SV [1], Fidelity [15]) and a possibility to use them in quite simple computers, as well as simple homogeneous or block models. With no regard to it our aim was not to strictly analyse presented phenomena, but only focus an attention of researchers upon the scale of the problem. From this point of view accepted tools and methods are fully correct and make it possible to present limitations in the exposure systems use and what is the most important, precautions in biomedical (and not only) experiments should be done.

In below presented estimations electrical parameters of animals and men were taken from [5] [6].

Biological object in a TEM cell

Studies of the effect discussed have been initiated by the authors [4]. The way of thinking was as follows: if a conducting medium close to an antenna is able to affect it's input impedance, the same phenomenon should exist in the case of any arbitrary medium. A twofold question was here formulated: what does it mean "an input impedance of a mouse" and "a mutual impedance of the mouse and it's mirror reflection", if an answer to the questions exists at all!

At the first step a cube model of a mouse immersed inside a TEM cell was studied. We assumed that the influence of the cell upon the object should be reflected by the power absorbed in it. The power is:

$$P_{abs} = 0.5\sigma \int_V E^2 dV \,, \tag{3}$$

where: P_{abs} – power absorbed by the object, σ – absorber conductivity, E – electric field intensity within the object, V - volume of the object.

Analysed homogeneous lossy model, in the form of a cube of side h = 1.5 cm, conductivity σ = 1 S/m and ε_r = 80, was immersed between two parallel, perfectly conducting plates of sizes 20x20 cm and E-field was kept constant: E = 1 V/m. Results of estimations are shown in Fig. 9. If dimensions of tested object are quite small (d>>h) P_{abs} approaches the value in the free space. However, while the object is large, as compare to d, the power may be remarkable different. The latter case has nothing common with results obtained in the free space. If distance between plates increases (ratio d/h increases) than power absorbed decreases and that means the committed error decreases.

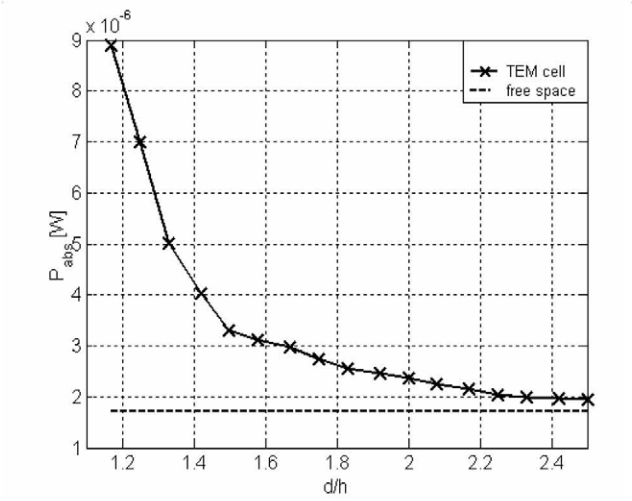


Fig. 9. Absorbed power by examined cube.

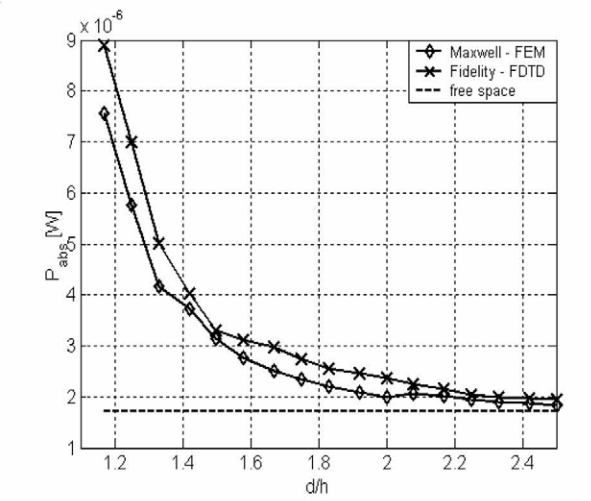


Fig. 10. Comparison of results obtained with different numerical methods.

Similar results are obtained for more complicated model (Fig. 7d) of a mouse - block model (Fig. 11) that was made of 76 cube pieces of side 1 cm. The tissue values are the same as above.

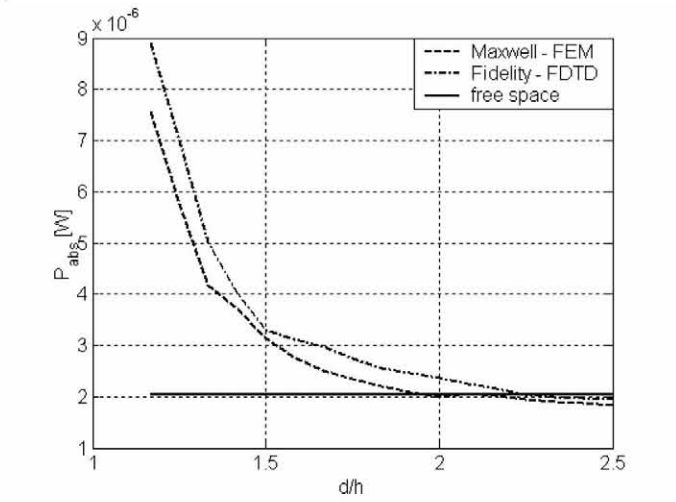


Fig. 11. Results of absorbed power by block model of a mouse.

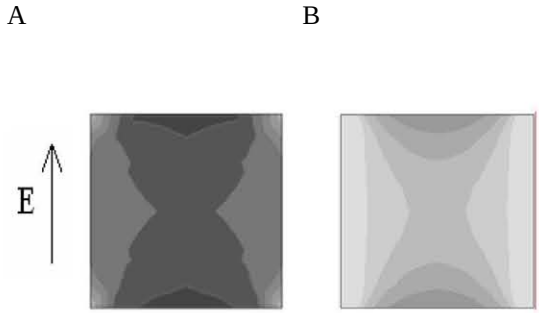


Fig. 12. Results of estimations of the E-field distribution: a) f = 100 MHz, b) f = 1 GHz.

In traditional approach, in biomedical investigations is assumed that the power absorbed within tested object is distributed homogeneously. It is not always acceptable. Lets analyse single object exposed in a TEM cell, in conditions while the proximity effects may be neglected. Results of estimations of the E-field distribution within the homogeneous cube, as described above, for two frequencies are shown in Fig. 12. Of course similar situations is for model of a man (Fig. 13). It is necessary to remind here that absorbed power, and the SAR, are proportional to E^2, that makes that their distribution inside the model is more inhomogeneous as compare to E one, shown in the figures.

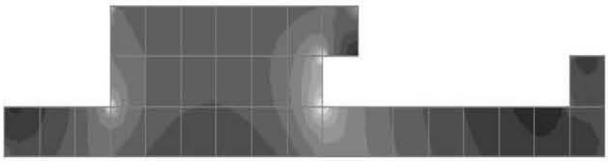


Fig. 13. Electric field inside model of a man.

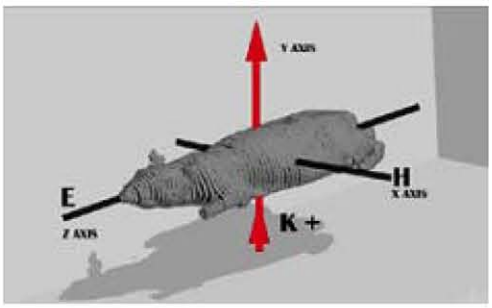


Fig. 14. Location a mouse in relation to vectors [12].

Even in the free space conditions electric field distribution inside a model is non-homogeneous, as a result can be observed fact that each of the organs absorb different power. Results of SAR, for voxel model of a rat that orientation is defined by the incident field vectors (Fig. 14), are shown in Fig. 15. The model was processed in the far-field conditions at frequency 450 MHz.

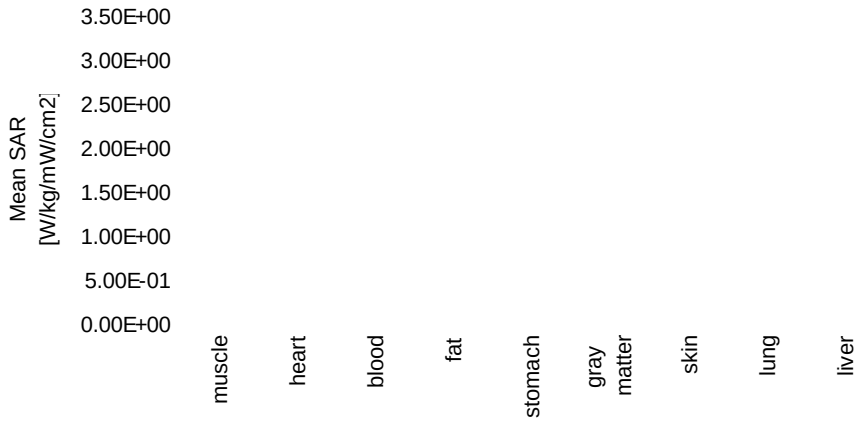


Fig. 15. SAR calculated for different organs in a one-millimetre rat model.

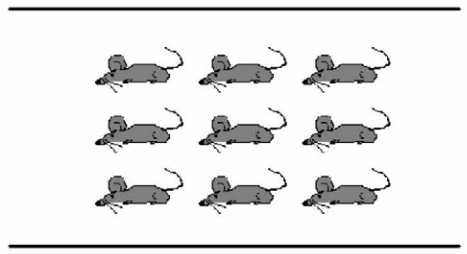


Fig. 16. TEM cell with n examined objects.

A typical condition, in biomedical investigations, is simultaneous exposure in a cell more than one object, sometimes the objects occupy whole volume of the cell. Let's consider the cell while exposed several objects in it, as shown in Fig. 16. In standard approach the power absorbed in the cell (P_{abs}) is calculated as difference of the input and the output power: P_{in} and P_{out} respectively:

$$P_{abs} = P_{in} - P_{out}\,. \tag{4}$$

Then, the power absorbed by i-th animal is calculated dividing the above by number of objects (n):

$$P_i = \frac{P_{abs}}{n}\,. \tag{5}$$

There is no proof that powers absorbed by animals are identical. A few simulations were done to illustrate the statement. Firstly we considered the case where two mice were placed inside a TEM cell (Fig. 17a). One of them is placed in the center of the exposure system and the other in the center between the first one and the wall of the system. Similarly to above estimations the mice are represented here by cubes (5x5x5 cm) that parameters are: $\sigma = 0.84$ and $\varepsilon_r = 80$. E-field intensity is constant and equals 1 V/m. Results, presented in Fig. 17b, confirm our doubts and show a magnitude of exposure estimation error while formula (5) is in use, in the worst conditions the power absorbed by mouse 2 is twice as much as power absorbed by mouse 1.

a) b)

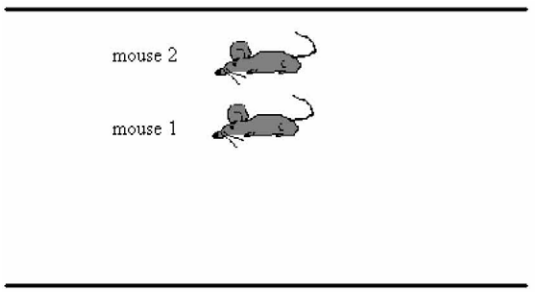
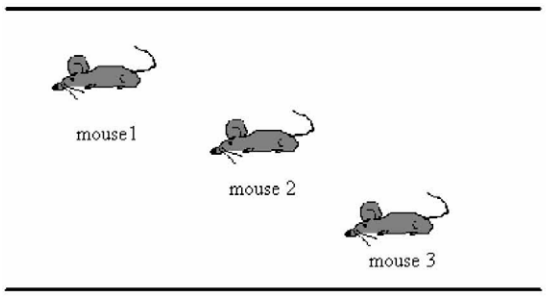


Fig. 17. Powers absorbed by two mice placed in TEM cell: a) model, b) results of calculations.

a) b)



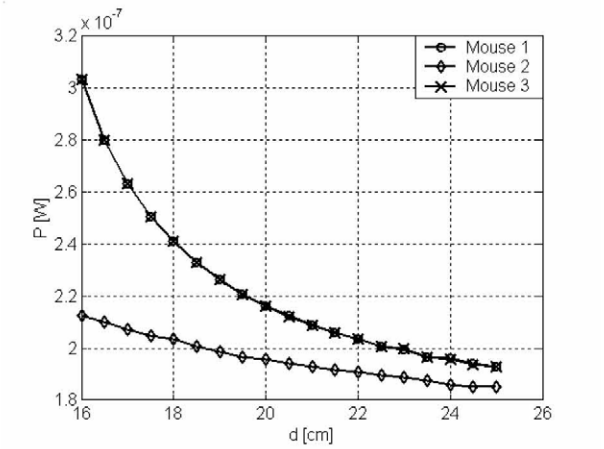


Fig. 18. Powers absorbed by three mice placed in TEM cell: a) model, b) results of calculations.

Similar effect exists in different space configuration of mice, like shown in Fig. 18. In this case the power absorbed by mouse 1 and 3 may be two times bigger than power absorbed by mouse 2. Again can be said that an assumption of identical power absorption in each examined object in discussed exposure system is not appropriate and it may lead to remarkable errors in experiments carried out in the conditions.

Conclusion

The paper discusses role of an affect, caused upon a tested object, by an exposure system due to existence of mirror reflections of the object in the walls of the system. The problem has never been considered before. The authors were inspired to start investigations in the field by estimations and experiments with the use of antennas in EMF measurements in close proximity of conducting objects or while the antennas were calibrated within a TEM cell or waveguide.

The question: what does it mean "input impedance of a mouse" remains unanswered, however, results of estimations, presented in the paper, show essential role of the phenomenon, especially in biomedical investigations while many animals are simultaneously exposed in an exposure system. Apart from different power absorbed by separate objects the absorbed power distribution within them is not homogeneous - especially at higher frequencies, even in the plane wave conditions.

Although the estimations were done for a TEM cell, their results are valid for any case while the discussed effect exists (waveguide, any conductivity media). Presented approach may allow to estimate a role of the phenomenon in any case and a possibility to refer results of exposure to the free space conditions.

Presented results lead to question:

- what is accuracy of biomedical investigations if do not take into account different exposure levels of different animals and even different their organs and tissues?
- what a way may be summarized very precise formulation of protection standards based upon such experiments?

References

[1] Ansoft, *„Maxwell 2D SV"*, simulation software for high performance electronic design http://www.ansoft.com.

[2] Chen Kun-Mu, Guru B.S., Nyquist D.P., *„Quantification and Measurement of Induced Fields Inside Finite Biological Bodies"*, Biological Effects of Electromagnetic Waves, USN/URSI Annual Meeting, Boulder, Colorado, October 20-23, 1975, pp. 19-43.

[3] Crawford M.L., *„Generation of Standard EM Fields Using TEM Transmission Cells"*, IEEE Trans. on Electromagnetic Compatibility, Vol. EMC-16, No. 4, 1974, pp. 189-195.

[4] Dlugosz T., Trzaska H., *„Mutual Interactions in EMF Dosimetry"*, International Conference and COST 281 Workshop on Emerging EMF-Technologies, Potential Sensitive Groups and Health, Graz, Austria, 20-21 April, 2006, (CD Proceedings).

[5] Federal Communications Commision, *„Tissue Dielectric Properties"*, http://www.fcc.gov/cgi-bin/dielec.sh.

[6] Gajšek P., Hurt W.D., Ziriax J.M., Mason P.A., *„Parametric Dependence of SAR on Permittivity Values in a Man Model"*, IEEE Trans. On Biomedical Engineering, Vol. 48, No. 10, October 2001, pp. 1169-1177.

[7] Gandhi O.P., Okoniewski M., *„Computation of Electromagnetic Fields in the Human Body"*, XXVIIth URSI GA, Maastricht, Netherlands, 17-24 August, 2002, (CD Proceedings).

[8] Gandhi O.P., Sedigh K., Beck G.S., *„Distribution of Electromagnetic Energy Deposition in Models of a Man with Frequencies Near Resonance"*, Biological Effects of Electromagnetic Waves, USN/URSI Annual Meeting, Boulder, Colorado, October 20-23, 1975, pp. 44-67.

[9] Grudzinski E. Trzaska H., *„EMF Probes Calibration in a Waveguide"*, IEEE Trans. On Instrumentation and Measurement, Vol. 50, No. 5, October 2001, pp. 1244-1247.

[10] Guy A.W., Johnson C.C., Lin J.C., Emery A.F., Kraining K.K., *„Electromagnetic power deposition in man exposed to HF fields and the associated thermal and physiologic consequences"*, USAF School of Aerospace Medicine, Brooks Air Force Base, Texas, Report SAM-TR-73-13, December 1973.

[11] Leicher-Preka A., Ho H.A., *„Dependence of Total and Distributed Absorbed Microwave Energy Upon Size and Orientation of Rat Phantoms in Waveguide"*, Biological Effects of Electromagnetic Waves, USN/URSI Annual Meeting, Boulder, Colorado, October 20-23, 1975, pp. 158-168.

[12] Luebbers R., Kunz K., *„FDTD99"*, ftp://starview.brooks.af.mil/

[13] United States Air Force Research Laboratory, *„EMF Dosimetry Research"*, http://www.brooks.af.mil/AFRL/HED/hedr/dosimetry.html.

[14] United States National Library of Medicine, National Institutes of Health, *„The Visible Human Project"*, http://www.nlm.nih.gov/research/visible/visible_human.html.

[15] Zeland Software, *„Fidelity”*, Electromagnetic Simulation and Electronic Design Automation, http://www.zeland.com .

ALTERATIONS IN HEMOLYSIS AFTER *IN VITRO* EXPOSURE OF HUMAN ERYTHROCYTES TO GSM900 ELECTROMAGNETIC FIELD

M. KOUZMANOVA[1], G. ATANASOVA[2], N. ATANASOV[3], S. TASHEVA[1]

[1]*Department of Biophysics and Radiobiology, Biological Faculty, Sofia University, 8 Dragan Tzankov blvd., 1164 Sofia, Bulgaria, e-mail* mkouzmanova@yahoo.com
[2]*Department of Telecommunication Technologies, e-mail* ghristova@hctp.acad.bg
[3]*Department of Wireless Communications and Broadcasting, e-mail* natanasov@hctp.acad.bg
Higher College of Telecommunications and Posts, 1 Acad. Stefan Mladenov str., 1700 Sofia, Bulgaria

Abstract

During the last decade the sources of radiofrequency electromagnetic (RF EM) radiation increased enormously both in residential and occupational environment. The study of the biological effects of RF EM radiation could contribute to better understanding of the possible health hazards. This study was designed to investigate the changes in hemolysis after *in vitro* exposure of human erythrocytes to GSM900 electromagnetic field (EMF).

Erythrocyte suspensions with two different cell concentrations (hematocrit 20% and 40 %) were exposed to EM radiation from GSM mobile phone (carrier frequency 902 MHz, 2 W output power in pulse) for 20 min. Alterations in haemolysis were registered 0, 10, 20, 30, 40, 50 and 60 min after the treatment. Hemolysis was determined by measuring the absorbance of hemoglobin at 413 nm in the supernatant obtained by centrifuging the suspensions. Hemolysis was expressed as a hemoglobin concentration.

Our data indicated statistically significant decrease in the hemoglobin level in irradiated suspensions. The GSM900 EMF exposure probably stabilized erythrocyte membrane and caused reduction in the hemolysis depending on the suspension water content (hematocrit) and on the time elapsed after irradiation.

Introduction

During the last decade the sources of radiofrequency electromagnetic (RF EM) radiation increased enormously both in residential and occupational environment. More and more people are exposed to EM radiation not only at work, but also at home. Particularly digital GSM (Global System Mobile) phones are biologically active, especially those with short, helical antennae [19]. To explore if the influence of mobile telephone is really hazardous for the human health, it is necessary to elucidate interaction mechanisms of electromagnetic field (EMF) with biological systems.

The study of the biological effects of RF EM radiation could contribute to better understanding of the possible health hazards. Research on the potential influence of EMF on living organisms and humans is performed at all different organization levels of organisms: from population studies via studies of individuals (humans and animals), cells and tissues (of humans, animals and plants; of unicellular organisms and bacteria) to the lowest, molecular level. Interaction mechanisms of low level EMF with biological systems are not clearly identified. Identifying them could help to find potential field targets in living material.

Reports from *in vitro* research indicate that low level high frequency fields may alter membrane structural and functional properties that trigger cellular responses. It was hypothesized that the cell membrane may be susceptible to low level high frequency fields, especially when these fields are amplitude modulated at extremely low frequencies [20]. There are abundant data on the effects of weak physical signals on cell functional activity. However cell targets for these signals are not established yet. Since water is the main component of biological systems and all metabolic processes take place in aqueous medium it was supposed that the minor changes in the physico-chemical properties of water could significant modify cell functional activity. The data about the effect of EMF on water specific electrical conductivity and wheat sprouting serve as an additional evidence for the hypothesis according to which the EMF-induced water structure changing is an important pathway through which the biological effect of EMF is realized [6].

Evidences for directly non-thermal interaction with living systems are obtained after investigation of the RF EMF effects on the membrane permeability [2, 15]. These effects have not been explained by integral heating of the samples. Some other mechanisms such as formation of local temperature gradients in membrane-water interface or existence of hot spots in the system should be considered [11]. Changes in the ion transport and in the osmotic fragility are considered as an indicator for alterations in the erythrocyte membrane [1, 13]. Structural alterations were found out under the action of microwaves in membranes of granulocytes [22], erythrocytes [8],

melanoma cells (B-16 melanoma) [17]. Investigations of influence of EMF on the cation transport, membrane structure and fluidity show direct interactions of the field with specific membrane macromolecules or macromolecule complexes, which very often lead to global changes in the membrane properties. Considering the frequency dependence of the effects, different models for interaction of high frequency EMF energy and membrane components were submitted. The model about absorption of EM energy from water, bounded to biomolecules, is most likely [4, 14].

Microwaves could initiate chemically important events, i.e. configurational changes, e.g. multiple transitions between closely spaced vibratory states at successively higher energy levels. In the 10^8– 10^{11}-Hz range, mono-water rotation occurs. Water-lattice vibrations (quasi-rotational or vibratory motions) may be important in the labialization of the primary and secondary structure of the biopolymers in the frequency range of 10^{11} – 10^{14} Hz. Other researchers believe bound water has a principal dispersion region in the range of 3×10^8 – 2×10^9 Hz [16].

The cell membrane, nervous cells and DNA molecules are considered in literature as most probably acceptors of microwave (MW) radiation. Cell activity and viability depend on the state of the cell membrane. Because of its unique bioelectrochemical properties the cell membrane is considered as primary acceptor of microwave radiation. A number of studies of EMF bioeffects have been performed on native and model membranes and substantial changes in membrane dielectric properties and membrane transport were reported.

Erythrocyte membrane is often used as a model membrane in investigating the structure and the functions of the biological membranes as well as in studying the influence of different physical and chemical factors on the membranes.

This study was designed to estimate the effects of GSM900 EMF *in vitro* exposure of human erythrocytes on hemoglobin release, their dependence on the suspension water content and on the time elapsed after irradiation.

Materials and methods

Erythrocyte concentrates were obtained from the National Center of Hematology and Transfusiology. Red blood cells were washed three times in 0.155 M NaCl (2000×g for 10 min). After the last centrifugation suspensions were diluted to final cell concentration – hematocrit 20% or 40%.

The exposure was performed by GSM mobile phone type NSM-3, which was connected to a personal computer through an interface cable. The mobile phone was programmed via special software to emit carrier frequency 902 MHz (60^{th} uplink channel of GSM900). The signal included standard GSM modulation. GSM signal was pulsed. The duration of the pulses was 577μs that corresponded to one time slot of TDMA frame. The TDMA frame in GSM systems has a duration 4.615 milliseconds (Fig. 1). Discontinuous transmission mode (DTX) was off during all exposures. Mobile phone pulse output power was 2 W.

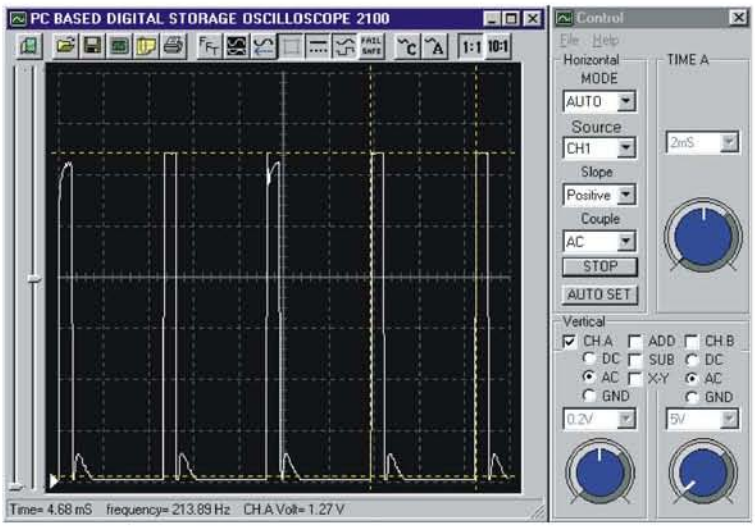


Figure 1. The emitted GSM signal, measured into mobile phone control circuit of the power amplifier.

Two milliliters of erythrocyte suspensions with different water content (hematocrit 20% or 40%) were transferred into two petri dishes (3 mm depth). One of them were control, another were exposed at 2 cm distance from the side of the mobile phone helical antenna. The exposure was 20 minutes. For eliminating of the influence of operator's hand on exposure conditions mobile phone was raised from the floor of 1 meter of the set up. The mobile phone and exposed erythrocyte suspensions were placed in the free space.

Alterations in hemolysis were registered 0, 10, 20, 30, 40, 50 and 60 min after the treatment. At given time intervals, 80 μl of the suspensions (control and irradiated) were transferred to 1.3 ml 0.155 M NaCl in Eppendorf

tubes and centrifuged at 10000rpm for 10s in a centrifuge MLW TH21. Hemolysis was determined by measuring the absorbance of hemoglobin in the supernatant at 413 nm. Hemolysis was expressed as a hemoglobin concentration (μM), calculated as follows:

$C = E\ V_2/\varepsilon\ l\ V_1$

where: C – hemoglobin concentration; E – absorbance of the supernatant at 413 nm; ε – molar extinction coefficient, for hemoglobin at λ = 413 nm ε = 120000 M^{-1} cm^{-1}; l – length of the optical way (1 cm), V_1 – volume of added erythrocytes, V_2 – final volume.

The presented data are average and standard deviations of 8 measurement of the released hemoglobin quantity for each term. The Student *t*-test was used to estimate the statistically significant differences between the experimental samples.

Results and discussion

During the study of hemolysis in the process of blood aging we observed an increase of the quantity of the released hemoglobin with the increase of the time of blood storage. After the construction of the graphics *hemoglobin / days after blood taken* for control samples it was found that the values of the released hemoglobin between 2nd and 10th days were close (Fig. 2, 3). In the latest terms the quantity of the released hemoglobin was about 5 times more than at early terms. Because of the great differences in the quantity of the released hemoglobin, averaging of the results from spontaneous hemolysis before and after 10th day of blood storage would result in large standard deviations and would mask effects of the investigated factor. Experiments related to influence of different factors on the hemolysis should be made in the first 10 days of *in vitro* storage of the blood.

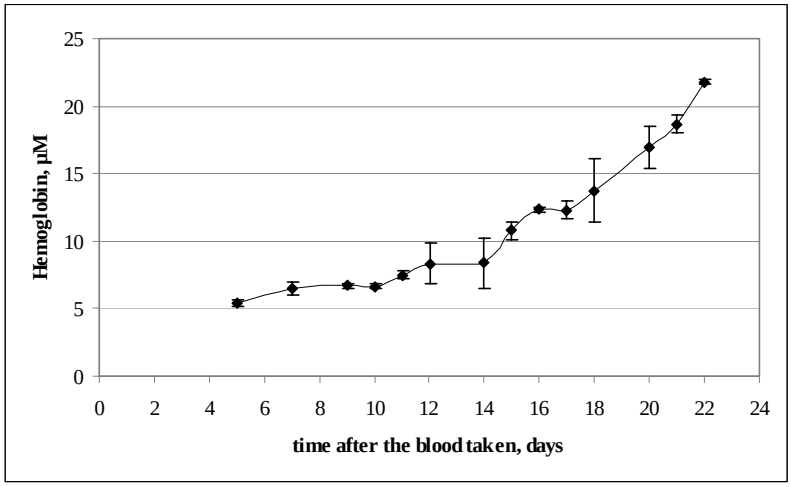


Figure 2. Quantity released hemoglobin from human erythrocytes in the process of *in vitro* blood aging (control, hematocrit 20%).

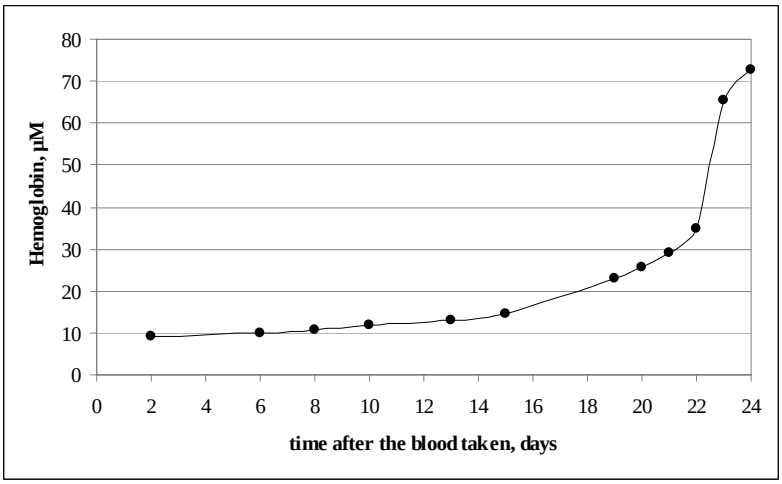


Figure 3. Quantity released hemoglobin from human erythrocytes in the process of *in vitro* blood aging (control, hematocrit 40%).

Represented data about the effects of GSM900 EMF (Figs 4, 5) are the averages and standard deviations of the values of released hemoglobin obtained in the first 10 days after the blood taken.

During the study of the hemolysis, we observed that the amount of the released hemoglobin increased with the time elapsed after the exposure to EMF both in the control and exposed erythrocytes. The differences between control and exposed cells are bigger at the beginning of the term of the blood storage at two studied hematorcits.

From the beginning of post exposure period to 60th min after irradiation the amount of released hemoglobin increased about two times in the erythrocyte suspensions with hematocrit 20%. There were no statistical significant alterations in irradiated erythrocytes immediately after termination of the exposure. Effects of EMF appeared 10 min after exposure and differences retains 30 min. There were no significant differences in the later terms (Fig. 4).

The *in vitro* exposure of erythrocyte suspensions with hematocrit 40% with GSM900 EMF for 20 min caused statistically significant decrease of the hemolysis (about 10-15%) compared to the control in all investigated terms (Fig. 5). Differences between control and exposed erythrocyte suspensions were more strongly expressed in suspensions with hematocrit 40%, which is close to physiological one (Table 1).

The obtained results showed that the EMF induces more significant changes in the suspensions with the lower water content (hematocrit 40%). These results contradict our previous results about the effects of 24 GHz MW *in vitro* exposure of human erythrocytes, where the most significant changes in erythrocyte electrophoretic mobility were observed in the suspensions with higher water content (hematocrit 20%) [12]. It is probably because the water content is of no importance in the realization of the effects of EMF on living organisms at this lower frequency (902 MHz). The decrease of the hemolysis is probably due to some stabilization of erythrocyte membrane after the irradiation with GSM900 EMF as a result of the field influence.

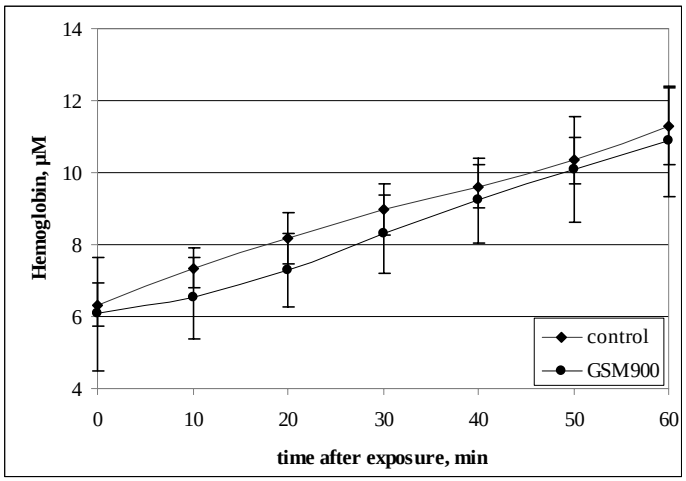


Figure 4. Quantity released hemoglobin from human erythrocytes after 20 min *in vitro* exposure to GSM900 EMF of the suspensions with hematocrit 20%.

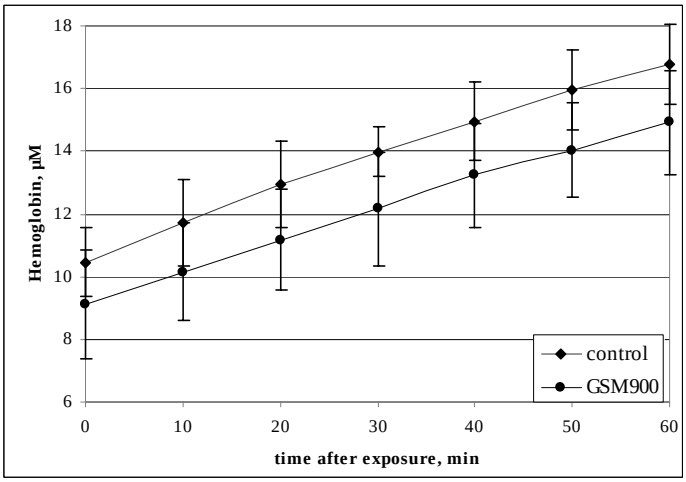


Figure 5. Quantity released hemoglobin from human erythrocytes after 20 min *in vitro* exposure to GSM900 EMF of the suspensions with hematocrit 40%.

Table 1. Rated decrease of the spontaneous hemolysis (compared to the control) and statistical significance of the differences between control and exposed to GSM900 EMF erythrocyte suspensions with hematocrit 20% and 40%.

Time after exposure, min	Hemolysis decrease compared to the control, %		Statistical significance (p)	
	Hematocrit 20%	Hematocrit 40%	Hematocrit 20%	Hematocrit 40%
0	4	15	-	0.99
10	10	13	0.98	0.99
20	11	14	0.99	0.99
30	8	14	0.95	0.999
40	10	11	-	0.99
50	3	12	-	0.999
60	3	11	-	0.999

These results are in consent with some authors. Microwave *in vitro* exposure (2.45 GHz, pulsed, power flux density: 5 mW/cm², exposure duration: 20 min, SAR: 400 µW/g) significantly decreased spontaneous hemolysis of human erythrocytes at 42°C, but had no effect at 37°C or 48°C [9]. Some authors find no effects of high frequency EMF on hemolysis. Heating erythrocytes to 43°C for 10 min with microwaves (2.45 GHz, CW, exposure duration: 15 min, SAR: 91 mW/g) or hot air did not significantly increase hemolysis, compared with hemolysis at 4°C. Hemolysis of cells coated with concanavalin A-luminol-bovine serum albumin and heated to 43°C for 10 min by use of microwaves or hot air was significantly greater than that of controls at 4°C [10]. Possible nonthermal effects of 434 MHz microwave radiation (CW, exposure duration: 6 h, electric field strength: 15 V/cm, power flux density: 100 – 600 mW/cm², time of investigation: after exposure) on human blood should be investigated *in vitro* [5]. Plasma levels of hemoglobin and sodium and potassium ions serve as an indicator of haemolysis, caused by an increased membrane fragility. Indicated by the measurements no increased membrane fragility was observed, which could be clearly assigned to nonthermal effects.

Our results contradict the results of another authors, who state that exposure to high frequency EMF increases hemolysis. Cleary et al. investigated the effects of RF irradiation (10, 50, and 100 MHz, CW, exposure duration: 2 h, electric field strength: 1; 4,5; 9 V/cm) on cation permeability and hemolysis of rabbit erythrocytes *in vitro*. Potassium and sodium release were not altered by exposure. Hemoglobin release as an indicator for hemolysis was statistically significant increased at 50 and 100 MHz at field strength of 9 V/cm. The mechanism of the observed hemolytic effect is unknown [3]. Low intensity radiation from mobile phones leads to release of hemoglobin from red blood cells and accumulation of the hemoglobin in the body could result in heart diseases or kidney stones [7]. It was found that 2.45 GHz irradiation induces a significant hemoglobin loss due to transient permeabilisation of irradiated erythrocytes rather than to their lysis [18]. The microwave induced hemoglobin loss by irradiated erythrocytes is up to 80% of the spontaneous hemoglobin loss by the controls. The rate of the increase of hemoglobin loss with increasing power density was found to be highly dependent on the initial level of spontaneous hemolysis. It seems that the membrane is as more sensitive to the radiation power as it was leaker at the start. Kinetics of hemolysis degree at three different power densities was studied. At low power densities (0.8 and 1.36 mW/cm^2) there is a quasi-linear increase of hemolysis degree with time of irradiation. At higher density (5 mW/cm^2) this tendency seems to reverse after first 10 hours of irradiation. The only reasonable explanation for this seems to be that the spontaneous hemoglobin loss of controls increases faster than that of the exposed samples. It appears like long-term irradiation would exert a protective action against spontaneous hemolysis caused by cells ageing. This observation is paralleled by the results of kinetic measurements of the osmotic resistance of irradiated erythrocytes, which show a progressive increase of the osmotic resistance with time of irradiation at exposures to 5 mW/cm^2. Sajin et al. studied the effects of long-term exposure of human blood to 2.45 GHz irradiation at athermal power densities (CW, exposure duration: 60 h (84 h kinetic measurements), power flux density: 10 mW/cm², max value (50 W/m², 25 W/m², 10 W/m², 5 W/m², 2.5 W/m², 1 W/m², 0.5 W/m², 0.25 W/m²)) [21]. A significant increase of the hemoglobin loss by irradiated erythrocytes as well as a strong dependence of the rate of the increase of hemoglobin loss on the initial level of spontaneous hemolysis were revealed. It was found that at low power densities, the hemolysis degree increases quasi-linearily with the exposure time, while at higher density (5 mW/cm²), this tendency is reversed after first 10 h of irradiation. Long-term irradiation seems to exert a protective effect against spontaneous hemolysis caused by blood ageing. The osmotic fragility test performed on samples exposed to 5 mW/cm² at different

irradiation times showed that the osmotic resistance increased in time, reaching a maximum at the end of irradiation (60 h), while the osmotic resistance of the controls was constant.

The data about the effects of EMF on hemolysis in available literature are contradictory. More research and additional methods are necessary to decide these contradictions and to explain the mechanisms of low level RF EMF interaction with erythrocyte membrane.

Summary

Our data indicate statistically significant decrease in the hemoglobin level in irradiated suspensions. The 900 MHz EMF exposure probably stabilized erythrocyte membrane and caused reduction in the hemolysis that depended on the suspension water content (hematocrit) and on the time elapsed after irradiation.

References

1. Baranski S., Szmigielski S., Moneta J., 1974, Effect of MW irradiation *in vitro* on cell membrane permeability, in: *Biological Effects and Health Hazards of Microwave Radiation*, P. Czerski, K. Ostrowski, C. Silverman, et al. (Eds.), Polish Medical Publishers, Warsaw, Poland, p. 173–177.
2. Cleary S.F., F. Garber, L.M. Liu, 1982, Effects of X-band MW exposure on rabbit erythrocytes, *Bioelectromagnetics*, 3: 453–466.
3. Cleary S.F., L.M. Liu, F. Garber, 1985, Erythrocyte hemolysis by radiofrequency fields, *Bioelectromagnetics*, 6 (3): 313–322 (*www.emf-portal.de*).
4. Cleary S.F., L.M. Liu, G. Cao, 1989, Functional alternation of mammalian cells by direct high frequency electromagnetic field interactions, in: *Charge and Field Effects in Biosystems-2*, M.J. Allen, S.F. Cleary, F.M. Hawkridge (Eds.), Plenum Press, N.Y., p. 211–221.
5. Dunscombe P.B., K. Gammampila, N.W. Ramsey, 1983, A search for nonthermal effects of 434 MHz microwave radiation on whole human blood, *Radiat Res*, 96 (2): 235–250 (www.emf-portal.de).
6. Hakobyan S., N. Baghdasaryan, A. Amyan, S. Ayrapetyan, 2001, The effect of EMF on water specific electrical conductivity and wheat sprouting, in: *Proceedings of WHO Meeting on EMF Biological Effects and Standard Harmonization in Asia and Okeania, Seul, Korea*, p.123.
7. Harris S., 1999, Now mobiles give you kidney damage, http://emfacts.com
8. Ismailov, E., 1987, Biophysical effects of VHF radiation, Moscow, p.84 (*in Russian*)
9. Kiel J.L., D.N. Erwin, 1984, Microwave and thermal interactions with oxidative hemolysis, *Physiol Chem Phys Med NMR*, 16 (4): 317–323 (*www.emf-portal.de*).
10. Kiel J.L., D.N. Erwin, 1986, Physiologic aging of mature porcine erythrocytes: effects of various metabolites, antimetabolites, and physical stressors, *Am J Vet Res*; 47 (10): 2155–2160 (*www.emf-portal.de*).
11. Kim Yu.A., Yu.V. Kim, B.S. Fomenko, E.L. Holmuhamedov, I.G. Akoev, 1989, Effects of microwave radiation on inducable ion transport of rat erythrocytes, in: *Charge and Field Effects in Biosystems – 2*, M.J. Allen, S.F. Cleary, F.M. Hawkridge (Eds), Plenum Press, New York and London, p. 223–232.
12. Kouzmanova M., M. Hristova, 2004, Effects of *in vitro* microwave exposure on electrophoretic mobility of human erythrocytes, *Annuaire de l'Universite de Sofia* (*10eme session scientifique, Sofia'03*), 96(4): 221–227.
13. Kovacs E., T. Savopol and A. Dinu, 1997, Lower Power Microwave Effects On Erythrocytes Membranes, in: *Abstract Book of II World Congress for Electricity and Magnetism in Biology and Medicine, Bologna, Italy*, p. 259.
14. Litvinov G.S., N.Ya. Gridina, G.I. Dovbeshko, et al., 1994, Millimeter wave effect on blood plasma solution, *Electro- and Magnetobiology*, 13(2): 167–174.
15. Liu L.M., F.G. Nickless, S.F. Cleary, 1979, Effects of microwave radiation on erythrocyte membranes, *Radio Sci*, 14: 109–115.
16. NCRP Reports №86, 1986, Biological Effects and Exposure Criteria for Radiofrequency Electromagnetic Fields, Recommendations of the National Council on Radiation Protection and Measurements (NCRPM), Bethesda, MD.
17. Phelan A.M., D.G. Lange, H.A. Kues, G.A. Lutty, 1992, Modification of membrane fluidity in melanin-containing cells by low-level MW radiation, *Bioelectromagnetics*, 13: 131–146.
18. Pologea-Moraru R., E. Kovacs, T. Savopol and A. Dinu, 1997, Lower power microwaves effects on erythrocytes membranes, in: *Abstract Book of II World Congress for Electricity and Magnetism in Biology and Medicine, Bologna, Italy*, p.259.
19. Prastalo R., G. Tesanovic, S. Sukalo, 2003, Mechanism of mobile phone radiation acting on biological systems, *TELSIKS, Serbia and Montenegro, Nis*, p. 675–678.
20. Repacholy M.H., 2001, Review of health effects and gaps in knowledge, in: *Proceedings of WHO Meeting on EMF Biological Effects and Standard Harmonization in Asia and Okeania, Seul, Korea*, 33–42.
21. Sajin G., E. Kovacs, R.P. Moraru, T. Savopol, M. Sajin, 2000, Cell membrane permeabilization of human erythrocytes by athermal 2450-MHz microwave radiation, *IEEE Trans Microwave Theory Tech*; 48 (11): 2072–2075 (*www.emf-portal.de*).
22. Szmigielski S., 1975, Effect of 10 cm (3 GHz) electromagnetic radiation (microwaves) on granulocytes *in vitro*, *Annals NY Acad Sci*, 247: 275–281.

ANALYTICAL METHOD FOR HUMAN EXPOSURE ASSESSMENT TO SHORT RANGE DEVICES

DINA SIMUNIC AND DAMIR ZRNO

UNIVERSITY OF ZAGREB, FACULTY OF ELECTRICAL ENGINEERING AND COMPUTING, UNSKA 3, HR-10000 ZAGREB, CROATIA

Abstract

Electromagnetic dosimetry and exposimetry quantify electromagnetic fields inside and outside of the biological material, i.e., human body, respectively. They are primarily used for evaluation of human exposures due to various devices generating electromagnetic fields. The both: dosimetry and exposimetry have their bases in experimental and/or numerical methods. In this paper a proposed new formula for a *SAR* of short-range radio-frequency devices in multiple reflection environment has been developed. The involved scenario assumed semi-infinite plane with properties of homogeneous muscle. The shown results indicate that a reliable human exposure assessment in the indoor environment requires an application of deterministic numerical methods, capable of calculation of multiple reflection conditions, such as ray-tracing.

Introduction

Dosimetry and exposimetry of high-frequency fields have been investigated for a number of years in variously shaped object, like the prolate spheres [1] and spheres [2]. The dipole-type normal excitation has been studied in the semi-infinite slab [3], even under near-field conditions [4]. Human body in vicinity of wireless communications devices acts as a disturbing element of wireless communications systems performance [5]. On the other hand, biological effects of electromagnetic fields are being investigated also for a number of years [6]. Some numerical techniques, which are excellent tools for a calculation of deposited electromagnetic energy in the human body, like FDTD, are being extensively used throughout years [7]. Insofar, the attention has been mostly focused to cellular telephony. The constant development of new wireless technologies introduces presence of wireless technologies in the total human environment, which further complicates calculations of deposited electromagnetic energy. This paper presents an analytically developed SAR formula for multiple reflections conditions, natural to indoor environment.

Oblique incidence of plane wave

Let us suppose that tissue is a homogeneous material, so that it acts like a semi-infinite plane to the impinging

electromagnetic wave. The considered technology is in the ISM frequency range of short range devices (SRD), i.e., ISM part at 2.5 GHz. Analytical formulas have been derived for *SAR* of the SRD base stations. The SRD technology usually uses half-wave antennas, which allows us to conclude that all the calculations related to human exposure to SRD base stations have to be performed for far-field propagation conditions. For a plane wave travelling in air (Fig. 1), induced SAR at a planar interface air/tissue is defined by tissue mass density ρ, tissue conductivity σ, tissue impedance (Z_t) and power density in the tissue (S_t):

$$SAR = \frac{\sigma}{\rho}\left(S_t Z_t\right) \tag{1}$$

Fig. 1 shows a vertically polarized EM wave impinging obliquely the air/tissue interface. Air is characterized by μ_0, ε_0; tissue by μ_0, ε_r, σ.

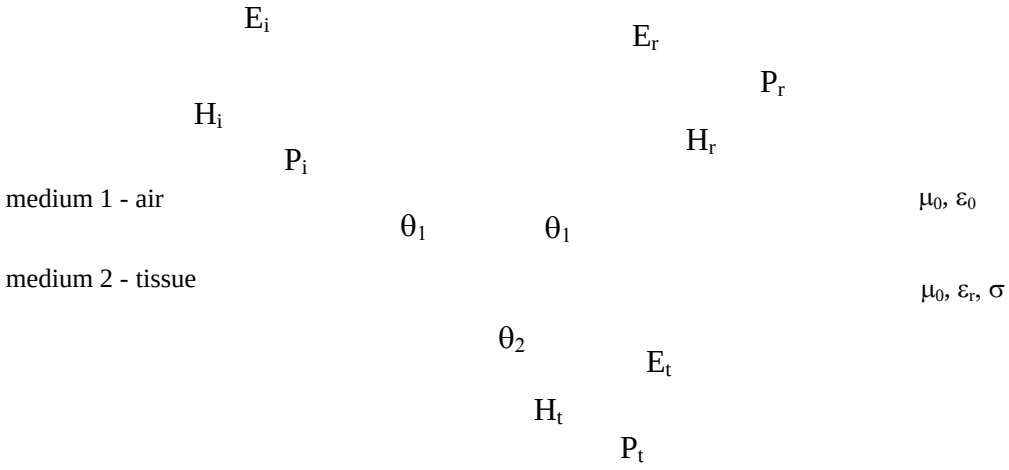


Fig. 1 Oblique incidence of a vertically polarized wave

Transmitted power density in the tissue (S_t) is defined as a difference of the incident (S_{inc}) and reflected (S_{refl}) power density:

$$S_t = S_{inc} - S_{refl} \tag{2}$$

The transmitted power density, S_t, is at the air-tissue interface defined in terms of S_{inc} by a reflection coefficient Γ:

$$S_t = S_{inc}\left(1 - \Gamma^2\right) \tag{3}$$

SAR is defined at the air-tissue interface as:

$$SAR = \frac{\sigma}{\rho} S_{inc} Z_t \left(1 - \Gamma^2\right) \tag{4}$$

Tissue impedance, Z_t, is for the plane wave exposure defined by tissue conductivity, σ, tissue permittivity, ε_r, tissue permeability, μ_0 and angular frequency, ω:

$$Z_t = \frac{\mu_0}{\varepsilon_r \varepsilon_0 - j\frac{\sigma}{\omega}} \tag{5}$$

Reflection coefficient depends on a wave polarization. For a vertically polarized wave impinging obliquely tissue, Γ_v, is defined by an incident angle (θ_1), free space permittivity ε_0, tissue conductivity σ, tissue permittivity ε_r, and angular frequency, ω:

$$\Gamma_v = \frac{\sin\Theta_1\left(\varepsilon_r - j\frac{\sigma}{\omega\varepsilon_0}\right) - \left(\varepsilon_r - j\frac{\sigma}{\omega\varepsilon_0}\right) - \cos^2\Theta_1}{\sin\Theta_1\left(\varepsilon_r - j\frac{\sigma}{\omega\varepsilon_0}\right) + \left(\varepsilon_r - j\frac{\sigma}{\omega\varepsilon_0}\right) - \cos^2\Theta_1} \tag{6a}$$

Reflection coefficient for horizontal polarization Γ_h is slightly differently defined:

$$\Gamma_h = \frac{\sin\Theta_1 - \left(\varepsilon_r - j\frac{\sigma}{\omega\varepsilon_0}\right) - \cos^2\Theta_1}{\sin\Theta_1 + \left(\varepsilon_r - j\frac{\sigma}{\omega\varepsilon_0}\right) - \cos^2\Theta_1} \tag{6b}$$

The graphs for the both reflection coefficients, depending on the incident angle, are given in Fig. 2.

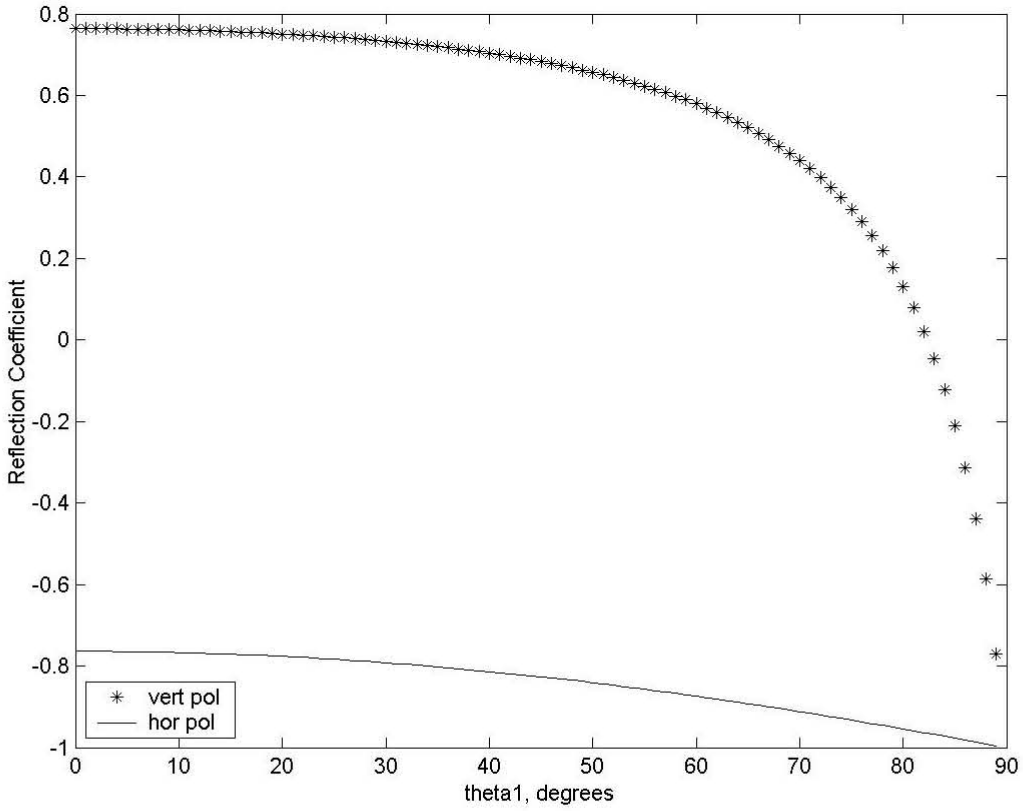


Fig. 2 Calculated reflection coefficient for vertically and horizontally polarized impinging wave

SAR in the tissue for a vertically polarized wave is defined as:

$$SAR_{\mathrm{v}} = \frac{\sigma}{\rho}\left(S_{\mathrm{inc}} \frac{\omega\mu_0}{\sigma^2 + \left(\omega\varepsilon_{\mathrm{r}}\varepsilon_0\right)^2} \left(1 - \frac{\sin\Theta_1 \left(\varepsilon_{\mathrm{r}} - j\frac{\sigma}{\omega\varepsilon_0} \right) - \left(\varepsilon_{\mathrm{r}} - j\frac{\sigma}{\omega\varepsilon_0} \right) - \cos^2\Theta_1}{\sin\Theta_1 \left(\varepsilon_{\mathrm{r}} - j\frac{\sigma}{\omega\varepsilon_0} \right) + \left(\varepsilon_{\mathrm{r}} - j\frac{\sigma}{\omega\varepsilon_0} \right) - \cos^2\Theta_1} \right)^2 \right) \quad (7a)$$

For a horizontally polarized wave *SAR* in the tissue is defined as:

$$SAR_{\mathrm{h}} = \frac{\sigma}{\rho}\left(S_{\mathrm{inc}} \frac{\omega\mu_0}{\sigma^2 + \left(\omega\varepsilon_{\mathrm{r}}\varepsilon_0\right)^2} \left(1 - \frac{\sin\Theta_1 - \left(\varepsilon_{\mathrm{r}} - j\frac{\sigma}{\omega\varepsilon_0} \right) - \cos^2\Theta_1}{\sin\Theta_1 + \left(\varepsilon_{\mathrm{r}} - j\frac{\sigma}{\omega\varepsilon_0} \right) - \cos^2\Theta_1} \right)^2 \right) \quad (7b)$$

Fig. 3 shows calculated surface *SAR* in dependence of impinging angle, θ_1, with used electrical parameters in the 2.45 MHz frequency band for the homogeneous all-muscle model (ε_{2r} = 53.57, σ_2 = 1.81 S/m, and ρ = 1040 kg/m^3) for the both polarizations.

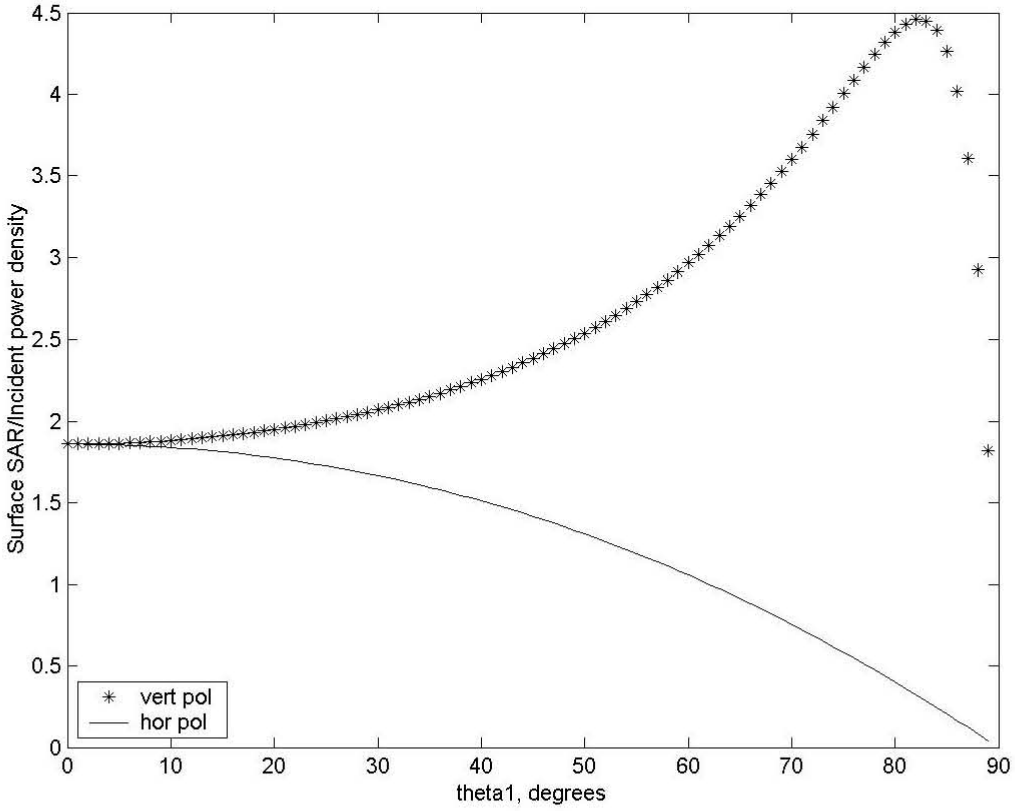


Fig. 3 Calculated ratio of surface *SAR* and incident power density in dependence of vertically and horizontally polarized obliquely impinging angle, θ_1, at 2.45 GHz, with electrical properties of homogeneous all-muscle model

The results indicate that for a range of incident angles the ratio of surface *SAR* and incident power density depends highly on the polarization and on angle of incidence.

Multiple oblique incidence of plane waves

In the case of multiple reflections environment, where all reflected and transmitted components have a general arrangement and thus statistical phase difference, it is necessary to define a position of human body in the indoor space. Fig. 4 depicts a situation with only one barrier (e.g., a wall), which is placed at a distance ζ from the human being.

Even under these very especial and simplified circumstances (only one perfectly conducting wall), the analytical calculation of the reflected components of electric field is quite complex. The reflected field is calculated from a number of reflected components, i.e., the first reflection E_{1r}, the second reflection E_{2r},... the n-th reflection E_{nr}, by using incident field (E_0), reflection (Γ) and transmission coefficient (T), as given by Eqs. (8a-n).

$$E_{1r} = E_0 \Gamma e^{j\omega t} \tag{8a}$$

$$E_{2r} = E_0 T\Gamma' T' e^{j(\omega t-\zeta)} \tag{8b}$$

$$E_{3r} = E_0 T\Gamma'^3 T' e^{j(\omega t-2\zeta)} \tag{8c}$$

…

$$E_{nr} = E_0 T\Gamma'^{(2n-3)} T' e^{j(\omega t-(n-1)\zeta)} \tag{8n}$$

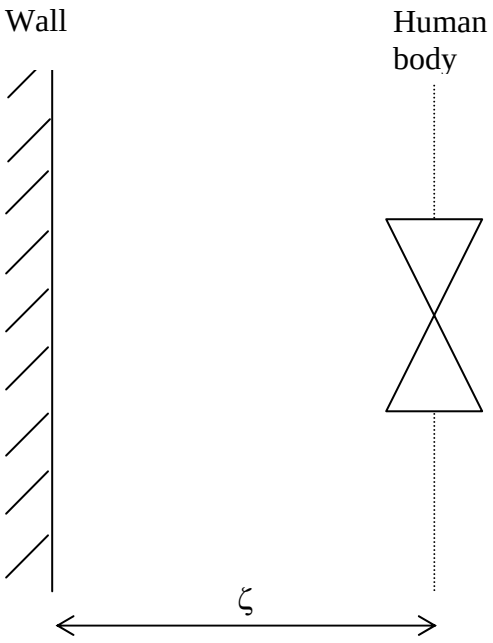


Fig. 4 Human body in a reflective environment with only one wall

Reflection and transmission coefficient depend on polarization and incidence angles. Reflection coefficient for vertically polarized field is given by:

$$\Gamma_{vm} = \Gamma_{1v} \frac{\left(\omega\varepsilon_0\left(\varepsilon_r - \cos^2\Theta_1\right) - j\sigma\right)\left(1-\Gamma_{1v}^2 t_d^2 t_s\right) - t_d^2 t_s \sin^2\Theta_1\left(1-\Gamma_{1v}^2\right)}{\left(\omega\varepsilon_r\varepsilon_0 - j\sigma\right)\cos^2\Theta_t\left(1-\Gamma_{1v}^2 t_d^2 t_s\right)} \tag{9a}$$

Reflection coefficient for horizontally polarized field is defined as:

$$\Gamma_{hm} = \frac{\Gamma_{1h}\left(1-t_d^2 t_s\right)}{1-\Gamma_{1h}^2 t_d^2 t_s} \tag{9b}$$

Fig. 5 shows reflection coefficients for the multiple incidence of waves of the both polarizations.

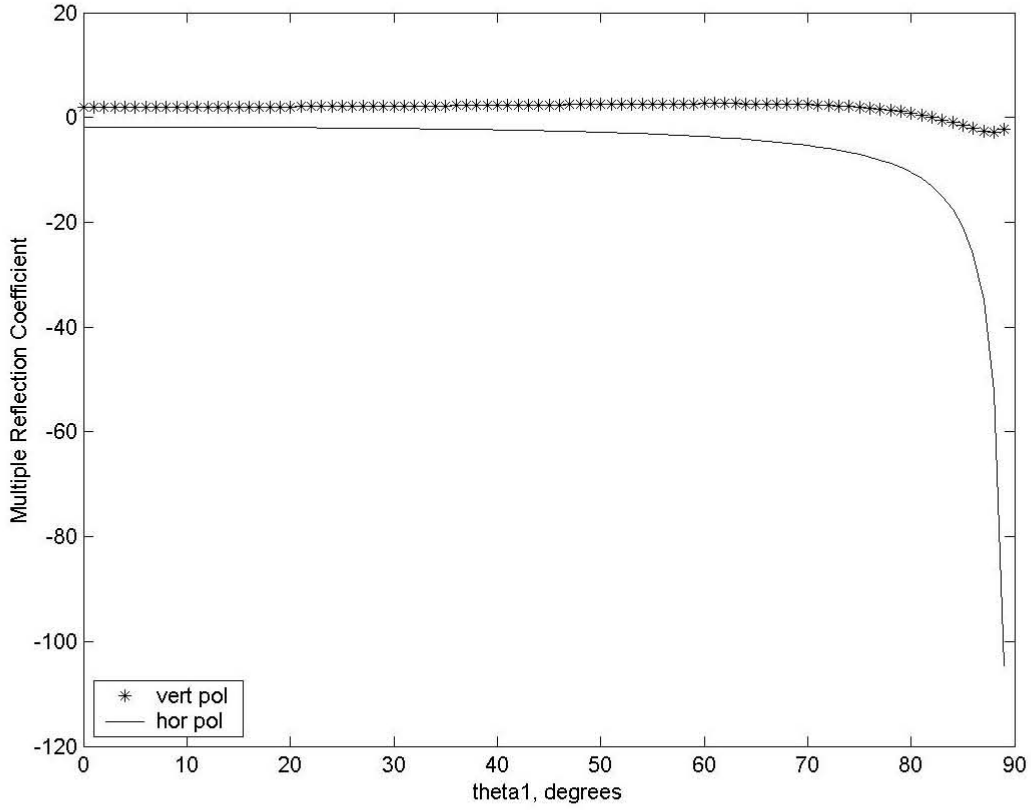


Fig. 5 Calculated reflection coefficient for multiple incidence of vertically and horizontally polarized wave

Results of application of relation (4) for *SAR* with the reflection coefficient of multiple reflection of electromagnetic waves (9a) and (9b) are shown in Fig. 6.

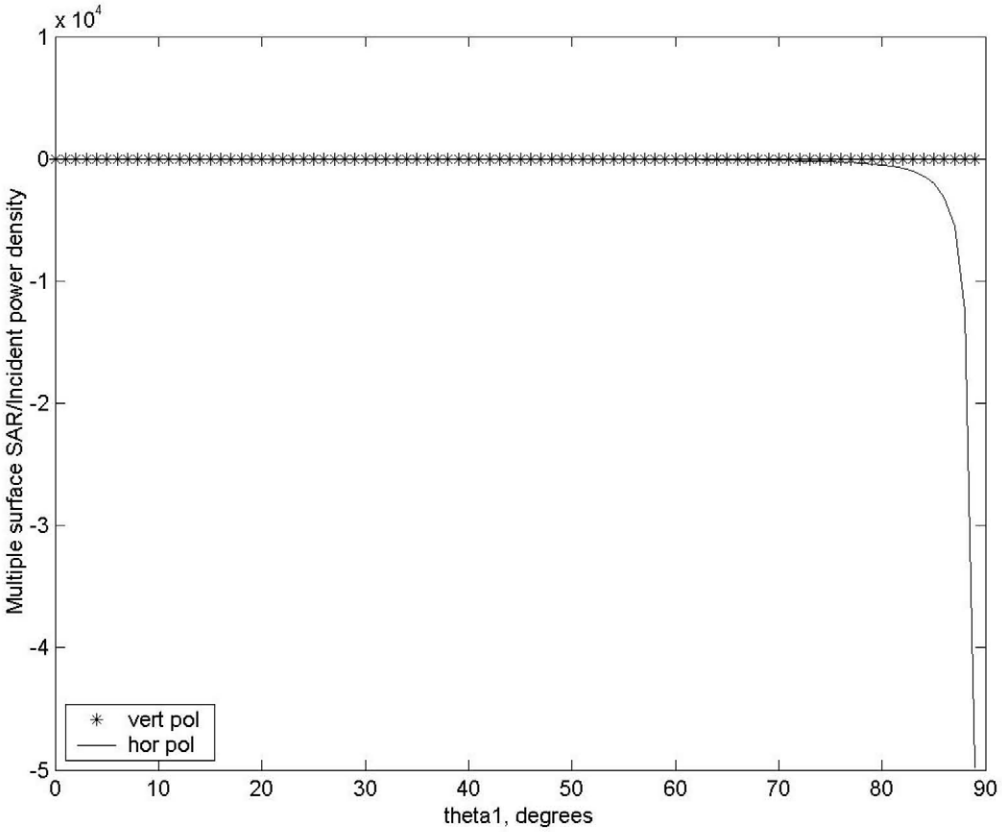
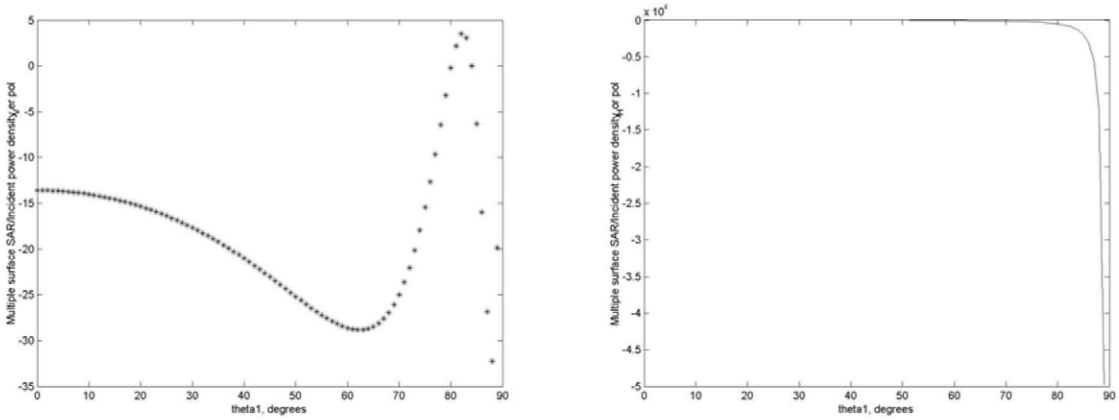


Fig. 6 Calculated ratio of surface *SAR* and incident power density in dependence of incident angle θ_1 of vertically and horizontally polarized obliquely impinging wave at 2.45 GHz, with electrical properties of homogeneous all-muscle model, for multiple reflection

The results on Fig. 6. show that for a range of incident angles the surface *SAR* is equal to incident power density except for horizontal polarization for angles higher than approximately 75 degrees.



a. b.

Fig. 7 Calculated ratio of surface *SAR* and incident power density in dependence of incident angle θ_1 of vertically (a) and horizontally (b) polarized obliquely impinging wave at 2.45 GHz, with electrical properties of homogeneous all-muscle model, for multiple reflection

Further inspection into the calculated results shows that there are differences in calculation of *SAR* for vertically polarized wave, following the reflection coefficient, where it can happen that for some angles (e.g., 82 degrees) the value of total *SAR* is up to 3.5 times higher than for the normal incidence.

These results show that for the relevant *SAR* calculation as many reflections as possible have to be taken into account. Also, it if utmost importance to realize that calculation of normal incidence of electromagnetic fields does not indicate the so-called “worst-case” *SAR*.

Summary
The formula for *SAR* has been developed under the conditions of multiple reflections in a semi-infinite plane with electrical properties of homogeneous all-muscle model. The calculated results show that at certain incidence angles the *SAR* values for vertically polarized wave can be up to 3.5 times higher than for the normal incidence. Thus, if is of importance for *SAR* calculation in multiple reflective environment, such as indoor, to take into account as many reflected rays as possible. This can be performed by introducing numerical methods, such as ray-tracing [9],[10].

References
[1] Iskander MF, Barber PW, Durney CH, Massoudi H. 1980. Irradiation of prolate spheroidal models of humans in the near field of a short electric dipole. IEEE Trans. on MTT. 28(7):801-807
[2] Kritikos HN, Schwan HP.1972. Hot spots generated in conducting spheres by electromagnetic waves and biological implications. IEEE Trans. Biomed. Eng., 19:53-58.
[3] Chatterjee I, Gandhi OP, Hagmann MJ, Riazi A. 1980. Plane-wave spectrum approach for the calculation of electromagnetic absorption under near-field exposure conditions. Bioelectromagnetics, 1:363-377.
[4] Kuster N, Balzano Q. 1992. Energy absorption mechanism by biological bodies in the near field of dipole antennas above 300 MHz. *IEEE Trans Vehicular Technol*, 41(1):17-23.
[5] Ziri-Castro KI, Scanlon WG, Evans NE. 2004. Indoor Radio Channel Characterization and Modeling for a 5.2-GHz Bodyworn Receiver. *IEEE Antennas and Wireless Propagation Letters*, 3:219-22.
[6] Radiofrequency Radiation Dosimetry Handbook, Fourth Edition, *USAF School of Aerospace Medicine, Aerospace Medical Division (AFSC), Brooks Air Force Base*, October 1986.
[7] Kunz KS, Luebbers RJ. The finite difference time domain method for electromagnetics, CRC Press, Boca Raton, FL, 1993.
[8] Sullivan DM, Borup DT, Gandhi OP. 1987. Use of the finite-difference time-domain method in calculating EM absorption in human tissues. *IEEE Trans. Biomed. Eng.*, 34:148–57.
[9] Zrno D, Šimunić D. 2003. Matrix Based Ray-Tracing Model for Indoor Propagation, ICECOM 2003. Dubrovnik, pp. 221-224
[10]Simunic D, Zrno D. A Novel Method for Electromagnetic Dosimetry Related to Human Exposure from Short-Range Devices. Submitted to Journal for Ecodynamics.

FULFILLING THE OCCUPATIONAL HEALTH TRAINING REQUIREMENTS OF EU DIRECTIVE 2004/40/EC

MICHAEL BANGAY
Radhaz Consulting Pty Ltd
Suite 5, 8 Clay Drive, Doncaster, Victoria 31 Australia
michael@radhaz.com.au

Abstract

This paper addresses the application of the European Union Directive 2004/40/EC in respect to worker information and training. The Directive has placed obligations on employers to protect their workers from risks to their health and safety arising from their workplace exposure to electromagnetic fields. Employers are required to meet particular health and safety requirements that include exposure assessment and worker training. This paper sets out an approach that achieves the employee training and information objectives described in Article 6 of Directive 2004/40/EC. An overview of training material provided in Australia by the author of this paper to meet similar requirements to Article 6 is presented.

Introduction

Governments around the world are reacting to the growing concerns over exposure to electromagnetic fields. While much of the concern has centred around the public's exposure to magnetic fields around high voltage power lines, mobile telephone emissions and radiated signals from telecommunications towers, there are new endeavours to address worker safety. Hazards associated with high-level exposure to radiofrequency (RF) fields have been well understood for many years. While the issue of injuries resulting from radiated low frequency fields like those around electrical power infrastructure is less clear, injuries caused by radiated RF fields and associated currents is quite clear and requires a response to protect both the employee and employer. The understanding about RF hazards and the way it can cause heating and burns extends back into the early days of radio use. Safety standards to guard against the heating effects of RF radiation have been in place for almost fifty years. The current preoccupation over possible athermal health effects alleged to be caused by exposure to levels of RF below the ICNIRP limits has possibly come at the expense of a more appropriate response to known RF hazards that need to be controlled.

During the mid 1980's Australia's government owned national telecommunications company faced a major occupational health and safety crisis with maintenance and installation staff refusing to climb masts/towers for fear that they may be physically harmed by the RFR radiation. The company responded by initiating a well-resourced hazard management program that included a hazard assessment and staff training. The training program has been continually refined over the past 20 years to produce training that establishes safe working procedures for all RF workers. This paper provides an outline of the training program conducted by Radhaz Consulting Pty Ltd over the past eight years.

Employers have an obligation to carryout an assessment of RF exposure levels around devices that emit RF radiation to determine if there is a risk that must be managed. Generally, a potential hazard is defined as an exposure situation that allows a worker to be exposed to levels that are in excess of the exposure limit values described in the Annex of Directive 2004/40/EC which were obtained from the ICNIRP guidelines ICNIRP7/99. These values are described as the occupational exposure limits and do not apply to members of the public. It is assumed that exposed workers have an intelligent awareness of the hazard and have their exposure controlled as a consequence of good engineering design, safe work procedures and training.

The initial assessment of the hazard by the employer to determine compliance or otherwise forms the basis of the measures needed to control the hazard. Depending on the circumstances, the assessment may be either performed by calculation or by measurement. Measurement is generally preferred for

frequencies below 110 MHz due re-radiation situations and the need to determine touch or induced current levels. The hazard assessment will determine the critical issues of frequency, applicable limit units and exclusion distance boundaries. For this reason the assessment should be performed by organisations with proven competences with accreditation from a suitable body. The accreditation requirements should ensure that the procedures, tools, instrumentation and personnel are of a sufficient standard to make certain that the assessment is credible.

Once an employer has established the possibility of a hazard there is an "duty of care" or obligation to control the hazard and apply the hierarchy of control these are:

- Elimination
- Substitution
- Isolation
- Engineering controls
- Administrative procedures
- Protective clothing and equipment

Concurrent with of the control the hazard is the education of the employees so that when they work with potentially high levels of RF radiation they may intelligently apply safe work procedures. In summary, the training of workers should cover the following topics:

- The properties of radiofrequency radiation
- The biological effects
- The safety standards that provide protection
- Clear presentation of the areas of high exposure in the worker's workplace
- Safe work procedures
- The characteristics of an RF source that effect exposure

Properties of Radiofrequency radiation

Most workers do not have an adequate understanding of the properties of RF radiation. It is neither practical nor necessary to give workers a comprehensive or scientific understanding of RF radiation. However, it is appropriate to describe the relevant properties that may cause health effects and remove the misunderstanding that can cause unnecessary worry and disruption to the workplace. Some of the fundamental properties that need to addressed are:

- RF radiation is part of the electromagnetic spectrum
- RF fields are energy waves composed of electric and magnetic fields that can be modulated
- The waves are described by their frequency/wavelength and intensity
- RF radiation is part of the non-ionising spectrum and not like the ionising part of the spectrum that includes x-rays, gamma rays and UV light
- RF radiation is not the same as power frequency magnetic fields
- Is more similar to IR light in that the main known effect is heating

Biological effects

The knowledge regarding the known short-term effects about RF radiation is well established. This knowledge should have a direct bearing on the work practices of employees who are exposed to it during the course of their employment. The WHO has identified three known effects where there is an extensive body of scientific evidence to support their existence. These effects are: tissue heating by various mechanisms, neuro-stimulatory and acoustic. When describing these effects it is important to point out the influence of frequency showing that the level of absorption and the effect are related to frequency.

The neuro-stimulatory effect that is caused by the induced RF currents in tissue stimulating the nerves and causing an involuntary reaction is limited to frequencies of about 100 kHz and is more related to those workers who work with induction heaters.

The acoustic effect is a particular phenomenon that manifests itself as a clicking or buzzing in then ears when the exposed person is subjected to high power pulsed microwave fields like those around radar antenna. While this is an established phenomenon, it is quite rare to encounter the exposure situation that generates this effect.

Of greater importance are the heating effects which can range from cataracts, burns and heat exhaustion. It is this particular effect where most importance should be directed as it is relevant to most

workers who are employed in the field of radio communications and broadcasting along with manufacturing industries that use RF welding and drying equipment. The more serious injuries that generally occur are a consequence of high limb or contact currents that cause burns or nerve damage. High currents are generally through physical contact with a reradiating metal objects or live conductors/antenna elements. There are many documented cases where RF welder operators have received bad burns that require medical involvement. Similarly, workers who work around high power MF, HF and VHF broadcast antennas have received bad burns though contacting live conductors and reradiating guy wires.

While the more serious injuries occur as a result of contact currents, whole body heating can occur as a result of being in a strong ambient field like that around a HF broadcast antenna. The heating effects will be felt as either a localised heating more commonly in the ankles and lower leg or as a core temperature rise in the body that if allowed to continue would result in heat exhaustion.

While many workers express the concern that RF exposure may lead to male fertility effects, eye damage and cancer induction, it is important that the training puts these concerns in their proper perspective and alleviate unnecessary worry. It would require extremely high levels of sustained exposure that is well above the ICNIRP limits to cause eye damage and short-term fertility effects. There is no substantiated scientific evidence that RF causes cancer.

An important part of training is to raise the issue of medical implants that may be either metal rods as in the case of bone breakages or active devices like pacemakers. In these circumstances workers are advised to speak with medical specialist before working in areas that have high fields. Similarly, the issue of pregnancy needs to be addressed. Some authorities consider the unborn child for purposes of the exposure limits to be a member of the general public that consequently requires the mother to restrict her exposure to the general public limits. Should this approach be taken it would be necessary for pregnant workers to notify their employer with the intention of ensuring that their work place exposure does not exceed the general public limits.

Safety standards

Article 6 of the EU Directive requires workers to be provided with information about “the values and concepts of the exposure limit values and action values”. This component of the training creates a potential challenge for workers in the various industries using RF radiation. Quite often workers do not have an educational background or familiarity with the units of measurement that would otherwise enable them to understand the measurement terms. While it is simple to present a table with exposure frequencies and related limit values it is necessary to provide an explanation for the concepts. The key points to present are:

- Exposure limit values which ICNIRP calls Basic Restrictions which relate to power density at the skin’s surface, energy and current densities in the body which are not easily measured. Although important at a theoretical level, exposure limit values need not be taught in much depth.
- Action values are described by ICNIRP as Reference Levels and are the units of measurement for the physical quantities of electric and magnetic field strength, equivalent plane wave power density, contact current and induced limb current. Measurement of these quantities will determine compliance with the limits. A clearer understanding of action values needs to be given to those workers participating in training.

A successful method used by the author when conveying the concepts of action values is to build on knowledge of common every-day experience. This method includes using the analogy of radiated heat from an electrical radiator and the use of a domestic microwave oven to heat food. This allows more complex and less familiar concepts to be built on the knowledge of familiar and readily understood experiences.

Clear presentation of exposure areas in the worker’s workplace

A further requirement of the Directive is that workers receive the results of the exposure assessment. This requirement logically seeks to provide the worker with an understanding of where the areas of non-compliant exposure occur so that they may avoid those areas. The adoption of a common reporting format of hazard zones greatly simplifies this aspect worker information. A common graphical presentation that is gaining worldwide acceptance and is standard practice in Australia is to show site/building plans marked with two colours. The colour yellow depicts areas where the exposure

levels exceed the time averaged ICNIRP general public limits but are less than the occupation exposure limits. The colour red on the drawing shows the areas where the time averaged exposure levels are in excess of the occupational exposure limits. The use of simplified colour coded scale drawings enables workers to understand the hazardous areas without having to interpret units of measurement. Employers who provide a graphical presentation of hazard areas will fulfil their requirement to assess/map exposure areas and also provide the necessary hazard assessment information to their workers.

Australia has developed a standard reporting format for identifying RF hazard zones around transmitting antennas. The assessment report is known as a radio communications site management book (RCSMB) and finds its major use with radio systems that enable calculation of the exposure levels based on antenna gain/aperture and input power. The RCSMB is also suitable for use where exposure levels are determined by measurement and its format allows its use for industrial applications of RF. The RCSMB is the one document that addresses all of RF safety issues related to a particular site. The RCSMB contains the following sections:

1. **Site Contact Details -** *who should be contacted when any information is required*
2. **Site RF EME Diagrams –** *plan and elevation drawings showing exclusion zones*
3. **Site Access Control** - *Access Control Procedure - RF Hazard Warning Signs Installed - Special Requirements / Local Rules*
4. **Equipment Installed at this Site -** *Summary of Physical Equipment Installed - Equipment List*
5. **Site Specific Documents –** *Photographs – additional measurements*
6. **Safe Work Procedure –** *The procedures that need to be followed to ensure a safe workplace*
7. **Additional Information Sources –** *generic RF hazard information – web based information etc*

Safe work procedures

Every worker whose duties require them to access areas of RF exposure that exceed the ICNIRP general public limits need to have a written set of understandable safe work procedures. The procedures can be generic and applicable for all RF workplaces. The procedures should include:

- Read the site safety documentation (RCSMB)
- All workers accessing the area must be trained
- All workers entering the area must be authorized
- Obey all warning signs
- Assume all RF sources/antennas are active
- Have transmitters/sources locked out/disconnected before working on them
- Do not pass in front of the radiating faces of antennas, always pass behind/below
- Use personal RF monitors (PPE) when working around transmitting antennas or unfamiliar antennas. Note: specific training is a prerequisite for correct use

The characteristics of an RF source that effect exposure

The majority of sites will not have sufficient documentation to identify the hazard zones and it will be up to the worker to conduct their job safety analysis (JSA). Training needs to provide a basic understanding of the properties and characteristics of RF transmitting sources/antennas. This will enable workers to enter a site and generally determine where potential hazard zones exist. An important part of this training is to educate workers about transmitting antennas. The training material on antennas should not be at an engineering level or involve complex mathematics. Rather, it should focus on the physical differences that allow antennas to be defined to be either omni directional or directional with the emphasis on where potential hazard zones exist. A brief introduction to the calculation of radiated power flux levels should be given with attention being given to the three variables in the equation. The variables of gain, power and distance from the source should be explained in sufficient detail to enable the worker to see how these variables may effect their exposure.

Summary

Training for workers who work around RF transmitting sources is essential for their safety. It is possible to pitch the training material at an educational level that captures the majority of workers. The use of graphical materials (power point slides) and analogies from every day life will help most workers meet the training objectives. Wherever possible, workers should be encouraged to discuss their experiences and draw on their knowledge during group discussions. The training should not be delivered as a lecture; preferably, the training should be presented as small group training.

The training can be delivered in less than one day (4 – 6 hr) and should be accompanied by a comprehensive set of training notes. The training objectives need to be clearly stated with a written assessment conducted at the conclusion of training. A certificate should be issued if the assessment indicates correct understanding of the material.

Where possible the material should be accredited by an external educational/advisory organisation. The person conducting the training should be able to demonstrate an in depth knowledge of the material and have obtained formal training qualifications.

Acknowledgements

Australian Centre for RF Bioeffects Research: Specification of Key Learning Objectives for Training on RF EME Awareness & Operating Procedures.

TRANSPARENCY FORUM - A RISK COMMUNICATION PROJECT IN SWEDEN

L. Mjönes and Lena Hyrke

Swedish Radiation Protection Authority
SE-171 16 Stockholm, Sweden

Abstract

The roll-out of the third generation system for mobile telephony has been fast in Sweden. The decision to build the UMTS system, 3G, was taken in 1999. In spring 2006 the population coverage for the system was over 90 percent. The rapid launching has created concern and opposition among parts of the general population. During 2004 and 2005 the Swedish Radiation Protection Authority, SSI, has arranged the "Transparency Forum", TF, a series of three open seminars regarding the 3G roll-out where all stakeholders were involved: authorities, industry and NGO:s, including interest groups. The basis for TF is a risk communication model (RISCOM) for delicate situations. A key element in TF is that all stakeholders are involved on equal terms in the planning and realization of the project. The three seminars covered: Roles and responsibilities of the different organisations, The scientific basis for risk assessment and Risk management and precautionary principles. An independent evaluation company evaluated the project. The conclusion was that TF had offered an arena for stakeholders to meet and that the dialogue had been valuable. The evaluators pointed out that it is the responsibility of SSI to carry on working in the transparent way opened up by the TF.

Recent Risk Communication Activities in Sweden

The Swedish Radiation Protection Authority, SSI, is the competent authority for radiation protection in Sweden, both for ionising and non-ionising radiation. During 2004 and 2005 SSI has made special efforts to inform and educate the public and the municipalities as well as arranging other kinds of dialogue-projects concerning mobile telephony and health.

In 2004 a series of six regional one-day training courses, "Mobile telephony and health", was organised by SSI and the National Board of Health and Welfare. The training course was offered to all Swedish municipalities. Altogether more than 300 regional and municipal employees and politicians attended the courses. The response from the attendants has been very positive.

Early the same year SSI took the initiative to a network of experts on mobile telephony and health in the five Nordic countries: Denmark, Finland, Iceland, Norway and Sweden. The work in this group resulted in a common position paper "Mobile Telephony and Health" (1). In short the Nordic authorities pointed out that there is no scientific evidence for adverse health effects from mobile telecommunication systems, but that some scientific uncertainty and knowledge gaps could justify a precautionary attitude regarding the use of handsets for mobile telephony.

During 2004 and 2005 SSI, arranged the "Transparency Forum for mobile telephone systems", TF, a series of three open seminars regarding the 3G roll-out where all stakeholders were involved: authorities, industry and NGO:s, including interest groups. The basis for TF was a risk communication model (RISCOM) for delicate situations. A key element in the RISCOM model is that all stakeholders are involved on equal terms in the planning and realization of the project. The three seminars in TF covered: Roles and responsibilities of the different organisations, The scientific basis for risk assessment and Risk management and precautionary principles.

This paper describes the Transparency Forum in more detail.

The process of defining the project

The roll-out of the third generation system for mobile telephony has been fast in Sweden. The decision to build the UMTS system was taken in 1999. The licences for the operators were distributed in 2000. In spring 2006 the population coverage for the system exceeded 90 percent in Sweden. The rapid launching has created considerable concern and opposition among certain parts of the general population. The media coverage of the

3G issue has been intensive. Interest groups have been active in the resistance towards the launching of the new system and sabotage against masts carrying UMTS base stations has occurred. Also, individuals that have reported a variety of health problems that they relate to exposure to electromagnetic fields have argued that the authorities have neglected their problems. The debate at the municipal level has been intensive, involving local civil servants as well as local politicians. The building of masts has been appealed in court etc. SSI and other central authorities, have received critical views concerning the authorities' role in the controversy on new mobile phone technologies. One reason for this is the perceived technocratic approach that is no longer accepted. The need for a dialogue was obvious.

The RISCOM model of transparency

For more than 15 years, SSI has been working with risk communication in the nuclear waste arena, trying to achieve a better dialogue between different stakeholders. Using this risk communication experience and methodology, SSI has been co-financier in the development of a communication model for dialogue in different areas of complex issues of society – RISCOM (from RISkCOMmunication). One suggestion of the RISCOM approach is to create an arena for dialogue and discussion for concerned parties (2,3,4).

Decisions on certain complex issues, for instance regarding nuclear waste management, involve both scientific/technical and value-laden parts. If this is evident, transparent, both to the public and the decision-makers the decisions taken will generally improve in quality. It is also important that all parties understand the roles and responsibilities of the different stakeholders.

According to the RISCOM model, appropriate procedures must be created in which the decision-makers and the public can validate claims of:

- Truth (technical-scientific issues: Is this true? Are we doing things right?
- Legitimacy (normative issues: What is fair, acceptable, legitimate)
- Authenticity (trust, no hidden agendas, personal integrity and organisational identity)

These are the three corner-stones (often illustrated as a triangle) in the RISCOM concept, they are equally important and interconnected.

It is seldom possible for the public to understand the scientific and technical issues in detail, or for the different scientists and experts to understand the details of each other's disciplines. Therefore, appropriate decision processes must be created; allowing the public to judge whether they can trust different scientists and experts. The public, and other stakeholders, must have the opportunity to evaluate the trustworthiness and authenticity of all parties involved. An important and useful tool to evaluate Truth, Legitimacy and Authenticity is the concept of "stretching". Stretching usually means that critical questions are raised from different perspectives and answered. All involved parties must allow themselves to be stretched. Public participation is essential for transparency and a satisfactory public involvement is not possible without transparency. The media is also important in a transparent process. Experienced journalists are vital for stretching scientists, experts and authorities but must also allow themselves to be stretched.

The RISCOM concept has been successfully applied in the nuclear waste management discussions in Sweden.

Transparency Forum

During 2004 SSI initiated a dialogue project outline on the launching of the third generation of mobile telephony, the "Transparency Forum for mobile telephone systems". The aim of this project was to improve the dialogue and transparency in society regarding electromagnetic fields, focusing on new mobile telephone systems, and to increase the mutual understanding of different stakeholders' roles and value judgements, so that different discussions will be addressed in the right arenas (political, technical, municipal etc.).

All kinds of relevant stakeholders have taken part in the project; authorities, industry and NGO:s, including interest groups. All were given the opportunity to express their opinions and ideas since a key element in RISCOM is that all stakeholders are involved on equal terms in the planning and realization of the project.

The reference group

A reference group was created, with a broad representation of the relevant stakeholders. The reference group did, at a series of regular meetings, take decisions on defining the process, program, timetable, meeting places, etc. A requirement for the Transparency Forum concept was that the project was to be defined and decided by this reference group, and not by SSI alone. The RISCOM principles were used all the way as the structure for

dialogue. Swedish authorities financed the project and SSI was the project manager, also using consultant experts.

A number of preparatory meetings were held to define the need for a dialogue process, starting with representatives from two municipalities experiencing a debate concerning the implementation of new mobile phone technologies. The municipal interest was very high, leading to widened meetings with other stakeholders, also approving the initiative (other authorities, municipal representatives, industry, NGO:s etc.). Therefore, a reference group with a broad range of stakeholders was established to define the Transparency Forum project. A project outline was created, that has been updated and accepted by the reference group, along with a formal agreement specifying the conditions for participating.

Organisations represented in the reference group:
Authorities

Swedish Radiation Protection Authority
National Board of Health and Welfare
National Electrical Safety Board
Swedish Work Environment Authority
National Post and Telecom Agency
National Institute of Public Health
Swedish Emergency Management Agency
Stockholm County Council (Medical expertise)
Nacka and Södertälje municipalities

Industry
Ericsson
MTB (Organises manufacturers and dealers of mobile phones)
Tele2 (Network operator)
TeliaSonera (Network operator)
Vodafone (Network operator)

NGO's
TCO Development (Labelling of mobile phones and other electronic products)
Vågbrytaren, Swedish for Breakwater (Interest group fighting unhealthy electromagnetic radiation)
FEB, Swedish Association for the Electro hypersensitive

Three interactive seminars

During the project preparation it was decided that three seminars should be organised where it would be possible for all stakeholders to state their true opinions and be questioned on their views by all others. The reference group decided on the following themes for the three seminars:

Seminar 1 - The roles and arenas of the different stakeholders
This first seminar was held late in 2004 and about thirty people attended. The seminar gave a description of the historical evolution of the new mobile telephone systems, focusing on decisions in political, technical, and economical areas that have led to the present situation.

To create a dialogue people have to meet, and be given the opportunity to understand other stakeholders' roles and responsibilities. Several Swedish national authorities are more or less involved when it comes to the question of UMTS, and the roles and interactions of these are not always easily understood. Therefore, a description of the interaction between different stakeholders and arenas was designed. Representatives for the involved authorities, industrial companies and NGOs gave accounts of their different views on the mobile telephone issue. A Member of Parliament representing the Green party presented that party's view.

After the presentations a number of interesting questions that had appeared during the day were discussed in working groups. Some of the questions were.

- How can Society take better care of people who claim to be electro hypersensivive?
- How can the precautionary principle be applied to mobile telephony?
- Who has the responsibility for weighing risk against benefits of new techniques?

- How should anecdotic reports and personal experiences be taken into account in the risk estimation process?

The discussion in the groups were loud and vivid, but were held in a good mood.

Seminar 2 - The research basis for the risk estimation

The second seminar was held for two days early in 2005 and about sixty people attended. The scope of the seminar was to discuss the research in the area of radiofrequency electromagnetic fields and health as a basis for the risk estimation for mobile telephony.

Risk evaluation and judgment is not a strictly technical and scientific issue, values also plays a very important role. It is important to understand how we, as individuals, perceive risks and makes personal risk judgments. The second seminar was therefore planned with a broad framing where the themes of discussion were:

- Radiation – physical and biological facts and risk estimations for electromagnetic fields
- Risk estimation concerning mobile telephone systems
- Different methods for risk estimation
- The basis for SSI´s risk estimation and regulations for electromagnetic fields
- The situation for individuals who find themselves hyper-sensitive to electromagnetic fields

Among the participating scientists were Anders Ahlbom and Maria Feychting from the Karolinska group, Lennart Hardell from Örebro University, Jacob Eberhardt from Lund University (the Salford-Persson group) and Igor Belyaev from Stockholm University. Lars-Erik Holm, director general of SSI presented the authority's risk estimation for exposure from mobile phones and from base stations. Representatives for the industry and the interest organisations presented their respective views on the risks. The discussions and stretching after the presentations were intensive and sometimes rather aggressive

Also at the second seminar discussions in working groups were an important part. The group discussions were held at the end of the first day. A specific scope this time was that the groups should present questions that could be used for the stretching the next day. Four groups were formed:

1. Research on health risks from base stations and antennas
2. Research on electrical hypersensitivity
3. Risk estimation procedures
4. Research, methodology and evaluation

The working groups were successful in formulating a number of relevant questions for the stretching.

Seminar 3 - Precautionary principles and exposure limits

The third and last seminar, also for two days, was held in spring 2005 and about a hundred people attended. The scope of this seminar was to discuss precautionary principles and exposure limits as applied to mobile telephony.

Precautionary principles are used in many different areas and there are many different interpretations on the practical use and consequences. The precautionary principles relate of course to the use of exposure limits for electromagnetic fields. Themes to discuss were:

- Legal aspects of exposure limits and the precautionary principle (EU and national legislation)
- Exposure limits for electromagnetic fields
- Different interpretations and practical implications

The seminar began with a very interesting presentation on the background and the legal aspects of the precautionary principle by Annika Nilsson, legal expert from Lund University. Maila Hietanen, vice chairman of ICNIRP (Internation Commission on Non-Ionizing Radiation Protection) presented ICNIRP's work and the 1998 guidelines. Igor Belyaev gave an account of the guidelines from RNCNIRP, the Russian commission on non-ionizing radiation protection. The proposal from the WHO EMF Project for a Precautionary Framework, was

also presented. The second day concluded with a panel discussion focussed on exposure limits and how to apply the precautionary principle.

At the beginning of the second day the Swedish minister of the environment, Lena Sommestad, gave the Government's view on precautionary principles and exposure limits applied to mobile telephony. Lars-Erik Holm gave an account of the scientific basis of SSI:s risk estimation and exposure limits. He also presented the role of SSI:s international expert group on electromagnetic fields (5). After that other central Swedish authorities involved in mobile telephony: the National Board of Health and Welfare, the National Electrical Safety Board and the Swedish Work Environment Authority gave their views on the risk estimation.

A representative from Stockholm municipality discussed the rights of those who claim to be electrically hypersensitive and the industry and the NGOs in turn presented their views on the risk estimation. The second day of the seminar concluded with a questioning of some of the speakers and a panel discussion.

The evaluation of the project

To investigate whether the aim of the project was fulfilled, an evaluation was made by an external company specialised in evaluations of different authorities dialogue projects. The evaluation method that was used included different kinds of interviews and telephone questionnaires. Special care was taken to make sure that as many of the project's participants as possible took part in the evaluation. It was also important for the credibility of the evaluation that personal opinions should be taken into consideration and analysed. A special focus was therefore put on subjective impressions of both the project's accomplishment as well as the effects of the project.

The evaluation clearly shows that the majority of the participants have the distinct opinion that the project has resulted in an improved dialogue of the UMTS issue. The project has contributed to that the stakeholders have been sitting at the same table actually meeting each other's different opinions and views in a way that not had occurred in Sweden prior this project. There have also been different forms of learning and a new forum for dialogue has been created. Due to the meeting between different stakeholders with different opinions and values there has been an increased understanding for other stakeholders' roles and values. The project did not have as an aim to reach consensus (6).

The final report

During the entire project the documentation of the process has been of the greatest importance. Some parts of the seminars have also been recorded to make sure that all aspects of the interesting discussions were not lost in mere notes. It was stated already in the beginning of the project that the documentation would result in a final report. The idea was that this report would try to capture the very essence of the Transparency Forum; the dialogue itself. The report is being written not only for the participants of the project but also for all those who did not have the opportunity to participate in the project, of for example geographic reasons. The report is expected to be released in the autumn of 2006.

How is the dialogue continued?

Originally there was an ambition to continue the dialogue of Transparency Forum in a more permanent way, as a regular part of the work of SSI and other stakeholders. But in December 2005 the project was concluded and the reference group resolved. The evaluation points out that it is important to continue the dialogue. The question is how. For this there are no readymade plans as of today, but SSI is determined to continue the work that has been started. SSI has the intention to summon the stakeholders regularly to discuss different aspects of electromagnetic fields and health in order to maintain the dialogue.

References

(1) Mobile telephony and Health – A common approach for the Nordic competent authorities. http://www.ssi.se/news/newsEntire.asp?ID=114&MenueType=5&menu2=Press

(2) R. Espejo and T.Gill The systematic roles of SKI and SSI in the Swedish nuclear waste management system, SSI Report 98:02, RISCOM pilot study, Stockholm 1998.

(3) K. Andersson (Ed), Review/decide and inquiry/decide- Two approaches to decision making, SSI Report 98:03, RISCOM pilot study, Stockholm 1998.

(4) K. Andersson, R. Espejo, C.-O. Wene, Building Channels for Transparent Risk Assessment, SSI Report 98:04, Final Report RISCOM pilot Project, Stockholm 1998.

(5) Reports from SSI:s International Independent Expert Group on Electromagnetic Fields 2003 and 2004, SSI Rapport 2005:01.

(6) P. Salino, S. Faugert, K. Eduards, H. Segerpalm, Transparensforum, An evaluation of the Transparency Forum project (in Swedish), Faugert & Co, 2006.

EFFECTS OF THE STATIC MAGNETIC FIELD GENERATED BY 0.5 T MRI UNIT ON HUMAN CD4$^+$ T CELLS ACTIVATION PATTERNS.

CARMELA LA MENDOLA[1], ANTONIO LO CASTO[2], SERGIO SALERNO[2], GIUSEPPE MAMONE[2], NADIA CACCAMO[1], ROBERTO LAGALLA[2]

[1]Dipartimento di Biopatologia - Università degli Studi di Palermo
[2]Sezione di Scienze radiologiche - Dipartimento di Biotecnologie mediche e Medicina legale - Università degli Studi di Palermo

Abstract

The aim of this study was to investigate the effects of a 0.5 T static magnetic field (SMF) of a MRI clinical unit on human CD4$^+$ T cell lines in terms of cytokines content, expression of surface markers, cell proliferation. Cells were sorted by immunomagnetic beads from peripheral blood mononuclear cells (PBMC). Cells were cultured in complete medium and split into 2 groups of samples, one to be exposed and the other one as control. After 2 hrs of exposure to the SMF at 37°C, cells were stimulated or non stimulated with a mitogen, and incubated for 48 and 72 hrs. After 48 hrs of incubation it was observed in exposed CD4$^+$ T cell lines: a decrease of IFN-γ production assayed by ELISA technique, a decrease of IFN-γ content, cell proliferation, expression of CD25 an activation surface marker- assayed by flow cytometry. After 72 hrs of incubation these effects were no statistically significant. This observation indicates that magnetic fields could have temporarily biological effects on T lymphocytes and that lymphocytes represent a sensitive model for the studying and understanding of the effects of magnetic fields on the immune system.

Introduction

The influence of static magnetic field (SMF) on biological systems has been a topic of considerable interest for many years [1-2]. We have previously demonstrated that SMF can influence the release of cytokines and intracellular calcium by human CD4$^+$ T cell lines [3-6]. Immune system cells represent a sensitive model for the study and understanding of immunophysiological effects of the SMF [7]. The aim of this study was to investigate the effects of a 0.5 T SMF of a MRI clinical unit on human CD4$^+$ T cell lines on cytokines content, expression of surface markers, cell proliferation.

Materials and methods

Peripheral blood mononuclear cells (PBMC) were isolated from heparinized blood by centrifugation on Ficoll-Hypaque (Pharmacia, Uppsala, Sweden). Cells were maintained in RPMI-1640 (Gibco, Grand Island, NY) supplemented with 10% heat-inactivated pooled human AB$^+$ serum, 2mM L-glutamine, 20mM HEPES, 100 U/ml penicillin, 100 μg/ml streptomycin, 5 x 10^{-5} M 2-mercaptoethanol and 150 IU/ ml rIL-2. CD4$^+$ T lymphocytes were sorted by immunomagnetic beads, using an anti-CD4 specific monoclonal antibody (mAb) and CD4$^+$ T cells were then expanded *in vitro* in IL-2/CM supplemented with a purified mitogen, phytohemagglutinin, PHA (Leucoagglutinin, 0,5 μg/ml, Sigma, St. Louis, USA) and irradiated (30 Gy from a Caesium source) allogeneic feeder cells (PBL and Epstein Barr Virus-B cells at a ratio of 10/1). Cells were maintained for 2 weeks without restimulation prior to functional analysis. Purity of the CD4$^+$ T cells was assessed by two colours flow cytometry. PE-conjugated anti-CD3 mAb was used with FITC-conjugated anti-CD4 (mAb Becton Dickinson, San Jose, CA). The cells were analysed by FACScan flow cytometer (Becton Dickinson, Mountain View, CA). This T cells expansion procedure, using PHA and allogeneic stimulation, induces expansion of virtually all CD4$^+$ T cells and does not introduce any bias in the T cell repertoire. Cell culture was split into two groups of samples, one to be exposed and the other one as control to be kept under isothermal conditions for the whole time of the experiment, before the exposure to the SMF. After 2 hrs of exposure to the SMF, cells were stimulated with PHA, employed at a 0.5 μg/ml suboptimal concentration. After 48 hrs and 72 hrs of cell culture, CD4$^+$ T cells were collected and incubated at 37°C for 48 hrs and 72 hrs. A superconducting MRI unit (Vectra, GE Medical Systems, Milwaukee, WI, USA) commonly employed for clinical examinations was the source of the 0.5 T SMF. A specific device for keeping the cell samples at 37° C was used; it was constituted by a thermostated water bath in which a plexiglass tube holder with the tubes

containing cell samples were placed before their introduction within the gantry of the MRI unit. The experiment was repeated twice in different days. Intracellular staining was used to determine the IFN-γ intracellular concentration at the single-cell level both on exposed and sham exposed cell samples, before and after exposure to the SMF. Staining for intracellular nuclear antigen was performed by incubation of fixed permeabilized cells with FITC-labelled anti-Ki67 antibody and/or with PE-labelled anti-CD25 antibody (Becton Dickinson). After two more washes in PBS 1% FCS, the cells were analysed by FACScan flow cytometer (Becton Dickinson). Viable lymphocytes were gated by forward and side scatter and analysis was performed on 100.000 acquired events for each sample. Cells were harvested and fixed with 4% (w/v) paraformaldehyde in PBS for 10 m at room temperature. Fixed cells were suspended and washed twice with permeabilization buffer containing 0.1% saponin (Sigma-Aldrich, Milano, Italy), 1% heat-inactivated FCS, and 0.1% NaN_3 in PBS. The permeabilized cells were then incubated in the presence of saponin with FITC-coniugated anti-IFN-γ , anti-Ki67 and anti-CD25 (Sigma-Aldrich, Milano, Italy) for 1 h at ice temperature. After two more washes in PBS 1% FCS, the cells were analysed by FACScan flow cytometer (Becton Dickinson, Mountain View, CA). Viable lymphocytes were gated by forward and side scatter and analysis was performed on 100,000 acquired events for each sample. The IFN-γ, CD25 expression and Ki67 concentration were monitored by single excitation flow-cytometer technique. The fluorescence was recorded at 490 nm excitation and 520 nm emission.

Results

In $CD4^+$ T cell lines exposed for 2 hrs to a 0.5 T SMF, after 48 hrs of *in vitro* culture, there was a decreased IFN-γ intracellular content and expression of CD25 surface marker with respect to sham exposed cells, that was enhanced in cells stimulated with PHA (Tab. 1, 2). The exposure also caused a decrease of the rate of proliferation of $CD4^+$ T cell lines in exposed cells with respect to sham exposed, stimulated and not stimulated with PHA, as demonstrated by typical FACS intracellular analysis of Ki67 expression (Fig. 1). After 72 hrs of exposure there were not significant differences of the above parameters analysed between the exposed and sham-exposed cells.

Discussion

In this study we investigated the bioeffects of the SMF on the intracellular content of IFN-γ, CD25 marker expression and cell proliferation, using an homogeneous cell population of human $CD4^+$ T cell lines. IFN-γ cytokine is a highly versatile homodimeric protein that plays an essential role in cell mediated immune responses to viral and mycobacterial infections [8]. The IFN-γ gene is located on chromosome 12 and codes for a 17 kDa protein, which then undergoes posttranslational glycolysis converting the IFN-γ to a 20-25 kDa glycoprotein. IFN-γ is produced by NK cells, dendritic cells, cytotoxic T cells, Th0 cells and Th1 cells. IFN-γ directs several immunoregulatory mechanisms that enhance the cytokine's function and increases the production of MHC class I and II, which in turn increase the likelihood that the infected cell will be recognized as such. Moreover, FACS analysis for CD25 expression, which is expressed as an early membrane marker of T cell activation, in exposed and sham exposed cells, treated and not treated with PHA, shows lower expression of CD25 marker surface in exposed cells. Furthermore, we evaluated the cells proliferation by the expression of Ki-67 protein. The Ki-67 protein is present during all active phases of the cell cycle (G1, S, G2 and mitosis), but is absent from resting cells (G0) and therefore it is an excellent marker for determining the so-called growth fraction of a given population. Although the functional role of Ki-67 protein during cell proliferation is unknown, it is unquestionable that Ki-67 protein expression and cell proliferation are closely linked. During the interphase, this antigen can be exclusively detected within the nucleus, whereas in mitosis most of the protein is relocated to the surface of the chromosomes [9]. In this paper, after 48 hrs of *in vitro* culture, a significant decrease of intracellular content of IFN-γ, CD25 expression and cell proliferation was observed in $CD4^+$ T cells exposed for 2 hrs to the 0.5 T SMF of a MRI clinical unit with respect to sham exposed cells, stimulated and not stimulated with PHA. However, after 72 hrs of exposure there were not significant differences of the above parameters analysed between the exposed and sham-exposed cells. These results indicate that $CD4^+$ T cell lines are a target population of SMF, and that the inhibitory effect of the latter is reversible.

References

1. Hong FT. Magnetic field effects on biomolecules, cells, and living organisms. Biosystems 1995; 36, 187–229.
2. Rosen AD. Mechanism of action of moderate-intensity static magnetic fields on biological systems. Cell Biochem Biophys 2003; 39, 163–173.
3. La Mendola C, Lo Casto A, Salerno S, Mamone G, Caccamo N, De Maria M. Effect of the static magnetic fields generated by 0.5 T MRI unit on intracellular calcium concentration and IFN-γ release of human CD4+ T cells. Proceedings Biological effects of EMFs – 3rd International Workshop, 4-8 October, Kos, Greece, 2004: 367-370.

4. Aldinucci C, Pessina F. Pulsed electromagnetic fields enhance the induction of cytokines by peripheral blood mononuclear cells challenged with phytohemagglutinin. Bioelectromagnetics 1998;19:445-51.
5. Salerno S, Lo Casto A, Caccamo N, D'Anna C, De Maria M, Lagalla R, Scola L, Cardinale AE. Static magnetic field generated by a 0.5T MRI unit affects in vitro expression of activation markers and interleukin release in human peripheral blood mononuclear cells (PBMC). Int J Radiat Biol 1999; 75: 457-463.
6. Salerno S, La Mendola C, Lo Casto A, Mamone G, Caccamo N, Cardinale AE, Salerno A. Reversible effect of MR and ELF magnetic fields (0.5 T and 0.5 mT) on human lymphocyte activation patterns. Int J Radiat Biol 2006; 82:77-85.
7. Cadossi R, Bersani F, Cossarizza A, Zucchini P, Emilia G, Torelli G, Franceschi C. Lymphocytes and low-frequency electromagnetic fields. FASEB J. 1992; 6:2667-74.
8. Suzue K, Asai T, Takeuchi T, Koyasu S. In vivo role of IFN-gamma produced by antigen-presenting cells in early host defense against intracellular pathogens. Eur J Immunol. 2003; 33:2666-75.
9. Ikeda K, Shinmura Y, Mizoe H, Yoshizama H, Yoshida A, Kanao S, Sumitani H, Hasebe S, Motomura T, Yamakawa T, Mizuno F, Otaka Y, Hirose H. No effects of extremely low frequency magnetic fields found on cytotoxic activities and cytokine production of human peripheral blood mononuclear cells in vitro. Bioelectromagnetics 2003, 24: 21-31.

Fig.1. FACS intracellular analysis of $CD4^+$ T cells exposed in vitro for 2 hrs to a 0.5 T SMF, stained with antibody anti-ki67 FITC conjugated.

A) **B)**

C) **D)**

A) Control: $CD4^+$ T cells in complete medium.

B) Control : $CD4^+$ T cells stimulated with PHA.

C) Exposed cells: $CD4^+$ T cells in complete medium.

D) Exposed cells: $CD4^+$ T cells stimulated with PHA.

Table 1. Assay of intracellular IFN-γ of $CD4^+$ T cells exposed in vitro for 2 hrs to a 0.5 T SMF.

Samples		Sham-exposed	Exposed
%IFN-γ^+CD4^+			
48 h at 37 °C	5	2.4 ± 2.5	1.5 ± 1.3
48 h at 37 °C,PHA	5	3.6 ± 2.8	2.4 ± 2.1

Table 2. Expression of surface activation marker on the membrane of $CD4^+$ T cells exposed in vitro for 2 hrs to a 0.5 T SMF.

Samples		Sham-exposed	Exposed
% $CD25^+CD4^+$			
48 h at 37 °C	5	4.2 ± 2.8	3.1 ± 1.7
48 h at 37 °C,PHA	5	9.0 ± 4.5	6.7 ± 2.6

INFLUECE OF ELECTROMAGNETIC FIELD EXPOSURE ON THE GROWTH OF OCIMUM BASILICUM AND ITS ESSENTIAL OIL

FAEZEH GHANATI[1], ELHAM RAJABBEIGI[1,2], PARVIZ ABDOLMALEKI[1]

[1]DEPT. BIOL. FAC. SCI. TARBIAT MODARES UNIV (TMU), POB:14115-175, TEHRAN IRAN

[2]YOUNG RESEARCHERS CLUB IN AZAD ISLAMIC UNIVERSITY, POB14515-775

Abstract

The effect of electeromagnetic field (1 kHz, square wave) on the growth and essential oils of sweet basil (Ocimum basilicum) was studied. The plants in vegetative growth phase were discontinuously exposed to the electeromagnetic field for 6 days, each 5 hours. The results showed decrease of the growth of shoots of treated plants compared to the control group. The activity of polyphenol oxidase was increased by the treatment, whereas the amount of volatiles, in particular of methyl chavicol was decreased. It can be suggested from the results that electeromagnetic field exposure of basil caused metabolism pathway shifted from producing essential oil to the synthesis of other metablites.

Introduction

Interaction between cells and extraneously applied electromagnetic fields (EMFs) have been investigated over last years and many of them have focused on their influence on the growth of organism (Hirano et al., 1998; Davis 1996). However, investigations, dealing with effect of EMF on the performance are scarce and the possible mechanism of he effects of electromagnetic fields on the cells are yet to be elucidated (Panagopoulos et al. 2002).

According to a simple hypothesis an oscillating, external electric field, by exerting an oscillating force on the free ions on both sides of the cell membranes can give a false signal for gating channels that leads in turn to disordering the membrane and therefore the whole cell function (Panagopoulos et al. 2002). Any slight membrane structure disturbance could potentially lead to detectable physiological and biochemical effect. In plants it has been shown that exposure to EMF can alter the metabolism of certain amino acids e.g., asparagines, glutamine, alanine and GABA (Ben-Izak Monselise et al. 2003).

The present study the effect of EMF on the growth, the quality and the quantity of essential oils of sweet basil (Ocimum basilicum), a plant of high economic value was studied.

Seeds of sweet basil were cultivated in a soil containing sand-clay and humus (2:1) and grown at 27 ± 2 ºC and 16 h photoperiodic with a photosynthetic photon flux of 58 μmol m^{-2} s^{-1} at the plant level. Micro- and micronutrients and physical parameters of the soil are shown in Table 1.

A locally designed electromagnetic wave generator capable to generate different wave shape including sinusoidal, triangular and quadratic, was used. This system could generate EMF in the range of 0.1HZ– 10 KHZ with a continuous fine control in stable conditions. It was consisted of two vertical coils each 28 turns of 0.3 mm copper wire rounded around a quadratic frame of 48 × 34 cm. One coil oriented in vertical plane (XOZ) with pointing vector in horizontal direction (anti parallel with the gravity) while the other coil oriented in horizontal plane (XOY) with pointing vector in vertical direction (perpendicular with the gravity). Impedance of each coil was 8 ohm. The maximum consuming power of the system was 9 watt controlled by a fine analog controller. The calibration of system was performed at three different frequency (50, 300 and 1000 HZ) in the center of the chamber. The consuming power was 8 watt at 1kHZ in which the average electric and magnetic strength were 96/3± 4.8(kV/m) and 984± 43(mA/m), respectively. A digital thermal sensor was used to control the temperature inside the chamber during the exposure. While the sample were exposed to the defined EMF, the control samples were placed in the same conditions (i.e., the same temperature, humidity and light intensity), but far enough from the apparatus, being shielded from possible exposure. The plants in vegetative growth phase were discontinuously exposed to the aforesaid EMF for 6 days, each 5 hours. After the period of exposure, plants were gathered and kept at –80 ^{0}C until used for biochemical and analysis. The rate of growth as well as the ratio of fresh weight to dry weight of

the samples before and after the treatment were measured (Table 2). Statistical analysis was done by SPSS and t-test and the differences were considered significant at the level of $p \leq 0.05$.

Polyphenol oxidase (PPO) was extracted from homogenized cells in freshly prepared 100 mM Na-phosphate buffer (pH 6.8) followed by centrifugation at 15,000 × g for 20 min (Kahn 1975). Aliquots of supernatant were added to 100 nM Na-phosphate buffer (pH 6.5) and freshly prepared 4-methylcatecol at a final concentration of 0.02 M. The increase in absorbance at 410 nm per min per mg protein content of the homogenate was the expression of Enzyme activity.

The essential oils were extracted from 50 g (dry weight) of shoot samples by steam-distillation for 3h using a Clevenger type apparatus and were analyzed by GC and GC-MS.

Analytical gas chromatography was carried out in a GC-9A (Shimadzu, Tokyo, Japan) equipped with a DB-5 fused silica column (30 m×0.25 mm, film thickness 0.25 µm, J & W scientific corporation). Oven temperature was held at 60 ºC for 5 minute and then programmed to 210 ºC at a rate of 3 ºC/min. Injector and detector (FID) temperature were 270 ºC; helium was used as carrier gas with a linear velocity of 32 cm/s. Percentages were calculated by area normalization method without the use of response factor correction. The retention indices were calculated for all compounds using a homologous series of n-alkanes.

GC-MS analysis was carried out on a GC-MS system (Varian 3400, USA) equipped with a DB-5 fused silica column (30 m × 0.25 mm, film thickness 0.25 µm, J & W scientific corporation); Oven temperature program was 50 º - 60 ºC at a rate of 3 ºC/min. Transfer line temperature 270 ºC, carrier gas helium with a linear velocity of 31.5 cm/s, split ratio 1/60, ionizing energy 70 ev, scan time 1 sec, mass range 40-300 amu.

The constituents were identified by comparison of their mass spectra with those in a computer library (LIBR-TR and Wiley5 lib.) or with authentic compounds. The identifications were confirmed by comparison of their Retention indices in table 3, either with those of authentic compounds or with data in the literature.

The result showed that the growth of the plants treated with EMF was decreased compared to that of the control group, whereas the ratio of fresh weight to dry weight of increased with EMF-exposed plants were higher than those of the control ones (Table 2).

There activity of PPO of EMF-exposed plants was also significantly higher than that of the control plants (Fig.1).

In comparison to control plants, the amount of the total volatiles of EMF-exposed plants was reduced. The major components of the essential oils of both control and EMF-treated plants were methylchavicol, nerol and geraniol, however the amount of methylchavicol was significantly enhanced by exposing to EMF (Table 3).

Table1. Characteristics of the soil in which the plants were cultivated.

Soil parameters [a]									
pH	EC(dsm^{-1})	%O.C	%Total N	P(ppm)	K(ppm)	Mn(mg/kg)	Fe(mg/kg)	Cu(mg/kg)	Zn(mg/kg)
7.6	4.85	1.79	0.153	52.4	670	13	12.4	0.94	3

Table 2. Effect of EMF on the growth and water content of *Ocimum basilicum*

	Ctrl	EMF
Net Growth (mm)	77.0±0.05	45.0 ±0.1
FW/DW	13.7±0.01	14.3±0.03*

Data are means of three independent experiments in triplicate ± SD, n=3. Asterisk refer to as statistically significant difference at the level of $p \leq 0.05$, by Student t.Test.

Table 3. Percentage of volatile compounds identified in the oil of *Ocimum basilicum* before and after treatment with EMF

Compound	%Eos	
	Control plants	EMF–exposed plants
α-pinene	0.23	0.33
myrcene	0.37	0.40
α-phellandrene	0.15	0.30
α-terpinene	0.11	0.23
limonene	trace	0.23
(E)- β-ocimene	0.44	0.45
trance linalool oxide	trace	-
(E)- β-ocimene	0.82	0.98
linalool	0.20	0.36
neo-allo-ocimene	0.20	0.17
cis-menth-2-en-1-ol	0.37	0.45
borneol	0.32	0.43
methyl chavicol	34.06	42.25
neral	0.16	-
nerol	28.80	19.03
geraniol	27.79	24.53
α-copaene	0.21	-
β-cubebene	0.29	0.66
β-caryophyllene	2.42	1.89
β-sesquiphellandrene	0.82	-
α-humulene	0.43	1.76
spathulenol	1.88	1.19
caryophylleneoxide	0.81	0.28

Retention indices on DB-5 capillary column , t= trace (≤ 0.05%)

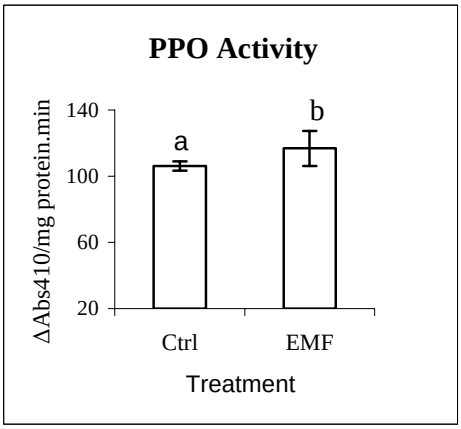


Fig 1. Effect of electromagnetic field on the activity of PPO of shoot of *Ocimum basilicum*. Data are means ± SD, n= 3, signs with different letters indicate significant differences at p≤0.05 according to t-Test.

EFFECT OF EMF ON ESSENTIAL OILS OF BASILE

Summary

The mechanism of the effect of EMF on plant metabolism is still unclear. However, it has been suggested that the production or enhancement of free radicals (Scott, 1993) and ferrous ions (Miyakoshi, 2005), ion change and mass resonance are involved in the adverse effects of EMF on the growth and metabolism of plants.

Decrease of growth can be resulted from damage DNA, proteins, cellular membranes and mutiple genes (Da Silva et al., 2000; Sahebjamie et al. 2006).

Polyphenol oxidase is responsible for tissue browning of raw fruits and vegetables (Mathew & Parpia 1971), which has been found in most higher plants. PPO is a bifunctional enzyme that hydroxylates monophenols to O-diphenols, the only specific reaction catalysed by this enzyme (cresolase or monophenolase) and also oxidizes self generated O-diphenols to the corresponding o-quinon (catecholase or diphenolase) (Gowda & Paul, 2002). Most phenolics that are oxidized by PPO, are intermediates or derivatives of the shikmate and phenyl propanoids pathway. In the present study the increase of the activity of PPO in EMF-exposed basils was not accompanied by an increased production of essential oils. From the results presented here it can be suggested that in EMF-treated plants the activity of PPO shifted from producing essential oil to the synthesis of other metabolites like quinines. Interestingly, despite to the reduction of the of total essential oil content in EMF-treated plants, the amount of methyl chavicol, a main medicinal volatile of basil increased by EMF. Taking all together, the results presented by this study suggest that EMF can be applied as a useful tool to manipulate the metabolism of medicinal plants in order to obtain more desired components.

References

Ben-Izak Monselise E., Parola AH., Kost D. 2003. Low-frequency electromagnetic fields induce a stress effect upon higher plants, as evident by the universal stress signal, alanin, BBRC, 302: 427-434.

Da Silva RL, Albano F., dos Santos LRL, Tavares AD, Felzenszwalb I. 2000. The effect of electromagnetic field exposure on the formation of DNA lesions. Redox Report, 5(5): 299-301.

Davies MS. 1996. Effects of 60 Hz Electromagnetic Fields on early growth in three plant species and replication of previous results. 17: 154-161.

Ghanati F., Morita A. & Yokota H. 2002. Induction of suberin and increase of lignin content by excess Boron in tobacco cells. Soil Sci. Plant Nutr. 48(3):357-364.

Gowda LR. & Paul B. 2002. Diphenol activation of the monophenolase and diphenolase activities of field bean (*Dolichos lablab*) polyphenol oxidase. Journal of Agricultural and Food Chemistry 50: 1608-1614.

Hirano M., Ohta A. and Abe K. 1998. Magnetic field effects on photosynthesis and growth of the Cyanobacterium *Spirulina platensis*. Journal of Fermentation and Bioengineering 86(3):313-316. Kahn V. 1975. Polyphenol oxidase activity and browning of tree Avocado varieties . J. Sci. Food. Agric. 26:1319-1324.

Mathew A.G.H.A.B., Parpia .1971. Food browning as a polyphenol reaction . Adv. Food Res. 19: 75-145.

Miyakoshi J. 2005. Effects of static magnetic fields at the cellular level . Progress in Biophysics and Molecular Biology 87:213-223.

Panagopoulos D., Karabarbounis A & Margaritis LH. 2002. Mechanism for action of electromagnetic fields on cell. Biochemical and Biophysiological Research Communications 298:95-102.

Sahebjamei H., Abdolmaleki P. and Ghanati F. 2006. Effects of static magnetic field on the oxidant enzymes activities of suspension-cultured tobacco cells, Bioelectromagnetics, in press.

Scott G., Free Radicals provide a mechanism for EMFs to promote cancer, In Electromagnetic News, Dec., 1992 (It was then republished in Open Forum on Health (prev. Hauora), Spring 1993.

BIOEFFECTS OF EXTREMELY LOW FREQUENCY ELECTROMAGNETIC FIELDS IN THE LIGHT OF NONEQUILIBRIUM THERMODYNAMICS LAWS

Yulia Chukova

Russian People's Academy of Science, Krasnopresnenskiy Ecological Fund, Malaya Gruzinskaya St. 6 – 42, 123242, Moscow, Russian Federation
Electronic address: y.chukova@mtu-net.ru

Abstract

It is found that reasons for a poor replicability of the nonthermal bioeffects of electromagnetic fields of the extremely low frequency (50-60Hz) have the fundamental basis, revealed by the thermodynamic theory of systems under the Rayleigh-Jeans radiation. It is shown the difference between the Rayleigh-Jeans region and the Wien region of electromagnetic radiation from the viewpoint of energy conversion. The rules and conditions of the good replicability of medical and biological experimental results are formulated.

1. Introduction

The discussion of the electromagnetic fields of extremely low frequency (50-60 Hz) effects on health had began in 1979 with the report by Wertheimer and Leeper [1], who noted that the incidence of cancer was much more in children living in houses where electromagnetic fields exposure was presumed to be higher than usual. This report has given rise to important problem because the exposure of increasingly larger human populations to higher mean levels of extremely low frequency electromagnetic fields is an outcome of the electrification of residential and commercial buildings, particularly in the well-developed countries of the world. The intensity of these man-made fields is substantially more than the ambient nature electric and magnetic fields. Later many epidemiological studies have been published concerning the effects of electromagnetic fields on health, mainly on possible carcinogenic effects. One part reported presence of an association between field exposure and human cancer (leukemia), brain tumor and breast cancer [2,3], but the second part had not found this association. The experimental researches both in vitro and in vivo in this sphere were conflicting too. And may be, that the findings of effects absence are more frequent [4]. So great length of this discussion shows the complication and importance of the problem. Prof. R. Reiter called this situation the Cheshire cat phenomenon [5].

Similar situation was presented in [6] and is connected with bioeffects under microwave radiation. To be more specific, we can say with reasonable confidence that in the present-day a matter of microwave region is more dramatic, as the some scientists do not study the nonthermal bioeffects since they are sure that they do not exist, while the others (Russian) scientists cure many illnesses (cancer etc) on these effects basis.

This conflicting situation may be changed for the better, if the experimentalists use the advances in the nonequilibrium thermodynamics of systems under electromagnetic radiation [7]. This theory shows that the large field of phenomena which were before considered as independent ones, follows a general law of nonequilibrium thermodynamics. This law governs the phenomena of conversion of electromagnetic radiation energy into electrical work, chemical bonds energy and luminescence. It is valid for living and inorganic systems. The qualitative and quantitative validity of this theory was tested in solar cells and it allowed to calculate the dependence of entropy generation rate on absorbed power of radiation due to the irreversibility of a process. This theory is useful in understanding the various aspects of human vision, protozoa photomovement, photosynthesis of plants, nonthermal bioeffects of radiofrequency radiation and other processes. The aim of this paper is to show the reasons of the Cheshire cat phenomenon existence.

2. The thermodynamic law of the isothermal processes under electromagnetic radiation

As it is known [8], the efficiency η of the isothermal conversion of electromagnetic energy into Helmholtz free energy F in open thermodynamic systems is defined as

$$\eta = \Delta F / \Delta W_a \qquad (1)$$

where ΔF is the change of the Helmholtz free energy of the products at the outlet from the system in relation to Helmholtz free energy of the reactants at the inlet of the open thermodynamic system and ΔW_a is the electromagnetic radiation energy, absorbed by the system. If $\Delta F > 0$, we have the endergonic process and if $\Delta F < 0$, we have the exergonic process.

In line with the first and second laws of nonequilibrium thermodynamics for the steady state of a system we have the relation [7]

$$\eta = 1 - T (\dot{S}_a + \dot{S}_i) / \dot{W}_a \qquad (2)$$

where T is the temperature of the system, $\dot{W}_a$ is the absorbed power, $\dot{S}_a$ is the flux of entropy of electromagnetic radiation absorbed by the system, $\dot{S}_i$ is the entropy generation rate as a result of the thermodynamic irreversibility of the process.

Usually in work concerning isothermal process, the thermodynamic method is used to analyse only the limiting efficiency η^* obtained from Eq. (2) under assumption of thermodynamic reversibility of the process, i.e. with the condition $\dot{S}_i = 0$ [9]. Then

$$\eta^* = 1 - T \dot{S}_a / \dot{W}_a \qquad (3)$$

We can find η^* for nonequilibrium electromagnetic radiation with arbitrary spectral characteristics, using follow equations

$$\dot{W}_a = \int E_\nu d\nu \qquad (4)$$

$$\dot{S}_a = 2\pi k c^{-2} \int \nu^2 [(1+\rho) \ln(1+\rho) - \rho \ln\rho] d\nu \qquad (5)$$

$$\rho = c^2 E_\nu / 2\pi h \nu^3 \qquad (6)$$

where k is the Boltzmann constant, h is the Planck constant, c is the speed of light, ν and E_ν are the frequency and the spectral density of absorbed radiation power respectively.

The analyse of Eq. (3) with Eqs. (4 – 6) shows that there are two regions of energy conversion, where the dependence of the η^* on absorbed power $\dot{W}_a$ is quite different because of the ρ may be both more and less than unity [6, 10].

For the $\rho >> 1$ we have

$$\dot{S}_a = 2\pi k c^{-2} \int (1 + \ln\rho) \nu^2 d\nu \qquad (7)$$

and for $\rho << 1$

$$\dot{S}_a = 2\pi k c^{-2} \int \rho (1 - \ln\rho) \nu^2 d\nu \qquad (8)$$

The region, which corresponds to the $\rho << 1$, is the Wien region and the other one, which corresponds to the $\rho >> 1$, is the Rayleigh-Jeans region. These regions are known to experimentalists as the regions, where $h\nu >> kT$ (the Wien region) and $h\nu << kT$ (the Rayleigh-Jeans region). It should be substituted the corresponding values in to Eq. (6) to be certain that is the case.

Fig. 1. Dependence of limit efficiency η^* on logarithm of absorbed power spectral density E_ν for the Wien region (solid line) and for the Rayleigh-Jeans region (dotted line). E_ν is measured in J/cm^2.

The upper limit of the η^* is equal to 1 in both the Wien region and the Rayleigh-Jeans one, but the dependence η^* on absorbed power (or the spectral density E_ν) is different. It is slow in the Wien region, where the limit efficiency and absorbed power $\dot{W}_a$ (or E_ν) have the logarithmic relationship. The dependence η^* on E_ν in semilogarithmic coordinates is the straight line, and the interval of E_ν, where the η^* takes the values from zero to unity, is very large (solid line in Fig. 1). In the Rayleigh-Jeans region the η^* dependence on the absorbed power $\dot{W}_a$ (or E_ν) is very strong until it flattens out on a plateau, where $\eta^* = 1$. The thermodynamic limit efficiency varies from 0 to 0.9 with a tenfold increase in E_ν (dotted curve in Fig. 1). Both these curves have the point, where $\eta^* = 0$ and exergonic process is balanced out by endergonic one. The geometry place of these points is defined by [10]

$$c^2 E_\nu^0 = 2\pi k T \nu^2 [(1 + \rho_0) \ln (1 + \rho_0) - \rho_0 \ln\rho_0] \qquad (9)$$

where the E_ν^0 is the spectral density of absorbed radiation and the ρ_0 is the function of distribution at the point $\eta^* = 0$. But the thermodynamic limit efficiency is of no interest for experimentalists.

The real efficiency η of irreversible process may be of interest to them. It is known that the entropy generation rate $\dot{S}_i$ rises at first linearly [7, 11]

$$\dot{S}_i = \alpha \dot{W}_a \qquad (10)$$

where α is constant. One should take into account, the linear changing of the entropy generation rate does not change the form of η^* dependence on E_v , but leads to a parallel shift of the whole curve of η^* along the logarithm absorbed power axis in the Rayleigh-Jeans region and along the η axis in the Wien region [6]. This shift changes the position of the endergonic and exergonic compensation point.

Allowance for nonlinear irreversibility of real process leads to a decrease of η sometimes up to zero in both regions [11].

Fig. 2 . Position of isothermal, nonthermal and thermal process in the line of logarithm of absorbed power (Rayleigh-Jeans region).

In the final analysis the η dependence on the absorbed power is complicate. Fig.2 gives it over a wide range of the absorbed power for the Rayleigh-Jeans region. Fig.2 shows different processes (isothermal exergonic process, isothermal endergonic one, nonthermal endergonic one, thermal one) and different dependences (increase, decrease and the lack of any dependence). As is known from experiment [12] the interval of endergonic process may be small (power windowing). Fig. 2 demonstrates the very complicate situation for bioeffect study in the Rayleigh-Jeans region.

The analyse of experimental results on bioeffects of extremely low frequency electromagnetic fields shows that experimentalists study the different ranges of the exciting power, and this is true that they have the different results, including the absence of any effects [4]. The up-to-date experimental results will allow in the future to define the boundary of different processes under the Rayleigh-Jeans radiation in different living systems. Then the general situation will be not like the Cheshire cat.

3. The influence of individual properties of subjects

The Rayleigh-Jeans region has many differences from the Wien one, sending the experimentalists in search of a new apparatus for the experiments. But they must search the new methods of research too, if they want to have the good replicability of the results. The fact is that the role of individual properties of living subject is different in the Wien and in the Rayleigh-Jeans regions.

The indicator of individual properties is the entropy generation rate $^0\dot{S}_i$ at the point of endergonic and exergonic processes balance in the real experiments. This point is very known in photosynthesis of green leaves and is called a compensation point. It is studying for human vision processes too. The experimental results for this point allows to calculate the entropy generation rate $^0\dot{S}_i$ at this point. In the null point of the real process the dissipative term is equal to the thermodynamic limit efficiency

$$1 - T\ {}^0\dot{S}_a / {}^0\dot{W}a = T\ {}^0\dot{S}_i / {}^0\dot{W}a \qquad (11)$$

and the value of $^0\dot{S}_i$ may be calculated. The entropy generation rate $^0\dot{S}_i$ is own characteristic of every individual and can change as a function of internal conditions, for example as age. For the group of individuals with different ^0S_i there are the family of curves $\eta = \eta (E_v)$. In Wien region (Fig. 3a) this family permits to find the average value of endergonic effect in ensemble. In Rayleigh-Jeans region the situation is more complicate (Fig. 3b). Averaging over the ensemble gives the zero result as a rule because of the endergonic and exergonic processes are the opposite ones, and averaging over the small group gives the chance result. This is (and will be always) the reason of poor replicability of the experimental results in conditions of low-level of excitation. Knowledge of thermodynamic theory allows to reduce the extent of poor replicability.

Fig. 3. The different role of the number of objects in experiment under the Wien (a) and the Rayleigh-Jeans radiation (b).

The phenomenon of poor replicability near the boundary of endergonic and exergonic processes depends on the sharpness of $\eta = \eta (E_v)$ dependence. This phenomenon is small in Wien region and would be taken into account by Gauss distribution (the inset in right part of Fig. 3a). This factor is great in Rayleigh-Jeans region. In this region the individual properties of subject are the main ones.

I think that the up-to-date figurative popular expression “the Cheshire cat phenomenon” may be in the future the strict scientific term, indicating that the experimentalist studies the initial stage of endergonic effect under Rayleigh-Jeans radiation without the selection of endergonic and exergonic processes. The selection of these processes allows to save from the Cheshire cat phenomenon.

4. Conclusion

Key features of energy conversion in Rayleigh-Jeans region are sharp dependence of efficiency on power and sharp change-over from exergonic process to endergonic one. On the basis of the thermodynamic theory it is thought that the Cheshire cat phenomenon will be seen in pilot studies of bioeffects under other frequencies of Rayleigh-Jeans region and will cloud the work of experimentalists. However the study of nonequilibrium thermodynamics allows them to understand the situation and reduce to zero (or minimum) the Cheshire cat phenomenon. May be, that the experimentalists, who works in the sphere of extremely low frequency, will be more well than the researchers of microwaves, where the microbiological researches are necessarily associated with the ensemble averaging. In such experiment only the experimentalist of extra class can see the effect.

As known, there is the melatonin synthesis reaction, which is the very good object for study. It enables to clear the influence of electromagnetic fields on the processes in animals and human. Melatonin synthesis will be used as a promoter in solution of discussed problem [13].

5. Acknowledgement

of the financial support from the Research and Writing Initiative of the Program on Global Security and Sustainability of the John D. and Catherine T. MacArthur Foundation

References

1. N. Wertheimer, E. Leeper, Electrical wiring configuration and childhood cancer. American Journal of Epidemiology, 109, 272 - 284 (1979).

2. D.A. Savitz, D.P. Loomis, Magnetic field exposure in relation to leukemia and brain cancer mortality among electric utility workers. American Journal of Epidemiology, 141, 123 (1995)

3. A. Ahlbom, M. Feychting, M. Koskenvuo, Electromagnetic fields and childhood cancer. Lancet, **342**, 1295 (1993)

4. H. Takebe, T. Shiga, M. Kato, E. Masada, Biological and health effects from exposure to power-line frequency electromagnetic fields. Confirmation of absence of any effects at environmental field strengths (Ohmsha, IOS press, 2001).

5. Reiter R. J. An assessment of the bioeffects induced by power-line frequency electromagnetic fields - Modern Radio Science, ed. By M.A. Stuchly. Oxford University Press, 1999, pp. 287 -307

6. Yu.P. Chukova. - Reasons of poor replicability of nonthermal bioefects by millimeter waves - Bioelectrochemistry and bioenergetics, 1999, v.48, p.349 - 353

7. Yu.P. Chukova, Advances in nonequilibrium thermodynamics of the systems under electromagnetic radiation (Khrizostom, Moscow, 2001, ISBN 5-7508-0285-X).

[8] L.N.M. Duysens - In *The photochemical apparatus. Its structure and function.* Brookhaven symp. in biology. (Upton -N.Y., 1959).

9. P.T.Landsberg , G.Tonge - Thermodynamic energy conversion efficiencies.- J. Appl. Phys. 1980, v.51, N7, p.R1 - R20

10.Chukova Yu.P. Effective non-equilibrium radiation temperature (Weinstein temperature) and fundamental thermodynamic prohibition of endergonic reactions.- Russian Journal of Physical Chemistry, 1990,v.64,p.16-19

11. Chukova Yu.P. Energetic and informational interactions in terms of thermodynamics.-Biophysics, 1992, v.37, N 5, p.889-893

12. W.R.Adey,- Frequency and Power Windowing in Tissue Interaction with Weak Electromagnetic Fields, - Proceedings of the IEEE, 1980, v.68, N1, p.119

13. Reiter R.J. Melatonin aspects of exposure to low frequency electric and magnetic fields – In: Advances in electromagnetic fields in living systems, ed. By J.C. Lin . Plenum Press, N.Y.,1997, v.2, pp 1-27

USE OF A MODEL ORGANISM FOR AN ESTIMATION OF ACTION OF THE PHYSICAL FACTORS OF VIDEODISPLAY TERMINALS

VOYCHUK S.I., GROMOZOVA E.N., PODGORSKIY V.S.
INSTITUTE OF MICROBIOLOGY AND VIROLOGY OF NAS OF UKRAINE
UKRAINE, KIEV, 03143, ZABOLOTNY STR., 154,
E-MAIL: VOYCHUK@SERV.IMV.KIEV.UA

Abstract

It is very important to understand whether the electric and magnetic fields generated by video display terminals (VDT) are capable to influence on the living organisms. The effect of VDT (17" computer monitor with cathode-ray tube) was studied on viability of *S. cerevisiae* cells, which is the model organism for studying of eukaryotes. The capacity of electric field at the 4 cm distance to the display was 6.4±3.57 V/m, 4.8±2.04 V/m at 30-40 cm, 0.1±0.02 V/m at 100 cm, and zero at 200 cm. Experimental samples were settled on the distance 4, 40 and 250 cm opposite to the central point of the monitor. Some samples were additionally treated with nystatin (20 μg/10^6 cells) just after exposure. Viability was determined by the colony forming units.

Exposure of the yeast cells to the VDT radiation only did not change their viability. Same time exposed cells showed much grater sensitivity to the nystatin than the control ones. Effect depended on the distance to the computer monitor and the time of exposure.

These results suggests that physical factors of VDT cause some changes in the yeast cells, which reduce their viability at the presence of the strong stress factors, such as nystatin.

Introduction

The problem of an overload of environment with anthropogenic electromagnetic fields (EMFs) grows together with development of scientific and technical progress and introduction of the newest electrical engineering devices. Anthropogenic EMFs, changing a natural electromagnetic background, can result in the origin of a number of disturbances at cellular, subcellular and molecular levels that reflects in the different diseases (cancers tumors, leukemia, dermatitises, mental decline, and so on) [4, 16]. Researches in this field carried out in the different laboratories of the world behind several directions depending on the frequency characteristics of EMFs. Special attention given to influence on the user of radiation emitted from video display terminals (in particular monitors of computers and TV sets) [3, 12]. Except for a mental fatigue, aggression and depression [16], work with video display terminals (VDT) influences a physiologic state of the user's organism changing frequency of heart rhythms, reducing concentration of melatonin in saliva and increasing maintenance in urine of 8-hydroxydeoxyguanosine, and also the number of leucocytes multiplying in a blood [7, 9, 14]. For today, VDT is possible to consider as a risk factor, which increases probability of origin of disease of skeletal-muscular and visual systems [13], skin [2, 10, 15] and reproductive system [11, 12]. In the publications, which generalize the new data on EMFs effects, absence of unique mind is marked in relation to the mechanisms of EMFs action on living objects. This results in the constant revision and perfection of the already established norms of allowable radiation on the living organism [8].

The situation arisen in the given direction of researches closely linked to absence of the biological system-indicator adequate to revealing of harmful effect of VDT on an organism. Multicellular organisms, because of complexity of their structure, not are able to be the sensors of EMFs action that is why attention of scientists aimed on the use as biosensors of separate cultures of human cells [6] or most studied microorganisms [1]. Microscopic biological objects are more conservative in the reactions to action of any factor, and that is why can be used as indicators of the negative/positive influence of EMFs. There are some rather simple and convenient microscopic modeling systems for research of various processes occurring in the eukaryotic cells, in particular cells of yeast *Saccharomyces cerevisiae* and *Schizosaccharomyces pombe* [5].

Studying of EMFs effects with eukaryotic modeling microorganisms will allow to use them as sensory/indicators systems for analysis of the radiation effects from different household devices (computers, mobile phones, the microwave-ovens, and so on) and accordingly to prevent originating the majority of the problems linked to the action of EMFs on the living organism.

The purpose of work was studying the reaction of the yeast *Saccharomyces cerevisiae* cells on the influence of emission of video display terminals.

Materials and methods.

Yeast *Saccharomyces cerevisiae* Y-517 from Ukrainian collection of microorganism at the Institute of Microbiology and Virology of NAS of Ukraine were used for studying. The culture of yeasts was preliminary cultivated on agar medium at 28 ^{o}C during 24 h, and then washed off with sterile distilled water, filtered through cotton wool for the separation of pieces of medium and diluted to 10^9 cells/ml (OD_{540} = 0,75). Cells were held in the distilled water in order to stop the process of division and accordingly to provide the condition of the work with the same organisms. The optical density of cell suspension measured on a wavelength 540±10 nm in a cuvette with optical way 3 mm.

Received cell suspension divided in equal amounts (5 ml) into the 20 ml glass vials. The vials placed (a) in metallic boxes – for shielding of EMFs and (b) simply in glass vial – for shielding of UV-radiation only.

The source of the electromagnetic fields was 17"-monitor with the cathode-ray tube SAMTRON 75E. The monitor was disposed on a wooden-table on 42 cm higher than system block. The screen of monitor was white-color with maximal brightness and contrast. For studying the influence of physical factors generated by VDT on the yeast cells, the diagrams of electromagnetic emission from the computer monitor were analyzed. Measurements carried out with a dosimeter of intensity of an electromagnetic field – NFM 1, in a range 60 kHz – 350 MHz. The readings were taken at 4, 40, 100 and 250 cm from a surface of the screen and walls of monitors. The exposed samples placed on distance 4, 40 and 250 cm to the center of monitor. Irradiation carried out at the room temperature of 24.5±0.5 ^{o}C and day light during maximum 24 h. Cell suspension periodically mixed.

Viability of the exposed and unexposed yeasts cells was determined by the colony forming units in absence and in presence of the fungicidal antibiotic nystatin. Nystatin (2-3 mg) was dissolved in 1 ml of dimethylis sulfoxidum and sterile distilled water added to the necessary volume to receive final concentration of 20 μg of nystatin in 1 ml of solution. This solution used for further researches.

Initially and after 3, 6 and 24 hours yeasts cells from each vial used for determination of viability and sensitivity to the fungicidal antibiotic nystatin. For this purpose 0.1 ml of cells added to 9.9 ml of the sterile distilled water or to 9.9 ml of water containing 20 μg/ml of nystatin getting the concentration of 10^6 cells/ml and mixed it during 10 min. After that, the series of dilutions was done and concentrations 10^3 and 10^2 cells/ml received. From these solutions, 0.1 ml added to the Petri dishes with agar and placed in a thermostat at 28 ^{o}C. The colonies counting and data analyses were done after 72 h.

Results and discussion.

Analysis of the yeast *Saccharomyces cerevisiae* viability in the distilled water showed that cells keep during a long time (more than 24 hours) in a wide range of temperatures (20 – 28 ^{o}C) stable physiologic state. Necessary to notice, that the opportunity of use of only water medium without admixtures is very important as, at first, simplifies process of carrying out of researches and, secondly, minimizes influence of additional physical and chemical factors, which take place at presence in medium of free ions.

As well as in previous our researches [17, 18] at optimum for yeast *Saccharomyces cerevisiae* conditions of an external environment (temperature, pH, and so on) action of EMFs generated by VDT did not reflect on standard parameters of the growth processes. Microscopy also has not given an opportunity to find any differences between the exposed and control samples.

Same times in the presence of the strong stress-factor, such as fungicidal antibiotic, the negative consequences of electromagnetic emission from the VDT were seen. The data concerning vitality of *Saccharomyces cerevisiae* cells at the presence of nystatin shown in Table 1.

Table 1. Percent of viable cells of *Saccharomyces cerevisiae* Y-517 in the presence of nystatin (20 μg/10^6 cells) and in dependence on the distance to the monitor and time of exposure
Values are the mean±SD from the minimum three separate experiments.

Time of an exposition, h	Distance to the monitor, cm			The control
	4	40	250	
0	-	-	-	28±9,9
3	4±2,8	14,8±6,7	25±9,9	28±9,9
6	12±1,2	42,5±5,3	40±2,2	55±7,3
24	29±29,7	22±4,2	45,5±3,5	25±9,9

The maximum of activity of an antibiotic and accordingly a minimum of a resistance of the cells were observed at minimal (4 cm) distance from the center of the monitor. After three hours nystatin suppressed growth of 70 % of cells in the control, and in the exposed samples – 96 %, 85 % and 75 % accordingly on the distance 4, 40 and 250 cm. After 6 and 24 hours these parameters reduced that, probably, testifies to increase of stability of cells to action of the external stress-factors of the physical and chemical nature.

It is necessary to note, that after 6 hours in control samples observed substantial increase (on 20 %) of viable cells. The cause of such phenomenon can be in change of some properties of the yeast cells. For example, the stay of living organisms in the distilled water results in decrease of permeability of cytoplasm membranes and cellular walls with the purpose of not allow an efflux of the intracellular compounds. It, in turn, complicates process of penetration and probability of attachment of polyene antibiotic to the molecules of cytoplasm membranes.

After 24 hours, vitality of cells in the controls diminished up to initial parameters while in the exposed samples remained at high level. This can testify to the presence of differences in character of flowing of intracellular processes in the exposed and unexposed yeast cells, what clearly recognized under action of the strong stress-factor such as fungicidal antibiotic.

Table 2. Doses of radiation in a range 60 kHz – 350 MHz from the SAMTRON 75E monitor with cathode-ray tube, V/m

Values are the means.

Distance from VDT, cm	Screen	Left side	Right side	Top side	Back side
4	6,4	15	9	3	7
40	4,5	2	3	3	7
100	0,1	0,5	0,5	0,5	0,5
250	0	0	0	0	0

The ability of cells to survive under action of an antibiotic is in direct dependence on the distance to the display. The data in Table 2 present doses of radiation received for the monitor with cathode-ray tube SAMTRON 75E used during experiments. Seen, that the intensity of EMFs in the same manner significantly decreased with the distance. Both these facts may suggest that electric fields generated by VDT may play a key role in the influence on the biological objects. It is very important to note that on the distances of 200 and 250 cm from the screen of the display the intensity of EMFs in the range 60 kHz – 350 MHz are equal zero, but biological action of VDT emission still obvious.

Summary

EMFs generated by VDT had the negative influence on the modeling organism *Saccharomyces cerevisiae* that especially seen in the presence of the stress-factor (antibiotic nystatin). Cells of *S. cerevisiae* Y-517 provides unique tools for understanding environmental effects on cellular systems and can be biological sensors at development of the bioanalytical systems for analyses of bioeffects from different electromagnetic devises such as computers, TV sets, mobile phones, microwave ovens and so on.

Other microorganisms may also be sensible to the action of the electromagnetic fields generated with different laboratory or industrial equipments. Therefore, during work with microbiological objects it is necessary to take into account and eliminate the possible influencing of emissions from VDT for avoidance of errors at the estimation of results of researches or during biotechnological processes.

References

1. Parkhomenko I.M., Zarubina A.P., Romanova N.A. et al., Perspectives of the microorganisms' use as biosensors of the low doses of ionizing radiation, *Moscow University Herald, Biology Ser. 16.*, No.2, 2001, pp. 33-40.
2. Aminian O., Mansoori P., Sharifian A. et al., The relationship between Video Display Terminals (VDTs) usage and dermatologic manifestations: a cross sectional study, *BMC Dermatol.*, Vol.5, No.1, 2005, pp. 1-3.

3. Eriksson N., Hoog J., Mild K.H. et al., The psychosocial work environment and skin symptoms among visual display terminal workers: a case referent study, *Int. J. Epidemiol*., Vol.26, No.6, 1997, pp. 1250-1257.
4. Feychting M., Ahlbom A., Kheifets L., EMF and health, *Annu. Rev. Public. Health*., Vol.26, 2005, pp. 165-189.
5. Forsburg S.L., The yeasts *Saccharomyces cerevisiae* and *Schizosaccharomyces pombe*: models for cell biology research, *Gravit. Space Biol. Bull*., Vol.18, No.2, 2005, pp. 3-9.
6. Guisasola C., Desco M., Millan O. et al., Biological dosimetry of magnetic resonance imaging, *J. Magn. Reson. Imaging*., Vol.15, No.5, 2002, pp. 584-590.
7. Higuchi S., Motohashi Y., Liu Y. et al., Effects of VDT tasks with a bright display at night on melatonin, core temperature, heart rate, and sleepiness, *J. Appl. Physiol.*, Vol.94, No.5, 2003, pp. 1773-1776.
8. Hill D.L., McLeish K., Keevil S.F., Impact of electromagnetic field exposure limits in Europe: is the future of interventional MRI safe? *Acad. Radiol.*, Vol.12, No.9, 2005, pp. 1135-1142.
9. Ishihara I., Ikushima M., Horikawa J. et al., A very low level of magnetic field exposure does not affect a participant's mental fatigue and stress as much as VDT work, *J. UOEH*., Vol.27, No.1, 2005, pp. 25-40.
10. Liden C., Wahlberg J.E., Work with video display terminals among office employees. V. Dermatologic factors, *Scand. J. Work. Environ. Health*., Vol.11, No.6, 1985, pp. 489-493.
11. Marcus M., McChesney R., Golden A., Landrigan P., Video display terminals and miscarriage, *J. Am. Med. Womens Assoc*., Vol.55, No.2, 2000, pp. 84-88.
12. Shaw G.M., Adverse human reproductive outcomes and electromagnetic fields: a brief summary of the epidemiologic literature, *Bioelectromagnetics*., Vol.5, 2001, pp. 5-18.
13. Signorelli C., Lepratto M., Summa A., Management of the visual risk in VDT workers and the role of the occupational physician, *Ann. Ig*., Vol.17, No.6, 2005, pp. 573-584.
14. Takahashi K., Sasaki H., Saito T. et al., Combined effects of working environmental conditions in VDT work, *Ergonomics*., Vol.44, No.5, 2001, pp. 562-570.
15. Tamez Gonzalez S., Ortiz-Hernandez L., Martinez-Alcantara S., Mendez-Ramirez I., Risks and health problems caused by the use of video terminals, *Salud. Publica Mex*., Vol.45, No.3, 2003, pp. 171-180.
16. Travers P.H., Stanton B.A., Office workers and video display terminals: physical, psychological and ergonomic factors, *AAOHN J*., Vol.50, No.11, 2002, pp. 489-493.
17. Voychuk S.I., Gromozova E.N., Lytvyn P.M., Podgorskiy V.S., Changes of surface properties of yeast cell wall under exposure of electromagnetic field (40.68 MHz) and action of nystatin, *The Environmentalist*, Vol.25, 2005. pp. 139-144.
18. Voychuk S.I., Gromozova E.N., Podgorskiy V.S., Effect of EMF (40,68 MHz) on the sensitivity to stress-factors, *Proceedings: 3rd International Workshop "Biological Effects of EMFs", Kos, Greece, 4 - 8 October 2004*, Vol.2, pp. 799 - 804.

INVESTIGATION INTO THE EFFECTS OF 900MHZ ELECTROMAGNETIC RADIATION ON MESENCHYMAL STEM CELLS.

E.F.ANDREWS (1), A.T. BARKER (2), G.G. COOK (1), L. COULTON (3), W. LIU (1), A. SCUTT(4)

(1) DEPT. OF ELECTRONIC & ELECTRICAL ENGINEERING, UNIVERSITY OF SHEFFIELD, SHEFFIELD, U.K.
(2) DEPT. MEDICAL PHYSICS & CLINICAL ENGINEERING, ROYAL HALLAMSHIRE HOSPITAL, SHEFFIELD, U.K.
(3) BONE BIOLOGY GROUP, UNVERSITY OF SHEFFIELD MEDICAL SCHOOL, SHEFFIELD, U.K.
(4) KROTO RESEARCH INSTITUTE, UNVERSITY OF SHEFFIELD, SHEFFIELD U.K.

ABSTRACT

The controversy over the safety of mobile phones and their base stations continues despite many years of study into the non-thermal interactions of radio frequency electromagnetic fields (RF-EMF) with biological tissue. This study exposes rat mesenchymal stem cells (MSC) to RF-EMF in a Crawford TEM cell at 900MHz. A robust dosimetric analysis of the exposure system is performed to determine the configuration which will optimise system efficiency, minimise heating and provide the most uniform specific absorption rate (SAR) across the cell monolayer. Data from exposure of MSC to continuous wave, GSM and intermittent (5mins on/ 10mins off) 900MHz RF-EMF is presented. SAR levels are all below the 2 W/kg ICNIRP guidelines for public exposure. Recruitment, proliferation and differentiation of MSC are measured using the CFU-f assay under osteogenic (bone stimulating) conditions. No effect is observed. Additionally, hydrogen peroxide is used as a model of oxidative stress in order to determine if GSM 900MHz RF-EMF is a cofactor in stressing cells. Again, no effect is observed on MSC recruitment, proliferation or differentiation into bone.

INTRODUCTION

There is continuing widespread debate concerning the possible biological effects of radio frequency electromagnetic fields (RF-EMF) emitted by mobile phones [1]. In-vitro studies are useful because they provide a simplified biological model that allows the exposure parameters to be more precisely defined and controlled compared with in-vivo exposure. This paper presents dosimetric analysis of a Crawford TEM cell [2] at 900MHz using finite difference time domain (FDTD) modelling, to determine the optimum dish separation and height off the septum, and level of culture medium so as to maximise both the power deposited and its uniformity in a monolayer of mesenchymal stem cells (MSC) in the bottom of each culture dish. A similar system has previously been used by the authors to expose human leukocytes in suspension [3]. Specific absorption rates (SAR) are calculated in the ~1mm layer of culture medium at the dish bottom using both in-house [4] and commercial SEMCAD [5] software, with subsequent experimentation based on the results using the fibroblastic-colony forming units (CFU-f) assay to quantify any effects on stem cell recruitment, proliferation and differentiation.

Exposures using continuous wave (CW), GSM type bursts and intermittent carrier (5 mins on / 10mins off) were performed at 900MHz, whilst maintaining a constant ambient temperature of 37°C. In order to ascertain if such non-thermal RF-EMF could also act as a co-factor in causing an effect, a common in-vitro model of oxidative stress was used. Hydrogen peroxide (H_2O_2) is an oxidative agent, known to cause stress to cells, and a concentration of this was added to the cells, sufficient to affect them with no RF-EMF applied whilst at the same time not killing them all.

Materials and Methods

RF Equipment

Briefly, the exposure system in Fig.1 utilises a GSM handset in engineering test mode as a source, which is then amplified and routed through a travelling wave TEM cell. Environmental control is achieved by placing the TEM cell inside an incubator which maintains 95% humidity, 37°C, and 5% CO_2, and real time thermal monitoring of internal TEM cell temperature is provided by a fluoroptic thermometer. To expose at higher SAR values non-thermally the system needs to deliver high efficiency, measured in W/kg per W of input power, while minimising the thermal load. Air fans are therefore attached to the TEM cell at its tapered ends to increase cooling. A second identical TEM cell provides sham exposure for control purposes.

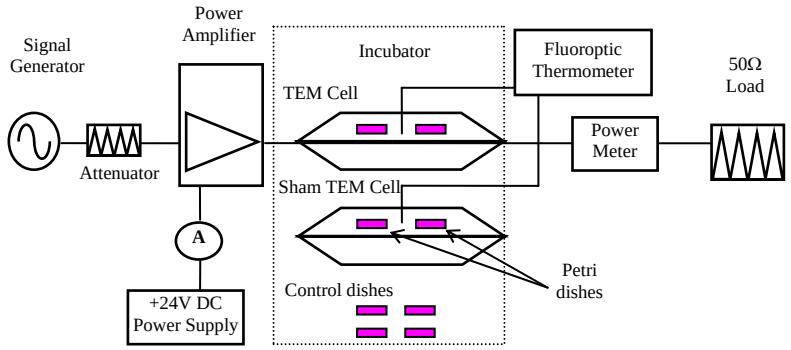


Figure 1: Schematic of Exposure system.

Fibroblastic Colony Forming Unit Assay

The fibroblastic colony forming unit (CFU-f) assay is a cell culture model which uses primary bone marrow seeded at low density. The low density seeding allows the cells to form colonies without contact inhibition. Each colony is assumed to grow in isolation from the others, and be derived from a single MSC, and the number of colonies is a measure of the number of colony forming units present in the original bone marrow cell suspension therefore. This MSC proliferates and differentiates depending on the stimulus [7] which can be chemical or physical. The colonies are then sequentially stained for alkaline phosphatase, calcium and collagen, which are all markers of osteogenic differentiation.

Primary BMSC were extracted from the femur and tibia of adult Wistar rats. Bone marrow was extracted using the method published in [7]. Briefly, the leg bones were removed and the bone marrow extracted and re-suspended in 1ml of Dulbecco's Minimum Essential Medium (DMEM) to create a single cell suspension. Cells from all bones were then pooled and 10ml supplemented DMEM per bone was added to create primary bone marrow suspension. The supplements added to the DMEM were 10% Serum Supreme, 1% Ultraglutamine, 1% Penicillin/Streptomycin and osteogenic stimuli, 50µg/ml ascorbic acid and 10^{-8}M dexamethasone.

The primary bone marrow suspension was used to seed the 90mm Petri dishes at a density of 1.2×10^6 cells, in 10ml supplemented DMEM. RF-EMF exposure was for five 3-hour periods over 5 consecutive days, after which the medium was changed, and thereafter twice a week. Cells were then cultured for a total of 16 days, after which the plates were washed in PBS and fixed with cold 70% industrial methylated spirits (IMS). After fixing, they were immediately histochemically stained for alkaline phosphatase (APase) activity, and then sequentially for calcium-positive, collagen-positive and total colonies. After each staining, the cultures were digitally photographed and the subsequent photographs processed to allow for automatic analysis. The images were then analyzed using Bioimage ''Intelligent Quantifier'' image analysis software [8]. The software counts the colony number and calculates each colony area. This data was subsequently analyzed using SPSS for significance testing using the ANOVA test at $p < 0.05$.

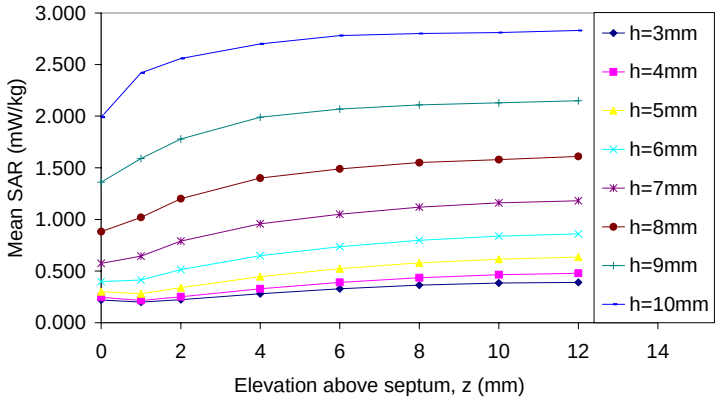
As a result of the dosimetric analysis (see results section), the required medium height in the Petri dishes had to be 10mm (60ml medium) instead of the standard 2-3mm (10ml medium). However, this amount of fluid above the monolayer hinders the gas exchange between the monolayer and atmosphere, causing hypoxia and cell death. In order to comply with the dosimetric analysis therefore, the extra 50ml of medium was added for the duration of the RF exposure and the hour-long temperature equalization pre-exposure period. Immediately after RF-EMF exposure, this extra medium was then removed from each dish and stored separately at 4°C overnight until the next exposure the following day, when it was returned to the same dish. This is because it has been shown that non-adherent cells in the medium are crucial to MSC recruitment and proliferation [7]. After the initial five days exposure however, this extra medium was no longer used. To control for the effect of the extra medium, a set of dishes were placed outside the TEM cells with 10ml of medium, in contrast to the dishes inside the exposed and sham exposed cells which contained 60ml.

The protocol for co-exposure of the MSC to GSM modulated RF-EMF and H_2O_2 was the same as for exposure to RF-EMF alone, with the following modifications. A third control group was added, where MSC were exposed to H_2O_2 alone, outside of the TEM cell, and a concentration of 10^{-5}M H_2O_2 was added to the MSC immediately before placing them in the TEM cells.

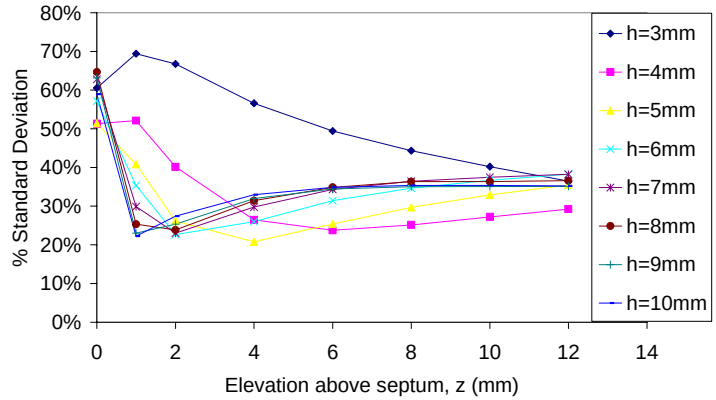
Results

Dosimetric analysis

The aim of the dosimetry analysis was to optimise the system to give high SAR efficiency and uniformity. The use of both in-house and commercially available SEMCAD FDTD code provides valuable control data for accuracy assessments, and also expedites analysis since the in-house code runs on a Unix super-cluster rather than the standard Windows PC, which our version of SEMCAD is configured for (although a Unix version is available). Uniformity can be quantified as the ratio of standard deviation of SAR to the mean (%SD), and is calculated for the bottom layer of voxels in a dish. Acceptable uniformity is 30% SD or less [6]. No software currently available can realistically grid to the micrometer scale (the thickness of the monolayer), however a grid size as small as 0.3mm is possible with reasonable simulation time in SEMCAD, which is better than the resolution achieved using physical measurements. It is assumed for the purposes of dosimetry that the SAR in this bottom layer of voxels is representative of the SAR in the monolayer. The volume of medium in the tissue culture dish affects the SAR uniformity and efficiency, as does its distance from the septum, as shown in Fig.2 for 1V peak excitation of the TEM cell. Here our in-house FDTD code has been used to calculate the SAR in the bottom 1mm layer of medium contained within a 90x18mm circular dish with a lid. The SAR clearly increases with medium height (h) and elevation above the septum (z), with bigger changes observed at higher medium levels, whereas the variation of uniformity with elevation converges towards a standard trend as the medium height increases. A medium level of h = 10mm was therefore chosen, at z = 5mm off the septum. A smaller elevation of z = 1mm would have provided the best uniformity of exposure, but with a reduced mean SAR. However, the CFU-f assay requires medium heights of 3mm or less in order to allow adequate oxygen diffusion to the stem cells. This would reduce the SAR by about 10dB and degrade the uniformity, so the medium height was temporarily increased to 10mm for the duration of the planned exposure (3 hours plus 1 hour warm up time) as mentioned previously.



(a)



(b)

Figure 2: Variation of (a) mean SAR and (b) SAR uniformity in bottom layer of culture medium as a function of dish elevation (z) for various medium heights (h).

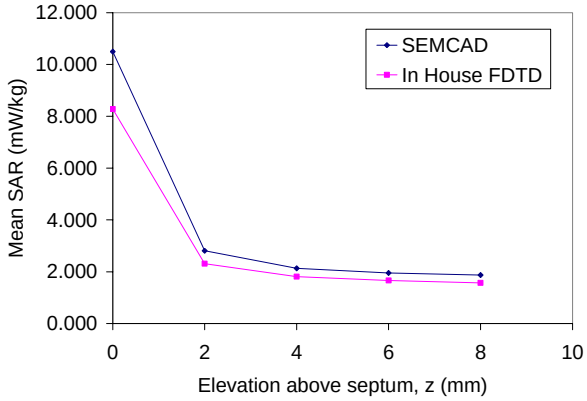


Figure 3: Comparison of in-house FDTD code and SEMCAD. Mean SAR for the whole medium volume varying with elevation above septum (h=10mm).

To increase the number of samples exposed simultaneously, two dishes were used, and SEMCAD was now employed to further refine the dosimetry and to investigate the effect of separation between the dishes on SAR and uniformity. As seen in Fig.3 our in-house and SEMCAD code agree reasonably well for a control example. Fig.4 shows the field interacting with the dishes to produce both dissimilar and non-uniform SAR distributions in the bottom layers. Increasing the separation reduces the coupling

and makes the distributions more alike, but edge effects from the tapered ends of the TEM cell begin to influence the uniformity at the furthest separation. The best uniformity is found at a separation of s = 50mm, where the mean SAR's in the bottom layers and their %SD's are similar, which allows the dishes to be treated almost identically. The CFU-f assay uses imaging software to analyse the colony formation of MSC, which excludes the outer 1mm of the dish bottom as the imaging process produces artefacts here. If this area is not taken into account the SAR values are slightly higher than those in Fig.4, with mean = 2.61 mW/kg, %SD = 31.9% for dish 1 and mean = 2.58 mW/kg, %SD = 32.7% for dish 2. The effective SAR efficiency is ~1.0 W/kg per Watt of TEM cell input power.

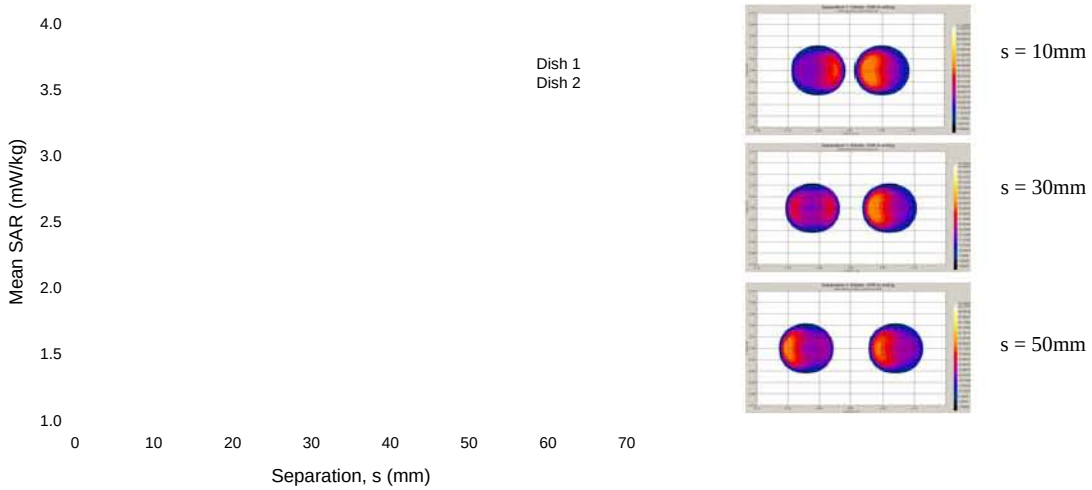


Figure 4: Variation of mean SAR in bottom layer of medium for 2 dishes as a function of separation (s) (h = 10mm, z = 5mm), with example SAR contrast plots shown at s = 10mm, 30mm and 50mm.

Biological Results

Having determined the optimum elevation, medium level and separation for the two dishes, MSC were then exposed to 900MHZ CW, GSM and intermittent CW (5mins on/10mins off) RF-EMF. Averaged SAR values were 1.6 W/kg for CW, 1.6W/kg for GSM and 0.9W/kg during the on period for the intermittent exposure (further work is planned with a higher SAR for the intermittent exposure scheme). After consecutive histochemical staining and image analysis, colony numbers and areas were calculated, and are shown in Figs.5-7.

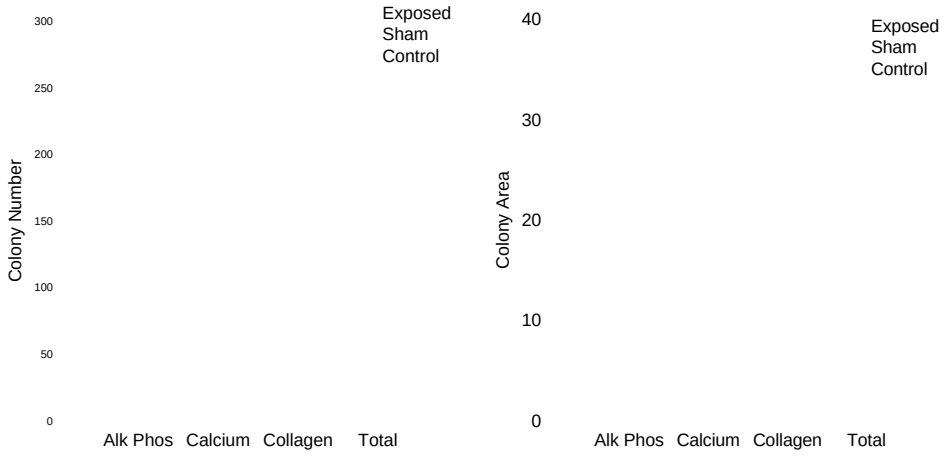


Figure 5: Colony number and area for a representative CW 900MHz RF-EMF exposure. (n = 3 or 4)

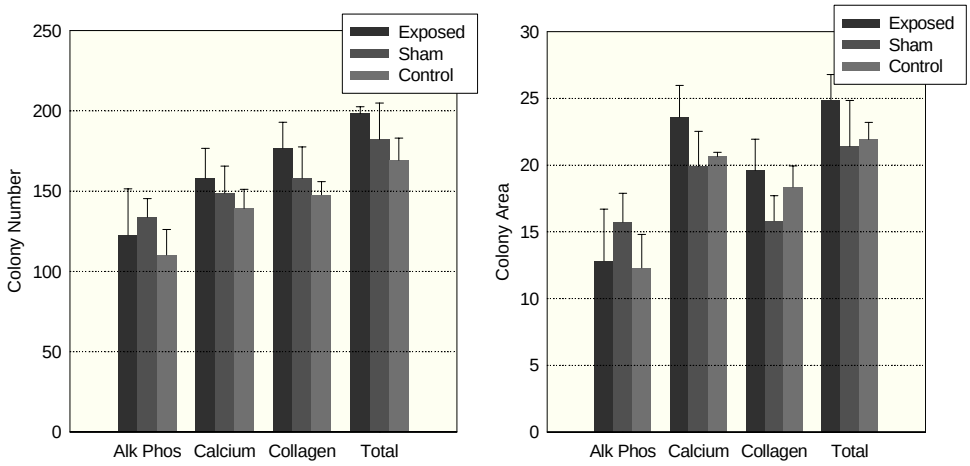


Figure 6: Colony number and area for a representative GSM 900MHz RF-EMF exposure (n = 4)

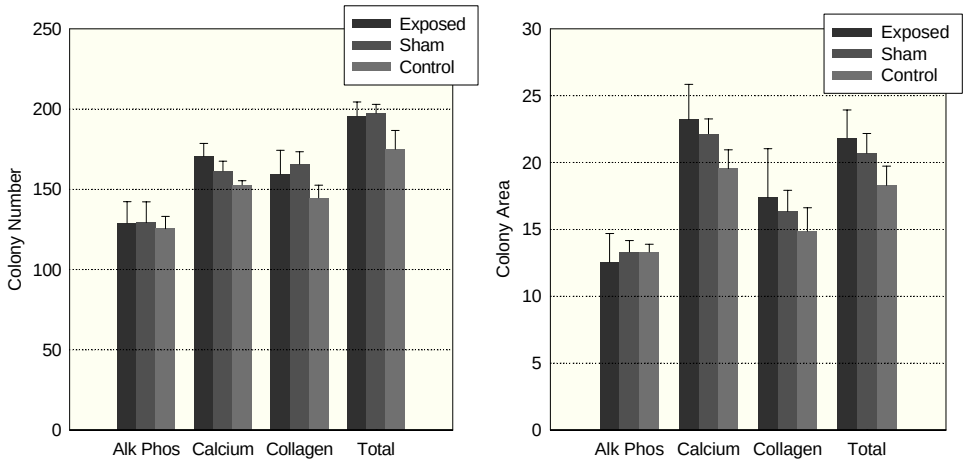


Figure 7: Colony number and area for a representative intermittent 900MHz RF-EMF exposure (n = 4).

Effect of simultaneous oxidative stressing by hydrogen peroxide

MSC were then co-exposed to 900MHz GSM RF-EMF at an averaged SAR of 1.6W/kg and to 10^{-5}M H_2O_2 in the same optimized configuration, and the results are shown in Fig.8.

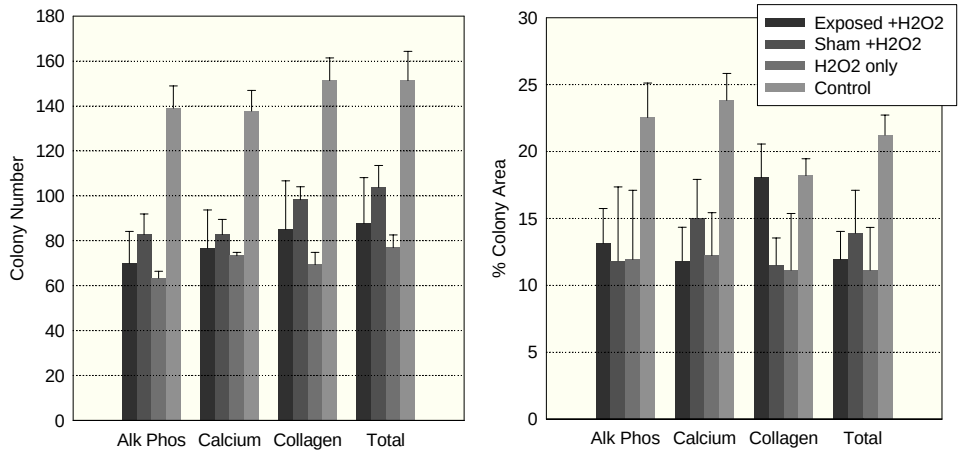


Figure 8: Colony number and area for a representative co-exposure of 900MHz GSM RF-EMF and H_2O_2 exposure (n = 4).

Discussion

Generally no significant differences in colony numbers or areas between exposed and sham exposed MSC are evident in Figs.5-7, although there does appear to be borderline differences in colony numbers between some controls and sham exposed MSC in Fig.7. This is to be expected, given the difference in conditions between these groups. Generally, in the control group, the colony number is slightly reduced, and the colony area slightly smaller. This suggests that the extra handling and medium levels of the exposed and sham groups could be affecting both the recruitment and the proliferation of the MSC. This is probably due to them receiving higher amounts of growth factors from the larger volume of medium. Another behavioural difference was seen in the distribution of the colonies; in the control group the colonies tended to be in the middle of the dish, whereas they were more evenly spread in the exposed and sham groups. This is likely to be due to moving the dishes in and out of the TEM cell, as well as stirring when the extra medium is added.

Diem et al, [10] used intermittent exposure to show that 1800MHz RF-EMFs could cause DNA breakages in both cultured human diploid fibroblasts and cultured rat granulosa cells at non-thermal levels after 16 hours continuous exposure (SAR =1.2 and 2 W/kg). Our experiments exposed MSC to daily 3 hour periods of intermittent RF-EMF for 5 consecutive days, at an SAR of 0.9 W/kg but found no significant effects. As the SAR levels for the data shown here is lower than that of [10], further exposures are ongoing at higher SAR's. While caution is required in comparing different frequencies, different cell types, and the responses of cultured and primary cells, this does suggest that a long continuous exposure is required to induce any effect, rather than an equivalent cumulative exposure.

Oxidative stress is known to play a role in stem cell differentiation [11]. It has been shown that there are interactions between oxidative stress levels and the ability of the stem cells to proliferate, and that antioxidants can increase the total number of cells. Stolzing and Scutt [11] showed that H_2O_2 reduces both alkaline phosphatase expression and total colony number. As expected, in our experiments H_2O_2 alone generally significantly reduced MSC number, as well as their proliferation, as shown by the reduced colony numbers and sizes in Fig.8. This also helps corroborate the assaying procedure itself.
Co-exposure with RF-EMF generally showed no additional effects compared with sham exposure, although some significant differences were again observed between H_2O_2 MSC colony numbers outside and inside the TEM cells. Finally it is worth noting the anomalous significant differential collagen area of H_2O_2 stressed MSC when exposed to GSM compared to sham exposure, although no conclusions may be drawn from this one result.

SUMMARY

A dosimetric analysis has been performed using a TEM cell based exposure system for in-vitro stem cell cultures, with subsequent experimentation based on the results. Optimal positioning and filling of the cell culture Petri dishes for maximum mean SAR and uniformity in the stem cell monolayer was calculated using both in-house and commercial FDTD modelling software. MSC recruitment, proliferation and differentiation were not affected by CW, GSM or intermittent CW exposure to 900MHz RF-EMF, even when the MSC were co-exposed with H_2O_2.

ACKNOWLEDGEMENTS

We would like to thank Dr A. Stolzing for her help in the preparation of this manuscript.

REFERENCES

[1] W. Stewart, "Mobile phones and Health", *Report of Independent Expert Group on Mobile Phones, NRPB*, 2000.
[2] H.B. Lim et al., "Effect of 900 MHz Electromagnetic Fields on Nonthermal Induction of Heat-Shock Proteins in Human Leukocytes", *Radiation Research*, Vol.163, pp. 45-52, 2005.
[3] E.F. Andrews, et al., "Investigation of SAR Uniformity in TEM Cell Exposed Culture Media", *Proceedings of Technical Seminar on Antenna Measurements and SAR (AMS 2004)*, pp.71-74, 2004.
[4] H.B. Lim et al, "FDTD design of RF dosimetry apparatus to quantify the effects of near fields from mobile handsets on stress response mechanisms of human whole blood", *International Journal of Numerical Modelling-Electronic Networks Devices and Fields*, Vol.15, pp. 562-577, 2002

[5] SPEAG, Zurich, Switzerland.
[6] N. Kuster and F. Schonborn, “Recommended minimal requirements and development guidelines for exposure setups of bio-experiments addressing the health risk concern of wireless communications” *Bioelectromagnetics* Vol.21, pp.508-514, 2000.
[7] A. Scutt, L. Reading, N. Scutt, and K. Still, "Mineralizing Fibroblast-Colony-Forming Assays," in *Bone Research Protocols*, vol. 80, Methods in Molecular Medicine, M. H. Helfrich and S. H. Ralston, Eds. Totowa, NJ: Humana Press Inc., 2003, pp. 29-40.
[8] K. Dobson, L. Reading, and A. Scutt, "A Cost-Effective Method for the Automatic Quantitative Analysis of Fibroblastic Colony-Forming Units," *Calcified Tissue International*, vol. 65, pp. 166-172, 1999.
[9] A. Scutt and P. Bertram, "Bone Marrow Cells Are Targets for the Anabolic Actions of Prostaglandin E2 on Bone: Induction of a Transition from Nonadherent to Adherent Osteoblast Precursors," *Journal of Bone and Mineral Research*, vol. 10, pp. 474-487, 1995.
[10] E. Diem, C. Schwarz, F. Adlkofer, O.Jahn, H. Rudiger, “Non-thermal DNA breakage by mobile-phone radiation (1800 MHz) in human fibroblasts and in transformed GFSH-R17 rat granulosa cells in vitro,” *Mutation Research* Vol.583, pp. 178-83, 2005.
[11] A. Stolzing and A. Scutt, “Effect of reduced culture temperature on antioxidant defences of mesenchymal stem cells”, *Free Radical Biology and Medicine*, Vol. 41, pp.326-338, 2006.

BIOPHYSICAL STUDIES OF LIGHT INTERACTION WITH MEMBRANE MODEL SYSTEMS BASED ON CHLOROPHYLL a

LAURA TUGULEA

Faculty of Physics - University of Bucharest
P.O.Box MG-11, Bucharest-Magurele, 077125 ROMANIA

Abstract
The interaction of light energy with plants results in the most important process on earth: the photosynthesis. Biophysical studies on membrane model systems bring relevant insights for *in vivo* primary reactions in photosynthetic membranes. Liposomes with chlorophyll *a* are biomembrane models, providing a hydrophobic environment for chlorophyll *a*, the major pigment in photosynthesis. The spectral features of chlorophyll *a* allow its use as sensor for physical properties of liposomes and for specific molecular interactions in the liposome bilayer. Supported lipid bilayers (SLB) can be obtained by deposition of liposomes on solid surfaces, using different supports. This new approach provides access to basic aspects of membrane biophysics and represents the basis for developing different applications. The objective of our work was to obtain SLB with chlorophyll *a* and to use chlorophyll as a marker in biophysical studies on these structures. Specific interactions occurring inside the lipid membranes, exposed to light (in the visible range of electromagnetic radiation) have been studied, using the strong absorption and emission of chlorophyll *a*. The most interesting application of SLB with chlorophyll *a* is represented by devices for light energy conversion, mimicking photosynthesis. Photovoltaic devices based on chlorophyll *a* are presented.

Introduction

Liposomes are phospholipidic vesicles which enclose an aqueous volume. They have been under extensive investigation for more than 20 years as carriers for the improved delivery of a broad spectrum of agents: chemotherapeutic agents, imaging agents, antigens, chelating compounds, hemoglobin and cofactors, lipids and genetic material [1]. Liposomes can be prepared so that they can entrap certain quantities of materials both within their aqueous compartment and within the membrane.

The value of liposomes as membrane model systems derives from the fact that they can be prepared of natural constituents and the liposome membrane forms a bilayer structure which is almost identical to the lipid portion of the natural cell membranes. The similarity between liposomes and natural membranes can be increased by chemical modification of the liposome membrane and can be exploited in different applications, both *in vivo* and *in vitro*, mimicking successfully the behaviour of natural membranes. Apart from their chemical constituents, which determine such properties as membrane fluidity, charge density and permeability, liposomes can be characterized by their size and shape. They can range in size from ~ 25 nm to 1000 nm or greater, which equals the dimensions of a living cell. Alternatively, liposomes can be prepared of entirely artificial components, chosen for their improved chemical properties.

The liposomes with chlorophyll a (Chla) are excellent models for biomembranes, specifically for photosynthetic membranes and are successfully used to study the influence of different agents on the bilayer structure at molecular level [2-5]. Chlorophyll a is a “valuable” molecule, but insufficiently exploited in biotechnological applications. The strong visible absorption and fluorescence of Chla allow its use as a sensor for the interactions at molecular level and as a fluorescence marker. It has been shown that Chla has also radioprotective, antimutagenic and anticarcinogenic activities. Chlorophyll's antioxidant

properties could be partly responsible for its protective effects in natural and artificial structures.

The deposition of liposomes on solid surfaces, by different techniques, conducted to a new approach: supported lipid bilayers (SLB) [6-8]. This new approach provides access to basic aspects of membrane biophysics and molecular ordering and may constitute a strategy for developing biotechnological applications [9].

Because it turns out that liposomes of diferent size require completely different methods of manufacture and because different applications demand the use of liposomes within particular size, an objective of our work was to prove that the spectral features of Chl*a* allow its use as a sensor for physical properties of liposomes (size, shape, molecular dynamics).

The main objective of the present work was to obtain stable Chla-liposomes and supported Chl-lipid membranes and to characterize the structures by using Chla as a marker and molecular sensor. Using the strong absorption and emission of chlorophyll *a*, specific interactions occurring inside the lipid membranes, exposed to light (in the visible range of electromagnetic radiation) have been studied. A particular application of SLB with chlorophyll *a* was developed by manufacturing devices for light energy conversion, mimicking the primary act in photosynthesis (separation of charges under the light irradiation).

Materials and Methods

Chl a - Liposomes preparation procedure

Chla- liposomes were prepared using the thin-film hydration method. The lipid and Chla were dissolved in chloroform, with Chla/lipid molar ratio varying from 1/100 to 1/10. Different types of thin films were obtained, by vacuum evaporation, using different lipids: ß-stearoyl-oleoyl L-phosphatidylcholine (SOPC), dimyristoyl phosphatidylcholine (DMPC), dioleoyl phosphatidylcholine (DOPC) or soybean lecithin. Chla was prepared from fresh spinach leaves by Strain&Svec method and checked for purity (absorption and fluorescence in VIS). The hydration (2 hours) of the lipid-Chla film was done by adding phosphate buffer, pH in the range: 6.2 - 7.6, in a rotary evaporator (BIOBLOCK SCIENTIFIC – Heildolph 94200, 60–90 rpm). Multilamellar vesicles (MLV) were obtained by mechanical dispersion (VIBRAX stirrer, 200rpm) of the hydrated films (30'). Intermediate unilamellar vesicles (IUV) or small unilamellar vesicles (SUV) were obtained from the multilamellar liposomes by using the exposure to ultrasonic in a bath (Branson 1210), above lipid Tc, for variable periods. For obtaining a homogenous population of liposomes, the suspension was collected after a centrifugation at 100000 g for 1 h.

Formation of supported lipid membranes

Chla-SLB have been obtained by adsorption method. A drop of Chla-SUVs suspended in phosphate buffer was spread on different solid supports: Silicon wafers and semitransparent SnO_2 or ITO glass. Chla-SLBs are formed by spontaneous deposition of Chla - SUVs.

Chla-SLBs on n-dopped silicon wafers have been covered by a semitransparent gold electrode (1.5 mm2 measurable area). Thus a photovoltaic device, sandwich type, was manufactured.

Spectral measurements

The optical absorption spectra were obtained on a double beam UV - VIS spectrophotometer Lambda 2S Perkin Elmer & PECSS software. A computer assisted Aminco Bowman was used for recording the fluorescence spectra. A front face geometry, on Perkin Elmer LS 55 fluorometer, was used for measuring the fluorescence, collected at 45^o from the solid support.

Photo-electrical measurements

The irradiation of Chla- liposomes in suspension was done by using a halogen lamp (650 W), a convergent lens and a water filter (5 cm thick). The photovoltaic devices were illuminated, within the visible range of the electromagnetic spectrum, by using a halogen lamp and a grating monochromator (Oriel). For the electrical measurements (photocurrents) a dedicated software and a Keithley 6517 electrometer were used.

Results and discussions

Characterisation of Chla - liposomes by light absorption in VIS

The liposomes will scatter light in the visible range of the electromagnetic spectrum, if their dimension is in the range of the respective wavelengths. Typical diameters for MLVs range between 100nm and 1000nm, each vesicle consisting of five or more concentric lamellae. Typical dimensions for SUVs are 15 nm (pure egg lecithin liposome in normal saline) or 25 nm (for DPPC liposomes). IUVs have

the order of magnitude around 100nm, according to R.R.C. New [1].

In order to do a rapid estimation of the size of the lipid vesicles, the absorption changes in the VIS spectra of Chl a were monitored and some spectral criteria were established. Inspecting the absorption spectrum of Chla in different liposomes, presented in Figure 1, major differences can be observed as regarding the base line (background) of the spectra. The main absorption bands of Chla (Soret band and red band) are present in the spectrum and confirm the localisation of the porphyrin ring of chl*a* at the lipid-water interface in the vicinity of polar lipid heads (the red band is shifted to longer wavelengths as comparing with solution, i.e. 670 nm).

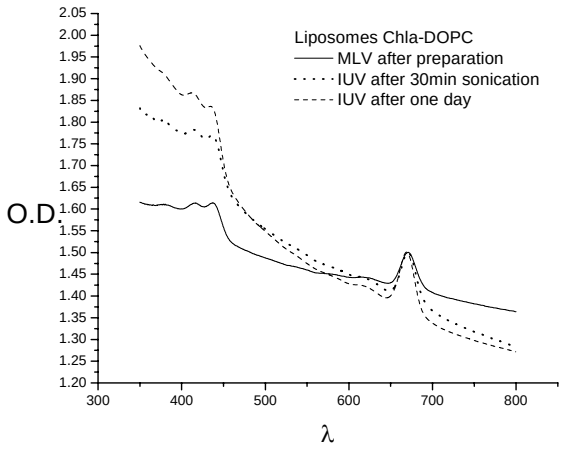


Figure 1. Absorption spectra of Chla liposomes

A $1/\lambda^4$ dependence of the baseline was observed in VIS absorption spectra of the Chl*a*-unilamellar vesicles (SUV or IUV), suggesting that the size of the vesicles is small enough to act as point sources of scattered light. And it was observed that smaller liposomes scatter shorter wavelengths (blue) more intensely, while larger liposomes scatter long (red) wavelengths. It is the case of Rayleigh scattering, applying to particles with a radius less than the wavelength of light / 20 ($R < \lambda/20$) [10]. The increase of the background scattering observed in the stability studies can be explained by the aggregation or fusion of the vesicles. The larger vesicles formed by aggregation strongly scatter light in comparison with the non-aggregated vesicles obtained after sonication.

Assuming a Rayleigh scattering, the over-estimated absorbances values can be corrected for the

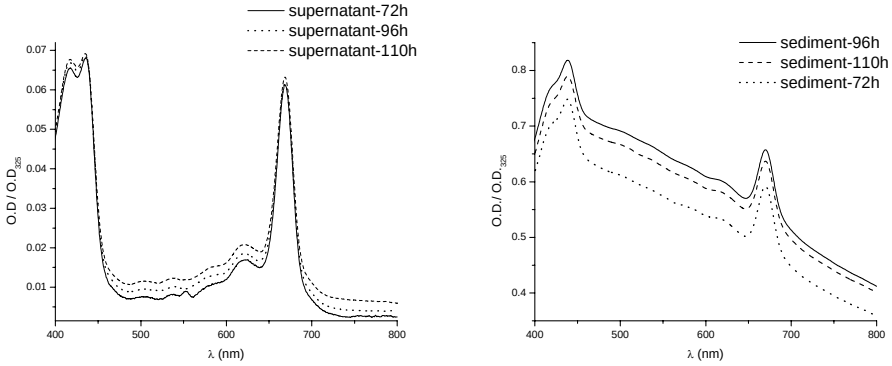


Figure 2. Corrected spectra of Chla liposomes in suspension, after centrifugation

contribution of light scattering on the basis of the OD measured at 325nm, where the scattering is the sole contributor to the O.D. (11):

$$(OD_{\lambda})_{corrected} = (OD_{\lambda})_{measured} - (OD_{325})_{measured} \times (325/\lambda)^4$$

In Figure 2 the corrected spectra are presented for 2 cases: supernatant and sediment, obtained after the centrifugation of Chla-liposomes. The suspension of Chla-liposomes (SUVs) was manufactured as described above, by sonicating the MLVs. By ultracentrifugation, the remained large vesicles are deposited on the bottom of the tube and a homogenous population of liposomes remains in the supernatant. The correction by the above formula of the absorption spectra works very well in the case of the supernatant, but does not correct the base line in the case of the sediment. As a conclusion, the average diameter of the liposomes in the homogenous population is around 60 nm.

Therefore, the spectral analysis of Chl a- liposomes, using the spectral properties of Chla, leads to a rapid monitoring of the liposome preparation. The Chla-liposomes prepared as described above are unilamellar and have diameters in the range 40-100 nm. The nature of lipids and pH value of the buffer are influencing the dimension of liposomes. The neutral pH values proved to be the best as concerning the stability of liposomes [12].

The influence of the lipid nature on Chla –liposome was also investigated. Figure 3 presents the normalized absorption spectra (corrected for the baseline) of Chla- IUVs, obtained by using different lipids. The background absorption is depending on the lipid nature. The difference between DMPC and DOPC is the presence of unsaturated acyl chains in the case of DOPC, thus providing a different environment for Chla in the lipid bilayer. This explains the lower background and therefore the smaller dimension of the DOPC liposomes.

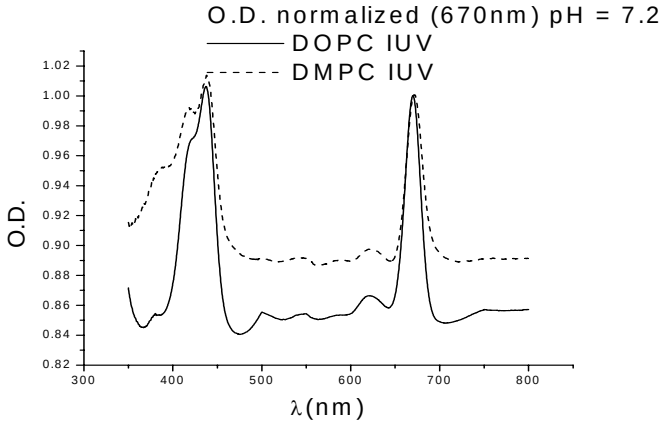
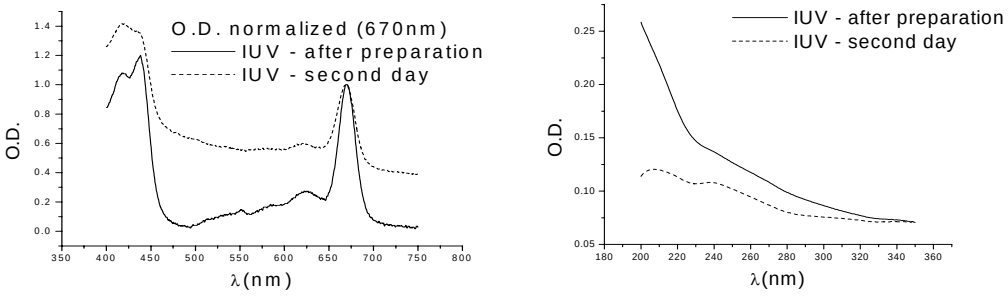


Figure 3. Absorption spectra of Chla- IUVs

Stability studies on liposomes with Chl a were performed by monitoring the changes in the Chl a spectra for different factors. The photooxidation of Chl a was monitored by comparing the absorbance ratio in the Soret band $O.D._{438}/O.D._{416}$. A correlation between Chl a oxidation and lipid oxidation was also observed by performing VIS and UV spectroscopy on the lipids - Figure 4.



(a) (b)

Figure 4. Absorption spectra of Chla - IUVs in VIS (a) and UV (b)

Light effect on liposomes with Chl a

In order to monitor the effect of light on Chla incorporated in liposomes as compared with Chla in solution (ethanol, polar solvent), aliquots of 4 ml suspension of Chla- liposomes were irradiated using a halogen lamp (white light). In order to prevent heating of the solution and consequences, a water filter was interposed between the sample and lamp. The irradiated cuvette was monitored by measuring the absorption spectrum, every 10 minutes. For comparison, Chla in ethanol solution (the same concentration as in the liposomes) was irradiated and monitored in the same conditions.
The combined effect of oxygen and illumination on the exposed liposomes was monitored by 2 spectral criteria: the ratio of absorbance in the Soret band of Chla (OD 438/ OD 416) and photobleaching % (at the maximum in red, 670 nm). The results are presented in Figure 5, for two cases: pH= 6.2 and pH= 7.35. In both cases, the photoxidation of Chla is pleading for the fact that Chla is photobleached by a slower rate when incorporated in the lipid bilayer.

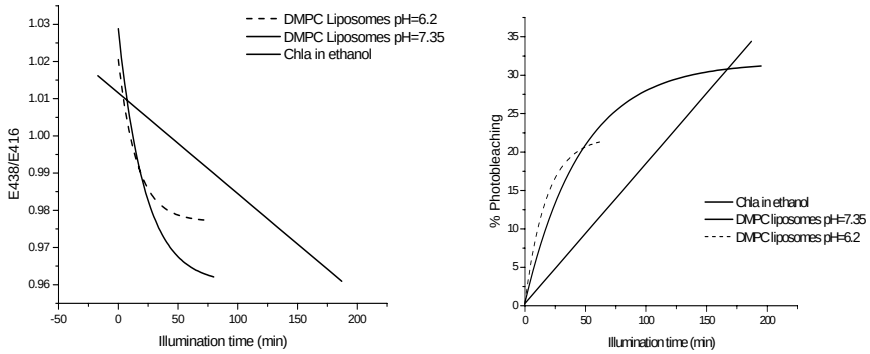


Figure 5. Dependence of spectral parameters upon illumination time

Formation of Chl a-supported lipid membranes:

The deposition of liposomes on solid surface was accomplished by the adsorption technique. Different events could take place in the process of unilamellar vesicles adsorption on the surface [9]:

- interaction of vesicles with other vesicles and with the substrate
- fusion and rupture of vesicles/ rupture of individual vesicles
- transformation of surface bound vesicles in a continuous supported lipid bilayer.

The concentration quenching of Chla fluorescence, in a suspension of Chla-SUVs, as presented in Figure 6,

could be explained by two possible mechanisms: transfer of energy or formation of molecular non-fluorescent Chla aggregates. The second mechanism could be considered in the case of liposome fusion or rupture of vesicles: Chla inserted in the lipid bilayer achieves more freedom to self-aggregate in fused or ruptured liposome membranes. Following this result, the optimum concentration for liposome adsorption was estimated.

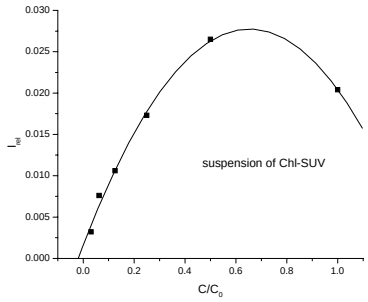
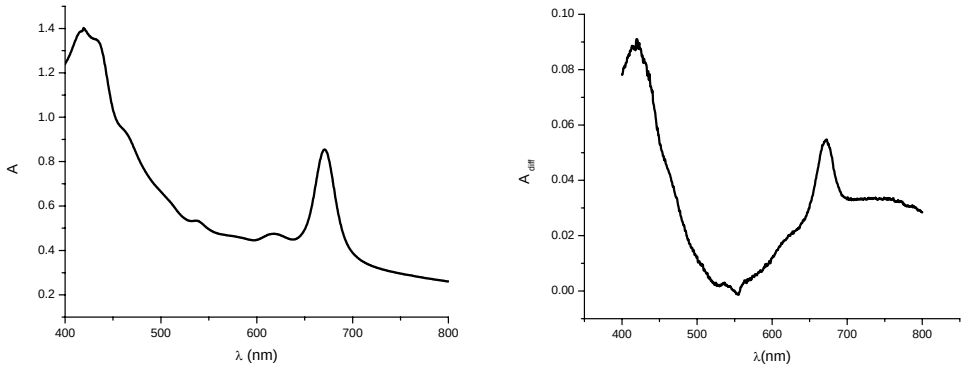


Figure 6. The dependence of Chla fluorescence on concentration, in a suspension of Chla-SUVs (λexc= 430 nm, λem= 680 nm)

To monitor the adsorption of Chla-liposomes on solid supports, the Chla absorption and emission properties have been used. In figure 7, the absorption spectra of Chla both in liposome suspension and on ITO covered by Chla-SLB are represented. The spectra are very similar. The red maximum is at 670 nm in both spectra, leading to the conclusion that after deposition on the solid support, Chla remains in the same environment as in the liposomes, i.e. with the porphyrin ring in the vicinity of lipid polar groups.



A. B.

Figure 7. Absorption spectra in VIS range

(A) Chla-SUVs in suspension, (B) Chla-SLB on ITO (ITO absorption was extracted graphically)

Also the emission spectra of Chla-liposome in suspension as compared with the Chla-SLB on silicon wafer, presented in Figure 8, are sustaining the above conclusion, that Chla is keeping the place in the lipid bilayer when liposomes are spread on the solid support surface.

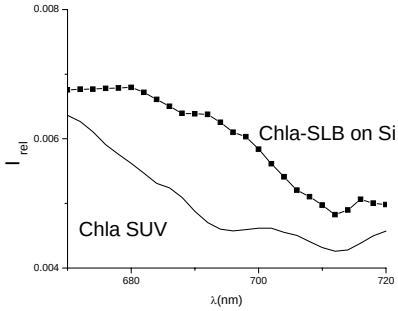


Figure 8. Emission spectra of Chla in SUVs and in BLS on Silicon wafer

(λexc= 430 nm)

Sensitization process at chlorophyll/Si hetero-junction

As already mentioned in the introduction, SLBs are envisaged as useful new structures for different biotechnological applications. By manufacturing a photovoltaic device, based on Chla-SLB deposited on Si wafer, some promising preliminary results have been obtained. The action spectrum presented in figure 9 (the photocurrent plotted as function of the wavelength of the illumination light) is pleading for an effect of sensitization at Chlorophyll/Si hetero-junction.

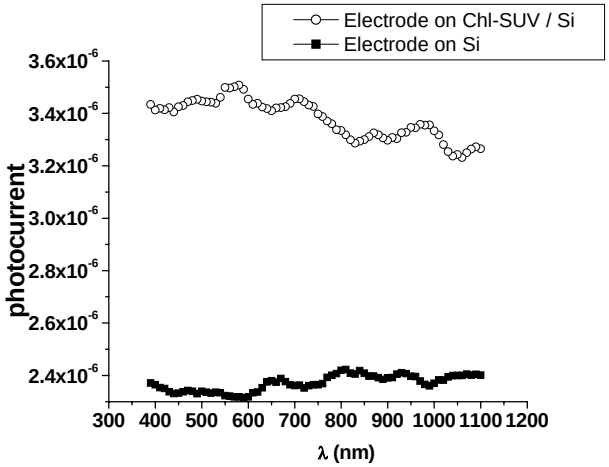


Figure 9. Action spectrum of the sandwich type cell (Si/Chla-SLB/Au)

Summary

Chlorophyll a incorporated in the liposome lipid bilayer was used to monitor the formation of both Chl- liposomes and supported Chl-lipid membranes.

The strong visible absorption and fluorescence of Chlorophyll a allow its use as a sensor for the interactions at molecular level and as a fluorescence marker.

Spectral criteria have been developed in order to monitor the size and shape of Chla-liposomes, the oxidation state of the components and for studying the effect of irradiation with light (VIS range).

Interaction of Chla with light and the Chla absorbance and fluorescence properties were successfully used to monitor the supported lipid membranes on ITO and Si substrate.

Preliminary photo-electrical measurements are pleading for successful utilization of supported Chl lipid membranes in building up photovoltaic devices using Chl a as a photo- sensitisation factor.

Acknowledgement

The Romanian National Council of Research in Higher Education (CNCSIS grant No.1148, theme 30 A/2006) and the Romanian Ministry of Education and Research (CEEX program, Contract 67/2005) are acknowledged for the financial support. The Perkin Elmer fluorescence equipment was purchased by a donation offered by the Department of Biophysical Chemistry, University of Bielefeld, Germany (Professor Dr. Eberhard Neumann). The author would like to thank to Adrian Enache and Andreia Popa (former master students) for their contribution to this work.

References

1. R.R.C. New (editor) "Liposomes - a practical approach"(1990), IRL at Oxford University Press
2. V.A. Nadtochenko et al. (1993) J.Photochem.Photobiol.B:Biol. **18**, 221
3. Laura Tugulea, Simona Pascanu (1996) Romanian Journal of Biophysics **6**, no.1-2, 1
4. Marcela Barbinta Patrascu, Manuela Voinea, Laura Tugulea (2003) Analele Universitatii din Bucuresti, Fizica, **LII**, 35
5. Barbanta-Patrascu Marcela, Tugulea Laura (2005) Romanian Journal of Physics **50**, Nos. 9-10
6. J.T.Groves, N.Ulman, P.S.Cremer, S.G.Boxer (1998), Langmuir **14**, 3347
7. N.Bergstrand, K.Edwards (2001) Langmuir 17, 3245
8. E. Reimhult, F.Hook, B.Kasemo (2002) J.Chem.Phys.**117**, no.16, 7401
9. R.P.Richter, J.Lai Kee Him, A. Brisson (2003) Materials today, November, 32
10. W. J. Moore "Physical Chemistry" Longmans Green and Co. Ltd., London (1962), pp. 761-763
11. O. Bittner et al. (2002) Chemistry and Physics of Lipids **114**, 81
12. Laura Tugulea, I.M. Iacovache (2002) W. Mejbaum-Katzenellenbogen's Molecular Biology Seminars "Liposomes, From Models to Applications", Wrocław/Piechowice by Szklarska Poręba, Poland, May 26-29, 2002

THE EFFECT OF TERAHERTZ RADIATION OF A FREE ELECTRON LASER ON THE LYOPHLIZED SAMPLES OF OX SERUM ALBUMIN

N.L.LAVRIK, E.M.NEMOVA

INSTITUTE OF CHEMICAL KINETICS AND COMBUSTION SBRAS, NOVOSIBIRSK, RUSSIA

lavrik@ns.kinetics.nsc.ru

The lyophilized samples of ox serum albumin (OSA) were IR irradiated at λ = 120 -140 mkm by a free electron laser of a power of 130-280 mw. The analysis of IR absorption spectra indicates a decrease in both the optical density of the bands of characteristic frequencies (2700 - 3100 cm^{-1}) and the value of background determined by scattering intensity. The analysis of UV absorption spectra indicates a decrease in the optical density of irradiated samples at λ = 270 nm as compared with the non-irradiated ones. The thermal heating of samples caused an increase in the scattering of IR spectra and no changes of absorption value in the region of characteristic frequencies and UV absorption spectra. The influence of terahertz radiation was did`t observed for water solution of OSA. The observed laser effects are interpreted in the framework of the hypothesis of the existence of photochemical destruction, laser swelling and ablation.

Introduction

Studying the influence of interaction between electromagnetic terahertzian radiation, THz (70 - 240mkm), and bioobjects is actual because of a feasible effect of this radiation on their functioning and structure [1-2]. However, the total number of works devoted to this problem is rather small [3]. A direct study on the interaction between terahertzian radiation and biomolecules is presented in a limited number of works [4-8]. Thus, in [5] it is shown that the irradiation of horse-radish DNA molecules, lysocyme and peroxidase leads to soft ablation under free electron laser irradiation (λ =100-200 mkm, pulse duration 50 pc, frequency 5,6 MHz, mean power 200 W). The existence of soft ablation is assigned to the fact [7] that the irradiated protein partially preserves a functional activity.

It is concluded then [8] that the irradiation of the lyophilized preparation of ox serous albumin (OSA) causes changes (deformation) in a secondary structure. In this work, a pulse laser with a generation wavelength of 90 mkm and a pulse energy of 5 mJ was used. The values of doses were varied from 0.2 to 3 J. This information was extracted from changes of the fluorescence properties of the probe whose interaction with an OSA molecule was dependent on the irradiation dose obtained by the OSA molecule. The deformation of substance structure under laser pulse can be followed by swelling and ablation [9]. Thus, according to [9] the action of laser radiation is likely to lead to the swelling of OSA samples.

The swelling (the formation of tubercles at the irradiated surface), i.e., the deformation of object macrostructure, can actually cause direct changes in the electron characteristics of the OSA molecule. Thus, of interest is to observe changes in the IR and UV absorption spectra of OSA samples under terahertzian radiation because these spectra contain direct information on the electron properties of the molecule under study. The goal of the present work is to compare the IR and UV absorption spectra of OSA samples before and after THZ irradiation.

Materials and Methods.

The lyophilized OSA preparation of the firm «PPP» was used without repurification. The starting preparation was represented by 3 mm flat plates. The samples were irradiated in teflon (fluoroplast) cells. The thickness of the windows was 3 mm. The sample irradiated (the preparation was preliminarily grinded in an agate mortar) was spread throughout a window with 50 mkm cylindrical cavities of a diameter of 30 mm.

A free electron laser (FEL) [10] produced terahertzian radiation with the parameters λ = 130-140 mkm, a pulse duration of 50 ps, a frequency of 5,6 MHz, and a mean power of 200 mW. The time of irradiation was 3, 6 and 9 min which corresponded to doses of 36, 72, and 108 J, respectively. The power was controlled by an power meter IMO-2. The laser beam half-width was 8 mm.

The thermal heating was realized by locating a cell in a thermostat at a given temperature under irradiation of a thermal gun. The heating temperature was measured using a differential thermocouple. The samples were heated to 55^0C.

The IR spectra of irradiated and test samples were analyzed in the cells used for irradiation. A Fourier-spectrometer ("Bruker") was employed for analysis. The UV spectra of irradiated and test samples were analyzed using aqueous OSA solutions whose concentration was 1mg/ml. The solutions were prepared by dissolving the weighted portions of irradiated and non-irradiated OSA powders in deionized water. The UV absorption spectra were obtained using a "Hewlette-Packard" spectrometer.

Results and discussion

Figure1a shows the IR absorption spectrum of albumin powder (control). The range of characteristic frequencies from 2700 to 3500 cm^{-1} is determined by the stretching vibrations of CH, NH and OH groups [11]. Figure1b shows the IR absorption spectrum of albumin powder after a 3 min irradiation by the FEL at λ = 130 mkm and with a power of 200 mW. A comparison of these spectra indicates a decrease in the intensities of both the background at 2800 cm^{-1} and the lines of characteristic frequencies at 2930 cm^{-1}. Note that the value of the absorption of the structurized spectrum region changes in proportion to the change in the background absorption. Heating the samples by either air convection in a thermostat or the directed stream of hot air from a heat gun with a temperature up to 55^{o}C causes another change in the IR absorption spectra, i.e., the background intensity increases and that of specific bands remains unchanged. Thus, the action of FEL radiation and the thermal heating of OSA samples lead to changes in the IR spectra with different signs. It is concluded then that the nature of changes in absorption spectra is quite different. The difference between the absorption spectra of the starting sample and the irradiated one depends on the time of irradiation (dose).

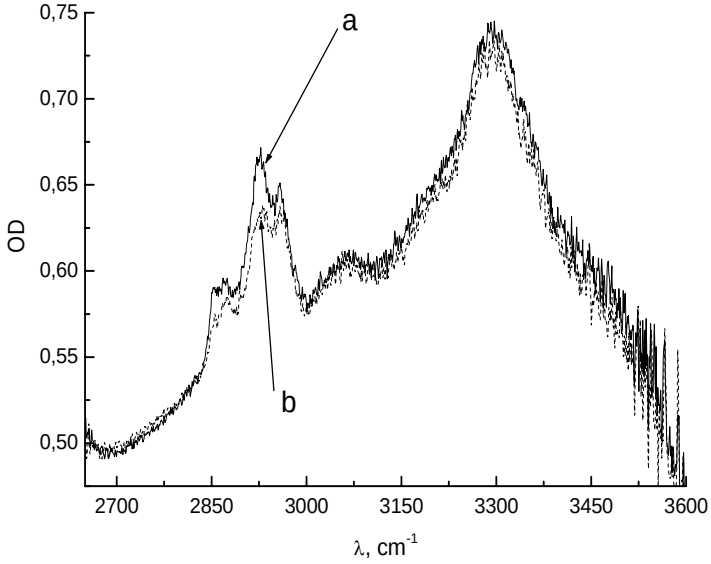


Fig.1. IR spectra of OSA before (a) and after (b) irradiation.

Both the increase in the intensity of background absorption, determined by cell absorption and sample scattering, and the absence of changes in the intensity in the area of absorption of CH, NH, and OH vibrations under heating can be assigned to either the appearance of fractures in the sample or the subdivision of the granules of laminar OSA. In this case, the background intensity is sure to increase and the intensity of the structurized spectrum region will remain constant because the concentration of characteristic groups remains unchanged.

A decrease in the absorption intensity of the background and the structurized spectrum region under FEL irradiation can be assigned to the fact that under irradiation a considerable heating causes carbonization, agglomeration, etc. Such “burning” or “agglomeration” can cause a decrease in the number of reflecting surfaces. In addition, the process of “agglomeration” can decrease the number of CH, NH, and OH groups if initial molecules are destructed and the products are formed in which a fraction of molecules containing the given structural fragments is smaller. This chemical process is e.g., well known for the process of humus-formation where chemical transformations in soil cause an increase of C/H, N/C ratios in time. An increase in the values of these ratios testifies to the increase in the aroma of the systems studied [12]. When the process of “burning” prevails in the effect of the decrease of OSA sample absorption, the presence of oxygen will be of major importance because the samples were irradiated from which oxygen was not removed. Therefore, it is interesting to perform experiments on THz irradiation of OSA samples in an oxygen-free medium.

Note that a feasible effect of conglomeration is in agreement with the concepts of the existence of the effect of laser ablation in the system under study. Indeed, since irradiation was performed in a closed volume, the possible products of ablation whose structure is sure to differ from the initial ones, remain in the same volume and can lead to a change in absorption spectra. As for the effect of laser swelling (the swelling of the irradiated sample surface at the irradiation site) which precedes laser ablation, it is also possible because the OSA powder is a set of laminar structures at the surface of which the swelling effect can be observed. However, our method of recording the effects of irradiation fails to reveal the manifestations of swelling because these cause no

changes in the value of absorption of both a substrate and the structurized part of the spectrum. Finally, the swelling can be absolutely absent because in our experiments the pulse energy and the dose substantially exceed those in [8].

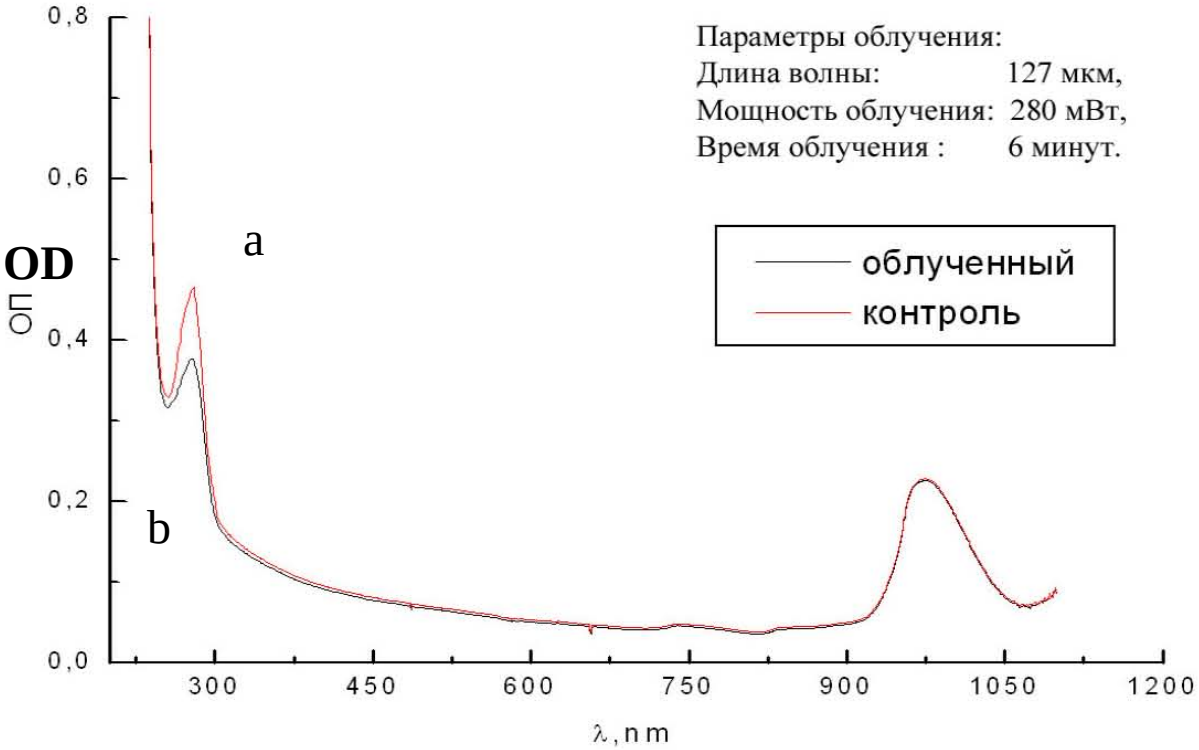


Fig.2. Electronic absorption spectra of OSA samples before (a) and after (b) irradiation.

Assumption of the effect of "agglomeration" accompanied by a significant chemical destruction of the initial structure of OSA molecule is confirmed by the effect of a decrease in the intensity of the UV spectrum absorption of the OSA molecule after irradiation (fig.2). As follows from the figure, after irradiation, the absorption intensity of the sample decreases by about 40%. This testifies to a decrease in the number of structural groups determining a characteristic "protein" absorption at λ = 270 nm. The tests performed using the thermally heated OSA samples indicate the absence of any changes in the UV absorption spectra.

Thus, the terahertzian radiation with a wavelength of 130 mkm and a power of 200 mW leads to the observed changes in the UV and IR absorption spectra that are opposite in their directivity to the influence of thermal heating. The changes in absorption spectra are likely to be due to the destruction of initial molecules.

References

1. C.F.Blackman, M.C.Surles, S.C.Bename. // Biol. Effects of Electromagnetic Waves, 1976, **1**, 406-413.
2. M.Zhengyu. // Infrared Phys., 1989, **29**, 631-636.
3. V.I.Fedorov, S.S.Popova, A.N.Pisarchik. // Intern. J. Infrared and Millimeter Waves. 2003, **24(8)**, 1235–1252.
4. D.D.Dlott, M.D.Fayer. // IEEEJ.Quantum Electron, 1991, **27**, 2697-2713.
5. A.Xie, A.F.G.Meer, W.Hoff, R.H.Austin.// Phys.Rev.Lett., 2002, **88**, 018102/1-4.
6. S.A.Ilyina, G.F.Bakaushina, V.I.Gaiduk, A.M.Hrapko, N.B.Zinovieva. // Biofizika, 1979, **24(3)**, 513 - 518 (in Russian).
7. A.K.Petrov, A.S.Kozlov, M.B.Taraban, T.N.Goryachkovskaya, S.B.Malishkin, V.M.Popik, S.E.Peltek. // Dokladi Akademii Nauk, 2005, **404(5),** 698-700 (in Russian).
8. V.M.Govorun, V.E.Tretiakov, N,N.Tulyukov, V.B.Fleurov, A.I.Demin, A.Yu.Volkov, V.A.Batanov, A.B.Kapitanov. // Infrared and Millimeter Waves, 1991,**12**, 1469-1474.
9. A.Yu.Malishev, N.M.Bituyrin.// Quntum Electronics, 2005, **35(9)**, 825-830 (in Russian).
10. V.P.Bolotin, D.A.Kairan, B.A.Knyazev et al. Status of Novosibirsk free electron laser and First Experiments with High Power Terahertz Radiation. Preprint of Institute of Nuclear Physik. Novosibirsk, 2004.
11. K.Nakamoto. // Infrared spectra of inorganic and coordination compounds. John Wiley & Sons, Inc., New York, London, 1965.
12. N.L.Lavrik, M.I.Dergacheva, E.I.Kovaleva. // Chemistry of stable development, 2000, **8**, 815-821.
13. A.Malyshev, N.Bityurin. // Appl. Phys. 2004, **A 79**, 1175-1179.

THE ROLE OF THE OPTICAL VISUAL SYSTEM IN RECOGNIZING THE THIRD DIMENSION OF THE OPTICAL IMAGE

Medhat ElMessiery and Manal M. Awad

Department of Engineering Mathematics and Physics Faculty of Engineering

Cairo University, Cairo Egypt

Abstract

Against the popular believe that the acute visual recognition takes place at the fovea this work examines the possible focusing effect of the visual system as a whole in the formation of clear image on the retina as a whole . Accordingly the image is affected by the curvature of the retina, the gradient of the index of refraction of the lens and other media as well as the curvature of the retina itself. The present approach utilizes the ray tracing technique to track the image at different levels until it reaches the curved surface of the retina. The results confirm that it is possible to have a focused image on considerable area of the retina. Also it gives a reasonable explanation to the third dimension recognition.

Introduction

The eye is the most efficient image system. The visual system in man is capable of reducing the dimensions of the external world to almost 0.3 % of its original size without losing acuity, resolution and sharpness of the formed image. It is so adjustable to distance so that it deals with objects that are large and small, far and near and bright and dull. It differentiates colours within the visible spectrum. the system is in a continuous process of adjusting its parameters to focus objects at different distances on the retina (accommodation), thus the refractive power of the lens increases for focusing a near object upon the retina. Most importantly it is capable of recognizing the third dimension of the perceived world.

Over the years, A number of models were introduced in order to explain the remarkable abilities of this system . Most of the classical approaches deal with the paraxial properties of image formation on the retina.

For example, the paraxial schematic eye is highly approximative and serves only in obtaining some parameters such as the equivalent power , the position of the cardinal points, the retinal image size , magnification factor. This model simplifies many mathematical difficulties and overlooks the problems of media inhomogeneity; geometrical considerations and the effect of the curved shape retina on image reception.

Rosenblum et al.[1] introduced a defined model of the human eye by including a inhomogeneous crystalline lens with a purely radial gradient index of refraction. The model has the same basic elements that Blaker[2] used and consists of a corneal refracting surface with a radius of 7.8 mm, an aqueous chamber that is 3.6 mm thick, and has an index 1.336. The crystalline is composed of an anterior thin lens of radius 10.0 mm with an index of 1.386, a radial gradient of a central index of 1.406 and an edge index of 1.375, and a posterior thin lens of radius 6.0 mm and an index of 1.386.

The index of refraction distribution within the radial gradient takes the form.

$$n(y)=n_0\left(1\pm\frac{V^2}{2}y^2\right)$$

Which describes a quadratic change in refractive index from a central value of n_0. The magnitude of the coefficient V depicts the type of gradient index lens being used. Rosenblum et al [3] used a value for V^2 of $41.58m^{-2}$. They found that the focal length, measured from the posterior of the crystalline lens, is 16.55 mm. This posterior focal length compares favourably with the 16.51 mm value that Blaker[2] obtained using both an axial and a radial gradient in his model of the eye.

Despite the difficulties in introducing a mathematical description to the different refracting surfaces of the system, Al-Ahdali and ElMessiery[3] introduced a model of the human eye for which they take into consideration the laminated nature of lens fibres. The thickness of each lamina is 0.0056 mm; thus lens comprises 300 eccentric lenses of minute dimensions. The index gradient of the lens is such that the index of refraction increases exponentially from the lens core to its peripheral zone. The radius of anterior and posterior group decreases exponentially from the pole toward the core.

The laminated lens model offers a plausible explanation to the image formation which is not only compressed but completely focused on a curved surface of the retina. The acuity of the image is usually examined by the spot diagram which is a plot of intersection points of rays from an object point with an image plane. The spot diagram is constructed by using finite ray tracing for all rays that emerge from the object and reach their final destination on the image plane. This diagram is very effectively in studying firstly, the distribution of light intensity on the image plane of a luminous object. Secondly, The imaging features, the possible defects, and limitations of an optical system.

The merit function is related to the image quality. The optimum form of image formation may be achieved by minimizing the merit function. Most commonly used merit functions are the RMS blur circle radius, the wave aberration function, and the sum of squares of the aberration coefficients.

It is based on determination of the central coordinates of the intersection of rays with the image plane. The RMS blur circle radius gives a measure of the transverse aberration among other optical defects of the system. In order to obtain reliable values for RMS blur circle radius, one needs to trace several hundred rays, uniformly distributed over the entrance pupil, through the optical system.

The least square deviation is given as :

$$(RMS)^2=\frac{1}{N}\sum_{I}^{N}\left[(X(I)-<X(I)>)^2+(Y(I)-<Y(I)>)^2\right]$$

Where X(I) and Y(I) are the coordinates of intersection of the ray at the image plane.

$<X(I)>$ and $<Y(I)>$ represent the average coordinates of the ray intercepting the image plane.

They are the result of tracing N rays passing through equal areas in the entrance pupil.

$$<X(I)>=\frac{1}{N}\sum_{I}^{N}X(I) \quad \text{and} \quad <Y(I)>=\frac{1}{N}\sum_{I}^{N}Y(I)$$

Al Ahadali [4] used caustic surfaces as a merit function and optimized the caustic points towards an Gaussian focal point. In this case the lens parameters are varied by a certain procedure.

Pomerantzeff et al [5] have introduced an eye model based on the wide angle of light entrance to the eye which was based on finding the square root of the distance between the Gaussian focal point and the caustic Kortez and Handelman[6] discussed the mechanism of eye accommodation and produced a simple model explaining the effect of such accommodation on image formation.

Manal and Essam[7] have used this model to examine the demagnification power of the eye for near and far vision they found that the image rotates and demagnifies as it formed on the curved retina.

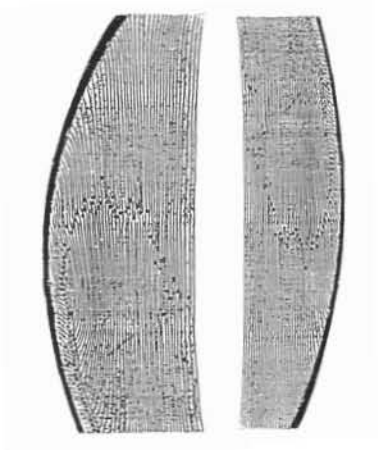


Figure1, the laminated distribution of the human lens

THE MODEL:

Since the dimensions of human eye are large in comparison to the visible wave length (λ = 4000 to 7000 A°, Iris diameter = 4 mm), the geometrical optics approach is applicable. In this work we use the laminated lens model, which was described previously and proved its accuracy and reliability in connection with the main parameters of

the visual system. This model is based mainly on the following:

1. The lens is not a homogenous medium, but in fact, there are many zones of optical discontinuity within it and they vary both in refractive index and in radius of curvature as shown if figure(1). In the absence of accurate information about the number of these zones or their curvature. This variation in the index of refraction is dealt with by assuming an exponential increase of the lens index of refraction from the core to the peripheral. The surfaces of both the cornea and the lens deviate from being spherical to ellipsoidal. The lens thickness varies as the lens changes from unaccommodated to the accommodated modes. Accordingly the image is formed with extra features that are it is compressed by an average value from 0.3 to 7 %. The radius of curvature R of the surfaces of the cornea and the lens ; are expressed mathematically as rotationally symmetric aspherical surface so that

$$x^2 + y^2 + (1+Q)z^2 - 2zR = 0$$

The degree of asphericity are examined by varying Q in order to give the optimum acuity of the image on the retina.

2. Vector ray-tracing technique is employed to study the optical characteristics of the system. Both paraxial and marginal rays are simulated, by considering 400 rays (which are equally distributed on the cornea) emerging from each point of the source and they were all traced through the system until they strike the retina. The angles of incidence vary from 0° to ± 20° and the maximum iris entrance radius was taken as 2mm.
3. Computer simulation technique studied the visual system under accommodation and unaccommodating modes also far and near objects were studied.
4. The constants introduced in this model, were obtained under the optimal conditions of; focusing the images on the curved surface of the retina; Minimum radius of the blur circle and caustic surface and finally minimal spherical aberration.
5. The spot diagram is constructed by using finite ray tracing for all rays that emerge from the object and reach their final destination on the image plane. This diagram is used in studying firstly, the distribution of light intensity on the image plane of a luminous object. Secondly, the imaging features, the possible defects, and limitations of an optical system.

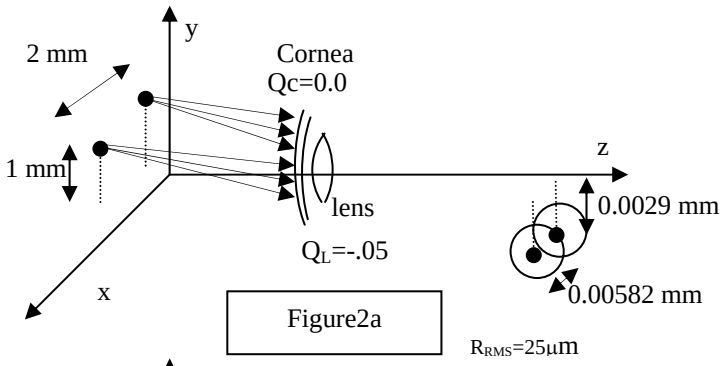


Figure2a

R_{RMS}=25μm

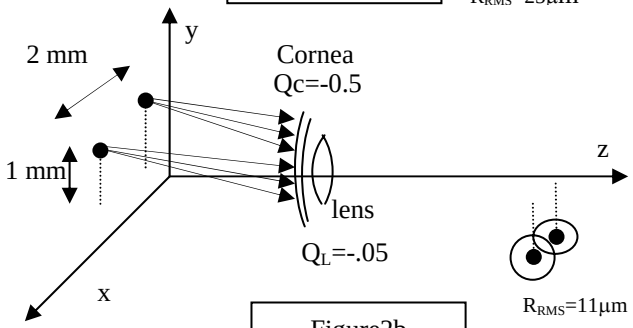


Figure2b

R_{RMS}=11μm

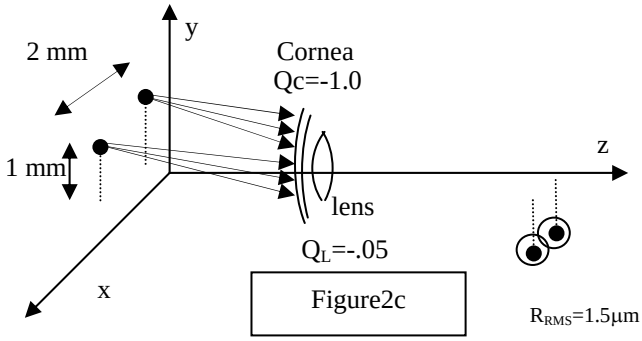


Figure2c

R_{RMS}=1.5μm

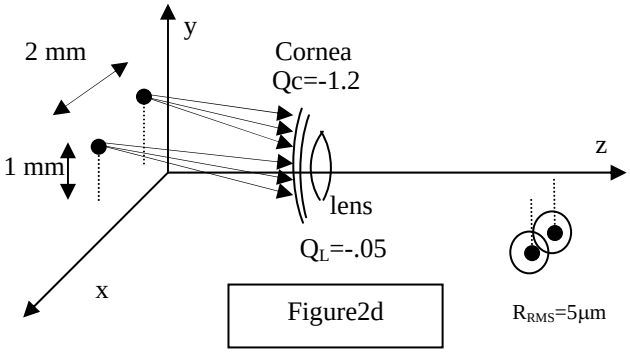


Figure2d

R_{RMS}=5μm

RESULTS:

Figure(2) represents the variations of RMS of the blur radius with lens asphericity for different values of both the cornea Q_c and the lens Q_L. Here, the object is considered at far vision, i.e. the incident rays are parallel to the optical axis and uniformly distributed at the entrance grid placed in front of the cornea.

A four hundred incident rays are used to construct the image of two point objects

(2 mm apart and height 1 mm); as they received on the retina. These objects are considered at far vision.
Figures (2a,b,c and d) show the variation of RMS value of the radius of the blur circle of the image point at the retina for different values of cornea asphericity represents; lens asphericity is kept constant at a value of -0.5.
It is clear that the cornea asphericity plays a dominate factor of the image acuity and there is a critical value of Q_C of -1.0 at which the blur circle has a minimum rms radius.
In order to examine the effect of the complicity of the eye in comparison with other optical system the image of a cube in the near vision is first received on a plane Figure(3a) and the second on the curved surface of the retina Figure(3b).

In the first case the projection of the cube is demagnified square that hide the far edges LKMN behind but in the second case the projection of the same object is firstly subjected to different demagnification factor that exhibits the all sides of the cube with different location. Secondly the straight edges are focused and curved and thirdly the image rotates with respect to the object with an angle that is proportional to the axial distance.

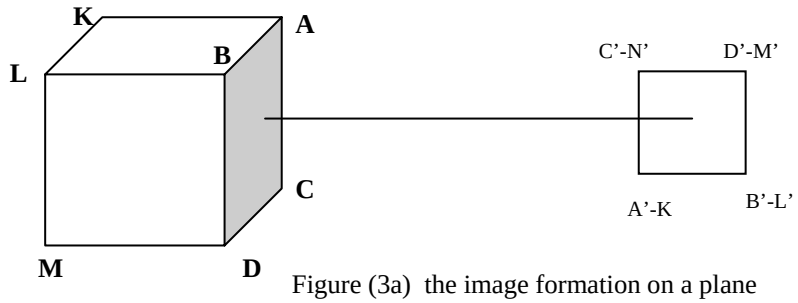


Figure (3a) the image formation on a plane

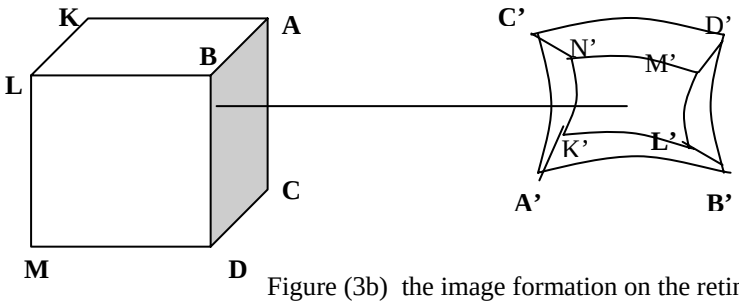


Figure (3b) the image formation on the retina

Figure (3) comparison between the image formation on a plane and on the curved retina

DISCUSION AND CONCLUSION

The present investigation aimed at producing a complete model to the image formation at the retina of human eye. The model suggests that:
1-The cornea acts as a very powerful converging lens. The aqueous humour has a refractive index differing slightly from the corneal substance, thus the posterior surface has a negligible refractive power. The focusing depends on the cornea curvature of lens surfaces curvature and the gradients of the lens index of refraction. Thus the asphericity of the system plays a strong role in the perfection of the eye as an optical system.

2- There is a linear dependence between corneal asphericity and lens asphericity that gives the optimum sharpness conditions as illustrated in figure(1).

3-The fovea is less than one half a millimetres (less than 500 micrometers) in diameter, which means that maximum visual acuity occurs in only 3 degrees of the visual field. Outside this fovea area the visual acuity is reduced five to tenfold, and it becomes progressively poorer as the periphery is approached.
The image blur circle of a point source could have a rms radius in the order of 5 micrometers. While the average diameter of cones in the fovea (the central part of the retina where vision is most highly developed), is approximately 1.5 micrometers. a person can distinguish two separate points if their centres lie approximately 2 micrometers apart on the retina, which is slightly greater than the width of a single cone in the fovea.

4- The blur circles for objects at far vision do not affect the image. However as the size of the object decreases the image itself as a whole lies within a very small area on the retina (in the order of 2 cones) so that it will not be recognized in full details. For bigger object the resolution improves and the blur circle does not seriously damage the details of the object. As the object comes nearer to the eye the problems of aberration appears more seriously.

6- The demagnification factor for far vision is almost constant ($0.29 \pm 0.003\%$) which means that all images will be demagnified equally irrespective of their geometry as long as they are in the far vision region.
For Near vision (object distance $\leq$ 25 cm). The demagnification factor is almost constant (6.8) for small object height up to 50 mm. But decreases linearly for object height greater than 50 mm.

The variation of lens height is not the main factor affecting the accommodation process but also the shape of the lens (lens asphericity) changes during accommodation in order to obtain the maximum sharpness of the image.

7- The accommodation process does not affect the demagnification factor where it is almost the same for both accommodated and unaccommodated lens. So the accommodation process affects only the sharpness of the image but not the size of the image.
8- The perception of the 3D of the image is not an absolutely mental process. But it is done by the variation of demagnification factor with the axial distance.

REFERENCES

1-Rosenblum, W, M., Blacker, J, W, & Block, M, G, "Matrix method for the evaluation of lens systems with radial gradient-index elements", *Am. J. Optomet.Physiol. Opt,* Vol 65, 1988, pp 661-665.

2-Blaker, J, W, "Toward an adaptive model of the human eye", *J.Opt.Soc.Am.*, Vol 70, 1980, pp 220-223.

3-AL-Ahdali, E, H, & EI-Messiery, M, A, "Examination of the effect of the fibrous structure of a lens on the optical characteristics of the human eye: a computer simulated model", *Applied Optics*, Vol. 34, No. 25, 1995, pp 5738-5745.

4-AL-Ahdali, E, H, "Optimization of three and four-element lens systems by minimizing the caustic merit function" PhD. Thesis, Birmingham, ALABAMA, 1989, pp 27-3 5.

5- Pomerantzeff, 0, Pankratov, M, & Dufault P, " Wide-Angle optical model of the eye", *Am.J. Of. Optom. & Physio. Optics*, Vol 61, No. 3, 1984, pp 166-176.

6- Kortez, J, F, & Handelman, G, H, "model of the accommodative mechanism 'in the human eye", *Vision Res.*, Vol 22, 1982, pp 917-927.

7-Manal , M and Essam G,"3Dcompressed image recognition and variable magnification power of the human vision system" 4th IEEE International Midwest Symposium",-ISBN 0-7803-8294-3/04, pp356-360 .

8-EI-Messiery, M, A, & Gomaa, E, "A computer model for the visual system of the eye", *Proc. ICEMP* , Vol1, 1998 pp 298-304.

CALCULATIONS OF OCULAR HEATING DUE TO COMMUNICATIONS HANDSETS

PETER WAINWRIGHT

HEALTH PROTECTION AGENCY, RADIATION PROTECTION DIVISION, CHILTON, DIDCOT, OXFORDSHIRE OX11 0RQ, UK

Exposure standards for radiofrequency radiation are framed in terms of acceptable specific energy absorption rate (SAR) in order to limit temperature rises in the body. The eye lens is particularly sensitive due to the lack of perfusion and limited capacity for repair. This work combines the FDTD method (for SAR computations) and finite element method (for thermal computations). A comparison is made between use of an isolated eye model, with convective boundary conditions, and a full head model. The resolution of the model is insufficient to describe the actual blood flow distribution at the choroid. However, an "equivalent perfusion rate" is used which is chosen to match the convective heat transfer coefficient used in other models. Calculations were made for exposure to a wireless handset with a monopole antenna at 380, 900 and 1800MHz, and with a helical antenna at 380MHz. A range of antenna positions was considered. Despite the range of different exposures, a consistent relationship was found between temperature rise in the eye, SAR averaged over the eye, and the 10g average SAR which is subject to restriction in ICNIRP guidelines.

Introduction

Recent years have seen a rapid increase in the use of personal wireless communications devices such as mobile phones. Unlike other sources of radiofrequency and microwave radiation, these are used in close proximity to the head. These sources can produce exposures which approach national or international safety guidelines (ICNIRP 1998, NRPB 2004, IEEE 2005) and therefore require fairly detailed safety assessment.

Over the past few years several authors (van Leeuwen *et al* 1999, Wainwright 2000, Bernardi *et al* 2000, Gandhi *et al* 2001, Hirata and Shiozawa 2003) have computed the temperature rises in the brain expected during use of a GSM mobile phone. In view of the high blood perfusion rate in the brain, temperature rises are likely to remain well within safe limits, indeed considerably less than the normal diurnal variation of brain temperatures.

The eye is more susceptible than most other organs to damage by microwave radiation. It lacks an internal blood supply, so that it is prone to the appearance of hot spots in the central regions (Hirata 2005). Furthermore, the lens has a limited capacity for repair, and the accumulation of cellular debris can lead to a loss of transparency. Animal experiments (Guy *et al* 1975) have shown the induction of cataracts with acute high level exposure.

Many models of the eye, for humans and other species, have been constructed over the years (Lagendijk 1982, Scott 1988a,b). Modelling the anatomy of the eye itself is relatively straightforward. However, a critical factor in the temperature calculation is the blood flow in the vessels surrounding the eye, particularly in the choroid, which has a dense network of vessels supplying the retina.

A new combined electromagnetic and thermal model of the human head has been developed at HPA. This model combines a finite difference time domain electromagnetic model with 2mm resolution and a finite element thermal model with 1mm resolution in the eye.

The aim of this study is to clarify the relationship between specific energy absorption rate (SAR) and temperature rises in the eye, and to determine whether the present basic restriction on SAR, recommended by ICNIRP, gives adequate protection against possible adverse effects such as cataract. To this end the new model has been used to compare the SAR and temperature rises due to radiation from antennas and handsets at frequencies produced by several widely used types of communication handset. The three frequencies studied

here are 380MHz (used by the Terrestrial Trunked Radio system, TETRA), 900MHz and 1800MHz (used by GSM mobile phones). The model has also been used to study the differences between two alternative antenna types, the monopole and helix.

Some older studies (Lagendijk 1982, Scott 1988a,b) have used a model of the eye in isolation from the head, and a boundary condition at the surface to take into account all heat losses to blood in the choroid and surroundings. The parameters of this boundary condition were chosen to fit temperature data obtained by measurement in the rabbit eye. In order to transfer this information to the full head model, an "equivalent" blood perfusion rate has been estimated for the layer of elements surrounding the eye. This perfusion rate produces a heat transfer approximately equivalent to that in the older truncated models.

Methods

The SAR in the head was calculated using the finite difference time domain (FDTD) technique implemented by a computer program developed at HPA and previously used to calculate SAR from TETRA exposures (Dimbylow *et al*, 2003). This technique uses a segmented voxel (VOlume piXEL) dataset to describe the human anatomy. The body is divided into a regular 3D array of hexahedral cells, and the tissue type of each cell is described by an integer code in the range 0 — 255. This tissue code is used as an index into several arrays which contain the electromagnetic and physical properties for each tissue, for example the density, permittivity and conductivity. Each program run is performed for one frequency. Prior to the run, the permittivity and conductivity at that frequency is calculated for each tissue. This is done using a 4-Cole-Cole model (Gabriel 1996). The open boundary was simulated using the "Perfectly Matched Layer" technique (Berenger 1994) using a 6-cell PML layer and a minimum 5-cell air gap between this and the nearest object.

The original voxel dataset of the head was derived from an MRI scan of an adult male. After initial segmentation as described in (Dimbylow and Mann 1994), a number of additional adjustments were made to correct shortcomings in the data acquisition and automatic tissue segmentation. For example, some voxels on the surface of the head had been erroneously labeled as CSF, and some inside the brain labeled as muscle. The original dataset did not distinguish the cartilage in the nose, and the eyes were half-closed. The original dataset did not show the orbital fat between the optic nerve and the orbital muscles; this region appeared as solid muscle.

The resolution of the original voxel dataset was 1 mm. However, in view of the large number of calculations to be performed it was found that a lower resolution of 2 mm was more appropriate for the majority of SAR calculations. Therefore, the dataset was resampled to the lower resolution using a simple voting algorithm to determine which of the 8 voxel tissue types would be assigned to the larger cube. In the course of this procedure the thin layer of skin covering the head was eroded in places. A subsequent automated procedure ensured a uniform 2 mm (1 voxel) covering of skin over the entire head.

For the thermal calculations a finite element technique was used, since this allows for non-uniform meshing and better conformance to curved interfaces (such as the surface of the eyeball). In this case accuracy of anatomical modeling far from the source is not critical, while the the structures of the eye must be represented in detail. The finite element mesh was derived by an automated procedure (Wainwright 1999) from the voxel dataset used for the SAR calculations. The SAR from the FDTD code was interpolated onto the finite element mesh in the following way: If an element lay entirely within one voxel, the SAR for that voxel was assigned to the element. If an element spanned several voxels, a simple numerical quadrature procedure was applied to integrate the power density over the element and derive the equivalent SAR.

The heat flow was modeled using the bioheat equation (Pennes 1948):

$$\rho c \frac{\partial T}{\partial t} = \nabla.(k \nabla T) + \rho S - \rho \rho_b c_b \omega (T - T_b) \quad (1)$$

together with the boundary conditions

$$k \frac{\partial T}{\partial n} = -(h_r + h_c)(T - T_{amb}) \quad (2)$$

where ρ, c, k and ω are respectively the density, specific heat, thermal conductivity and blood perfusion rate, T is the temperature and S the SAR. The suffices "b" and "amb" indicate the parameters of blood and the ambient temperature. The radiative and convective heat transfer coefficients h_r and h_c may vary over the surface of the body. However, in this work it has been assumed that the total value h is 20 W kg^{-1} for the cornea (Lagendijk 1982) and 8 W kg^{-1} elsewhere. In this paper all results are shown for the steady state, $\partial T/\partial t=0$.

Choroidal blood flow

Although a very thin layer, the choroid has a particularly high blood perfusion rate, which is necessary to supply the oxygen demands of the retina. This has a significant impact on the temperature distribution in the posterior chamber of the eye. The actual value and distribution of choroidal blood flow in humans is still a matter of debate. Many papers have used a model of the eye in isolation from the head, and a boundary condition at the surface to take into account all heat losses to blood in the choroid and surroundings (Lagendijk 1982, Scott 1988a,b). More recently, the value of the heat transfer coefficient has been questioned. It is not clear whether the extrapolation from rabbit to human models is valid. The anesthesia used in the original study may have had a significant effect on the measured blood flow (Kojima *et al* 2004).

Despite these shortcomings, the isolated eye models have been widely used, and a definitive improvement on this approach has not yet been forthcoming. Therefore the model in this study has been designed to replicate as closely as possible the effect of the choroid in the older models, while adding a complete model of the head. By examining simple analytical models of planar layers or concentric spheres it is possible to derive an "equivalent perfusion" for the choroid which replicates the heat loss of the older models in the simplest cases. This is then applied to the realistic SAR distribution in the whole head model.

First consider the steady-state one-dimensional bioheat transfer problem with two regions: region 1 the "choroid" ($0<x<d$), and region 2 the "head" ($x>d$). Assume a known heat flux F incident from the left at the interface $x=0$. In each region the temperature rise ΔT can be expressed as a sum of exponentials:

$$\Delta T(x) = A_i \exp(\alpha_i x) + B_i \exp(-\alpha_i x) \tag{3}$$

where in each region $i=1,2$

$$\alpha_i = \sqrt{\frac{\rho_b c_b \rho_i \omega_i}{k_i}} \tag{4}$$

The coefficients A_i and B_i can then be obtained using the continuity of temperature and heat flux at the tissue interfaces. Note that in the "infinite" region $x>d$ the solution cannot have an exponentially increasing part, so it is necessary that $A_2=0$. When this is done, we have a relationship between heat flux F and $\Delta T(0)$:

$$h = \frac{F}{\Delta T(0)} = k_1\alpha_1 \frac{k_1\alpha_1 \sinh(\alpha_1 d) + k_2\alpha_2 \cosh(\alpha_1 d)}{k_1\alpha_1 \cosh(\alpha_1 d) + k_2\alpha_2 \sinh(\alpha_1 d)} \tag{5}$$

Assume the rest of the "head" contains tissue of very low perfusion, so $\alpha_2 \approx 0$. Then in order to generate a heat transfer coefficient of h=65 W m^{-1} ºC^{-1} (Lagendijk 1982) it is necessary to set α_1=341 m^{-1}, or ω_1=16.3 ml kg^{-1} s^{-1}. If the "head" contains tissue similar to fat, ω_2=0.467 ml kg^{-1} s^{-1} (Duck 1990, Appendix A). Then α_1 must have a somewhat smaller value of 284 m^{-1}.

It is possible to derive a similar analytical solution for a more realistic spherical model of the eye, where the "eye" is the region $r<a$ and the "choroid" is $a<r<a+d$. In this case

$$h = \frac{k_1}{a} \frac{(k_1\alpha_1^2 a + k_2\alpha_2)\sinh(\alpha_1 d) + (k_2\alpha_1\alpha_2 a + k_1\alpha_1)\cosh(\alpha_1 d)}{k_1\alpha_1 \cosh(\alpha_1 d) + k_2\alpha_2 \sinh(\alpha_1 d)} \tag{6}$$

Interestingly, the change from planar to spherical geometry has a major effect on the heat transfer coefficient. For an eye of radius 1.25 cm surrounded by fat, this predicts h=67 W m^{-1} ºC^{-1} *even when* $\alpha_1=0$. This means that the coefficient proposed by Lagendijk (1982), 65 W m^{-1} ºC^{-1}, could be entirely accounted for by a sufficiently large volume of relatively low-perfusion material surrounding the eye. Since the surroundings include higher-perfusion tissues such as muscle and brain, and the choroid itself, it seems likely that the true value of the effective h is considerably higher than this.

As a control value, this paper uses a blood perfusion rate of 16.3 ml kg^{-1} s^{-1} in the choroid. Using the simple spherical model in Equation (6), this corresponds to h=130 W m^{-1} ºC^{-1}, a value which is twice that used in Lagendijk's rabbit model. The sensitivity of the results to this parameter has been investigated by either doubling, or eliminating entirely, the blood flow to the choroid.

Results

First, several computations were made to validate different aspects of the method. The basic configuration was a monopole, radiating at 380 MHz, on top of a metal box. This is a simplified representation of the Motorola MTP700 TETRA handset (Dimbylow *et al* 2003). As a worst-case scenario the handset model was placed as close as possible to the eye in a vertical orientation.

There was some concern initially that the 5-cell (1cm) air gap between the objects and the PML layer might not be sufficient for adequate accuracy in the FDTD calculations. Therefore one typical calculation was performed with both a 5-cell and a 10-cell gap. However, the resulting change in the computed SAR averages was found to be less than 1%. It was therefore concluded that the 5-cell gap was indeed adequate for the present study.

Some comparisons were done to investigate the effect of the improvements made to the segmentation of the anatomical model. The original model contained muscle in place of the cartilage of the nose and the orbital fat behind the eyeball. Inserting the orbital fat had relatively little impact. The maximum change in temperature was

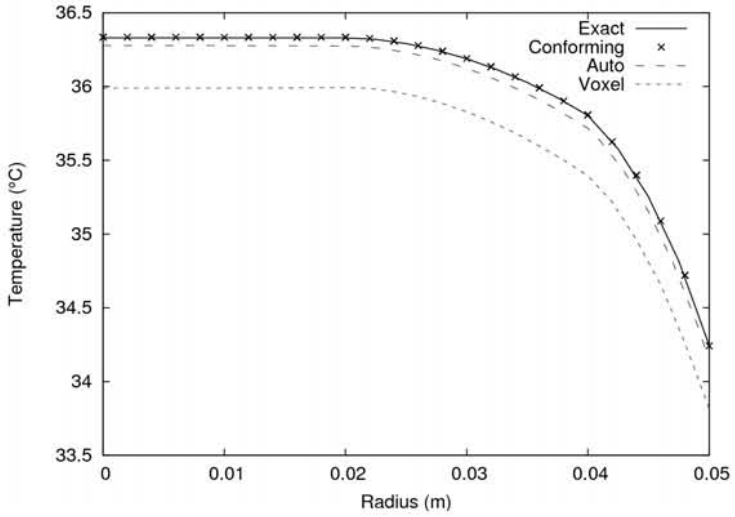


Figure 1: Finite element and exact solution for temperature in a sphere

about 10% of the peak temperature rise in the eye. A similar result was found for the cartilage.

The finite element thermal method was validated by comparison with the exact solutions derived by Durkee *et al* (1990) for spherical shell models. A uniform SAR of 1 W kg^{-1} was injected into a homogeneous sphere of muscle-equivalent material with a radius of 5 cm. The arterial blood temperature was 37ºC, the ambient temperature was 20 ºC and the convective heat transfer coefficient h at the surface was 8 W m^{-1} $ºC^{-1}$. Several finite element meshes were created to model this sphere. These meshes each had a nominal resolution of 2 mm. However, one (the "conforming mesh") was chosen to conform as closely as possible to the spherical boundary. The others were created by the automeshing procedure (Wainwright 1999) and by simply subdividing a mesh of cubical voxels. The latter meshes do not have a continuous normal vector at the surface, and as a result the surface area is somewhat greater than that of the real sphere. This causes a slight overestimate of heat loss from the surface, and slightly lower predicted temperatures as seen in .

A range of different thermal models were compared, ranging from a simple analytic solution with a spherical "eye", to a finite-element solution in an anatomically realistic head. This comparison shows the effects of the factors which are included at each stage of development of a realistic model. The differences between each model and the next can be explained, and this provides some reassurance that the final finite-element calculation correctly implements the model. Each model was applied to a test case consisting of a uniform SAR, 1 W kg^{-1}, applied within the eye alone. For each model, the maximum and minimum ΔT within the eyeball was calculated. The maximum occurs at or near the centre of the eyeball, and the minimum at the periphery.

The successive models were:

1. A homogeneous spherical "eye", of 26mm diameter. A constant convective heat transfer coefficient h=65 W m^{-2} $ºC^{-1}$ was assumed at the surface (Lagendijk 1982). This model was solved using the analytic method (Durkee *et al* 1990).
2. A finite element model containing the eye tissues only, extracted from the full head model, with the same constant h.
3. The same model as in 2, but using a different coefficient h= 20 W m^{-2} $ºC^{-1}$ on the cornea (Lagendijk 1982).
4. The complete head model, with SAR in the eye alone, with no special blood supply to the choroid.

5. The complete head model, with SAR in the eye alone, using the equivalent choroidal blood flow suggested above.

The results are shown in Table 1.

	Min. ΔT (°C)	***Max. ΔT (°C)***
1. Spherical	0.067	0.114
2. Isolated eye, constant *h*	0.046	0.110
3. Isolated eye, variable *h*	0.060	0.135
4. Eye in head	0.063	0.137
5. Eye in head, choroidal BF	0.031	0.102

Table 1: Comparison of eye models

Good agreement is seen between the maximum temperature rise in models 1 and 2. Errors are due to the finite element discretization, as discussed above. The greatest discrepancy arises in those areas of the eye surface where the staircasing effect is most noticeable. The difference between models 2 and 3 arises from the reduction of the heat transfer coefficient at the cornea. The temperature profile is now asymmetric, with the maximum being located toward the anterior part of the eye.

The agreement between models 3 and 4 is at first sight the most surprising feature of these calculations, because model 4 contains no special blood supply for the choroid. However, this result does agree with the argument made in the previous section. There it was shown that the fatty tissue surrounding the eye has a sufficient blood flow to generate an effective heat transfer coefficient of 67 W m^{-1} $^oC^{-1}$, nearly equal to the value used in the isolated eye models. Figure 2 shows the maximum and minimum ΔT in the eye for a range of choroidal blood perfusion. The central value, in particular, is relatively insensitive to this value. The difference between the central and peripheral temperature is almost constant because there is a constant thermal resistance between the centre and periphery; this cannot be eliminated however large the choroidal perfusion.

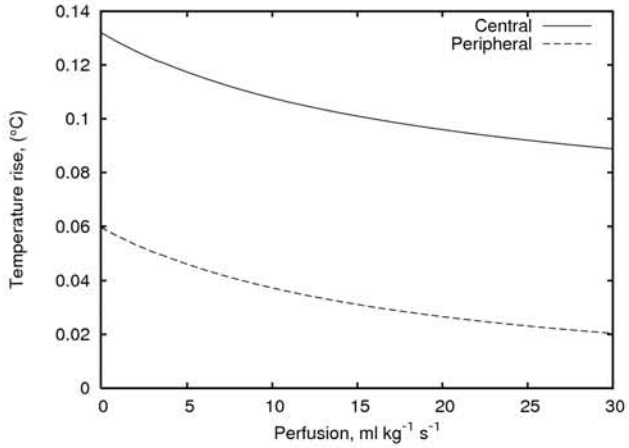


Figure 2: Effect of choroidal perfusion on ΔT

Figure 3 shows the TETRA handset placed as close as possible to the eye; the antenna feed point is 2.4 cm from the surface of the eye. Only the metallic parts of the antenna and handset are shown here. The handset is covered with a plastic casing and this prevents it from being moved any closer to the eye. In the following figures, this position is used as the origin for displacements of the antenna. The length of the monopole is about 3λ/16, where λ is the free-space wavelength. As seen from the figures this leads to quite a long and unwieldy antenna at the TETRA frequency, 380MHz. A more compact design uses a helical antenna (Dimbylow *et al* 2003). The temperature and SAR quoted here have been calculated for an antenna input power normalized to 1W. In order to study the effect of frequency on the temperature distribution, calculations were also performed using appropriately scaled monopole antennas at the GSM frequencies, 900 and 1800MHz, mounted on the same metal box.

Figure 4 and Figure 5 show the relative SAR profiles for the TETRA monopole handset located at 2.4 cm and at

8.4 cm. The greyscale values are not to the same scale. In Figure 4 the maximum (white) represents 4 W kg^{-1}, while in Figure 5 it represents 1 W kg^{-1}. It can be seen here that when the handset is held well away from the face the maximum SAR occurs not in the eye but in superficial structures such as the nose. Also, for a distant source, the SAR distribution in the eye becomes much more uniform, since the penetration depth at 380MHz is comparable to the eye size.

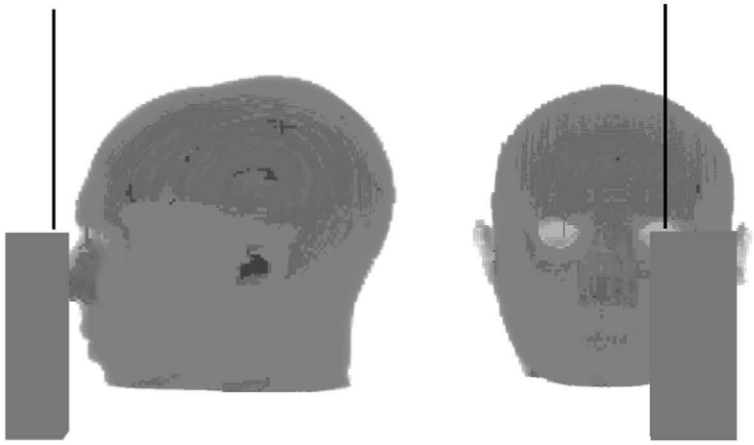


Figure 3: TETRA handset close to eye



Figure 4: TETRA at 2.4cm



Figure 5: TETRA at 8.4cm

An investigation was made into the relative contributions made to the temperature rise by the SAR inside and outside the eye. A plot of temperature rise along the central AP axis of the eye (Figure 6) shows heat conduction from outside the eyeball accounts for about 40% of the temperature rise in the lens. A detailed examination of the SAR and temperature profiles (not shown) has been done and reveals that this heat comes mainly from the orbital muscles above and below the eye.

Figure 7 shows the temperature rise along the central axis of the eye for various values of the choroidal perfusion rate. The middle curve is for the control value; the other curves show ΔT for the case of no perfusion or of double perfusion. As previously seen in Figure 2, it is apparent that increments in the perfusion rate become successively less effective, and in fact that ΔT for the lens converges to a nonzero value.

Figure 8 shows the central axis temperature rises for TETRA monopole and helical antennas, and GSM900 and GSM1800 monopole antennas (with appropriately scaled size) mounted on the same metal box. The profiles are very similar. The main difference arises from the fact that the penetration depth is smaller at 1800MHz, and therefore in this case the temperature rise is noticeably more peaked in the anterior part of the eye.

Table 2 summarises the SAR averages and temperature rises obtained for three frequencies, two antenna types and two values of the antenna-eye distance. The ICNIRP basic restriction (ICNIRP 1998) is framed in terms of the maximum SAR average over any 10g of tissue in the head. However, also listed is the average over the eye alone, which has been calculated by other authors (Hirata 2005). The maximum ΔT is always found near the posterior pole of the lens. For sufficiently small values of SAR and ΔT, thermoregulatory changes to blood flow are negligible and the relationship between these quantities is therfore linear. The slope of this linear curve is

also shown in the table, using both the ICNIRP SAR average and the eye averaged SAR.

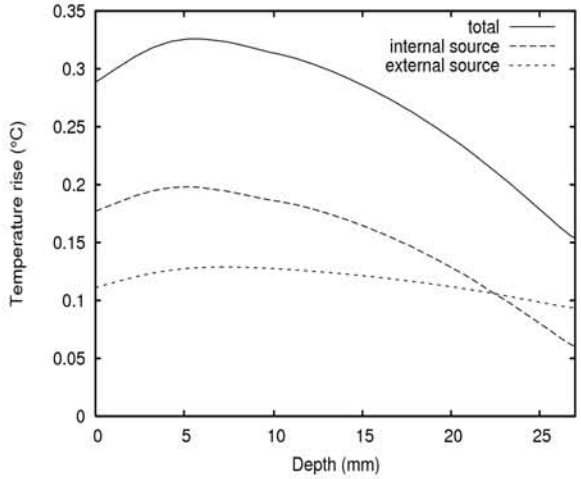


Figure 6: Contribution of internal and external SAR to ΔT

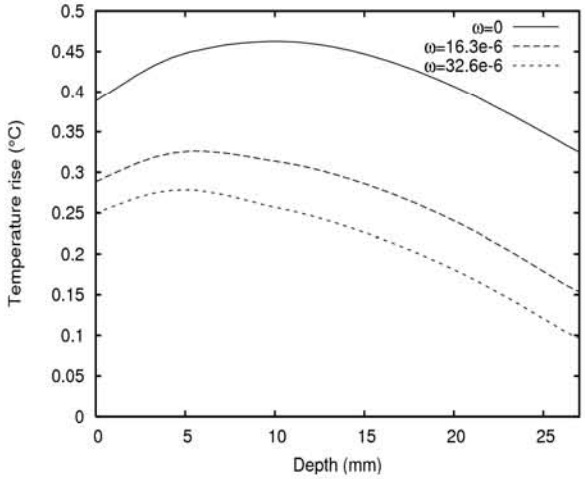


Figure 7: ΔT for various values of choroidal perfusion rate

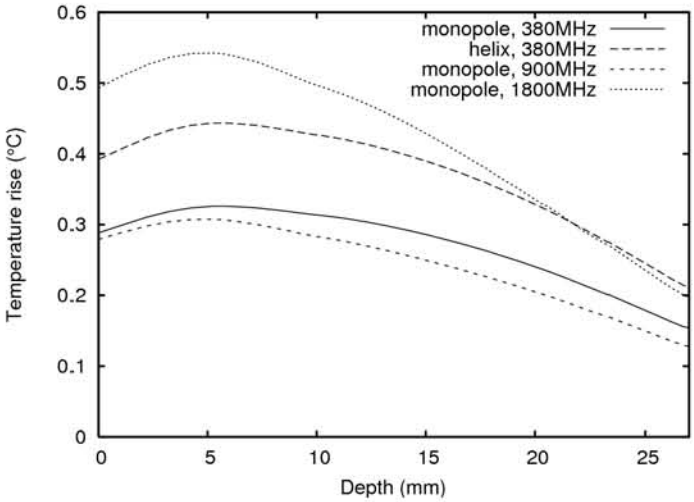


Figure 8: Temperature rises for various antenna types and frequencies

	SAR_{eye} (W kg^{-1}, ~10g)	SAR_{head} (W kg^{-1}, 10g)	Max. ΔT(eye) (°C)	$\frac{\Delta T}{SAR_{eye}}$	$\frac{\Delta T}{SAR_{head}}$
Monopole, 380MHz, 24mm	1.73	2.95	0.33	0.19	0.11
Monopole, 380MHz, 84mm	0.42	0.85	0.077	0.18	0.09
Helix, 380MHz, 24mm	2.35	3.97	0.44	0.19	0.11
Helix, 380MHz, 84mm	0.51	1.04	0.09	0.18	0.09
Monopole, 900MHz, 24mm	1.65	2.71	0.31	0.19	0.11
Monopole, 900MHz, 84mm	0.09	0.55	0.017	0.18	0.03
Monopole, 1800MHz, 24mm	2.97	4.00	0.55	0.19	0.14
Monopole, 1800MHz, 84mm	0.24	0.70	0.043	0.18	0.06

Table 2: Temperature rise and SAR summary

When the eye-averaged SAR is 10W kg^{-1}, the temperature rise in the eye is generally greater than 1°C but less than 2°C. However, when the ICNIRP occupational exposure restriction is respected (10W kg^{-1} in the head), the temperature rise in the eye is limited to about 1°C for all the TETRA exposures. However, it might reach 1.4°C if an antenna at 1800MHz were held very close to the eye.

Summary

These calculations have shown that the temperature rise in the eye is due not only to the energy directly absorbed by the eye tissues, but also by heat conduction from adjacent tissues which also absorb significant energy from the electromagnetic field. In some cases, about 40% of the temperature rise in the lens can be attributed to conduction from tissues outside the eye. Some studies have cited the SAR average over the eye as a predictor of thermal effect. This is because the mass of the eye is similar to the 10g averaging mass specified by ICNIRP. However, the present results show that the absorption in the orbital muscles must also be taken into account.

Under most circumstances the SAR average over the eye is substantially lower than the maximum SAR average in the head. Then, if the ICNIRP occupational exposure restriction is followed (10 W kg^{-1} in the head), the temperature rise in the eye is generally less than about 1ºC . However, at 1800MHz, it is theoretically possible to place an antenna very close to the eye and to produce larger temperature rises in the anterior part of the eye. However, this is still below the threshold which has been determined for cataractogenesis under acute exposures.

References

Berenger J. P. (1994), A perfectly matched layer for the absorption of electromagnetic wave, *J. Comput. Phys.* **114**, 185–200.

Bernardi P., Cavagnaro M,. Pisa S. & Piuzzi E. (2000). Specific absorption rate and temperature increases in the head of a cellular-phone user. I*EEE Trans. Microw. Theory Tech.*, **48**(7), 1118 – 1126.

Dimbylow P. J. & Mann S. M. (1994), SAR calculations in an anatomically realistic model of the head for mobile communication transceivers at 900 MHz and 1.8 GHz, *Phys. Med. Biol.* **39**, 1537–53.

Dimbylow P., Khalid M. & Mann S. (2003), Assessment of specific energy absorption rate (SAR) in the head from a TETRA handset, *Phys. Med. Biol.* **48**, 3911–3926.

Duck F. A. (1990), *Physical Properties of Tissue*, Academic Press.

Durkee J. R. Jr., Antich P. P. & Lee C. E. (1990), Exact solutions to the multiregion time-dependent bioheat equation. I: Solution development, *Phys. Med. Biol.* **35**(7), 847–867.

Gabriel S., Lau R. W. & Gabriel C. (1996), The dielectric properties of biological tissues: 3. Parametric models for the dielectric spectrum of tissue, *Phys. Med. Biol.* **41**, 2271–2293.

Guy A. W., Lin J. C., Kramar P. O. & Emery A. F. (1975), Effect of 2450-MHz radiation on the rabbit eye, *IEEE Trans. Microw. Theory Tech.* **MTT-23**(6), 492–498..

Gandhi O.P., Li Q.-X. & Kang G (2001). Temperature rise for the human head for cellular telephones and for peak SARs prescribed in safety guidelines. *IEEE Trans. Microw. Theory Tech.* **49**(9), 1607 – 1613.

Hirata A. (2005), Temperature increase in human eyes due to near-field and far-field exposures at 900 MHz, 1.5 GHz, and 1.9 GHz, *IEEE Trans. Electromag. Compat.* **47**(1), 68–76.

Hirata A. & Shiozawa T. (2003) , Correlation of maximum temperature increase and peak SAR in the human head due to handset antennas, *IEEE Trans. Microw. Theory Tech.* **51**(7), 1834 – 1841.

ICNIRP (1998). Guildelines for limiting exposure to time-varying electric, magnetic, and electromagnetic fields (up to 300 GHz). *Health Phys.* **74**, 494-522.

IEEE (2005). Standard for Safety Levels with Respect to Human Exposure to Radio Frequency Electromagnetic Fields, 3 kHz to 300 GHz. Std C95.1 – 2005.

Kojima M., Hata I., Wake K., Watanabe S., Yamanaka Y., Kamimura Y., Taki M., Sasaki K. (2004). Influence of Anesthesia on Ocular Effects and Temperature in Rabbit Eyes Exposed to Microwaves. Bioelectromagnetics **25**, 228-233.

Lagendijk J. J. (1982), A mathematical model to calculate temperature distributions in human and rabbit eyes during hyperthermic treatment, *Phys. Med. Biol.* **27**(11), 1301–1311.

NRPB (2004). Advice on limiting exposure to electromagnetic fields (0 – 300 GHz). *Documents of the NRPB,* **15**(4).

Pennes H. H. (1948), Analysis of tissue and arterial blood temperature in the resting human forearm, *J. Appl. Physiol.* **1**, 93–122.

Scott J. A. (1988a), A finite element model of heat transport in the human eye, *Phys. Med. Biol.* **33**(2), 227–241.

Scott J. A. (1988b), The Computation of Temperature Rises in the Human Eye Induced by Infrared Radiation. *Phys. Med. Biol.* **33**(2), 242–257.

van Leeuwen G. M. J., Lagendijk J. J. W., van Leersum G. J. A. M., Zwamborn A. P. M., Hornsleth S. N. & Kotte A. N. T. J. (1999), Calculation of change in brain temperatures due to exposure to a mobile phone. *Phys. Med. Biol.* **44**, 2367–2379.

Wainwright P. R. (1999), Localized specific absorption rate calculations in a realistic phantom leg at 1–30 MHz using a finite element method, *Phys. Med. Biol.* **44**, 1041–1052.

Wainwright P. R. (2000), Thermal effects of radiation from cellular telephones, *Phys. Med. Biol.* **45**, 2363–2372.

NUMERICAL EVALUATION OF EXTERNAL ELECTROMAGNETIC FIELDS INFLUENCE ON BRAIN ELECTRICAL ACTIVITY

Marina Rezinkina
National Technique University "KPI", Frunze st., 21, Kharkov 61002, Ukraine,
e-mail: marinar@kpi.kharkov.ua

Eleonora Bydianskaya
Kharkov Scientific Research Institute of Hygiene of Labour and Industrial Diseases
Trinklera st., 6, 61022, Kharkov, Ukraine

Anatoliy Shcherba
Institute of Electrodynamics, avenue Pobedy, 56, Kiev, Ukraine

Abstract

Hodgkin-Huxley model, describing generation of action potentials in the nerve cell membranes has been used for appreciation of the possible EMF influence mechanisms on the brain own electric activity. The carried calculations have shown that at simultaneous passing through a nerve cell of action potentials and external ac, suppression of the own excitation pulses is possible starting from the certain level of the external current value, which depends on its frequency. To avoid such suppression of action potentials, their levels may be increased relatively minimum limit level. It may be supposed that brain "tunes up" its work at presence of external ac, increasing amplitudes of its own excitation signals so that their suppression does not occur. It is possible also that this "tuning" acts some time after external EMF removing while brain adapts again to its absence, as it is observed in experiment.

1. Introduction.

There are studies connected with influence of electromagnetic fields (EMF) on the activity of cerebrum of animals (see for instance [1]) and people (see for instance [2-5]). As it is shown in these works, low frequency or amplitude modulated radio-frequency EMF of the defined strength and frequency may influence bioelectrical activity of mammals' cerebrum. It is expressed in changes observed by means of electroencephalography (EEG) [1-5]. However, literature data on the character of the EMF influence are discrepant. Thus, it is mentioned about blocking of cerebrum bioelectrical activity upon action of magnetic field with 10 Hz frequency and 0.1 мТл stress [4]. At the same time it is shown in [2] that influence of the magnetic field with frequency f=0-500 Hz and 0.2 мТл magnetic field stress was expressed in increase of the potential levels, registered by EEG after lifting of the exposure. It is shown in [3] that magnetic fields of 60 Hz frequency and 1 Ga stress cause reliable change of EEG of people after lifting of the exposure.

As it is shown in [6], heterogeneity of the electrical properties of cortex tissues and, in particular presence of the intercellular fluid, leads to low frequency filtration of electromagnetic field. As a result, EEG has only low frequency components. It is possible that the answer of the cerebrum neurons to the influence of radio-frequency electromagnetic fields is suppressed also by the low frequency filter, which serves cerebrum intercellular fluid, so it is not registered by EEG. However, influence on the people's EEG of high frequency electromagnetic fields in the limited time diapason $t < 300$ ms after lifting of the exposure has been fixed [5].

The purpose of this work is estimation of the parameters of electrical processes in the membrane of a brain neuron for evaluation of the limit levels of current density, induced as a result of external EMF application, which do not influence own bioelectric processes, occurring at normal cortex operation in absence of an external EMF. To understand the mechanism of EMF influence on the own electrical activity of cerebrum, it is suggested to use simple, but demonstrative Hodgkin-Huxley model [7], describing passage of bioelectric pulses through the neuron membrane.

2. Evaluation of the neuron membrane charges and potentials at external current flow.

Let's consider influence of the external EMF on the cellular level. The author of [8] has made estimation of Q_R – charge density of the cell membrane: $Q_R=V_m \cdot C_m$, where $C_m=10^{-2}$ F/m^2 - specific membrane capacitance, V_m=-60 mV - resting potential of the membrane: $Q_R \sim 6 \cdot 10^{-4}$ K/m^2. Let's evaluate Q_p – value of the charge density in brain tissues at flowing in them of the normalized, for instance in [9], permitted level of current density J_p=10 mA/m^2 at f ≤ 1000 Hz: $|Q_p|=|J_p|/\omega$. For industrial frequency 50 Hz $|Q_p| \sim 0.3 \cdot 10^{-4}$ K/m^2, i.e. makes up about 5 % from Q_R. For lower frequencies, for instance 10 Hz, as in the experiments described in [1,2], $|Q_p|$ is even greater: $|Q_p| \sim 0.16 \cdot 10^{-3}$ K/m^2, i.e. makes up nearly 27 % from Q_R. Such a change of charge may influence own electrical processes, occurring at cerebrum functioning.

Let's perform evaluative calculations of the levels of potential, appearing in intercellular medium and membrane of a nervous cell at flowing in the cerebrum tissues of the very low frequency (f ≤ 1000 Hz) current with the density J^{ext}=10 mA/m^2, equal to the permitted level. It is necessary to take into account that an external current J^{ext} passes both through the membrane and through the nucleus of the cell. Let's consider that specific conductivity of the intercellular fluid does not exceed $\gamma_i \sim 0{,}03 – 0{,}1$ С/м at frequencies f ≤ 100 Hz (see for instance [10]). Then G_i^* - conductivity of the intercellular medium corresponding to the unit area, makes up: $G_i^*=G_i/S=\gamma_i \cdot S/(L \cdot S) \sim 10^4$ S/m^2 (at L~10^{-5} m - transverse size of a cell, S – the area of a cell). At the same time, capacitive conductivity of a membrane, corresponding to a unit area at frequency, for instance 10 Hz, is equal to: $\omega \cdot C_m^* = \omega \cdot C_m/S \sim 0{,}6$ S/m^2. So, at outside current J^{ext} flowing, Ohm's law for a cell membrane and intercellular medium may be expressed as follows, taking into account that $G_i^* >> \omega \cdot C_m^*$:

$$U = I^{ext} \cdot [1/(\omega \cdot C_m)+1/G_i] = I^{ext} \cdot S \cdot [1/(\omega \cdot C_m \cdot S)+1/(G_m \cdot S)] = J^{ext} \cdot [1/(\omega \cdot C_m^*)+1/G_i^*] \sim J^{ext}/(\omega \cdot C_m^*) \sim 16 \text{ мВ},$$

where I^{ext} – external current.

Thus, at very low frequencies of the external current flowing through a cell, the main drop of voltage is in its membrane (see [8] also). So, at flowing of the induced by external sources current with density 10 mA/m^2, which is normalized as permitted, drop of voltage in a membrane may reach 16 mV at f=10 Hz and about 3 mV at f=50 Hz.

The same result may be obtained at evaluation of the field problem. In 1D approach: $J_i=J_m=J^{ext}$ (where J_i - current density in the intercellular medium; J_m - current density in the cell membrane) and $J_i=\gamma_i \cdot E_i$; $J_m=j \cdot \omega \cdot \varepsilon \cdot \varepsilon_0 \cdot E_m$ (where E_i - electric field stress in the intercellular medium, E_m - electric field stress in the cell membrane, ε=81). From this $\gamma \cdot |E_i|=\varepsilon \cdot \varepsilon_0 \cdot \omega \cdot |E_m|$. For very low frequencies $E_m >> E_i$, thus for f=10 Hz and γ_i =0.1 S/m:

$$|E_m| = |E_i| \cdot [\gamma_i/(\varepsilon \cdot \varepsilon_0 \cdot \omega)] \sim |E_i| \cdot 0.2 \cdot 10^7. \quad (1)$$

General fall of voltage in a cell:

$$U_c = d_m \cdot |E_m| + d_i \cdot |E_i|, \quad (2)$$

where d_i - thickness of a cell ($d_i \sim 10^{-5}$ м); d_m - membrane thickness ($d_m \sim 10^{-8}$ м).

Substituting (1) in (2), we get: $U_c = |E_m| \cdot (10^{-8}+10^{-5} \cdot 5 \cdot 10^{-7})$, thence $E_m \cdot d_m \sim U_c$. As a result we get:

$$U_m \sim U_c \sim [J^{ext}/(\varepsilon \cdot \varepsilon_0 \cdot \omega)] \cdot d_m,$$

where U_m- voltage drop in a membrane,

that at f=10 Hz gives $U_m \sim 16$ mV.

Considering that this value has the same order as, for instance potential difference, caused by the presence of K^+ ions inside a cell, $E_K \sim$ -12 mV (see for instance [11]), such change of the membrane potential may cause change of its conductivity to K^+ ions.

3. Calculations with the help of Hodgkin-Huxley model.

Let's use the known Hodgkin-Huxley model [7] describing electric processes in the membrane of neuron (see fig. 1). The equivalent electrical circuit of a patch of the axon membrane is shown in fig. 2.

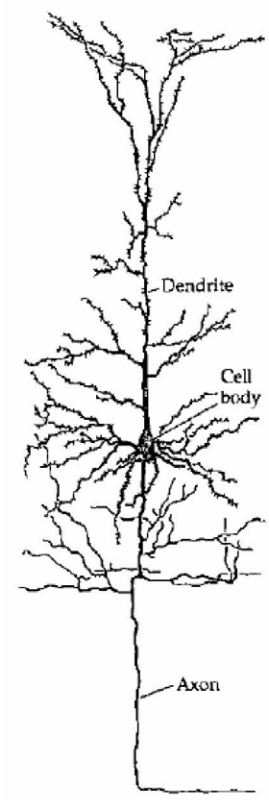


Fig. 1. A real neuron.

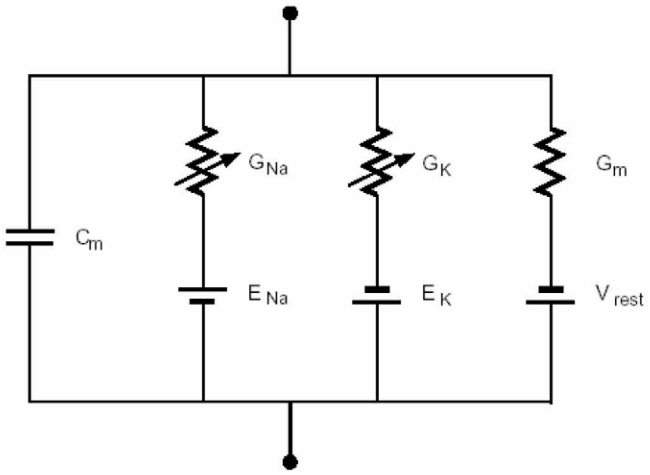


Fig. 2. Equivalent electrical circuit of a patch of axon.

It is known that high concentration of potassium ions as well as low concentration of sodium and chlorine ions exists inside a neuron cell in the state of rest. The membrane of a cell performs the role of a barrier, preventing ions penetration from the intercellular medium inside a cell and vice versa. The rest potential E_m settles in a cell membrane as a consequence of presence on its both sides of different concentration of Na^+ and K^+ ions. If it is considered that membrane potential V is equal to 0 in the rest state, $E_K \sim -12$ mV, $E_{Na} \sim 115$ mV, $E_{rest} \sim 10.613$ mV, $G_m \sim 3$ Sm/m^2, $C_m \sim 10^{-2}$ F/m (see for instance [11]), where E_K - potential difference, connected with presence of potassium ions inside a cell; E_{Na} - potential difference, connected with presence of sodium ions inside a cell; E_{rest} – value, chosen by calculations, which provides equality to zero of the membrane

potential in the rest mode; G_K - conductivity of a unit area to K^+ ions; G_{Na} - conductivity of a unit area to Na^+ ions; G_m – leak conductivity of a unit area; C_m - membrane capacity of a unit area (see fig. 2).

Let's take into account presence in the equivalent circuit of a cell of the additional current sources, imitating current of axon excitation, as well as current, running in cortex at application of an external EMF. As all quantities in the equivalent scheme are expressed as specific values, we suppose that external source is characterized by density J^{ext} and frequency f, and the source of axon excitation current is characterized by density J^{ax} and duration τ^{ax}.

It is supposed in Hodgkin-Huxley model that full current through a membrane consists of a capacitive current, as well as conductivity currents of K^+, Na^+ ions and leak current through active resistance of a membrane. Nonlinear dependencies of the conductivities to K^+ and Na^+ ions relatively the value of the membrane voltage V are entered in this model. These dependencies assume that transition from non-conducting state of a membrane to its conducting state occurs at certain voltage on the membrane. According to Hodgkin-Huxley model, this transition complies with the first-order kinetics. The equation of such transition for K^+ ions may be written down as follows:

$$\frac{dn}{dt} = \phi(T) \cdot [\alpha_n(V) \cdot (1 - n) - \beta_n(V) \cdot n], \tag{3}$$

where $\phi(t) = 3^{(T-6.3)/10}$ - coefficient depending on the temperature; T - temperature in the Celsius degrees; $\alpha_n(V)$, $\beta_n(V)$ - coefficients depending on the voltage level.

Specific conductivity to potassium ions G_K is supposed to be equal to $G_K = \overline{G}_K \cdot n^4$ ($\overline{G}_K$ =36 mS/cm^2), and coefficients $\alpha_n(V)$, $\beta_n(V)$ are written as follows:

$$\alpha_n(V) = \frac{10 - V}{100 \cdot \{\exp[(10 - V)/10] - 1\}}; \qquad \beta_n(V) = 0.125 \cdot \exp(-V/80),$$

where V - in millivolt.

Specific conductivity to sodium ions G_{Na} is written in the form $G_{Na} = \overline{G}_{Na} \cdot m^3 \cdot h$ ($\overline{G}_{Na}$ =120 mS/cm^2), and it is supposed also that transition from m condition to (m-1) condition and from h to (h-1) condition also complies with the first-order kinetics:

$$\frac{dm}{dt} = \phi(T) \cdot [\alpha_m(V) \cdot (1 - m) - \beta_m(V) \cdot m]; \tag{4}$$

$$\frac{dh}{dt} = \phi(T) \cdot [\alpha_h(V) \cdot (1 - h) - \beta_h(V) \cdot h], \tag{5}$$

where $\alpha_m(V)$, $\beta_m(V)$, $\alpha_h(V)$, $\beta_h(V)$ - coefficients depending on the voltage level.

Coefficients $\alpha_m(V)$, $\beta_m(V)$, $\alpha_h(V)$, $\beta_h(V)$ are written as follows:

$$\alpha_m(V) = \frac{25 - V}{10 \cdot \{\exp[(25 - V)/10] - 1\}}; \qquad \beta_m(V) = 4 \cdot \exp(-V/18);$$

$$\alpha_h(V) = 0.07 \cdot \exp(-V/20); \qquad \beta_h(V) = \frac{1}{\exp[(30 - V)/10] + 1},$$

where V - in millivolt.

Let's write down the equation for all current densities, flowing through a membrane (equivalent scheme is shown in fig. 2):

$$C_m \cdot \frac{dV}{dt} = \overline{G}_{Na} \cdot m^3 \cdot h \cdot (E_{Na} - V) + \overline{G}_K \cdot n^4 \cdot (E_K - V) + G_m \cdot (V_{rest} - V) + J^{ext} + J^{ax}. \tag{6}$$

Let's replace derivatives in the expressions (3)-(6) by their differential analogues and express volumes of the sought functions at the time step t for $T=6.3^0$ C as follows:

$$n_t = \frac{n_{t-\Delta t} + \alpha_n(V_t)\cdot\Delta t}{1+\Delta t\cdot[\alpha_n(V_t)+\beta_n(V_t)]};\ m_t = \frac{m_{t-\Delta t} + \alpha_m(V_t)\cdot\Delta t}{1+\Delta t\cdot[\alpha_m(V_t)+\beta_m(V_t)]};$$

$$h_t = \frac{h_{t-\Delta t} + \alpha_h(V_t)\cdot\Delta t}{1+\Delta t\cdot[\alpha_h(V_t)+\beta_h(V_t)]};\ V_t = \frac{V_{t-\Delta t}\cdot C_m/\Delta t + \overline{G}_{Na}\cdot m^3\cdot h\cdot E_{Na} + \overline{G}_K\cdot n^4\cdot E_K + G_m\cdot V_{rest} + J^{ext}(t) + J^{ax}}{C_m/\Delta t + \overline{G}_{Na}\cdot m^3\cdot h + \overline{G}_K\cdot n^4 + G_m},$$

where Δt [ms] - step in time domain; C_m [μF/cm^2]; J^{ext}, J^{ax} [μA/cm^2]; $\overline{G}_K$, $\overline{G}_{Na}$ [mS/cm^2]; V [mV].

The obtained system of nonlinear equations was solved by the iterative method in each time step. The value of Δt was chosen equal to 0.01 ms.

An example of the calculated axon membrane voltage at application to it of the excitation current with density J^{ax}_{min} = 14 μA/cm^2 and duration τ^{ax} = 0.5 ms is shown in fig. 3.

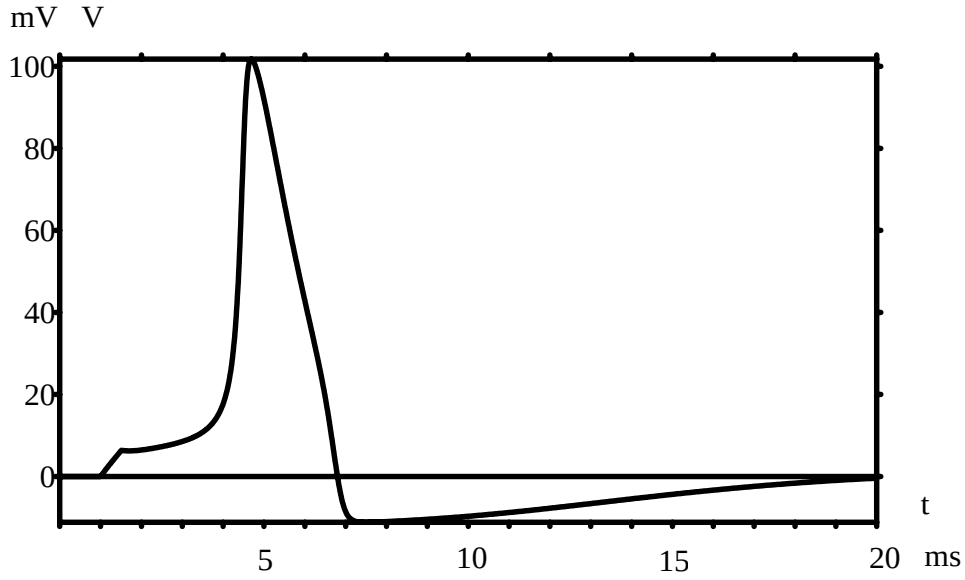


Fig. 3.

The calculated dependencies of n, m, h change in time domain for this case are presented in fig. 4.

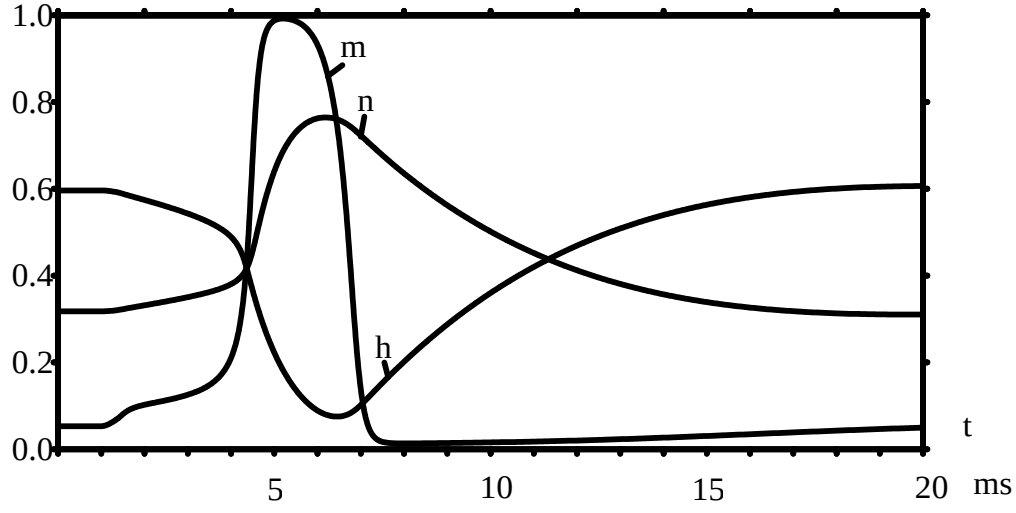


Fig. 4.

It is known that excitation potentials with certain periodicity are generated in an axon at application of an external dc. The same phenomenon is present also at application of an external ac. The calculated boundary levels of the external currents densities J^{ext}_{lim1} and J^{ext}_{lim2}, such that presence of an external field does not cause appearance of induced excitation potentials in an axon if $J^{ext} < J^{ext}_{lim1}$, but potentials with certain periodicity depending on J^{ext} value are generated in an axon if $J^{ext} > J^{ext}_{lim2}$ are presented in the table for different frequencies. Generation of a single induced excitation pulse or a transition stage occurs at $J^{ext}_{lim1} < J^{ext} < J^{ext}_{lim2}$.

Table.

f [Hz]	J^{ext}_{lim1} [mA/m^2]	J^{ext}_{lim2} [mA/m^2]
10	50	60
30	20	25
50	15	20
100	20	30
1000	65	70

Calculated changes in time domain of the potentials in the neutron's membrane at application of the external current of 10 Hz frequency with the amplitude 60 mA/m^2 and 100 mA/m^2 are presented in fig. 5 and 6 correspondingly.

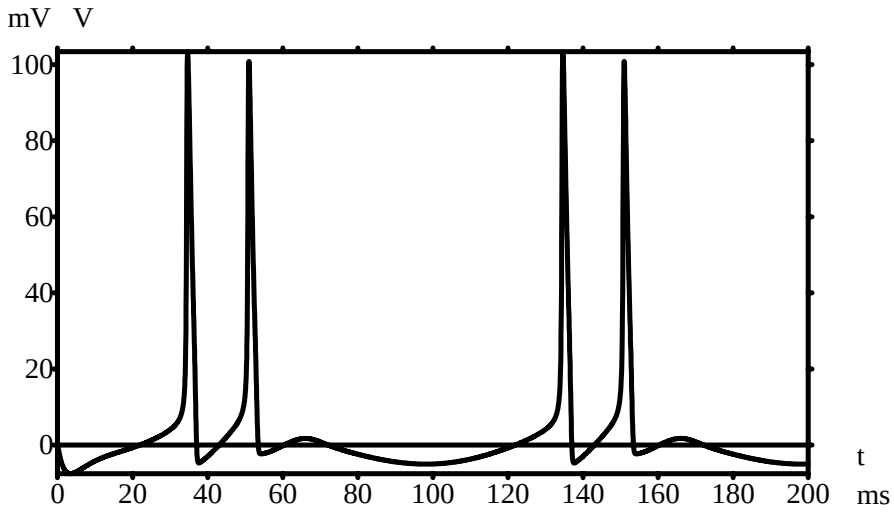


Fig. 5. Dependence of the axon membrane voltage from time at flowing of the external current with frequency 10 Hz and amplitude 60 mA/m^2.

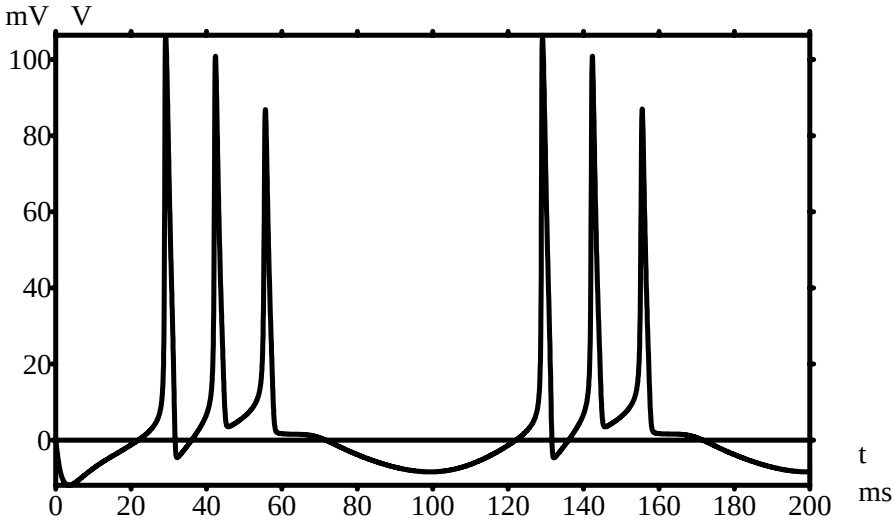


Fig. 6. Dependence of the axon membrane voltage from time at flowing of the external current with frequency 10 Hz and amplitude 100 mA/m^2.

As carried calculations have shown, at simultaneous passage through an axon of an external current J^{ext}, as well as axon excitation current J^{ax}, starting from the defined level of an external current, depending on its frequency, suppression of the excitation pulses occurs if they pass through the axon membrane during negative half-waves of external current (see fig. 7 moment t_1). The same external current does not affect excitation pulses if they appear during positive half-waves (see fig. 7 moment t_2). The carried calculations have shown that current caused by the presence of external field ceases to suppress brain own excitation pulses only when $J^{ext} < J^{ext}_{lim0}$ (where J^{ext}_{lim0} - limit level of current density). For the industrial frequency of 50 Hz this limit level is equl to: J^{ext}_{lim0} =1.5 mA/m^2, for other frequensies it should be calculated.

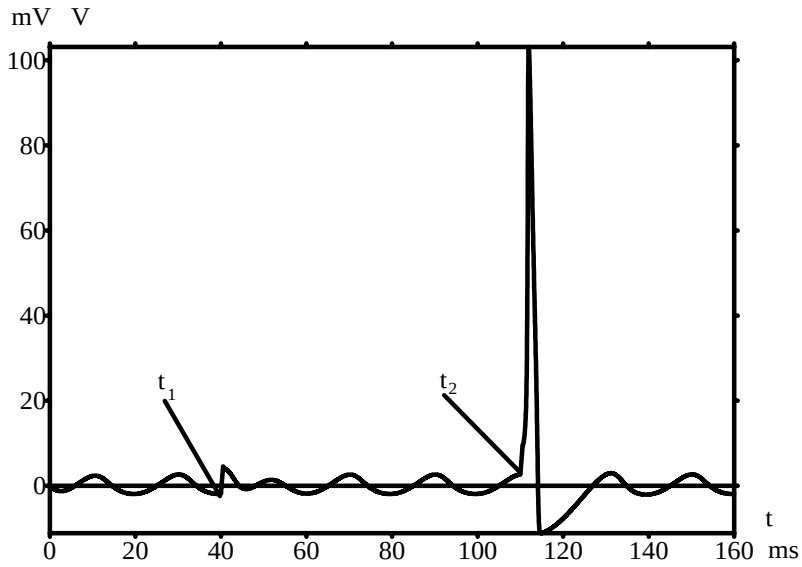


Fig. 7. Dependence of the axon membrane voltage from time at flowing of the external current with frequency 50 Hz and amplitude 10 mA/m^2 and simultaneous flowing of excitation pulses of amplitude J^{ext}=14 μA/cm^2 in the moments t_1, t_2.

It was obtained from the calculations also that to prevent suppression of brain own excitation pulses by the external current of permitted density J^{ext} = 10 mA/m^2, their levels should be increased up to J^{ax} = 18 μA/cm^2 - approximately on 30 % relatively the minimum limiting level of J^{ax}_{min} = 14 μA/cm^2 at which excitation pulses of duration τ^{ax} = 0.5 ms still pass (see fig.8).

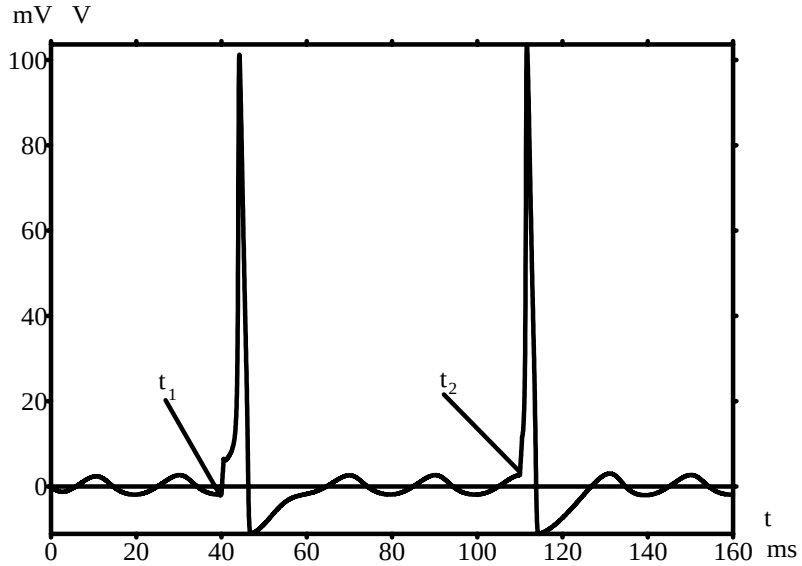


Fig. 8. Dependence of the axon membrane voltage from time at flowing of the external current with frequency 50 Hz and amplitude 10 mA/m^2 and simultaneous flowing of excitation pulses of amplitude J^{ext} = 18 μA/cm^2 in the moments t_1, t_2.

From certain level of external current density, full suppression of the own brain electrical activity has been observed in the calculations. It may be a cause of the analgesic effect during application of the external low frequency EMF due to blocking of action potential propagation.

Thus, from an example of simple calculations, it may be seen that at certain conditions of irradiation, flowing through the membrane of axon of the low frequency external ac can cause suppression of the own excitation signals passing through the membrane. It can cause also generation of the induced excitation signals, as well as increase of the levels of brain own excitation potentials so that they would not be suppressed by the presence of external current, i.e. all phenomena observed in experiment (see [1-5]).

Conclusions.

1. As calculations with the help of Hodgkin-Huxley model have shown, flowing through nervous cells of current with density 10 mA/m^2 and frequency f < 100 Hz in absence of own brain excitation pulses does not cause appearance of the induced excitation potentials. However, simultaneous flowing through an axon of the external very low frequency current $J^{ext}_{lim0} < J^{ext} \leq 10$ mA/m^2 and excitation pulses can cause suppression of the excitation pulses, moreover minimum low frequency current at which this phenomenon still exists, corresponds approximately to 50 Hz, i.e. the most wide-spread industrial frequency.

2. It is possible that at presence of the external very low frequency current, which density level lays in the limits: $J^{ext}_{lim0} < J^{ext} < J^{ext}_{lim1}$ including smaller or equal to the permitted level, brain "adjusts" its work so that suppression of its own excitation signals does not occur, enlarging amplitude of these signals: $J^{ax} > J^{ax}_{min}$. It is possible also that this "tuning" acts some time after removal of the external EMF while brain will not adapt again to the EMF absence, as it was observed in experiment when EEG levels were greater some time after lifting of the low frequency EMF irradiation [2]. It may be also a cause of pain and sensitivity thresholds decrease some time after removal of the low frequency magnetic field exposure (see [12]) as at greater levels of action potentials brain may be more sensitive to lower levels of external pain effects.

References

[1] Bell G., Marino A., Chesson A., Struve F., *"Electrical states in the rabbit brain can be altered by light and electromagnetic fields"*, Brain Research, v. 570, p. 307-315, 1992.
[2] Cook C.M., Thomas A.W., Prato F.S., *"Resting EEG is affected by exposure to a pulsed ELF magnetic field"*, Bioelectromagnetics, v. 25, p. 196-203, 2004.
[3] Marino A.A., Nilsen E., Chesson Jr A.L., Frilot C., *"Effect of low-frequency magnetic fields on brain electrical activity in human subjects"*, Clinical Neurophysiology, v. 115, p. 1195-1201, 2004.
[4] Bell G., Marino A., Chesson A., *"Frequency-specific blocking in the human brain caused by electromagnetic fields"*, NeuroReport, v. 5, No 4, p. 510—512, 1994.
[5] Marino A.A., Nilsen E., Frilot C., *"Nonlinear changes in brain electrical activity due to cell phone radiation"*, Bioelectromagnetics, v. 24, p. 339-346, 2003.
[6] Bédard C., Kröger H., Destexhe A., *"Modeling extracellular field potentials and the frequency-filtering properties of extracellular space"*, Biophysical Journal, v. 86, p. 1829-1842, 2004.
[7] Hodgkin A.I., Huxely A.F., *"A quantitative description of membrane current and its application to conduction and excitation in nerve"*, J. Physiol, v. 117, p. 500-544, 1952.
[8] Adair R.K., *"Biophysical limits on athermal effects of RF and microwave radiation"*, Bioelectromagnetics, v. 24, p. 39-48, 2003.
[9] *"Board statement on restrictions on human exposure to static and time varying electromagnetic fields and radiation"*, Documents of the NRPB, Chilton. Didcot. Oxon, v. 4, No 5, 69 p., 1993.
[10] Gabriel S., Lau R.W., Gabriel C., *"The dielectric properties of biological tissues: II. Measurements in the frequency range 10 Hz to 20 GHz"*, Phys. Med. Biol., v. 41, p. 2251-2269, 1996.
[11] Peasgood W., Dissado L.A., Lam C.K., Armstrong A., Wood W., *"A novel electrical model of nerve and muscle using Pspice"*, J. Phys. D: Appl. Phys., v. 36, p. 311-329, 2003.
[12] Ghione S., Seppia C., Mezzasalma L., Emdin M., Luschi P. *"Human head exposure to a 37 Hz electromagnetic field: effects on blood pressure, somatosensory perception and blood parameters"* Bioelectromagnetics, v. 25, p. 167-175, 2004.

EFFECT OF A SPECIALLY PULSED MAGNETIC FIELD ON WOUND HEALING IN RAT SKIN

*OZLEM ULUKUT

*SELCUK COMLEKCI

**SULEYMAN DEMIREL UNIVERSITY, FACULTY OF ENGINEERING, DEPARTMENT OF ELECTRICAL & COMMUNICATIONS ENGINEERING, 32260, CUNUR, ISPARTA, TURKEY*

e-mail:oulukut@mmf.sdu.edu.tr *e-mail:scom@mmf.sdu.edu.tr*

Abstract

The exact mechanism by which electromagnetic fields affect bone and other tissues has yet to be cleared. Several mechanisms have been proposed, among them changes in cellular ionic calcium, modified receptor and messenger behavior, increased synthesis or degradation of substances, and even direct interaction with genes. Several in vivo studies were conducted to evaluate the effect of pulsed electromagnetic field (PMF) on the healing of skin wounds in rats. Variable results were reported. In some of these studies, exposure of wounds to PMF resulted in a higher rate of wound contraction (WC), enhanced cellular organization, and earlier collagen formation and maturation. However, several other reports failed to show any beneficial effect of PMF on the healing of skin wounds in rats. The aim of this study was to investigate the possible effects of a specially pulsed magnetic field (PMF) on skin wound healing in rats. Thirty male Sprague-Dawley male rats were used in this study. After anaesthetizing and shaving a paired full thickness incision wound (30 mm in length) was made on each side of the dorsal midline of the rats. The rats were randomly divided into three groups each containing 10 rats. Control and two treatment groups which were exposed to 0.45 ms pulse rates of 2.2 kHz. Treatment group1 were exposed PMF (5 mT) for 30 min a day for seven days and treatment group 2 were exposed PMF (2.5 mT) 1 hour a day for seven days after surgery. Control group were subjected to the same procedure, but with the PMF device not activated.

Key words: PMF, wound healing

Introduction

The process of regeneration and repair following injury represents one of the most fundamental defense mechanisms of an organism against environmental damage. Biological processes such as inflammation, proliferation, wound contraction and remodeling lead to the scar formation. Certain systemic diseases, such as injuries to the nervous system, metabolism and aging, have negative influence on the healing process, and lead to chronic wound formation. The use of pulsed magnetic field (PMF) for selective control of cellular function has given biology and medicine a new dimension. PMF stimulators with different characteristics were designed to induce voltages similar to those produced normally, during mechanical deformation of connective tissue. Researchers have used PMF stimulators to promote healing, but the results differ significantly from one another and there are discrepancies between the uses of PMF parameters. Further studies are needed to determine the optimal PMF parameters for the acceleration of wound healing. This study was designed to compare the different PMF pulse rates on skin wound healing in rats.

Milgram et al., (2004), objected to examine the effect of high intensity, short duration PMF on the healing of full thickness skin wounds in rats. Certain type of PMF did not have a significantly beneficial effect on wound healing. Wound healing is characterized by the restoration of the epithelial surface. The process of second intention wound healing consists of contraction and epithelialization.

Basset et al., (1974) including peripheral nerves for regeneration. The influence of PMF on nerve regeneration in vivo has been reported to be acceleration of the recovery of function following peripheral nerve crush or transection and exposure of the proximal nerve segment.

De Haas W.G., Lazarovici M.A., and Morrison D.M. (1979) the object of this experimental work was to evaluate the effect of a noninvasive method of electrical stimulation on the healing of freshly- created osteotomies of the rabbit radius. The apparatus consisted of a solid core electromagnet energized by a square wave unidirectional current. The magnetic field was pulsed transversely across the osteotomy site of the radius while the animal was confined to a restraining device 6 hours daily for 5 days per week. In one group of animals the influence of different pulse frequencies, using 0.1 Hz, 1 Hz, and 4 Hz, was evaluated, while the period of stimulation was kept constant at 2 weeks. In another group of animals, exposure was continued for 3 and 4 weeks while the pulse frequency was kept constant at 1 Hz. Histologic and radiologic comparison with control animals revealed that the initiation of the healing process can be accelerated in magnetic fields pulsed at 1 Hz, but that this effect is not maintained, and that the total period of time required for union is not significantly shortened. In view of these findings, this form of treatment is not recommended for clinical use in the treatment of recent fractures of long bones.

Ieran et al., (1990) PMF have been used clinically for the treatment of chronic skin ulcers of venous origin in humans. In a double blind study PMF have been used clinically for the treatment of chronic skin ulcers of venous origin in humans. In a double blind study the PMF treated group showed no worsening of any the ulcers, whereas four ulcers worsened in the control group.

Stiller et al., (1992), Ieran et al., (1990) by the end of the study, the treated group showed an increased number of healed wounds and a decrease in the rate of recurrence of venous ulcers, compared to the control group. In a multi centre study, a portable PMF device for home use was tested. Fifty percent of the ulcers in the treatment group healed or markedly improved, while none of the ulcers in the placebo group had healed. In the treatment group, no worsening was seen in any of the ulcers, while 54% of the ulcers in the control group exhibited worsening of the ulcers.

PMF Signal Generation and Exposure

The system was fed by a function generator (custom made in the department), producing a 2.2 kHz sine wave with 0.45 ms repetition time. The output of the function generator was connected to the Helmholtz coils: two identical coils (each of 300 turns of enameled copper wire with 0.4 mm radius) were mounted coaxially at a distance of one coil radius (13 cm) from each other to produce a highly uniform horizontal field between them. The coils were connected to the PMF generator.

The pulse duty was defined as the percentage of the time during which the voltage is switched on in one cycle. Helmholtz coil, producing 2.5 mT and 5 mT field effective intensity on the surface of rat skin. During the experiments, field intensity was measured by Philip Harris Probe (Shenstone/England) and Chauvin Arnoux Max3000 TRMS Multimeter (Paris/France). Unilab, Digital Gauss/Tesla Meter (Blackburn/England) was used for purity of the field. Maximum variation was less than 1%. Validation of the intensity measurement, axial magnetic field between the coils was also calculated.

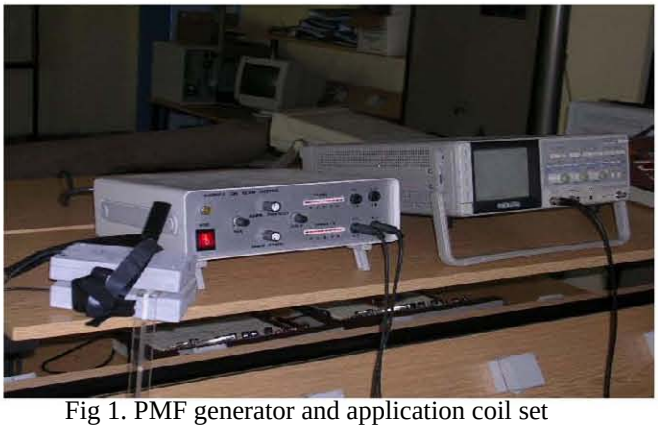


Fig 1. PMF generator and application coil set

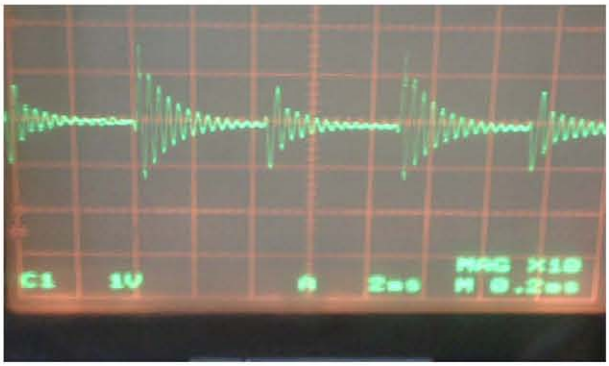


Fig 2. PMF source wave shape

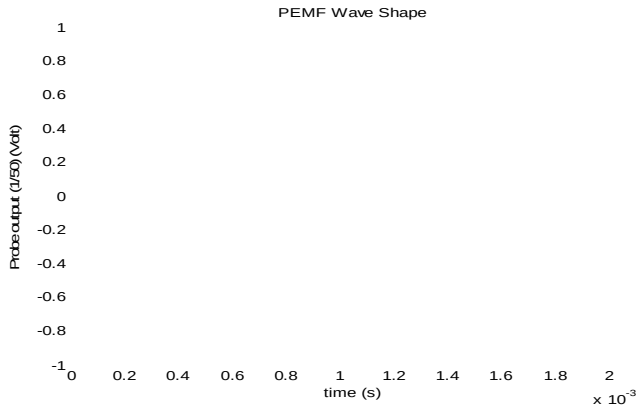


Fig 3. PMF wave shape (MATLAB)

Material and Methods

Thirty Sprague-Dawley male rats, 8-10 weeks old, weighing 200-250 g were used. They were kept in standard cages, food and water were available to them without any restriction. The temperature in the room was 20 ± 2^{o} C, the light cycle was 12/ 12-h light/dark schedule. Anesthesia was performed by the intra-peritoneal injection of ketamine HCL, 100 mg/kg and pompun, 10 mg/kg, 10 minutes before surgery. After shaving and cleaning, a pair of full thickness incisions (30 mm in length) was made parallel to and at a distance of 1.5 cm on each side of the dorsal midline. Then the animals were divided into three groups**.** Treatment group1 were exposed PMF (5 mT) for 30 min a day for seven days and treatment group2 were exposed PMF (2.5 mT) 1 hour a day for seven days after surgery. Control group were subjected to the same procedure, but with the PMF device not activated..

Discussion

Published reports indicated that the PMF stimulators may promote wound healing, but this depends on parameters such as frequency, intensity, exposure time and orientation of PMF. It was suggested that the suitable dosage and optimum PMF parameters involved in wound healing be found. The purpose of this study was to investigate the effects of pulse rates of PMF on skin wound healing in rats.

The animals in the sham group were kept in the restrainer inside the unenergized coil. These conditions may increase stress or temperature of animals, they did not affect wound healing time significantly and it was seen that the animals adapted to these conditions very soon.

Goldman et al.,(1998) have shown enhancement of fibroblast proliferation in response to certain conditions of the electric field (41 mv/m, 10 Hz) and Katsir et al. showed that chick embryo fibroblast proliferation was modified by EMF (60 Hz, 0.7 mT).

Berg et al., (1997) showed that the proliferatory response of yeast to electromagnetic field is frequency dependent and there is a window so that a high proliferation is detected at 15 Hz and a minimum proliferation at 40 Hz. These reports confirm our results in that there is a window between 10 to 80 Hz pulse rates (which is around 20 Hz). The significance in the absolute values and the normalized wound maximal lengths for the 20 Hz group compared to the sham group, verifies that the PMF with 20 Hz pulse rate accelerates wound healing. Our results on the wound surface area indicate that PMF stimulation does not affect wound contraction in rats which is in keeping with Scardino et al. that showed PMF had a positive effect on epithelilization only.

Based on the results obtained in this study it could be concluded that PMF stimulators (which could later become a practical tool for clinical use) are effective devices for the acceleration of wound healing but further studies are required to determine the optimal frequency, direction and intensity of the PMF to be used in soft tissue healing and two clarify the exact mechanisms in involved in this phenomenon.

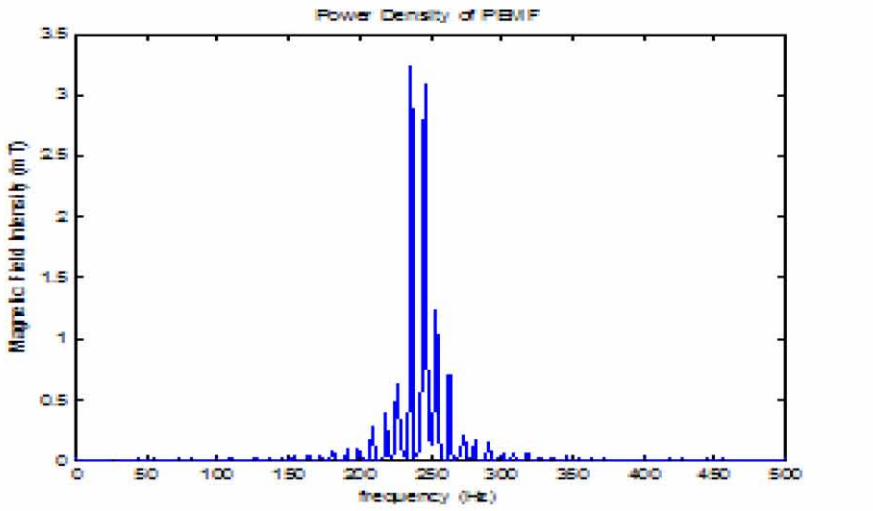


Fig 4. PMF power density

Power spectrum investigation has been conducted by using MATLAB software. Obtained spectrum density of pulsed magnetic field has been shown in Figure 4. As shown in Figure 4 fundamental component of RF energy must be in frequency about 250 Hz. So the main effective portion might be affected calcium permeability of cell membrane .It is known that permeability of cell membrane provides calcium efflux. Consequently target tissues related to wound healing affected by our used waveform.

Fig.5 and Fig. 6 shows the effect of various pulse rates on wound healing.

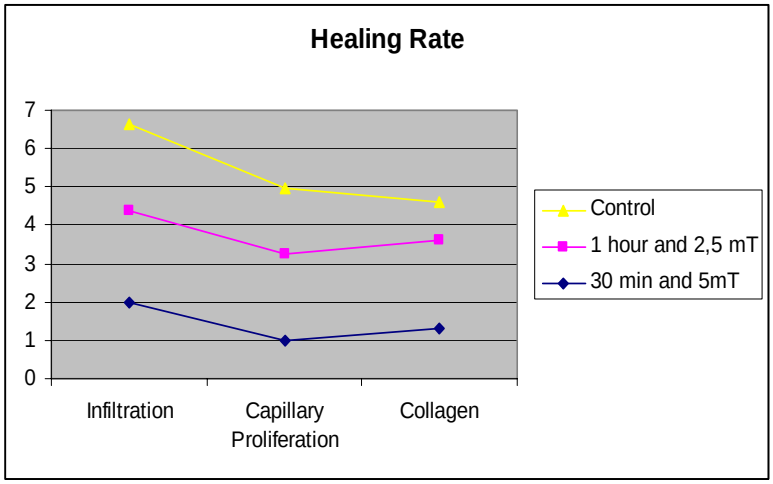


Fig 5. 3rd day's healing results

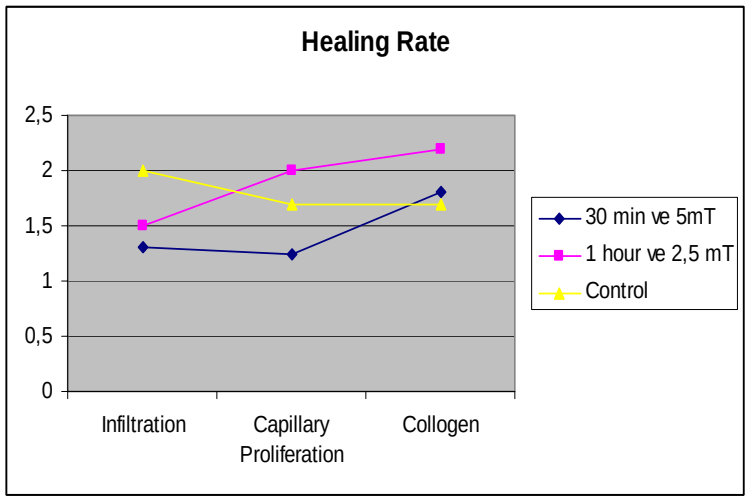


Fig 6. 7rd day's healing results

Conclusions

Changing rate of collagen fibrous and inflammation infiltration are shown in Fig 5. and Fig 6. At the end of the one-week process, decreasing in inflammation infiltration and increasing in collagen fibrous was observed. At incision on dorsal midline, 5 mT a day exposure can decrease healing rate half amount compare to control group. Exposure of 2.5 mT a day can increase the healing rate double amount to control group. The result of beneficial effect about wound healing was found in case of giving exposure with proper PMF. In the study similar results were found as in the scientific literature. Wave shape is as known the waveform which is used by Basset. Using proper exposure type can augment healing rate. The lower the exposure duration, the faster the healing occurs. It is agreeable that in the future, accelerated studies focused on waveform, frequency, power density, and different cell type will give reasonable interesting results.

References

[1] Basset CAL, Pawluk RJ, Pilla AA. 1974. Augmentation of bone repair by inductively-coupled electromagnetic fields. Science 184:575±577.

[2] Berg H, Mehedintu M .Proliferation response of yeast saccharomyces cerevisiae on electromagnetic field parameters. Bioelectrochem.Bioenerg 1997; 43: 67-70.

[3] De Haas W.G., Lazarovici M.A., and Morrison D.M. (1979) The effect of low frequency magnetic fields on the healing of the osteotomized rabbit radius. Clin. Orthop. 245-251.

[4] Goldman RJ, Cheng K. Electric fields and proliferation in a dermal wound model. Bioelectromagnetics 1998*;* 19:68-74.

[5] Ieran M, Zaffuto S, Bangnacani M. Effect of low frequency pulsing electromagnetic fields on skin ulcers of venous origin in humans. J Orthop Res 1990; 8: 276-82.

[6] Milgram, J., Shahar, R., Harrus, T., Kass, P., 2004. The Effect of Short, High Intensity Magnetic Field Pulses on the Healing of Skin Wounds in Rats. Bioelectromagnetics, 25:271 277.

[7] Stiller MJ, Pak GH, Shupack JL, Thaler S, Kenny C, Jondreau L. 1992.Aportable pulsed electromagnetic field (PMF) device to enhance healing of recalcitrant venous ulcers: A doubleblind, placebo-controlled clinical trial. Br J Dermatol 127:
147–154.

[8] Trostel, C. T., Mc Laughlin, R.,M., Lambert, J. G., Cooper, R.C., Elder, S. H., Pool, R. R., Cromiak, J. A., Boyle, C. R., 2003. Effects of Pico-Tesla Electromagnetic Field Treatment on Wound Healing in Rats, Am. J Vet Res, 64: 845-54.

CALCIUM HOMEOSTASIS IN CULTURED EXCITABLE CELLS EXPOSED TO ELF

MARIA A. MARIGGIÒ*•, CATERINA MORABITO*•, GUGLIELMO DI TANO*•, SILVIA BELIA*•, FRANCO CUCCURULLO* AND GIORGIO FANÒ*•

Laboratorio di Fisiologia, *Centro di Studi dell'Invecchiamento – Università "G.d'Annunzio", via Colle dell'Ara, 66013 Chieti – •Istituto Interuniversitario di Miologia (IIM)

Corresponding Author: Prof. Maria A. Mariggiò Lab Fisiologia, Centro di Studi dell'Invecchiamento – Università "G.d'Annunzio"-Chieti-Pescara
via Colle dell'Ara
Chieti 66013, Italy
Tel +39 0871 3554048 Fax +39 0871 3554043
e-mail: mariggio@unich.it

Abstract
It was abundantly but also roughly reported that extremely low-frequency magnetic fields interact with biological systems and in particular with excitable cells, but it remains obscure the mechanism(s) by which ELF are transduced into biological signals. To test if the presence of 50Hz ELF modulates in vitro the activity of excitable cell models, we analysed some features concerning the intracellular calcium homeostasis. In fact, the spatially and temporally defined intracellular calcium variations are the transductive events of numerous extracellular stimuli and this ion can modulate cellular excitability.
Using a single cell approach and a confocal microscope supplemented with a specially designed Helmholtz coils, we recorded intracellular calcium variations during ELF exposure of PC12, GL15 and C2C12 cell lines resembling neuron-like, glial and muscle model respectively. The acute cellular response to ELF was different in each cell line. We observed a differently modulated spontaneous calcium oscillations related to the ELF presence in differentiated C2C12 cells or in undifferentiated GL15 ones; in the other cell models there were not any significant effect in the same experimental conditions. These effects, probably, differently influenced the chronic response on calcium channels, as was revealed by experiments on cell-free samples from 10 days exposed cells.

Introduction
The biological effects of extremely low frequency electromagnetic fields (ELF-EMF) have fascinated scientists for a long time. But it is only during the past decade that the study of EMF interactions with whole organisms or isolated cells has become an increasingly recognized area of research within the biological sciences thank to an increasing number of experimental findings confirming that, under certain conditions, the non-ionizing electromagnetic energy can influence physiological processes in organisms (Gartzke and Lange, 2002; Vaughan et al, 2005). Even if numerous hypotheses have been suggested, none are convincingly supported by experimental findings. Various cellular processes, and systems can be affected by ELF-EMF exposure: i.e. cell membranes, general and/or specific gene expression, cell proliferation and differentiation, metabolic pathways and many other physiological mechanisms correlated directly or indirectly with cell viability (Repacholi and Greenebaum, 1999; Sieron at al, 2004; Ivancsits et al, 2005).
More recently, Simko and Mattsson (2004) suggested that ELF-EMF exposure is capable of increasing intracellular production of free radicals. These are intermediates in natural processes and could be the initial stimulus inducing a first response which then enhances (depending on cell type and status) the release of free radicals (Wolf et al, 2005) in turn leading to different biological events (Droge W, 2002). Mitochondria are the main sites of reactive oxygen species (ROS) formed as a side-product of oxidative phosphorylation, since electrons flowing from reduced substrates are occasionally transferred to oxygen to form superoxide anion and derived products (Chen et al, 2003).
If ROS generation and accumulation can be considered the first cellular event of an ELF-EMF exposure, the modification of Ca^{2+} homeostasis is surely one of the most important mechanisms by which ROS explicate their multiple actions into the cell (Camello-Almaraz et al, 2006). In the past years, many data obtained in various laboratories, showed that the ELF-EMF exposure was able to induce modifications of cytoplasmic Ca^{2+} levels which can be related to different physiological mechanisms: i.e. differentiation of chromaffin cells into neuronal-like cells (Morgado-Valle et al, 1998); cell death by apoptosis induced by several agents in different human cell systems (Fanelli et al, 1999); functional modifications of cells of the immune system (Walleczek J, 1992); etc. All these effects, and more others, can be attributed to modifications of Ca^{2+} homeostasis by ELF-EMF exposure throughout different mechanisms such as the involvement of P2Y membrane receptors (Takahashi et al, 2005); the activation of mechanically operated stretch-activated Ca^{2+} channels (Sun and Cho, 2004); the enhancing of the expression of voltage-gated Ca^{2+} channels (Grassi et al, 2004). All these pathways are constituted at least in part of ionic transmembrane channels that, above all in excitable cells, represent the main way for cell communication. The goal of this paper is to analyse some features involved in the homeostasis of intracellular calcium in excitable cells exposed to ELF-EMF at different intensities (0.1-1.0 mT). In particular we checked if

1. intracellular Ca^{2+} levels are changed
2. alterations of active or passive Ca^{2+} transport through cell membranes can be postulated
3. levels of some proteic factors, directly linked to Ca^{2+} activation, were modified

Results. The experimental plane regards the study of the possible influences of ELF-EMF on calcium homeostasis of excitable cells. For this reason, we used PC12, GL15 and C2C12 cell lines resembling neuron-like, glial and muscle model respectively. The presence of ELF-EMF influences the oxidative system of some excitable cells (Mariggiò et al., 2006) and also in this study some tested cell lines showed ROS production and/or mitochondrial membrane potential variations. Using a confocal microscope equipped with Helmholtz coils, we monitored the cells producing ROS (DCF labelled cells) or their mitochondrial membrane potential (JC-1-labelled cells) during a short exposure time (30 min) to 1.0 mT ELF-EMF. In these conditions, PC12 and GL15 populations showed an increased percentage of cells revealing increased ROS production (3 fold or 10

fold increase compared to PC12 or GL15 controls respectively), while in C2C12 cells no differences compared to control cells were detectable. In addition mitochondrial membrane potential variations were undetectable in PC12 cells, while GL15 and C2C12 cells showed a decreased potential compared to control cells.
The tested cell lines have a peculiar feature common to other excitable cells, which is to show spontaneous intracellular calcium ($[Ca^{2+}]i$) variations. Using the above described experimental single cell approach and a calcium specific fluorescent dye (FLUO4/AM), we assayed spontaneous $[Ca^{2+}]i$ variations during 30 min exposure to 0.1 or 1.0 mT ELF-EMF. Figure 1 shows selected representative frames (0, 15 and 30 min) depicting Fluo4-loaded cells (A) and temporal analysis of single cells (B). Data derived from these experiments showed that the spontaneous $[Ca^{2+}]i$ variations were increased in differentiated cells, above all in NGF-differentiated PC12 cells and in C2C12 myotubes in all experimental conditions (Fig. 1, C). In addition, while no PC12 phenotype was sensible to the presence of ELF-EMF (0.1-1.0 mT), both undifferentiated and differentiated GL15 cells and C2C12 myotubes showed increased spontaneous $[Ca^{2+}]i$ variations during short ELF-EMF exposure time (30 min) (Fig. 1, C).

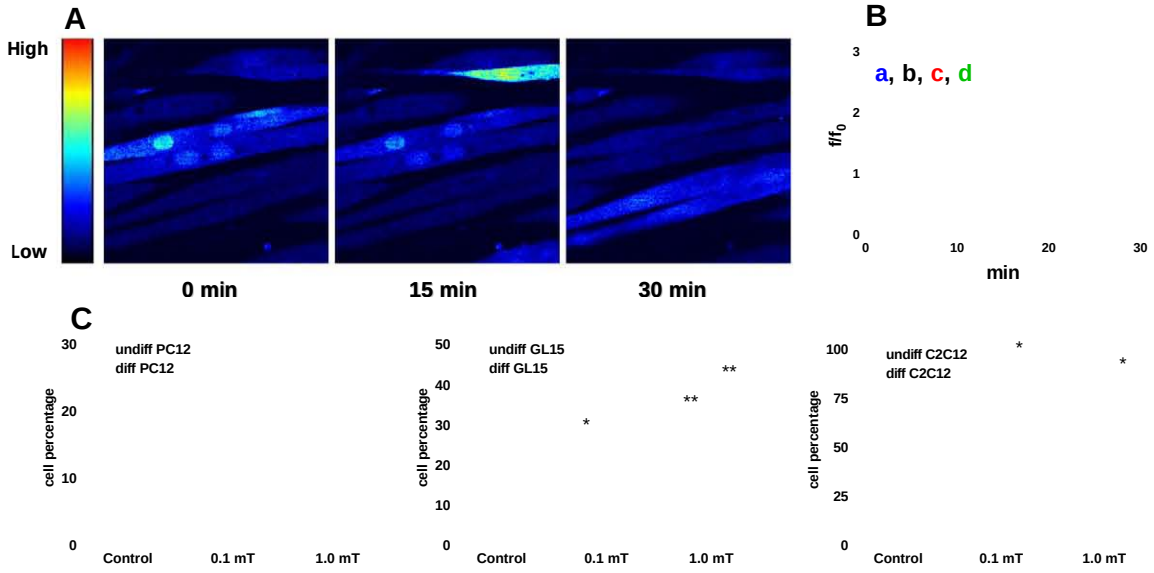


Figure 1: Temporal $[Ca^{2+}]i$ analysis. A: Confocal representative images, acquired at 0, 15 and 30 min, show a pseudo-color representation of Fluo4-loaded cells during a temporal analysis; the pseudo-color bar located to the left of the confocal images indicates a color scale from blue to red related to low (blue) and high (red) Ca^{2+} levels. B: Traces represent the possible $[Ca^{2+}]i$ variations in cells observed in presence or absence of ELF-EMF: a represents no calcium variations, b high frequency calcium variations, c a slow calcium increase and d a single increased pulse of calcium; the traces are the ratio of the single Fluo4-loaded cell fluorescence at time range from 2 to 30 min (*f*) to the mean value of fluorescence intensities after 2 min when, in exposed cells, ELF-EMF were produced (*f*0), as a function of time. C: Graphs represent the cell percentage of spontaneous variations (shown in B) in undifferentiated (undiff) or differentiated (diff) PC12, GL15 and C2C12 cells; bars are mean±SEM, n=5, *p<0.05 and **p<0.01.

Longer cell exposure (3 and 10 days) to ELF-EMF modified basal $[Ca^{2+}]i$ (Fig. 2, A and B). In particular after 3 days exposure at 0.1-1.0 mT ELF-EMF, GL15 cells showed significantly higher basal $[Ca^{2+}]i$ compared to controls; PC12 cells revealed the same increased when exposed to 1.0 mT ELF-EMF after 3 or 10 days exposure, no significant difference was observed after 0.1 mT ELF-EMF exposure. C2C12 cells didn't show any differences at 3 days ELF-EMF exposures, while these cells showed increased basal $[Ca^{2+}]i$ in respect to controls after 10 days exposure to 0.1 or 1.0 mT (Fig. 2, A and B).

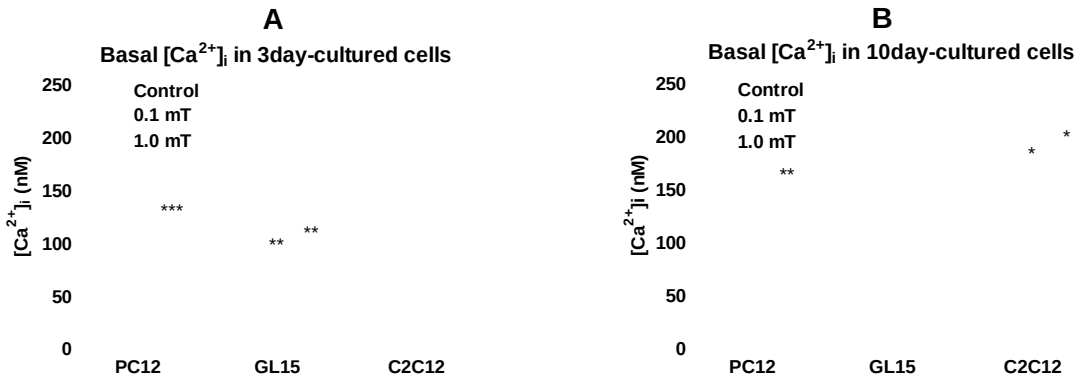


Figure 2: Basal $[Ca^{2+}]$i recorded in cell suspensions after 3 (A) or 10 (B) days (3day- or 10day-cultured) exposure to 0 (Control), 0.1 or 1.0 mT ELF-EMF. Bars are mean±SEM, n=5, *p<0.05, **p<0.01 and ***p<0.001.

The changes in basal $[Ca^{2+}]$i after ELF-EMF exposure could be determined by modifications in the calcium homeostatic system. For this reason we checked some elements involved in calcium homeostasis on long time exposed cells (3 or 10 days to 0.1 or 1.0 mT ELF-EMF). They were: two calcium regulated proteins (calmodulin and calcineurin); the functionality of calcium channels characteristic of excitable cells, voltage-gated dihydropyridine-sensible calcium channel (DHPR) and store ryanodine-sensible channel (RYR); Ca^{2+}/Mg^{2+} ATPase pump activity.

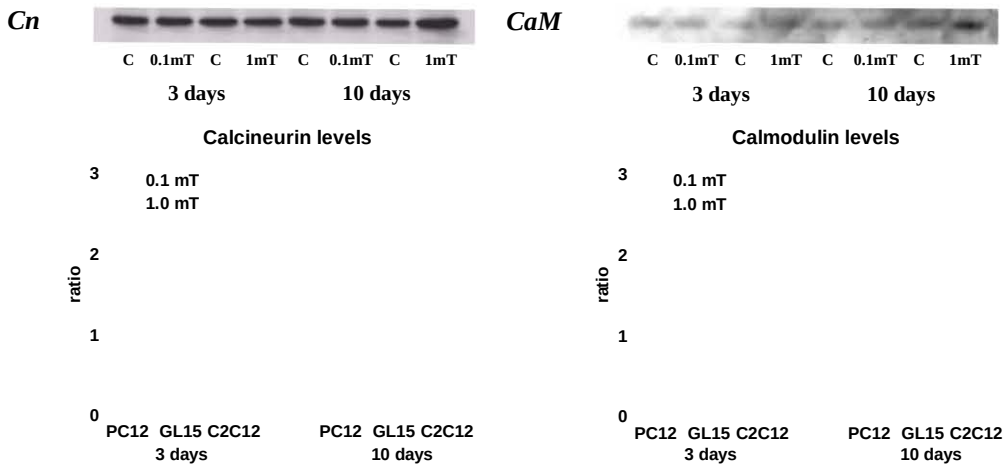


Figure 3: Representative Western blots of calcineurin (Cn) and calmodulin (CaM) in PC12 cells grown in absence (C) or in presence (0.1 or 1.0 mT) of ELF-EMF for 3 or 10 days. The graphs show the summarized densitometric analysis of Western blots of calcineurin and calmodulin in the tested cells. Bars are ratios between ODxmm^2 of each band related to control (C) proteins and ODxmm^2 of the band related to 0.1 or 1.0 mT exposed cells proteins.

Calcineurin levels revealed by Western blot analysis appeared increased in extracts from GL15 cells exposed for 3 days at 1.0 mT ELF-EMF or in those from PC12 cells exposed for 10 days to 1.0 mT ELF-EMF; in the other tested cells no modification was observed in any experimental conditions (Fig. 3). The calmodulin levels appeared increased only in PC12 cells exposed to 1.0 mT for 3 or 10 days (Fig. 3).
Figure 4 shows the data collected from experiments on cell extracts assayed for the functionality of DHPR and RYR channels and ATPase activity.

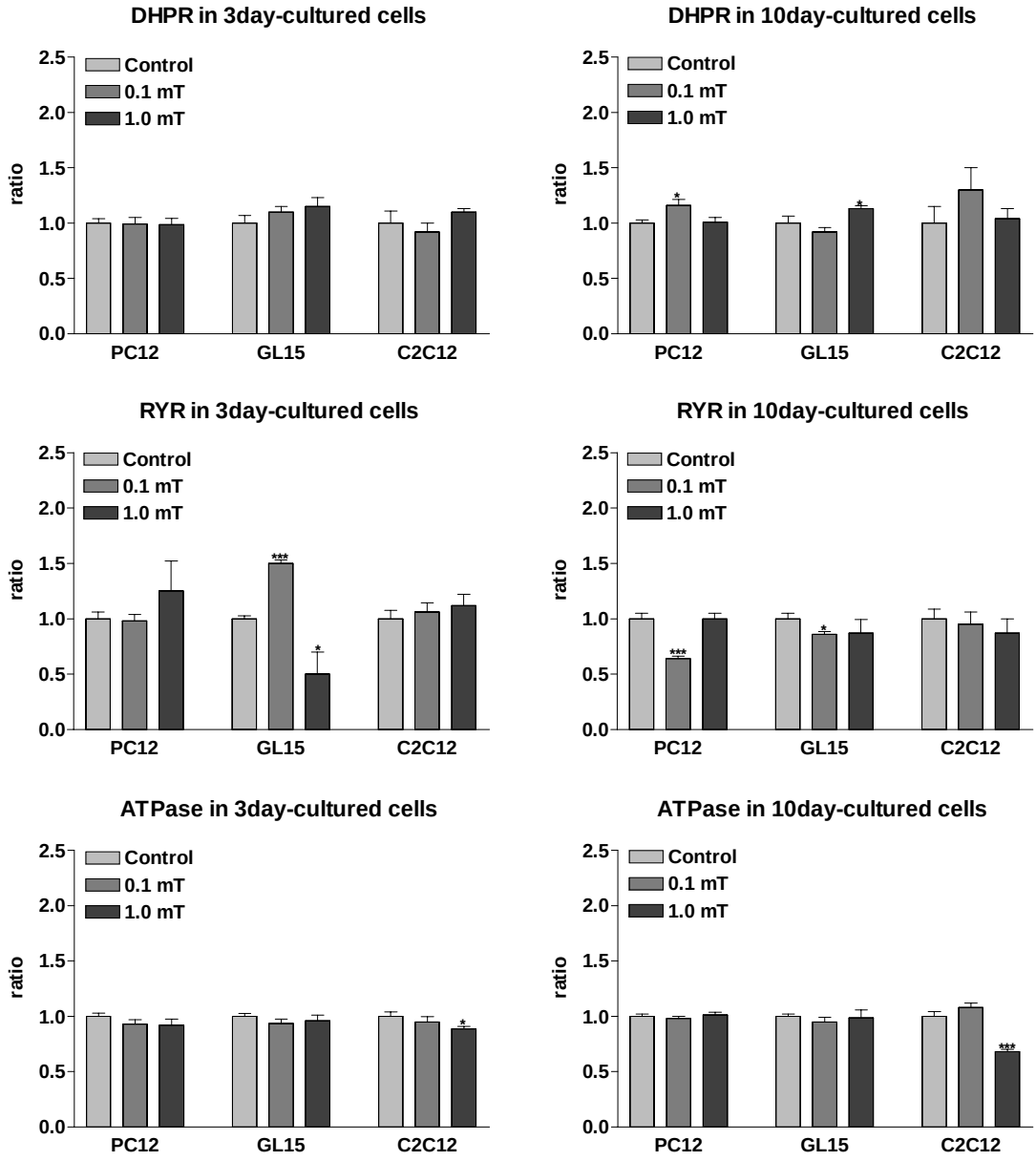


Figure 4: Functional assays on PC12, GL15 and C2C12 cells extracts. After 3 or 10 days (3day- or 10day-cultured cells respectively) exposure to 0 (Control), 0.1 mT or 1.0 mT ELF-EMF, cells were collected, homogenized and assayed for DHPR or RYR binding (calculated as pmol/mg protein and reported as ratio between treated and control cells) and ATPase activity (calculated as specific activity and reported as ratio between treated and control cells). Bars are mean±SEM, n=5, *p<0.05, **p<0.01 and ***p<0.001.

The DHPR and RYR binding assays permitted to monitor the presence of these channels on tested cells, in addition RYR binding experimental protocol revealed the functionally opened RYR channels. The number of DHPR appeared significantly increased on 10 days exposed PC12 and GL15 cells treated with 0.1 and 1.0 mT respectively. Fewer opened RYR channels appeared on 10 days and 0.1 mT exposed PC12 and GL15 cells, in the latter cells this result was evident also at 3 days and 1 mT exposure, while the opened RYR channels increased on 3 days and 0.1 mT exposed GL15 cells. The ATPase assay revealed a decreased ATPase activity on 3 or 10 days and 1 mT exposed C2C12 cells.

In conclusion each cell line showed a peculiar pattern of functional activities probably depending on their biological features.

Discussion. In the excitable cells, the Ca^{2+} ion has shown to play an important role in a wide variety of cellular

functions, such as that related to cell differentiation which involves nerve or muscle growth factors. For this reason, all changes to its cytoplasmic levels and/or transport can be the beginning of modifications able to modify, sometimes also radically, the functional capacity of the cell.
Cells exhibit several Ca^{2+}-mobilizing messengers, which transduce a large variety of extracellular stimuli regulating various intracellular Ca^{2+}-sensitive targets. Recent studies suggest that agonists differentially select their characteristic Ca^{2+} signals but it is still unclear whether different messengers mediate different functions or whether they act in a redundant fashion (Berridge et al, 2000). It is also possible that Ca^{2+} variations, induced by a specific source, are able to activate a sort of negative feed-back mechanism by which the cause of these variations can be suppressed. If this does not happen, then a measurable effect on some specific functional aspects of cell life must take place.
Under our conditions the first cause of Ca^{2+} overload can be found in the ROS generation triggered by ELF-EMF exposure. In fact, in at least two of three tested cell lines (PC12 and GL15), a significant increase of ROS, probably generated from the uncoupling of mitochondrial activity, was evident. As reported by several authors, a close relation between cytoplasmic Ca^{2+} variations and increase of ROS production exists under different experimental conditions. For example: (i) in cardiac tissue, a cytosolic, and subsequently mitochondrial, Ca^{2+} overload impaired mitochondrial bioenergetics (Solaini and Harris, 2005); (ii) in neurons, transient deprivation of oxygen and glucose during temporary ischemia coupled with elevation in cytosolic Ca^{2+} concentration triggers ROS generation and mitochondrial permeabilization, resulting in neural cell death (Brailoiu et al, 2006). Also under our experimental conditions, a significant modification of $[Ca^{2+}]i$ probably dependent on ELF-EMF intensity and/or exposure time, can be observed. Thereafter also some aspects of basal Ca-dependent activity as well as the spontaneous spikes generations, seemed to be influenced from the presence of electromagnetic fields. In fact, we observed differently modulated spontaneous calcium oscillations related to the ELF-EMF presence in differentiated C2C12 cells or in undifferentiated GL15 ones. In this case, it is important to note that modulations of calcium activity was observed during ELF-EMF exposure of single living cells, and the unique experimental procedure used, permitted to strictly correlate, for the first time, the Ca^{2+} variations and the presence of the electromagnetic field. On the other hand, the results from experiments carried out to detect some modifications of Ca^{2+} transport system remain without a clear and complete explanation. This fact could be due to physiological adaptive mechanisms present in the cells. Moreover, it is worth noting that these experiments were performed on cell-free substrate after several days exposure to ELF-EMF, so that the slight, but significant effects observed could be considered other proof of the existence of an interference mechanism induced by ELF-EMF on Ca^{2+} homeostasis

Summary
Cells possess several Ca^{2+}-mobilizing messengers, which couple stimulation at the cell surface, by a multitude of extracellular factors, to the regulation of intracellular Ca^{2+}-sensitive targets. As reported by several authors, a tight relation between cytoplasmic Ca^{2+} variations and an increase of ROS production under different experimental conditions, exists. In particular, the presence of ELF-EMF, with an intensity ranging from 0.1 to 1.0 mT, was able to induce qualitative and quantitative modifications of Ca^{2+} homeostasis (with different features in different cell lines) probably dependent on ELF-EMF intensity and/or time exposure.

Acknowledgments
We wish to thank Dr Cristina Puglielli for her technical assistance in basal $[Ca^{2+}]i$ measurements. This study was supported by grants from MATT (5376/2002/SIAR; DSA/2004/0026772)

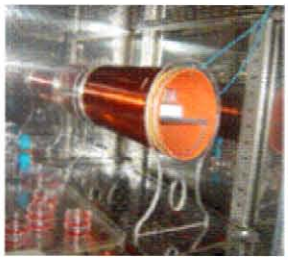
References

1. Berridge MJ, Lipp P, Bootman MD. The versatility and universality of calcium signalling. Nat Rev Mol Cell Biol. 2000; 1:11-21.
2. Brailoiu E, Churamani D, Pandey V, Brailoiu GC, Tuluc F, Patel S, Dun NJ. Messenger-specific role for nicotinic acid adenine dinucleotide phosphate in neuronal differentiation J Biol Chem. 2006 Jun 9;281(23):15923-8. Epub 2006 Apr 4.
3. Camello-Almaraz C, Gomez-Pinilla PJ, Pozo MJ, Camello PJ. Mitochondrial reactive oxygen species and Ca^{2+} signalling Am J Physiol Cell Physiol (June 7, 2006). doi:10.1152/ajpcell.00217.2006.
4. Chen Q, Vazquez EJ, Moghaddas S, Hoppel CL, Lesnefsky EJ. Production of reactive oxygen species by mitochondria: central role of complex III. J Biol Chem. 2003; 278:36027-36031.
5. Droge W. Free radicals in the physiological control of cell function. Physiol Rev. 2002; 82:47-95.
6. Fanelli C, Coppola S, Barone R, Colussi C, Gualandi G, Volpe P, Ghibelli L. Magnetic fields increase cell survival by inhibiting apoptosis via modulation of Ca^{2+} influx. FASEB J. 1999; 13:95-102.

7. Gartzke J, Lange K. Cellular target of weak magnetic fields: ionic conduction along actin filaments of microvilli. Am J Physiol Cell Physiol. 2002; 283:C1333-C1346.
8. Grassi C, D'Ascenzo M, Torsello A, Martinotti G, Wolf F, Cittadini A, Azzena GB. Effects of 50 Hz electromagnetic fields on voltage-gated Ca^{2+} channels and their role in modulation of neuroendocrine cell proliferation and death. Cell Calcium. 2004; 35:307-315.
9. Ivancsits S, Pilger A, Diem E, Jahn O, Rudiger HW. Cell type-specific genotoxic effects of intermittent extremely low-frequency electromagnetic fields. Mutat Res. 2005; 583:184-188.
10. Mariggiò MA, Amicarelli F, Grossi MR, Falone S, Morabito C, Fanò G, Cuccurullo F, Di Ilio C. Extremely low frequency electromagnetic fields and oxidative stress in excitable cell lines. Proceedings of 4th International Workshop on Biological Effects of Electromagnetic Fields. 16-20 October 2006, Crete, Greece.
11. Morgado-Valle C, Verdugo-Diaz L, Garcia DE, Morales-Orozco C, Drucker-Colin R. The role of voltage-gated Ca^{2+} channels in neurite growth of cultured chromaffin cells induced by extremely low frequency (ELF) magnetic field stimulation. Cell Tissue Res. 1998; 291:217-230.
12. Repacholi MH, Greenebaum B. Interaction of static and extremely low frequency electric and magnetic fields with living systems: health effects and research needs. Bioelectromagnetics 1999; 20:133-160.
13. Sieron A, Labus L, Nowak P, Cieslar G, Brus H, Durczok A, Zagzil T, Kostrzewa RM, Brus R. Alternating extremely low frequency magnetic field increases turnover of dopamine and serotonin in rat frontal cortex. Bioelectromagnetics 2004; 25:426-430.
14. Simko M, Mattsson MO. Extremely low frequency electromagnetic fields as effectors of cellular responses in vitro: possible immune cell activation. J Cell Biochem. 2004; 93:83-92.
15. Solaini G and Harris DA. Biochemical dysfunction in heart mitochondria exposed to ischaemia and reperfusion. Biochem J. 2005; 390:377-394.
16. Sun S, Cho M. Human fibroblast migration in three-dimensional collagen gel in response to noninvasive electrical stimulus. II. Identification of electro coupling molecular mechanisms. Tissue Eng. 2004; 10:1558-1565.
17. Takahashi K, Doge F, Yoshioka M. Prolonged Ca2+ transients in ATP-stimulated endothelial cells exposed to 50 Hz electric fields. Cell Biol Int. 2005; 29:237-243.
18. Vaughan TE, Weaver JC. Molecular change signal-to-noise criteria for interpreting experiments involving exposure of biological systems to weakly interacting electromagnetic fields. Bioelectromagnetics. 2005; 26:305-322. l
19. Walleczek J. Electromagnetic field effects on cells of the immune system: the role of calcium signaling FASEB J. 1992; 6:3177-3185.
20. Wolf FI, Torsello A, Tedesco B, Fasanella S, Boninsegna A, D'Ascenzo M, Grassi C, Azzena GB, Cittadini A. 50-Hz extremely low frequency electromagnetic fields enhance cell proliferation and DNA damage: possible involvement of a redox mechanism. Biochim Biophys Acta. 2005; 1743:120-129.

Appendix

Instrumentation. The 50Hz electromagnetic fields were generated by two different devices: a solenoid and a pair of Helmholtz coils. These devices were planned and built to deliver variable, homogeneous, sine-wave alternate current magnetic fields with 50 Hz frequency and intensities ranging between 0.1-1.0 mT±2%. The horizontal cylindrical solenoid (length=340mm, diameter=113mm), on a supporting base, was supplied by a power supply Elgar Electronics (mod. CW-801P). The solenoid was used in an incubator (5% CO_2 and 37°C) for long time continuous cell exposures (1-10 days) during which the solenoid's eventual added temperature was negligible (photo A). The pair of Helmholtz coils (r=445mm, distance between coils=400mm), producing homogeneous magnetic field over the specified volume-under-test corresponding to the cell chamber, were located in the working zone of a confocal microscope and connected to a power supply Elgar Electronics (mod. CW-1251P) (photo B). The coils were used to generate 0.1-1.0mT ELF-EMF for short time cell exposure (30 min) during in vivo cell analysis (ROS production, mitochondrial membrane potential variation, $[Ca^{2+}]i$ variation).



A: Solenoid in a CO_2 incubator







B: Confocal microscope equipped with Helmholtz coils

Cell culture. C2C12 and PC12 (American Culture Collection) and GL15 (functionally characterized in our lab, Mariggiò et al BMC Physiology 1:4, 2001) were cultured as exponentially growing cells in growth medium (GM). The GM for C2C12 and GL15 contains Dulbecco's modified Eagle's medium (DMEM), 10-20% foetal calf serum (FCS), 2-4 mM L-glutamine and 100 UI mL^{-1}-100 μg mL^{-1} Penicillin-Streptomycin. The differentiative phenotype was induced in C2C12 and GL15 cells in GM supplemented only by 2% FCS for 7-10 days. The GM for PC12 cells contains RPMI 1640 with 5% FCS and 10% horse serum, glutamine and antibiotics as mentioned previously. Reagents for cellular cultures were purchased from Gibco (Paisley, Scotland, UK). In PC12 cells, the differentiative phenotype was induced in GM containing 50ng/ml nerve growth factor for 7 days. The cells were seeded on Petri dishes in GM and routinely sub-cultured every three days C2C12 and GL15 and weekly PC12 (Mariggiò et al, BMC Physiology 1:4, 2001; Guarnieri et al, Neuroscience 128:697–712, 2004; Pietrangelo et al., J Physiol.572.3:721-733, 2006). The PC12 cells were cultured on Falcon flask and plated for experiments on collagen-treated wells.

$[Ca^{2+}]i$ and ROS measurements. We plated the cells on glass coverslips that were incubated for 30 min at 37°C in normal external solution (NES) supplemented with 10 mg mL^{-1} BSA and 5 μM FLUO4 AM or H_2DCF-DA (Molecular Probes, Eugene, OR, USA) for $[Ca^{2+}]i$ or ROS determination respectively. The NES solution consisted of 10 mM glucose, 140 mM NaCl, 2.8 mM KCl, 2 mM $CaCl_2$, 2 mM $MgCl_2$, and 10 mM HEPES, pH 7.4. After Fluo4-AM incubation, cells were rinsed with NES and observed. The images were collected using a Bio-Rad MRC-1024 ES confocal system (Bio-Rad Microscience Ltd, Hemel Hempstead, UK) connected to an inverted microscope Zeiss Axiovert 100 equipped with 63x/1.25 PLAN NEOFLUAR oil immersion objective and Helmholtz coils described above. For Fluo4 fluorescence, as well as that of DCF, excitation was fixed at 488 nm and emission was set at 522 nm using a bandpass filter (bandwidth±32 nm). The laser potency, photomultiply and pinhole size were kept constant for the whole experiments. Images were acquired, stored and off line analyzed. Traces deriving from total cell area were calculated as $f/f0$ where f is the fluorescence emission of a single FLUO4 (or H_2DCF-DA) loaded cells at times ranging from two to x seconds and $f0$ is the mean value of fluorescence intensities of the same cell calculated among all the images before turning on the coils. Graphs were plotted using Prism 2.0 (GraphPad Software, San Diego, CA, USA).

Spectrofluorimetric determination of basal $[Ca^{2+}]i$. For basal $[Ca^{2+}]i$ determination on cell suspensions, after 3 or 10 days ELF-EMF exposure, the cells (PC12, C2C12 and GL15) were detached and washed by gentle centrifugation. The cells, resuspended in NES, were loaded with 5 μM Fura 2-AM for 30 min at 37°C and treated for 5 min with 250 μM sulphynpirazone then collected in the quartz cuvette and analysed using LS-5B Perkin-Elmer spectrofluorimeter. The $[Ca^{2+}]i$ was calculated using the formula: $[Ca^{2+}]i = Kd\ (F-F_{min})/(F_{max}-F)$, where F_{max} and F_{min} were the fluorescences recorded at the end of each experiment, after the addition of 1 μM Ionomicin and 5 mM EGTA respectively; Kd (224 nM) is the dissociation constant of Fura2 for calcium (Grynkiewicz et al, J Biol Chem. 260:3440-3450, 1985).

Mitochondrial membrane potential measurements. These were determined using a carbocyanine dye JC-1 (Molecular Probes, Eugene, Oregon, USA) which is taken up by the mitochondria. When the transmembrane potential is high, like in normal cells, JC-1 forms red fluorescence dimers (J-aggregate), while when it is low the red fluorescence disappears and green fluorescence emission appears (monomer). Briefly, the cells on coverslips were incubated in growth medium containing 5 mM of JC-1 for 10 min. After being rinsed three times with PBS, each coverslip was observed and images were recorded with or without the ELF-EMF generated by Helmholtz coils applied to a confocal microscope (excitation was fixed at 488 nm and emission was set to either 522 nm, for green monomer, or 605 nm, for red J-aggregate, using a bandpass filter). To estimate the modification of fluorescence in mitochondria, the change in green and red areas was calculated for the whole image using Scion Image ver. beta 3b (Scion Corporation, Frederick, Maryland, USA). The red/green area ratio, resulting from each single image of the experiment was plotted against time (Castellano et al., Arch. Pharm. Pharm. Med. Chem. 333:373–380; 2000).

Western blots. PC12, C2C12 and GL15 cells were exposed to 0.1 or 1.0 mT ELF-EMF for 3 or 10 days. At the

end of the exposure the cells were collected, rapidly washed on ice with pre-cooled PBS and lysed in buffer containing (mM): 50 Tris-HCl, 100 NaCl, 50 NaF, 40 β-glycerolphosphate, 5 EDTA, 1% Triton X-100, 200 μM NaOrthovanadate, 100 μg/ml phenylmethylsulfonyl fluoride, 10 μg/ml leupeptin, 5 μg/ml pepstatin A, 10 μg/ml benzamidine, pH 7,4. After vortexing for 5 min, the sample were centrifuged at 12,000 rpm for 10 min at 4°C. The protein content of the supernatant was quantified by a colorimetric assay (Bio-Rad Laboratories Srl, Milano, Italy). Samples containing 40 μg of proteins were suspended in Laemmli buffer (8% SDS, 10% glycerol, 5% β-mercaptoethanol, 25 mM Tris-HCl and 0.003% Bromophenol Blue, pH 6,5), boiled for 5-10 min and electrophoresed on 10% SDS polyacrylamide homogenous slab gel (SDS-PAGE). Proteins were electroblotted onto a hydrophobic polyvinylidene difluoride membrane (Hybond-P Amersham-Pharmacia Biotech). The calmodulin and calcineurin proteins levels were detected with specific antibodies (monoclonal mouse anti-Calmodulin and polyclonal rabbit anti-Calcineurin, CALBIOCHEM, Germany). The antibodies were detected by chemiluminescence (ECL Amersham-Pharmacia Biotech).

Binding experiments and ATPase activity measurements**.** For [^{3}H]PN200-110 and RyR binding, and Ca^{2+}-ATPase activity the cells cultured in growth medium were exposed for 3 or 10 days to ELF-EMF electromagnetic fields at 0.1 and 1.0 mT intensity. At the end of the exposure times, the cells were sonicated (1 pulse 2 s^{-1}, 20-40 pulses) in a buffer solution containing 10 mM Hepes and 150 mM KCl. The dihydropyridine receptor (DHPR) concentration was determined according to the procedure of Renganathan et al. (J Membr Biol 157(3):247-253, 1997) using the radioligand [^{3}H]PN200-110. Sonicated cell proteins (40 μg) were incubated in a final volume of 250 μl binding buffer in the presence of 1nM [^{3}H]PN200-110 per 1 h at room temperature, then the samples were filtered with Whatman GF/C filters and washed with 6 volumes of ice-cold washing buffer. Radioactivity was determined by liquid scintillation counting. Non-specific [^{3}H]PN200-110 binding was assessed in the presence of 10 μM unlabeled nifedipine.

The sonicated cell proteins (25 μg), in a final volume of 250 μl, were incubated in a binding buffer (200 mM KCl, 10 mM HEPES pH 7.4, 100 μM $CaCl_2$, 1μg/ml pepstatin, 1μg/ml leupeptin) in agitation with 5 nM [^{3}H]ryanodine for 120 min at 37°C, then filtered with Whatman GF/C filters and washed with 6 volumes of ice-cold 200 mM KCl, 10 mM HEPES, pH 7.4 as described by Fanò et al. (J Muscle Res Cell Motil 22:345-351, 2001). The amount of bound [^{3}H]ryanodine was determined by liquid scintillation counting (Treves et al., Biochemistry 36:11496-11503, 1997).

Ca^{2+}-ATPase enzymatic activity was measured on total sonicated cell proteins according to the procedure of Fanò et al. (J Muscle Res Cell Motil 22:345-351, 2001). The assay was carried out in 1 ml incubation medium (in mM: 5 ATP, 1 $CaCl_2$, 50 Tris-HCl buffer, pH 7.4) containing 25 μg of proteins/sample. After 15 min at 37 °C, the reaction was stopped by the addition of 1 ml of 5% TCA and the precipitate removed by centrifugation at 5000g for 10 min. The released orthophosphate was estimated on 1 ml of clear supernatant, according to Saini and Van Etten (Arch. Biochem. Biophys 191:613-624, 1978). Enzyme specific activity was expressed as μmol of Pi released per min per mg of proteins (A.S.).

Statistical analysis of data was performed using Student's paired t-test, and automatically derived with Prism 2.0 software (GraphPad Software, Inc., San Diego, CA, USA).

THE EFFECTS OF DIFFERENT MAGNETIC FIELD INTENSITY TREATMENTS ON RAT ELECTROPHYSIOLOGICAL PARAMETERS

SEVGI GUNES, BELGIN BUYUKAKILLI

MERSIN UNIVERSITY, MEDICAL FACULTY, DEPARTMENT OF BIOPHYSICS, TURKEY

gunessevgi@yahoo.com, bbuyukakilli@mersin.edu.tr

Abstract

In this study, we investigated the effects of different densities at daily life exposure of sinusoidal magnetic fields on the mass of rats and peripheral nerve regeneration. Magnetic field was applied to 40 rats for 4 hours per day for a week. One of the rat groups were separated as a control the others were separated for 10, 20, and 30 Gauss (G) magnetic field treatment. All of the rats were exposed to crush injury just before the treatment.

In the study, after crush injury of sciatic nerve in the period of first 3 days treatments of magnetic field showed no mass differences compared to control. But 7 days treatment of 30 G magnetic field decreased mass of the rats when compared to control while the other groups did not.

When the electrophysiological results were estimated, in terms of nerve regeneration, it could be suggested that both after 3 days exposition to injury and 7 days treatments of different magnetic field densities have no statistically important effect on the CMAP (Compound Muscle Action Potential) amplitude, area and the rate of conduction.

As a result, it is observed that the density and frequency of magnetic fields used in this study had no effect on transmission and stimulation of nerves consequently so was not effecting the nerve regeneration.

Key words: Electromagnetic field, nerve regeneration, rat mass.

Introduction

All members of modern societies constantly live in electromagnetic fields and waves which intensities are much higher than those found in the nature. The potential negative effects of those on human health continue to be the subject of controversy (1). Most public exposure to ELF fields comes from electrical appliances, household wiring, and AC transmission and distribution lines (2).

In this study we tested whether magnetic fields created with 50 Hz alternating current (AC) affects regeneration of the sciatic nerve or not.

Exposure to PEMF as a pretreatment prior to crush injury also resulted in acceleration of axonal regrowth (3;4). Research in cats and rats suggests that pulsed electromagnetic fields may accelerate the rate of peripheral nerve regeneration (5,6). Stimulation with a 50–Hz alternating magnetic field stimulated regeneration of sensory nerve fibers in the rat sciatic nerve (7). A high-intensity static magnetic field of 1 Tesla has no effect on peripheral nerve regeneration as determined by myelinated axon counts and electrophysiologic studies in our rat sciatic nerve model. Specific orientation of the sciatic nerve with respect to the magnetic field also has no effect on the rate of nerve growth. Periods of restraint of 12 hours per day for 4 weeks inhibit weight gain by rats but have no effect on nerve regeneration in this experimental system (8).

Kolosova at al. [1996] reported that the stimulation observed in the study may not be a direct effect of MWR on regenerating nerve fibers. In their study data show a stimulating effect of low-intensity MWR on regeneration of the rat sciatic nerve. MWR treatment of the femoral skin in the area of suture accelerates the growth rate of the regenerating nerve fibers and their functional maturation (9).

The biological mechanism of action of magnetic fields is poorly understood. Reports of changes in cell membrane permeability suggest that the physiological effect is connected with electrolyte ion exchange (10).

Mean body weights of exposed groups of male and female mice were similar to those of the control groups throughout the study (11). In the another study the data indicated that over 21 days, the PEMF field inhibited young rats ability to recover from the mass loss normally associated with stress from the start of the experiment. In contrast all older rats recovered more slowly than the control young rats in the same study (12).

Materials and Methods

Animals

In present study 40 female Wistar Albino rats (150–200 g) were used. 30 of them were experiment group and the others were the control group. The rats were 12 weeks of age. They lived at 12h light-dark cycle with diet and water available *ad libitum*, without any additional medication. Before the experiment, they are adapted these conditions in a week. The experiment group was divided into three groups. They were given 10, 20 and 30 G respectively. The magnetic field generation coils were not energized, and the control rats were exposed only to the ambient magnetic field in laboratory (0.4-0. 5 G).

Surgical Procedure

All rats were operated on under intramuscular (i.m.) 50 mg/kg Ketamine Hydrochloride anesthesia. The sciatic nerve was exposed to biceps femoris muscle splitting incision unilaterally. Crush lesions were performed using a jeweler's forceps to prevent cutting when applied 15 sec, and the site of the injury was labeled with a 10/0 prolene suture attached to the epineurium. Following recovery from anesthesia, the rats were randomly assigned as a control group or experimental groups.

Magnetic Field Stimulation

A field of 10, 20 and 30 G as calculated from voltages induced in pick up standardized coil probe, placed midfield, was generated in a pair of Helmholtz coils 45 cm in diameter, with 160 turns of 2.2 mm gauge copper wire each. The coils were mounted on a plastic framework, 22.5 cm apart, and connected in series to a generator delivering a sine wave output current of 4.8 A at 50 Hz. Five rats were simultaneously put in a square, nonconductive plastic cage (35x20x45 cm) within the coils and left unrestrained. The coils were placed perpendicular to the table so the magnetic field was horizontal.

The rats were put in square plastic cages (20x20x30 cm) within the coils and exposed to the magnetic field for four hours on every seven days from the day of operation. The action potentials were recorded before experiment and after 3rd, 7th days of exposure to the electromagnetic fields by using a BIOPAC MP 100 Acquisition System Version 3.5.7 (Santa Barbara, USA).

Statistical Analysis

All statistical tests were performed with SPSS software (Statistical Package for the Social Sciences, SPSS, Inc., Chicago, IL, USA). Data obtained from study were compared by one-way ANOVA in term of differences. Bonferroni test was used for determining that the differences between each groups.

Results

The extent of nerve regeneration was studied by CMAPs. The amplitude, duration, area, and latency period of CMAPs were measured, and the conduction velocity of the nerve was calculated.

Table 1

Conduction Velocity (Effect of 50 Hz sinusoidal magnetic field exposure on regeneration of rat sciatic nerve)

Groups	Treatments (h/day)	Magnetic field intensity (G)	Before experiment measurements (m/s)		3rd day measurements (m/s)		7th day measurements (m/s)	
			Average	S D	Average	S D	Average	S D
Control	4	0	103.50	28.55	111.36	0.80	94.44	26.84
Group I	4	10	35.18	18.67	71.15	49.57	87.39	37.03
Group II	4	20	59.74	46.53	101.11	26.75	90.56	41.60
Group III	4	30	101.90	31.36	114.51	23.60	108.33	12.50

S D: Standard Deviation

CMAP rate analysis have showed that 3 days of 10 G treatment elongated duration compared to other three groups and 20 G treatment increased duration more than 30 G treatment. This results show that CMAP period increases while the intensity of magnetic field decreases. When compared to control, 7 days treatment of 20 G decreases total CMAP period more than the other groups. As a result, it is observed that the density and frequency of magnetic fields used in this study had no effect on transmission and stimulation of nerves consequently so was not effecting the nerve regeneration (Table 1).

In the study, after crush injury of sciatic nerve in the period of first 3 days treatments of magnetic field showed no mass differences compared to control. But 7 days treatment of 30 G magnetic field decreased mass of the rats when compared to control while the other groups did not (Table 2).

Table 2

Effect of 50 Hz sinusoidal magnetic field exposure on rats weights

Groups	Measurements	Average weights (g)	Standard deviation
Control (n=10)	1.	152.40	17.57
	2.	159.10	17.02
	3.	161.70	15.83
10 G Group (n=10)	1.	143.70	18.84
	2.	141.30	18.86
	3.	142.70	15.04
20 G Group (n=10)	1.	148.20	19.91
	2.	155.20	20.51
	3.	166.50	19.21
30 G Group (n=10)	1.	169.91	15.27
	2.	172.36	17.77
	3.	175.30	21.32

Conclusions:

We could not prove a neuroprotective effect of electromagnetic field in rat crush injury model using electrophysiological method.

Summary

In this study effects of weak, sinusoidal low frequency magnetic field (MF) stimulation on regeneration of the rat sciatic nerve were investigated. Forty Wistar rats were used: they were underwent unilateral sciatic nerve transaction injury, 30 of them were experiment group and the remaining 10 were control group. The experiment group with sciatic nerve lesion was divided into 3 groups randomly. After the injury all of the experiment groups were exposed to sinusoidal 50 Hz magnetic field of 10, 20 and 30 G respectively. During the experiment the rats were put between a pair of Helmholtz coils for a week for 4 h/day. The other ten rats were used for control.

When the electrophysiological results were estimated on the 3rd and 7th days after the injury, in terms of nerve regeneration, it could be suggested that treatments of different magnetic field densities have no statistically important effect on the CMAP amplitude, area and the rate of conduction.

CMAP rate analysis have shown that 3 days of 10 G treatment elongated duration compared to other three groups and 20 G treatment increased duration more than 30 G treatment. These results show that CMAP period increases while the intensity of magnetic field decreases. 7 days of treatment of 20 G found to decrease total CMAP period more than the control group. As a result, it is observed that the density and frequency of magnetic fields used in this study has no effect on transmission and stimulation of nerves, and also to the peripheral nerve regeneration.

In the study, after crush injury of sciatic nerve in the period of first 3 days treatments of magnetic field showed no mass differences compared to control. But 7 days treatment of 30 G magnetic field decreased mass of the rats when compared to control while the other groups did not.

References

1) Topcu C, Gurbilek M, Akoz M, Acıkgozoglu S. Effect of magnetic fields on the Na^+ K^+- ATPase activity of eritrocyte membrane and the levels of malondialdehyde and glutathione. *T Klin J MED Res*, 2002; 20:119-124.
2) Repacholi MH, Greenebaum B. Interaction of static and extremely low frequency electric and magnetic fields with living systems: health effects and research needs. *Bioelectromagnetics*, 1999; 20:133-160.
3) Sisken BF, Kanje M , Lundborg G, Herbst E, KURTZ W. Stimulation of rat sciatic nerve regeneration with pulsed electromagnetic fields. *Brain Res.* 1989; 24;485(2):309-16.
4) Kanje M, Rusovan A, Sisken B, Lundborg G. Pretreatment of rats with pulsed electromagnetic fields enhances regeneration of the sciatic nerve. *Bioelectromagnetics*, 1993*;* 14:353-359.Michael H. Repacholi B. Greenebaum 1993
5) Raji AM. An experimental study of the effects of pulsed electromagnetic field (diapulse) on nerve repair. *Journal of Hand Surgery.* 1984; 9(2):105-112.
6) Orgel MG, O'Brien WJ, Murray HM. Pulsing electromagnetic field therapy in nerve regeneration: an experimental study in the cat. *Plast Reconstr Surg.* 1984: 73(2):173-83.
7) Rusovan A, Kanje M. Stimulation of regeneration of the rat sciatic nerve by 50 Hz sinusoidal magnetic fields. *Exp Neurol*. 1991; 112(3):312-6.
8) Cordeiro PG, Seckel BR, Miller CD, Gross PT, Wise RE. Effect of a high-intensity static magnetic field on sciatic nerve regeneration in the rat. *Plast Reconstr Surg* 1989; 83(2):301-8
9) Kolosova LI, Akoev GN, Avelev VD, Riabchikova OV, Babu KS. Effect of low-intensity millimeter wave electromagnetic radiation on regeneration of the sciatic nerve in rats. *Bioelectromagnetics*, 1996; 17(1):44-7.
10) Gmitrova A., Ivanco I., Gmitrorov J., Murin M. Biological effect of magnetic field on laboratory animals. Journal of Bioelectricity. 1988 7(1):123-124
11) National Toxicology Program. NTP Toxicology and Carcinogenesis Studies of 60-HZ Magnetic Fields IN F344/N Rats and B6C3F1 Mice (Whole-body Exposure Studies). Natl Toxicol Program Tech Rep Ser. 1999 Apr;488:1-168.
12) Sandrey MA, Vesper DN, Johnson MT, Nindl G, Swez JA, Chamberlain J, Balcavage WX. Effect of short duration electromagnetic field exposures on rat mass. *Bioelectromagnetics.* 2002; 23(1):2-6.

TEMPERATURE AND MICROWAVE FIELD EFFECT ON THE RED FLUORESCENT PROTEIN (DsRed) PHOTOLUMINESCENCE IN SOLUTION

I. BARAK, A.B. COPTY, M. GOLOSOVSKY, AND D. DAVIDOV

The Racah Institue of Physics, The Hebrew University of Jerusalem, 91904 Jerusalem, Israel

Abstract

We compared the effect of microwave irradiation on the red fluorescent protein (DsRed) placed in a cylindrical resonant cavity with that of conventional heating. Our measurements show that the fluorescence intensity in either case decreases by ~ 1% per degree centigrade, indicating that the microwave effect on the sample is mostly a thermal one.

1. Introduction

In this work we studied the influence of microwave field on the DsRed, a red fluorescent protein (RFP) from Discosoma coral[1]. The DsRed has a very stable three dimensional beta-can barrel structure, but its emission spectrum is shifted to longer wavelength , with a maximum intensity at λ=583 nm [2, 3] . The sample, placed in a cylindrical cavity, was excited by the CW excitation at 488 nm by an Argon laser. We performed our experiments on RFP in a buffer solution, and have monitored changes in its photoluminescence under microwave irradiation and compared it to the changes in fluorescence under conventional heating. Previous studies indicate that the microwave field effect on proteins in solution and on living tissues can not be entirely reduced to heating [4, 5, 6,7] , while when the biomolecule is in the crystalline form, the effect of microwave irradiation is indistinguishable from conventional heating[8]. Our group has recently found a specific effect of the microwave field on the Enhanced Green Fluorescent Protein fluorescence in solution [9]. it is surprising since the theoretical analysis of microwave interaction with biological system does not leave many possibilities for non-thermal microwave effect on biological system. Adair [10] showed that the resonance excitation of biological molecules in solution at microwave frequency is highly improbable. Foster[11] demonstrated that thermal gradients on the nanometric scale are exceedingly small. The pupose of our present approach is to study the effect of microwave field on the protein fluorescence in solution in real time.

2. Experimental Setup

We placed a transparent glass pipette filled with buffer solution containing DsRed inside an X-band TE_{011} cylindrical resonant cavity (Fig. 1.). We drilled two small holes in the sidewalls of the cavity to introduce laser beam and to observe fluorescence. The pipette is mounted slightly off-center. The cavity is fed using a HP 83623A synthesized sweeper. We directed a 488 nm Argon laser beam (Omnichrome Series 43) through the pipette and picked up the fluorescence at 90^o using an objective lens coupled to a monochromator (DK480) through an optical fiber (Oriel, Model 77539). The monochromator is connected to a cooled photomultiplier (Product for Research, Model TE177RF) operating in the counting mode (SR400 Two channel Gated photon counter). In some experiments we also used a stereo microscope (Zeiss, Stemi 2000-c) connected to a digital camera.

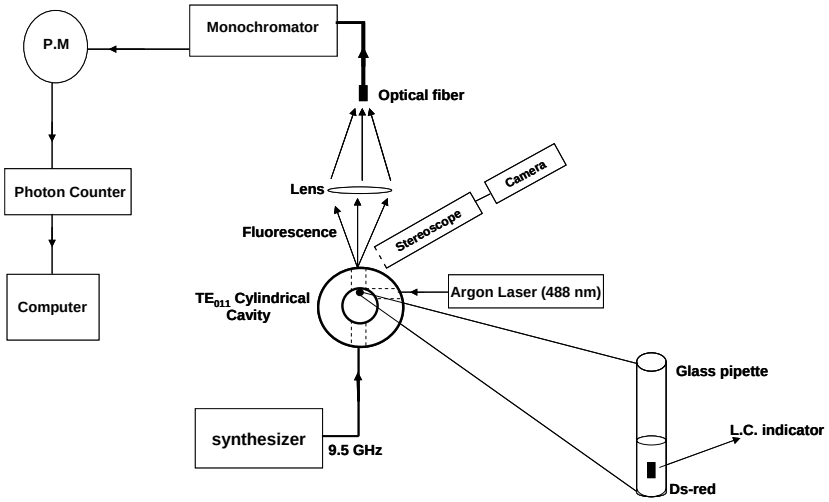


Fig. 1. Experimental setup - Top view. The pipette with a fluorescing solution is mounted in the cylindrical microwave cavity operating at 9.5 GHz. The pipette is slightly off-center of the cavity and it is irradiated by the laser beam through a small hole in the cavity sidewall. The photoluminescence under microwave field is analyzed. The sample is visualized using a stereomicroscope and a digital camera.

3. Mode of operation

Our 63.5 mm diameter cylindrical cavity operates in the TE_{011} mode. Under this mode of operation the currents are annular and there is no electrical current flow in either the radial or longitudinal direction (Fig. 2.). This property enables us to fine tune the frequency by moving the piston-like end plate in and out. A brass screw is used to maximize the coupling between the cavity and the coaxial adaptor.

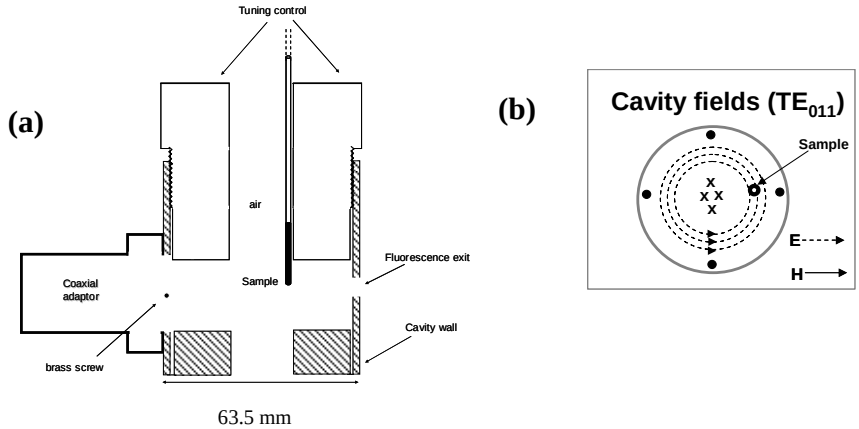


Fig. 2. **(a)** Cavity design – Cross sectional view. The microwave enters the cavity through a coax-to-waveguide adaptor and a coupling hole while the fluorescence exits from the other side of the cavity. **(b)** Cavity fields- Top view.

We measured microwave reflectivity using a vector network analyzer (HP 8510 C). Knowing the field distribution in the cavity, we placed the sample (10 mm long and 1.5 mm wide) slightly off-center where there is some electric field. Note, that the electric field in the center of cavity is zero. Care was taken not to destroy the Q-factor of the cavity (Fig. 3.).

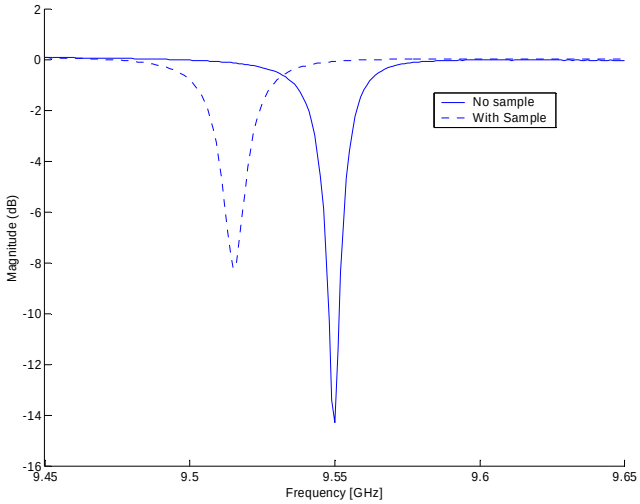


Fig . 3. Microwave reflectivity, S_{11}, with (dashed line) and without (solid line) the sample in a TE_{011} cylindrical cavity. When the sample is placed inside the cavity the resonance curve is slightly perturbed.

Liquid crystal as a temperature indicator

A very important issue in our experiments is independent control of the sample temperature under microwave irradiation. The important requirement here is that the temperature sensor should not perturb microwave field. Therefore, rather than to use a thermocouple, we looked for other methods. We took a thin sheet of commercial film of cholesteric liquid crystal (LC) indicator which changes its color when its temperature is between 35^{o}C- 36^{o}C . Using a stereomicroscope and a digital camera, we first verified that the dry LC indicator alone doesn't change color even under a maximum microwave power of 250 mW. Since our buffer solution consists mainly of water, we filled the same amount of distilled water in a thin glass pipette (just as with the RFP sample), put it inside the cavity together with a small piece of LC (1.3 x 3.3 mm^2) inside and watched for color changes as the incident microwave power is varied. Under maximal incident power the indicator changes its color. When the incident power gets smaller than ≈100mW, the indicator changes. This means that at the incident power of ≈100mW the temperature of the indicator is 35^{o}C- 36^{o}C, i.e. it exceeds ambient temperature (22^{o}C) by 13^{o}C- 14^{o}C. Since the temperature rise is proportional to the incident microwave power, we conclude that each 1 mW of the incident microwave power results in the solution temperature rise of ~ 0.07 ^{0}C.

Fluorescence Spectrum measurement under conventional heating

To observe the temperature dependence of the RFP fluorescence upon conventional heating and in the absence of microwave irradiation, we used a CCD detector (MS 125 ^{TM} 1/8m spectrograph, model 77400 Newport). The glass tube, which is sealed on one side and opened from another allows introduction of a small thermocouple inside the sample (RFP) near the laser-illuminated spot. The pipette with the solution was placed in a heated water bath. The fluorescence was picked up at 90^o to the laser beam by a fiber bundle focusing assemblies (model 77799 Newport), coupled to the CCD detector and to the computer. As we slowly varied the water bath temperature, between 26^o C and 36^o C, we measured the fluorescence spectrum.

4. Experimental Results

The Fig.4 shows the DsRed fluorescence spectrum in the absence and in the presence of the microwave field. First we measured the spectrum without microwave irradiation (dashed line). Then we turned on the microwave for 30 sec., performed the measurement (solid line) and turned it off. Under microwave irradiation the fluorescence intensity is reduced. Having the relation between the microwave power and the temperature we see that there is ~1% fluorescence decrease per one degree centigrade. The process is reversible as can be seen by the spectrum marked by the squares.

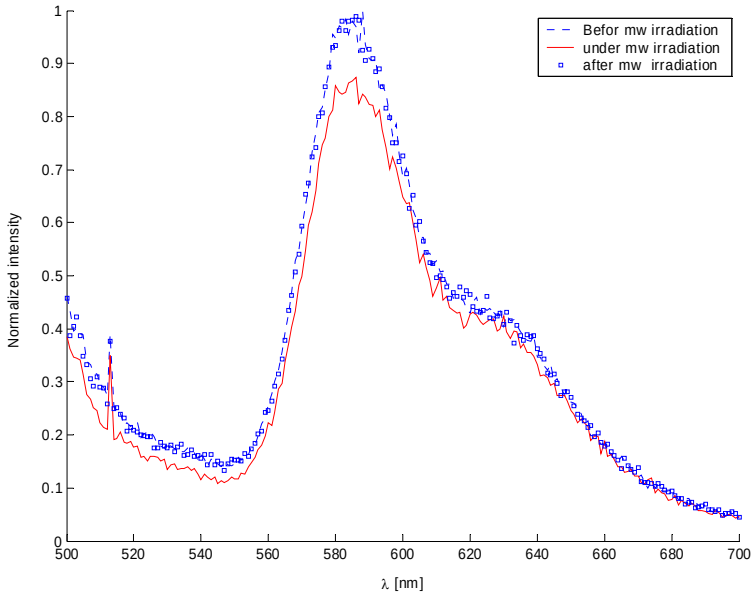


Fig. 4. RFP fluorescence spectrum (normalized with respect to the fluorescence at 583 nm before irradiation) under 488 nm excitation at room temperature before, during and after microwave field. It is seen that under 100 mW microwave irradiation the spectrum is reduced mainly in the peak (λ=583 nm). Note a "valley" at 540 nm.

The next step was to measure the kinetics of microwave effect on the RFP fluorescence (**Fig. 5.**). We picked the wavelength of maximum intensity, turned on the microwave (100mW) and monitored the fluorescence decrease. Then we turned off the microwave and observed how the fluorescence reaches its pre-exposure level. As the power increases the fluorescence "valley" decreases.

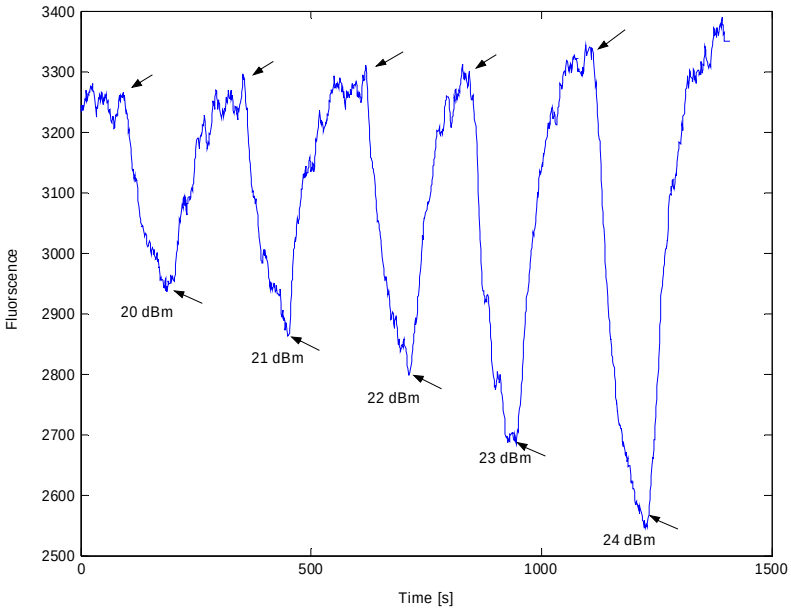


Fig 5. Fluorescence (at λ=583 nm) variation upon switching the microwave field on/off. First arrow on the left upper side indicates the moment when the microwave irradiation is switched on while the arrow at the bottom indicates a moment when the microwave irradiation is switched off.

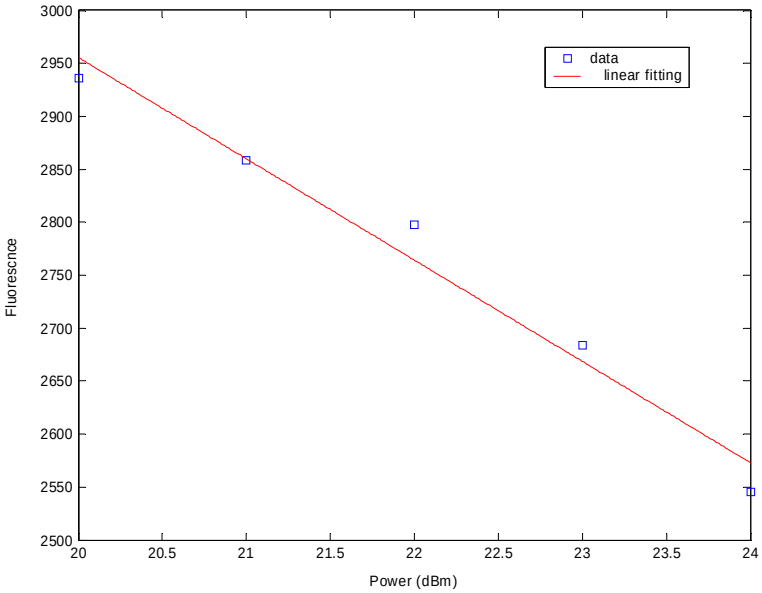


Fig. 6. A decrease in fluorescence (at 583 nm) as a function of the microwave power (dBm).

The effect of microwave on the DsRed should be compared to conventional heating of the protein. Figure 7 below shows the RFP fluorescence spectrum for two different temperatures measured with a CCD detector. Since the glass tube is placed inside a water thermal bath with a thermocouple inside the sample we can measure the fluorescence spectrum for different temperature. When the temperature is slowly increased

from 26°C to 36°C the fluorescence decreases by about 10%. Therefore there is a ~1% decrease per one degree centigrade.

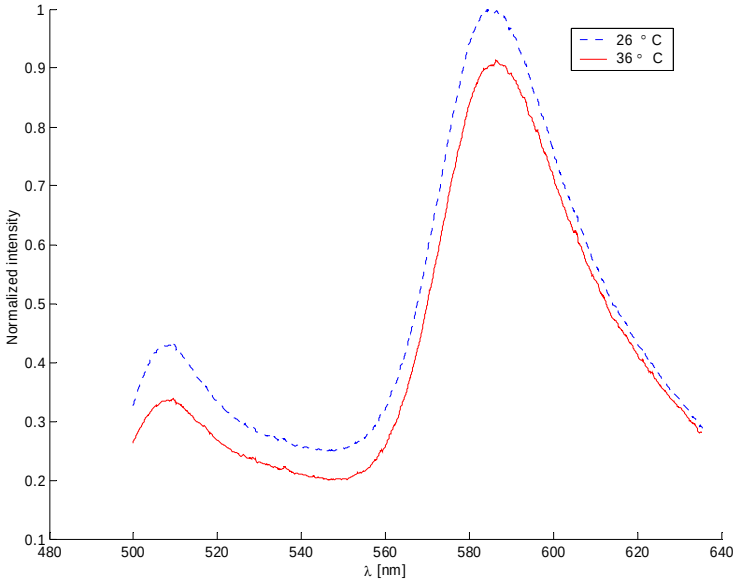


Fig. 7. RFP fluorescence spectrum (normalized) under 488 nm excitation. The glass tube with the protein solution was placed in a heat water bath and the spectrum was measured for two different temperatures using a thermocouple inside the sample. Upon increasing the temperature the fluorescence decreases mainly in the peak (~583 nm).

Since the effect of conventional heating on the fluorescence spectrum of the RFP is wavelength-dependent we present below the temperature dependence of the fluorescence for several wavelengths.

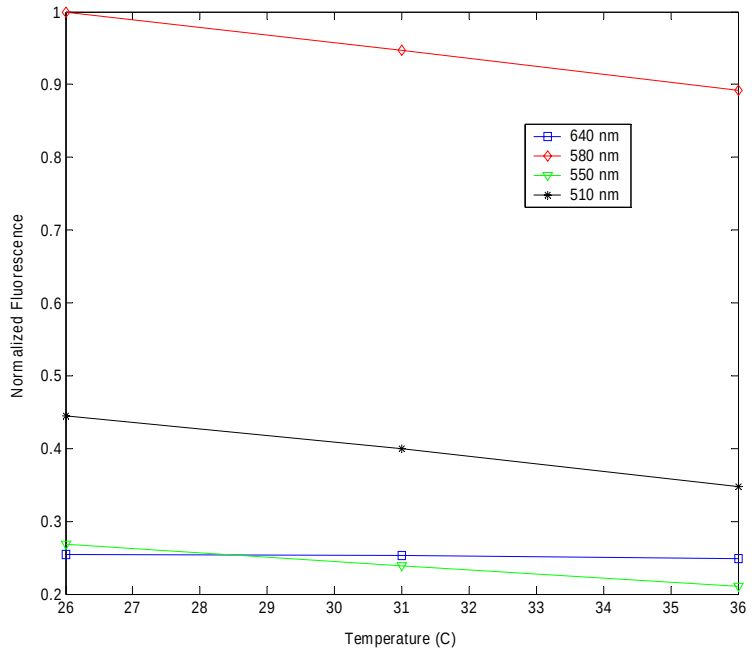


Fig. 8. Normalized fluorescence as a function of the temperature for different wavelengths. Upon increasing temperature the fluorescence does decrease but in different proportion around the spectrum. Watch for example difference of the 580 nm and the 640 nm line.

Summary

Our present experiments indicate that the effect of microwave irradiation on the dsRed fluorescence in solution can be reduced to thermal heating. This is different from our recent experiments with another fluorescent protein [9], EGFP, where we observed that the effect of microwave irradiation was stronger than the heating which accompanies microwave irradiation. Even though the GFP and the DsRed seem to share the same "barrel" form, the latest is known for his greater stability due to his oligomeric structure to elevated temperature and other physical factors [2]. We are now studying the effect of microwave field on the EGFP in our cavity-based set-up as well as the microwave effect on the well-known fluorescence anisotropy of both proteins.

Acknowledgment

We are grateful to F. Sakran for all the technical help and to Dr. Tsafi Danieli and her group for there assistance with RFP handling. We are grateful to O. Popov and V. Lirtsman for the help in optical experiments and for the samples of RFP.

References

[1] Fradkov, A.F. *et al FEBS Lett.* **479**, 127–130 (2000).

[2] V.V. Verkhusha & K.A. Lukyanov, nature Biotechnology **22**,289- 296 (2004).

[3] W. MA, M. Socolich , R. Ranganathan , Nat Struct Biol. 2000 Dec;7(12):1133-8.

[4] H. Bohr and J. Bohr, Phys. Rev. E **61**, 4310, (2000).

[5] D. de Pomerai, C. Daniells, H. David, J. Allan, I. Duce, M. Mutwakil, D. Thomas, P. Sewell, J. Tattersall, D. Jones, and P. Candido, Nature **405**, 417(2000).

[6] M. Porcelli, G. Cacciapuoti, S. Fusco, R. Massa, G. d'Ambrosio, C. Bertoldo, M. DeRosa. and V. Zappia, FEBS Lett**. 402**, 102(1997).

[7] F. Mancinelli, M. Caraglia, A. Abbruzzese, G. d'Ambrosio, R. Massa, and E. Bismuto, J. Cell. Biochem. **93**, 188 (2004).

[8] R. Weissenborn, K. Diederichs, W. Welte, G. Maret, and T. Gisler, Acta Crystallogr. Sect. D (Biol. Cryst.) **61**, 163 (2005).

[9] A.B. Copty, Y. Neve Oz, I. Barak, M. Golosovsky, and D. Davidov Biophys. J. 2006 **91**: 1413-1423.

[10] R.K. Adair Bioelectromagnetics. 24:39-48 (2003).

[11] K.R. Foster , IEEE Trans. Plasma Sci. 28:15-23 (2000).

STUDYING THE EFFECTS OF THE STATIC MAGNETIC FIELD ON THE ENZYMES CATALASE (CAT) AND SUPEROXIDE DISMUTASE (SOD) ACTIVITY IN SUSPENTION CULTURE OF TOBACCO CELLS

PARVIZ ABDOLMALEKI, FAEZEH GHANATI

FACULTY OF SCIENCE, TARBIAT MODARES UNIVERSITY, P.O. BOX 14115/175, TEHRAN, IRAN.

The influence of the magnetic field on the enzyme activity depends on the intensity as well as the period of exposition. In this research the effect of a static magnetic field (SMF) with intensity of 10mT and 30mT on the enzyme activity of superoxide dismutase (SOD) and catalase (CAT) in suspension-cultured of the tobacco cells were investigated. Suspension cultures in the exponential phase of the growth were exposed continuously for 5 days each 5 hours to SMF of 10 and 30 mT. The result showed that the exposure to SMF caused an increase in the activity on the treatment cells (n=24) compared with the controls (n=24). The best obtained average for enzymes activity of SOD on treatment group was 0.88 ± 0.01 (ΔAbs/mg. protein) while the best obtained average for enzymes activity of SOD on control group was 0.55±0.02 (ΔAbs/mg. protein). Similarly, the best obtained average for enzymes activity of CAT on treatment group was 296.61±122.87 (ΔAbs/mg. protein) while the best obtained average for enzymes activity of CAT on control group was 162.72±24.06 (ΔAbs/mg. protein). Our results showed that the exposure of treated cells with a SMF with 10 and 30 mt can cause an increase in the enzyme activity of SOD and CAT.

Introduction

Magnetic fields (MF) are widely distributed in environment and their effects are interesting with the burgeoning development of electrical machines [Ishisaka et al. 2000].There are arguments for both positive and negative effects of EMF on living systems[Yoshikawa et al. 2000]. The exact mechanism of these effects remains unknown and still under investigation. The effects of electromagnetic field exposure on cells can be difficult to interpret because findings are often contradictory. Difficulties may arise because effects are small and because of variations in magnetic field parameters such as strength, duration of exposure and the type of magnetic field (AC or DC). Confounding variables can also arise from differences in the cell type and from the effects of differentiation cues [Mcfarlane et al. 2000]. One of the most important hypotheses is such fields cause an increase the average concentration of free radicals (oxygen free radicals), lengthen their life time, in living organisms which results in the formation of excessive amounts of active oxygen forms [Sobczak et al. 2002, Scaiano et al. 1994, Lee et al. 2004]. They induce change in enzyme activity, gene expression, and release of calcium from intracellular storage sites; affect membrane structure, cell growth, and cell death [Kwee and Rashkmark 1998, Olivares-Barnuelos 2004, [Robison et al. 2002]. Free radicals are very reactive and unstable molecular species that can initiate chain reactions to form new free radicals. Although formed as a result of a wide range of normal biochemical process, they are potentially damaging .Several mechanisms are in place to neutralize and endogenous enzymatic antioxidant defenses that generally hold the production of free radicals and prevent oxidant stress and subsequently tissue damage. The balance between the oxidants and the antioxidants may be disturbed by an increase in free radical production or by a reduction in antioxidants. This imbalance between the oxidants and the antioxidants can lead to oxidative stress which is a series of peculiar and potentially damaging biochemical reactions [Moustafa et al. 2001].

These mechanisms have been initially studied on plants after they used as target model in different stresses. The previous results showed that they produce large amounts of active oxygen species such as superoxide anion (-O2), hydroxyl radical (°OH) and hydrogen peroxide (H2O2) that can result in photoinhibition and photooxidation. We considered the magnetic field as a physical stress and we intended to study the response of the selected cell plant in antioxidant defense systems. We assumed that this response is a protective mechanism that enables cells to survive .It is activated by a wide variety of environment stimuli, such as high temperature,

oxygen starvation, and heavy metals, as well as EMFs. We intended to clarify this point because we know that most organism have enzymatic systems associated with SOD and CAT to scavenge such active oxygen species.
In the present research suspension-cultured tobacco cells (Nicotiana tabacum) were used as a model to evaluate the response of tobacco cells when it exposed to a static magnetic field. Also the intensity of the magnetic field on the rate of enzymes activity was investigated. Tobacco cells were considered as model because there is a potential to extract a homogenate and undifferentiated embryonic batches of cells through carrying out too many subcultures. Thus, the present study was designed to evaluate the effects of exposure to SMF on some parameters indicative of oxidative stress (SOD and CAT) in tobacco cells.
Suspension–cultured tobacco cells (Nicotiana tabacum) were initially grown in Linsmaier & skoog (LS) medium. The calli from which suspensions were established had been maintained in our laboratory for several years. We extract the suspension cultures after 52 subcultures. This provided a homogenate and undifferentiated embryonic batches of cells which could be considered as a good target for our study. Furthermore by doing so, it seems that no longer have they kept their original properties and their physiological response to static magnetic field resembles physiological response of a plant cells regardless of it species. The prepared cells were then incubated at 25°Cin darkness on an orbital shaker at 100 rpm. The suspension of cells were then transferred (1.3gr fresh weight) at 7 day intervals [Kuboi and KAji 1994] into 30ml of fresh medium in a 100ml Erlenmeyer flask. We initially extracted the growth and the differentiation indices of tobacco cell by studying the tobacco growth cells curve. The cells in the exponential phase of the growth curve were then exposed continuously for 5 days (from 3 to 7 sub-cultured) with exposure rate of 5 day to 10 and 30mT in a local designed SMF. The cells were harvested after 5day of treatment and frozen in liquid N2 and kept at – 80 °C until used for biochemical measurements.
The apparatus (Fig.1) which we used to create the static magnetic field had two coils each with 3000 turns of 1mm of enameled copper wire. This provided a highly homogenous field enabling us to put our prepared cells into a large and homogenous field. To intensify the field we used iron surfaces that had been separated by diamagnetic materials to avoid the turbulence currents.
Thirty milliliter cell culture flasks containing tobacco cell cultures were put into the center of cylinder container (length 17cm) that allowed the placement of multiple or single flasks within apparatus simultaneously. The flasks were placed so that laid perpendicular to the direction of the generated magnetic field. The control samples were kept in the same condition regarding the temperature, humidity and light. Using the prepared calibration curve obtained for the apparatus to initialize a magnetic field with the intensity of 10mT and 30mT, a current of 5 ampere and 25 ampere were transferred through the circuit respectively.
Frozen samples (200 mg fresh weight) were homogenized in 3 ml HEPES-KOH buffers (pH 7.8) containing 0.1 mM EDTA. The homogenate was centrifuged at 15000 × g for 15 min. All operation was performed at 4 °C. The supernatant was used for SOD (EC 1.15.1.1) activity [Giannopolitis and Ries 1977]. Reaction mixture (3 ml) consisted of 50 mM HEPES-KOH buffer (pH 7.8), 0.1 mM EDTA, 50 mM Na2CO3 (pH 10.2), 12 mM L-methionine, 75 µM NBT, 300 µL enzyme extract and 1 µM riboflavin. One unit SOD activity was defined as the amount of enzyme required to result in a 50% inhibition of the rate of NBT reduction measured at 560 nm. Activity of CAT (EC 1.11.1.6) was measured in a reaction mixture containing 25 mM Na-phosphate buffer (pH 6.8), 10 mM H2O2 and enzyme extract in a total volume of 1 mL. The decomposition of H2O2 was followed by the decline in absorbance at 240 nm [Cakmak and Horst 1991]. In brief, samples were homogenized in 1 mL of 50 mM Na-phosphate buffer (pH 7.8) containing 5 mM ascorbate, 5 mM DTT, 5 mM EDTA, 100 mM NaCl and 2% (W/V) PVP. The homogenate was centrifuged at 15000 × g for 15 min at 4 °C. The reaction was initiated by adding H2O2 to a final concentration of 44 µM. The reaction rate was monitored by the decrease in absorbance at 290 nm. The rate constant was calculated using the extinction coefficient of 2.8 mM-1 cm-1and corrected for the rate obtained prior to the addition of H2O2. The protein contents were determined by the method of Bradford [1976], using bovine serum albumin (BSA) as standard. All experiments were repeated with at least three independent repetitions and all data were expressed as the mean values ± standard deviation (SD). The Statistical analysis was performed using student's t-test at $p<0.05$ significant level of the difference.
The results showed that the exposure of the magnetic field caused an increase in the antioxidant enzymes activity (SOD & CAT) on the treatment cells (n=24) compared with the controls (n=24). The obtained average for enzymes activity of SOD on treatment group was 0.88 ± 0.01 (nm/mg. protein) while the obtained average for enzymes activity of SOD on control group was 0.55±0.02 (nm/mg. protein) (Fig.2). Similarly, the best obtained average for enzymes activity of CAT on treatment group was 296.61±122.87 (nm/mg. protein) while the best obtained average for enzymes activity of CAT on control group was 162.72±24.06 (nm/mg. protein) (Fig. 3). The average results for the enzymatic antioxidative activity of SOD and CAT for treatment as well as control in two intensities of 10 and 30 mT were presented in table 1. These results showed that the activity of SOD in tobacco cells has been increased for both intensities (10 and 30 mT) in treatment cells. In contrast the activity of CAT showed a significant decreasement in treatment cells compared with control. Our results showed significant difference of enzymes activity in treatment and control cells for SOD (two-tailed $p<0.05$) and CAT (two-tailed $p<0.03$) at 30 mT. Similarly, the enzymes activity in treatment and control cells for SOD

(two-tailed $p<0.04$) and CAT (two-tailed $p<0.01$) at 10 mT showed a significant difference. Regardless of enzyme activity obtained for CAT which show a bigger difference at 30 mT compared to 10 mT (fig3), there was not reasonable difference of enzyme activity for SOD as far as the intensity is concern (fig2). These results show that the enzymes activity is not directly dependent to intensity at these two selected intensity of 10 and 30 mT.



Fig.1. Locally designed static magnetic field generator

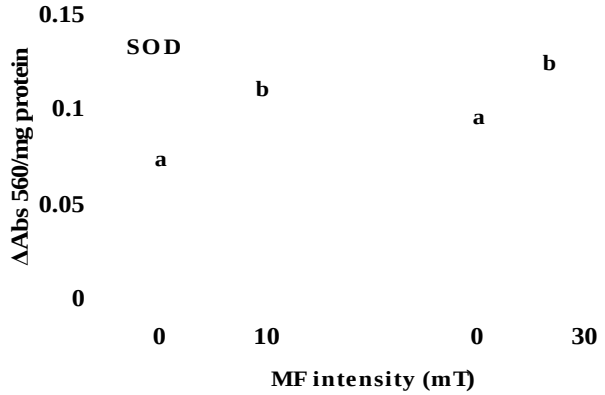


Fig.2. Effect of SMF with different intensities on the activity of SOD in tobacco cells. Data are means of three different experiments in triplicate ± SD. Different letters In each group shows significant difference.

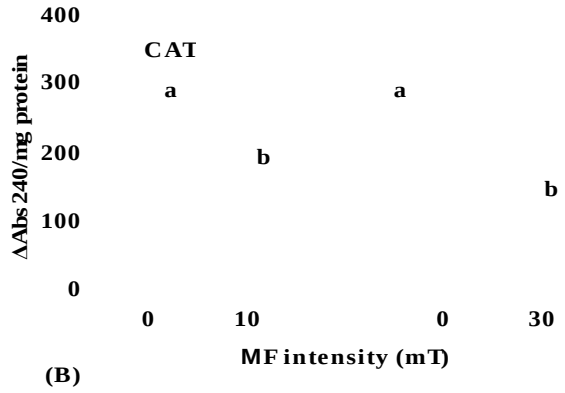


Fig.3. Effect of SMF with different intensities on the activity of CAT in tobacco cells Data are means of three different experiments in triplicate ± SD. Different letters In each group shows significant difference.

Summary

In recent years, the results of experimental studies have revealed that magnetic fields of moderate amplitudes (B=1-100mT) may alter the activity of certain enzyme reactions. An interpretation of the magnetic field activity observed in the enzyme reactions is based on the radical pair mechanisms [Zmyslony et al. 2000]. We actually tried 10 and 30mT in the initial stage of our *in vivo* experiment because these strengths are in the range that humans most often experience in our daily lives [Li and Chow 2001]. Compared to the pervious works which dealing with alternative current (AC) we assume that the effect of static magnetic field using DC current on enzymes activity is more severe. This is justifying because the cycle of 50HZ takes 20ms and the lifetime of a radical pair encounter is no longer than a few microseconds. It is therefore clear that the radical pairs may be affected for a long and continuous time interval by the static magnetic field [Zmyslony et al. 2000]. This may extend the life time of the free radical and its potential damage could be exaggerated.

Plants have several antioxidant enzymes and metabolites located in different plant cell compartments, the main ones being SODs a family metalloenzymes that convert O°2 to H2O2. Because superoxide is the first product of univalent reduction of oxygen, SOD is considered as the "primary defense" against oxygen radicals [Banister et al. 1989]. The product of SOD, hydrogen peroxiode, requires further detoxification. This is achieved by other enzymes and non-enzymatic antioxidants that may differ among the various cellular compartments. H2O2 is reduced to water by ascorbate peroxidase (APX).This enzyme uses a large pool of 10mM ascorbate present in the chloroplast and oxidizes it to monodehydroxyascorbate[Noctor and Foyer 1998]. Also, catalases (CATs) which are tetrameric heme-containing enzymes that similarly catalyze the removal of H2 O2 [Willekens et al. 1995]. Changes in catalase in response to other stress conditions have also previously been reported. Willekens and coworker studied the three isoenzymes of catalases in response to environmental challenges such as UV-B, O3, and SO2 [Willekens et al. 1995]. As a consequence of its sensitivity to environmental conditions, early loss of catalase was suggested as a signal for antioxidant defenses stimulus [Feierabend et al. 1996]. In a similar way, we tried the effect of the exposing to the SMF as another physical stress on catalase inhibition to investigate whether it can mediate defenses in tobacco cells or not.

In our study, a statistically significant CAT activity decrease was observed. Such a condition may indicate abnormal function of the antioxidant system caused by SMF which can lead to a high concentration of H2 O2 in the cells. This incensement in H2 O2 can cause a toxic condition. Spychalla and Desborogh [1990] emphasized that the overproduction of the H2O2–generating SOD must always be combined with increased levels of H2 O2 –metabolizing catalase and/or peroxidase. Such combination can generate a powerful scavenging of toxic oxygen forms. On the contrary, an increase in SOD activity alone might enhance cytotoxicity by active oxygen species likely owing to the accelerated H2 O2 generation and subsequent OH˚ overproduction by the metal catalyzed Haber-Weiss reaction [Piacentini et al. 2001]. Indeed, H2 O2 accumulation may itself lead to higher active oxygen species (AOS) production [Spychalla and Desborogh 1990]. The inconsistent action SOD and CAT enzymes as happened in our study due to the exposing to the static magnetic field contributes to increase the deteriorate effect of H2 O2 and above all the risk of OH˚ formation, the decrease survival and the appearance of signs of senescence. This could be happened through reactivating few oxygen species that cause change vital functions. As a result we can consider that tobacco cells may efficiently metabolize superoxide but may have difficulties in eliminating the hydrogen peroxide when exposing to SMF. Evidence is reviewed here showing that SMF can increase free radicals and alter enzyme reactions which could highlight the activity of oxidant radicals.

Although formed in normal cell metabolism, free radicals are potentially damaging and can initiate chain reactions to form new free radicals. A main protective role against free radicals is attributed to SOD in catalyzing and dismutation of superoxide anions to O2 and H2O2 (Sreenivasulu et al., 2000). The activity of SOD increased from 0.05 ± 0.004 to 0.09 ± 0.005 in 10 mT and from 0.07 ± 0.002 to 0.11 ± 0.006 in 30 mT MF treatments. It means that exposure to MF caused increases by 74% and 87% in unit of SOD activity in 10 and 30 mT-treated tobacco cells, respectively. It implies the first step of the increased production of free radicals by MF in tobacco cells. An increase in SOD activity might enhance cytotoxicity by active oxygen species likely owing to the accelerated H2 O2 generation and subsequent OH• overproduction by the metal catalyzed Haber-Weiss reaction (Piacentini et al. 2001). Likewise, the activity of CAT was also reduced from 247± 15 to 146 ± 8 in 10 mT and from 264 ± 37 to 80 ± 11 in 30 mT MF treatments. Interestingly, the ratio of the reduction of CAT activity in 30 mT-treated cells was remarkably more than those treated with MF of 10 mT (70% versus 41%).

Further experiments involving exposure of cells for a different time and at various magnetic field flux densities make it possible to establish threshold values for this biological effect [Jajte et al. 2001].

References

Banister J.V., Banister W.H., Rotilio G . Aspects of the structure, function, and applications of superoxide dismutase .CRC Crit .Rev.Biochem, 22(1989), 111-180.

Bradford M.B. .A rapid and sensitive method for the quantitation of microgram quantities of protein utilizing the principle of protein-dye binding. Anal. Biochem. 72(1976)248-254.
Cakmak I .. Horst W. J.. Effect of aluminum on lipid peroxidation, superoxide dismutase, catalase and peroxidase activities in root tips of soybean (Glycine max). Plant Physiol. 83(1991)463-468.
Feierabend J ., Streb P ., Schmidt M., Dehne S., Shang W .. Expression of catalase and its relation to light stress and stress tolerance .In: physical Stresses in Plants: Genes and Their Products for Tolerance.In:Physical Stresses in Plants:Genes and Their Products for tolerance, (1996)pp. 223-234. Grillo S.and Leone A.(eds),Springer,Berlin.
Giannopolitis C. N., Ries S. K.. Superoxide dismutase. I. Occurrence in higher plants. Plant Physiol. 59(1977)309-314.
Ishisaka RKanno,T., Inai Y., Nakahara H., Akiyama J.,.Yoshioka T, Utsumi K.,Effects of a magnetic fields on the various functions of subcellular organelles and cells,Pathophysiology 7(2000) 149-152.
Jajte J., Grzegorczyk J., Zmyslony M., Rajkowska E., Kowalska M.S., Kowalski M.L., Influence of a 7mT static magnetic field ,and irons on apotosis and necrosis in rat blood lymphocytes,J Oceup Health 43(2001) 379-381
Kuboi T ., Kaji M.. Establishment of tea cell lines with high growth rate. Tea Res. 80(1994) 1-8 (in Japanese).
Kwee S., Raskmark P. Changes in cell proliferation due to environmental non-ionizing radiation 2.Microwave radiation.Bioelectrochemistry and Bioenergetics 44(1998) 251-255.
Lee B.C.,.Johng H.M,.Lim J.K,.Jeong J.H Effects of extremely low frequency mafnetic field on the antioxidant defense system in mouse brain :a chemiluminescence study.Journal of photochemistry and Photobiology B:Biology 73(2004)43-48.
Li S.H., Chow K.C. Magnetic field induces DNA degradation.Biochemical and Biophysical and Research Communictions 280(2001) 1385- 1388.
Mcfarlane E.H, Dawe G.S., Marks M., Campbell I.C. Changes in neuritis outgrowh but not in cell division induced by low EMF exposure :influence of field strength and culture conditions on responses in rat PC12 pheochromocytoma cells,Bioelectrochemistry 52(2000) 23-28.
Moustafa Y.M., Moustafa R.M., Belacy A., Abou-EI-Ela S.H., Ali, F.M. Effects of acute to the radiofrequency fields of cFellular phones on plasma lipid peroxide and antioxidase activities in human erythrocytes, Journal of pharmaceutical and biomedical analysis 26(2001)605-608.
Noctor G., Foyer C.H. Ascorbate and glutathione: Keeping active oxygen under control .Annu.Rev.Plant Physiol.Plant Mol.Biol. 49(1998)249-279.
Olivares-Barnuelos T., Navarro L., Gonzales A., Drucker-Colin.,R.. Differentiation of chromaffin cells elicited by ELF MF modifies gene expression pattern.Cell Biology International 28(2004) 273-279.
Piacentini M.P., Fraternale D., Piatti E., Ricci D., Vetrano F. Senescence delay and change of antioxidant enzyme levels in Cucumis sativus L.etiolated seedling by ELF magnetic fields. Plant Science 161(2001) 45-53
Robison J.G., Pendleton A.R.,Monson K.O.,.Murray B.K.,.O'Neill K.L. Decreased DNA repair rates and protection from heat induced apoptosis mediated by electromagnetic field exposure.Bioelectromagnetics 23(2002)106-112.
Scaiano Cozens J.CF.L, Mclean J. Model for the rationalization of magnetic field In vivo. Application of the radical-pair mechanism to biological systems .Photochemistry and Photobiology. (1994) Vol.59,pp.585-589.
Sobczak A., Kula. B, Dancii A. Effects of electromagnetic field on free-radical processes in steelworkers.Part II: Magnetic field influence on vitamin A,E and selenium concentrations in plasma .J Occup health 44(2002) 230-233.
Spychalla J.P.,.Desborough S.L. Superoxide dismutase,catalase ,and ;-tocopherol content of stored potato tubers,Plant Physiol.94(1990) 1214-1218.
Sreenivasulu N, Grimm B, Wobus U and Weschke W 2000 Differential response of antioxidant compounds to salinity stress in salt-tolerant and salt-sensitive seedlings of foxtail millet (Setaria italica). Physiol. Plant. 109, 435-442.
Willekens H ., Inze D., Van Montagu M., Van Camp W. Catalases in plants .Mol.Breed. 1(1995)207-228.
Yoshikawa T., Tanigawa M.,.Tanigawa T.Imai,A, Hongo H.,.Kondo, M. Enhancement of nitric oxide generation by low frequency electromagnetic field , Pathophysiology 7(2000) 131-135.
Zmyslony M., Palus J., Jajte J., Dziubaltowska E., Rajkowska E. DNA damage in rat lymphocytes treated in vitro with iron cations and exposed to 7mT magnetic fields (static or 50HZ), Mutat. Res.453 (2000) 89-96.

Analysis of Radiation Hazards to Personnel on Surface Combatants

Avigdor Shechter
Alion Science and Technology
4300 King St.
Alexandria, VA, USA

Moshe Netzer
EMC and Safety Engineering
11 Avigail St.
Haifa, Israel

Abstract: The large number of radio frequency (RF) transmitters employed in combat systems of modern Naval surface combatants requires that they operate in mutual coexistence while posing no danger to operators and equipment despite the limited available physical space. A key to the successful combat system integration is the control of the electromagnetic environment on the combatants' topsides, which might pose radiation hazards (RADHAZ) to personnel (HERP). HERP are caused by transmitter antenna installations that generate intentional EM radiation in excess of the safe levels in zones of personnel activity. Radiation safety to personnel is achieved when the average radiation power density is below the permissible exposure limits (PEL) for HERP at locations of personnel activity and medical equipment operation. This paper describes the analysis tools and techniques for the evaluation of HERP on surface combatants. The same approaches could be employed in the analysis of land site antenna deployment scenarios.

Introduction

Modern surface naval combatants employ a vast array of electronic systems in order to accomplish their warfare missions. Toward this end, electronic systems utilized in combatants comprise powerful transmitters, some of which are broadband such as radar and ECM systems. These systems operate at frequencies from HF to Ka-band in order to perform an assortment of tasks: data and voice communications, radar search and track operations, fire control and weapon guidance activity, electronic warfare, etc.

As the electromagnetic radiation (EMR) sources on combatants' topsides are confined to extremely limited space on the combatants' topsides, they might compromise the EMR safety. Therefore, the EM environment on combatant topsides has to be controlled by either the proper placement of the effectors (hard solutions) or/and by establishing suitable system operational procedures (soft solutions).

RADHAZ are caused by transmitter antenna installations that generate intentional EMR in excess of safe levels in zones of personnel activity, ordnance storage and handling regions, or fueling operations areas. Correspondingly, RADHAZ is categorized according to the following three major groups of hazards of EMR to:

- Personnel (HERP) - harmful effects to humans,
- Ordnance (HERO) – initiation of electro-explosive devices by induced currents,
- Fuel (HERF) – ignition of flammable atmosphere–fuel vapors mixed with air.

In the context of EMR hazard to personnel, HERO and HERF pose indirect hazard; therefore, they will not be discussed.

It follows that during the process of combatant topsides integration, the electromagnetic compatibility (EMC) engineering should address HERP issues by controlling the EM environment, by design. EM Safety is achieved when either all the EMR levels onboard the ship are below the HERP PEL's at topside test point (TP) locations where personnel activity takes place.

From the engineering point of view, the analysis of the EM environment on the combatant topsides should reflect "worst case scenarios". Due to its complexity, combatant topside design is performed by means of computer analysis tools. The methods utilized in the software for topside EM analysis are discussed herein.

Topside EMR and Its Control

The potential for sustained HERP related problems on combatant topsides is due to the high level of EM energy emitted by the onboard intentional topside communications and combat system transmitters. Consequently, the EM environment on the topsides of surface combatants is the aggregate of a variety of RF components of time periodic EMR characterized by either modulated continuous wave (CW) (time harmonic), or repeated pulse (pulse train) modulated EM waves of period T within the range of 1.6 MHz to 36 GHz. Both the CW and pulsed modulated EMR represent finite bandwidth signals having approximate power spectral density (PSD) of similar shape ([1]).

Generally, EMR can be classified into one of the following two categories: ionizing radiation, and non-ionizing radiation. This classification is based on whether the EMR is capable of ionizing atoms and breaking chemical bonds. The EM environments onboard combatants is non-ionizing; thus, its biological effect is to cause dielectric heating. Consequently, the basic interaction of EMR with human tissue is by absorption of the EM energy. Exposure of humans to intense fields produces increased heating whose deposition in the tissue can lead to effects ranging from discomfort, through burns, to protein denaturation. As the human body does not have internal sensors for the sensation of heat, a major source of HERP danger is when the body absorbs

excess radiation, the awareness of the exposed individual. Consequently, as the victim does not feel the need to evacuate the RADHAZ area; thereby, the chance to biological damage increases due to the inability of the victim's body to dissipate the excess heat. Furthermore, strong EMF's induce electric currents in metal objects. The induced currents can cause RF burns or even electric shock to personnel whenever they touch surfaces of high current while standing on the "grounded" deck.

Combatants constitute an environment where personnel are aware of the potential danger of RF exposure associated concurrently with either their routine activity, or incidental transient passage through an area of high EMF. Accordingly, the regulations specifying acceptable limits of EMR exposures in such circumstances are lax as compared to those established for general public environments. Nevertheless, the corresponding RADHAZ permissible exposure limits (PEL's) serve as requirements for certification of combatants. HERP regulations are being regularly updated with the advance of the complex effects of EMR on the human body.

The current industrial specifications for HERP, contained in [1], were used as reference to create the combined HERP regulations for combatants. The resulting frequency dependent PEL's are based on a safety factor of ten over the specific absorption rate (SAR), which might cause bodily harm to humans at each EMR frequency. The graphs in **Figure 1** specify the PEL's for personnel, in terms of the electric field (E-field) strength, for both public and occupational exposure in accordance with [1].

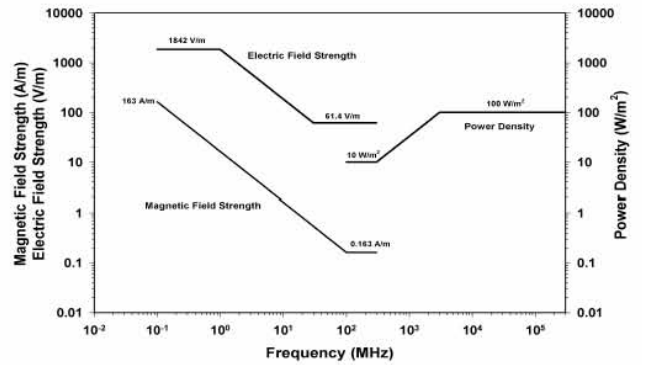


Figure 1 Permissible Exposure Standard for Personnel, IEEE Standard C95.1, 2005

Nevertheless, exceptions to the maximum limits specified in **Figures 1** which allow higher EMR levels do exist ([1]). For example, the power density is allowed to violate the PEL in case of pulsed RF fields, while for cases in which the source is a rotator the power considered for HERP (only!) is reduced according to the following rule:

$$\mathrm{PEL}_{\mathrm{scan}}(f) = \mathrm{PEL}_{\mathrm{fixed}}(f)^{\frac{2\times \mathrm{Beam\,Width}}{\mathrm{Scan\,Angle}}} \qquad (1)$$

where, f is the frequency of the EMR.

Computational EM (CEM) in Topside RADHAZ Analysis

The estimation of HERP from crowded multiple antenna sites can be performed either graphically ([2]), or purely computationally ([3], [4]) based on the following rule ([1], [2]):

$$\left(\frac{E_1}{E_{s1}}\right)^2 + \left(\frac{E_1}{E_{s2}}\right)^2 + \ldots + \left(\frac{E_N}{E_{sN}}\right)^2 < 1 \qquad (2)$$

where, $E_1,E_2,...,E_N$, are the E-field strength levels for the frequencies $f_1,f_2,...,f_N$, respectively, and $Es_1,Es_2,...,Es_N$ are the PEL's for the frequencies f_1, $f_2,...,f_N$, respectively. The application of Equation (2) requires the knowledge of the EMF strength or power received at various topside locations from the onboard transmitters. These are obtained via computer-aided predictions based on mathematical models of the topside HERP problem.

Mathematically, the HERP problem is expressed as a radiation/scattering field problem defined over an unbounded domain. However, due to the complexity of the conducting structures, closed form solutions of the topside integration problem are not accessible nor can they be generated using a single method. Thus, topside HERP analyses utilize an array of mathematical methods each suitable to the solution of a different aspect of the topside EMR problem. Due to the complexity of the domain of the topside integration problem, its solution is performed with the aid of numerical analysis tools executed on powerful computers.

The prevalent approach practiced in engineering analysis favors the investigation of the behavior of dynamical systems in the frequency domain (FD) over the time domain (TD). The key to the selection of a suitable FD numerical method is the electrical size of the problem, defined as the ratio of the physical size of the conducting structure to the wavelength, $\lambda \approx 300/f$, of the radiated RF carrier wave where, f is in MHz. At low RF frequencies, the EM wavelengths are of the order of magnitude of the dimensions of the conductor; thus, they interact with it strongly by exciting global resonances; at high RF frequencies, the interactions between the various parts of the conductor are weak; consequently, parts of the structures remote to the RF source location act as scatterers of EMR (i.e., they reflect and diffract the EM waves).

The starting point of all CEM methods are the TD linear Maxwell's curl equations (partial differential equations). The FD CEM methods use the FD version of Maxwell's equations after assuming separation of the time and space dependent variables in conjunction with time-harmonic response postulation. FD CEM methods applied to combatant topside scattering problems are classified according to their FD applicability to the RADHAZ problem as follows:

- Numerical Methods – applied to low frequency analysis,
- Analytically Based Methods – for high frequency analysis.

FD numerical methods belong mostly to the methods known as direct numerical methods. These methods use approximate discrete expressions (interpolations) of the solution functions. The analytically based methods on the other hand, use closed form models (formulae) of wave front propagation (reflection, refraction, and diffraction) in order to calculate EMR fields from EM sources in the presence of scatterers.

In light of the wide range of frequencies of interest in topside RADHAZ analysis in conjunction with the conductor size, the applicability of numerical methods to combatant topside analysis is generally limited to the HF and low VHF (LVHF) ranges (f=2-88 MHz). Consequently, the prediction of topside RADHAZ at UHF and up has to be performed by analytically based methods, as these methods have no applicability limitation in terms of conductor and domain sizes, and the frequency of the source.

Numerical Analysis

Within the framework of the FD modeling of scatterers in unbounded domains, the most popular direct numerical method is known as the method of moments (MoM) ([3]). The method, whose major advantage is the circumvention of the need to model the surrounding non-conducting space, is based on the premise that the total electric field, $\boldsymbol{E}^t$, at any point in space is the sum of the incident and the scattered electric fields. Furthermore, it assumes that the E-field scattered from metallic surfaces is produced by currents induced in the scatterer by the incident field such that the total tangential E-field on its surfaces vanishes (a boundary condition with the unbounded free space); i.e., $\boldsymbol{E}^t = \boldsymbol{E}^s + \boldsymbol{E}^i = 0$. Hence, MoM is a CEM method that uses a specialized analytical solution of Maxwell's equations.

The application of MoM to real conducting structures is accomplished by representing the conducting surfaces of the scatterer as a fine mesh of M thin cylindrical conducting wires of radii a. Consequently, the complete structure can be represented as the sum of the contributions of M wires assuming that their currents are compatible at the nodes of the mesh. Subsequently, the mathematical model, in the sense of MoM, is a system of linear algebraic equations of the general form:

$$[Z]\{I\} = \{E\} \qquad (3)$$

where, $[Z]$ is the global impedance matrix, $\{I\}$ is the unknown global current vector, and $\{E\}$ is the excitation vector.

The impedance matrix in Equation (3) is full rank. It is solved either by means of LU decomposition, or by a more efficient nonlinear programming method such as the conjugate gradient method ([5]). Once the M wire currents are known, the E-field at any TP on the topside can be calculated from the definition of the potential vector $\boldsymbol{A}$:

$$\boldsymbol{E}^s(\boldsymbol{r}) = -j\frac{2\pi}{f}\left[\boldsymbol{A} + j\frac{1}{\mu\varepsilon}\nabla(\nabla\cdot\boldsymbol{A})\right] \quad . \qquad (4)$$

Analytically Based Methods

The solutions obtained via the analytically based methods (also known as semi-analytical methods) are valid for high EMR frequencies in the sense that the EM waves are well formed and locally planar with respect to the conducting structure. It can be inferred that for scatterer sizes larger than two wavelengths, ray-tracing techniques can be utilized in order to calculate the fraction of the EM power reaching topside TP's from topside sources in the presence of scattering obstacles. In order to obtain realistic predictions of the levels of radiation at specified locations, the following source and propagation parameters, among others, should be considered:

- The radiation pattern of each transmitting antenna,
- The near-field (Fresnel Zone) boundaries and intensities,

- Antenna polarization, and cross polarization,
- In-band, out-of-band antenna performance,
- Blockage of line of sight by metallic structural components,
- Presence of radiation absorbing materials (RAM).

The (far-field) pattern of EMR from wanted topside radiation sources is either omni-directional, or directional as depicted in **Figure 2**. Far enough from the source the EMR propagates as a plane wave; nevertheless, often, the topside victims of the excessive radiation are positioned within the near-field regions of the topside sources, which are characterized, irregular field intensities.

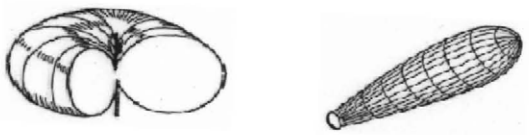


Figure 2 – Omni (left), and Directional (right) Radiation Pattern

The calculations of transmission losses of EMR power density due to propagation from topside sources to TP's follows Friis' modeling. Accordingly, the power density, Φ_D, received at a TP located a distance r from a Tx antenna is given by ([4]):

$$\Phi_D = \frac{P_T G_T}{4\pi r^2 L_F} \qquad (5)$$

Where, P_t is the transmitted power, G_T is the (far-field) gain of the Tx antenna, which is a metric characterizing the directivity, $D=4\pi/\Omega_b$ (Ω_b is the 3-dB beam solid angle), and L_F is a path loss factor. Subsequently, the power received at the victim location is just given by $P_R = A_{eff}\Phi_D$ where, A_{eff} is the effective receiving area.

As distances between the EMR sources and victim TP are relatively small for the topside RADHAZ problem, atmospheric propagation losses are negligible. Consequently, the path loss factor is determined by the extent of physical blockage along the line of sight (LoS) between the source and the victim. **Figure 3** (left) shows the possible paths and geometries of EM rays emanating from a generic point source to various observation positions in the presence of a wedge scatterer ([8]). As indicated in **Figure 3** (left), three radiation zones can be identified around the obstacle: direct/reflection/diffraction zone, direct/diffraction zone, and diffraction only zone.

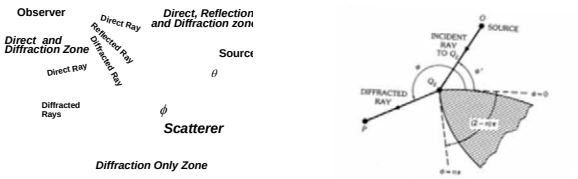


Figure 3 EMR Past a Wedge (left), and Wedge Diffraction (right)

Accordingly, diffraction coefficients are calculated based on the uniform/geometric theory of diffraction (U/GTD). The parameters determining the values of the diffraction coefficients are mainly:

- The incident and diffracted ray angels (found by ray tracing),
- The wave frequency and polarization,
- The wedge angle (where applicable).

A simple analytic GTD expression for wedge diffraction of tip angle $(2\text{-}n)\pi$ (n being some real number) is given by ([8]):

$$D_{\substack{e\\m}} = \frac{\sin\left(\frac{\pi}{n}\right)}{2\pi n\left(\frac{f}{300}\right)^2}\left(\left[\cos\left(\frac{\pi}{n}\right)-\cos\left(\frac{\phi-\phi'}{n}\right)\right]^{-1} \mp \left[\cos\left(\frac{\pi}{n}\right)-\cos\left(\frac{\phi+\phi'}{n}\right)\right]^{-1}\right) \qquad (6)$$

With the incident and diffracted angles indicated in **Figure 3** (right).

Modeling of the Topside RADHAZ Problem

The application of FD methods to the topside EMR problem requires the modeling of EM sources, EMR propagation, and scatterers. The modeling procedure corresponding to the application of both MoM and UTD to RADHAZ analysis is described herein.

Topside transmitting antennas are the sources of the intentional EMR components comprising the topside EM environment. In order to analyze the topside RADHAZ they have to be modeled over the entire RF range. Generally, in MoM analysis the models of sources are constructed to "reproduce" the physics of the real device, whereas in the case of the analytically based methods the models merely reflect the device typical operational characteristics. Once the models of the source of EMR are established, the propagation loss of the radiation from sources to observer (test) points in the presence of scatteres has to be ascertained.

MoM Modeling

Low frequency topside antennas are sources of E-fields. The modeling of E-field sources is implement by inserting a gap of infinitesimal length at the midpoint of a wire located at the position in the wire model corresponding to the real source location and assigning an E-field across it. **Figure 4** depicts the current distribution and the radiation pattern of a 10-wire lineal structure (antenna) radiating in free space in response to a 20 MHz source located at its bottom wire.

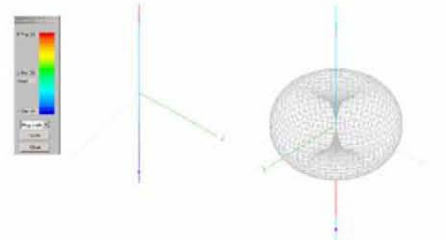


Figure 4 – 10-Wire Model of Monopole Free Space Antenna: Current Distribution (left), Radiation Pattern (right) at 20 MHz

MoM is based on first principles of physics, the correctness of their solutions is indisputable. However, in order to reduce numerical dispersion effects on the approximate solution the use of at least ten sample points within a wavelength is required. Consequently, the maximum length of the longest wire in the model is required to be L=0.1λ, at least. Furthermore, the successful application of the MoM requires that the network of wires representing the conducting structure (including all the topside antennas) follow a specific set of modeling restrictions in order to keep the modeling errors within the engineering acceptable range (a few percent). Furthermore, the ship structure from the waterline up has to be modeled in order to avoid the generation of spurious modes corresponding to any arbitrarily imposed boundaries. An example of a wire mesh model is shown in **Figure 5** for a nominal design of a 50m ship. The model discretizes the ship outer surfaces all the yaw to the waterline using 6,758 wires. The surface of the water is represented as an infinite ground plane having seawater permittivity and conductivity.

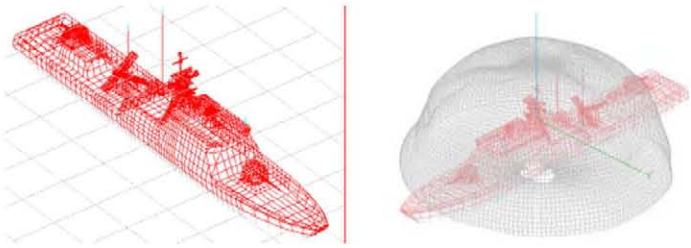


Figure 5. MoM Discretzation of a Nominal Combatant and the Radiation Pattern Of a HF Whip Antenna at 20 MHz

The frequency limitation on the applicability of the MoM is due to its inherent disadvantage that the memory requirement for the discrete model depends quadratically on the size of the conducting structure, while the computational complexity depends on the sixth power of the source frequency. This leads to high computational costs both in terms of computer resources and computation time. Furthermore, as the increase of frequency leads to a numerical model whose spatial resolution exceeds the geometrical confidence level of the design.

Analytically Based Methods Modeling

The limitation of the applicability of the numerical methods to low frequency analyses, requires supplemental methods for handling high frequencies (UHF and up for ships). The idea is to take advantage of the small wavelength relative to the scattering structure in order to generate analytical models that follow geometric arguments.

The general radiation pattern from an EMR source (antenna) is characterized by the presence of a main beam shaped to deliver RF energy along its axis. Nevertheless, due to local diffraction effects, sidelobes and backlobes regions exist as well as depicted

in **Figure 6** (left). Normally the spurious regions show a reduction of 10 dB from mainlobe gain in conjunction with half the beamwidth.

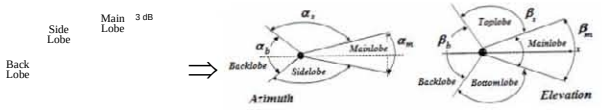


Figure 6 – Simplified Model of Antenna Radiation Patterns

The radiation pattern can be characterized by various analytical approaches. Nonetheless, satisfactory results are also obtained via simplified models based on physical arguments. Accordingly, radiation patterns are classified according to their EM properties via the notion of the antenna gain of the radiation pattern and the effect of its impedance mismatch. Consequently, it is possible to determine the radiation pattern parameters of topside antennas using merely three necessary input parameters: the directional mainlobe gain ($G_0=\eta D$, η radiation efficiency), the azimuth 3dB beamwidth angle (α), and the elevation 3dB beamwidth angle (β) as shown in **Figure 6** (right).

Nevertheless, as often the EMR field at the near-field of the antenna is of interest, the above far field models are corrected to account for near-field EMR. In addition, in order to account for nonlinear effects, empirical harmonic order correction factors for both CW and pulsed transmitter harmonic order attenuations are available.

Due to proximity of the topside transmitters to locations where personnel activity and/or mission critical equipment operate, it is important to consider the location of the near-field border (the point in which a planar wave front is received) corresponding to each topside emitter. The near-field/far-field border location, R_{FF} is determined according to [7] for the two antenna groups:

$$R_{FF}=\begin{cases}5\lambda & \text{for lineal antennas}\\ \frac{2D^2}{\lambda} & \text{for 2D and 3D aperture antennas}\end{cases} \qquad (7)$$

where, D is the maximal lineal dimension of the aperture, and λ is the wavelength. Calculating the "near-field correction", there are different models for three groups of antennas: reflector-aperture antennas, horn-aperture antennas, and lineal antennas.

As the high frequency methods are formulated based on the application of formulae, these methods offer low computational cost both in terms of computing time and machine resources.

Summary

In light of the complexity of topside configurations of modern surface combatants, analysis of topside EM environment is mandatory in order to assure the safety and functionality of the platform. Topside HERP analysis is based on the CEM prediction of EMR levels on the topside. Due to the large physical size of combatants and the wide frequency range employed by their combat systems, topside EMR analysis requires the employment of both low frequency methods, consisting of numerical analysis methods based on MoM, and high frequency methods that are based on ray-tracing algorithms in conjunction with analytically derived formulae. The latter offers high computational efficiency while the former provides accurate physical modeling requiring significant computational resources. HERP safety is achieved as a combination of adequate antenna placement and operating procedures.

References

[1] "IEEE Standard for Safety Levels w.r.t. Human Exposure to RF EM fields, 3 kHz to 300 MHz", IEEE C95.1-2005.

[2] M. Netzer at-al, "A Graphical Method for the Estimation of Radiation Hazards from a Crowded Multiple Antenna Site", Kos Workshop, 2004

[3] R F Harrington, "Field Computation by Moment Methods", IEEE Press, 1992.

[4] J.L.N. Violette et al, "Electromagnetic Compatibility Handbook" Van Nostrad Reinhold Co., NY, 1987.

[5] J.G. Burke, and A.J. Poggio, NEC - Method of Moments Parts I, II and III Technical Document No 116, LLNL, USA 1981.

[6] Balanis, "Antenna Theory – Analysis & Design", Wiley, 2nd Ed., 1997.

[7] "Reference Data for Radio Engineers", 5th ed., ITT, 1973, Howard W. Sams & Co. Inc.

[8] Balanis, "Adv. Engineering. Electromagnetics", Wiley & Sons, 1977.

THEORETICAL ANALYSIS OF VOLTAGE INDUCEMENT ON ORGANELLE MEMBRANES

TADEJ KOTNIK and DAMIJAN MIKLAVČIČ

UNIVERSITY OF LJUBLJANA, FACULTY OF ELECTRICAL ENGINEERING, TRŽAŠKA 25, SI-1000 LJUBLJANA, SLOVENIA

Abstract

Several reports have recently been published on effects of very short and intense electric pulses on cellular organelles; in a number of cases, the cell plasma membrane appeared to be affected less than certain organelle membranes, while with longer and less intense pulses the opposite is the case. The effects are the consequence of the voltages induced on the membranes, and in this paper we investigate the conditions under which the induced voltage on an organelle membrane could exceed its counterpart on the cell membrane. This would provide a possible explanation of the observed effects of very short pulses.

Frequency-domain analysis yields an insight into the dependence of the voltage inducement on the electric and geometric parameters characterizing the cell and its vicinity. The calculations show that at sufficiently high field frequencies, for a range of parameter values the voltage induced on the organelle membrane can indeed exceed the voltage induced on the cell membrane. Particularly, this can occur if the organelle interior is electrically more conductive than the cytosol, or if the organelle membrane has a lower dielectric permittivity than the cell membrane, and we discuss the plausibility of these conditions.

Time-domain analysis is then used to determine the courses of the voltage induced on the membranes by pulses with risetimes and durations in the nanosecond range. The particularly high resting voltage in mitochondria, to which the induced voltage superimposes, could contribute to the explanation why these organelles are the primary target of many observed effects.

1. INTRODUCTION

An exposure of a biological cell to an electric field of sufficient strength can lead to a significant increase in the permeability of the cell plasma membrane (40). If such an exposure is neither too strong nor too long, this phenomenon — referred to as *electroporation* or *electropermeabilization* — is reversible. This allows many otherwise nonpermeant molecules to enter into the cytosol or be inserted into the plasma membrane. Due to its efficiency, electroporation is rapidly becoming an established approach for treatment of solid cutaneous and subcutaneous tumors (22, 47), and it also holds great promise for gene therapy (17).

The mechanism underlying electroporation is the inducement of a voltage on the cell plasma membrane. This voltage is proportional to the field strength and superimposes onto the resting voltage present on the membrane under physiological conditions, typically about –70 mV (37). According to the theory of electroporation, a voltage on the membrane reduces the energy necessary for rearrangements of the membrane lipids that result in formation of aqueous passages (hydrophilic pores) and consequently in increased conductivity and permeability of the membrane. Consequently, as the voltage increases, so does the probability of formation of such passages. The resting voltages normally present on the cell membrane and on the organelle membranes — the largest is in mitochondria, about –140 mV (1) — are insufficient for this, and electroporation is not observed physiologically. However, with exposures to electric fields inducing voltages of several hundreds of millivolts, electroporation of the cell membrane becomes readily achievable and observed in experiments. Both the theory of electroporation (57, 41) and recent computational studies based on molecular dynamics (52, 53, 50) corroborate that as the membrane voltage increases, so does the rate of formation of metastable aqueous passages in the membrane.

The fields used for electroporation are most often delivered as rectangular pulses, with typical amplitudes of several hundred volts per centimeter, durations from tens of microseconds to milliseconds, and risetimes in microseconds. In the first few microseconds after the onset of the pulse, such exposures induce a voltage in the range of several hundred mV on the cell membrane, and this voltage persists until the end of the pulse. Also within microseconds, this leads to the onset of electroporation, detected as a steep increase in electrical conductivity and permeability of the membrane (24, 25).

The exposure of a cell to an electric field also induces voltages on the organelle membranes in the cell interior, but in their steady state, these are several orders of magnitude smaller than the voltage induced on the cell membrane. Thus when the cell membrane is electroporated with typical electroporation pulses with durations of hundreds of microseconds or several milliseconds, the organelle membranes are left unaffected. However, in a number of recent papers it has been reported that with much stronger (typically tens or hundreds of thousands of volts per centimeter) but much shorter (typically tens or hundreds of nanoseconds) pulses, the situation seems to be reversed, with the cell membrane affected less than some internal cell structures (46, 11, 7, 10, 19, 51). In many cases, a mitochondria-dependent apoptosis was observed, which could be due to electroporation of these organelles (6, 8, 58). For brevity, the high-intensity, nanosecond-duration pulses used in these experiments are often referred to as nsPEF (nanosecond-duration pulsed electric fields), and we will also adopt this practice here.

In this paper we explore one possible explanation of the observed effects of nsPEF on intracellular membranes. As discussed above, the steady-state value of the voltage induced on the cell membrane is always much larger than its counterpart on an organelle membrane. But the pulses with durations in the submicrosecond range are too short for the two voltages to approach their steady states, and their time courses become important. These depend on a number of geometric and electric parameters, and here we investigate whether there is a range of plausible parameter values for which the voltage on an organelle membrane can temporarily exceed the voltage on the cell membrane. This explanation has been proposed before, based on considerations of a more qualitative nature (46) and later on finite-elements modeling (29). Here, we derive analytical expressions for the induced voltages and analyze the role of each parameter. In Section 2 we present the expressions for the induced voltages, and in Section 3 we analyze the dependence of these voltages on each of the parameters.

2. DERIVATION OF THE INDUCED VOLTAGES

2.1 The model of a cell with an organelle

For a valid treatment of the membrane voltage induced by alternating fields with frequencies in the MHz and GHz range, or by pulsed fields with risetimes below 1 μs, both the electric conductivities and the dielectric permittivities of the membranes and the surrounding aqueous media have to be taken into account. An analytical treatment of such a system is possible only if the cell is the only object distorting the uniform electric field, and only in geometries where all the boundaries can be expressed as coordinate surfaces. Throughout this work, we will treat a single spherical cell, which meets these requirements. A spherical cell with a uniform interior (i.e. containing no organelles) is widely used in theoretical studies of cells exposed to electric fields, e.g. in derivation of the Schwan equation (38, 31) and its extensions (18, 32, 33, 34). The model with an organelle is then obtained by incorporating into the cell interior another spherical body with a concentric shell. This model (Fig. 1) consists of five regions, each characterized by an electric conductivity (σ, in S/m) and a dielectric permittivity (ε, in As/Vm). From the center outwards, the regions are the organelle interior (subscript 1i), the organelle membrane (1m), the cytosol (2i), the cell plasma membrane (2m), and the cell exterior (e). The radii of the organelle and the cell are denoted by R_1 and R_2, and their membrane thicknesses by d_1 and d_2. Although simplistic, this model is adequate for analyzing the voltages induced on the cell membrane and on organelle membranes (13, 29).

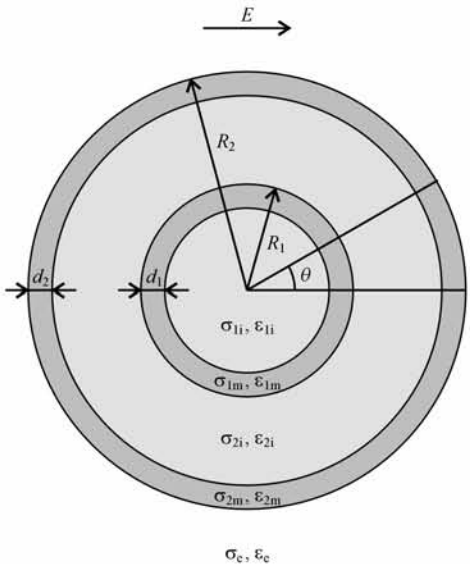


Figure 1

The spatial distribution of the electric potential in and around a spherical cell exposed to a uniform electric field is obtained by solving the Laplace equation in spherical coordinates (39). In each of the five regions of the model shown in Fig. 1, it has the general form

$$\Psi(r,\theta) = \left(A_k r + \frac{B_k}{r^2} \right) \cos\theta \ , \qquad (1)$$

with r the radius measured from the center, θ the angle with respect to the direction of the field, and with constants A_k and B_k specific for each regions. Finiteness of the electric potential at $r = 0$ implies $B_{i1} = 0$, and from uniformity of the field at $r \to \infty$ it follows that $A_e = -E$. The remaining constants A_{1i}, A_{1m}, B_{1m}, A_{2i}, B_{2i}, A_{2m}, B_{2m}, and B_e are determined by the requirement of continuity of the potential, Ψ, and of the normal component of the current density, $\Lambda(\partial\Psi/\partial r)$, at all four boundaries between the regions. In frequency-domain (FD) analysis, Λ is the complex

conductivity (admittivity), $\sigma + j\omega\varepsilon$, where ω is the angular frequency of the field, and in time-domain (TD) analysis, it is the admittivity operator, $\sigma + \varepsilon(\partial/\partial t)$, where $\partial/\partial t$ is the operator transforming a function into its time derivative. The continuity requirements for the boundary between the organelle membrane and the cytosol can be written as

$$\begin{aligned} A_{1m} r + \frac{B_{1m}}{r^2} &= A_{2i} r + \frac{B_{2i}}{r^2} \ , \\ \Lambda_{1m}\left(A_{1m} - \frac{2B_{1m}}{r^3} \right) &= \Lambda_{2i}\left(A_{2i} - \frac{2B_{2i}}{r^3} \right) \ , \end{aligned} \tag{2}$$

where in the FD $\Lambda_{1m} = \sigma_{1m} + j\omega\varepsilon_{1m}$, $\Lambda_{2i} = \sigma_{2i} + j\omega\varepsilon_{2i}$, and in the TD $\Lambda_{1m} = \sigma_{1m} + \varepsilon_{1m}(\partial/\partial t)$, $\Lambda_{2i} = \sigma_{2i} + \varepsilon_{2i}(\partial/\partial t)$. Analogous pairs of conditions characterize the other three boundaries. The direct dealing with operators in the TD can be avoided by transferring the treatment into the complex-frequency space, as described in Section 2.3.

The solutions for the eight constants are relatively lengthy expressions, as in general each of them incorporates the geometric and electric parameters of all five regions of the model, but algebraically their determination is elementary, since they form a well-defined system of eight equations with eight unknowns. The derivation and the solutions for the spherical cell with an organelle as shown in Fig. 1 are available at the web address `http://www.biophysj.org/cgi/content/full/biophysj.105.070771/DC1`

Once all the constants are determined, the voltage induced on a membrane is determined as the difference between the potentials $\Psi(r, \theta)$ at the inner and outer surface of this membrane. For the voltage induced on the cell plasma membrane this yields

$$\Delta\Psi_{cell} = \frac{3ER_2 d_2 \left(\begin{array}{l} (R_1 - d_1)^3 (\Lambda_{1i} - \Lambda_{1m}) \left(\begin{array}{l} 2(3R_2^2 - 3R_2 d_2 + d_2^2) \left(\begin{array}{l} (R_2 - d_2)^3 (\Lambda_{1m} - \Lambda_{2i}) \\ + R_1^3 (2\Lambda_{1m} + \Lambda_{2i}) \end{array} \right) \Lambda_{2i} \\ + (3R_2 d_2 - d_2^2) \left(\begin{array}{l} 2(R_2 - d_2)^3 (\Lambda_{1m} - \Lambda_{2i}) \\ - R_1^3 (2\Lambda_{1m} + \Lambda_{2i}) \end{array} \right) \Lambda_{2m} \end{array} \right) \\ + R_1^3 (\Lambda_{1i} + 2\Lambda_{1m}) \left(\begin{array}{l} (3R_2^2 - 3R_2 d_2 + d_2^2) \left(\begin{array}{l} (R_2 - d_2)^3 (\Lambda_{1m} + 2\Lambda_{2i}) \\ + 2R_1^3 (\Lambda_{1m} - \Lambda_{2i}) \end{array} \right) \Lambda_{2i} \\ + (3R_2 d_2 - d_2^2) \left(\begin{array}{l} (R_2 - d_2)^3 (\Lambda_{1m} + 2\Lambda_{2i}) \\ - R_1^3 (\Lambda_{1m} - \Lambda_{2i}) \end{array} \right) \Lambda_{2m} \end{array} \right) \end{array} \right) \Lambda_e}{M} \cos\theta \tag{3}$$

and for the voltage induced on the organelle membrane

$$\Delta\Psi_{org} = \frac{27ER_1 R_2^3 d_1 (R_2 - d_2)^3 \left(3R_1^2 \Lambda_{1i} - d_1 (3R_1 - d_1)(\Lambda_{1i} - \Lambda_{1m}) \right) \Lambda_{2i} \Lambda_{2m} \Lambda_e}{M} \cos\theta \tag{4}$$

where both in (3) and (4)

$$\begin{aligned} M = {} & 2(R_1 - d_1)^3 (\Lambda_{1i} - \Lambda_{1m}) \left(\begin{array}{l} (R_2 - d_2)^3 (\Lambda_{1m} - \Lambda_{2i}) \left(\begin{array}{l} 2(R_2 - d_2)^3 (\Lambda_{2i} - \Lambda_{2m})(\Lambda_{2m} - \Lambda_e) \\ + R_2^3 (\Lambda_{2i} + 2\Lambda_{2m})(\Lambda_{2m} + 2\Lambda_e) \end{array} \right) \\ + R_1^3 (2\Lambda_{1m} + \Lambda_{2i}) \left(\begin{array}{l} (R_2 - d_2)^3 (2\Lambda_{2i} + \Lambda_{2m})(\Lambda_{2m} - \Lambda_e) \\ + R_2^3 (\Lambda_{2i} - \Lambda_{2m})(\Lambda_{2m} + 2\Lambda_e) \end{array} \right) \end{array} \right) \\ & + R_1^3 (\Lambda_{1i} + 2\Lambda_{1m}) \left(\begin{array}{l} (R_2 - d_2)^3 (\Lambda_{1m} + 2\Lambda_{2i}) \left(\begin{array}{l} 2(R_2 - d_2)^3 (\Lambda_{2i} - \Lambda_{2m})(\Lambda_{2m} - \Lambda_e) \\ + R_2^3 (\Lambda_{2i} + 2\Lambda_{2m})(\Lambda_{2m} + 2\Lambda_e) \end{array} \right) \\ + 2R_1^3 (\Lambda_{1m} - \Lambda_{2i}) \left(\begin{array}{l} (R_2 - d_2)^3 (2\Lambda_{2i} + \Lambda_{2m})(\Lambda_{2m} - \Lambda_e) \\ + R_2^3 (\Lambda_{2i} - \Lambda_{2m})(\Lambda_{2m} + 2\Lambda_e) \end{array} \right) \end{array} \right) \end{aligned} \tag{5}$$

The substitution $\Lambda = \sigma + j\omega\varepsilon$ for each of the five regions provides the starting point for analysis of $\Delta\Psi_{cell}$ and $\Delta\Psi_{org}$ in the FD, and the substitution $\Lambda = \sigma + \varepsilon(\partial/\partial t)$ does the same for the TD.

2.2 Analysis in the frequency domain

The frequency domain (FD) is the natural setting for an exposure of a cell to a sinusoidal electric field. Fixing the geometric and electric parameters of the model, inserting for E the amplitude of the field, and writing explicitly $\Lambda = \sigma + j\omega\varepsilon$, the induced voltages $\Delta\Psi_{cell}$ and $\Delta\Psi_{org}$ become functions of a single variable, namely ω, the angular frequency of the field. For a fixed ω, the values of $\Delta\Psi_{cell}$ and $\Delta\Psi_{org}$ are complex numbers, with $|\Delta\Psi_{cell}|$, $|\Delta\Psi_{org}|$ corresponding to the amplitudes of the induced voltages, and $\arg(\Delta\Psi_{cell})$, $\arg(\Delta\Psi_{org})$ to their phase shifts with respect to the external field. It should be emphasized that these values characterize the sinusoidal steady states that are established after the transients occurring at the onset of the field are over.

By considering $\Delta\Psi_{cell}$ and $\Delta\Psi_{org}$ as functions of ω, it is then determined very straightforwardly whether there is a range of parameter values and field frequencies where $\Delta\Psi_{org}$ can — at least temporarily — exceed $\Delta\Psi_{cell}$. The results of such analysis are presented in Section 3.1.

The approach described above can be extended to other periodic time courses of the field representable as uniformly convergent Fourier series. The induced voltages are then given by the series of voltage components induced by individual field components in the Fourier series.

2.3 Analysis in the time domain

The time domain (TD) is the natural setting for exposures of a cell to aperiodic fields, as well as to periodic fields for which the Fourier series is nonuniformly convergent.[*] This class clearly contains a rectangular and a trapezoidal (i.e. having non-zero risetime and falltime) pulse, but it also contains periodic trains of such pulses, as the uniform convergence requirement fails at the pulse edges, which is usually referred to as the Gibbs phenomenon (23). As mentioned in Section 2.1, the most convenient approach here is an interim transfer of the treatment to the complex-frequency space. Denoting the complex frequency by s, the differentiation with respect to time is thereby transformed into multiplication by s, and time courses are replaced by their Laplace transforms. Fixing again the geometric and electric parameters of the model, inserting for E the Laplace transform of the time course of the electric field, $L[E(t)] = E(s)$, and writing explicitly $\Lambda = \sigma + \varepsilon s$, the expressions for $\Delta\Psi_{cell}$ and $\Delta\Psi_{org}$ become functions of s. The time courses of the induced voltages are then obtained as inverse Laplace transforms, $\Delta\Psi_{cell}(t) = L^{-1}[\Delta\Psi_{cell}(s)]$ and $\Delta\Psi_{org}(t) = L^{-1}[\Delta\Psi_{org}(s)]$. This yields the complete time courses, including the transients.

Provided that $E(s)$ is a polynomial in s, $\Delta\Psi_{cell}$ and $\Delta\Psi_{org}$ are rational functions (i.e. fractions of polynomials) of s, and the inverse Laplace transforms are obtained easily. The method is also applicable to all other cases for which the Laplace transform of $E(t)$ and the inverse Laplace transforms of $\Delta\Psi_{cell}$ and $\Delta\Psi_{org}$ can be obtained explicitly. For many of the conceivable time courses of the electric field, the transforms can be found in standard tables (43), while for other sufficiently regular functions they can be derived by means of the Laplace transform integral and the Bromwich integral, respectively (2). For more intricate cases, discretization of time and application of the unilateral Z-transform instead of the Laplace transform would yield approximate solutions.

3. RESULTS AND DISCUSSION

The aim of this paper is to evaluate the voltages induced by nsPEF, which will be approximated as having a trapezoidal shape. As described in the preceding sections, the natural setting for this is the TD, in which this aim will be pursued in Section 3.2. However, there are four geometric and ten electric parameters that have to be investigated with respect to their influence on $\Delta\Psi_{cell}$ and $\Delta\Psi_{org}$, and a trapezoidal pulse is characterized by a risetime, an amplitude, a duration pertaining to this amplitude, and a falltime. For a first insight into the role of the parameters, and for a selection of those to be investigated further, a clearer picture is provided by treating an exposure of a cell to a sinusoidal field, which is characterized only by its amplitude and frequency. Along these lines, Section 3.1 investigates the influence of each of the parameters in the FD, and a much smaller subset of parameters chosen on the basis of this investigation is then used in Section 3.2 in the TD with trapezoidal pulses.

[*] For other periodic fields, the analysis in the frequency domain is simpler, yet the analysis in time domain is nonetheless applicable, due to which it may be viewed as the more general of the two.

3.1 Voltages induced by a sinusoidal field

The purpose of this section is to determine whether in an exposure of a cell to a sinusoidal field, there is a range of parameter values for which $|\Delta\Psi_{org}|$ can exceed $|\Delta\Psi_{cell}|$, or equivalently, for which the ratio $|\Delta\Psi_{org}| / |\Delta\Psi_{cell}|$ can exceed the value of 1. The expressions for $\Delta\Psi_{cell}$ and $\Delta\Psi_{org}$ in Section 2.1 show that this ratio depends on practically all the geometric and electric parameters of the model. The only exceptions are σ_e and ε_e, as the numerators of $\Delta\Psi_{cell}$ and $\Delta\Psi_{org}$ are proportional to $\Lambda_e = \sigma_e + j\omega\varepsilon_e$, while their denominators are identical, so that in the ratio $|\Delta\Psi_{org}| / |\Delta\Psi_{cell}|$ all occurrences of Λ_e cancel out. The simplest method for investigation of the role of the remaining twelve parameters is by means of parametric studies, in which one parameter is varied through a given range while the others are kept at their default values. Restriction to one variable at a time does not completely elucidate the behavior of a function of twelve variables, but the results of such parametric studies are easy to interpret, and will also suffice for the aims of this paper.

Table 1 gives the default values and variation ranges of the parameters. The default values are based on the typical data found in the literature, and the limits of the variation ranges were chosen as physically plausible values. For the reasons discussed above, σ_e and ε_e do not enter the parametric studies, for which the table gives only the default values, which are needed when the two voltages are of interest, and not only their ratio.

Table 1. Default values and variation ranges for parametric studies

Parameter	Default value	Variation range	Parameter	Default value	Variation range
σ_{1i} [S/m]	0.3 [a]	0.1 – 1.0	ε_{1i} [As/Vm]	6.4×10^{-10} [b]	$(3.5 – 7.0) \times 10^{-10}$
σ_{1m} [S/m]	3×10^{-7} [c]	$10^{-8} – 10^{-5}$	ε_{1m} [As/Vm]	4.4×10^{-11} [d]	$(1.8 – 8.8) \times 10^{-11}$
σ_{2i} [S/m]	0.3 [e]	0.1 – 1.0	ε_{2i} [As/Vm]	6.4×10^{-10} [b]	$(3.5 – 7.0) \times 10^{-10}$
σ_{2m} [S/m]	3×10^{-7} [f, g]	$10^{-8} – 10^{-6}$	ε_{2m} [As/Vm]	4.4×10^{-11} [g]	$(1.8 – 8.8) \times 10^{-11}$
σ_e [S/m]	1.2 [h]	—	ε_e [As/Vm]	6.4×10^{-10} [b]	—
R_1 [µm]	3	1 – 8	d_1 [nm]	5	3 – 15
R_2 [µm]	10	5 – 100	d_2 [nm]	5 [k]	3 – 7

[a] set equal to σ_{2i}
[b] physiological saline at 35°C (42, 9)
[c] set equal to σ_{2m}
[d] set equal to ε_{2m}
[e] (21, 26)
[f] from (27), using the conversion given in (3)
[g] (15)
[h] blood serum at 35°C (49)
[k] (1)

Each of the parametric studies was performed for ω spanning the range from 10^5 to 10^{10} s^{-1}, yielding a set of data that can be visualized clearly in a contour plot of the ratio $|\Delta\Psi_{org}| / |\Delta\Psi_{cell}|$ as a function of frequency and the studied parameter. As shown in Figure 2, with the default values assigned to all parameters, this ratio does not exceed the value of 1 for any frequency. A similar result is obtained if the two membranes are assigned realistic dielectric permittivities but zero electric conductivities (13).

However, in eight of the twelve parametric studies, for sufficiently high frequencies the ratio $|\Delta\Psi_{org}| / |\Delta\Psi_{cell}|$ does exceed 1 in a certain range of parameter values. The contour plots showing the results of the parametric studies are given in Figure 3, from which two clear properties emerge. First, in the higher MHz range, either a small increase of σ_{1i} above its default value, or a small decrease of σ_{2i} below its default value suffices for $|\Delta\Psi_{org}|$ to exceed $|\Delta\Psi_{cell}|$. And second, in the higher MHz range and in the GHz range the same is the case for a decrease of ε_{1m} and for an increase of ε_{2m}. A more general

Figure 2

formulation is that the ratio $|\Delta\Psi_{org}|$ / $|\Delta\Psi_{cell}|$ can exceed the value of 1 if the organelle interior has a higher electric conductivity than the cytosol, or if the organelle membrane has a lower dielectric permittivity than the cell membrane. The effect of $\sigma_{1i} > \sigma_{2i}$ is due to the fact that with the increase of frequency, the shielding of the cell interior by the plasma membrane weakens, and the electric current flowing through the cell becomes concentrated in the organelle interior. The effect of $\varepsilon_{1m} < \varepsilon_{2m}$ is also easily explained, as the voltage inducement is faster on the membrane with the lower dielectric permittivity.

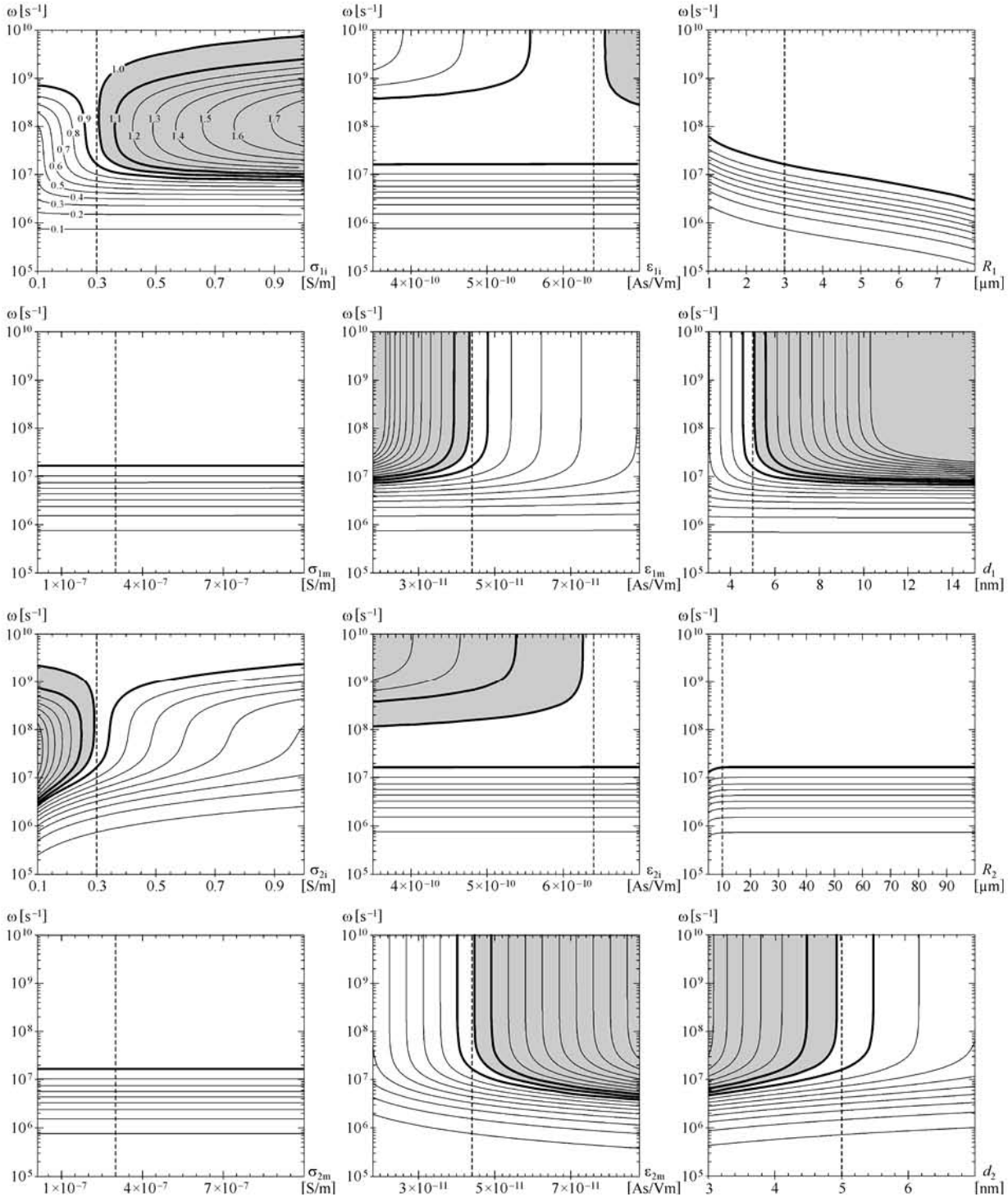


Figure 3

For $\sigma_{1i} > \sigma_{2i}$, the organelle interior would have to contain either a higher total concentration of ions with respect to the cytosol, or a larger fraction of ions with higher mobility (e.g. more potassium and less sodium). In a recent computational analysis, the concentration of potassium ions in the intermembrane space of the mitochondria was

estimated at between 175 and 207 mM (36), which is indeed significantly higher than in the cytosol, where it is typically about 140 mM (37). Among the membranes, the ones with the lowest dielectric permittivity are pure lipid bilayers, and hence for $\varepsilon_{1m} < \varepsilon_{2m}$, the membrane of the organelle under consideration would generally have to contain a smaller fraction of proteins than the cell plasma membrane. This is, however, markedly not the case for the inner mitochondrial membrane, where proteins represent about 76% of the mass — a higher fraction than in any other membrane (37).

The parametric studies also show that $|\Delta\Psi_{org}| / |\Delta\Psi_{cell}|$ can exceed 1 if d_1 is significantly larger than its default value of 5 nm. More generally, a sufficient condition is that the organelle membrane should be thicker than the cell membrane, $d_1 > d_2$. This is realistic for some organelles, such as the nucleus and the mitochondria, as they have a double membrane, and in mitochondria the two membranes are moreover separated by several nanometers of intermembrane space (1). Still, with a thicker membrane, a proportionally larger voltage is required for the same electric field within the membrane. As a consequence, if the electric field in the membrane is the decisive factor in electroporation, with $d_1 > d_2$ the condition $|\Delta\Psi_{org}| / |\Delta\Psi_{cell}| > 1$ is not sufficient for the organelle membrane to be electroporated, but instead roughly $|\Delta\Psi_{org}| / |\Delta\Psi_{cell}| > d_1 / d_2$ would be required.

Finally, a region with $|\Delta\Psi_{org}| > |\Delta\Psi_{cell}|$ is also reached in the parametric studies of ε_{1i} and ε_{2i}, namely at sufficiently high frequencies provided that $\varepsilon_{1i} > \varepsilon_{2i}$. However, as the organelle interior and the cytosol are both aqueous solutions, it is reasonable to assume that ε_{1i} and ε_{2i} are very similar. The choice of variation ranges for these two parameters primarily reflects the dependence of dielectric permittivities on the temperature, but since the cell is too small to contain significant temperature differences, change of the temperature by cooling or heating the cell suspension or a tissue will have nearly the same effect on the two permittivities.

Further analysis reveals that if the cell and organelle membranes are identical in their electric properties and their thickness, and if the cytosol is electrically identical to the organelle interior, then $|\Delta\Psi_{org}| < |\Delta\Psi_{cell}|$ at any field frequency. It should perhaps be stressed here that for such parameter values, the faster charging of the organelle membrane can not cause $\Delta\Psi_{org}$ to exceed $\Delta\Psi_{cell}$, even if the shielding of the organelle by the cell membrane is disregarded. Namely, without shielding, the rate of voltage inducement on a spherical object is inversely proportional to its radius, but the voltage plateau is directly proportional to the radius, so that on a larger object the induced voltage is necessarily larger at all times.[***] As a consequence, the voltage induced on the cell membrane is always larger than its counterpart on the organelle membrane. At low field frequencies the shielding intensifies this effect, as the voltage on the organelle membrane starts decreasing even during the exposure (Fig. 5 illustrates this for an exposure to a direct field).

However, as Figure 3 shows, if some parameters are shifted from their default values, the outcome can change significantly. As an illustration, in Figure 4 we assume that $\sigma_{1i} = 0.5$ S/m, $\varepsilon_{1m} = 3.0 \times 10^{-11}$ As/Vm, and $d_1 = 10$ nm, while keeping the other nine parameters at their default values. This study shows that on a cell characterized by the chosen parameter values, with an exposure to an alternating field with a frequency in the range of tens and hundreds of MHz, the induced voltage on the organelle could exceed its counterpart on the cell membrane by a factor of more than 3. Obviously, this is only relevant provided that σ_{1i} can actually differ that much with respect to σ_{2i}, and similarly for ε_{1m} with respect to ε_{2m}. We discuss the plausibility of this at the end of the paper, whereas we now turn to the voltages induced by a trapezoidal pulse.

[***] This follows from the fact that for $K > 1$ and $t > 0$, we have $1 - \exp(-t/\tau) < K(1 - \exp(-t/(K\tau)))$. Namely, the two functions are equal at $t = 0$, and for their respective derivatives at $t > 0$ we have $\exp(-t/\tau)/\tau < \exp(-t/(K\tau))/\tau$.

Figure 4

3.2 Voltages induced by a trapezoidal pulse

Before focusing on specific nsPEF, it is instructive to consider the general characteristics of the voltage inducement on a nanosecond time scale. For this, we treat an onset of a direct electric field, and to keep $E(t)$ continuous, we assume that this onset is trapezoidal with a risetime T. Such a time course of the field can be described as a sum of two ramp functions, the first one with a positive slope and starting at the time 0, and the second one with the negative slope of the same size and starting at the time T,

$$E(t) = E_0 \left[\frac{t}{T} u(t) - \frac{t-T}{T} u(t-T) \right] \tag{6}$$

where E_0 is the amplitude of the field that is reached at the end of the risetime. In the complex-frequency space, this becomes

$$E(s) = E_0 \frac{1-e^{-sT}}{s^2 T} \tag{7}$$

In analogy with the FD study shown in Figure 2, we assume that the field amplitude is $E_0 = 5 \times 10^4$ V/m, and treat the situation at $\theta = 0$. In addition, we take $T = 1$ ns, which is on the order of magnitude of the shortest risetimes achievable with nsPEF generators. Proceeding as described in Section 2.3, we insert $E(s)$ into the expressions for $\Delta\Psi_{cell}$ and $\Delta\Psi_{org}$, write all the admittivity operators as $\Lambda = \sigma + \varepsilon s$, assign all the parameters their default values, and apply the inverse Laplace transform to obtain the time courses of the two induced voltages for such an onset of the field. Shown in the top panel of Figure 5, these time courses reveal that the inducement on the cell plasma membrane is a monotonic process, while the inducement on an organelle membrane is transient; with the onset of the field, $\Delta\Psi_{org}$ increases for several hundred nanoseconds, and then recedes back to zero even if the external field persists. This is consistent with the simpler, widely used steady-state consideration of a DC exposure, where the voltage induced on the plasma membrane is given by the static Schwan equation, $\Delta\Psi_{cell} \approx 1.5\ E\ R \cos\theta$, while everywhere in the cell interior the electric potential is practically constant.

The time courses of the two induced voltages also show that with default parameter values, $\Delta\Psi_{org}$ remains below $\Delta\Psi_{cell}$ at all times, as could be expected from the results obtained in the FD (see Fig. 2). However, if in analogy to the second FD study we set $\sigma_{1i} = 0.5$ S/m, $\varepsilon_{1m} = 3.0 \times 10^{-11}$ As/Vm, $d_1 = 10$ nm, and keep the other nine parameters at their default values, the situation changes quite radically. As shown in the bottom panel of Figure 5, $\Delta\Psi_{org}$ now exceeds $\Delta\Psi_{cell}$ considerably during the first tens of nanoseconds. The general properties of the two voltages — a monotonic increase of $\Delta\Psi_{cell}$ and a transient increase of $\Delta\Psi_{org}$ followed by a decrease to zero — are unchanged.

The FD analysis (see Section 3.1) reveals that $\Delta\Psi_{org}$ can only exceed $\Delta\Psi_{cell}$ if either the cell membrane differs from the organelle membrane, or the cytosol differs from the organelle interior. From the results shown in Figure 5 it transpires that moreover, this can only occur during the first hundreds of nanoseconds after the onset of the pulse. Thus only pulse durations shorter than this can allow for selective targeting of intracellular structures, while with longer pulses the cell plasma membrane is always affected to a larger extent.

Further time courses of voltages induced by trapezoidal nsPEFs can be found in (35b).

Figure 5

3.3 Resting voltage on organelle membranes

It was already mentioned in Section 1 that the resting voltage normally present on the mitochondrial membrane is considerably larger than its counterpart on the cell plasma membrane. On each membrane, the voltage induced by an external electric field superimposes to the resting voltage, due to which the total voltage can be higher on a mitochondrial membrane than on the cell plasma membrane even with $\Delta\Psi_{org}$ equal to, or slightly below $\Delta\Psi_{cell}$. As the membrane voltages required for electroporation by nsPEF appear to be in the range of volts (28, 29), it is disputable whether a high resting voltage on an organelle membrane can alone be decisive in making this organelle the primary target of the field. Still, it could be among the reasons why mitochondria are the primary target of many observed effects of the nsPEF. This possibility has been discussed previously by Weaver (56).

3.4 Curvature of organelle membranes

Some theoretical studies suggest that the threshold value of membrane voltage required for electroporation can decrease if the membrane curvature is sufficiently high (54, 41). As the organelles are significantly smaller than the cell, the typical curvatures found in organelle membranes are generally also higher than those in the cell membrane. Due to this, it is conceivable that even with $\Delta\Psi_{org}$ somewhat lower than $\Delta\Psi_{cell}$, electroporation could affect an organelle membrane, but leave the cell membrane intact.

3.5 Voltage-gated channels in organelle membranes

This paper is mainly concerned with the conditions that would allow for electroporation of the organelle membranes, but for completeness it should be noted that some effects caused by nsPEF could also be explained without involving electroporation. Weaver (56) proposed that the membrane voltage induced on the inner mitochondrial membrane could open the mitochondrial permeability transition pore complex (MPTP). As this molecule is voltage sensitive (45, 44) and involved in the induction of apoptosis (20), apoptosis could in this manner be induced also without electroporation of the mitochondrial membranes.

4. CONCLUSIONS

In Sections 3.1 and 3.2, we investigated the circumstances under which the voltage induced by the external field on an organelle membrane can exceed its counterpart on the cell plasma membrane. The results imply that this can not occur if the electric properties of the organelle interior are very similar to those of the cytosol, and if the organelle membrane is very similar to cell membrane. On an organelle membrane considerably thicker than the cell membrane, as in mitochondria, the induced voltage can be higher even under these circumstances, but the electric field in the organelle membrane will remain below the electric field in the cell membrane, making electroporation of the former but not the latter unlikely.

However, if the organelle interior is more electrically conductive than the cytosol, or if the organelle membrane has a detectably lower dielectric permittivity than the cell membrane, the situation changes. For exposures to sinusoidal fields in the MHz range, and for the first tens of nanoseconds of exposures to pulsed fields, the voltage induced on the organelle membrane can easily exceed its counterpart on the cell membrane, as illustrated in Figure 4 and in bottom panels of Figures 5 and 6. These findings are of course only relevant provided that the assumed differences between the organelle interior and the cytosol, or between the cell and organelle membranes are realistic. Higher ionic concentrations in the interior of some organelles could result in higher conductivity of this region with respect to the cytosol, which appears to be a realistic assumption at least in the case of potassium ions in the mitochondria. Experimental estimates obtained by dielectric spectroscopy for the mitochondria (4) and the nucleus (5, 12) also corroborate that the differences between the electric conductivities of the organelle interiors and the cytosol can be considerable, and suggest that organelle membranes can also differ significantly from the cell plasma membrane in their dielectric permittivities.

Finally, as discussed in Sections 3.3, 3.4, and 3.5, there are at least three additional factors that could lead to an organelle membrane being electroporated but the cell membrane left intact: high resting voltage on the organelle membrane, high curvature of the organelle, and voltage sensitivity of certain proteins in the organelle membrane. The first and the third of these factors could also contribute to the explanation why particularly mitochondria often appear to be the primary targets of nsPEF.

References

1. Alberts, B., et al. 1994. *Molecular Biology of the Cell (3rd ed.)*. Garland Publishing, New York.
2. Arfken, G. B., et al. 1995. *Mathematical Methods for Physicists (4th ed.)*. Academic Press, San Diego.
3. Arnold, W. M., et al. 1987. *Biochim. Biophys. Acta.* 905:454–464.
4. Asami, K., and A. Irimajiri. 1984. *Biochim. Biophys. Acta.* 778:570–578.
5. Asami, K., et al. 1989. *Biochim. Biophys. Acta.* 1010:49–55.
6. Beebe, S. J., et al. 2002. *IEEE Trans. Plasma Sci.* 30:286–292.
7. Beebe, S. J., et al. 2003. *DNA Cell Biol.* 22:785–796.
8. Beebe, S. J., et al. 2003. *FASEB J.* 17:1493–1495.
9. Büchner, R., et al. 1999. *J. Phys. Chem. A.* 103:1–9.
10. Chen, N., et al. 2004. *Biochem. Biophys. Res. Commun.* 317:421–427.
11. Deng, J., et al. 2003. *Biophys. J.* 84:2709–2714.
12. Ermolina, I., et al. 2001. *IEEE Trans. Dielect. Elect. Insul.* 8:253–261.
13. Foster, K. R. 2000. *IEEE Trans. Plasma Sci.* 28:15–23.
14. Fröhlich, H. 1958. *Theory of Dielectrics (2nd ed.)*. Oxford University Press, Oxford.
15. Gascoyne, P. R. C., et al. 1993. *Biochim. Biophys. Acta.* 1149:119–126.
16. Gimsa, J., and D. Wachner. 2001. *Biophys. J.* 81:1888–1896.
17. Golzio, M., et al. 2004. *Methods.* 33:126–135.
18. Grosse, C., and H. P. Schwan. 1992. *Biophys. J.* 63:1632–1642.
19. Hall, E. H., et al. 2005. *DNA Cell Biol.* 24:283–291.
20. Halestrap, A. P., et al. 2002. *Biochimie.* 84:153–166.
21. Harris, C. M., and D. B. Kell. 1983. *Bioelectrochem. Bioenerg.* 11:15–28.
22. Heller, R., et al. 1999. *Adv. Drug. Deliv. Rev.* 35:119–129.
23. Hewitt, E., and R. E. Hewitt. 1979. *Arch. Hist. Exact Sci.* 21:129–160.
24. Hibino, M., et al. 1991. *Biophys. J.* 59:209–220.
25. Hibino, M., et al. 1993. *Biophys. J.* 64:1789–1800.
26. Hölzel, R., and I. Lamprecht. 1992. *Biochim. Biophys. Acta.* 1104:195–200.
27. Hu, X., et al. 1990. *Biochim. Biophys. Acta.* 1021:191–200.
28. Joshi, R. P., et al. 2001. *Phys. Rev. E.* 64:011913.
29. Joshi, R. P., et al. 2004. *Phys. Rev. E.* 69:051901.
30. Klösgen, B., et al. 1996. *Biophys. J.* 71:3251–3260.
31. Kotnik, T., et al. 1997. *Bioelectrochem. Bioenerg.* 43:285–291.
32. Kotnik, T., et al. 1998. *Bioelectrochem. Bioenerg.* 45:3–16.
33. Kotnik, T., and D. Miklavčič. 2000. *IEEE Trans. Biomed. Eng.* 47:1074–1081.
34. Kotnik, T., and D. Miklavčič. 2000. *Bioelectromagnetics.* 21:385–394.
35. Kotnik, T., and D. Miklavčič. 2000. *Biophys. J.* 79:670–679.

35b. Kotnik, T., and D. Miklavčič. 2006. *Biophys. J.* 90:480–491.

36. Lemeshko, S. V., and V. V. Lemeshko. 2000. *Biophys. J.* 79:2785-2800.
37. Lodish, H., et al. 1999. *Molecular Cell Biology (4th ed.)*. W. H. Freeman, New York.
38. Marszalek, P., et al. 1990. *Biophys. J.* 58:1053–1058.
39. Morse, P. M., and H. Feshbach. 1953. *Methods of Theoretical Physics*. McGraw-Hill, New York.
40. Neumann, E., et al. 1989. *Electroporation and Electrofusion in Cell Biology*. Plenum Press, New York.
41. Neumann, E., et al. 1999. *Bioelectrochem. Bioenerg.* 48:3–16.
42. Nörtemann, K., et al. 1997. *J. Phys. Chem. A.* 101:6864–6869.
43. Oberhettinger, F., and L. Badii. 1973. *Tables of Laplace transforms*. Springer, Berlin.
44. Palmeira, C. M., and K. B. Wallace. 1997. *Toxicol. Appl. Pharmacol.* 143:338–347.
45. Petronilli, V., et al. 1994. *Biochim. Biophys. Acta*. 1187:255–259.
46. Schoenbach, K. H., et al. 2001. *Bioelectromagnetics.* 22:440–448.
47. Serša, G., et al. 2003. *Cancer. Ther.* 1:133–142.
48. Stratton, J. A. 1941. *Electromagnetic Theory*. McGraw-Hill, New York.
49. Sunderman, F. W. 1945. *Am. J. Clin. Path.* 15:219–222.
50. Tarek, M. 2005. *Biophys. J.* 88:4045-4053.
51. Tekle, E, et al. 2005. *Biophys. J.* 89:274–284.
52. Tieleman, D. P., et al. 2003. *J. Am. Chem. Soc.* 125:6382–6383.
53. Tieleman, D. P. 2004. *BMC Biochemistry* 5:10.
54. Tönsing, K., et al. 1997. *Eur. Biophys J.* 26:307–318.
55. Tsong, T. Y. 1991. *Biophys. J.* 60:297–306.
56. Weaver, J. C. 2003. *IEEE Trans. Diel. El. Insul.* 10:754–768.
57. Weaver, J. C, and Y. A. Chizmadzhev. 1996. *Bioelectrochem. Bioenerg.* 41:135–160.
58. White, J. A., et al. 2004. *J. Biol. Chem.* 279:22964–22972.

TREATMENT PLANNING OF RADIOFREQUENCY ABLATION

T. SAMARAS

ARISTOTLE UNIVERSITY OF THESSALONIKI
RADIOCOMMUNICATIONS LABORATORY, DEPT. OF PHYSICS,
GR-54124 THESSALONIKI, GREECE

ABSTRACT

The treatment of cancer with the use of radiofrequency ablation under imaging guidance has attracted a lot of attention among oncologists in the recent years, as it is a minimally invasive technique of rare complications to the patients. In this work we present the results of treatment planning for the case of liver cancer treated with one electrode operating at 450kHz. We use the finite element method (FEM), implemented in a commercially available software package, to solve the combined electromagnetic and thermal problems. We explore the effect of voltage excitation, as well as of the temperature-dependent conductivity, on the resulting maximum temperature in the tissue. The influence of the blood perfusion term is also taken into consideration in our analysis. The results show that several parameters play a role in the production of a realistic treatment planning and in the investigation of the efficiency of this oncotherapeutic modality, but with the use of the necessary computer resources it is possible to study most of its aspects.

I. INTRODUCTION

The removal of tumor ('tumor ablation') is the destruction of cancerous tissue in an effort to cure the disease. It is clinically applied mainly to non-resectable tumors with the use of either thermal or chemical methods (e.g. ethanol). The thermal methods include the cooling of tissue to temperatures below –40^{o}C (cryoablation) or its heating to temperatures higher than 50^{o}C (thermoablation). The latter is achieved with electromagnetic radiation (RF or microwave), ultrasound and laser. More details on the techniques and the physical principles of tissue ablation can be found in [1].

Apart from liver tumors, where it is considered an established treatment modality, thermoablation is finding an increasing application in other sites like kidney, lung and bone. Most commercially available devices operate with the radiofrequency (RF) current which flows between an electrode (inserted into the tumor under the guidance of medical imaging) and a dispersive electrode (grounding pad), which is placed distally on the body surface of the patient and serves as the return path for the current. The heating of the tissues is larger where the current density is higher, i.e. next to the electrode in the tumor. The temperature can exceed 100^{o}C, although cell death due to coagulative necrosis occurs already above 50^{o}C. However, high tissue temperature may result in tissue carbonization (charring), which is an unwanted situation, not only because it is an irreversible effect, but mainly because it leads to an electrically insulating area which prevents the current from flowing.

There are currently several limitations in tumor thermoablation. Imaging techniques should be improved to allow better guidance of the electrode inside the tumor and evaluation of the thermal lesion. New techniques must be employed (e.g. multiple electrode systems) in order to increase the coagulative zones, instead of inserting a single electrode more than once in the tumor. Finally, the treatment efficiency is compromised next to large blood vessels, which advect a large portion of the heat developed in the target area, leading to lower than expected temperatures [2]. Such shortcomings make the introduction of treatment planning an important factor in securing quality assurance of the treatment and maximizing its outcome.

In this work we will present some of the numerical aspects and problems in the treatment planning of RF ablation with a single electrode inserted inside the liver.

II. METHODOLOGY

Formulation

At first look treatment planning of RF ablation appears like a two-step procedure. In the frequency range of 450–550 kHz, where most probes operate, the wavelength of the electromagnetic field inside the tissue is several orders of magnitude larger than the size of the ablation electrodes, i.e. we deal with a quasi-static problem. At these frequencies conduction current is more important in living tissues (due to electrolyte ions present in them) than displacement current. Therefore, in order to solve the electrical problem it is necessary to use Laplace's equation,

$$\nabla(\sigma \nabla V) = 0 \tag{1}$$

where σ is tissue conductivity (S/m) and V is the electric potential (V). It is assumed that no current sources at the same frequency like the externally imposed current are present inside the human body. Having calculated the electric field, the power per unit mass (W/kg) dissipated in the tissues, i.e. the Specific Absorption Rate (SAR), evaluates to

$$SAR = \frac{\sigma}{\rho} E^2 = \frac{1}{\sigma \rho} J^2 \tag{2}$$

where ρ is the mass density (kg/m^3) and J the current density (A/m^2). This term can be used as an input to the Bioheat Transfer Equation (BHTE) of Pennes' [3]

$$\rho c \frac{dT}{dt} = \nabla \cdot (k \nabla T) - \rho_b c_b \omega_b (T - T_b) + Q_m + Q_{RF} \tag{3}$$

where k is the thermal conductivity (W/(m K)), c is the specific heat (J/(kg K)), ω_b is the blood perfusion rate (in m^3 of blood per m^3 and per s), Q_m is the metabolic heat generation rate (W/m^3) and Q_{RF} is the volumetric heat generation rate (W/m^3) due to the RF current:

$$Q_{RF} = \rho \, SAR \tag{4}$$

The subscript b denotes 'blood'.

However, equations (1) and (3) are coupled, because electrical conductivity σ changes with temperature, i.e. the problem is non-linear and this can affect the final temperature calculated with numerical techniques [4],[5].

Numerical model

The coupled differential equations were solved numerically with the commercially available software package FEMLAB 3.1i (COMSOL AB, Stockholm, Sweeden), which implements the Finite Element Technique (FEM). The assumed electrode (probe) is shown in Figure 1. The probe had a diameter of 0.3cm and consisted of two parts. The lower tip of 2cm in length was set at a constant voltage V_0, whereas the upper part of 4cm in length was supposed to be insulated electrically. The whole probe was assumed thermally insulated, which is not far from reality for electrodes inserted in catheters.

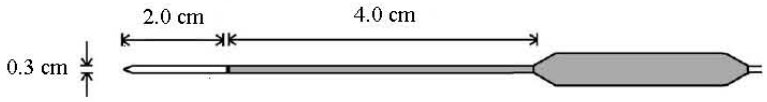


Figure 1. The electrode (probe) assumed in the numerical simulations

The probe was inserted inside a cubical volume of liver tissue with edge dimension of 12cm (Figure 2). The properties of the tissue and blood are given in Table 1. At the sides of the cube Dirichlet boundary conditions were set for both the electric and the thermal problem: The temperature was set at 37^{o}C and the voltage at 0V.

Table 1. Physical properties of model

Property	Value
Electrical conductivity of liver (37^{o}C)	0.143 S/m
Thermal conductivity of liver	0.502 W/(m K)
Specific heat of liver	3600 J/(kg K)
Mass density of liver	1060 kg/m^3
Specific heat of blood	4180 J/(kg K)
Mass density of blood	1000 kg/m^3
Blood perfusion rate	0.0064 1/s
Blood temperature	37^{o}C

The variation of electrical conductivity with temperature was adopted from [4] and can be summarized in

$$\sigma(T) = 0.1151 - [0.00226 \times (25 - T)] + [0.00000925 \times (25 - T)^2] \tag{5}$$

where T is the tissue temperature in ^{o}C. The conductivity and the temperature were sampled every 10 or 30s during the whole simulation of a treatment lasting 15min.

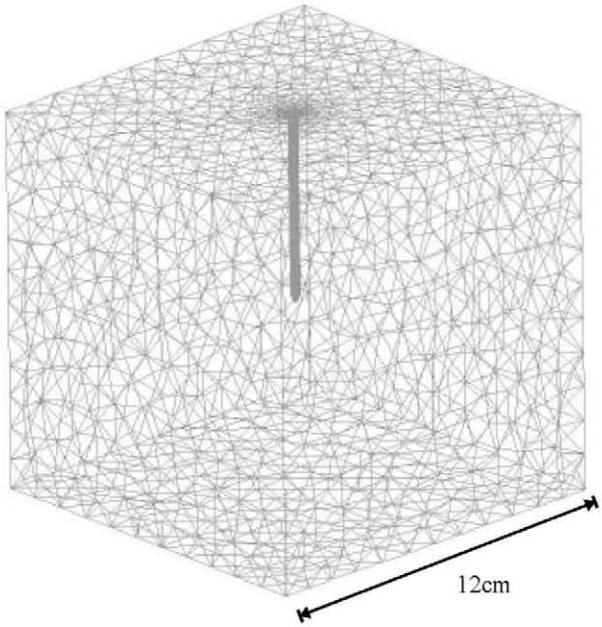
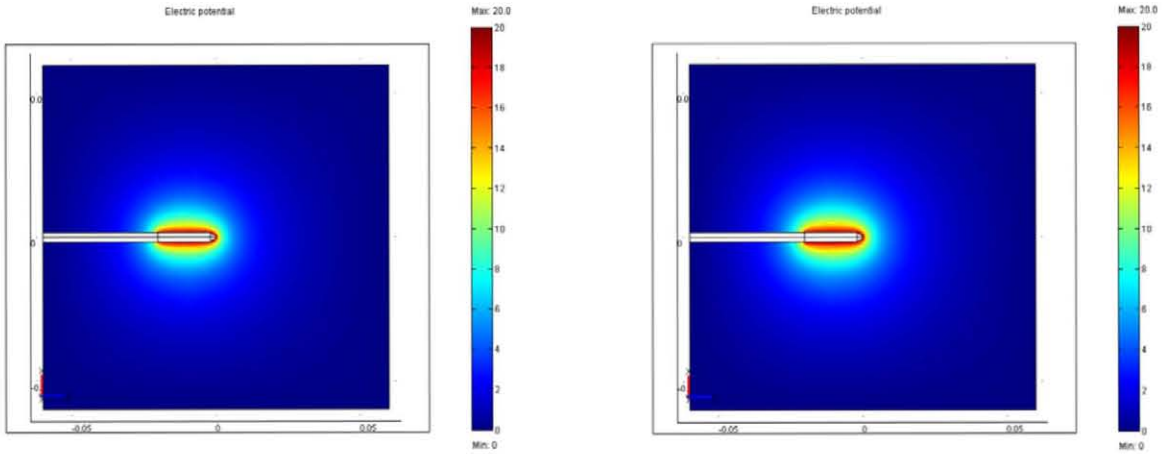


Figure 2. FEM model used for solving the problem

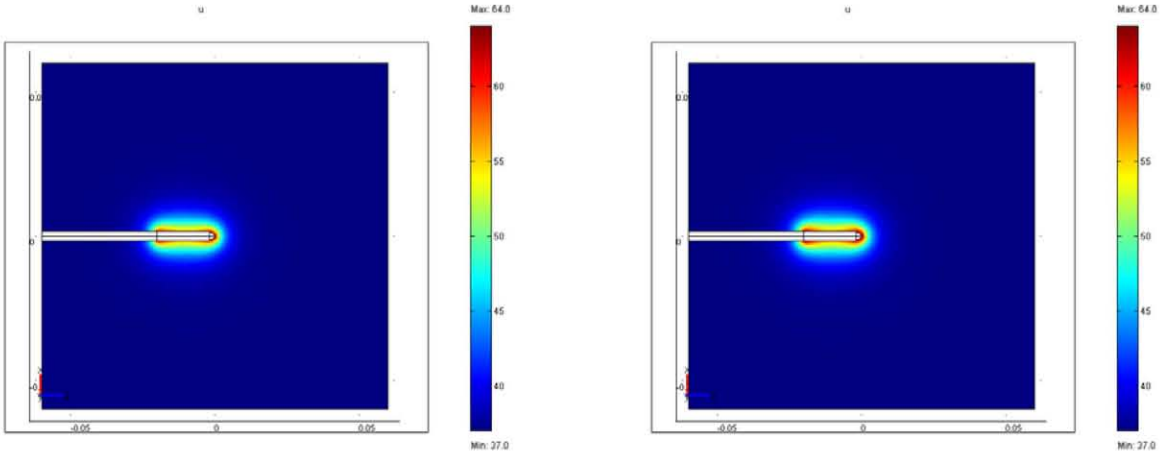
IV. RESULTS

In order to show the differences between the linear and the non-linear problem, the equations were solved both for constant electrical conductivity of liver and for temperature dependent according to equation (5). The shape of the distribution of the electric potential inside the computational domain does not change very much in the two cases (Figure 3), nor does the distribution of the final temperature (Figure 4).
However, the maximum temperature (calculated at the tip of the probe) is different in the two cases for the same voltage V_0 applied. Figure 5 shows that when the conductivity does not vary with temperature the maximum temperature is underestimated; this is especially true for higher probe voltages V_0. It is also clear from Figure 5 that the maximum temperature does not depend linearly on V_0.



(a) (b)

Figure 3. Distribution of electric potential in the tissue for (a) constant and (b) temperature dependent electrical conductivity



(a) (b)

Figure 4. Final (after 15min) temperature distribution in the tissue for (a) constant and (b) temperature dependent electrical conductivity

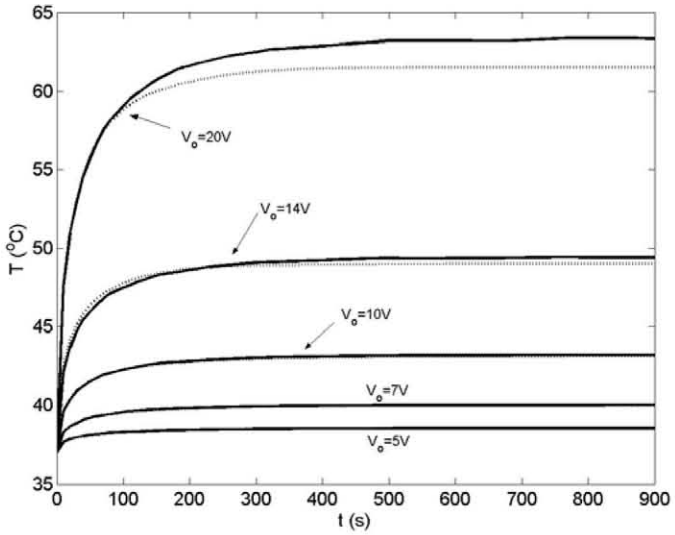


Figure 5. Time course of the temperature at the probe's tip for constant (dashed lines) and temperature dependent (solid lines) electrical conductivity at various source voltages

REFERENCES

[1] D. Haemmerich, "Tissue Ablation", in *Encyclopedia of Medical Devices and Instrumentation*, (John G. Webster, ed.), 2nd Edition, vol. 6, pp. 362-379, John Wiley & Sons, Hoboken, New Jersey, 2006

[2] S. Tungjitkusolmun, S. T. Staelin, D. Haemmerich, Tsai Jang-Zern, Cao Hong, J. G. Webster, F. T. Lee Jr., D. M. Mahvi, V.R. Vorperian, "Three-dimensional finite-element analyses for radio-frequency hepatic tumor ablation", *IEEE Trans. Biomed. Eng.*, vol. 49, no. 1, pp. 3-9, 2002

[3] H. H. Pennes, "Analysis of tissue and arterial blood temperatures in the resting human forearm", *J. Appl. Physiol.*, vol. 1, pp. 93-122, 1948

[4] I. Chang, "Finite Element analysis of hepatic radiofrequency ablation probes using temperature-dependent electrical conductivity", *Biomedical Engineering Online*, vol. 2, 12, 2003

[5] I. A. Chang and U. D. Nguyen, "Thermal modeling of lesion growth with radiofrequency ablation devices", *Biomedical Engineering Online*, vol. 3, 27, 2004

TRANSMIT POWER CONTROL IN MOBILE COMMUNICATIONS AND ITS POTENTIAL FOR A REDUCTION OF EMF EXPOSURE

MICHAEL A. BALDAUF, SANDRA KNÖRZER, THORSTEN KAYSER, AND WERNER WIESBECK

INSTITUT FÜR HÖCHSTFREQUENZTECHNIK UND ELEKTRONIK, UNIVERSITÄT KARLSRUHE (TH), KAISERSTR. 12, 76131 KARLSRUHE, GERMANY

Abstract

The application of transmit power control in mobile communications allows a decrease of the maximum output power to a lower level per link. Technical reasons to utilize transmit power control are the reduction of co-channel interference and an increase in the battery lifetime of the mobile terminal. Considering the well known COST-Hata wave propagation model the steady state transmit powers for base and mobile stations in typical scenarios are calculated. It is shown that for GSM base stations the optional transmit power control has only a small impact onto the human exposure to electromagnetic fields. In contrast to this the transmit power of a GSM mobile phone can be lowered clearly compared to the maximum output power, when applying transmit power control. For UMTS mobile phones there is even a higher potential for an exposure reduction.

Introduction

In mobile radio networks there are basically two sources of electromagnetic fields (EMF). On the one hand there is a fixed base station which transmits a signal with a constant level at all times to allow the mobile station to identify it. The more users there are in a cell the more transmit power is needed to serve the customers with user specific information. On the other hand, there is a mobile station which transmits generally only when the user actively uses the mobile phone e.g. by having a voice connection.

For the far field exposure due to base stations the exposure can be conveniently described by the electric field strength (E) or the power density (S). For the human head held close to a mobile phone there is a strongly varying near field over different tissue types. Therefore, a determination of the specific absorption rate (SAR) is necessary. The exposures which encounter in real life due to base and mobile stations are very different compared to the limit values. Safety distances to base stations based on the ICNIRP Guidelines [1] are typically just a few meters [2]. Thus, the exposures due to base stations are usually well below the limits. However, concerning the exposure to mobile phones some phones are quite close to the SAR limit [3]. In conformance tests the mobile phone transmits with it's maximum transmit power to simulate worst case conditions [4].

The possibility of transmit power control (TPC) allows a reduction of the transmit power. Hence, TPC is a means to reduce interference in mobile cellular networks. Additionally there is a remarkable increase in battery lifetime for mobile terminals. In 3rd generation's UMTS networks TPC at the mobile terminal is a must in order to allow a reception of all users with the wanted signal to noise plus interference ratio (SNIR) at the base station. This paper deals with the potential of the exposure reduction of TPC.

Network layout

In the simulations a simplified hexagonal network layout with three sector antennas in each hexagon is considered. Base stations are placed at the centers of the hexagons (cf. Fig. 1). There are two rings of hexagons surrounding a center hexagon to take the exposure of surrounding cells into account. The technical configuration is the same for all base stations. The exposure is evaluated for the center hexagon. Therefore, this hexagon is overlayed with a regular grid of about 100 000 equidistant points.

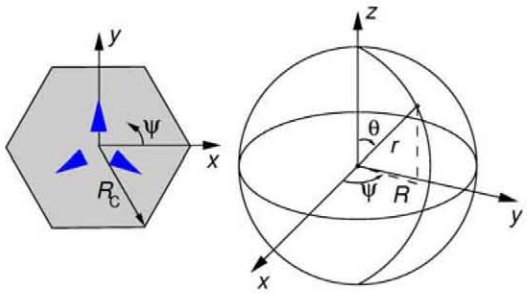


Fig. 1: Left: Hexagonal cell showing the orientation of the sector antennas (arrows). Right: Convention for angles in a spherical coordinate system.

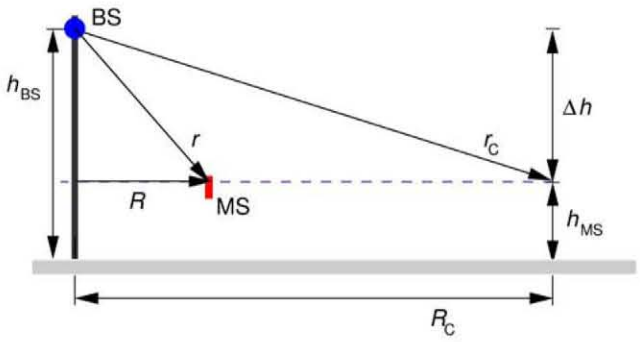


Fig. 2: Exposure scenario.

Exposure Scenario

Fig. 2 shows the considered exposure scenario in a side view. All base stations (BS) are mounted at a height h_{BS}, the mobile stations (MS) are at a height h_{MS} = 1.5 m. The horizontal separation of the MS to the BS is given by the distance R. The variable R_C denotes the cell radius, which is defined in Fig. 1. In the simulations cell radii of R_C = 1 km and R_C = 6.3 km are regarded. Since for smaller cell sizes the antennas are typically mounted at a lower height the antenna heights h_{BS} of the BS are chosen to be dependent on the cell radius R_C. For the smaller cell radius (R_C = 1 km) the antenna height h_{BS} = 12.6 m for the larger cell radius (R_C = 6.3 km) h_{BS} = 41 m.

At the BS there are three Kathrein 742212 antennas [5] mounted with $\psi = \{90°, 210°, 330°\}$ to cover three sectors (cf. Fig. 1). The pattern of the antenna with a gain G_{BS} = 18 dBi is shown in Fig. 3. For the simulation the pattern is smoothed and limited to take an increased field strength due to multipath propagation into account. To concentrate more energy on the ground a declination of the antenna pattern can be done electrically. The considered sector antennas are tilted down slightly. The downtilt angle is chosen in such a manner that the direction where the antenna has its half power beamwidth above the main beam direction is directed at the height of a MS's antenna at the cell radius R_C.

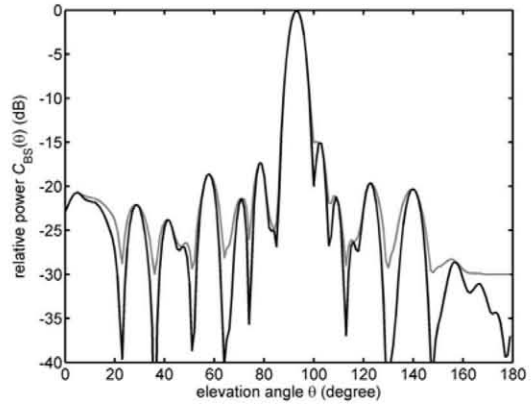


Fig. 3: Elevation pattern of Kathrein's 742212 with 3° electrical downtilt. Shown is the pattern $C_{BS}(\theta)$ for one polarization of the X-polarized antenna. Dark line: unmodified manufacturer data; light line: smoothed and limited pattern data.

Emission versus Exposure

A measure of the biological relevance of electromagnetic fields is the exposure. Transmitters are often classified by their transmit power (emission). In situations where there is no change in the loss between transmitter and the

human body the change in transmit power is directly proportional to the change in exposure. An example is a mobile station held close to the head. As long as the terminal is not moved the exposure is proportional to the transmit power. However, moving e.g. the mobile terminal further away from the head will typically lead to a lower absorption loss of the head. As a result of this, the transmit power can be lowered. Furthermore, the distance to the head is increased. Both facts will lead in sum to an exposure that is lower compared to the situation where the mobile phone is closer to the human head. However, the change in exposure is no longer directly proportional to the change in emission.

Considering two cell radii R_C with different BS antenna heights h_{BS} yields different path losses in the scenarios. Since the exposure is in the far field it can be expressed as power density S. Comparing the power density S allows a direct comparison of the exposure. In contrast to this, for the human exposure due to the mobile phone a constant position of the phone to the head will be assumed. Therefore, the change in exposure is then directly proportional to the change in transmit power.

Path loss model

In order to derive the exposure a knowledge of the path loss L between all sources of EMF and the points that are defined for an evaluation is necessary. The path loss model chosen for the simulations is the well known COST-Hata model [6]. The model takes a correction term for open areas into account [7]. For this reason, the building development can be described by a parameter b. This parameter ranges from $b = 0...1$, $b = 0$ corresponds to an open area whereas $b = 1$ corresponds to an urban area. For more information about the parameter b see [8]. The uplink and downlink frequencies are chosen to be $f = 2$ GHz. A deviation between uplink and downlink frequency is not considered since the frequency difference is usually small in prevalent frequency division duplex (FDD) systems, and therefore has only a negligible influence on the path loss. The isotropic path loss L_i according to the COST-Hata model is given by:

$$\frac{L_i}{\mathrm{dB}} = 158.16 - 13.82 \log\left(\frac{h_{BS}}{\mathrm{m}}\right) + \left(44.9 - 6.55 \log\left(\frac{h_{BS}}{\mathrm{m}}\right)\right) \log\left(\frac{R}{\mathrm{km}}\right) + 32.52\, b \tag{1}$$

where use of the fixed MS antenna height and frequency has been made. Formula (1) gives the path loss for isotropic antennas, therefore the name isotropic path loss L_i. Using directional antennas will change the path loss to:

$$\frac{L}{\mathrm{dB}} = \frac{L_i}{\mathrm{dB}} + \frac{G_{BS} C_{BS}^2(\theta_{BS}, \psi_{BS})}{\mathrm{dB}} + \frac{G_{MS} C_{MS}^2(\theta_{MS}, \psi_{MS})}{\mathrm{dB}} \tag{2}$$

Herein G_{BS} and G_{MS} are the gains of the base and mobile stations, respectively. The gains have to be weighted by the square of the antenna patterns C^2. Since the patterns depend on the viewing angle different indices for the angles θ and ψ are used for the base and mobile station. Depending on the gains G and patterns C the path loss L can be larger or smaller than the isotropic path loss L_i. Typically the base station antennas are directed in order to radiate much energy into directions were the isotropic path loss L_i is large. For the antenna of the mobile station an isotropic radiator is assumed, therefore, the last term in (2) vanishes for the calculation of the path loss L.

For distances close to the base station (1) might yield path losses which are smaller than for a free space propagation (unobstructed line of sight). If this happens the path loss in the model is replaced by the value of the path loss for free space condition.

Path Loss in a Cell

Four cell types were considered for an evaluation of the path loss L in a cell. These are:

- a large urban cell
- a small urban cell
- a large rural cell
- a small rural cell

The term “large” refers to a cell size of $R_C = 6.3$ km, whereas the term “small” refers to a cell size of $R_C = 1$ km. For the urban cell the parameter b in (1) is chosen to be $b = 0.8$ for the rural cell $b = 0.2$. Figs. 4-7 show the distribution of the path losses in the four types of regions for different antenna types. Fig. 4 shows the probability density function (PDF) of the path loss according to (1) with $b = 0.2$. Figs. 5-7 include a log-normal fading with a standard deviation $\sigma = 7$ dB. The left hand sides (LHS) of the figures show the PDF for the larger cell sizes whereas the right hand sides (RHS) show the PDF for the smaller cell sizes. Whereas Figs. 4 and 5 refer to an isotropic antenna at the BS the Figs. 6 and 7 regard the Kathrein 742212 as BS antenna. Comparing

Figs. 4 and 5 shows that considering a log-normal fading shows broader distribution of the PDF. The installation of sector antennas with a high gain will allow a significant reduction of the path loss (compare Figs. 5 and 6). Increasing the building development would yield higher path losses (cf. Fig. 7).

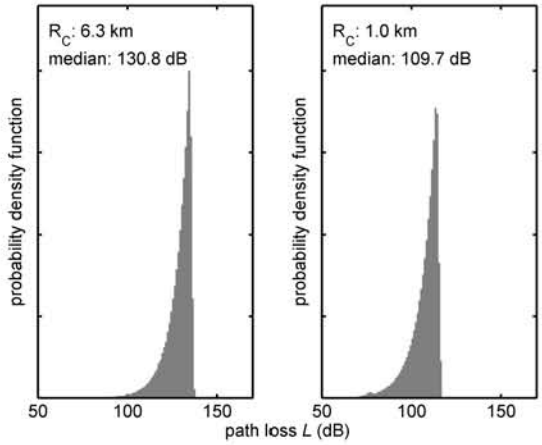


Fig. 4: PDF of the isotropic path loss in a rural region. Parameters: $b = 0.2$. LHS: $R_C = 6.3$ km, RHS: $R_C = 1$ km. No log-normal fading.

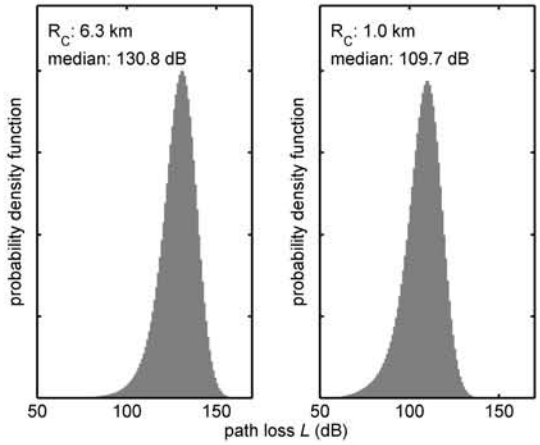


Fig. 5: PDF of the isotropic path loss in a rural region. Parameters: $b = 0.2$. LHS: $R_C = 6.3$ km, RHS: $R_C = 1$ km. Log-normal fading ($\sigma = 7$ dB).

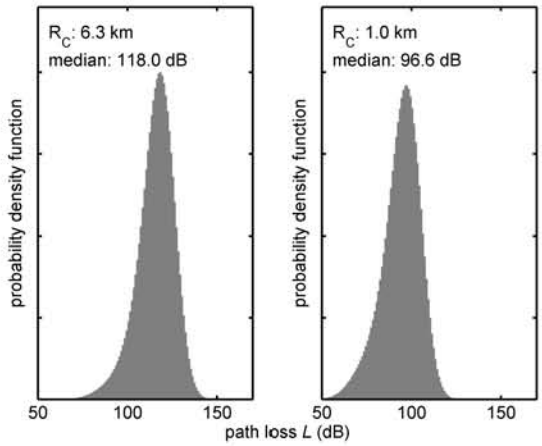


Fig. 6: PDF of the path loss for the considered directional antenna in a rural region. Parameters: $b = 0.2$. LHS: $R_C = 6.3$ km, RHS: $R_C = 1$ km. Log-normal fading ($\sigma = 7$ dB).

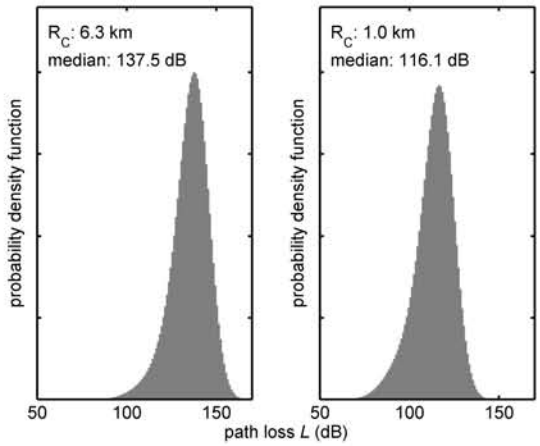


Fig. 7: PDF of the path loss for the considered directional antenna in an urban region. Parameters: $b = 0.8$. LHS: $R_C = 6.3$ km, RHS: $R_C = 1$ km. Log-normal fading ($\sigma = 7$ dB).

Link budget

To decode a signal correctly a minimum required signal quality must be reached. This quality can be given in general as a SNIR (signal-to-noise-plus-interference-ratio). The noise is thermal noise and can't be reduced below a certain value which is dependent on the system temperature and bandwidth. For CDMA systems (e.g. UMTS) where a lot of users share the same frequency at the same time interference has to be taken into account. Interference can be interpreted as noise and vice versa.

GSM systems use frequency division multiple access (FDMA) and time division multiple access (TDMA) to separate users. Assuming sufficient carriers are available the effect of interference needs not to be considered. To determine the required transmit powers at the base and mobile stations it is sufficient to regard the necessary received power P_R per user at the receiving end in combination with the path loss. P_R is independent of the network load and given by the transmit power P_T minus the path loss L between the transmitter and the receiver. Knowing the path loss the minimum required P_T can be determined.

For the determination of the maximum path loss L and therefore also for the mandatory channel no log-normal fading is considered. The transmit power of the base and mobile stations are increased by 20 dB to account for additional propagation losses as the absorption of energy in the human body and effects of small-scale fading. For simplicity fading is not explicitly considered in the determination of the transmit powers. For the mobile stations fading is considered in a later step.

The transmit power of the BS is labeled by $P_{T,BS}$ and the transmit power of the MS by $P_{T,MS}$.

TPC at the BS

If there is no TPC implemented the PDF of the received signal has the same shape as the path loss. Power control can be used only for dedicated channels which don't have to be received at all MS.

The channel configuration of the considered GSM system is shown in Fig. 8. Shown are two carriers which are allocated to different frequencies around $f = 2$ GHz. On the LHS there is the BCCH carrier. Each of the eight bins corresponds to one time slot. Via this carrier information about the cell is transmitted in one slot. The seven other time slots on this carrier are reserved for additional signaling purposes or e.g. SMS services. If the information of these slots is not needed they are filled up with dummy bits and transmitted with full power. This carrier can't be power controlled. Active users having a voice connection are put on another carrier on which power control is available. The transmit power in a power controlled slot is decreased by ΔPC compared to the power of the BCCH carrier. The maximum power reduction which is possible is given by ΔPC_{max}. The simulations were done assuming a varying range of the parameter ΔPC_{max}.

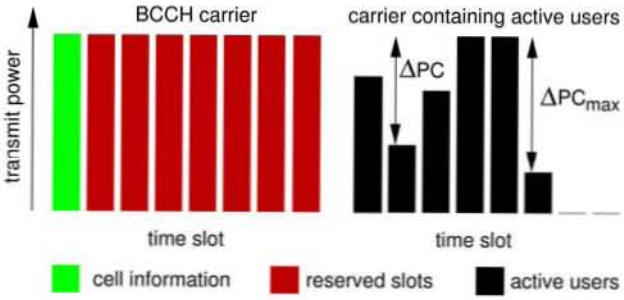


Fig. 8: Channel configuration of the considered GSM system.

In the following three different numbers of carriers N are investigated. The numbers chosen are $N = 1$, 4 and 6. In the case of $N = 1$ only the BCCH carrier is transmitting. $N = 4$ and 6 correspond to typical channel configurations. The required user densities n for these three cases are:

- $n = 0$ ($N = 1$)
- $n = 0.70$ /km^2 ($R_C = 6.3$ km, $N = 4$)
- $n = 1.16$ /km^2 ($R_C = 6.3$ km, $N = 6$)
- $n = 27.71$ /km^2 ($R_C = 1$ km, $N = 4$)
- $n = 46.18$ /km^2 ($R_C = 1$ km, $N = 6$)

Whereas in the large cell ($R_C = 6.3$ km) the considered number of carriers can be filled with small user densities much higher user densities are needed for the smaller cell size ($R_C = 1$ km).

Figs. 9-14 show the transmit power $P_{T,BS}$ per sector and the average power density S_{avg} versus the maximum possible power reduction ΔPC_{max}, respectively, for three cases. There are no results given for the case of the large urban cell. For this case the path loss would be too high for a lot of mobile stations to reach the base stations.

If there is only the mandatory BCCH carrier on air TPC would yield no power reduction since this carrier can't be power controlled ($N = 1$ in the figures). If there are active users in time slots which can be power controlled the total transmit power fed into the sector antenna can be lowered typically by just 3 to 4 dB. A higher value of ΔPC_{max} allows lower transmit powers. Choosing ΔPC_{max} larger than 10 dB shows no further positive effect in terms of transmit power reduction.

The more channels that are in use, the higher is the reduction of the transmit power when using TPC. The increase from 4 carriers to 6 carriers shows no significant effect. A change in transmit power within one configuration is directly proportional to the change in exposure (compare the figures in one row).

Furthermore, the results show that there is no one-to-one equivalence of emission (transmit power) and exposure

(power density). In the case of the rural cell the transmit power of the BS $P_{T,BS}$ in the large cell (cf. Fig. 9) is much higher than in the smaller cell (cf. Fig. 11). However, the exposures in both network configurations are almost the same (compare Figs. 10 and 12). In the small urban cell the transmit power is much higher than in the small rural cell but the exposure is higher by just a small amount. This is due to the fact that in the urban network not only the transmit power is higher but also the path loss is much higher than in the rural case.

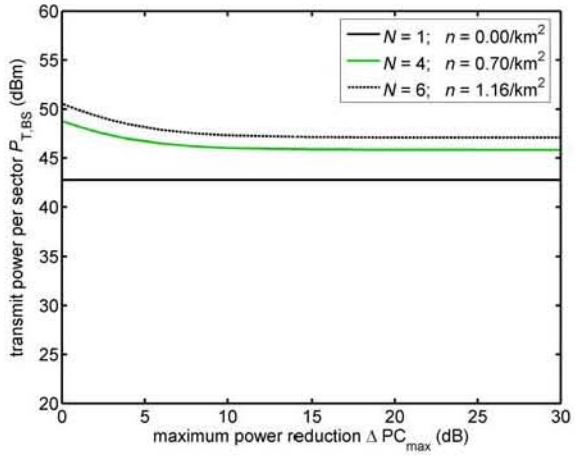


Fig. 9: Transmit power per sector versus the maximum power reduction. Parameters: R_C = 6.3 km, b = 0.2 (rural area).

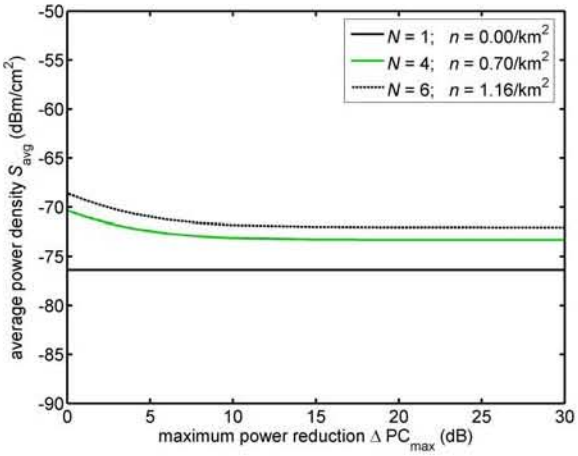


Fig. 10: Average power density versus the maximum power reduction. Parameters: R_C = 6.3 km, b = 0.2 (rural area).

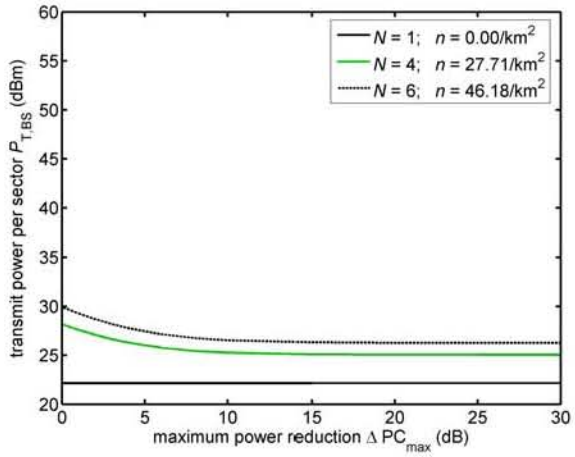


Fig. 11: Transmit power per sector versus the maximum power reduction. Parameters: R_C = 1 km, b = 0.2 (rural area).

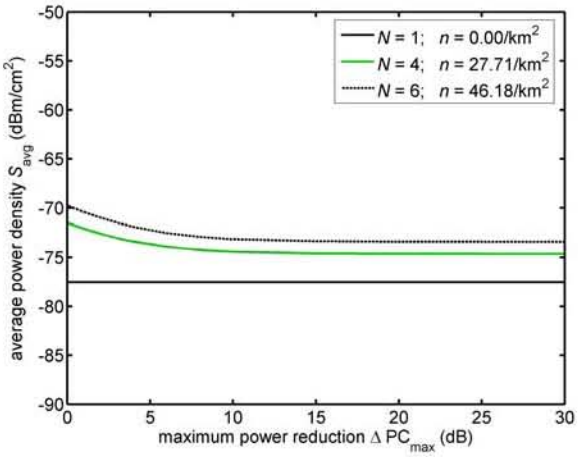


Fig. 12: Average power density versus the maximum power reduction. Parameters: R_C = 1 km, b = 0.2 (rural area).

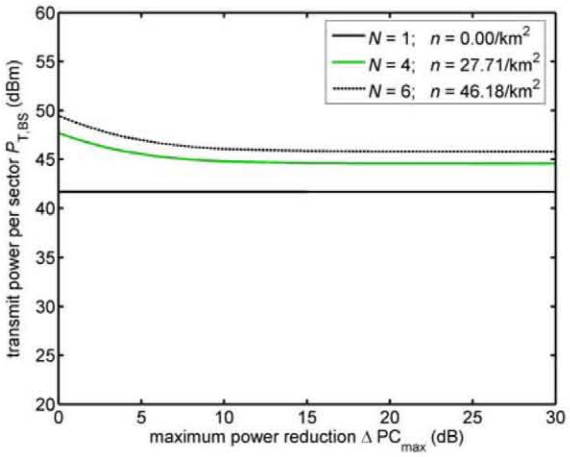


Fig. 13: Transmit power per sector versus the maximum power reduction. Parameters: R_C = 1 km, b = 0.8 (urban area).

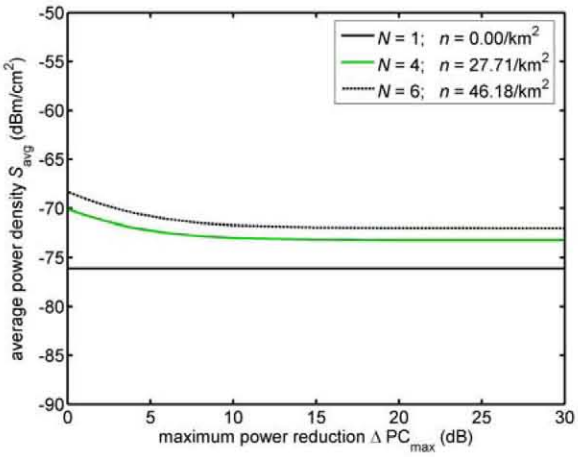


Fig. 14: Average power density versus the maximum power reduction. Parameters: R_C = 1 km, b = 0.8 (urban area).

For UMTS there are also some channels which are transmitted at all times with a constant level. As in GSM, user specific channels can be also power controlled. Simulations have shown that the results for UMTS are very similar to those shown for GSM.

TPC at the MS

The mobile station can adjust it's transmit power in a given range. For GSM 1800 mobile phones the transmit power $P_{T,MS}$ can be adjusted according to the specifications from 0 dBm to 30 dBm [9]. Fig. 15 shows the transmit power of the mobile station when there is no restriction on power control. In the large cell there are some MSs which would transmit with a very high transmit power (LHS of Fig. 15). In practice the maximum TPC is restricted to 30 dBm [9] (LHS of Fig. 16). Since 20 dB are added to the transmit powers as a safety margin there might be a quality decrease for MSs demanding a higher transmit power than possible. MSs that would need more than 50 dBm of transmit power definitely can't be served due to their restriction of the maximum output power of 30 dBm. However, this is only a relatively small part. Comparing large and small cell sizes shows that the transmit power in the smaller cell can be lowered by about 20 dB. Furthermore, comparing the Figs. 15 and 16 it is clear that the implemented lowest transmit power for MSs in GSM networks is not exposure optimized since a lot of MSs would be able to lower their transmit power below $P_{T,MS}$ = 0 dBm in small cells.

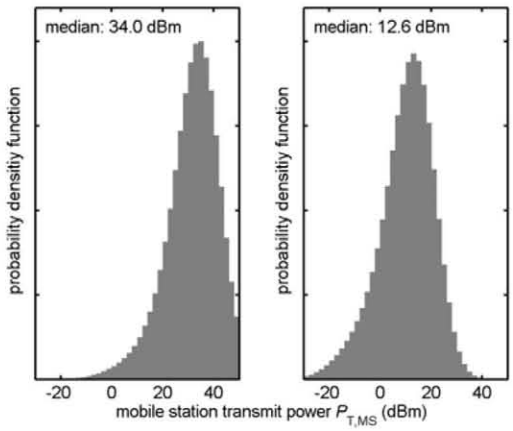


Fig. 15: PDF of the mobile station's transmit power in a rural GSM network. The transmit power can reach arbitrary values. Parameters: b = 0.2; LHS: R_C = 6.3 km, RHS: R_C = 1 km.

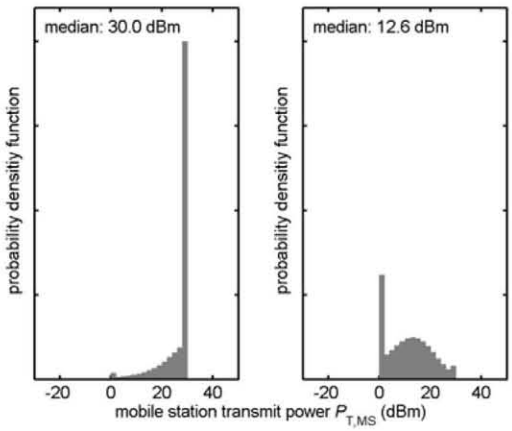


Fig. 16: PDF of the mobile station's transmit power in a rural GSM network. The transmit power can be in the range of the specified TPC. Parameters: b = 0.2; LHS: R_C = 6.3 km, RHS: R_C = 1 km.

For UMTS mobile phones the maximum output power typically used for voice transmissions is $P_{T,MS}$ = +21 dBm. Since every transmitting mobile station produces interference an optimum received power at the base station is a must. The specifications [10] demand a minimum transmit power of $P_{T,MS}$ = -50 dBm or lower. Fig. 17 shows the chosen transmit power of the MS $P_{T,MS}$ if there is no restriction of the TPC. Setting a lower limit of $P_{T,MS}$ = -50 dBm shows that a very small part of the mobile stations in the small cell is then transmitting with a higher power than necessary (cf. Fig.18). Since a transmit power that is too high would cause interference at the BS this situation should be avoided. Therefore, the range of the TPC in UMTS should be extended even further.

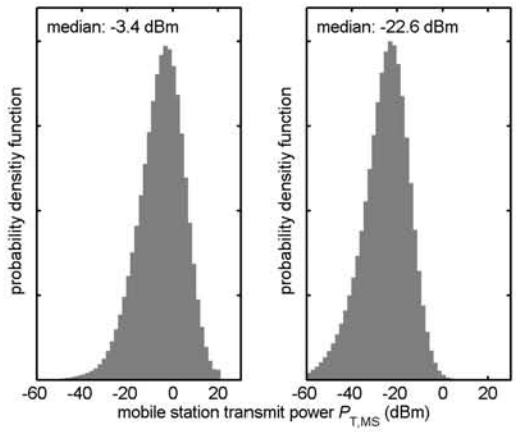


Fig. 17: PDF of the mobile station's transmit power in a rural UMTS network. The transmit power can reach arbitrary values. Parameters: b = 0.2; Channel model: Veh. A, MS speed = 3 km/h. LHS: R_C = 6.3 km, RHS: R_C = 1 km.

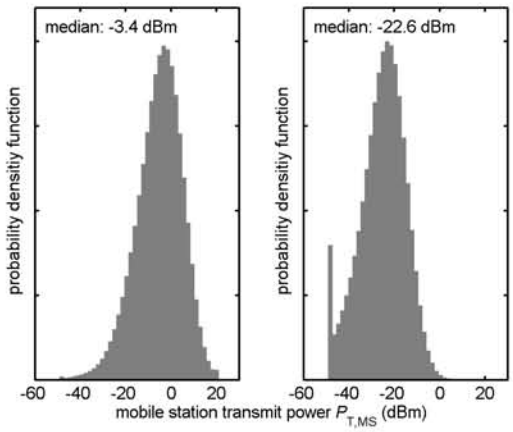


Fig. 18: PDF of the mobile station's transmit power in a rural UMTS network. The transmit power can be lowered only to -50 dBm. Parameters: b = 0.2; Channel model: Veh. A, MS speed = 3 km/h. LHS: R_C = 6.3 km, RHS: R_C = 1 km.

Comparing the results for GSM and UMTS suggests that UMTS MSs need much lower transmit powers than GSM MSs. The reason for this is that typical configurations of the MSs are assumed. Since interference due to the reception of multiple MSs at the same frequency and time is not a dominant problem at GSM BSs, network operators tend to choose transmit powers at the MS which are clearly higher than those needed at a certain instant of time. This is due to fact that the implemented power control can only react very slowly on changing propagation conditions. In contrast to this interference in UMTS networks at the BS is really a problem. Therefore, network operators have to choose the MS's transmit power as low as possible. Fast TPC at the MS helps to adjust the transmit power every 1/1500 seconds. For this reason there is no need for adding a large security factor to account for fading effects as long as the MS is moving with a low speed.

Conclusion

Interference reduction and an increase in battery lifetime are technical reasons to implement transmit power control. The reduction of the human exposure to electromagnetic fields is rather a side effect. It is shown that the decrease in exposure using power control at the base station is rather small since the base station has to transmit site specific information in a broadcast mode at all times. From an exposure point of view a maximum power decrease of 10 dB per power controlled link is sufficient. A larger power reduction will not help to decrease the exposure to electromagnetic fields. Taking advantage of transmit power control at the mobile station the transmit power and, therefore, the exposure due to the mobile phone can be lowered clearly by several orders of magnitude. Whereas the power control range of UMTS mobile phones corresponds in a very good manner to the path loss the power control range of GSM phones is clearly not exposure optimized.

References

[1] ICNIRP, “Guidelines for limiting exposure to time-varying electric, magnetic, and electromagnetic fields (up to 300 GHz)”, *Health Physics*, vol. 74, no. 4, pp. 494-522, 1998

[2] M.A. Baldauf, A. Herschlein, W. Sörgel, W. Wiesbeck, “Safety Distances in Mobile Communications”, *Proceedings of 2nd International Workshop on Biological Effects of Elektromagnetic Fields*, pp. 148-156, Rhodes, Greece, Oct. 2002

[3] http://www.mobile-phones-uk.org.uk/sar.htm

[4] *IEEE Recommended Practice for Determining the Peak Spatial-Average Specific Absorption Rate (SAR) in the Human Head from Wireless Communications Devices: Measurement Techniques*, IEEE Std. 1528-2003, Dec. 2003

[5] KATHREIN Werke KG, Available Online, www.kathrein.de

[6] COST 231, Digital mobile radio towards future generation systems, *European Commission, Directorate General XIII*, EUR 18957, 1999

[7] M. Hata, “Empirical Formula for Propagation Loss in Land Mobile Services”, *IEEE Transactions on Vehicular Technology*, vol. 29, pp. 317-325, 1980

[8] M. A. Baldauf, S. Knörzer, W. Sörgel, and W. Wiesbeck, “Cell Splitting and Exposure in GSM networks”, *13th International Conference on Telecommunications*, published on CD-ROM, Madeira, May 2006

[9] *3rd Generation Partnership Project; Technical Specification Group GSM/EDGE Radio Access Network; Radio transmission and reception (Release 1999)*, Technical Specification, 3GPP TS 05.05, 2003

[10] *3rd Generation Partnership Project; Technical Specification Group Radio Access Networks; User Equipment (UE) radio transmission and reception (FDD) (Release 4)*, 3GPP TS 25.101, 2004

ELECTRIC FIELD ANALYTICAL FORMULAS FOR SINGLE-CIRCUIT POWER LINES WITH TRIANGULAR CONDUCTORS' ARRANGEMENT

A. TZINEVRAKIS **D. TSANAKAS** **E.MIMOS**

Tsanakas@ee.upatras.gr

DEPARTMENT OF ELECTRICAL AND COMPUTER ENGINEERING
UNIVERSITY OF PATRAS
26500, RION, GREECE

Abstract
The electric field produced by electric power lines is usually calculated with the use of numerical methods. However, the analytical calculation of the electric field is preferable, because it leads to a mathematical expression, which shows the field's dependencies from all the line parameters.

Initially, a method to derive the analytical formulas of the intensity of the electric field produced by electric power lines, is presented in this paper. This method is based on the analysis of the intensity of the electric field into the sum of two multipole expansions and in the use of double complex numbers for the simplification of the mathematical expressions. Due to the asymmetry of conductors' charges, they are analyzed in their symmetrical components. Afterwards, accurate analytical formulas of the intensity of the electric field for simple circuit power lines with conductors in triangular arrangement are given, which are valid at any point in the vicinity of lines. Beyond the accurate formulas, simpler approximate formulas are presented, which give the electric field with known precision.

1 Introduction

During the last 25 years the electric and magnetic fields are considered more and more as environmental factors. The International Commission on Non–Ionizing Radiation Protection (ICNIRP) published in 1998 the guidelines [1]. In these guidelines, the limit values are 5kV/m and 100μT for the public exposure and 10kV/m and 500μT for the occupational exposure. The World Health Organization (WHO) and the European Union (E.U.) have adopted the limits of ICNIRP [2,3]. These limits are included in the national legislations of the most countries in the E.U.

In the present paper analytical formulas are developed for the calculation of the intensity of the electric field in the vicinity of single circuit power lines. Corresponding analytical formulas for the calculation of magnetic flux density were published in [4]. The analytical formulas provide the advantage of easy and precise calculation of the field intensities and of a simpler parametrical investigation for evaluating the effect of various parameters, without the use of numerical methods. Therefore, they are appropriate for the assessment of the public exposure, e.g. in the frames of epidemiological studies.

2 Calculation procedure

2.1 Electric field produced by power lines

Figure 1 shows the model of a simple circuit power line and a point of interest P for the calculation of the intensity of the electric field. It is considered that the line route is straight and that its length is very big in comparison with the distances between the conductors and the distances of conductors from the ground. The three conductors in figure 1 bring charges $\underline{Q}_1$, $\underline{Q}_2$ and $\underline{Q}_3$, which are sinusoidal varying in time, while their distances from the point P are R_1, R_2 and R_3 respectively. The intensity of electric field $\underline{\mathbf{E}}_k$ in point P, produced by a conductor k, is given by

$$\underline{\mathbf{E}}_k = \frac{\underline{Q}_k}{2\pi\varepsilon_0}\left(\frac{1}{R_k^{'2}}\mathbf{R}_k^{'} - \frac{1}{R_k^{2}}\mathbf{R}_k\right) \tag{2.1}$$

where $\varepsilon_0 = \frac{1}{36\pi}10^{-9}\frac{A\cdot s}{V\cdot m}$ is the electric permittivity of free space, $\mathbf{R}_k$ the vector distance from the k conductor to the point P, $\mathbf{R}_k^{'}$ the vector distance from the image of the k conductor to point P and R_k, $R_k^{'}$ the modulus of vectors $\mathbf{R}_k$ and $\mathbf{R}_k^{'}$ respectively.

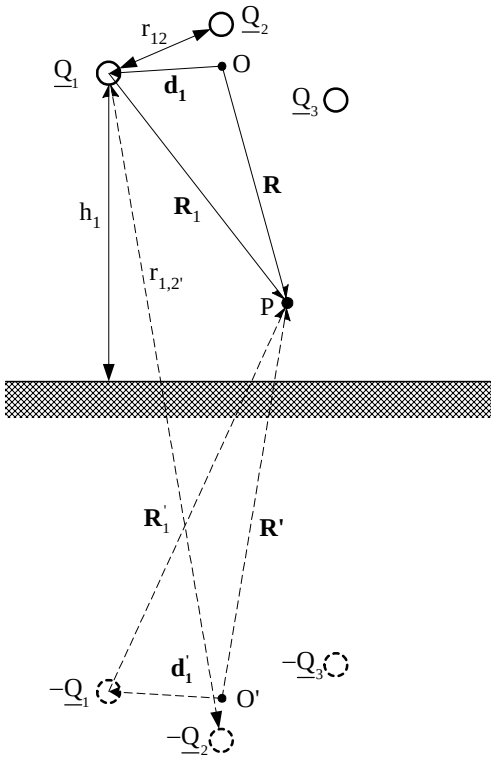


Figure 1. Model of a single circuit power line with the conductors' images

In the general case, a line with n conductors may be considered. Using the superimposition theorem, the intensity of electric field $\underline{\mathbf{E}}$, produced by the line is equal to the sum of the fields produced by each conductor separately,

$$\underline{\mathbf{E}} = \sum_{\kappa=1}^{n}\underline{\mathbf{E}}_k = \frac{1}{2\pi\varepsilon_0}\sum_{\kappa=1}^{n}\underline{Q}_k\left(\frac{1}{R_k^{'2}}\mathbf{R}_k^{'} - \frac{1}{R_k^{2}}\mathbf{R}_k\right) \Rightarrow$$

$$\underline{\mathbf{E}} = \frac{1}{2\pi\varepsilon_0}\sum_{\kappa=1}^{n}\underline{Q}_k\left(\frac{1}{\underline{\mathbf{R}}_k^{'}} - \frac{1}{\underline{\mathbf{R}}_k}\right) \tag{2.2}$$

Relation (2.2) is usually used for the numerical calculation of the intensity of the electric field. However, the summing operation doesn't allow this formula to be readily applied for the calculation of the electric field and makes it unsuitable for reaching general conclusions for the electric field properties and its dependencies on the various parameters of the line.

2.2 Double complex numbers and multipole expansions

The relations for the electric field vector are simplified if complex numbers are used for the representation of vector distances. On the other hand, complex numbers are used for the representation of sinusoidal varying quantities in time (phasors), such as conductors' charges, so finally double complex numbers are required. Book [5] contains the theoritical basis of double complex numbers, in [4] they are used for the calculation of magnetic flux density and in [6] to express the elliptically polarized vector of the electric field of light.

For the representation of space vectors the set of complex numbers C_1 is used, with the imaginary part j, for example $\mathbf{R}_k=x_k+jy_k$, while for the representation of sinusoidal varying quantities in time, the set C_2 with the imaginary part i is used, for example $\underline{Q}_k=Q_k e^{i\varphi_K}$.

Figure 1 shows that each conductor k may characterized by the vector distance $\mathbf{d}_k$ from the reference point O, which is a central point of the real conductors' system. The image of each conductor k may characterized by the vector distance $\mathbf{d}_k^{'}$ from the reference point O΄, which is a central point for the conductors' images' system. The points O and O΄ are close to but not necessarily the centers of the conductors' systems. Their choice is a matter of experience and is made in order to simplify the mathematical expressions.

Replacing $\mathbf{R}_k=\mathbf{R}-\mathbf{d}_k$ and $\mathbf{R}_k^{'}=\mathbf{R}^{'}-\mathbf{d}_k^{'}$ in (2.2), it becomes (2.3).

$$\underline{\mathbf{E}}=\frac{1}{2\pi\varepsilon_0}\sum_{k=1}^{n}\underline{Q}_k\left(\frac{1}{\overline{\mathbf{R}}^{'}-\overline{\mathbf{d}}_k^{'}}-\frac{1}{\overline{\mathbf{R}}-\overline{\mathbf{d}}_k}\right) \tag{2.3}$$

Using the well-known relations (2.4) in (2.3), the intensity of the electric field results as the sum of two multipole expansions, one from the real conductors' system and the other from the conductors' images' system, relation (2.5).

$$\left(\overline{\mathbf{R}}^{'}-\overline{\mathbf{d}}_k^{'}\right)^{-1}=\sum_{\lambda=1}^{\infty}\frac{\overline{\mathbf{d}}_k^{'\,\lambda-1}}{\overline{\mathbf{R}}^{'\,\lambda}} \tag{2.4a}$$

$$\left(\overline{\mathbf{R}}-\overline{\mathbf{d}}_k\right)^{-1}=\sum_{\lambda=1}^{\infty}\frac{\overline{\mathbf{d}}_k^{\,\lambda-1}}{\overline{\mathbf{R}}^{\lambda}} \tag{2.4b}$$

$$\underline{\mathbf{E}}=\frac{1}{2\pi\varepsilon_0}\sum_{k=1}^{n}\underline{Q}_k\left(\sum_{\lambda=1}^{\infty}\frac{\overline{\mathbf{d}}_k^{'\,\lambda-1}}{\overline{\mathbf{R}}^{'\lambda}}-\sum_{\lambda=1}^{\infty}\frac{\overline{\mathbf{d}}_k^{\,\lambda-1}}{\overline{\mathbf{R}}^{\lambda}}\right)\Rightarrow$$

$$\underline{\mathbf{E}}=\sum_{\lambda=1}^{\infty}\underline{\mathbf{E}}_{(\lambda)}^{'}+\sum_{\lambda=1}^{\infty}\underline{\mathbf{E}}_{(\lambda)} \tag{2.5}$$

The terms $\underline{\mathbf{E}}_{\lambda}^{'}$ and $\underline{\mathbf{E}}_{\lambda}$ are called λ order terms and are given by the relations (2.6)

$$\underline{\mathbf{E}}_{(\lambda)}^{'}=\frac{1}{2\pi\varepsilon_0}\cdot\frac{\underline{\mathbf{M}}_{\lambda}^{'}}{\overline{\mathbf{R}}^{'\lambda}} \tag{2.6a}$$

$$\underline{\mathbf{E}}_{(\lambda)}=-\frac{1}{2\pi\varepsilon_0}\cdot\frac{\underline{\mathbf{M}}_{\lambda}}{\overline{\mathbf{R}}^{\lambda}} \tag{2.6b}$$

where the factors $\underline{\mathbf{M}}_{\lambda}^{'}$ and $\underline{\mathbf{M}}_{\lambda}$ are called λ order moments for the conductors' images' system and the real

conductors' system respectively and are given by the relations (2.7).

$$\underline{\mathbf{M}}'_{\lambda} = \sum_{\kappa=1}^{n} \underline{Q}_k \, \underline{\mathbf{d}}'^{\,\lambda-1}_k \tag{2.7a}$$

$$\underline{\mathbf{M}}_{\lambda} = \sum_{\kappa=1}^{n} \underline{Q}_k \, \underline{\mathbf{d}}^{\,\lambda-1}_k \tag{2.7b}$$

The multipole expansion, which appears in relation (2.5), is a series of infinite terms, each inversely proportional to an increasing power of the distance and has been used in [4] and [7] for the calculation of magnetic field produced by electric power lines.

2.3 Analysis of charges in symmetrical components

The calculation of the conductors' charges is necessary in order to calculate the intensity of the electric field. In the case of a single circuit power line, figure 1, the conductors' charges $\underline{Q}_1$, $\underline{Q}_2$ and $\underline{Q}_3$ are given by the relations (2.8).

$$\underline{Q}_1 = \frac{\underline{D}_1}{D} \quad , \quad \underline{Q}_2 = \frac{\underline{D}_2}{D} \quad , \quad \underline{Q}_3 = \frac{\underline{D}_3}{D} \tag{2.8}$$

The terms $\underline{D}_1$, $\underline{D}_2$, $\underline{D}_3$ and D are calculated by the relations (2.9)

$$D_1 = \begin{vmatrix} V_1 & S_{12} & S_{13} \\ V_2 & S_{22} & S_{23} \\ V_3 & S_{32} & S_{33} \end{vmatrix} \quad , \quad D_2 = \begin{vmatrix} S_{11} & V_1 & S_{13} \\ S_{21} & V_2 & S_{23} \\ S_{31} & V_3 & S_{33} \end{vmatrix} \quad , \quad D_3 = \begin{vmatrix} S_{11} & S_{12} & V_1 \\ S_{21} & S_{22} & V_2 \\ S_{31} & S_{32} & V_3 \end{vmatrix} \quad , \quad D = \begin{vmatrix} S_{11} & S_{12} & S_{13} \\ S_{21} & S_{22} & S_{23} \\ S_{31} & S_{32} & S_{33} \end{vmatrix} \tag{2.9}$$

where V_1, V_2 and V_3 are the voltages of the conductors 1, 2 and 3 respectively, and

$$S_{ii} = \frac{\ln(2h_i/r_i)}{2\pi\varepsilon_0} \quad , \quad S_{ij} = S_{ji} = \frac{\ln(r_{i,j'} / r_{ij})}{2\pi\varepsilon_0} \quad (i=1,2,3 \text{ and } j=1,2,3) \tag{2.10}$$

The factors h_i, r_i, r_{ij} and $r_{i,j'}$ that appear in relation (2.10) are:
- h_i, distance of the conductor i from the ground
- r_i, radius of the conductor i
- r_{ij}, distance between the conductors i and j
- $r_{i,j'}$, distance between the conductor i and the j conductor's image.

Figure 1 shows, for example, three characteristic distances h_1, r_{12} and $r_{1,2'}$.

The conductors' charges $\underline{Q}_1$, $\underline{Q}_2$ and $\underline{Q}_3$ constitute an asymmetrical system, which impedes the calculation of the intensity of the electric field. The asymmetrical system of charges is analyzed in three symmetrical three phase systems, the positive, the negative and the zero sequence system, according to relation (2.11).

$$\begin{bmatrix} \underline{Q}_{(0)} \\ \underline{Q}_{(1)} \\ \underline{Q}_{(2)} \end{bmatrix} = \frac{1}{3} \cdot \begin{bmatrix} 1 & 1 & 1 \\ 1 & \underline{a} & a^2 \\ 1 & \underline{a}^2 & \underline{a} \end{bmatrix} \cdot \begin{bmatrix} \underline{Q}_1 \\ \underline{Q}_2 \\ \underline{Q}_3 \end{bmatrix} \tag{2.11}$$

where $\underline{Q}_{(0)}$, $\underline{Q}_{(1)}$, $\underline{Q}_{(2)}$ are the zero, the positive and the negative sequence charge respectively and $\underline{a} = e^{i2\pi/3}$.

The intensity of the electric field is calculated for each one of the components of charges separately and the final accurate formulas arise from the superimposition of the results.

3 Electric field of single circuit power lines with conductors in triangular arrangement

3.1 Accurate formula of the electric field

Figure 2 shows a single circuit line with the conductors placed on the corners of an equilateral triangle. The voltages of the three conductors constitute a symmetrical system and are given by relation (3.1).

$$V_a = V\angle 120^0 \quad , \quad V_b = V\angle 0^0 \quad , \quad V_c = V\angle -120^0 \tag{3.1}$$

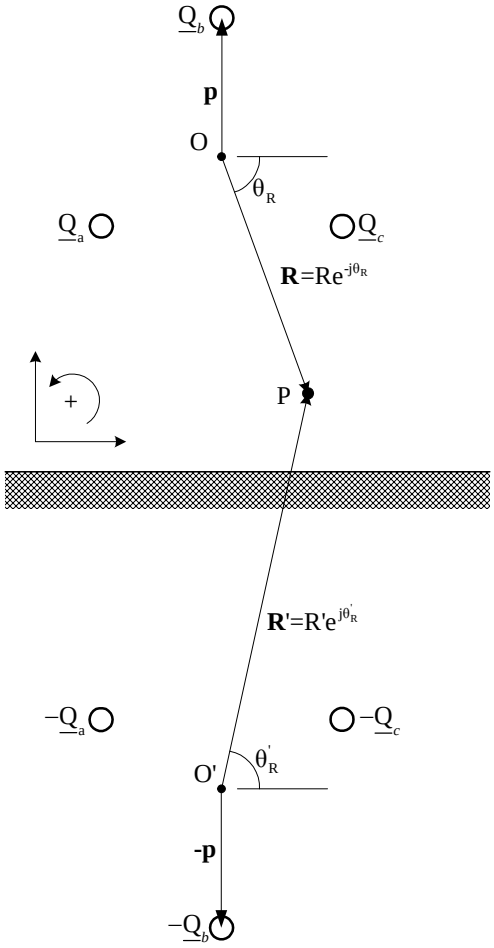


Figure 2. Model of a single circuit power line with the conductors placed on the corners of an equilateral triangle

Choosing the center of the arrangement as the reference point for both the real conductors' system and the conductors' images' system, as shown in figure 2, the distances of the conductors from these points are given in (3.2).

$$\mathbf{d}_a = \mathbf{p}e^{j\frac{2\pi}{3}} \quad , \quad \mathbf{d}_b = \mathbf{p} \quad , \quad \mathbf{d}_c = \mathbf{p}e^{-j\frac{2\pi}{3}} \tag{3.2a}$$

$$\mathbf{d}'_a = \mathbf{p}e^{j\frac{\pi}{3}} \quad , \quad \mathbf{d}'_b = -\mathbf{p} \quad , \quad \mathbf{d}'_c = \mathbf{p}e^{-j\frac{\pi}{3}} \tag{3.2b}$$

where $\mathbf{p}=jp$ is the distance vector between the reference point O and the upper conductor, as shown in figure 2.

Due to $\mathbf{d_k} \neq \mathbf{d}'_k$, the moments $\underline{\mathbf{M}}_\lambda$ and $\underline{\mathbf{M}}'_\lambda$, which are given in relations (2.7), are different,

$$\underline{\mathbf{M}}_\lambda \neq \underline{\mathbf{M}}'_\lambda \tag{3.3}$$

From relation (3.3) results that the real conductors' system is calculated separately from the conductors' images' system.

The conductors' charges are calculated through relations (2.8)-(2.10) and the assymetrical system that results is analyzed in its symmetrical components according to relation (2.11). For all the changes of the distance between the conductors as well as the height h from the ground of the real conductors, it results that the negative sequence charge is practically zero($Q_{(2)}$=0) and that the charges' angles for the positive and zero sequence system, $\theta_{(1)}$ and $\theta_{(0)}$ respectively, remain constant and equal to

$$\theta_{(1)} = \frac{2\pi}{3} \quad , \quad \theta_{(0)} = \pi \tag{3.4}$$

Thus, the intensity of the electric field is calculated only for the positive and zero sequence charges for the two conductors' systems (real conductors and conductors' images) separately.

Considering that the conductors bring only the positive sequence charges, then each conductor's charge is given in relation (3.5)

$$\underline{Q}_a = \underline{Q}_{(1)} \quad , \quad \underline{Q}_b = \underline{a}^2 \underline{Q}_{(1)} \quad , \quad \underline{Q}_c = \underline{a}\underline{Q}_{(1)} \tag{3.5}$$

where according to relation (3.4), results

$$\underline{Q}_{(1)} = Q_{(1)} \cdot e^{i\frac{2\pi}{3}} \tag{3.6}$$

Replacing relations (3.2), (3.5) and (3.6) in relations (2.7), (2.6) and (2.5) and taking into consideration relation (3.3), results the intensity of the electric field that comes from the positive sequence charge and is given in (3.7) for the conductors' images' system and in (3.8) for the real conductors' system.

$$\underline{\mathbf{E}}'_{(1)} = -\frac{3Q_{(1)}\bar{\mathbf{p}}}{4\pi\varepsilon_0\left(\bar{\mathbf{R}}'^{3} + \bar{\mathbf{p}}^{3}\right)} \cdot \left[\bar{\mathbf{R}}'(1+ij) - \bar{\mathbf{p}}(1-ij)\right] \tag{3.7}$$

$$\underline{\mathbf{E}}_{(1)} = -\frac{3Q_{(1)}\bar{\mathbf{p}}}{4\pi\varepsilon_0\left(\bar{\mathbf{R}}^{3} - \bar{\mathbf{p}}^{3}\right)} \cdot \left[\bar{\mathbf{R}}(1-ij) + \bar{\mathbf{p}}(1+ij)\right] \tag{3.8}$$

Considering that the conductors bring only the zero sequence charges, then each conductor's charge is given in relation (3.9)

$$\underline{Q}_a = \underline{Q}_{(0)} \quad , \quad \underline{Q}_b = \underline{Q}_{(0)} \quad , \quad \underline{Q}_c = \underline{Q}_{(0)} \tag{3.9}$$

where according to relation (3.4), results

$$\underline{Q}_{(0)} = Q_{(0)} \cdot e^{i\pi} \tag{3.10}$$

Replacing relations (3.2), (3.9) and (3.10) in relations (2.7), (2.6) and (2.5) and taking into consideration relation (3.3), results the intensity of the electric field that comes from the zero sequence charge and is given in (3.11) for the conductors' images' system and in (3.12) for the real conductors' system.

$$\underline{\mathbf{E}}'_{(0)} = -\frac{6Q_{(0)}\bar{\mathbf{R}}'^{2}}{4\pi\varepsilon_0\left(\bar{\mathbf{R}}'^{3} + \bar{\mathbf{p}}^{3}\right)} \tag{3.11}$$

$$\underline{\mathbf{E}}_{(0)} = \frac{6Q_{(0)}\bar{\mathbf{R}}^{2}}{4\pi\varepsilon_0\left(\bar{\mathbf{R}}^{3} - \bar{\mathbf{p}}^{3}\right)} \tag{3.12}$$

The intensity of the electric field $\underline{\mathbf{E}}$, at any point in the vicinity of the line, arises finally from the

superimposition of all intensities from relations (3.7), (3.8), (3.11) and (3.12), as shown in (3.13).

$$\underline{\mathbf{E}} = \left(\underline{\mathbf{E}}_{(1)} + \underline{\mathbf{E}}_{(0)}\right) + \left(\underline{\mathbf{E}}'_{(1)} + \underline{\mathbf{E}}'_{(0)}\right) \tag{3.13}$$

From (3.13), results the final expression (3.14), which represents the intensity of the electric field as a double complex number.

$$\begin{aligned}\underline{\mathbf{E}} = -\frac{3}{4\pi\varepsilon_0\left(\bar{\mathbf{R}}^{-3} - \bar{\mathbf{p}}^{-3}\right)\left(\bar{\mathbf{R}}'^{-3} + \bar{\mathbf{p}}^{-3}\right)} \cdot [&(Q_{(1)}\bar{\mathbf{p}}\bar{\mathbf{R}}^{-3}\bar{\mathbf{R}}' + Q_{(1)}\bar{\mathbf{p}}\bar{\mathbf{R}}\bar{\mathbf{R}}'^{-3} - Q_{(1)}\bar{\mathbf{p}}^{-2}\bar{\mathbf{R}}^{-3} + Q_{(1)}\bar{\mathbf{p}}^{-2}\bar{\mathbf{R}}'^{-3} + 2Q_{(0)}\bar{\mathbf{R}}^{-3}\bar{\mathbf{R}}'^{-2} \\ &- 2Q_{(0)}\bar{\mathbf{R}}^{-2}\bar{\mathbf{R}}'^{-3} - Q_{(1)}\bar{\mathbf{p}}^{-4}\bar{\mathbf{R}}' + Q_{(1)}\bar{\mathbf{p}}^{-4}\bar{\mathbf{R}} + 2Q_{(1)}\bar{\mathbf{p}}^{-5} - 2Q_{(0)}\bar{\mathbf{p}}^{-3}\bar{\mathbf{R}}'^{-2} - 2Q_{(0)}\bar{\mathbf{p}}^{-3}\bar{\mathbf{R}}^{-2}) + \\ &+ ij(Q_{(1)}\bar{\mathbf{p}}\bar{\mathbf{R}}^{-3}\bar{\mathbf{R}}' + Q_{(1)}\bar{\mathbf{p}}^{-2}\bar{\mathbf{R}}^{-3} - Q_{(1)}\bar{\mathbf{p}}^{-4}\bar{\mathbf{R}}' - Q_{(1)}\bar{\mathbf{p}}\bar{\mathbf{R}}\bar{\mathbf{R}}'^{-3} + Q_{(1)}\bar{\mathbf{p}}^{-2}\bar{\mathbf{R}}'^{-3} - Q_{(1)}\bar{\mathbf{p}}^{-4}\bar{\mathbf{R}})]\end{aligned} \tag{3.14}$$

The rms value of the electric field E is equal to the modulus of the double complex number $\underline{\mathbf{E}}$ and is given in relation (3.15).

$$\begin{aligned}E = \frac{3\sqrt{2}}{4\pi\varepsilon_0} \cdot \left[\frac{1}{\left(R^6 + p^6 - 2R^3p^3\sin 3\theta_R\right)\left(R'^6 + p^6 - 2R'^3p^3\sin 3\theta_{R'}\right)}\right]^{1/2} \cdot \\ [(Q_{(1)}pR^3R'\sin(3\theta_R - \theta_{R'}) - Q_{(1)}p^2R'^3\cos 3\theta_{R'} - Q_{(1)}p^4R'\cos\theta_{R'} + Q_{(0)}R^3R'^2\cos(3\theta_R - 2\theta_{R'}) \\ - Q_{(0)}R^2R'^3\cos(2\theta_R - 3\theta_{R'}) - Q_{(0)}p^3R'^2\sin 2\theta_{R'} + Q_{(0)}p^3R^2\sin 2\theta_R)^2 + \\ + (Q_{(1)}pRR'^3\sin(\theta_R - 3\theta_{R'}) + Q_{(1)}p^2R^3\cos 3\theta_R + Q_{(1)}p^4R\cos\theta_R + Q_{(0)}R^3R'^2\cos(3\theta_R - 2\theta_{R'}) \\ - Q_{(0)}R^2R'^3\cos(2\theta_R - 3\theta_{R'}) - Q_{(0)}p^3R'^2\sin 2\theta_{R'} + Q_{(0)}p^3R^2\sin 2\theta_R)^2 + \\ + (-Q_{(1)}pR^3R'\cos(3\theta_R - \theta_{R'}) + Q_{(1)}p^2R'^3\sin 3\theta_{R'} + Q_{(1)}p^4R'\sin\theta_{R'} - Q_{(1)}p^5 + Q_{(0)}R^3R'^2\sin(3\theta_R - 2\theta_{R'}) \\ - Q_{(0)}R^2R'^3\sin(2\theta_R - 3\theta_{R'}) - Q_{(0)}p^3R'^2\cos 2\theta_{R'} - Q_{(0)}p^3R^2\cos 2\theta_R)^2 + \\ + (-Q_{(1)}pRR'^3\cos(\theta_R - 3\theta_{R'}) + Q_{(1)}p^2R^3\sin 3\theta_R + Q_{(1)}p^4R\sin\theta_R - Q_{(1)}p^5 + Q_{(0)}R^3R'^2\sin(3\theta_R - 2\theta_{R'}) \\ - Q_{(0)}R^2R'^3\sin(2\theta_R - 3\theta_{R'}) - Q_{(0)}p^3R'^2\cos 2\theta_{R'} + Q_{(0)}p^3R^2\cos 2\theta_R)^2]^{1/2}\end{aligned} \tag{3.15}$$

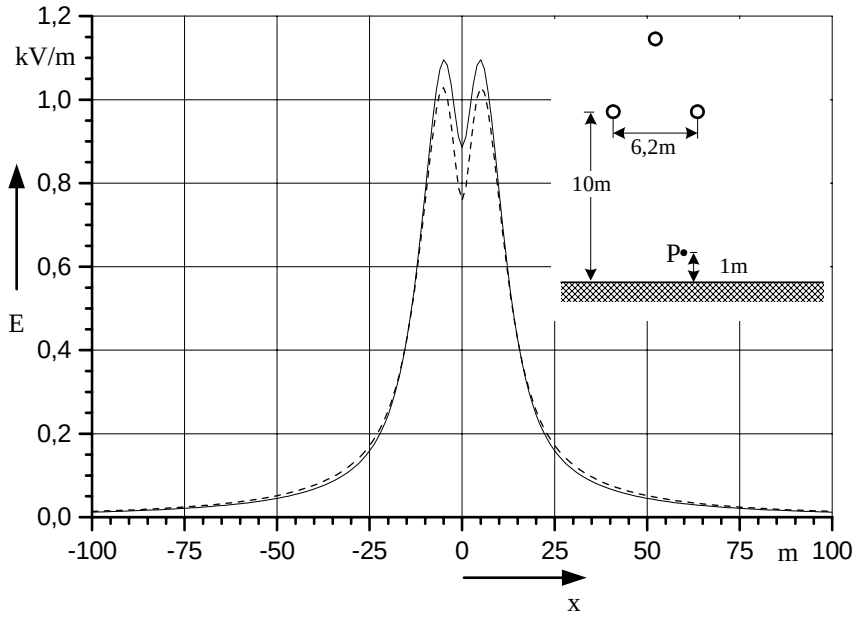
The angles θ_R and $\theta_{R'}$ are shown in figure 2. Relation (3.15) is valid only for the case where the equilateral triangle has the arrangement of figure 2. If the triangle has a different placement in space, then the relative positions of the images would also be different and the calculation of the intensity of the electric field should remade from the beginning.

3.2 Approximate formulas of the electric field

Relation (3.15) is the accurate formula of the intensity of the electric field and depends on the positive and zero sequence charges. This formula is very extensive. A simpler approximate formula may derive taking into account only one of the symmetrical components of the charges.

Figure 3 shows the effect of the positive and zero sequence charge in the intensity of the electric field, for a typical 150kV power line with the conductors in triangular arrangement. From figure 3 results that the positive sequence charge has the bigger effect in the electric field not only close to but also far from the line. However, choosing only the positive sequence charge for the calculation of the electric field, the deviation from the accurate values, mainly close to the line, is considerable.

a)



b)

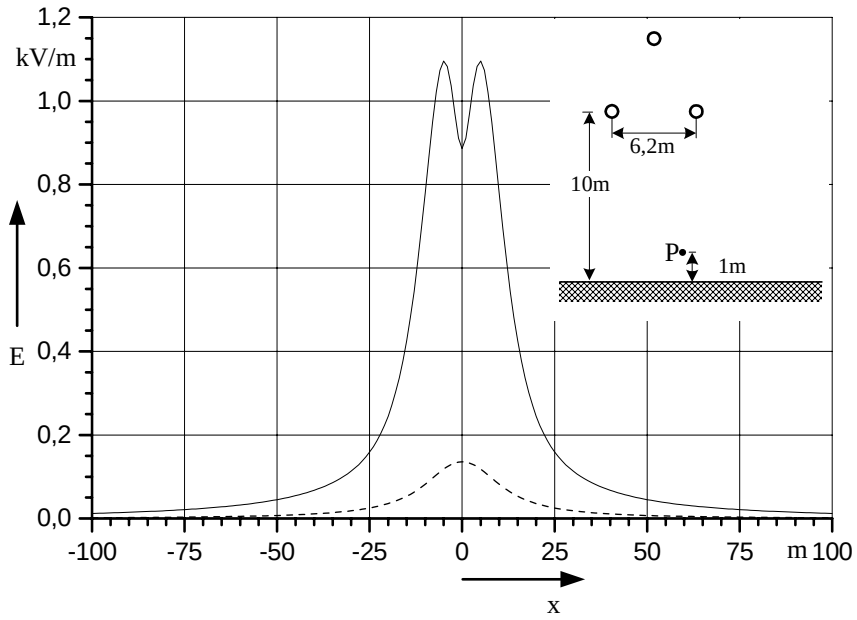


Figure 3. a) Positive and b) zero sequence charge effect in the electric field E that produced by a typical 150kV single circuit line with triangular arrangement of conductors.
——————— Accurate values by formula (3.15) ---------- Symmetrical component's effect

Replacing $Q_{(0)}=0$ in (3.15), the intensity of the electric field by the positive sequence charge is derived in (3.16).

$$E=\frac{3\sqrt{2}Q_{(1)}p}{4\pi\varepsilon_0}\cdot\left[\frac{1}{\left(R^6+p^6-2R^3p^3\sin3\theta_R\right)\left(R'^6+p^6-2R'^3p^3\sin3\theta_{R'}\right)}\right]^{1/2}\cdot$$

$$\left[\left(R^3R'\sin(3\theta_R-\theta_R')-pR'^3\cos3\theta_{R'}-p^3R'\cos\theta_{R'}\right)^2+\left(RR'^3\sin(\theta_R-3\theta_{R'})+pR'^3\cos3\theta_R+p^3R\cos\theta_R\right)^2+\right.$$
$$\left.+\left(-R^3R'\cos(3\theta_R-\theta_R')+pR'^3\sin3\theta_{R'}+p^3R'\sin\theta_{R'}-p^4\right)^2+\left(-RR'^3\cos(\theta_R-3\theta_{R'})+pR'^3\sin3\theta_R+p^3R\sin\theta_R-p^4\right)^2\right]^{1/2} \quad (3.16)$$

Relation (3.16) is also quite extensive. Taking into account the considerable deviation between the approximate values and the accurate values of the electric field, it results that the approximate formula (3.16) is not efficient.

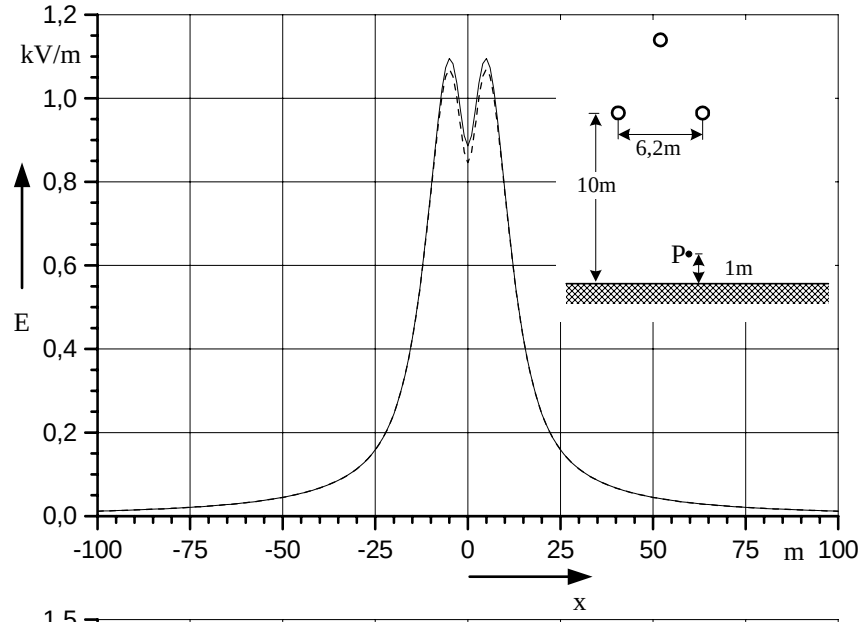
Another formula may derive considering R=R´ and $\theta_R=\theta_{R'}$. Thus, replacing R=R´ and $\theta_R=\theta_{R'}$ in (3.15), the simpler formula (3.17) arises.

$$E=\frac{3}{2\pi\varepsilon_0}\cdot\frac{1}{\left|R^6+p^6-2R^3p^3\sin3\theta_R\right|}\cdot[Q_{(1)}{}^2p^2\left(R^4\sin2\theta_R-pR^3\cos3\theta_R-p^3R\cos\theta_R\right)^2+$$
$$\left(-Q_{(1)}pR^4\cos2\theta_R+Q_{(1)}p^2R^3\sin3\theta_R+Q_{(1)}p^4R\sin\theta_R-Q_{(1)}p^5+2Q_{(0)}R^5\sin\theta_R-2Q_{(0)}p^3R^2\cos2\theta_R\right)^2]^{1/2} \quad (3.17)$$

Relation (3.17) is the accurate formula of the intensity of the electric field on the surface of ground. This relation can also be a very good approximate formula for the electric field, for low calculation heights (up to 1m), as well as for far distances from the line.

Figure 4 shows the comparison of the electric field E produced by a single circuit line with the conductors in triangular arrangement, as it is calculated by the accurate formula (3.15) and the approximate formula (3.17). In figure 4a the comparison between the two formulas is made for calculation height 1m from the ground, while in figure 4b the comparison is made for calculation height 3m from it.

a)



b)

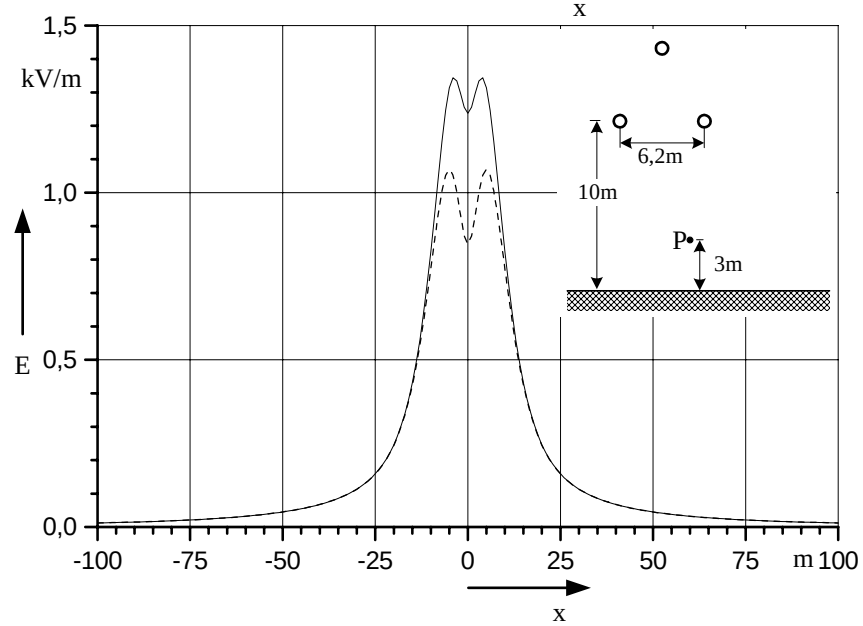


Figure 4. Intensity of the electric field E produced by a typical 150kV single circuit line with triangular arrangement of the conductors, as it is calculated from the accurate formula (3.15) and the approximate formula (3.17) for height a) 1m and b) 3m from the ground.

——————— Accurate formula (3.15) ---------- Approximate formula (3.17)

Figure 4a shows that for low calculation heights (up to 1m), the approximate formula (3.17) gives the intensity of the electric field with exceptional precision, not only far from the line, but also close to it. Figure 4b shows that for bigger calculation heights, the formula (3.17) gives satisfying results only for far distances from the line, while close to it the deviation is significant.

4 Conclusions

The electric field produced by power lines of big length in comparison with the distances between the conductors and the distances between the conductors and the ground, can be expressed with extensive analytical formulas. In the present paper a method to derive the analytical formulas of the electric field has been developed. This method is based on the analysis of the intensity of the electric field into two multipole expansions, one from the real conductors' system and the other from the conductors' images' system. For the simplification of the mathematical expressions double complex numbers are used. Due to the asymmetry of conductors' charges, they are analyzed in their symmetrical components.

Using this method the accurate analytical formula for the intensity of the electric field produced by single circuit lines with the conductors in triangular arrangement is given. This relation may be used for the accurate calculation of the intensity of the electric field, at any point in the vicinity of the lines, close to or far from them. From the accurate formula, a simpler approximate formula with very good precision is derived, which is valid either for low calculation heights (up to 1m) either for bigger heights in far distances from the line.

References

[1] ICNIRP: Guidelines for limiting exposure to time-varying electric, magnetic and electromagnetic fields (up to 300GHz*), Health Physics*, Vol. 74, No 4, pp 494 -522, April 1998.

[2] European Union Council: Recommendation of 12 July 1999 on the limitation of exposure of the general public to electromagnetic fields (0Hz – 300GHz), (1999/519/EC).

[3] European Parliament and Council: Directive 2004/40/EC of 29 April 2004 on the minimum health and safety requirements regarding the exposure of workers to the risks arising from physical agents (electromagnetic fields).

[4] G. Filippopoulos and D. Tsanakas, *Analytical calculation of the magnetic field produced by electric power lines. IEEE Trans. on Power Delivery*, Vol. 20, pp. 1474-1482, 2005.

[5] I. L. Kantor and A.S. Solodovnikov, *Hypercomplex numbers-An Elementary Introduction to Algebras*. Berlin, Germany: Springer –Verlag, 1989

[6] J. Bojanowski, "Vector description of polarized and unpolarized light in double – complex calculus", Optics Lasers Eng., vol. 22, pp. 291-304, 1995.

[7] W. T. Kaune and L. E. Zaffanella, *"Analysis of magnetic fields produced far from electric power lines," IEEE Trans. on Power Del.*, vol. 7, no. 4, pp. 2082-2091, Oct. 1992.

ON THE ANALYSIS OF EMF GENERATED BY POWER LINES

ALESSANDRO MORI

MARIO CALAMIA

DEPARTMENT OF ELECTRONICS AND TELECOMMUNICATIONS,
UNIVERSITY OF FLORENCE,
VIA DI SANTA MARTA, 3
50139 FIRENZE (ITALY)
alessandro.mori@unifi.it
mario.calamia@unifi.it

Abstract
In this paper we discuss the human exposure level for electric and magnetic fields generated by power lines. In particular, we consider the real case of a populated area in Tuscany (Italy) crossed by two high voltage (380 kV) power lines. We carried out a wide measurement campaign and also estimated the electric and magnetic fields generated by the power lines by means of simple and full-wave models (based on the Method of Moments).
The measurement data are used to verify the accuracy of the models. The estimated electric and magnetic fields are then used to evaluate the field exposure in the whole area.
In this paper, we briefly describe the models used in the analysis. We then compare and examine the results obtained from the measurements and the models. Finally, we discuss the model exploitation.

Introduction

The problem of evaluating the power line field exposure is complicated for two reasons. The strong variation of the electric current in a power line reflects on the variation of the generated magnetic field, and the accurate estimation of the electric field generated by a power line can be a very complicated problem due to the complexity of the environment. If the area to be analyzed is large (in our case about 700 m × 250 m) an accurate evaluation of the human exposure level only by measures can be impracticable. Moreover, in case of evaluation of the exposure level for the magnetic field, it is necessary to analyze the field over a large time span (several months – one year). Even for this reason an accurate evaluation of the human exposure level only by measures can be impracticable. On the contrary, the combined utilization of measurements and numerical models allows the characterization of the electric and magnetic fields generated by power lines and the evaluation of the field exposure.

In Italy, the electric and magnetic fields generated by power lines are subjected to the D.P.C.M. (Decree of the Prime Minister) 8th July 2003. It states that the maximum electric field generated by power lines (in accessible areas) has not to exceed the effective value of 5 kV/m. For the effective value of the magnetic flux density (here, for sake of brevity, the magnetic field), the D.P.C.M. establishes three limits. The maximum value has not to exceed 100 μT. In babies playing fields, schools, houses and, in general, in areas where people can stay more than 4 hours/day, the value of 10 μT, evaluated as median over a time span of 24 hours, has not to be exceeded. Finally, in case of a new power line near babies playing fields, schools, houses and, in general, in areas where people can stay more than 4 hours/day, and/or new buildings the median value of 3 μT has not to be exceeded.

The fact to have to evaluate the median value of the magnetic field over 24 hours makes hard to carry out a measurement campaign in a large area. The Italian regulations CEI 211-6 gives suggestions about a measurement campaign and allow the use of a numerical model, recommending measurements where a numerical model estimates a field intensity greater than 50% of the limit value. In our case we have collected a large measurement set (one hundred points / two heights for point / two dates per point), we have used these data in order to evaluate the numerical model accuracy, and we have used the numerical model to estimate the human

exposure level [1], [2].
The Italian regulations CEI 211-4 describes two models (for the magnetic and electric field, respectively) to estimate the fields generated by power lines. These models are two-dimensional, i.e. consider the two-dimensional problem obtained from a perpendicular plane cut of the power line, containing the test point. In order to estimate the magnetic field, the terrain is considered completely transparent, so the Biot-Savart law for a infinite straight wire can be directly used. In order to estimate the electric field, the terrain is assumed as an infinite plane parallel to the power line wires and with an electric potential of 0 V. In order to use these (and the others) numerical models, we have collected all the geometrical and electrical characteristics of the power lines, including the line current and voltage recording (one sample per hour for one year).
We have also used others models, to represent in more detail the real situation. In particular, we have used a three dimensional Biot-Savart model in order to estimate the magnetic field, and a 2D full wave model, based on the Method of Moments [3], in order to estimate the electric field. In this model the profile of the terrain and of buildings on the plane perpendicular to the power line wires and containing the test points are considered at 0 V and are discretized by linear segments with an unknown uniform electric charge distributed on. Also, a three dimensional model is considered, where the AIM (Adaptive Integral Method) [4], [5] approach is used to overcome the computational time and dynamic memory requests of the classical Method of Moments in case of a large number of unknowns.
In the following sections we briefly described the models used, comparing the results with the measurements.

Magnetic field model
We have used two numerical models to estimate the magnetic field generated by power lines. Both models use the Biot-Savart law, in two and three dimensions, respectively. In the following, we describe these models and the results obtained.

Two dimensional model
The two dimensional model follows the Italian regulations CEI 211-4. The fields are considered almost static, the wires of the power lines are assumed as infinite straight wires with uniform current and passing by the intersection between the real wire and the perpendicular plane containing the test point. The terrain and other objects (buildings, etc.) are considered having the same magnetic permeability of the air. So, they are completely transparent to the magnetic field and the classical Biot-Savart law can be employed to evaluate the contribution of a wire to the total magnetic field. This situation is sketched in Fig. 1.
The magnetic field generated by the power line is given by

$$\vec{B}(\vec{r}) = \sum_{i=1}^{M} \vec{B}_i(\vec{r}) = \frac{\mu}{2\pi} \sum_{i=1}^{M} I_i \frac{\hat{u}_i}{d_i} \quad ,$$

where M is the number of wires, I_i is the current phasor flowing on wire i, d_i is the distance between the wire i and the test point on the plane perpendicular to the wire, and

$$\hat{u}_i = \hat{x} \times \hat{d}_i = \hat{x} \times \frac{\vec{d}_i}{d_i} \quad .$$

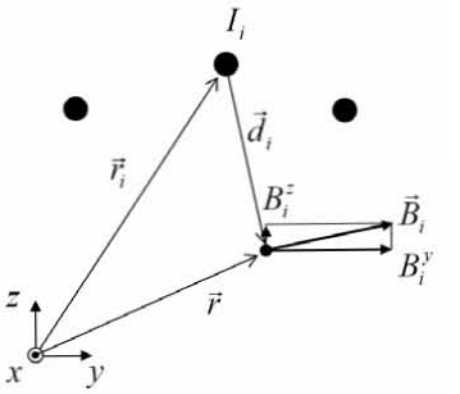


Fig. 1**:** Two dimensional model geometry for the evaluation of the magnetic field.